

Advances in Science, Technology & Innovation  
IEREK Interdisciplinary Series for Sustainable Development

Ali Al-Maktoumi · Osman Abdalla · Anvar Kacimov · Slim Zekri ·  
Mingjie Chen · Talal Al-Hosni · Kaveh Madani *Editors*

# Water Resources in Arid Lands: Management and Sustainability

---

# Advances in Science, Technology & Innovation

## IEREK Interdisciplinary Series for Sustainable Development

### Editorial Board

Anna Laura Pisello, Department of Engineering, University of Perugia, Italy

Dean Hawkes, University of Cambridge, Cambridge, UK

Hocine Bougdah, University for the Creative Arts, Farnham, UK

Federica Rosso, Sapienza University of Rome, Rome, Italy

Hassan Abdalla, University of East London, London, UK

Sofia-Natalia Boemi, Aristotle University of Thessaloniki, Greece

Nabil Mohareb, Faculty of Architecture - Design and Built Environment,  
Beirut Arab University, Beirut, Lebanon

Saleh Mesbah Elkaffas, Arab Academy for Science, Technology, Egypt

Emmanuel Bozonnet, University of la Rochelle, La Rochelle, France

Gloria Pignatta, University of Perugia, Italy

Yasser Mahgoub, Qatar University, Qatar

Luciano De Bonis, University of Molise, Italy

Stella Kostopoulou, Regional and Tourism Development, University of Thessaloniki,  
Thessaloniki, Greece

Biswajeet Pradhan, Faculty of Engineering and IT, University of Technology Sydney,  
Sydney, Australia

Md. Abdul Mannan, Universiti Malaysia Sarawak, Malaysia

Chaham Alalouch, Sultan Qaboos University, Muscat, Oman

Iman O. Gawad, Helwan University, Egypt

Anand Nayyar , Graduate School, Duy Tan University, Da Nang, Vietnam

### Series Editor

Mourad Amer, International Experts for Research Enrichment and Knowledge Exchange  
(IEREK), Cairo, Egypt

**Advances in Science, Technology & Innovation (ASTI)** is a series of peer-reviewed books based on important emerging research that redefines the current disciplinary boundaries in science, technology and innovation (STI) in order to develop integrated concepts for sustainable development. It not only discusses the progress made towards securing more resources, allocating smarter solutions, and rebalancing the relationship between nature and people, but also provides in-depth insights from comprehensive research that addresses the **17 sustainable development goals (SDGs)** as set out by the UN for 2030.

The series draws on the best research papers from various IEREK and other international conferences to promote the creation and development of viable solutions for a **sustainable future and a positive societal** transformation with the help of integrated and innovative science-based approaches. Including interdisciplinary contributions, it presents innovative approaches and highlights how they can best support both economic and sustainable development, through better use of data, more effective institutions, and global, local and individual action, for the welfare of all societies.

The series particularly features conceptual and empirical contributions from various interrelated fields of science, technology and innovation, with an emphasis on digital transformation, that focus on providing practical solutions to **ensure food, water and energy security to achieve the SDGs**. It also presents new case studies offering concrete examples of how to resolve sustainable urbanization and environmental issues in different regions of the world.

The series is intended for professionals in research and teaching, consultancies and industry, and government and international organizations. Published in collaboration with IEREK, the Springer ASTI series will acquaint readers with essential new studies in STI for sustainable development.

**ASTI series has now been accepted for Scopus (September 2020). All content published in this series will start appearing on the Scopus site in early 2021.**

More information about this series at <http://www.springer.com/series/15883>

---

Ali Al-Maktoumi · Osman Abdalla ·  
Anvar Kacimov · Slim Zekri ·  
Mingjie Chen · Talal Al-Hosni ·  
Kaveh Madani  
Editors

# Water Resources in Arid Lands: Management and Sustainability



*Editors*

Ali Al-Maktoumi  
Water Research Center  
Sultan Qaboos University  
Al-Khod, Oman

Anvar Kacimov  
Department of Soils, Water, and  
Agricultural Engineering  
College of Agricultural and Marine Sciences  
Sultan Qaboos University  
AlKhod, Oman

Mingjie Chen  
Water Research Center  
Sultan Qaboos University  
Al-Khod, Oman

Kaveh Madani  
Henry Hart Rice Senior Fellow  
The MacMillan Center  
Department of Political Science  
Yale University  
New Haven, CT, USA

Osman Abdalla  
Department of Earth Sciences  
College of Science  
Sultan Qaboos University  
Al-Khod, Oman

Slim Zekri  
Department of Natural Resources Economics  
College of Agricultural and Marine Sciences  
Sultan Qaboos University  
Al-Khod, Oman

Talal Al-Hosni  
Department of Earth Sciences  
College of Science  
Sultan Qaboos University  
Al-Khod, Oman

ISSN 2522-8714 ISSN 2522-8722 (electronic)  
Advances in Science, Technology & Innovation  
IEREK Interdisciplinary Series for Sustainable Development  
ISBN 978-3-030-67027-6 ISBN 978-3-030-67028-3 (eBook)  
<https://doi.org/10.1007/978-3-030-67028-3>

© The Editor(s) (if applicable) and The Author(s), under exclusive license to Springer Nature Switzerland AG 2021  
This work is subject to copyright. All rights are solely and exclusively licensed by the Publisher, whether the whole or part of the material is concerned, specifically the rights of translation, reprinting, reuse of illustrations, recitation, broadcasting, reproduction on microfilms or in any other physical way, and transmission or information storage and retrieval, electronic adaptation, computer software, or by similar or dissimilar methodology now known or hereafter developed.

The use of general descriptive names, registered names, trademarks, service marks, etc. in this publication does not imply, even in the absence of a specific statement, that such names are exempt from the relevant protective laws and regulations and therefore free for general use.

The publisher, the authors and the editors are safe to assume that the advice and information in this book are believed to be true and accurate at the date of publication. Neither the publisher nor the authors or the editors give a warranty, expressed or implied, with respect to the material contained herein or for any errors or omissions that may have been made. The publisher remains neutral with regard to jurisdictional claims in published maps and institutional affiliations.

This Springer imprint is published by the registered company Springer Nature Switzerland AG  
The registered company address is: Gewerbestrasse 11, 6330 Cham, Switzerland

---

## Editorial Board of Conference Proceedings

- (1) Dr. Ali Al Maktoumi  
Director of Water Research Center  
Associate Professor  
Department of Soils, Water and Agricultural Engineering  
College of Agricultural and Marine Sciences  
Sultan Qaboos University  
[ali4530@squ.edu.om](mailto:ali4530@squ.edu.om)
- (2) Dr. Osman Abdalla  
Associate Professor  
Earth Sciences Department  
College of Science  
Sultan Qaboos University  
[osman@squ.edu.om](mailto:osman@squ.edu.om)
- (3) Prof. Anvar Kacimov  
Professor  
Department of Soils, Water and Agricultural Engineering  
College of Agricultural and Marine Sciences  
Sultan Qaboos University  
[anvar@squ.edu.om](mailto:anvar@squ.edu.om)
- (4) Prof. Slim Zekri  
Professor  
Head of the Department of Natural Resource Economics  
College of Agricultural & Marine Sciences  
Sultan Qaboos University  
[slim@squ.edu.om](mailto:slim@squ.edu.om)
- (5) Dr. Mingjie Chen  
Research Scientist  
Water Research Center  
Sultan Qaboos University  
[mingjie@squ.edu.om](mailto:mingjie@squ.edu.om)
- (6) Dr. Talal Al Hosni  
Assistant Professor  
Department of Earth Sciences  
College of Science  
Sultan Qaboos University  
[hosni@squ.edu.om](mailto:hosni@squ.edu.om)

- (7) Dr. Kaveh Medani  
Henry Hart Rice Senior Fellow  
MacMillan Center for International and Area Studies  
Yale University  
[kaveh.madani@yale.edu](mailto:kaveh.madani@yale.edu)

---

## Reviewers List

Abdelaziz Hirich  
Abdulrahim Al-Ismaili  
Ahmed Douaik  
Ahmed Hadidi  
Alaba Boluwade  
Alexander Osadchiv  
Ali Sulaiman  
Anwar Ahmed  
Arash Malekian  
Azizallah Izady  
Balai Chandra Das  
Elsayed Abu El Ella  
Eman Hasan  
Farhad Hosseinali  
Furat Ahmed Mahmood Al-Faraj  
Furat Al-Faraj  
George Zaimes  
Hamdan Al-Wahaibi  
Ibrahim Al-Helal  
Iswar Chandra Das  
Khadija Semhi  
Luminda Hewawasam  
Mansour Al-Haddabi  
Mohamed Chiban  
Mohammad Mahdi Rajabi  
Mohammed Farfour  
Mushtaque Ahmed  
Nalusamy Sivakumar  
Narasimman Sundararajan  
Pankaj Pathare  
Peter Zavialov  
Rashid Al-Yahyai  
Rashid Umar  
Rifaat Abdalla  
Roohollah Noori  
Said Al-Ismaily  
Slim Zekri  
Sundarajan Narasimman  
Yaseen Al-Mulla  
Yassine Charabi

---

## Preface

The scarce freshwater resources in arid areas are under increasing pressure from population and economic growth, food demand, expanding irrigated agricultural areas, and climate change. The water deficit is especially drastic in arid areas characterized by low precipitation and high evaporation rates. In arid areas, groundwater is usually the only natural water resources and is endangered by excess agricultural extraction and seawater intrusions to coastal aquifers. Climate change leads to temperature increase and shifts of precipitation patterns, and likely increases the frequency of flooding and drought seasons. It is important to understand the impact of climate changes on irrigation, subsurface hydrology, flood risk, salinization, as well as mitigation approaches to cope with the above-mentioned challenges. Desalination of seawater is a popular way to supplement insufficient domestic water supply in urban areas. In recent years, desalination of brackish water and reuse of treated wastewater are also becoming popular as a non-conventional source of water for mainly for farming activities along with other feasible purposes. In addition, economical management and associated policy reforms are critical to induce water conservation and adoption of water-saving and reuse technologies.

This book entitled *Water Resources in Arid Land: Management and Sustainability* aims to address multiple water issues and challenges in arid land discussed above by selecting excellent studies presented at the 2nd International Conference on Water Resources in Arid Areas (WRAA2020) held online during November 9–11, 2020. This book consists of 6 parts with 31 chapters presenting contributions to a wide range of water sciences in arid regions. The following themes represent the six parts in the book ordered as:

Hydroinformatics  
Water Desalination and Purification Technologies  
Climate Change and Water Resources  
Economics and Management of Wastewater  
Urban Water  
Subsurface Hydrology.

Hopefully, the most recent innovation, trends, and concerns, practical challenges encountered, and the solutions adopted in the field of water sciences presented in this book can enlighten water researchers and authorities in management of water resources in arid land.

Thanks!

Al-Khod, Oman  
Al-Khod, Oman  
Al-Khod, Oman  
Al-Khod, Oman  
Al-Khod, Oman  
Al-Khod, Oman  
New Haven, USA

Ali Al-Maktoumi  
Osman Abdalla  
Anvar Kacimov  
Slim Zekri  
Mingjie Chen  
Talal Al-Hosni  
Kaveh Medani



---

## Acknowledgements

This book assembles selected papers presented at “the 2nd International Conference on Water Resources in Arid Areas” during November 9–11, 2020, in Muscat, Oman, jointly organized by Water Research Center, Sultan Qaboos University (SQU) and Ministry of Agriculture, Fisheries, and Water Resources in Oman. The highly appreciated generous support provided by SQU for the conference has paved the ground for this book. The review of papers conducted by a pool of experts in various fields of water science (names of reviewers are listed in the book) has significantly improved the quality and provided constructive criticism important for quality assurance. We would like to also express our deepest thanks and gratitude to the authors of the selected papers for their valuable contribution. We are also indebted to the office work and support of Ms. Maria Diana Austria, the WRC office coordinator.

---

## Contents

### Hydroinformatics

<b>Statistical Approach for Water Quality Evaluation of Irrigation Canals in Egypt</b> . . . . .	3
Eman A. Hasan, Marwa M. Aly, and A. M. I. Abd El Hamid	
<b>Eutrophication Status and Control of Egyptian Northern Lakes</b> . . . . .	15
Eman A. Hasan	
<b>An Integrated System Dynamics Model to Predict the Effects of Management Scenarios on Economic Assessment of Water and Soil Resources in Hableh-Rud River Basin, Iran</b> . . . . .	25
Ebrahim Karimi Sangchini, Majid Ownegh, Amir Sadoddin, and Mahdi Zarghami	
<b>Seasonal Variation for Trace Metals Contamination of Groundwater Using GIS Technology in Pissurlem, Sonshi, Cudnem, Velguem, Surla Watersheds, North Goa District, Goa State, India</b> . . . . .	37
E. Kuppusamy and S. M. Hussain	
<b>The Impact of Different Design Approaches on Fine Sediment Transport in Gezira Scheme, Sudan</b> . . . . .	55
Awad M. Ali, Ishraga S. Osman, Hozaifa Khalid, Maab Albager, and Amal Ibrahim	
<b>Remote Sensing Approach for Estimating Evapotranspiration Using Satellite-Based Energy Balance Models in Al Hamra, Oman</b> . . . . .	73
Ahsan Ali, Yaseen Al-Mulla, Yassin Charabi, Ghazi Al-Rawas, and Malik Al-Wardy	
<b>Application of Dipole–Dipole, Schlumberger, and Wenner–Schlumberger Arrays in Groundwater Exploration in Karst Areas Using Electrical Resistivity and IP Methods in a Semi-arid Area, Southwest Iran</b> . . . . .	81
Leila Mirzaei, Mohammad Kazem Hafizi, and Mohammad Ali Riahi	
<b>A Comparative Study on Regional Drought Characterization Using Estimated Drought Indices in Conjunction with Trend Analysis in Peninsular India</b> . . . . .	91
M. P. Akhtar, L. B. Roy, and Abhishek Sinha	
<b>An Investigation Standardized Precipitation Index Trend in Arid and Semi-arid Region of Pakistan Applying the Innovative Trend Analysis (ITA) Technique</b> . . . . .	111
Kashif Hussain and Muhammad Shahab	
<b>The Impacts of Land-Use Change on the Runoff Characteristics Using HEC-HMS Model: A Case Study in Wadi Al-Mulaikhy Sub-Watershed in Sana’a Basin, Yemen</b> . . . . .	121
Ibrahim Al-Samawi, Abdullah Noman, Khaled Khanbari, Hadi Quriaa, Nabil Al-Areeq, and Musaed Aklan	

<b>Evaluation of Groundwater Quality Variations Using Geographical Information System (GIS) and Multivariate Statistical Techniques: A Case Study from Qa’Jahran Basin, Dhamar, Yemen</b> . . . . .	131
Nabil M. AL-Areeq, Hadi A. Quriaa, Ahmed M. AL-Areeq, and Amer M. Al-Sabri	
<b>Development and Calibration of Transient Groundwater Flow Model for Al Kufrah Region, Southeast Libya</b> . . . . .	147
Abdalraheem M. Huwaysh and Zuhair B. Hafi	
<b>A Multivariate Analysis of Groundwater Chemistry Data</b> . . . . .	167
Ahmed Garba, Muhammad Mukhtar, and Aishatu Hussein Santuraki	
<b>Water Desalination and Purification Technologies</b>	
<b>Successfully Mutual Cooperative Collective Action: Principle of Institutional Arrangement of the Aflaj Irrigation System in Sultanate of Oman</b> . . . . .	175
Ahmed S. Al-Marshoudi, Suzyrman Bin Sibly, and Hamoon Khelghat-Doost	
<b>Monitoring and Counting <i>E. coli</i> Bacterial Growth During Low-Pressure Events in Drinking Water Distribution Networks</b> . . . . .	185
Ashraf Farahat	
<b>Use of Bio-fabricated Silver Nanocomposite Capped with Mud Crab Shell (<i>Scylla serrata</i>) Chitosan for Water Purifications and Sustainable Management of Mosquito Vectors at Stagnant Water System in the Semiarid Zone of Tamil Nadu, India</b> . . . . .	195
Kadarkarai Murugan, Lan Wang, Jiang Shiou Hwang, Jaganathan Anitha, Devakumar Dinesh, Pandiyan Amuthavalli, Murugan Vasanthakumaran, Suresh Kumar, and Hans-Uwe Dahms	
<b>Sulphate Removal from Aqueous Solution Using Modified Bentonite</b> . . . . .	203
Suaibu O. Badmus and Bassam Tawabini	
<b>Climate Change and Water Resources</b>	
<b>Rainfall Change and Spatial-Temporal Aspects of Agricultural Drought in Syria</b> . . . . .	215
Safwan Mohammed, Karam Alsafadi, Seyed Mohammad Nasir Mousavi, and Endre Harsányi	
<b>Rainwater Resources of India’s Desert Area in the West Rajasthan</b> . . . . .	223
P. R. Rakhecha	
<b>Deficit Irrigation as a Strategy in Irrigating Citrus Tree Plantings Under Water Scarcity Conditions</b> . . . . .	235
Mohamed El-Otmani, Fatima Alahian, Charif Azrof, Chouaibi Anouar, and Redouane Choukrallah	
<b>Economics and Management of Wastewater</b>	
<b>Comparative Analysis on Adsorption Properties and Mechanisms of Nitrate and Phosphate Ions by a Zn Fe<sub>3</sub>O<sub>4</sub>/SiO<sub>2</sub> MCM-48 Magnetic Composite: Kinetic and Isotherm Studies</b> . . . . .	247
Mahmoud F. Mubarak and Rasha Hosny	

---

<b>Effect of Treated Wastewater on the Growth and Yield of Two Sweet Corn Varieties: Impact of Doses and Systems of Irrigation</b> .....	263
Afaf Belabhir, Imane Mansir, Lhoussaine Bouchaou, Mohamed El Otmani, Bouchra Yaacoubi, and Redouane Choukr-Allah	
<b>Ecotoxicological Assessment of Three Types of Wastewater Effluents: Catalase as a Biomarker of Oxidative Stress in Marine Bivalves</b> .....	277
Abdellah Meknachi, Mustapha Djellali, and Abdelmalek Badis	
<b>Preparation and Characterization of Activated Carbon Derived from Sewage Sludge for Pollutant Removal from Wastewater</b> .....	289
Abdulbari A. Ahmad and Marwan Alraggad	
<b>Urban Water</b>	
<b>Water Quality Investigation of Recent Wells Which Were Randomly Dug at the Left Side of Mosul City</b> .....	297
Mohammed F. O. Khattab, Eman Sami Al-Sarraj, Hazim J. Mahmood, and Oliver Wiche	
<b>Social Network Analysis of Collaborative Management: Assessment of Human Network Stability in Water Resources Management of Iran</b> .....	307
Iman Islami	
<b>Techno-economic Analysis of Membrane Distillation to Provide Potable Water to the Hormuz Island</b> .....	317
Ramin Haghighi Khoshkhoo, Ameneh Mouvivand, and Mohammad Namazizadeh	
<b>Subsurface Hydrology</b>	
<b>Groundwater Pollution in an Arid Region, Southwest of Iran</b> .....	329
Hassan Daneshian, Nasrollah Kalantari, and Farshad Alijani	
<b>Aquifer Characteristics and Evidence of Saltwater Intrusion in Coastal Groundwater of Niger Delta (Nigeria) Based on Historical and Recent Data</b> .....	345
Aniekan Edet	
<b>Hydrogeophysical Investigation of Fractured Shale Aquifers in Ikwo and Environs, South-Eastern Nigeria</b> .....	367
Amobi C. Ekwe, Georgebest Azuoko, Olufemi V. Omonona, Obialo S. Onwuka, and Julius Onwuka	

---

## About the Editors



**Dr. Ali Al-Maktoumi** is an associate professor of groundwater hydrology at the Department of Soil, Water, and Agriculture Engineering, and Director of Water Research Center, Sultan Qaboos University, Oman. His research focuses on water resources management in an arid area, which includes groundwater modeling/hydrology, the efficiency of recharge dams, and hydro-pedology. Through a number of awarded grants, he established scientific collaboration with Utrecht University, Delft University of Technology, UNESCO-IHE, California Institute of Technology, Jet Propulsion Laboratory-NASA, University of Nebraska-Lincoln, and University of Jordan. This international collaboration resulted in a number of excellent publications and professional scholarly activities.



**Dr. Osman Abdalla** holds B.Sc. (1988) and M.Sc. (1993) in geology from University of Khartoum and Ph.D. (2000) in hydrogeology from University of Technology, Berlin. He is Director of Water Research Center at Sultan Qaboos University since 2012 and Associate Professor of hydrogeology at the Department of Earth Sciences, College of Science. His research bridges several areas of physical and chemical hydrogeology in arid areas and intends to develop a solid platform for hydrogeological and environmental research and training of an international standard with emphasis on groundwater recharge and discharge. Dr. Abdalla has established many international and regional collaborations, been awarded over 10 major grants including His Majesty Trust Fund, and published several articles in reputable international journals.





**Dr. Anvar Kacimov** completed his B.Sc., M.Sc., Ph.D. (fluid mechanics) from Kazan University, USSR, 1982, 1987. He worked at Kazan University, Departments of Seepage and Mathematical Analysis for the period 1982–1998. Since 1998, he worked at SQU, Oman, as assistant–associate full professor, Department of Soils, Water and Agricultural Eng; administratively, HoD (2007–2012); director of Water Research Centre (2011–2012); and dean (2012–2015). His areas of interest include fluid, heat, and mass transfer through porous media (soils, aquifers, oil formations) and of applications in hydroecology, soil physics, irrigation and drainage, hydraulic and hydrologic engineering, groundwater hydrology, fluid mechanics, and reservoir engineering. He has published 128 papers in refereed journals (in English) and has co-authored two books (in Russian). He has been awarded Omani Green Research Award with a Special Commendation of Mitsubishi Corporation (2010) and Best Reviewer of *Vadose Zone Journal* (2005) and *Journal of Irrigation and Drainage Engineering*, ASCE (2013). Research and Innovation Award in Water Sciences, The Research Council, Oman (2018).



**Dr. Slim Zekri** is Professor and Head of the Department of Natural Resource Economics at Sultan Qaboos University (SQU) in Oman. He earned his Ph.D. in Agricultural Economics and Quantitative Methods from the University of Cordoba, Spain. He is Associate Editor of the *Journal of Water Economics and Policy*. Dr. Zekri has worked as a consultant for a range of national and international agencies on natural resource economics, policy and governance, agriculture, and water economics in the Middle East and North Africa. He is member of the Scientific Advisory Group of the FAO's Globally Interesting Agricultural Heritage Systems. His main research interests are in Water Economics and Policy and Environmental Economics. In 2017, he was awarded the Research and Innovation Award in Water Science from the Sultan Qaboos Higher Center for Culture and Science in the Scientific Publications Category.



**Dr. Mingjie Chen** holds a B.E. in Environmental Engineering (1997) from Tsinghua University China, a M.Sc. in Environmental Sciences (2000) from Peking University (China) and a Ph.D. degree in Hydrogeology (2005) from University of California, Santa Barbara (USA). After 10 years of research experiences in Los Alamos National Lab, Tufts University, Lawrence Livermore National Lab in USA, Dr. Chen joined Water Research Center, Sultan Qaboos University (Oman) in 2014 as a senior hydrogeologist. Dr. Chen's research focuses on using laboratory experiments, mathematical models, and numerical techniques to study multiple fluids (water, oil, gas) flow and contaminant transport in subsurface area. He has conducted more than 20 research projects on underground environment remediation, hydrocarbon reservoirs, CO<sub>2</sub>utilization and sequestration, geothermal reservoir, groundwater modeling and management. At present, Dr. Chen serves as Associate Editor for *Arabian Journal of Geosciences*, *Hydrogeology Journal*, and *Journal of Hydrology*.



**Dr. Talal Al-Hosni** holds a B.Sc. in earth sciences (1999) from Sultan Qaboos University (Oman) and a M.Sc. in hydrogeology (2001) from Birmingham University (UK). He received a scholarship from Oman government in 2003 to continue with his Ph.D. study in chemical hydrogeology at Melbourne University (Australia). After his Ph.D. in 2007, Al-Hosni joined the Department of Earth Sciences at Sultan Qaboos University as an assistant professor in the area of hydrogeology and environmental geology. He worked as Theme Supervisor (Omani Land) in the Omani Encyclopedia for the period 2008–2009. Since 2012, he is a member of the scientific committee for the Oman Mountains Atlas Project. Talal is one of the Oman representatives in Group B of the CTBTO. He was the deputy director in the Center for Environmental Studies and Research at Sultan Qaboos University (2018–2019) and is now the head of Earth Sciences Department. He is a geology expert in the courts of Oman. Areas of interest include mainly hot springs, groundwater recharge, intra-aquifers mixing, and usage of bottled water and its impact. Al-Hosni contributed to teaching a number of courses including environmental geology and hydrogeology and developed a number of training courses in the area of EIA of mining and groundwater management.



**Kaveh Madani** is an environmental scientist, educator, and activist, working at the interface of science, policy, and society. He has previously served as the Deputy Vice President of Iran in his position as Deputy Head of Iran's Department of Environment, Vice President of the UN Environment Assembly Bureau, and Chief of Iran's Department of Environment's International Affairs and Conventions Center. He is currently a Henry Hart Rice Senior Fellow at the MacMillan Center for International and Area Studies of Yale University and a Visiting Professor at the Centre for Environmental Policy (CEP) of Imperial College London. He has received a number of awards for his research, teaching, as well as outreach and humanitarian activities, including the New Faces of Civil Engineering recognition in 2012, the Arne Richter Award for Outstanding Young Scientists in 2016, the Walter Huber Civil Engineering Research Prize in 2017, and the Hydrologic Sciences Early Career Scientist Award in 2019.

# Hydroinformatics



# Statistical Approach for Water Quality Evaluation of Irrigation Canals in Egypt

Eman A. Hasan, Marwa M. Aly, and A. M. I. Abd El Hamid

## Abstract

Surface water quality is a vital issue worldwide due to increasing population and development plans. The objective of this study is to develop a statistical approach for assessing irrigation water canals through monitoring pollutant concentrations and a water quality index. Water samples were collected monthly for the two years 2012/2013 and 2013/2014, from fixed locations along the studied canals in Eastern Delta as a case study. The statistical approach used in this work includes weighted arithmetic water quality index (WAWQI), hierarchical clustering analysis (HCA) and principal component/factor analysis (PC/FA). The study revealed that according to the cluster analysis considering WAWQI, 61.11% of the monitoring locations were grouped under cluster A which has the best water quality among the cluster groups. Furthermore, the results of the principal component analysis identified five principal components which were responsible for 81.24% of water quality status in the studied locations. The results obtained from this study can assess the decision makers in applying water quality strategy to control the presence of pollutants from different sources.

## Keywords

Water quality index • Cluster analysis • Principal component analysis • Factor analysis • Eastern Nile Delta canals

E. A. Hasan (✉)

Professor Irrigation and Hydraulics Engineering, Drainage Research Institute, National Water Research Center, Awal Shubra Al Kheimah, Egypt

M. M. Aly

Faculty of Engineering, Helwan University, Matareya, Egypt

A. M. I. Abd El Hamid

Hydraulic Research Institute, National Water Research Center, Awal Shubra Al Kheimah, Egypt

## 1 Introduction

In developing countries, millions of people die annually from water-related diseases (WHO, 2017); for this reason, protection of freshwater resources is an essential aspect. In Egypt, observing water quality of the Nile system began in 1980 using monitoring network (Abdel-Dayem, 2011). The purpose of monitoring network is to measure 34 water quality parameters such as physical, chemical, biological parameters, heavy metals and nutrients to be compared with Egyptian standards. Consequently, water quality index (WQI) is used to reduce the higher number of parameters, rate the health of a stream with a single number and assist in the development of water management strategies (Tyagi et al., 2013; Elshemy, 2016).

Several researchers worldwide assess the water quality of different canals and rivers using WQI (Goher et al., 2014; Manju et al., 2014). Meanwhile, Oketola et al. (2013) reported that hierarchical cluster analysis (HCA), principal component/factor analysis (PC/FA) and correlation matrix are used widely worldwide to illustrate the variations in the water quality as a statistical tool. In Bangladesh, the HCA and WQI were used to evaluate the water quality of an industrial area in Dinajpur (Howladar et al., 2017). FA was used to illustrate the water quality index parameters of the Nile River in Egypt (Yousry & El Gammal, 2015). In China, the water quality of the Tiaoxi River was evaluated by HCA and PCA for physicochemical and microbiological parameters (Vadde et al., 2018).

The research problem is the issue of water quality in the Eastern Nile Delta to support decision makers in taking the appropriate action regarding the protection of water resources. Several researchers assessed water quality of water-courses using different statistical analyses as mentioned before, but the objective of this research is to develop a statistical approach for assessing irrigation water canals through monitoring pollutant concentrations and water quality index.



## 2 Methodology

### 2.1 Study Area

The status of water quality for ten canals in the Eastern Delta region was evaluated. These canals are Tawfiki Rayah, Mansouria Canal, Sharkawiya Canal, Bahr Mois Canal, Daffan Canal, Ismailia Canal, Port Said Canal, Suez Canal, El-Wadi El-Sharky Canal and El-Salam Canal. The research gets to benefit from the GIS technique; the available database of the canals and drains of Egypt is generating a map for the study area using the ArcMap software as shown in Fig. 1. El Salam Canal is the backbone of an agriculture developing project in Egypt that aims at reclaiming more than six hundred thousand Feddans in the north-eastern part of the country. The water sources of El-Salam Canal are from mixing agricultural drainage water and freshwater from

the River Nile (Damietta Branch) with variable mixing ratio through the year, up to 1:1.

### 2.2 Studied Locations and Parameters

Eighteen monitoring locations of water quality along the ten investigated canals in the Eastern Delta irrigation system are shown in Table 1. Seventeen water quality parameters were studied, namely dissolved oxygen (DO), biological oxygen demand (BOD), chemical oxygen demand (COD), nitrate ( $\text{NO}_3$ ), ammonium ( $\text{NH}_4$ ), total phosphorus (TP), total dissolved solid (TDS), sulfate ( $\text{SO}_4$ ), the power of hydrogen (pH), boron (B), cadmium (Cd), copper (Cu), iron (Fe), manganese (Mn), zinc (Zn), lead (Pb) and nickel (Ni).

Monthly water quality parameters for the two years 2012/2013 and 2013/2014 were obtained from the database



Fig. 1 Eastern Delta region and studied locations

**Table 1** Studied locations in the Eastern Delta irrigation system

No	Location code	Canal name	Description
1	EI01	Tawfiki Rayah	Downstream of the built-up area of Banha city
2	EI02	Tawfiki Rayah	Downstream of the built-up area of Zifta/Mit Ghamr city
3	EI03	Mansouria Canal	Downstream of the built-up area of Mansoura city
4	EI04	Sharkawiya Canal	Upstream of the built-up area of Damietta city
5	EI05	Sharkawiya Canal	Upstream of the drinking water intake of Matariya city
6	EI06	Bahr Mois Canal	Upstream of the Zagazig drinking water intake
7	EI07	Bahr Mois Canal	Downstream built-up area of Zagazig city and inflow from East Wadi Irrigation Canal
8	EI08	Bahr Mois Canal	Upstream of drainage reuse PS* EH02
9	EI09	Daffan Canal	Upstream of drainage reuse PS EH12
10	EI10	Ismailia Canal	Ismailia Canal—at km 15
11	EI11	Ismailia Canal	Downstream of the built-up area of Bilbais city
12	EI12	Ismailia Canal	Upstream the branching and the built-up area of Ismailia city
13	EI13	Port Said Canal	Upstream the built-up area and the drinking water of Port Said city
14	EI14	Suez Canal	Upstream the built-up area and the drinking water intake of Suez city
15	EI15	El-Wadi El-Sharky Canal	Upstream of drainage reuse PS EB03
16	EI18	El-Salam Canal	Upstream of drainage reuse PS ESL02
17	EI19	El-Salam Canal	Upstream of drainage reuse PS ESL04
18	EI21	El-Salam Canal	El-Salam Canal intake from Damietta Branch of the River Nile

\*PS pump station

of the Drainage Research Institute and the Central Water Quality Unit in the Ministry of Water Resources and Irrigation (MWRI).

### 2.3 Statistical Approach

The statistical approach used in this study began with investigating water quality status using WAWQI and then applying statistical techniques (HCA and PC/FA).

#### 2.3.1 Investigating Water Quality Status

The objective of this part is to investigate and evaluate the water quality status of each location along the studied canals using the WAWQI and taking into consideration the Egyptian guidelines (law 48 for 1982 and ministerial decree in 92/2013).

Over the years, several WQIs have been proposed and used appropriately by governmental agencies and researcher; Canadian Council of Ministers of Environment Water Quality Index—CCMEWQI (CCME, 2001), National Sanitation Foundation Water Quality Index—NSFWQI (Brown et al., 1972), Oregon Water Quality Index—OWQI

(Dunnette, 1979) and Weighted Arithmetic Water Quality Index Method—WAWQIM are commonly used (Howladar et al., 2017).

The average WQI of the studied locations was computed by weighted arithmetic method, for the above-mentioned seventeen parameters during the two years. The weighted arithmetic water quality index (WAWQI) was used as it is considered a robust method in water quality analysis (Howladar et al., 2017; Chauhan & Singh, 2010; Chowdhury et al., 2012; Rao et al., 2010; Balan et al., 2012). After Rown et al. (1972), WAWQI was calculated according to Eq. (1).

$$WQI = \frac{\sum_{i=1}^n QiWi}{\sum_{i=1}^n Wi} \quad (1)$$

where

$Qi$ : the quality rating scale

$Wi$ : the unit weight

$N$ : number of parameters.

Equation (2) is used to calculate the quality rating scale (Rown et al., 1972), while for calculating the unit weight for each parameter Eq. (3) is used.

$$Qi = 100[(Vi - Vo)/(Si - Vo)] \quad (2)$$

where

$V_i$ : actual measured value of  $i$ th parameter in the analyzed water

$V_o$ : the ideal value of the parameter in pure water,  $V_o = 0$  except pH = 7 and

$DO = 0.146 \text{ kg/m}^3$  (Tripathy & Sahu, 2005)

$S_i$ : the standard value of its parameter of Egyptian quality guidelines (MWRI, 2013).

$$Wi = \frac{K}{Si} \quad (3)$$

$K$  is proportionally constant and is calculated from Eq. (4).

$$K = \frac{1}{\sum (1/Si)} \quad (4)$$

At the end of this part, the rating (status) of water quality for the studied locations can be obtained after using Table 2.

### 2.3.2 Hierarchical Cluster Analysis (HCA)

Cluster analysis (CA) is one of the large families of statistical techniques whose main purpose is to categorize sampling locations into distinct groups or clusters according to some criteria, such that the within-group similarity is maximized and among-group similarity is minimized. CA joins the most similar observations and successively the next most similar observations (Oketola et al., 2013).

In this study, CA was applied using the monthly values of the seventeen water quality parameters measured at eighteen monitoring locations along Eastern Delta canals for the two years 2012/2013 and 2013/2014 by means of Ward's method using squared Euclidean distance for similarity measurements (Singh et al., 2004). The data used were checked first to be normally distributed ensuring its validity to apply the multivariate statistical techniques (HCA and PC/FA). Kolmogorov–Smirnov and Shapiro–Wilk tests were used to examine the normality status.

### 2.3.3 Principal Component/Factor Analysis (PC/FA)

PCA is a powerful pattern recognition technique that attempts to explain the variance of a large dataset of inter-correlated variables with a smaller set independent variable (principal component) (Simeonov et al., 2003). Factor analysis (FA) generally helps to reduce and simplify the outcomes from the PCA.

For the purposes of this paper, PCA has been carried out upon seventeen parameters for identifying the most significant parameters for the assessment of the water quality of the Eastern Nile Delta canals. Through FA, varimax rotation was applied to determine the varimax factors (VFs) with strong positive loading that can account for high variability.

An eigenvalue gives a measure of the significance of factors with the highest eigenvalues, those are the most significant. Eigenvalues of 1.0 or greater are considered significant (Shrestha & Kazama, 2007). Classification of principal components is thus “strong,” “moderate” and “weak,” corresponding to absolute loading values of >0.75, 0.75–0.50 and 0.50–0.30, respectively (Liu et al., 2003).

It is worth to mention that the STATISTICA 10 software program was used to perform the statistical analysis (HCA and PC/FA) for the water quality parameters.

## 3 Results and Discussion

### 3.1 Investigating Water Quality Status

Table 3 shows the descriptive statistics of the measured parameters at the eighteen studied locations. The basic statistics are described, namely the mean, median, maximum, minimum, variance, standard deviation and variance coefficient of the selected water quality parameters. Regarding the Egyptian guidelines of law 48/1982 and its ministerial decree amendment 92/2013, it must be emphasized that the mean concentrations of some variables such as DO, BOD, COD,  $\text{NO}_3$ ,  $\text{NH}_4$ , TDS, Cu and Pb are higher

**Table 2** Water quality rating according to WAWQI (Brown et al., 1972)

WQI value	Rating of water quality	Grading
0–25	Excellent	A
26–50	Good	B
51–75	Poor	C
76–100	Very poor	D
Above 100	Need treatment	E

**Table 3** Descriptive statistics for water quality parameters measured at Eastern Delta locations

Parameters	Mean*	Median	Min	Max	Variance	Std dev	Var coef	Standard values**
DO	6.490	5.990	3.240	8.020	2.020	1.420	21.879	6
BOD	9.093	6.583	6.000	17.250	16.180	4.022	44.233	6
COD	11.725	8.833	7.833	21.500	23.850	4.883	41.647	10
pH	7.858	7.870	7.770	7.930	0.00	0.041	0.525	6.5–8.5
NO <sub>3</sub>	5.284	4.130	1.820	12.770	13.300	3.647	69.022	2
NH <sub>4</sub>	1.777	1.590	0.950	4.770	0.850	0.920	51.791	0.500
TP	0.316	0.230	0.050	0.640	0.040	0.207	65.484	2
TDS	535	435	306	1172	751	274	51	500
SO <sub>4</sub>	1.829	1.520	1.190	3.310	0.50	0.704	38.504	200
B	0.117	0.124	0.062	0.171	0.00	0.034	29.475	0.5
Cd	0.0004	0.000	0.000***	0.001	0.000	0.001	123.201	0.001
Cu	0.094	0.054	0.000	0.560	0.020	0.128	136.207	0.010
Fe	0.014	0.016	0.000	0.029	0.000	0.008	57.967	0.5
Mn	0.001	0.000	0.000	0.006	0.000	0.002	199.018	0.2
Zn	0.000	0.000	0.000	0.001	0.000	0.000	282.290	0.01
Ni	0.0001	0.000	0.000	0.001	0.000	0.0002	412.311	0.02
Pb	0.024	0.000	0.000	0.168	0.000	0.054	228.754	0.01

\*All the parameters are in milligrams per liter except pH

\*\*Law 48/1982 amended in 2013

\*\*\*Number approximately equal to zero

than the standards; therefore, the water resource needs extensive monitoring process.

### 3.2 WAWQI

The method of calculation of WQI assigned unit weights for the considered parameters of the studied locations in the Eastern Delta. Table 4 shows an example of WAWQI calculation of the monitoring location (EI14) along the Suez Canal; the WAWQI for EI14 was 44.8. It is obvious from the table that the weighted value of copper affected mainly the calculation of WAWQI at EI14.

The results of WAWQI calculation ranged from 25.73 to 135.9 for all the monitoring locations as shown in Fig. 2. Its highest value was at location EI18 that represents water quality of El-Salam Canal after the mixing process of fresh and drainage water from the Nile River and Farsqur drain, respectively, resulting in high water salinity according to Shaban (2017). The lowest WAWQI was at monitoring location EI15 along El-Wadi El-Sharky Canal upstream of drainage reuse PS EB03. According to the calculated values of WAWQI, 30% of the considered locations fall under good quality, poor quality for another 30% and very poor for 20% and the rest 20% of the monitoring locations need more investigation and long-term monitoring to control any source of pollution in the future.

Figure 2 shows also that the three studied locations, namely EI01, EI06 and EI18, have the extreme values of the WAWQI. Table 5 shows the percentages of compatible measurements with the Egyptian water quality guidelines for these locations. From these percentages for (DO, BOD, COD), (NO<sub>3</sub>, NH<sub>4</sub>, TDS) and (Cu) measured at EI01, EI06 and EI18, respectively, there was pollution resulted from domestic, agriculture and industrial activities. Meanwhile, it is clear that the location EI18 has the least percentages of compatible for the above-mentioned water quality parameters according to its location on El-Salam Canal which is fed by reused water as previously explained.

### 3.3 HCA

Since HCA requires the examined data to be normally distributed, Kolmogorov–Smirnov and Shapiro–Wilk tests were used to check the normality status of the seventeen water quality parameters. The results showed that COD, BOD, Fe, B, TP and NO<sub>3</sub> were normally distributed while other studied parameters were transformed to be normally distributed. Then, all the seventeen water quality parameters were used for clustering process.

The relationships between the monitoring locations were resulted from the cluster analyses and were presented in the dendrogram plot, Fig. 3. It is obvious that the whole studied

**Table 4** Calculation of WAWQI at monitoring location EI14 along Suez Canal

Parameters	*Actual measured values ( $V_i$ )	**Standard values ( $S_i$ )	Unit weight ( $W_i$ )	Quality rating ( $Q_i$ )	Weighted values ( $Q_iW_i$ )
DO	4.480	6	0.0001	117.674	0.014
BOD	6.000	6	0.0001	100.000	0.012
COD	8.000	10	0.0004	80.000	0.006
pH	7.840	6.5–8.5	0.0015	168.000	0.016
NO <sub>3</sub>	12.770	2	0.0004	638.500	0.234
NH <sub>4</sub>	1.530	0.5	0.0000	306.000	0.449
TP	0.540	2	0.0000	27.000	0.010
TDS	946.000	500	0.0015	189.200	0.000
SO <sub>4</sub>	2.820	200	0.7340	1.410	0.000
B	0.092	0.5	0.0734	18.400	0.027
Cd	0.000	0.001	0.0015	0.000	0.000
Cu	0.060	0.01	0.0037	600.000	44.034
Fe	0.014	0.500	0.073	2.800	0.004
Mn	0.000	0.200	0.037	0.000	0.000
Zn	0.000	0.010	0.073	0.000	0.000
Ni	0.000	0.020	0.0001	0.000	0.000
Pb	0.000	0.010	0.0001	0.000	0.000
					WAWQI = 44.88

\*All the parameters are in milligrams per liter except pH, multiply all parameters except pH by  $10^{-2}$  to convert and follow S.I units ( $\text{kg}/\text{m}^3$ )

\*\*Law 48 for 1982 and ministerial decree in 92/2013

**Fig. 2** Weighted arithmetic water quality index for monitoring locations

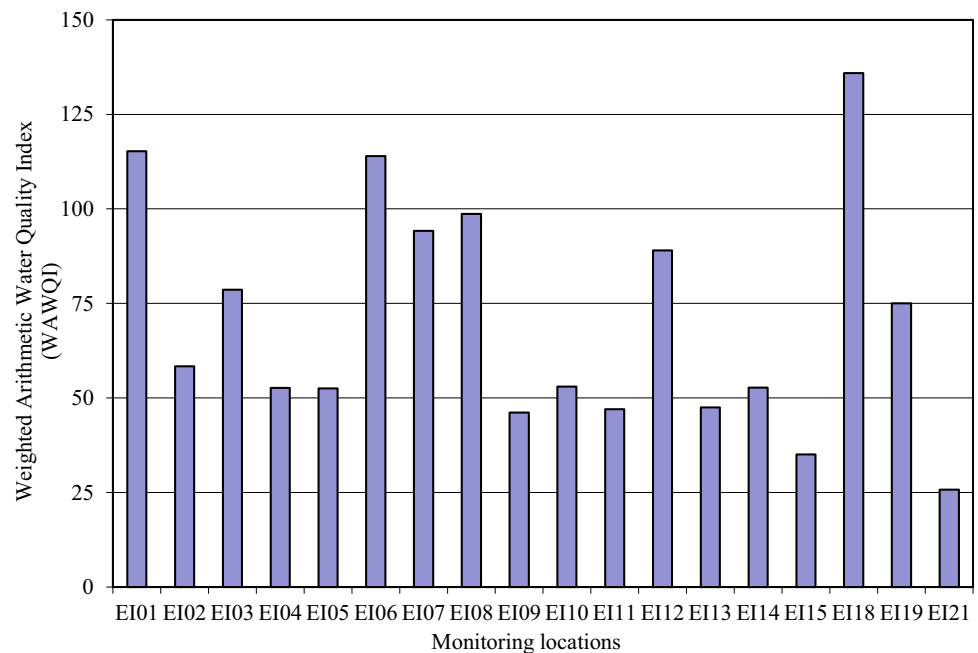


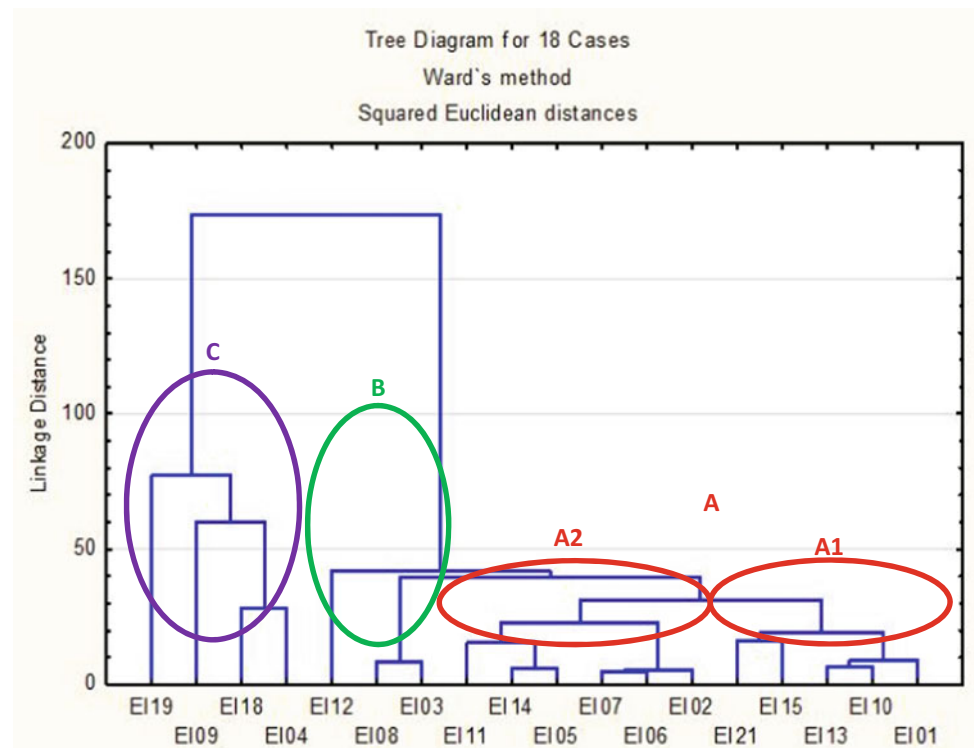


**Table 5** Percentages of compatible measurements for water quality parameters measured at EI01, EI06 and EI18

Parameters	*Egyptian water quality guidelines	Percentage of compatible measurements		
		EI01	EI06	EI18
DO	6	0	0	0
BOD	6	84	75	17
COD	10	67	59	17
pH	6.5–8.5	100	100	100
NO <sub>3</sub>	2	17	0	0
NH <sub>4</sub>	0.50	59	100	0
TP	2	100	100	100
TDS	500	38.89	82	0
SO <sub>4</sub>	200	100	100	100
B	0.50	100	100	100
Cd	0.001	100	100	100
Cu	0.01	12	17.50	0
Fe	0.50	100	100	100
Mn	0.20	100	100	100
Zn	0.01	100	100	100
Ni	0.02	100	100	100
Pb	0.01	100	100	100

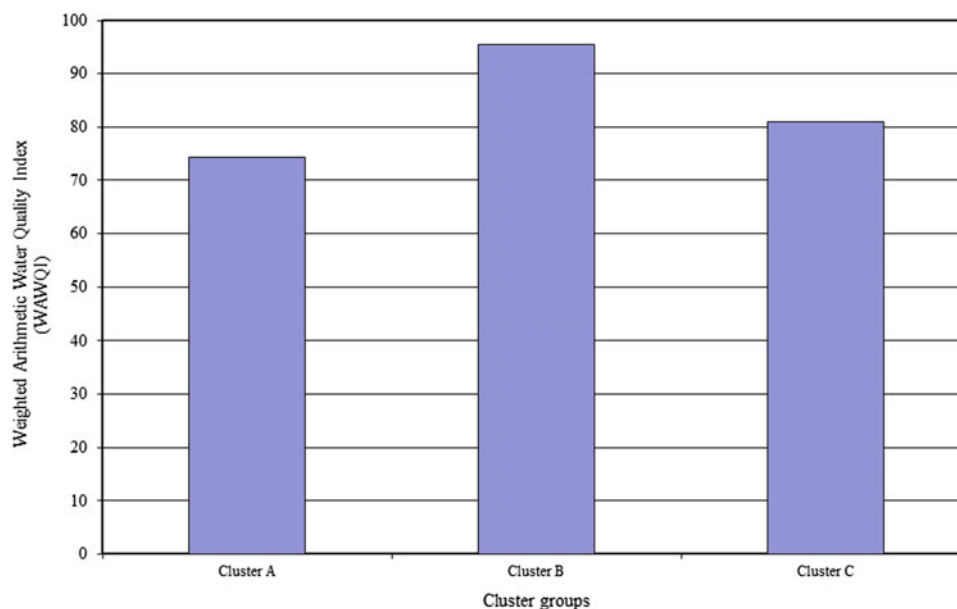
\*Law 48 for 1982 and ministerial decree in 92/2013

**Fig. 3** Dendrogram shows the relationship between monitoring locations in Eastern Delta



**Table 6** Cluster analysis of monitoring locations

Group	Location code	Cluster	Cluster percentage	Water quality status
A1	EI01, EI10, EI13, EI15, EI21	Cluster A	61.11	Poor
A2	EI02, EI06, EI07, EI05, EI14, EI11			
B	EI03, EI08, EI12	Cluster B	16.67	Very poor
C	EI04, EI18, EI09, EI19	Cluster C	22.22	Very poor

**Fig. 4** Weighted arithmetic water quality index of cluster groups

locations formed three main groups of the cluster. Table 6 shows that cluster A groups 61.11% of the studied locations whereas cluster B represents 16.67% of locations and finally cluster C includes 22.22% of the total locations.

Figures 4 and 5 show the classifications of different studied locations according to their WAWQI and cluster group, and cluster group A has the best water quality among the cluster groups as it has the lowest value of the WAWQI. This result can assess the decision maker in management of water quality in the Eastern Delta.

### 3.4 PC/FA

According to PC/FA, five principal factors were detected to be responsible of 81.24 of the total variances in the water quality data. Table 7 shows that each of the five factors has eigenvalue greater than 1, and Factor1 (PC 1) is the most significant variables which explain 37.25% of the total variance and was strongly loaded with DO, NO<sub>3</sub>, TP, TDS and SO<sub>4</sub>, moderately loaded with BOD and COD and

weakly loaded with B and Cu, while Factor2 (PC 2) contains 18.56% of the total variance which was strongly loaded with Cd and Cu, moderately loaded with BOD, COD and Pb and weakly loaded with DO, TP and Ni. Factor3 (PC 3) accounts 11.25% of the total variance and was strongly loaded with Zn and Ni and moderately loaded with B and Pb. Factor4 (PC 4) possesses 7.95 of the total variances and was strongly loaded with NH<sub>4</sub>, moderately loaded with pH and weakly loaded with Cd, BOD and COD. Finally, Factor5 (PC 5) represents 6.23% of the total variance, weakly loaded with Fe, BOD and COD as shown in Table 8. The previous analysis proves the presence of organic contamination and wastewater from domestic, agricultural and industrial sources.

## 4 Conclusion

In this research, a comprehensive statistical approach was applied to classify, evaluate and identify the significant parameters in water quality of irrigation canals in Eastern

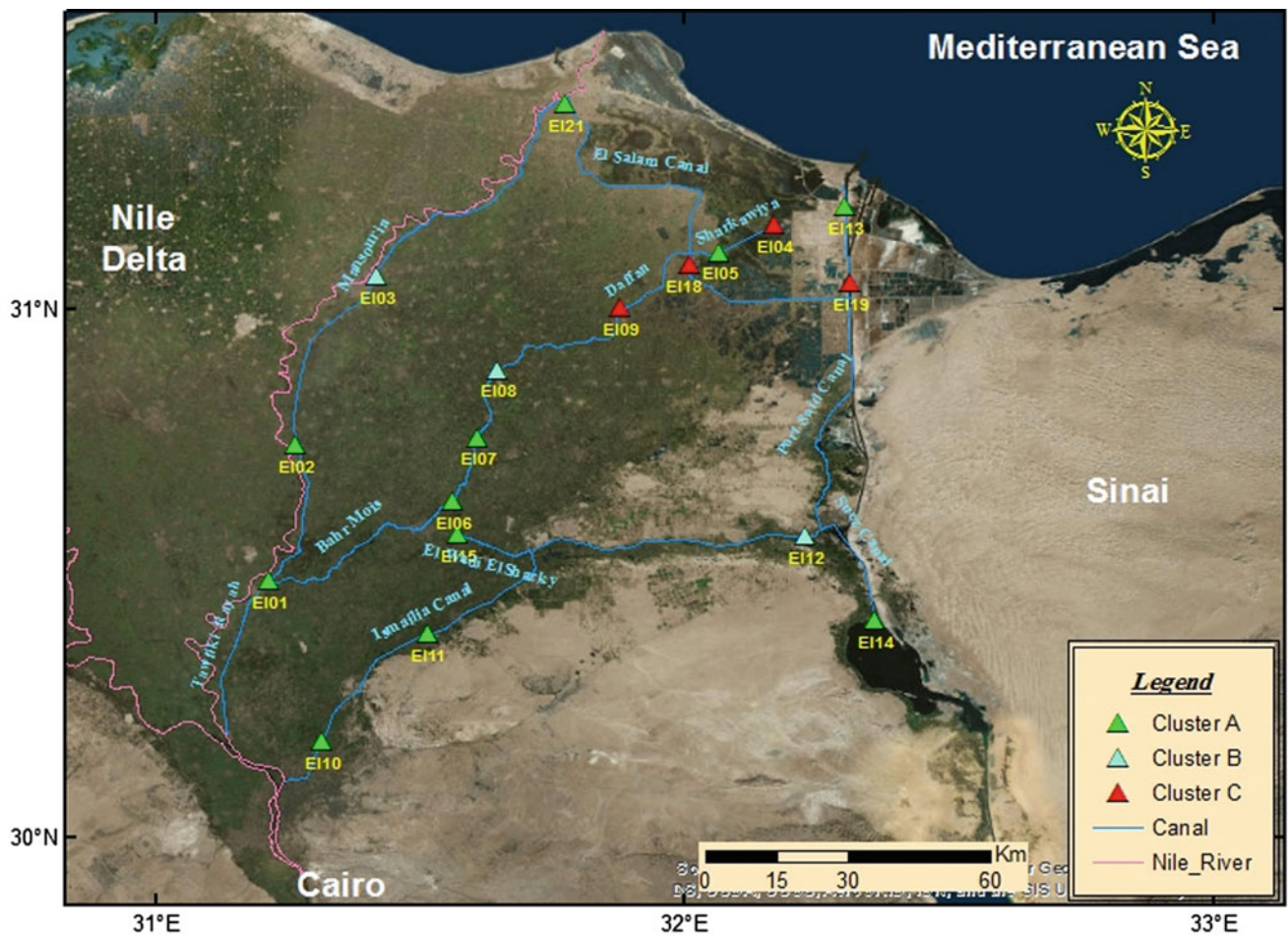


Fig. 5 Water quality clustering in Eastern Delta

Table 7 Eigenvalues and variance percentage

Principal components	Eigenvalue	% total variance	Cumulative eigenvalue	Cumulative percentage
1	6.3321	37.2479	6.3321	37.2479
2	3.1555	18.5618	9.4876	55.8097
3	1.9129	11.2523	11.4005	67.0620
4	1.3509	7.9461	12.7514	75.0081
5	1.0592	6.2305	13.8106	81.2386

Delta of Nile River taking into consideration the Egyptian guidelines of law 48/1982 and ministerial decree in 92/2013. The study revealed that the calculated WAWQI varied along the studied canals, according to the effect of each pollutant to the index calculation. This variation is due to organic pollution, nutrients and sometimes heavy metal concentration. According to the HCA, 61.11% of the studied locations were

grouped under cluster A which has the best water quality among the cluster groups. Furthermore, the results of the PC/FA proved the presence of five principal components responsible for 81.24% of the variation in water quality. The results obtained from this study can assess the decision makers in applying water quality strategy to control the presence of pollutants from different sources.

**Table 8** Factor loadings after varimax rotation

	Factor1	Factor2	Factor3	Factor4	Factor5
DO	-0.717	0.377	-0.295	0.157	-0.100
BOD	0.570	0.502	0.277	0.385	0.312
COD	0.547	0.559	0.265	0.348	0.311
pH	0.088	0.174	0.230	<b>0.675</b>	-0.279
NO <sub>3</sub>	<b>0.955</b>	0.214	-0.007	-0.015	-0.029
NH <sub>4</sub>	0.066	0.021	-0.016	<b>0.849</b>	0.166
TP	<b>0.841</b>	0.305	0.228	0.076	0.012
TDS	<b>0.933</b>	-0.185	0.075	0.053	-0.061
SO <sub>4</sub>	<b>0.938</b>	-0.085	0.134	0.140	0.036
B	0.319	-0.170	<b>0.687</b>	-0.101	-0.327
Cd	0.068	<b>0.766</b>	0.197	0.336	0.013
Cu	0.455	<b>-0.724</b>	-0.005	0.262	-0.011
Fe	-0.024	0.079	<b>-0.622</b>	-0.012	0.311
Mn	-0.012	-0.068	-0.075	-0.001	<b>-0.933</b>
Zn	0.272	0.131	<b>0.895</b>	0.157	0.186
Ni	-0.014	0.434	<b>0.846</b>	0.055	0.119
Pb	0.250	<b>0.638</b>	0.473	-0.016	0.095

\*Significant factor loadings are in bold

**Acknowledgements** The authors are grateful to the staff of the Drainage Research Institute (DRI), special thanks to Professor Dr. Esam Khalifa and Professor Dr. Hussein El Gammal Director of the institute for their continuous support and making all the required data available.

## References

- Abdel-Dayem, S. (2011). Water quality management in Egypt. *International Journal of Water Resources Development*, 27(1), 181–202. <https://doi.org/10.1080/07900627.2010.531522>.
- Balan, I., Madan Kumar, P., & Shivakumar, M. (2012). An assessment of groundwater quality using water quality index in Chennai, Tamil Nadu, India. *Chronicles of Young Scientists*, 3(2), 146–150. <https://doi.org/10.4103/2229-5186.98688>.
- Brown, R. M., McClelland, N. J., Deininger, R. A., O'Connor, M. F. (1972). A water quality index—crossing the psychological barrier. In S. H. Jenkis (Ed.), *Proceedings of International Conference on Water*.
- CCME. (2001). Canadian Environmental Quality Guidelines for the Protection of Aquatic Life, CCME Water Quality Index: technical report, 1.0.
- Chauhan, A., & Singh, S. (2010). Evaluation of Ganga water for drinking purpose by water quality index at Rishikesh, Uttarakhand, India. *Report Opinion*, 2(9), 53–61.
- Chowdhury, R. M., Muntasir, S. Y., & Hossain, M. M. (2012). Water quality index of water bodies along Faridpur-Barisal road in Bangladesh. *Global Engineers and Technologists Review*, 2(3), 1–8.
- Dunnette. (1979). A geographically variable water Quality Index used in Oregon. *Journal Water Pollution Control Federation*, 51(1), 53–61.
- Elshehy, M. (2016). Water quality assessment of Lake Manzala, Egypt: a comparative study. *International Journal of Scientific Research in Environmental Sciences*, 4(6), 196–207. <https://doi.org/10.12983/ijres-2016-p0196-0207>
- Goher, M. E., Hassan, A. M., Abdel-Moniem, I. A., Fahmy, A. H., & El-Sayed, S. M. (2014). Evaluation of surface water quality and heavy metal indices of Ismailia Canal, Nile River, Egypt. *Egyptian Journal of Aquatic Research*, 40(3), 225–233.
- Howladar, M. F., Al Numanbakhth, Md. A., & Faruque, M. O. (2017). An application of water quality index (WQI) and multivariate statistics to evaluate the water quality around Maddhapara Granite Mining Industrial Area, Dinajpur, Bangladesh. *Environmental Systems Research*, 6(1), 6–13. <https://doi.org/10.1186/s40068-017-0090-9>
- Liu, C. W., Lin, K. H., & Kuo, Y. M. (2003). Application of factor analysis in the assessment of groundwater quality in a blackfoot disease area in Taiwan. *Science of the Total Environment*, 313(1–3), 77–89.
- Manju, E. K., George, A. V., & Rekha, V. B. (2014). A comparative study of water quality index (Wqi) of Vagamon and peermade sub-watersheds of Meenachil and Pamba River basins of Western Ghats, Kerala, South India. *IOSR Journal of Environmental Science, Toxicology and Food Technology*, 8(1), 53–58. <https://doi.org/10.9790/2402-08125358>.
- MWRI. (2013). Egyptian Ministry of Water Resources and irrigation, law 48/1982, Protection of the River Nile and Waterways from Pollution “Decree No. 49” (2013) in the amended executive regulations of the law by Minister Decision No. 92/2013. (Arabic Edition).
- Oketola, A. A., Adekolurejo, S. M., & Osibanjo, O. (2013). Water quality assessment of river ogun using multivariate statistical techniques. *Journal of Environmental Protection*, 4(5), 466–479. <https://doi.org/10.4236/jep.2013.45055>.
- Rao, C. S., Rao, B. S., Hariharan, A. V. L. N. S. H., & Bharathi, N. M. (2010). Determination of water quality index of some areas in Guntur district Andhra Pradesh. *International Journal of Applied Biology and Pharmaceutical Technology*, 1(1), 79–86.
- Rown, R. M., McClelland, N. J., Deiniger, R. A., & O'Connor, M. F. A. (1972). Water quality index—Crossing the physical barrier. In S. H. Jenkis (Ed.), *Proceedings in International Conference on water pollution Research Jerusalem*, Vol. 6, pp. 787–797.

- Shaban, M. (2017). Statistical framework to assess water quality for irrigation and drainage canals. *Irrigation and Drainage*, 66(1), 103–117. <https://doi.org/10.1002/ird.2042>.
- Singh, K. P., Malik, A., Mohan, D., & Sinha, S. (2004). Multivariate statistical techniques for the evaluation of spatial and temporal variations in water quality of Gomti River (India)—A case study. *Water Research*, 38(18), 3980–3992.
- Shrestha, S., & Kazama, F. (2007). Assessment of surface water quality using multivariate statistical techniques: A case study of the Fuji river basin, Japan. *Environmental Modelling and Software*, 22(4), 464–475.
- Simeonov, V., Stratis, J. A., Samara, C., Zachariadis, G., Voutsas, D., Anthemidis, A., et al. (2003). Assessment of the surface water quality in Northern Greece. *Water Research*, 37(17), 4119–4124.
- Tripathy, J. K., & Sahu, K. C. (2005). Seasonal hydrochemistry of groundwater in the barrier spit system of the Chilika Lagoon, India. *Journal of Environmental Hydrology*, 13, 1–9.
- Tyagi, S., Sharma, B., Singh, P., & Dobhal, R. (2013). Water quality assessment in terms of water quality index. *American Journal of Water Resources*, 1(3), 34–38. <https://doi.org/10.12691/ajwr-1-3-3>.
- Vadde, K. K., Wang, J., Cao, L., Yuan, T., McCarthy, A. J., & Sekar, R. (2018). Assessment of water quality and identification of pollution risk locations in TiaoxiRiver(Taihu Watershed), China. *Water (Switzerland)*, 10(2), 183. <https://doi.org/10.3390/w10020183>
- WHO (World Health Organization). (2017). *World Water Day Report*. Available at: [www.who.int/water\\_sanitation\\_health/takingchange.html](http://www.who.int/water_sanitation_health/takingchange.html)
- Yousry, M. M., & El Gammal, H. A. A. (2015). Factor analysis as a tool to identify water quality index parameters along the Nile River, Egypt. *Journal of American Science*, 11(2), 36–44. [https://free-journal.umm.ac.id/files/file/005\\_27939am110215\\_36\\_44.pdf](https://free-journal.umm.ac.id/files/file/005_27939am110215_36_44.pdf)





# Eutrophication Status and Control of Egyptian Northern Lakes

Eman A. Hasan

## Abstract

Four coastal lakes fringe the north coast of the Nile Delta, Egypt: Manzala, Maruit, Edku and Burullus. These lakes receive huge amounts of direct and indirect drainage: agriculture, industrial and domestic. Eutrophication of these lakes can have significant negative ecological, social and economic impacts on human. The objective of this paper is to quantify and classify the Carlson trophic state index of the Egyptian northern lakes. Also, control actions to reduce deterioration of northern lakes will be recommended. Data of water quality variables of different lakes are taken from the formal reports of the Egyptian Environmental Affairs Agency (EEAA) Web site. The calculation and classification of Carlson trophic state index (CTSI) are made for the period from 2011 until 2015 according to Carlson method, United States Environmental Protection Agency (USEPA) classification and other variables associated with trophic levels in lakes. These variables are total phosphorus, total nitrogen, chlorophyll-a and Secchi depth. The study revealed that northern lakes suffer from different degrees of eutrophication. Regression analysis results showed that Carlson trophic state index trend is increasing which indicates deteriorating water quality in Lake Maruit, Burullus and Bardawil, declining or improving in Lake Edku and Lake Manzala.

## Keywords

Carlson trophic state index • Eutrophication • Northern lakes • Regression analysis

## 1 Introduction

Carlson's trophic state index (CTSI) is a common method for characterizing a lake's trophic state or overall health. This method uses Secchi's disk transparency, chlorophyll-a and phosphorus measurements (Carlson, 1977). The average values of CTSI of these three parameters will be considered in determining Carlson's trophic state index.

Eutrophication was recognized as a pollution problem in European and North American lakes and reservoirs in the mid-twentieth century. Since then, it has become more widespread. Surveys showed that 53% of lakes in Europe, 48% in North America and 41% in South America are found in eutrophic state (Colin et al., 2007).

The productivity of Kaw Lake, Oklahoma, USA, was evaluated through the interaction of nutrient concentration, mainly total phosphorous, chlorophyll-a and Secchi disk transparency as defined in Carlson trophic state index for the year 2013–2015. The results showed that the lake is eutrophic to hyper-eutrophic (Alemayehu & Francine, 2016).

Eutrophication problem in the Egyptian lakes (except Bardawil Lake) is attributed mainly to the large volumes of wastewaters discharged through land-based effluents to coastal lakes that are connected directly or indirectly to the Mediterranean coastal area. These effluents are loaded by variable amounts of nutrient salts, which promote intensive phytoplankton growth.

In this regard, the Egyptian government has taken action through preparing a comprehensive database for environmental parameters. This was done by implementing the periodic monitoring program of water quality of Egyptian lakes, starting with northern lakes (Maruit—Edku—Burullus—Manzala—Bardawil) with four seasons of field campaigns during each year (EEAA, 2015).

The research problem studied in this work is the deterioration of Egyptian northern lake's status as a result of dumping huge amounts of untreated wastewater into lakes

E. A. Hasan (✉)  
Professor, Irrigation and Hydraulics Engineering, National Water Research Center, Awal Shubra Al Kheimah, Egypt

leading to a loss in fish production. Several researchers tackled different aspects for each lake regarding its eutrophication. Water classification of Lake Manzala was studied through calculation of the TSI and the spatial distribution of eutrophication condition in Lake Environment (Donia & Hussein, 2004).

The eutrophication profile of Lake Burullus was established using a remote sensing approach (Farg & El-Gamal, 2012). They estimated and mapped the reflectance response of chlorophyll-a and transparency. They proved that there was a change in the eutrophic profile of Lake Burullus due to changing the environmental factors affecting the lake. Serious eutrophication levels were assessed in Lake Maruit (Ahmed & Kaiser, 2014). Chlorophyll spatial distribution and corresponding water surface temperatures in polluted water were extracted from 1986 to 2012 satellite images. Their results showed that surface areas exhibiting algal bloom were 29.2 km<sup>2</sup> and surface water temperatures were 22 °C in 1986 and in 2012 increased to 32.5 km<sup>2</sup> and 24 °C.

This work differs from predecessor works that used only one or two parameters in their studies and were limited to study only one lake. The objective of this paper is to quantify and classify the recent trophic state index of the Egyptian northern lakes. Also, control actions to reduce deterioration of northern lakes will be recommended.

## 2 Methodology

### 2.1 Study Area

The study area of this work covers the Egyptian northern lakes that extend along the Mediterranean coastal region of Egypt for about 970 km, from Sallum in the west to Rafah in the east. These natural lakes are Maruit—Edku—Burullus—Manzala and Bardawil as in Fig. 1. The northern lakes receive drainage water from different drainage systems in the Nile Delta. Lake Maruit receives drainage water from El-Qalaa drain, El Umouim drain, and east and west treatment plants of Alexandria and Nubaria canal. Meanwhile, Lake Manzala accommodates the drainage water of the east Delta (except few sub-catchments) through Baher El-Baker and Baher Hadous drain systems (Abdel Ghaffer, 2006).

The drainage water in Lake Burullus is from El Burullus and El Nasser drains in the eastern side of the lake, drains 7, 8, 9 and 11 in the southern side of the lake, Brimbil canal in the western extremity of the lake and Gharbya drain as shown in Fig. 1.

Two drains, namely El-Khairiy and Barzik, convey water to Lake Edku, while Lake Bardawil does not receive any drainage water. The water sources of El-Khairiy Drain are from three drainage waters coming from El-Bousely, Edku and Damanhour sub-drains.

### 2.2 Data Sources and Collection

Data of water quality variables of different lakes are taken from the formal reports of the Egyptian Environmental Affairs Agency (EEAA) Web site. The total number of monitoring and sampling points along the northern lakes is fifty-four points, ten points for Maruit, nine points for Edku, eleven points along Manzala and twelve points for each of Lake Burullus and Bardawil, Fig. 1. Water samples were taken from these monitoring points four times per year during the period from 2011 to 2015 for water quality analysis.

In this work, measures of water quality parameters including chlorophyll-a, total phosphorus, total nitrogen and Secchi depth of five Egyptian lakes along five years (2011–2015) are used in classification of trophic state of Egyptian lakes. Table 1 shows the statistical indices of water quality parameters used in this research.

### 2.3 Data Analysis

To fulfill the objective of this research, Carlson trophic state index (CTSI) for the Egyptian northern lakes is calculated according to Carlson (1977) as explained in the following equations:

$$\text{TSI}(\text{SD}) = 60 - 14.41 \ln(\text{SD}) \quad (1)$$

$$\text{TSI}(\text{Chl-a}) = 9.81 \ln + 30.6 \quad (2)$$

$$\text{TSI}(\text{TP}) = 14.42 \ln(\text{TP}) + 4.15 \quad (3)$$

$$\text{Average (CTSI)} = \left[ \frac{(\text{TSI}(\text{SD}) + \text{TSI}(\text{Chl-a}) + \text{TSI}(\text{TP}))}{3} \right] \quad (4)$$

where

ln = natural log

SD is the Secchi depth (m)

Chl-a is the chlorophyll-a average concentration ( $\mu\text{g L}^{-1}$ )

TP is the total phosphorus average concentration ( $\mu\text{g L}^{-1}$ ).

Classification of trophic state is carried out according to average CTSI, United States Environmental Protection Agency (USEPA 1974) and the variables associated with trophic levels in lakes. These variables are total phosphorus, total nitrogen, chlorophyll-a and Secchi depth (Vollenweider & Kerekes, 1980).

Three trophic state categories are used to describe lakes as they grow progressively greener: oligotrophic, mesotrophic and eutrophic (Brown & Simpson, 2011). These categories reflect a lake's nutrient and clarity levels. The CTSI index ranges from zero to 100, and lakes with CTSI values less than 40 are usually classified as oligotrophic. CTSI values

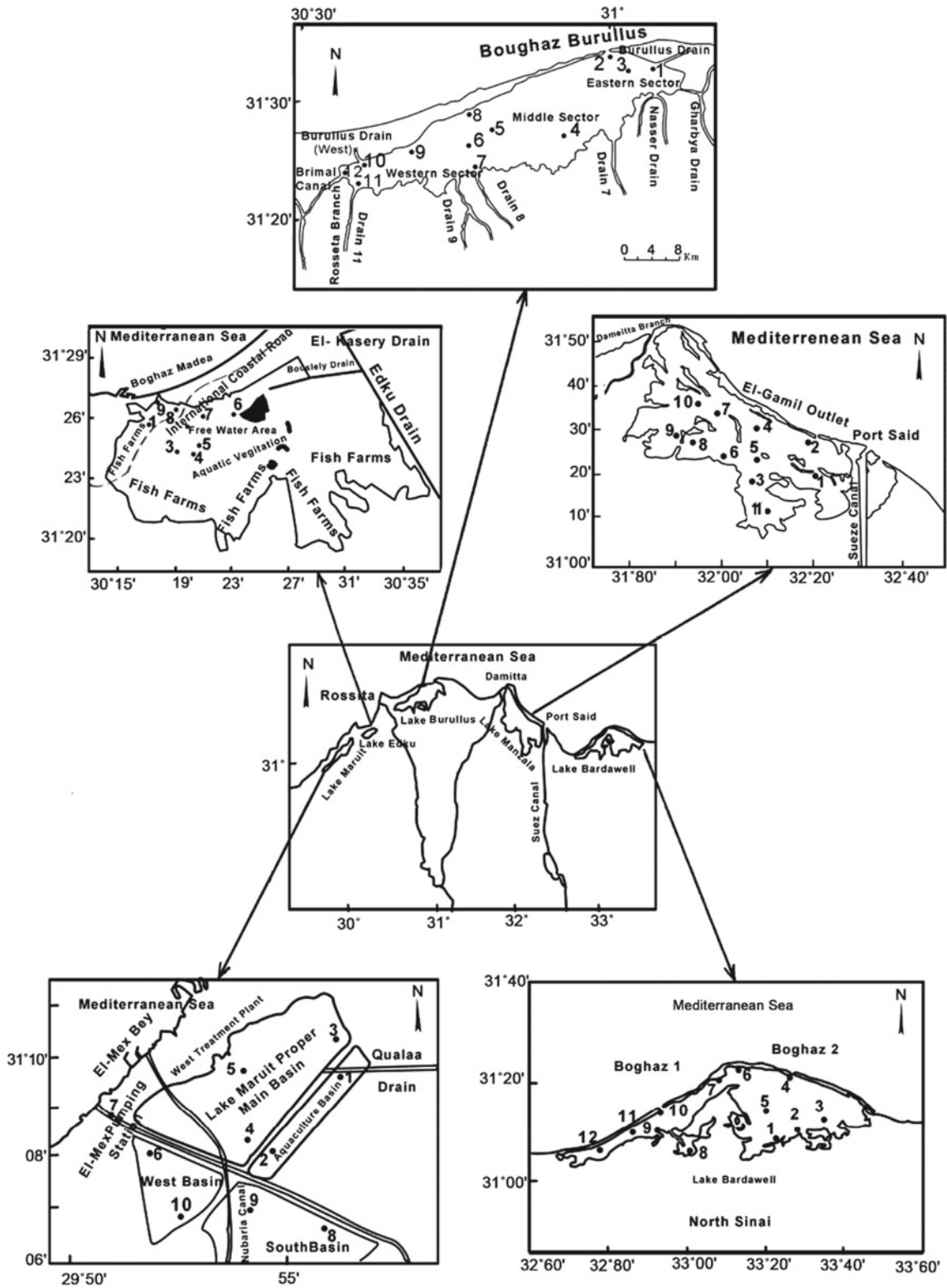


**Fig. 1** Northern lakes of Egypt and sampling point's locations modified after Shreadah et al. (2012)



**Table 1** Statistical indices of water quality parameters used in the classification of trophic state of lakes

Northern lakes/WQP	Chlorophyll-a ( $\mu\text{g/L}$ )			Total phosphorus ( $\mu\text{g/L}$ )			Total nitrogen ( $\mu\text{g/L}$ )			Secchi depth (m)		
	Min.	Mean	Max.	Min.	Mean	Max.	Min.	Mean	Max.	Min.	Mean	Max.
Burullus	15.62	73.46	508.07	126.49	44,067	889.77	2510	4672.77	7330	0.17	0.27	0.48
Manzala	15.82	42.97	135.76	144.29	440.67	901	2090	4896.66	9100	0.17	0.37	0.76
Edku	80.18	195.57	416.95	126.94	548.58	889.77	2359	5096.05	9400	0.05	0.14	0.25
Maruit	10.65	35.8	66.12	126.49	548.58	889.77	4300	7105	17,660	0.15	0.40	0.67

greater than 50 are generally defined as eutrophic lakes. Mesotrophic lakes have CTSI values between 40 and 50.

Carlson classified lakes and reservoirs into oligotrophic (low productive), mesotrophic (moderately productive), eutrophic (very productive and fertile) and hyper-eutrophic (extremely productive) based on nutrient enrichment and algal productivity (Carlson, 1977).

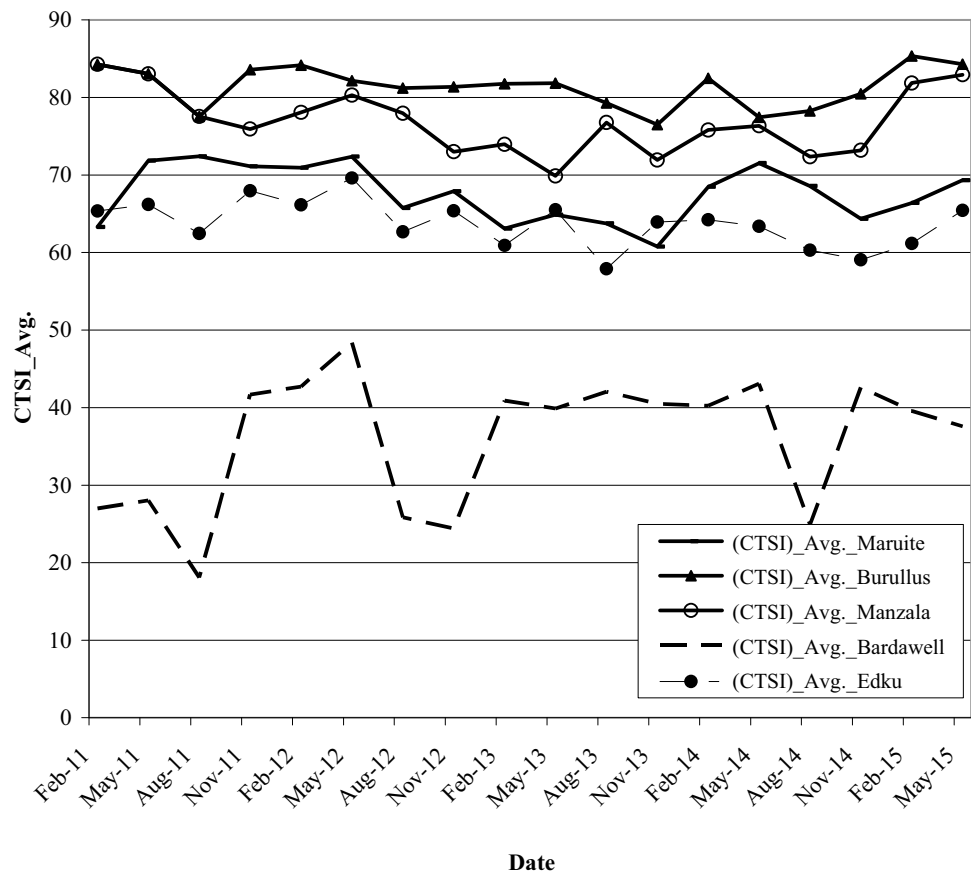
Regression analysis of CTSI is performed to detect the deterioration trend of each lake. Regression analysis of the measured water quality variables is also performed to characterize the relation between clarity, Chl-a and TP of each lake under study.

### 3 Results and Discussion

#### 3.1 Trophic State Index

Figure 2 shows the average Carlson trophic state index (CTSI) for the northern lakes and illustrates that Lake Bardawil has the smallest value of average CTSI in the range from 20 to 40 (oligotrophic). Then, lakes Edku and Maruit have nearly the same trend with a value from 60 to 70 (eutrophic) and finally Manzala and Lake Burullus lie in the range from 70 to 85 (hyper-eutrophic eutrophic).

**Fig. 2** Average Carlson trophic state index (CTSI) for Egyptian northern lakes



### 3.2 Total Nitrogen and Total Phosphorus

Figure 3 shows the range and the mean value of the total nitrogen of the Egyptian northern lakes. Lake Maruit has the highest mean value of about (7000  $\mu\text{g/L}$ ) as it received huge quantities of wastewater from east and west treatment plants in Alexandria, while the lowest mean value of total nitrogen is in Lake Bardawil of less than (2000  $\mu\text{g/L}$ ). Lake Edku and Lake Burullus have equal mean values of total nitrogen. However, all mean values of total nitrogen are above 1900, the limit value of the eutrophic state of lakes (Vollenweider & Kerekes, 1980) except Lake Bardawil.

According to USEPA classification, all northern lakes, except Lake Bardawil, are of eutrophic state as total phosphorus is more than 20  $\mu\text{g/L}$  as shown in Fig. 4, while lake Bardawil is of oligotrophic state. Lake Edku has the widest range of TP and the highest mean value of 500  $\mu\text{g/L}$  among all northern lakes, while Lake Bardawil has the narrowest range of TP and the lowest mean value of less than 200  $\mu\text{g/L}$ .

The N/P value is calculated for the five lakes for the period from 2011 to 2015 as in Table 2, and there is a variation of these values at different dates for each lake. Consequently, it is difficult to determine whether nitrogen or phosphorus is the limiting nutrient of lakes (Smith &

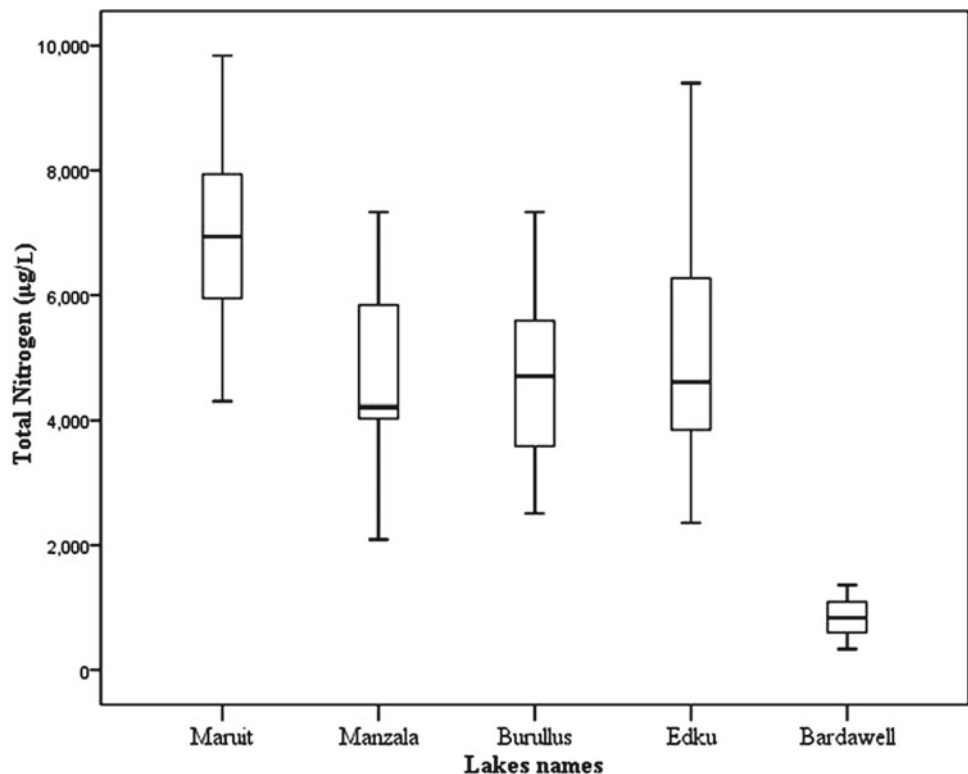
Shapiro, 1980; Donia & Hussein, 2004) or decide that the studied lakes are nutrient-balanced lakes (City of Maitland, 2006).

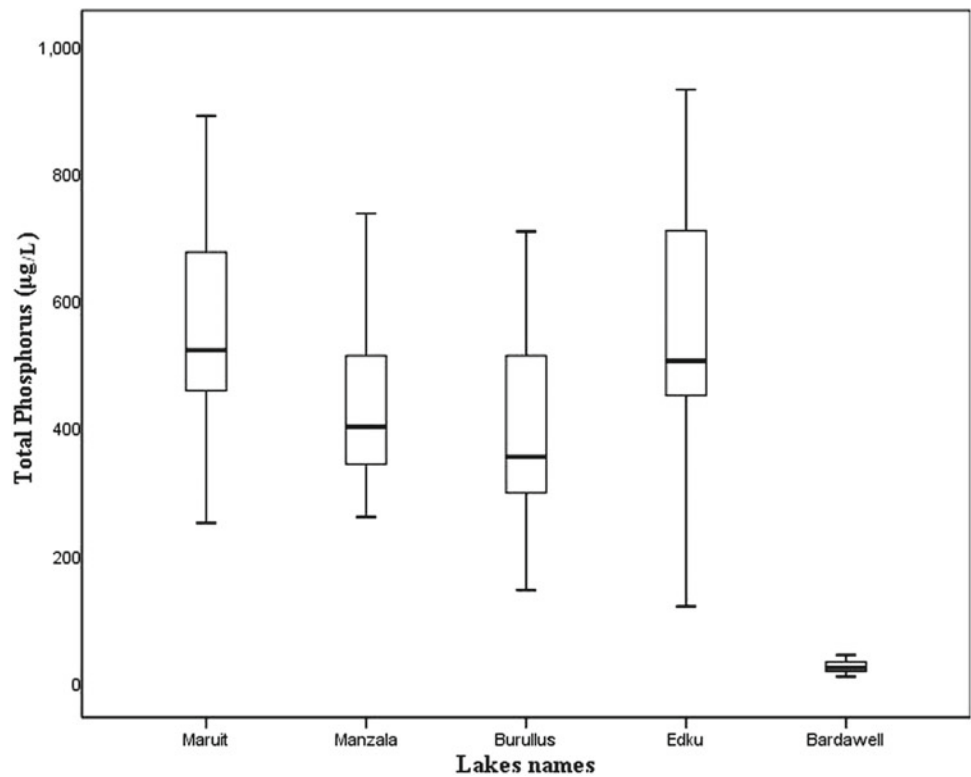
### 3.3 Regression Analysis

The objective of regression analysis here is to determine the trend of water quality of Egyptian northern lakes and to investigate if lake water quality is improving, deteriorating or stable. Regression results showed that CTSI is increasing in Lake Maruit, Burullus and Bardawil, indicating deteriorating water quality. Meanwhile, it is declining (improving) in Lake Edku and in Lake Manzala as shown in Fig. 5. For Lake Edku, CTSI values had a fluctuating trend, the lowest value of 60.93 in the year 2013 and the highest value of 66.15 in the year 2012. For Lake Manzala, the CTSI ranges between 74 and 84. CTSI values had a decreasing trend in the period from 2011 to 2013 and are followed by an increasing trend in the period from 2013 to 2015.

Regression analysis was carried out on the collected data to characterize the relation between total phosphorus as a nutrient and each of water clarity (SD) and chlorophyll-a (Chl-a) concentration of each lake. The relation of chlorophyll-a (Chl-a) and water transparency (SD) for each

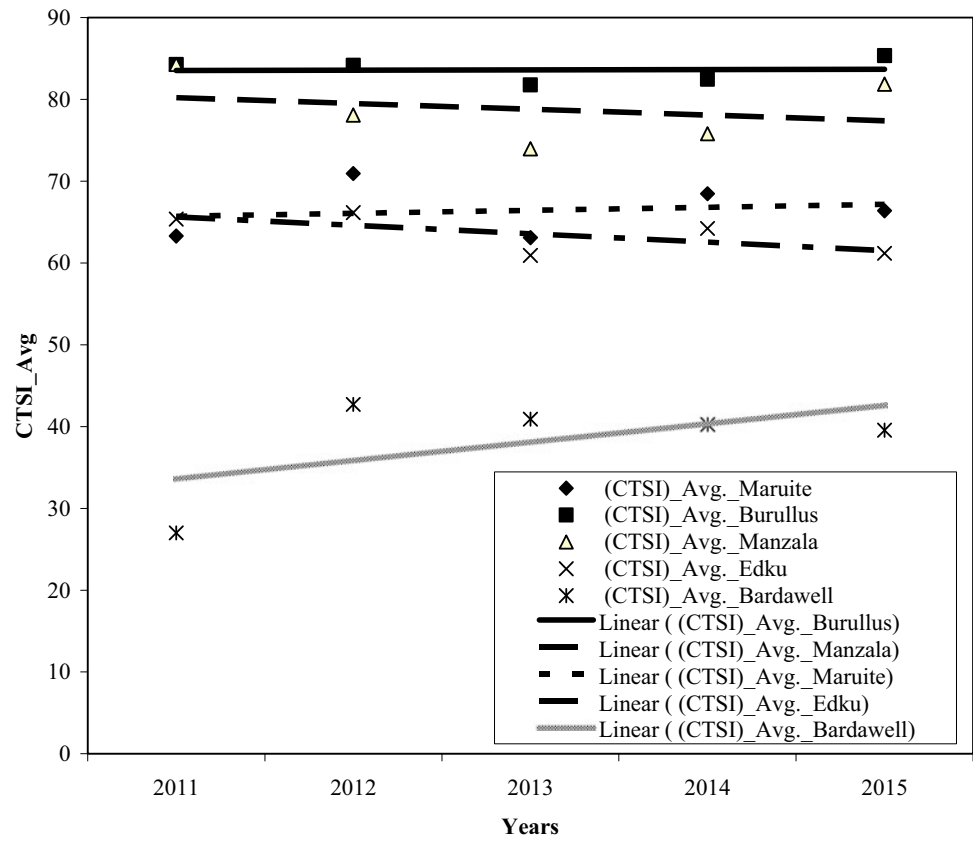
**Fig. 3** Total nitrogen of the Egyptian northern lakes



**Fig. 4** Total phosphorus of the Egyptian northern lakes**Table 2** (N/P) of northern lakes

Date	N/P_Maruit	N/P_Edku	N/P_Burullus	N/P_Manzala	N/P_Bardawil
February 2011	23.72	15.97	13.80	13.80	34.92
May 2011	8.05	9.81	8.28	8.28	28.34
August 2011	16.11	7.02	6.16	6.16	32.10
November 2011	19.85	5.89	9.19	9.19	113.05
February 2012	37.24	3.66	11.64	7.18	70.25
May 2012	10.49	4.15	8.68	10.33	10.94
August 2012	12.37	8.08	9.57	9.18	19.62
November 2012	12.36	8.61	36.18	15.54	15.08
February 2013	10.80	8.23	12.34	14.00	25.27
May 2013	15.30	7.87	32.44	12.24	32.51
August 2013	12.64	7.53	9.92	12.08	29.27
November 2013	10.01	5.78	9.46	5.21	20.93
February 2014	13.11	9.99	9.94	11.94	52.48
May 2014	15.57	7.29	20.34	13.46	48.33
August 2014	19.33	6.53	11.46	9.14	22.42
November 2014	13.88	9.69	14.57	10.23	57.54
February 2015	10.94	78.98	10.30	8.12	52.89
May 2015	0.32	4.73	1.46	6.03	200.37

**Fig. 5** Yearly Carlson trophic state indices for Egyptian northern lakes



lake was also estimated. These relationships are presented in Table 3 and can be used in a future work for water quality management scenarios.

### 3.4 Controlling Eutrophication of Northern Lakes

Based on the results of this work, Lake Edku has the highest value of phosphorus concentrations. This problem can be solved by pollutant reduction of El-Khairi and Barzik drains before entering the lake using “bio-filter” in the upstream.

The TSI (TP) value of 60 is used as the cutoff between eutrophic and Hypertrophy Lake (Ossman & Badr, 2010). TSI analysis is used to determine the necessary phosphorus reduction targets for the lake. By substituting in Eq. (3) with TSI (TP) of 60, we get the value of TP equal to 48.09 ( $\mu\text{g L}^{-1}$ ), and then the reduction in lake total phosphorus concentration (X) can be calculated from Eq. (5).

$$TP = \sum_{n=0}^n (X * TP * Q) / \left( \sum_{n=0}^n Q \right) \quad (5)$$

where

TP: Total phosphorus concentration ( $\mu\text{g/L}$ )

Q: Drainage water discharge flow rate ( $\text{m}^3/\text{day}$ )

X: Required load reduction [0.0, 1.0]

n: No. of point sources (two point sources, El-Khairi and Barzik drains).

Research results showed that Lake Maruit, Manzala and Burullus suffer from different degrees of high nitrogen concentration values. In-lake wetland treatment can be used for Lake Manzala and Burullus. For Lake Maruit, treatment of drainage water from El-Qalaa drain is a recommended solution. Treatment can be achieved by using in-stream/drain aeration to increase the level of dissolved oxygen in El-Qalaa drain (EEAA 2009).

## 4 Conclusion and Recommendations

This work studied the Egyptian northern lake’s status regarding water quality and eutrophication state. The research results revealed that the Carlson trophic state index trend is increasing, indicating deteriorating water quality in Lake Maruit, Burullus and Bardawil, and declining (improving) in Lake Edku and Lake Manzala.

According to USEPA and Carlson classification, Lake Bardawil is of oligotrophic state. Based on the Carlson TSI values of the northern lakes, Lake Maruit and Edku are of eutrophic status while Lake Manzala and Burullus are of hyper-eutrophic. According to USEPA classification, all

**Table 3** Interrelationship between TP, SD and Chl-a in Egyptian northern lakes

Lake name	SD as a function of Chl-a	SD as a function of TP	Chl-a as a function of TP
Maruit	$SD = 0.014 * \ln(\text{Chl-a}) + 1.583$ $R^2 = 0.994$	$SD = -0.004 * \ln(\text{TP}) + 0.433R^2 = 0.911$	$\text{Chl-a} = 0.1494 * \ln(\text{TP}) + 1.3576$ $R^2 = 0.997$
Edku	$SD = -3.705 * \ln(\text{Chl-a}) + 30.165R^2 = 0.955$	$SD = 0.0095 * \ln(\text{TP}) + 0.0831R^2 = 0.874$	$\text{Chl-a} = 70.376 * \ln(\text{TP}) - 251.67R^2 = 0.874$
Burullus	$SD = 1.60914 * \ln(\text{Chl-a}) + 20.284$ $R^2 = 0.926$	$SD = 0.0322 * \ln(\text{TP}) + 0.075$ $R^2 = 0.96$	$\text{Chl-a} = 49.808 * e \wedge (0.00071(\text{TP}))$ $R^2 = 0.993$
Manzala	$SD = -9.824 * \ln(\text{Chl-a}) + 77.975$ $R^2 = 0.882$	$SD = -0.056 * \ln(\text{TP}) + 0.7099$ $R^2 = 0.93$	$\text{Chl-a} = 22.568 * e \wedge (0.014(\text{TP}))$ $R^2 = 0.976$
Bardawil	$SD = 35.331 * \ln(\text{Chl-a}) + 160.74$ $R^2 = 0.936$	$SD = -0.207 * \ln(\text{TP}) + 1.9087$ $R^2 = 0.85$	$\text{Chl-a} = 0.002 * \ln(\text{TP}) + 0.459$ $R^2 = 0.85$

northern lakes except Lake Bardawil are of eutrophic state. Finally, for eutrophication control of the Egyptian northern lakes, it is recommended to reduce or treat pollutants from their sources before reaching lakes using drain bio-film or to apply in-lake wetland treatment.

## References

- Abdel Ghaffer, E. (2006). Impact of climate change on the hydrology of Lake Manzala. In *1st International Conference on Environmental Change of Lakes, Lagoons, and Wetlands of the Southern Mediterranean Region*, Cairo, Egypt.
- Ahmed, S., & Kaiser, M. (2014). Monitoring water pollution of lake Maryout on the Mediterranean Coast of Egypt. *International Journal of Remote Sensing Applications*, 4(1), 36–40.
- Alemayehu, D., & Francine, H. (2016). Water quality and trophic state of Kaw Lake. *Journal of Environmental Studies*, 1(7), 1–7.
- Brown, T., & Simpson, J. (2011). Determining the trophic state of Your Lake, watershed protection techniques. *Urban Lake Management*, 3 (4).
- Carlson, R. E. (1977). A trophic state Index for Lakes. *Limnology Oceanography*, 22, 361–369.
- City of Maitland. (2006). *Stormwater/lakes management plan, existing system water quality analysis*. Available from: <https://www.itsmymaitland.com/lakesplan/SLMPSec4.pdf>
- Colin, R. B., Robert, E., Wreede, D., et al. (2007). Do changes in seaweed biodiversity influence associated invertebrate epifauna? *Journal of Experimental Marine Biology and Ecology*, 344, 206–214. <https://doi.org/10.1016/j.jembe.2007.01.002>.
- Donia, N., & Hussein, M. (2004). Eutrophication assessment of lake manzala using GIS techniques. In *Eighth International Water Technology Conference*, Alexandria, Egypt.
- Egyptian Environmental Affairs Agency (EEAA). (2009). Alexandria Integrated Coastal Zone Management Project (AICZMP), Environmental and Social Impact Assessment. Available from: <https://www.eeaa.gov.eg>
- Egyptian Environmental Affairs Agency (EEAA). (2015). Egyptian lakes, Egypt state of environment 2012. Ministry of State of Environmental Affairs, Arab Republic of Egypt. Available from: [https://www.eeaa.gov.eg/portals/0/eeaaReports/SoE2013En/SOEREport\\_2012\\_english.pdf](https://www.eeaa.gov.eg/portals/0/eeaaReports/SoE2013En/SOEREport_2012_english.pdf)
- Farag, H., & El-Gamal, A. (2012). Assessment of the Eutrophic status of Lake Burullus (Egypt) using remote sensing. *International Journal of Science and Engineering (IJESE)*, 2, 61–74.
- General Authority for Fish Resources Development. (2012). Annual Report. Available from: <https://www.gafrd.org>
- Ossman, M., & Badr, N. B. E. (2010). Lake Edku water-quality monitoring, analysis and management model for optimizing drainage water treatment using a genetic algorithm. *International Journal of Environment and Waste Management*, 1(2), 152–162.
- Shreadah, M. A., Abdel Ghani, S. A., El Samie Taha, A. A., El Moniem M. Ahmed, A., Hamada, B., & Hawash, I. (2012). Mercury and methyl mercury in sediments of Northern Lakes-Egypt. *Journal of Environmental Protection*, 3, 254–261.
- Smith, V. H., & Shapiro, J. (1980). Chlorophyll a-phosphorus relations in individual lakes. *Environment Science and Technology*, 15, 444–451.
- U.S. Environmental Protection Agency (USEPA). (1974). The relationships of phosphorus and nitrogen to Trophic State of Northeast and North–Central Lakes and Reservoirs, National Eutrophication Survey Working Paper No.23, USEPA, Washington, DC.
- Vollenweider, R. A., & Kerekes, J. J. (1980). Background and summary results of the OECD cooperative program on eutrophication. In *Proceedings of an International Symposium on Inland Waters and Lake Restoration*. U.S. Environmental Protection Agency. EPA 440/5-81-010, pp. 26–36.



# An Integrated System Dynamics Model to Predict the Effects of Management Scenarios on Economic Assessment of Water and Soil Resources in Hableh-Rud River Basin, Iran

Ebrahim Karimi Sangchini, Majid Ownegh, Amir Sadoddin, and Mahdi Zarghami

## Abstract

System dynamics modeling facilitates the integrated and sustainable management of soil and water resources by enhancing the understanding of watershed systems. The Hableh-Rud river basin, an important watershed of Iran located across Tehran and Semnan provinces, was chosen for the present research. Reference diagrams were created to represent causal relationships and feedbacks based on which the conceptual model for the integrated management of soil and water resources of the Hableh-Rud river basin was developed. The conceptual model was then converted into a model of stocks and flows and run in the Vensim software. The model is comprised of by the biophysical and the economic subsystems. The main components of the physical subsystem include water balance, groundwater, erosion, sedimentation and water quality. In the economic subsystem, total costs and benefits were taken into account. Model verification was carried out through extreme condition tests and behavior reproduction tests. Having the Nash–Sutcliffe and  $R^2$  coefficients with greater values than 0.62 and 0.63, respectively, model tested. Different scenarios including vegetation management, climate, water resources management and cropping patterns were simulated, and the outputs of each scenario were compared to the outputs of

the existing condition. The results of scenario analyses for a 30-year period reveal that payment for 50% of the ecosystem services by the government to expand alternative jobs and reduce damage to natural resources was determined as the best scenario. Scenario of payment for 25% of the ecosystem services by the government to expand alternative jobs and reduce damage to natural resources was chosen as the next best scenario. After evaluating the vegetation management scenarios, it was determined that farm management actions were considered as the best vegetation scenario. The research indicates that the system dynamic model, as an integrated approach for management of water resources in a basin, is pragmatic.

## Keywords

Integrated water resources management • System dynamics • The economic situation • Hableh-Rud river basin

E. Karimi Sangchini (✉)  
Soil Conservation and Watershed Management Research  
Department, Lorestan Agricultural and Natural Resources  
Research and Education Center, AREEO, Khorramabad, Iran  
e-mail: [e.karimi64@areeo.ac.ir](mailto:e.karimi64@areeo.ac.ir)

M. Ownegh  
Arid Zone Management, Gorgan University of Agricultural  
Sciences and Natural Resources, Gorgan, Iran

A. Sadoddin  
Watershed Management Department, Gorgan University of  
Agricultural Sciences and Natural Resources, Gorgan, Iran

M. Zarghami  
Faculty of Civil Engineering and Institute of Environment,  
University of Tabriz, Tabriz, Iran

## 1 Introduction

Water and soil are important resources that play a vital role in fulfilling basic human needs and are essential for sustainable agricultural development. Management of water and soil resources in an integrated manner is crucial for sustainable economic development. In many developing countries, population growth has led to overexploitation of water and soil resources (Brooks & Tayaa, 2002; Savenije & Zaag, 2008).

System dynamics (SD) is an effective approach to study, analyze, model and improve dynamic socioeconomic and management systems using a feedback perspective (Barlas & Yasarcan, 2006). In 1960, Forrester and his colleague proposed SD modeling at the Sloan School of Management at the Massachusetts Institute of Technology, which refers to a



set of conceptual and numerical methods used to understand the structure and behavior of complex systems.

There are several software applications such as Stella, Dynamo, Vensim and Powersim to develop and simulate the SD model. They explain a set of graphical themes with their mathematical operators for easy representation of system structure and computer code development (Wang et al., 2011). SD is an integrated management approach which is capable of simulating complex water resources systems and also facilitates collaborative learning. This simulation is useful to reveal unknown outcomes of decision-making processes. It works toward facilitating system behavior learning at present and future temporal scales (Wolstenholme, 1990). SD behavior is a function of time and dynamic system modeling attempts to describe and understand the system through quantitative and qualitative models. Moreover, the simulation can be used to select those policies that should be implemented. SD focuses on causal linkages between different components and finally studies whole system behavior over time (Sterman, 2000). SD modeling denotes to a set of numerical and conceptual methods generally used to understand the structure and behavior of complex systems. This methodology has four key principles: feedback control theory, understanding the decision-making process, use of mathematical models to simulate complex processes and the use of computer-based technologies to develop simulation. Such modeling is commonly used to understand systems and social learning, but can be used in decision-making processes as well (Keli et al., 2013).

As for environmental and natural resource management, this methodology has been cited in many studies as environmental management (Vanden Belt, 2004; Stave, 2008, 2010; Jin et al., 2019; Cao et al., 2019), water resources management (Elmahdi et al., 2007; Fiorillo et al., 2007; Winz et al., 2009; Beall et al., 2011; Wang et al., 2011; Hassanzadeh et al., 2012; Liu et al., 2015; Sun et al., 2016; Bakhshianlamouki et al., 2019), flood management (Ahmad & Simonovic, 2000; Phonphotona & Pharino, 2019; Pagano et al., 2019; Perrone et al., 2020), drought management (Keyes & Palmer, 1993; Adl & Parvizian, 2009; Gies et al., 2014; Connell et al., 2019), ecological modeling (Chang et al., 2008; Settle et al., 2002; Baron et al., 2002; Mavrommati et al., 2013; Cordier et al., 2017; Lu et al., 2019), and erosion and nutrient management (Yeh et al., 2006; Xuan et al., 2012; Findlay et al., 2015; Zhang et al., 2018).

The Hableh-Rud is a permanent river passing through Garmsar city at Semnan Province. The Hableh-Rud river basin has significant natural, social, and economic value, such as soil fertility, medicinal plant species, natural rangelands, water resources and irrigation for the city of Garmsar. It is fraught with natural and anthropogenic issues

in soil and water resources including low water quality and increased salinity, soil salinity and land degradation, loss of soil fertility in lowlands, overgrazing, decreased water resources, conversion of rangelands to inefficient rainfed farming, deforestation, urbanization and industrial development (Keshtkar, 2013). The purpose of this research is to economically evaluate the water and soil resources for the Hableh-Rud river basin using a comprehensive SD approach. Therefore, this research is of a practical nature with a focus on achieving benefits that increase the system understanding of watershed development planning. This approach can also assist policy makers to manage watersheds.

---

## 2 Material and Methods

### 2.1 Study Area

Doab Samsami Watershed is located between 35° 1' to 36° 10' latitudes and 51° 39' to 53° 8' longitudes, occupying an area of 12,662 km<sup>2</sup> in Semnan and Tehran Provinces, north of Iran (Fig. 1). This watershed is one of the major sub-basins of central Iran. Altitude in the study area ranges from 739 to 4053 m above sea level. Based on the Iranian meteorological organization report, the average annual rainfall in the study area is 211 mm. The average annual temperature is 7.8 °C. The Hableh-Rud River, which originates from the Alborz Mountains, flows north to south, is bound by mountains and eventually empties into the Garmsar Plain. The catchment area is dominated by degraded rangelands, and intense salinity outbreaks occur in the southern parts of the catchment. The Hableh-Rud River supplies water for the municipal consumption of Garmsar city with a population of over 84,000, as well as for the industry and farmlands of the Garmsar Plain (about 5.2 km<sup>2</sup>). Basin formations are generally of the Cenozoic era. It contains parts of the Quaternary and Tertiary periods. The most effective factors on the Hableh-Rud river catchment's problems are overgrazing, intensive farming on the Garmsar Plain and urban development due to population growth in the city of Garmsar.

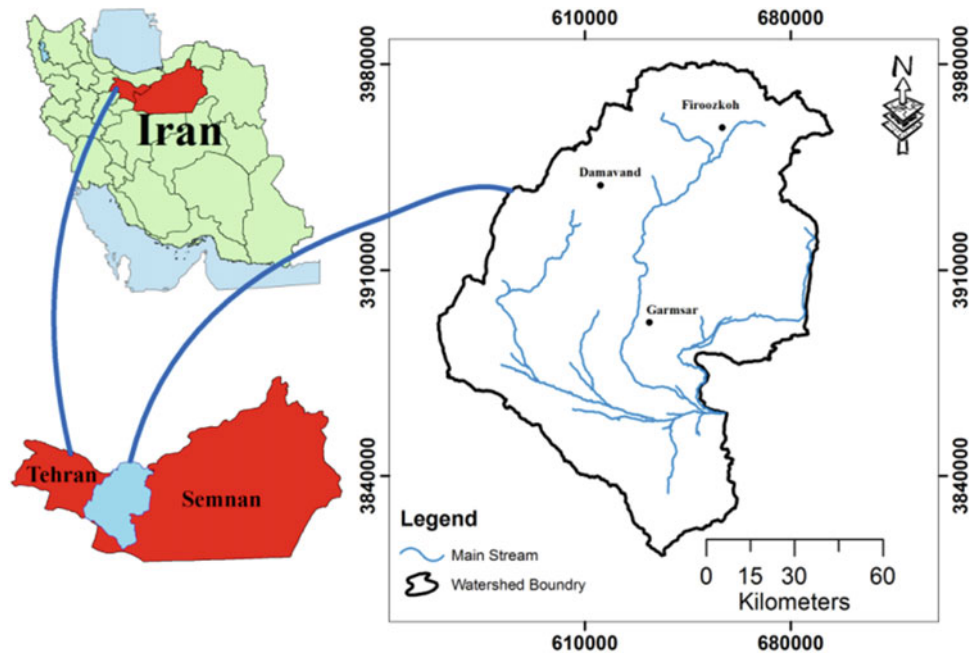
---

## 3 Problem Definition

Physical and socioeconomic subsystems were used to construct an integrated water and soil management model in the Hableh-Rud river basin. The method of quantifying the variables of these subsystems is described in the following. Curve number method was used to calculate runoff. The Long-Term Hydrological Impact Assessment (L-THIA) Model has been used to assess water quality (Youa et al.,



**Fig. 1** Location map of the study area



2012). The actual evapotranspiration was estimated annually using the torque equation (Eslamian et al., 2018). EPM model was used to predict erosion (Yeh et al., 2006). The socioeconomic subsystem includes population, total cost and total income. The costs of soil erosion, sediment production, water pollution and the implementation and maintenance of management scenarios were considered. Total income includes income from existing activities and income from executing management scenarios.

### 3.1 Model Development

This study purposes to develop a system dynamics simulation model using Vensim software, which can evaluate economic impacts of water and soil resources for Hableh-Rud river basin. SD model configuration is further partitioned into two subsystems: physical and socioeconomic. The cause–effect diagram shows subsystem relationships. This diagram performs certain scenario analysis following SD model formulation and validation. The SD modeling approach uses causal loop diagrams to show a system’s feedback structure. A causal loop diagram is similar to a network chart, showing cause–effect relations among system variables (represented as nodes) using causal links (displayed as oriented arcs). Cause–effect variable pairs positively related are represented by a plus sign added to the link; otherwise, a minus sign results. A causal loop diagram generally comprises several positive–negative–feedback-loop structures with closed circulation configurations. A positive feedback loop could trigger an embedded system variable growth process over time, possibly leading to

system loss of control and collapse. A negative feedback by contrast seeks a goal and responds through achieving a stable state. Figure 2 shows the cause and effect of the water and soil resource management model. Management scenarios are proposed to improve the physical, economic and social status of the watershed and aim to improve the performance of the model components.

### 3.2 Preparing a Stock and Flow Diagram and Model Performance

After defining the feedback loops, a conceptual model was developed which was quantified as flowcharts. In the next step, the model was implemented by SD approach and the results were examined. The method of quantifying economic variables is presented in Tables 1, 2, 3 and 4. Nutrition replacement cost method was used to estimate the costs of soil erosion. In this method, the cost of purchasing the fertilizer needed to maintain and restore soil productivity is calculated. Urea fertilizer contains 46% nitrogen, superphosphate fertilizer contains 24% pure phosphorus without oxygen, potassium sulfate fertilizer contains 42% potassium, and magnesium sulfate fertilizer contains 16% magnesium. Fertilizers were calculated at retail prices in Iran. The costs of filling Namrood Dam and waterways were calculated to estimate the outlet sediment costs. How to calculate the dredging cost of the sediment produced in Namrood Dam and Hableh-Rud river basin is presented in Table 2. Information on average yield, crop prices and costs is needed to calculate gross income and agricultural expenditure (Table 3).

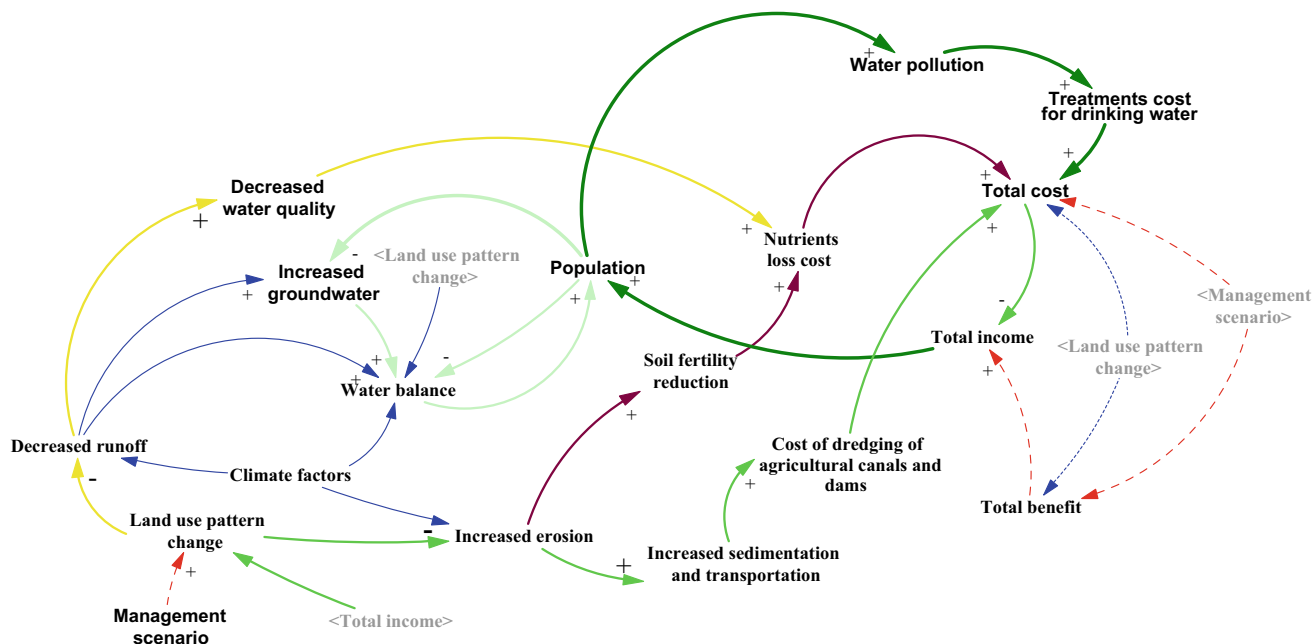


**Fig. 2** Causal diagram of conceptual model

**Table 1** Average concentration of minerals in soil (Fageria, 2009)

Element	Average concentration (g/kg)
Nitrogen	33
Phosphorus	23
Potassium	3

**Table 2** Estimation of dredging cost of sediment production in Namrood Dam and Hableh-Rud river basin (Vice-Presidency for Strategic Planning and Supervision, 2017)

Sediment type	Dredging costs (Iranian Rial/m <sup>3</sup> )
Namrood Dam	90,050
Hableh-Rud river basin	35,470

### 3.3 Model Validation Tests

Model verification was carried out through extreme condition tests and behavior reproduction tests. Limit condition test shows the logical performance of the model under limit condition. In this study,  $R^2$  and Nash–Sutcliffe tests were used to evaluate the model behavior (Sterman, 2000).

### 3.4 Scenario Planning for Integrated Management of Soil and Water Resources

In this study, different scenarios of vegetation management, climate, water resources management and cropping patterns were simulated and the outputs of each scenario were compared to the outputs of the existing condition (Table 5).

The effects of management activities on the physical, economic, social and ecological status of water and soil resources were analyzed using these scenarios.

## 4 Results and Discussion

### 4.1 Feedback Loops in Soil and Water Resources Management

SD mostly communicates feedback loop systems by means of causal loop diagrams (Figs. 3, 4, 5, 6, 7 and 8). The core building blocks of CLDs are variables and the direct causal relationships between them. These relationships are either positive or negative. The meaning of the terms positive and negative does not correspond to their everyday meaning

**Table 3** Average yield and prices of agricultural products in Hableh-Rud river basin (Ministry of Agriculture Jihad, 2017)

Crop name	Yield (kg/ha)	Water requirement (m <sup>3</sup> /ha)	Price per kg (Iranian Rial)
Wheat	1756	2235	11,550
Potato	16,905	6125	3600
Barley	1440	1775	9200
Sheathed corn	43,461	6510	9600
Alfalfa forage	14,500	7180	9500
Tomato	32,598	4260	8000
Rangeland forage production	87.57	–	5250
Apple	16,000	5845	15,000
Peach	14,000	6240	20,000
Walnuts	6000	7450	210,000
Pomegranate	20,000	5680	20,000

**Table 4** Average price of water in Hableh-Rud river basin (Tehran Regional Water Board, 2017)

Type of use	Price (Iranian Rials/m <sup>3</sup> )
Drinking water	4915
Industrial water	1037
Agricultural water	1152

(Gohari et al., 2013). Feedback loops in the model included population–economic, economic quality and quantity of water, water balance–population, economic–erosion and water balance–economic. The population–economy loop shows population changes related to the economy (Fig. 3). As population grows, drinking water demand increases; as a result, more water becomes contaminated and therefore a higher cost is required for water purification, which reduces the revenue generated from the basin. As a result, these interactions affect and slow down population growth. This loop follows the “limits to growth” archetype.

The water balance–population loop considers the factors contributing to growth and decline of population in relation to water balance (Fig. 4). Population has a negative effect on water resources and consequently on water balance in this model. However, water balance has a positive effect on population. This means that as water resources increase, so does the population. In another loop, population has a negative impact on groundwater resources. Increasing groundwater resources increases water balance, which inevitably increases population. Nevertheless, the realities in the Hableh-Rud river basin indicate that the water balance has declined due to the competitive and multilateral use (drinking, industry and agriculture) of the basin. It follows the archetype of “tragedy of the commons.”

Inappropriate changes in land use pattern and degradation of natural resources increase runoff which consequently

decreases water quality in economic quality and quantity of water loop. Decreasing water quality increases total cost (by increasing soil nutrient loss), followed by a reduction in total revenue. It is assumed that the lower the total revenue, the greater the change in land use will lead to destruction of natural resources. Implementation of management scenarios and improvement of land use patterns can mitigate these detrimental effects (Fig. 5). It follows the archetype of “tragedy of the commons.”

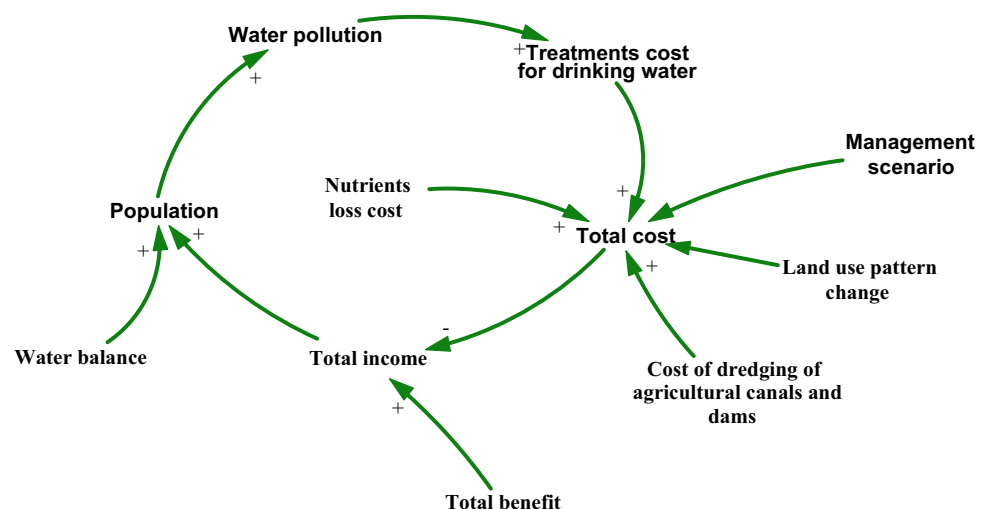
In the economic–erosion loop, inappropriate land use changes increase erosion and sedimentation, which have a positive effect on total cost through the loss of soil nutrient depletion costs and dredging costs. The total cost also has a negative effect on the total revenue of the basin (Fig. 6). Implementation of the proposed management scenarios to improve land use patterns will lessen damages and increase basin income. This loop follows the “escalation” archetype.

Water balance–economic loop considers changing land use patterns causes changes to surface and groundwater resources, which disrupts the water balance (Fig. 7). It causes changes to the population and the economy of the watershed (Woodruff & Halland, 2008). The watershed economy also has an impact on land use change. Applying management scenarios to modify the land use pattern leads to positive changes. It follows the archetype of “tragedy of the commons.”

**Table 5** Scenarios of vegetation management, climate, water resources management and cropping patterns for integrated management of soil and water resources

Number	Scenario	Implementation area
1	Rangeland restoration	Entire catchment is potentially suitable, not in the natural resources rehabilitation areas including bunch seeding, contour furrowing, grazing exclusion, seeding, drill seeding
2	Natural resources rehabilitation areas	Entire catchment is potentially suitable for riparian restoration, tree plantation and saxaul plantation
3	Farm management activities	Only in areas currently under dry farm including terracing, forage growing, orchard development and agroforestry
4	Management of agricultural cropping pattern	The agricultural cropping pattern will change to the ideal cropping pattern based on the land use planning model
5	Unsuitable management of agricultural water	Decrease 20% of agricultural water efficiency
6	Agricultural water management	Increase 20% of agricultural water efficiency
7	Climate change	Decrease 10% of precipitation and increase 1 degree in temperature
8	Pay 25% of the proceeds from ecosystem services to stakeholders	25% of ecosystem services are paid to stakeholders in order to motivate better rangeland management by the government to expand alternative jobs and reduce damage to natural resources
9	Pay 50% of the proceeds from ecosystem services to stakeholders	50% of ecosystem services are paid to stakeholders in order to motivate better rangeland management by the government to expand alternative jobs and reduce damage to natural resources

**Fig. 3** Population–economy loop of Hableh-Rud river basin



## 4.2 Stock and Flow Diagram (SFD)

The SFD of the physical and socioeconomic subsystems is shown in Figs. 6 and 7, respectively. Stock variables of the system include available surface water, available groundwater, total nitrate–nitrite, total phosphorus, water balance, population, erosion, sedimentation and income (Figs. 8 and 9). These stock variables increase or decrease in response to

changes in inflow and outflow rate variables. This diagram was drawn in the Vensim software environment.

## 4.3 Results of Model Validation Tests

Model verification was carried out through extreme condition tests and behavior reproduction tests. Having the Nash–

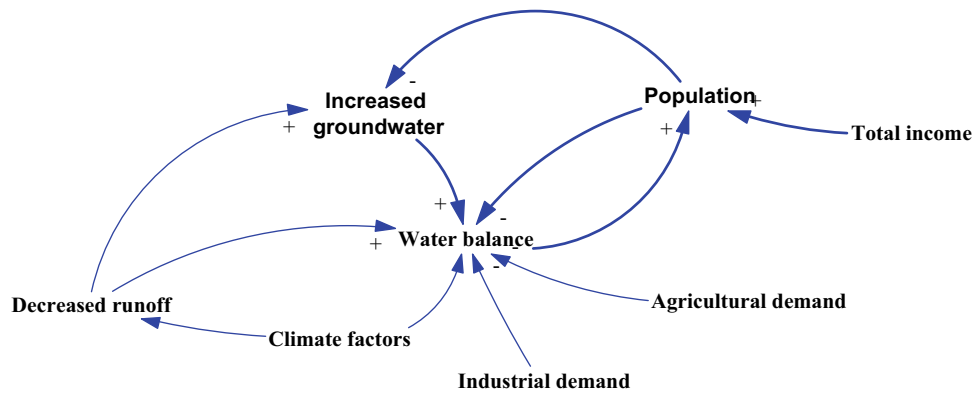


Fig. 4 Water balance–population loop of Hableh-Rud river basin

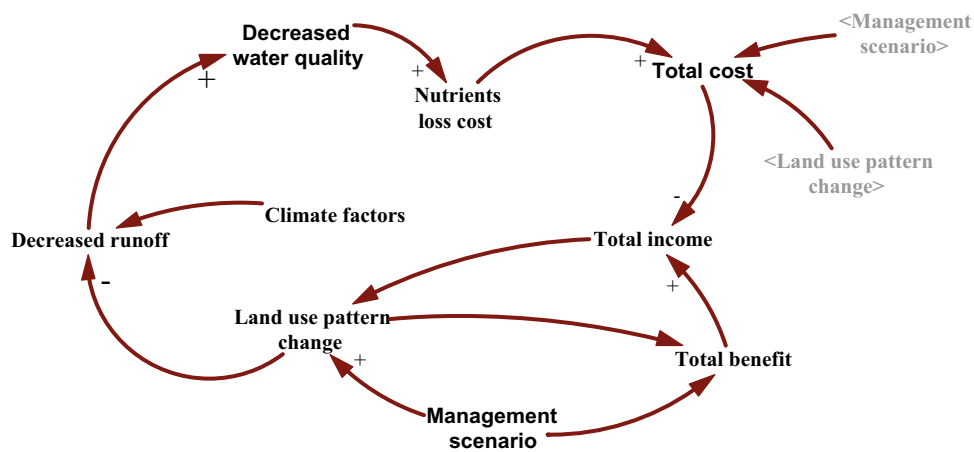


Fig. 5 Economic quality and quantity of water loop of Hableh-Rud river basin

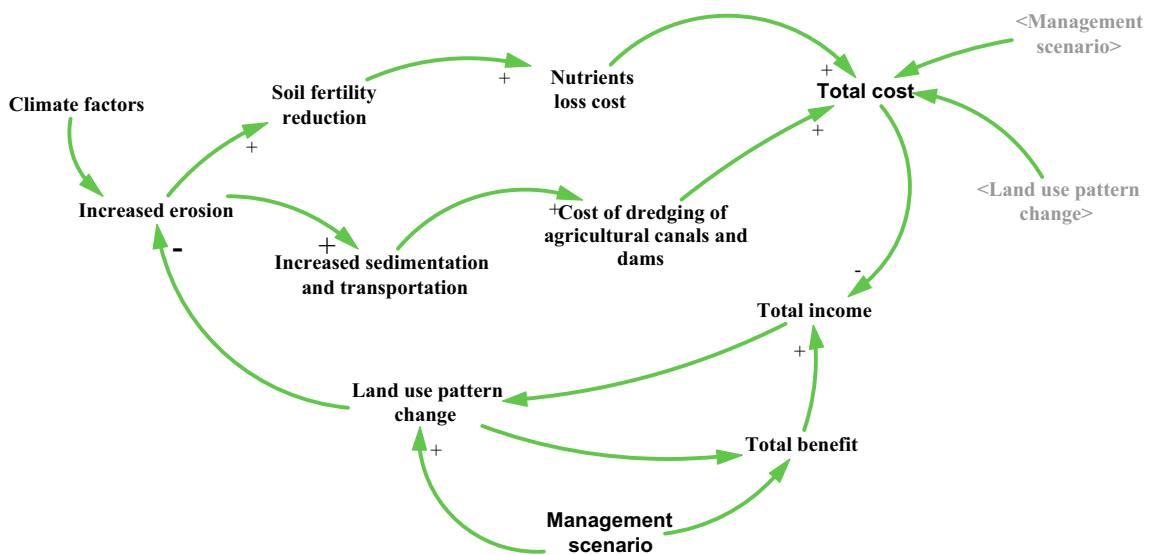


Fig. 6 Economic erosion loop of Hableh-Rud river basin

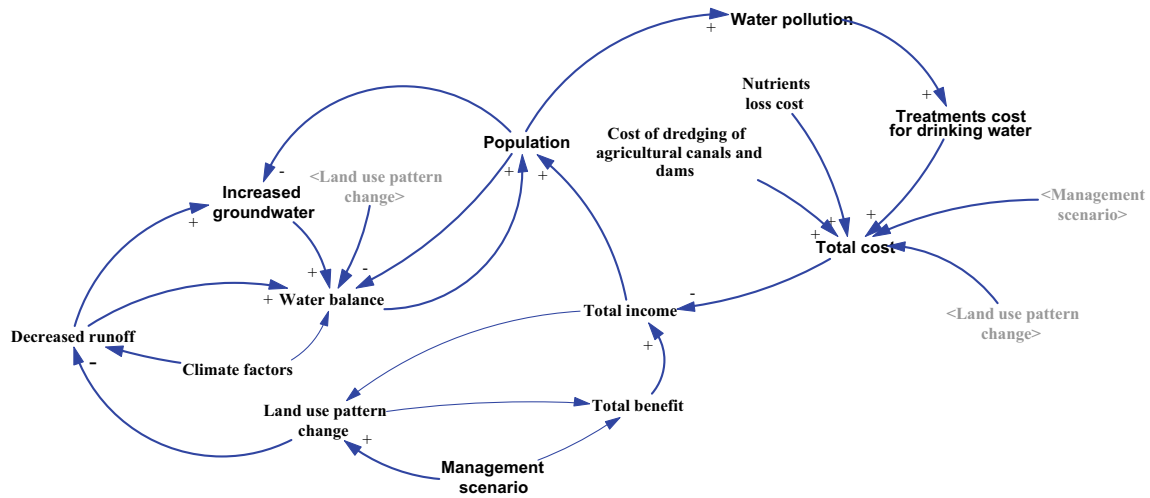


Fig. 7 Water balance–economic loop of Hableh-Rud river basin

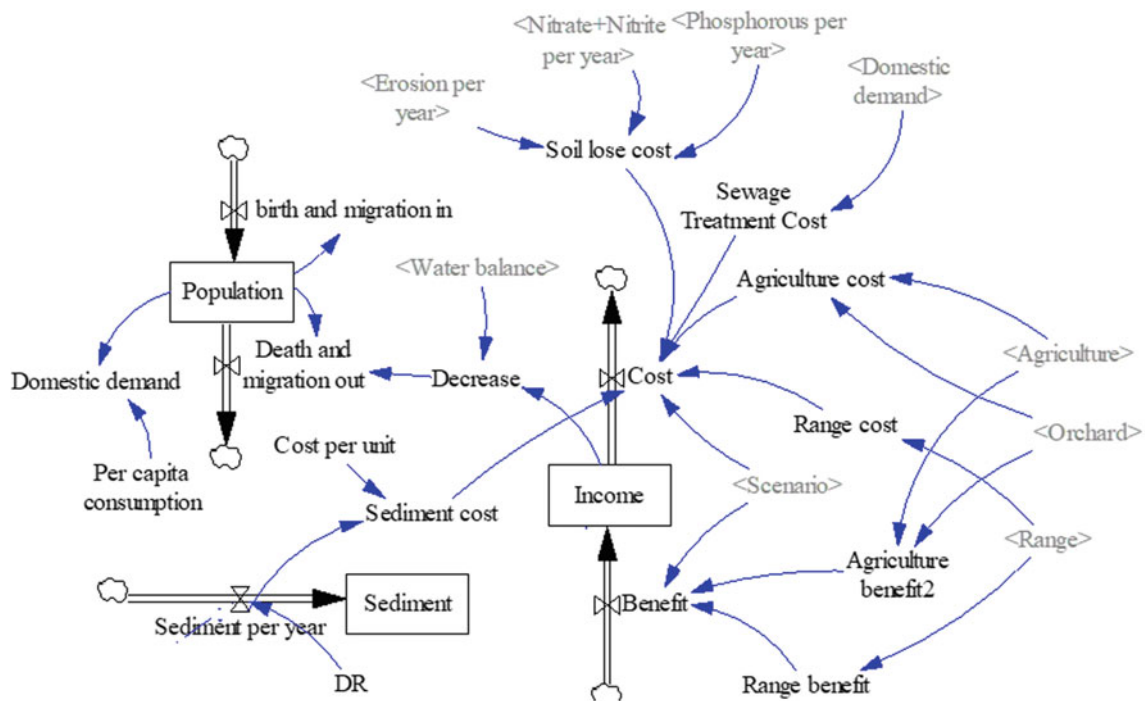


Fig. 8 Stock and flow diagram of the socioeconomic subsystem

Sutcliffe and  $R^2$  coefficients with greater values than 0.62 and 0.63, respectively, the system dynamic model satisfactorily simulates all variables (Table 6).

#### 4.4 Results of Implementation of Scenarios

After evaluating the model validation, the proposed scenarios were tested. These scenarios were assumed to be implemented over a 10-year period from 2015. Their effects

were also evaluated over a 30-year period. Figure 10 shows the spatial distribution of the proposed management activities in the Hableh-Rud river basin. Table 7 and Figs. 11 and 12 show that if the economic concerns of the watershed stakeholders are important, the scenario of paying 50% of the proceeds from ecosystem services to stakeholders is best applied.

Rangeland ecosystem service payment scenarios improve the economic status of the basin more than the other proposed scenarios. This scenario can be expanding alternative



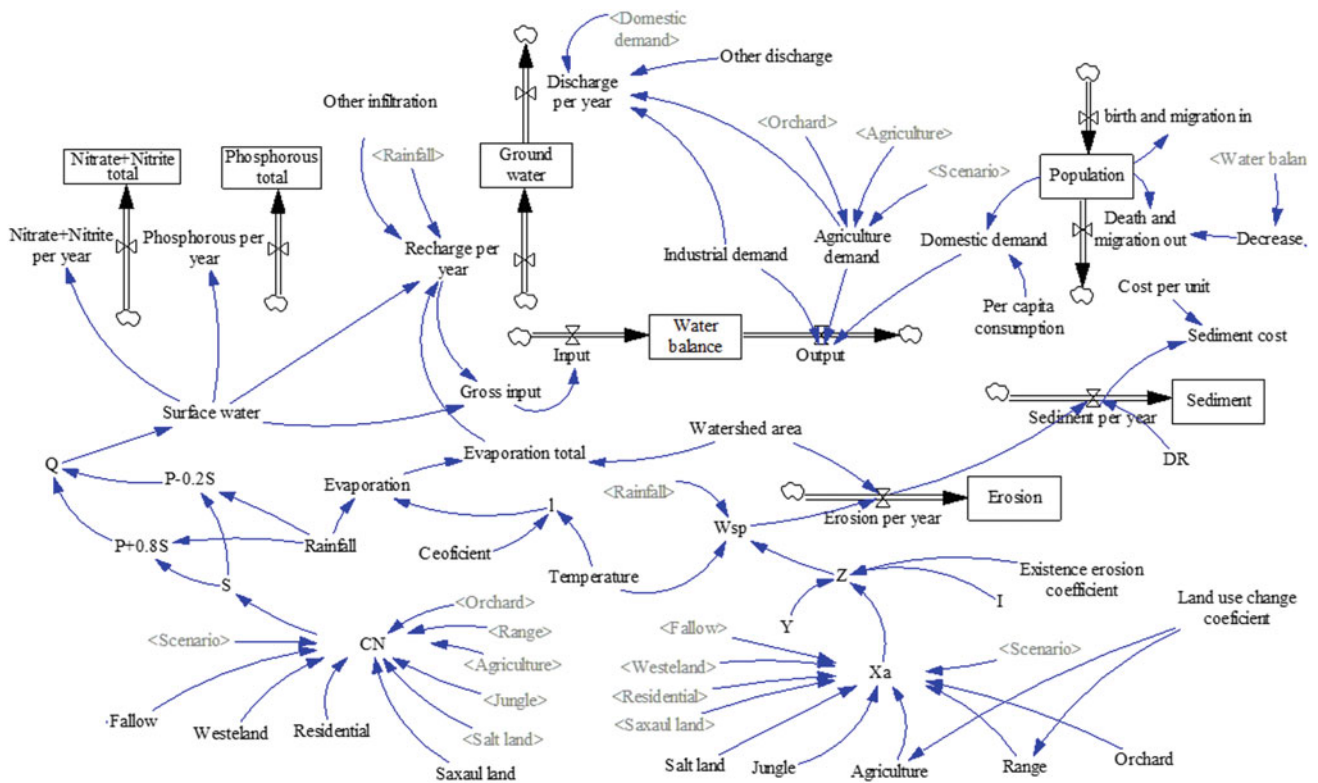


Fig. 9 Stock and flow diagram of the physical subsystem

Table 6 Values of Nash–Sutcliffe and  $R^2$  coefficients for model variables in Hableh-Rud river basin

Variable	Test				
	Water discharge	Nitrate–nitrite	Phosphorus	Sedimentation	Groundwater
$R^2$	0.68	0.63	0.7	0.7	0.89
Nash–Sutcliffe	0.67	0.62	0.62	0.79	0.86

jobs and reduce damage to natural resources. Management of agricultural water efficiency ranked second for improving economic situation. Gohari et al. (2013) emphasized the importance of managing agricultural water efficiency and management of agricultural cropping pattern in their research. Yeh et al. (2006) also noted the role of crop pattern management in reducing erosion and sedimentation. Inappropriate agricultural water management scenario was identified as the worst scenario.

## 5 Conclusion

Minimizing the cost of soil and water resources will require considering the full range of options for management of the upstream of the basin. However, the complexities and uncertainties of watershed problems seriously constrain

efforts to utilize traditional economic incentives to reach cost-efficiency goals. Thus, considering watershed economic issues is of critical importance for watershed decision makers. The economic aspects of soil and water resources management practices need to be quantified and better understood by decision makers if we are to see such practices become integral parts of resource development projects. Economic analysis of watershed management actions requires a comprehensive evaluation of many resources both at the site of implementation and at downstream sites. By integrating the simulation discipline and the feedback control theory into a dynamic consideration of soil and water resources, this paper proposes a system dynamics (SD) model for strategic capacity planning in watershed management. The SD model captures physical stocks and flows apparent in real-world soil and water resources networks and includes the feedback mechanisms which regulate

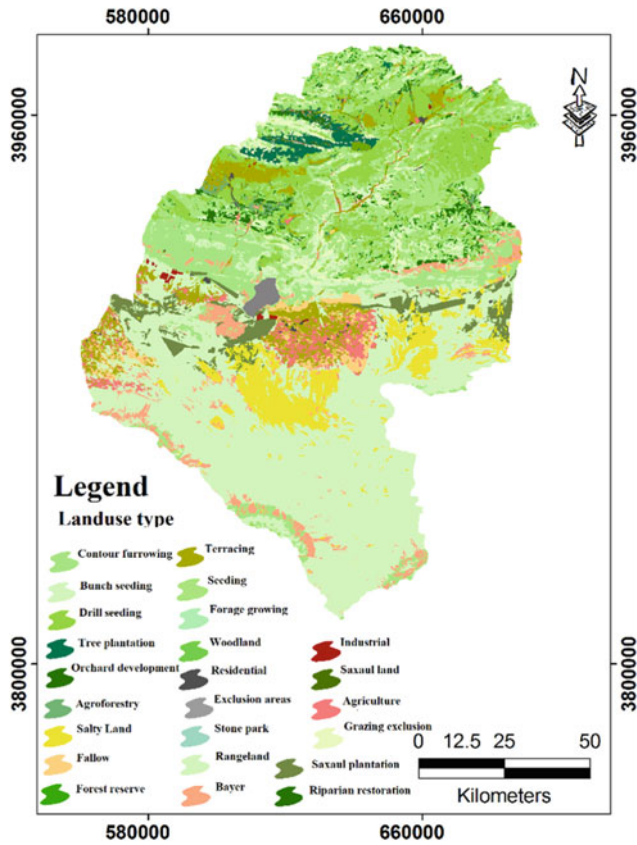


**Fig. 10** Map of the spatial distribution of the vegetation management activities in the Hableh-Rud river basin

these flows. The CLD developed in this study provides a good view of the Hableh-Rud river basin problem as well as different drivers of the system and their consistent relations. The objective was to test the proposed scenarios that address the issues of vegetation management, agricultural patterns,

economic of watershed, unsuitable management of agricultural water and climate change.

From an economic perspective, paying 50% of the ecosystem services by the government to expand alternative jobs and reduce damage to natural resources was determined as the best scenario. Scenarios of paying 25% of ecosystem services by the government to expand alternative jobs and reduce damage to natural resources and farm management activities were chosen as the next best scenarios, respectively. This demonstrates the economic importance of preserving natural ecosystems in many ways. If even part of this revenue is given to stakeholders to protect rangelands, it will help the watershed economy. Rangeland protection improves water quality, erosion, sedimentation and stability of natural ecosystems. Inappropriate management of agricultural water inflicts the highest economic loss to the current condition. After evaluating the vegetation management scenarios, it was determined that farm management actions were considered as the best scenario. The agroforestry, orchard development, forage growing and terracing activities have a high income which has made this scenario a better choice. Farm-related activities are in a good position for offering direct economic benefit to the stockholders. There will have to be a lot of costs for soil and water resource management if the conditions in the Hableh River Basin continue to exist. The Hableh-Rud river basin can pay for soil and water resource management, or it can pay more to continue this situation. No single solution will fix the Hableh-Rud river basin's soil and water problems. The research indicates that the SD model, as an integrated approach for management of soil and water resources of the basin, is a pragmatic and beneficial approach which helps stakeholders enhance their understanding of the causal relationships and feedbacks in the system.

**Table 7** Results of ranking of the proposed scenarios based on economic assessment of water and soil resources in Hableh-Rud river basin

Number	Scenario	Scenario rank
1	Current condition	8
2	Rangeland restoration	6
3	Natural resources rehabilitation areas	7
4	Farm management activities	5
5	Management of agricultural cropping pattern	4
6	Unsuitable management of agricultural water	10
7	Agricultural water management efficiency	3
8	Climate change	9
9	Pay 25% of the proceeds from ecosystem services to stakeholders by the government to expand alternative jobs and reduce damage to natural resources	2
10	Pay 50% of the proceeds from ecosystem services to stakeholders by the government to expand alternative jobs and reduce damage to natural resources	1



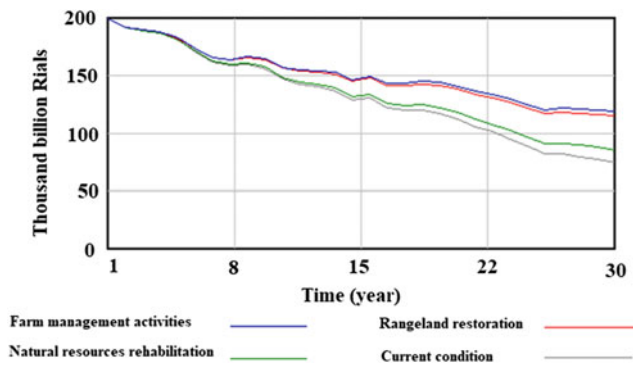


**Fig. 11** Comparison chart of the effect of vegetation management scenarios on the economic status of Hableh-Rud river basin

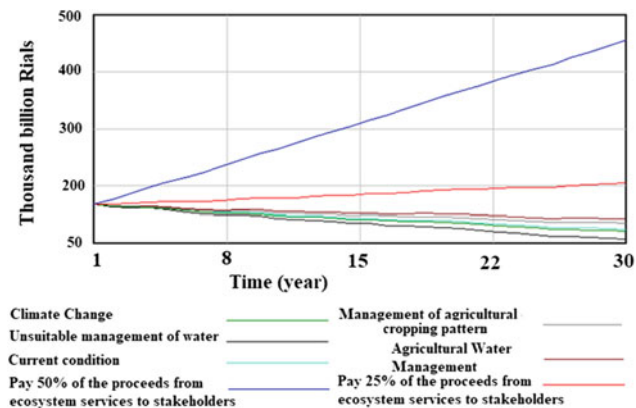


**Fig. 12** Comparison chart of the effect of climate change, water resources management and cropping pattern scenarios on the economic status of Hableh-Rud river basin

## References

- Adl, A., & Parvizian, J. (2009). Drought and production capacity of meat: A system dynamics approach. In *27th System Dynamics Conference* (p. 12).
- Ahmed, S., & Simonovic, S. P. (2000). System dynamics modeling of reservoir operation for flood management. *Journal of Computing in Civil Engineering*, *14*(3), 190–198.
- Bakhshianlamouki, E., Masia, S., Karimi, P., van der Zaag, P., & Sušnik, J. (2019). A system dynamics model to quantify the impacts of restoration measures on the water-energy-food nexus in the Urmia Lake Basin, Iran. *Science of The Total Environment*, 134874. <https://doi.org/10.1016/j.scitotenv.2019.134874>
- Barlas, Y., & Yasarcan, H. (2006). Goal setting, evaluation, learning and revision: A dynamic modeling approach. *Evaluation and Program Planning*, *29*, 79–87.
- Baron, J. S., Poff, N. L., Angermeier, P. L., Dahm, C. N., Gleick, P. H., Jackson, R. B., et al. (2002). Meeting ecological and social needs for fresh water. *Applied Ecology*, *12*(5), 1260–1274.
- Beall, A., Fiedler, F., Boll, J., & Cosens, B. (2011). Sustainable water resource management and participatory system dynamics. Case study: Developing the Palouse Basin participatory model. *Sustainability*, *3*, 720–742.
- Brooks, K. N., & Tayaa, M. (2002). Planning and managing soil and water resources in dry lands: role of watershed management. In *IALC Conference published in the Arid Lands Newsletter, International Arid Lands Consortium* (p. 18).
- Cao, Y., Zhao, Y., Wen, L., Li, Y., Li, H., Wang, S., Liu, Y., Shi, Q., & Weng, J. (2019). System dynamics simulation for CO<sub>2</sub> emission mitigation in green electric-coal supply chain. *Journal of Cleaner Production*, *232*, 759–773. <https://doi.org/10.1016/j.jclepro.2019.06.029>
- Chang, Y. C., Hong, F. W., & Lee, M. T. (2008). A system dynamic based DSS for sustainable coral reef management in Kenting coastal zone, Taiwan. *Ecological Modelling*, *211*, 153–168.
- Connell, O., Voisin, N., & Fu, M. (2019). Sensitivity of Western U.S. power system dynamics to droughts compounded with fuel price variability. *Applied Energy*, *247*, 745–754. <https://doi.org/10.1016/j.apenergy.2019.01.156>.
- Cordier, M., Uehara, T., Weih, J., & Hamaide, B. (2017). An input-output economic model integrated within a system dynamics ecological model: feedback loop methodology applied to fish nursery restoration. *Ecological Economics*, *140*, 46–57. <https://doi.org/10.1016/j.ecolecon.2017.04.005>.
- Elmahdi, A., Malano, H., & Etchells, T. (2007). Using system dynamics to model water-reallocation. *The Environmentalist*, *27*, 3–12.
- Eslamian, S., Najafi, M., Salariyan, M., Ostad-Ali-Askari, K., & Singh, V. P. (2018). Evaluation of radiation methods for calculating the water requirement of grass in two different climates using REF-ET software. *Journal of Plant Breeding and Agriculture*, *2*(1), 1–7.
- Fageria, N. K. (2009). *The use of nutrients in crop plants* (p. 431).
- Findlay, H., Hennige, S., Wicks, L., et al. (2015). Fine-scale nutrient and carbonate system dynamics around cold-water coral reefs in the northeast Atlantic. *Science and Reports*, *4*, 3671. <https://doi.org/10.1038/srep03671>.
- Fiorillo, F., Palestini, A., Polidori, P., & Socci, C. (2007). Modeling water policies with sustainability constraints: A dynamic accounting analysis. *Ecological Economics*, *63*, 392–402.
- Gies, L., Agusdinata, D. B., & Merwade, V. (2014). Drought adaptation policy development and assessment in East Africa using hydrologic and system dynamics modeling. *Natural Hazards*, *74*, 789–813. <https://doi.org/10.1007/s11069-014-1216-2>.
- Gohari, A., Eslamian, S., Mirchi, A., Abedi-Koupaei, J., Massah Bavani, A., & Madani, K. (2013). Water transfer as a solution to water shortage: A fix that can Backfire. *Journal of Hydrology*, *491*, 23–39.
- Hassanzadeh, E., Zarghami, M., & Hassanzadeh, Y. (2012). Determining the main factors in declining the Urmia lake level by using system dynamics modeling. *Water Resources Management*, *26*, 129–145.
- Jin, E., Mendis, G. P., & Sutherland, J. W. (2019). Integrated sustainability assessment for a bioenergy system: A system dynamics model of switch grass for cellulosic ethanol production in the U.S., Midwest. *Journal of Cleaner Production*, *234*, 503–520. <https://doi.org/10.1016/j.jclepro.2019.06.205>.
- Kelly, R. A., Jakeman, A. J., Barreteau, O., Borsuk, M. E., Elsawah, S., Hamilton, S. H., et al. (2013). Selecting among five common modelling approaches for integrated environmental assessment and management. *Environmental Modelling and Software*, *47*, 159–181.
- Keshtkar, A. R., Salajegheh, A., Sadoddin, A., & Allan, M. G. (2013). Application of Bayesian networks for sustainability assessment in catchment modeling and management (Case study: The Hablehrood river catchment). *Ecological Modelling*, *268*, 48–54.
- Keyes, A. M., & Palmer, R. (1993). The role of object oriented simulation models in the drought preparedness studies. In *Proceedings of 20th Annual National Conference on Water Resource Planning and Management Division* (pp. 479–482). ASCE.
- Liu, H., Benoit, G., Liud, T., Liu, Y., & Guo, H. (2015). An integrated system dynamics model developed for managing lake water quality

- at the watershed scale. *Journal of Environmental Management*, 155, 11–23.
- Lu, S., Qin, F., Chen, N., Yu, Z., Xiao, Y., Cheng, X., & Guan, X. (2019). Spatiotemporal differences in forest ecological security warning values in Beijing: Using an integrated evaluation index system and system dynamics model. *Ecological Indicators*, 104, 549–558. <https://doi.org/10.1016/j.ecolind.2019.05.015>.
- Mavrommati, G., Bithas, K., Panayiotidis, P. (2013). Operationalizing sustainability in urban coastal systems: A system dynamics analysis. *Water Research*, 1–16.
- Ministry of Agriculture Jihad. (2017). *Average yield and prices of agricultural products in Tehran province* (p. 50).
- Pagano, A., Pluchinotta, I., Pengal, P., Cokan, B., & Giordano, R. (2019). Engaging stakeholders in the assessment of NBS effectiveness in flood risk reduction: A participatory System Dynamics Model for benefits and co-benefits evaluation. *Science of the Total Environment*, 690, 543–555. <https://doi.org/10.1016/j.scitotenv.2019.07.059>.
- Perrone, A., Inam, A., Albano, R., Adamowski, J., & Sole, A. (2020). A participatory system dynamics modeling approach to facilitate collaborative flood risk management: A case study in the Bradano River (Italy). *Journal of Hydrology*, 580, 124354. <https://doi.org/10.1016/j.jhydrol.2019.124354>.
- Phonphoton, N., & Pharino, C. (2019). A system dynamics modeling to evaluate flooding impacts on municipal solid waste management services. *Waste Management*, 87, 525–536. <https://doi.org/10.1016/j.wasman.2019.02.036>.
- Savenije, H. H. G., & Zaag, P. V. (2008). Integrated water resources management: Concepts and issues. *Physics and Chemistry of the Earth*, 33, 290–297.
- Settle, C., Crocker, T. D., & Shogren, J. F. (2002). On the joint determination of biological and economic systems. *Ecological Economics*, 42, 301–311.
- Stave, K. A. (2010). Participatory system dynamics modeling for sustainable environmental management: Observations from four cases. *Sustainability*, 2, 2762–2784.
- Stave, K. A. (2008). Zero waste by 2030: A system dynamics simulation tool for stakeholder involvement in Los Angeles 'solid waste planning initiative. In *Proceedings of the 26th International Conference of the System Dynamics Society* (pp. 20–24), Athens, Greece.
- Sterman, J. (2000). *Business dynamics: Systems thinking for a complex world* (p. 1008). Irwin/McGraw-Hill.
- Sun, Y., Liu, N., Shang, J., & Zhang, J. (2016). Sustainable utilization of water resources in China: A system dynamics model. *Journal of Cleaner Production*. (In press).
- Tehran Regional Water Board. (2017). <https://www.tpww.ir>
- Vanden Belt, M. (2004). *Mediated modeling: A system dynamics approach to environmental consensus building*. Island Press.
- Vice-Presidency for Strategic Planning and Supervision. (2017). *Price list of watershed operations* (p. 151).
- Wang, X. J., Zhang, J. Y., Liu, J. F., Wang, G. Q., He, R. M., Elmahdi, A., & Elsawah, S. (2011). Water resources planning and management based on system dynamics: A case study of Yulin city. *Environment, Development and Sustainability*, 13, 331–351.
- Winz, I., Brierley, G., & Trowsdale, S. (2009). The use of system dynamics simulation in water resources management. *Water Resources Management*, 23(7), 1301–1323.
- Wolstenholme, E. (1990). *System enquiry: A system dynamics approach*. Wiley.
- Woodruff, A., & Halland, P. (2008). Benefit-cost analysis for improved natural resource decision-making in pacific island countries. In *CRISP Economic Workshop* (p. 10). 26th–30th May, Suva, Fiji.
- Xuan, Z., Chang, N. B., & Wanielista, M. (2012). Modeling the system dynamics for nutrient removal in an innovative septic tank media filter. *Bioprocess and Biosystems Engineering*, 35(4), 545–552. <https://doi.org/10.1007/s00449-011-0627-7>.
- Yeh, S. C., Wang, C. A., & Yu, H. C. (2006). Simulation of soil erosion and nutrient impact using an integrated system dynamics model in a watershed in Taiwan. *Environmental Modeling and Software*, 21, 937–948.
- Youa, Y. Y., Jin, W. B., Xiong, Q. X., Xu, L., Ai, T. C., & Li, B. L. (2012). Simulation and validation of on-point source nitrogen and phosphorus loads under different land uses in Sihou Basin, Hubei Province, China. In *The 18th Biennial Conference of International Society for Ecological Modelling Procedia Environmental Sciences* (Vol. 13, p. 1781).
- Zhang, L., Wu, L., Wu, C., Jin, J., Huo, S., & Zhou, Y. (2018). Construction of lake reference conditions for nutrient criteria based on system dynamics modelling. *Ecological Modelling*, 383, 69–79. <https://doi.org/10.1016/j.ecolmodel.2018.05.005>.



# Seasonal Variation for Trace Metals Contamination of Groundwater Using GIS Technology in Pissurlem, Sonshi, Cudnem, Velguem, Surla Watersheds, North Goa District, Goa State, India

E. Kuppusamy and S. M. Hussain

## Abstract

Groundwater quality and availability is one of the most important environmental and sustainability issues of the twenty-first century. Over the last few years, trace elements have increased in groundwater by human activities, such as agriculture, mining, fossil fuel burning and industrial effluent. The present study is focused on the pollution of groundwater by heavy metals. Seasonal variations of groundwater quality studies have been performed in Pissurlem, Sonshi, Cudnem, Velguem and Surla Watersheds, which are the primary watersheds of Mandovi and Cudnem rivers in Goa State. A maximum of 98 samples has been obtained at a rate of 49 samples per season (summer and winter). Trace elements are measured using the atomic absorption spectrophotometer (AAS). Measured groundwater traces of metals results were brought to the GIS to create spatial maps. Aluminum, barium, boron, copper, manganese, selenium, zinc, cadmium, lead, nickel, arsenic and chromium spatial maps shows that all groundwater levels in the study area were within the allowable limit. Iron spatial maps show all groundwater Fe research areas within the limit quality except in and around Kumbharwada, Vagheri and Morlem Colony sites (4.62 km<sup>2</sup>/summer and 5.96 km<sup>2</sup>/winter) for WHO 2011 norm. The study area is situated in the lower part of the Cudnem River with the Mandovi river portion. Research region for groundwater Trace metals contamination within the limits except iron for the WHO 2011 standard. Trace elements in groundwater are characterized as chemical components dissolved in very small quantities in water. The levels of aluminum, barium, boron, copper, manganese, selenium, zinc, cadmium, lead, nickel, arsenic and chromium are well within the permissible limits. All the water samples are favorable for drinking in both of the seasons. Iron levels in

groundwater are distinguished by a favorable quality for drinking in all samples, except for three test sites, such as Kumbharwada (S. No. 17), Vagheri (S. No. 22) and Morlem Colony (S. No. 40) in both seasons. The entire study area is widely distributed for the occurrence of iron ore and falls in the active mining belt.

## Keywords

Trace metals • Mandovi River • Spatial map • Groundwater • Contour values

## 1 Introduction

Trace metals in groundwater are defined as chemical components dissolved in water in very small quantities, always or almost always, with concentrations of less than one mg/L (U.S.G.S., 1993; Marcovecchio et al., 2007; Momodu & Anyakora, 2010). While present in a limited amount, but optimal intake, it is necessary for the proper functioning of the human body. Abundance or lack, or both, can pose a risk to health. The heavy metal element of groundwater is becoming one of the major concerns due to its adverse effects on human physiology. Excessive trace metal can also be found in groundwater near polluted sources posing serious health risks (Vadiati et al., 2016; Haritash & Garg, 2016; Modassir et al., 2015).

Trace metals derive mainly from source rocks due to weathering and are generally harmless to species at moderate levels of contamination; but, once their concentration increases, they are significantly harmful to human and other living organisms. Over the last few years, trace metals have risen in groundwater as they have become polluted by human activities, such as farming, fossil fuel burning and industrial effluent. It is clear that trace elements are entering aquatic environments either from point sources or from nonpoint sources. Trace elements enter groundwater from

E. Kuppusamy (✉) · S. M. Hussain  
Mineral Exploration Corporation Limited, Dr. Babasahab  
Ambedkar Bhavan, Seminary Hills, Nagpur, 440006, India

organic, anthropogenic and mining activities (Mahato et al., 2014; Verma & Singh, 2013; Adaikpoh et al., 2005; Goyal et al., 2008).

### 1.1 Study Area Details

The study area (Fig. 1) is situated in the northeastern part of the Goa State located between  $15^{\circ} 26' 47.142''$  N to  $15^{\circ} 36' 21.911''$  N and  $73^{\circ} 57' 8.676''$  E to  $74^{\circ} 7' 29.228''$  E. The total geographical area of the study area is  $185.48 \text{ km}^2$ . The present study area includes the watersheds in Pissurlem, Sonshi, Cudnem, Velguem and Surla, which are the major watersheds of the Mandovi River. The research area is shown in Fig. 1.

### 1.2 Mandovi River

The Mandovi River is the lifeline of the state, as its watershed covers about 42% of the total area of the state, and its water is widely used for drinking, transport, agriculture, fisheries, etc. It has five major tributaries, Mhadei, Khan-depar, Valvati, Mapusa and the Sinqerim River.

The Mandovi River is one of the important rivers of the Goa State, which rises in the Parwar Ghats of Sattari Taluk

at an altitude of 888 mts. southwest. The Mandovi River forms several islands in Bardez and Tiswadi Taluks, and enters the Arabian Sea through the Bay of Aguada, near Panaji, after a length of about 70 km. The length of the estuary is 3.2 km, it narrows down to 0.25 km in the downstream, and it is the biggest drainage basin in Goa.

Administratively, Goa State is divided into two districts, the North Goa District and the South Goa District. North Goa consists of six talukas such as (1) Tiswadi, (2) Bardez, (3) Pernem, (4) Bicholim, (5) Sattari and (6) Ponda. South Goa is subdivided into five talukas, such as (1) Sanguem, (2) Canacona, (3) Quepem, (4) Salcete and (5) Marmugao. It is situated to the west of the state of Karnataka and to the southwest of the state of Maharashtra, 100 km long in the west of the sea.

The state of Goa is divided into three physiological units. The major geomorphological characteristics are the coastal plains, the southern undulating regions and the Western Ghats.

### 1.3 Physicochemical Analysis of Groundwater

The water quality analysis of groundwater samples has been carried out the trace elements such as aluminum ( $\text{Al}^{3+}$ ), copper ( $\text{Cu}^{2+}$ ), iron ( $\text{Fe}^{2+}$ ), manganese ( $\text{Mn}^{2+}$ ), selenium ( $\text{Se}^{2+}$ ), zinc ( $\text{Zn}^{2+}$ ), cadmium ( $\text{Cd}^{2+}$ ), lead ( $\text{Pb}^{2+}$ ), nickel

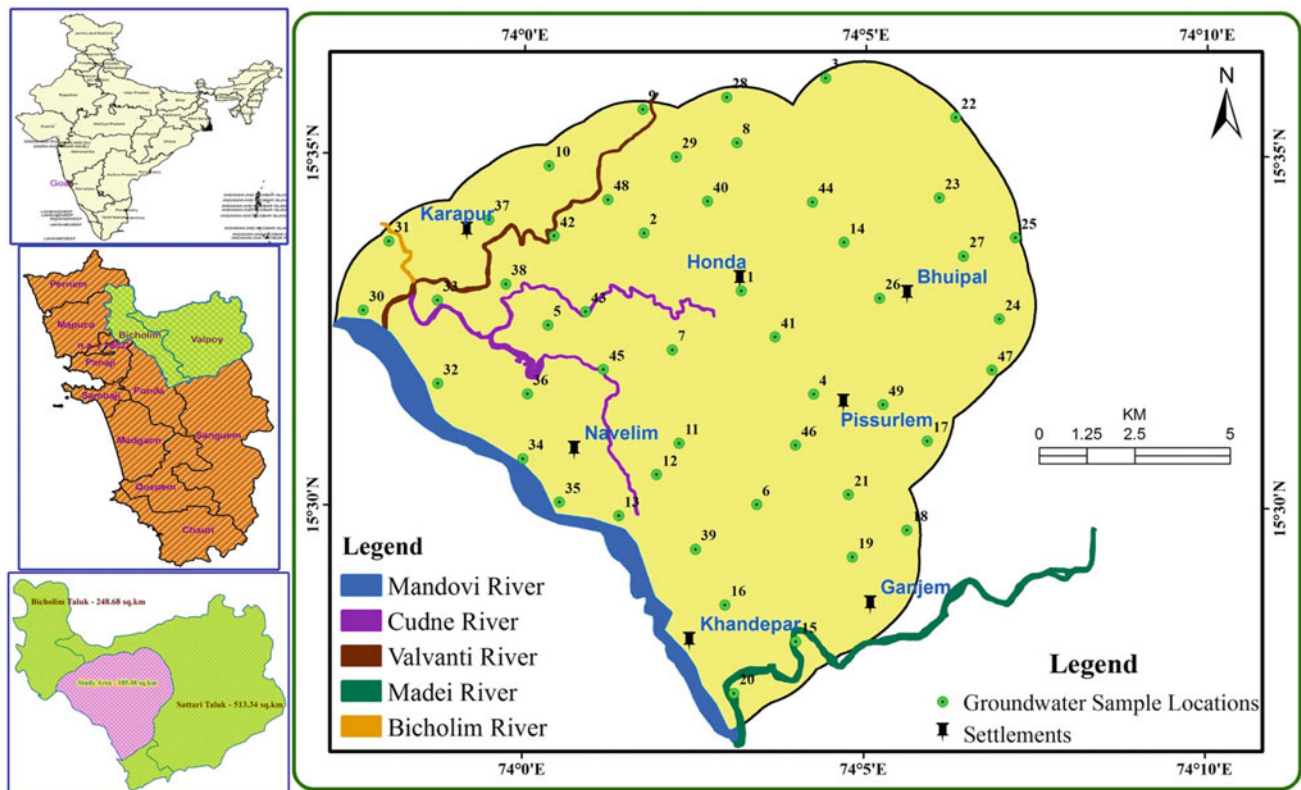


Fig. 1 Study area with groundwater sample locations



(Ni<sup>2+</sup>), arsenic (As<sup>2+</sup>), chromium (Cr<sup>2+</sup>) and their analyzed winter–summer seasons. The results of statistical parameters for trace elements are shown in Table 1. The data were used to understand the spatial distribution of ions and to classify those not permitted for drinking purposes in the study area.

## 2 Results and Discussion

Groundwater contamination is one of the most significant environmental issues in the world today, where substantial heavy metal exposure is of major concern due to its high hazard, even at low levels of fixation (Panigrahy et al., 2015; Kumar et al., 2014; Tiwari & Sing, 2014). The trace element concentration in groundwater was therefore calculated for Pissurlem, Sonshi, Cudnem, Velguem and Surla Watersheds.

### 2.1 Aluminum (Al)

Aluminum is one of the most accommodating metallic elements on earth crust and is widely distributed in soil and

rock. It enters the groundwater from the soil, weathering rock-forming minerals, industrial waste and anthropogenic activities. The source of aluminum is derived geologically from leaching of deposit and decomposition of various minerals. The aluminum concentration of more than 0.07 mg/L makes the water unsuitable for drinking purpose because it causes severe health problems.

According to WHO (2011) guidelines, the aluminum concentration <0.07 mg/L is classified as a desirable limit. Based on the above, all the samples are under a desirable category in the study area. In the winter season, groundwater aluminum values start from 0.010 to 0.017 mg/L. In the summer season, groundwater aluminum values are from 0.011 to 0.019 mg/L. These values are characterized by desirable nature for drinking purpose of all the samples in both the seasons.

The spatial distribution maps of aluminum during both the seasons are shown in Figs. 2 and 3. The aluminum spatial maps show that in all the study area, groundwater aluminum concentration is within the limit value as per WHO 2011 standards. But small changes occur in contour values in the summer season.

**Table 1** Result of the statistical parameters

Parameters	Seasons	Mean	Median	Minimum	Maximum	Std. dev.
Aluminum (Al)	Winter	0.012	0.012	0.010	0.017	0.002
	Summer	0.013	0.014	0.011	0.019	0.002
Copper (Cu)	Winter	0.008	0.008	0.007	0.009	0.001
	Summer	0.009	0.009	0.008	0.010	0.001
Iron (Fe)	Winter	0.086	0.060	0.045	1.000	0.145
	Summer	0.100	0.070	0.050	1.130	0.164
Manganese (Mn)	Winter	0.026	0.026	0.021	0.029	0.002
	Summer	0.029	0.029	0.024	0.033	0.002
Selenium (Se)	Winter	0.004	0.005	0.004	0.005	0.000
	Summer	0.005	0.005	0.005	0.006	0.000
Zinc (Zn)	Winter	0.005	0.005	0.004	0.005	0.000
	Summer	0.005	0.005	0.005	0.006	0.000
Cadmium (Cd)	Winter	0.002	0.002	0.002	0.003	0.000
	Summer	0.003	0.003	0.002	0.003	0.001
Lead (Pb)	Winter	0.005	0.005	0.004	0.005	0.000
	Summer	0.005	0.005	0.005	0.006	0.001
Nickel (Ni)	Winter	0.008	0.009	0.005	0.010	0.001
	Summer	0.010	0.010	0.006	0.011	0.001
Arsenic (As)	Winter	0.002	0.002	0.001	0.002	0.000
	Summer	0.002	0.002	0.002	0.002	0.000
Chromium (Cr)	Winter	0.028	0.028	0.024	0.030	0.001
	Summer	0.032	0.032	0.028	0.035	0.001

**Fig. 2** Winter season Al spatial map

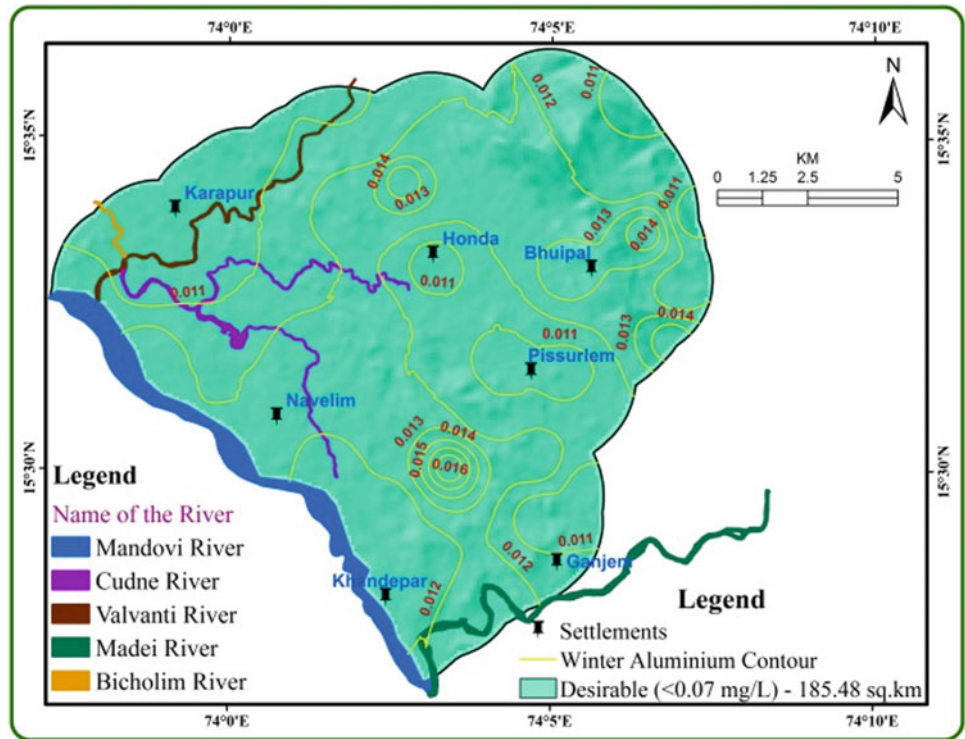
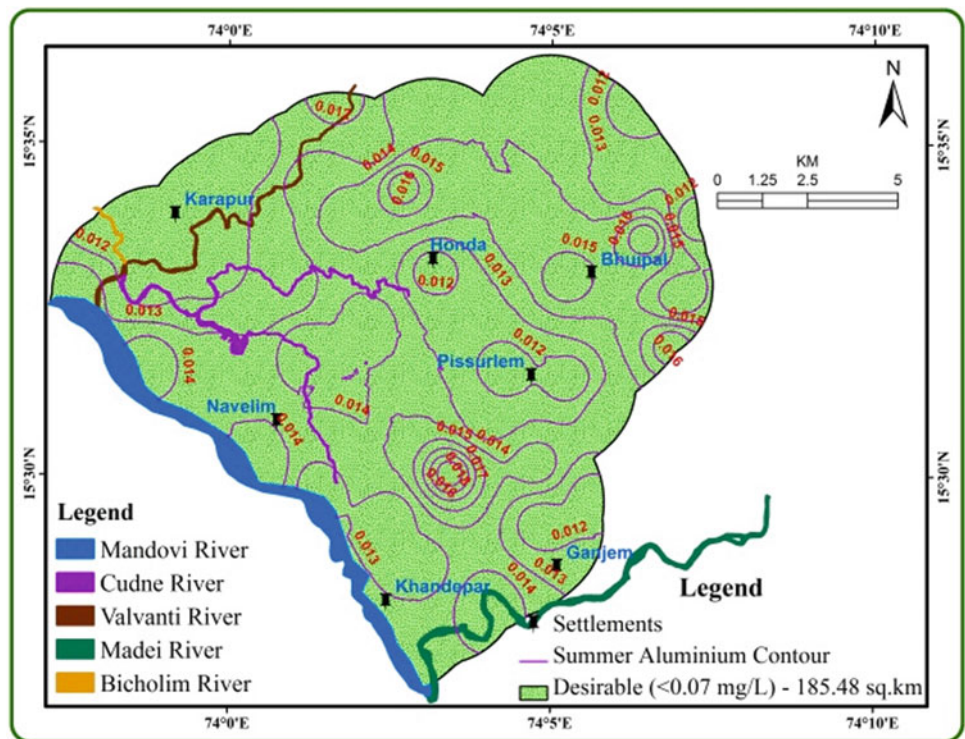


**Fig. 3** Summer season Al spatial map

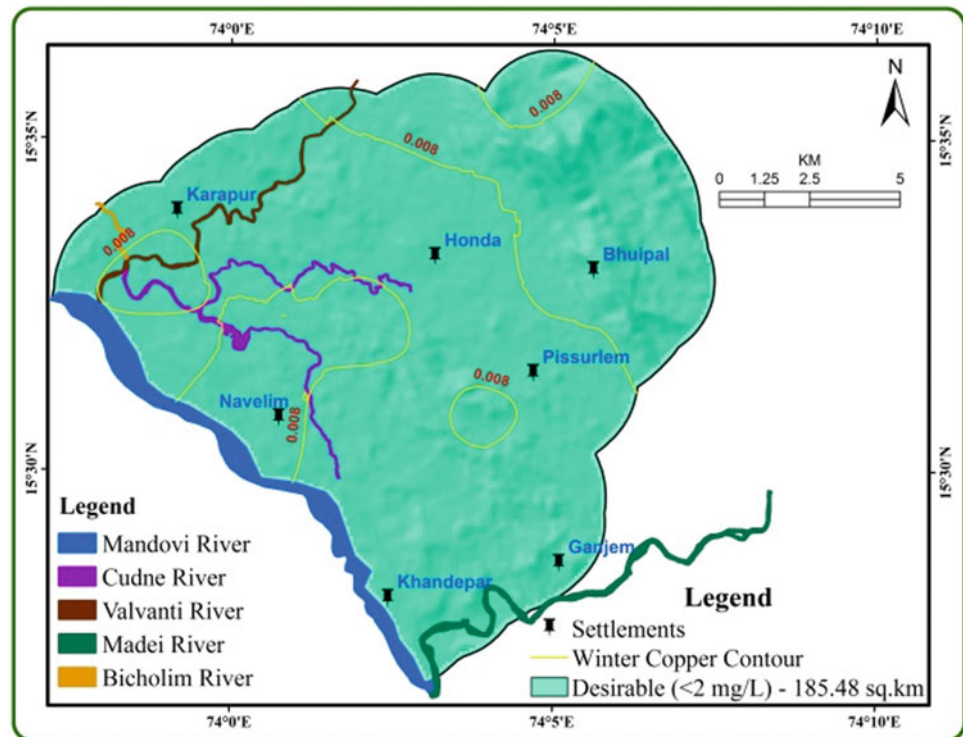


**2.2 Copper (Cu)**

Copper is a common trace metal on the earth and is broadly disseminated in rock-forming minerals. It enters the

groundwater from weathering rock-forming minerals, industrial waste and corrosive effect copper pipes. Copper is necessary for human health. But excess amount of copper is found to be the cause of liver and kidney injury in humans.

**Fig. 4** Winter season Cu spatial map



Kids who are less than one year are widely affected. It has a toxic effect on human health if the concentration is below the desirable limit. The diseases of anemia, diarrhea, etc., can be caused due to Cu deficiency (Abdullah Khan & Ahmad, 2010).

According to WHO (2011) guidelines, copper concentration  $<2$  mg/L is classified as a desirable limit. Based on the above, all the samples are under a desirable category in the study area. During the winter season, groundwater copper values start from 0.007 to 0.009 mg/L and in the summer season groundwater copper values are from 0.008 to 0.010 mg/L. These values are characterized by a desirable nature for drinking purpose of all the samples in both the seasons.

The spatial distribution maps of copper during both seasons are shown in Figs. 4 and 5. The copper spatial maps show that in all the study area, groundwater copper concentration is within the limit value as per WHO 2011 standards. But small changes occur in contour values in the summer season.

### 2.3 Iron (Fe)

Iron occurs chiefly in all stage of rock forms (igneous, metamorphic and sedimentary) origin. Iron is also a part of our life style, and iron is necessary for human health. Iron is a necessary component for nutritional requirement for most of the organisms. It enters the groundwater from weathering

rock-forming minerals, industrial waste products and corrosive copper pipes. It affects target organs which are the liver, cardiovascular system and kidneys. Its deficiency causes anemia. The entire study area is widely distributed for iron ore and potential belt for iron ore mining.

A maximum permissible Fe concentration is 0.3 mg/L for drinking purpose (WHO, 2011). Based on this, the results of the samples are under the desirable category in the study area. In the winter season, groundwater iron values start from 0.05 to 1.00 mg/L. During summer season, groundwater iron values are from 0.05 to 1.13 mg/L. These values are characterized by a desirable nature for drinking use of all the samples except three sample locations which are Kumbharwada (S. No. 17), Vagheri (S. No. 22) and Morlem Colony (S. No. 40) in both the seasons.

The spatial distribution maps of Fe during both the seasons are shown in Figs. 6 and 7. The iron spatial maps show that in all the study area groundwater Fe is within the limiting value except in and around the Kumbharwada, Vagheri and Morlem Colony locations (4.62 and 5.96 km<sup>2</sup>) as per WHO 2011 standards. But small changes occur in contour values in the summer season.

### 2.4 Manganese (Mn)

Manganese is one of the generous metals on the earth and is broadly disseminated in the form of oxides and hydroxides.

**Fig. 5** Summer season Cu spatial map

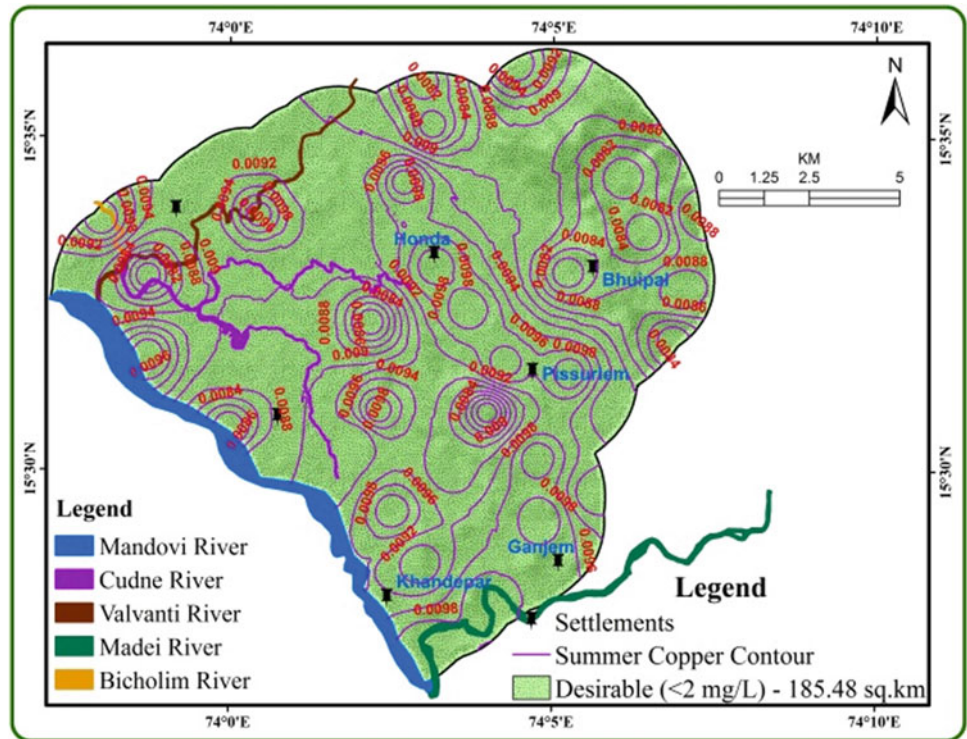
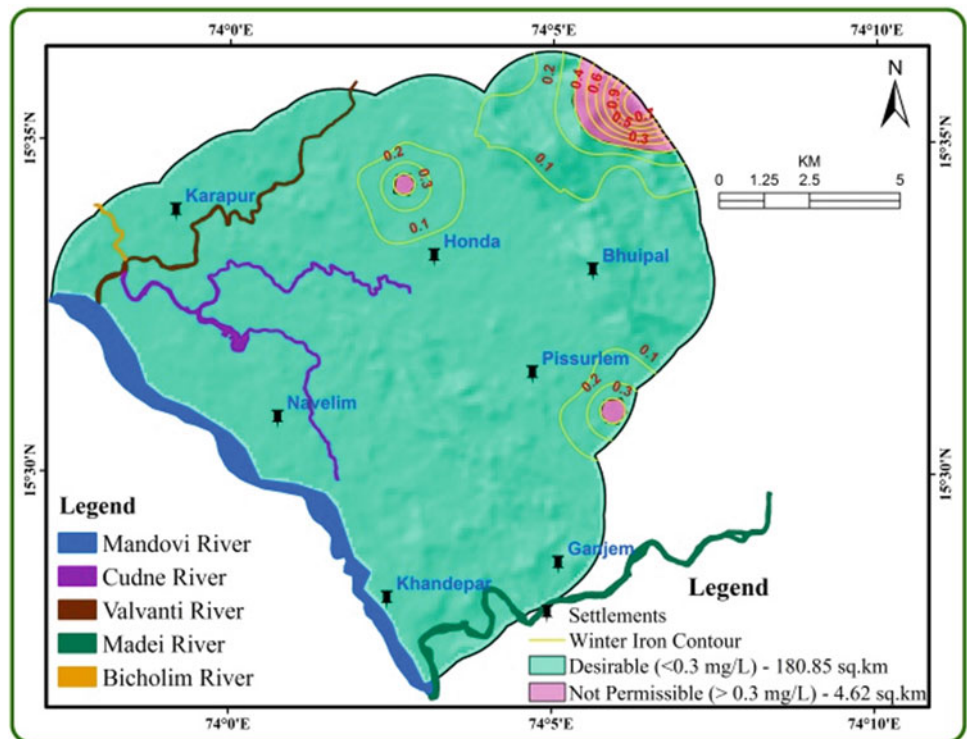


**Fig. 6** Winter season Fe spatial map

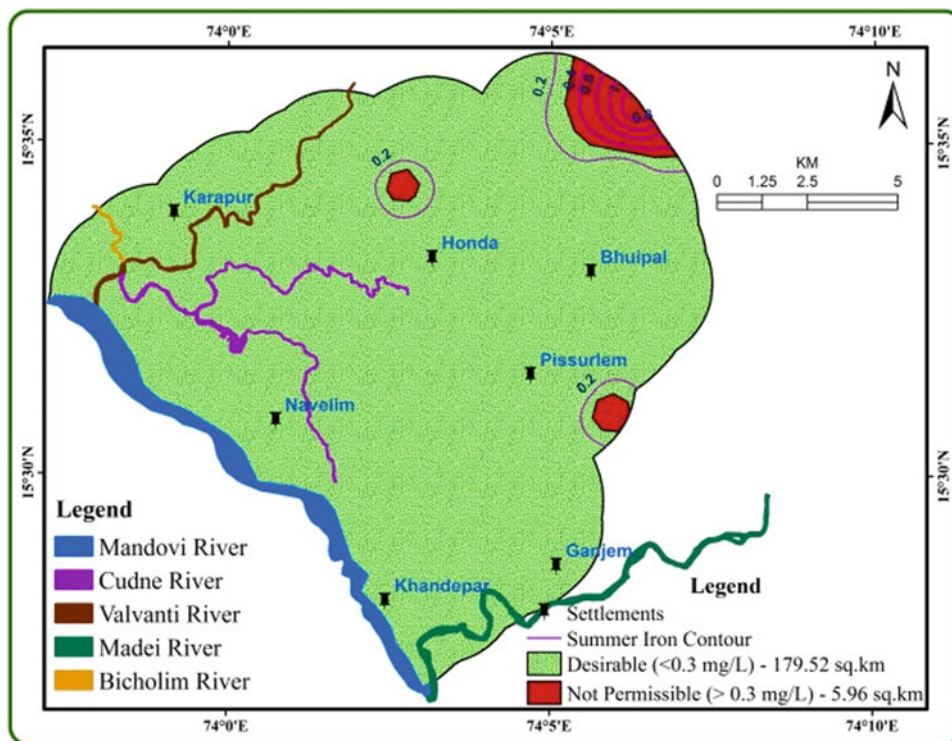


The atmosphere is the main source of manganese, so rain-water carries the manganese to reach the earth's surface. Another form of the source in earth's crust is dust particles of industrial discharge, volcanic ash, smoke of the burning

of garbage waste and soil erosion. The manganese concentration of more than 0.04 mg/L makes the water unsuitable for drinking use because it causes severe health problems. However, slight rise in its level may be accounted for by the



**Fig. 7** Summer season Fe spatial map



influence of domestic waste, natural geological rocks and industrial effluent. Sometimes, water containing manganese is not suitable for domestic purpose. Manganese is an essential nutrient for humans; Mn deficiency can disrupt the central nervous system and reproductive functions (McNeely et al., 1979).

A maximum amount of Mn concentration of 0.4 mg/L is permissible for drinking purpose (WHO, 2011). Based on this, it is found that the samples are under a desirable category in the study area. In the winter season, groundwater Mn values start from 0.02 to 0.03 mg/L. During summer season, groundwater Mn values are from 0.02 to 0.03 mg/L. These values are characterized by a desirable nature for drinking use of all the samples in both the seasons.

The spatial distribution maps of Mn during both the seasons are shown in Figs. 8 and 9. The Mn spatial maps show that in all the study area groundwater Mn is within the limit as per WHO 2011 standards. But small changes occur in contour values in the summer season.

## 2.5 Selenium (Se)

Selenium is a minor trace metal in water. The main sources of selenium in the groundwater are from erosion of natural deposits, discharge from mines and petroleum refineries. Selenium is an important nutrient food for fish, birds and animals. Selenium generally is similar to sulfur in its

chemical behavior (Lakin, 1973). The selenium concentration more than 0.01 mg/L makes the water unsuitable for drinking use because it causes severe health problems like hair loss, nail inflammation, vomiting, irritability, garlic breath odor, etc.

A maximum amount of Se concentration of 0.01 mg/L is permissible for drinking purpose (WHO, 2011). Based on this, the results of the samples are under the desirable category in the study area. During winter season, groundwater Se values start from 0.004 to 0.005 mg/L. In the summer season, groundwater Se values are from 0.005 to 0.006 mg/L. Those values are characterized by a desirable nature for drinking use of all the samples in both the seasons.

The spatial distribution maps of Se during both the seasons are shown in Figs. 10 and 11. The Se spatial maps show that in all the study area groundwater Se is within the limit as per WHO 2011 standards. But small changes occur in contour values in the summer season.

## 2.6 Zinc (Zn)

Zinc is an essential element for human health and agriculture; it plays an important role in protein synthesis and carbohydrate metabolism (Tylor & Demayo, 1980). The main source of zinc is industrial wastewater, fertilizers, pesticides and herbicides used for agricultural purposes. Zinc is relatively pre-toxic up to 3 mg/L in drinking water

**Fig. 8** Winter season Mn spatial map

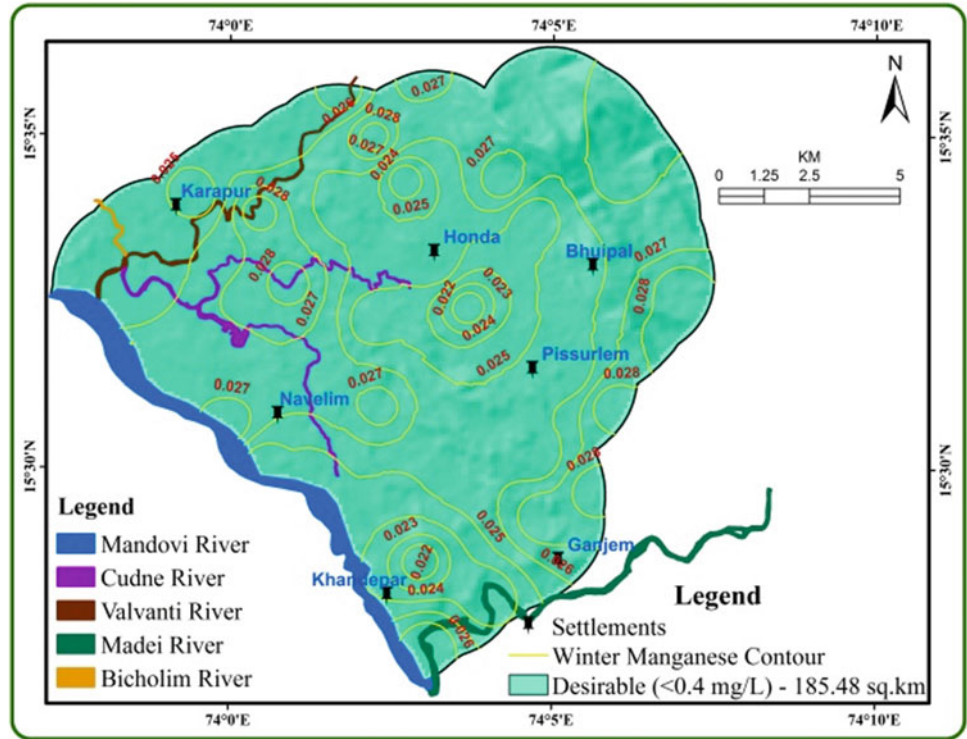
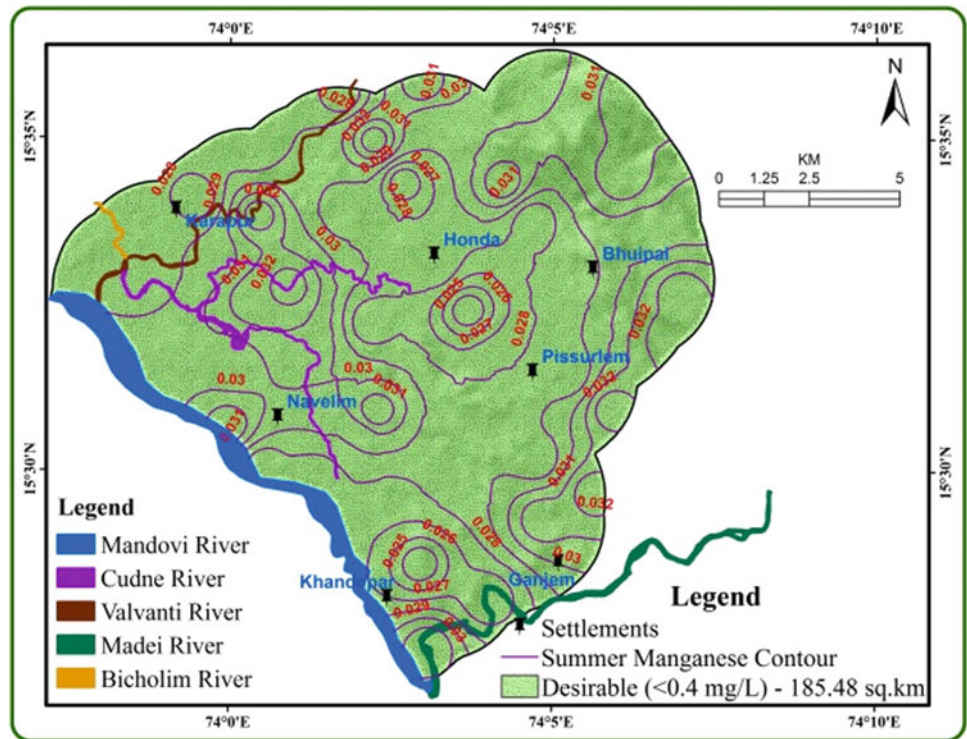


**Fig. 9** Summer season Mn spatial map



(McNeely et al., 1979). Zinc concentration more than 3 mg/L makes the water unsuitable for drinking use because it causes severe health problems like stomach pain, vomiting, fever and diarrhea.

A maximum permissible zinc concentration of 3 mg/L for drinking purpose is permissible (WHO, 2011). Based on this, the samples are under the desirable category in the study area. During winter season, groundwater Zn values

**Fig. 10** Winter season Se spatial map

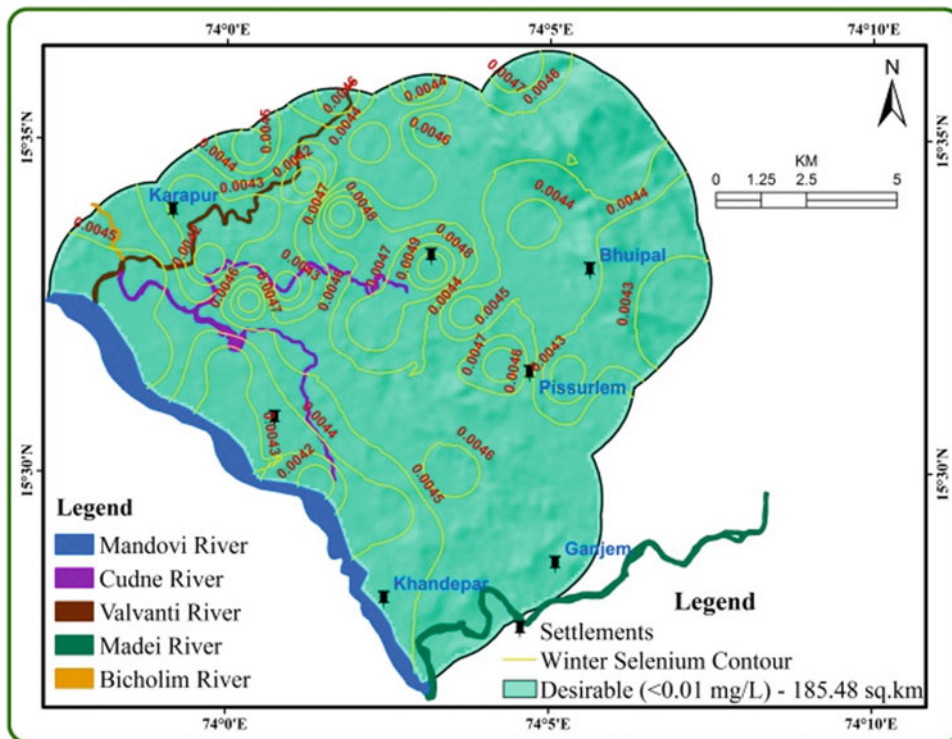
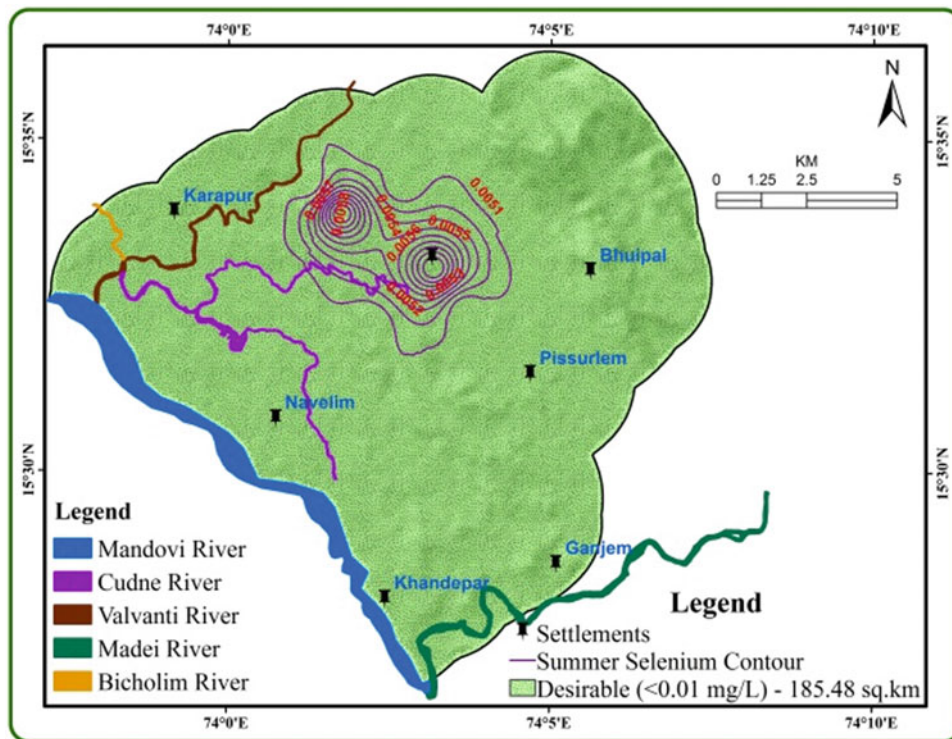


**Fig. 11** Summer season Se spatial map



start from 0.004 to 0.005 mg/L. In the summer season, groundwater Zn values are from 0.004 to 0.005 mg/L. That values are characterized by desirable nature for drinking purpose of all the samples in both the seasons.

The spatial distribution maps of Zn during both the seasons are shown in Figs. 12 and 13. High concentration contour is clustered in NNE to NW direction, because of the flow of rivers in this direction (Valvati River and Cudnem



**Fig. 12** Winter season Zn spatial map

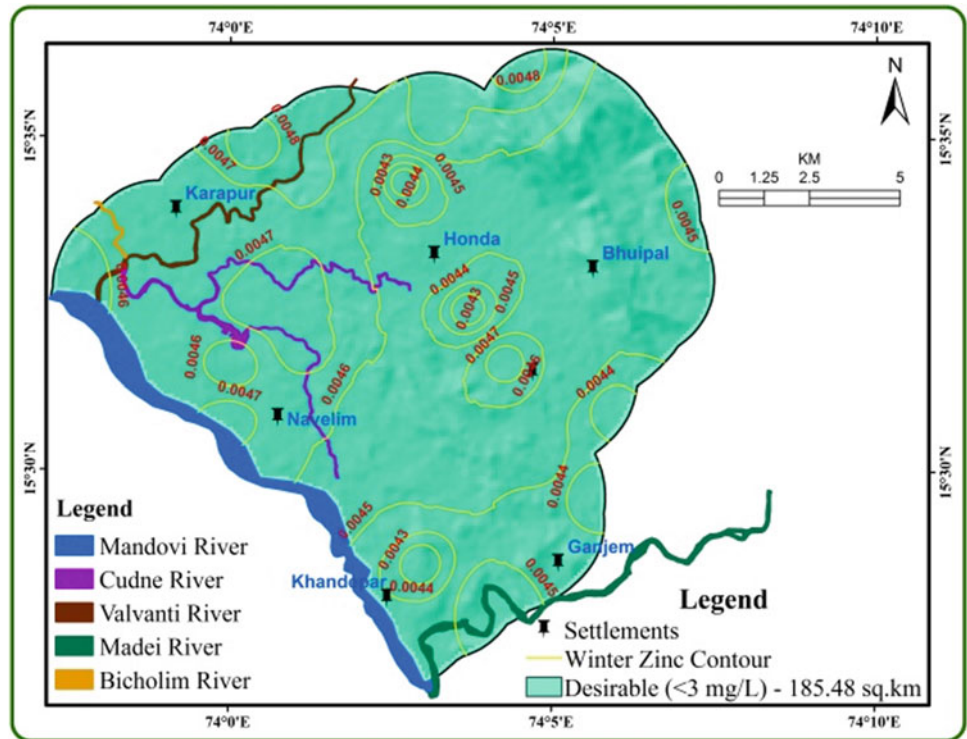
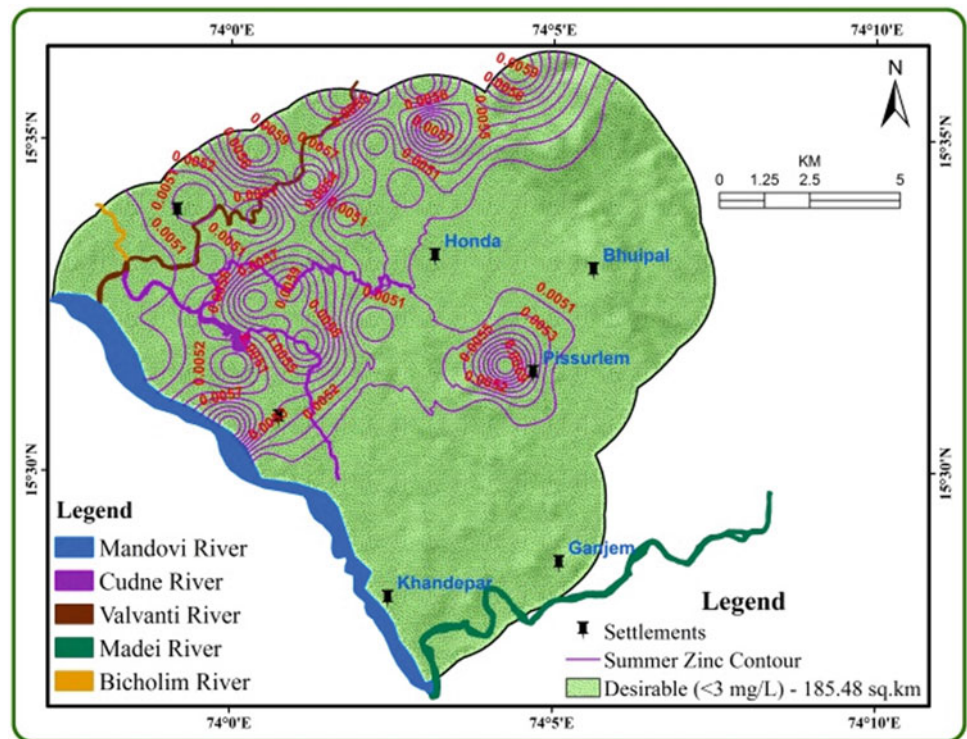


**Fig. 13** Summer season Zn spatial map



River). The Zn spatial maps show that in all the study area groundwater Zn is within the limit as per WHO 2011 standards. But small changes occur in contour values in the summer season.

### 2.7 Cadmium (Cd)

Cadmium is a common trace metal on the earth. Cd is found in very low concentrations in most rocks; other sources of

cadmium in groundwater come from burning fossil fuels and applying fertilizer, etc. Cd is found in basaltic rock (0.15 ppm) (Krasukopf & Bird, 1994), but is not essential for plants, animals and humans. Long-term exposure (over years or decades) to cadmium in drinking water may cause kidney damage (WHO, 2011) and can also lead to anemia, cardio vascular disease and hypertension (Mielke et al., 1991; Robards & Worsfold, 1991). Cadmium’s effect on the cardio vascular system can be explained by relating nutritional cadmium to hypertension (Schroeder, 1965).

A maximum cadmium concentration of 0.003 mg/L for drinking purpose is permissible (WHO, 2011). Based on this, the samples are under the desirable category in the study area. During winter season, groundwater cadmium values start from 0.002 to 0.0029 mg/L. In the summer season, groundwater cadmium values are from 0.002 to 0.003 mg/L. These values are characterized by a desirable nature for drinking purpose of all the samples in both the seasons.

The spatial distribution maps of cadmium during both the seasons are shown in Figs. 14 and 15. Higher concentration contour is clustered in the adjoining portion of Cudnem River. The cadmium spatial maps show that in all the study area groundwater cadmium is within the limit as per WHO 2011 standards. But small changes occur in contour values in the summer season.

### 2.8 Lead (Pb)

A naturally occurring toxic trace metal is lead. A very meager amount of lead occurs in natural resources such as soil, biological materials, water, plants and animals. The main source of lead contamination is due to transport burning and fossil fuel (Smirjakova et al., 2005). The lead concentration more than 0.01 mg/L makes the water unsuitable for drinking use because it causes severe health problems. Lead and its compounds are known to target the organs such as bones, brain, blood pressure and kidney damage, cardiovascular system and biosynthesis of hemoglobin (Homady et al., 2002; Massadeh et al., 2004).

A maximum lead concentration of 0.01 mg/L for drinking purpose is permissible (WHO, 2011). Based on this, the samples are under the desirable category in the study area. During winter season, groundwater lead values start from 0.0041 to 0.0049 mg/L. In the summer season, groundwater lead values are from 0.005 to 0.006 mg/L. These values are characterized by a desirable nature for drinking purpose of all the samples in both the seasons.

The spatial distribution maps of lead during both the seasons are shown in Figs. 16 and 17. The carbonate-bound fraction has significant values of Pb in the lower part of the Cudnem River with a portion of the Mandovi River. The Pb

**Fig. 14** Winter season Cd spatial map

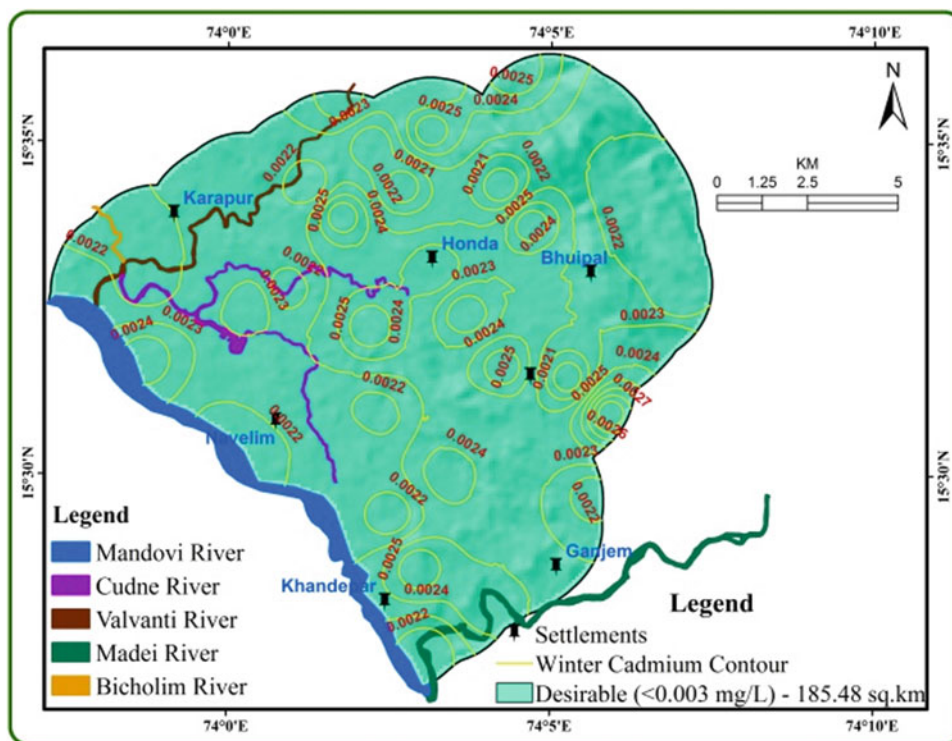


**Fig. 15** Summer season Cd spatial map

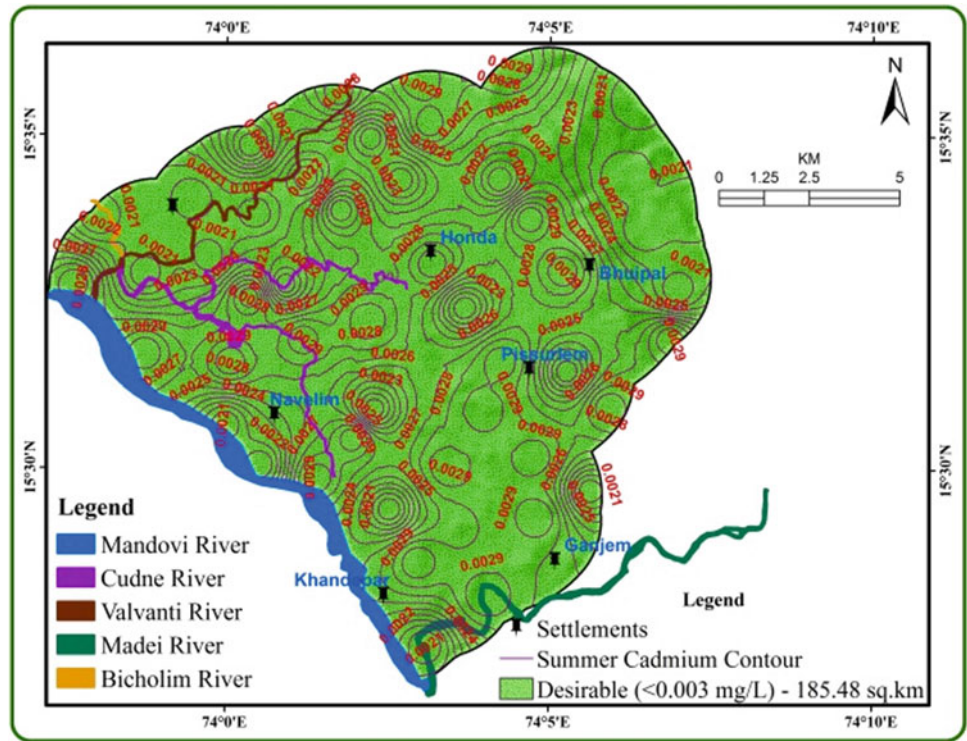


**Fig. 16** Winter season Pb spatial map

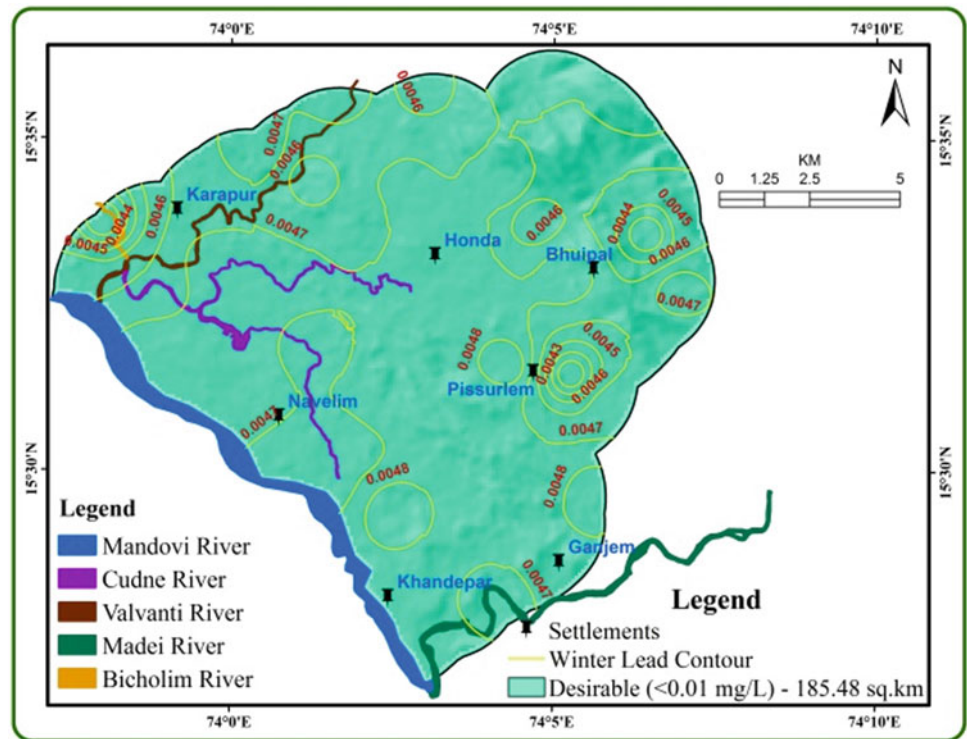
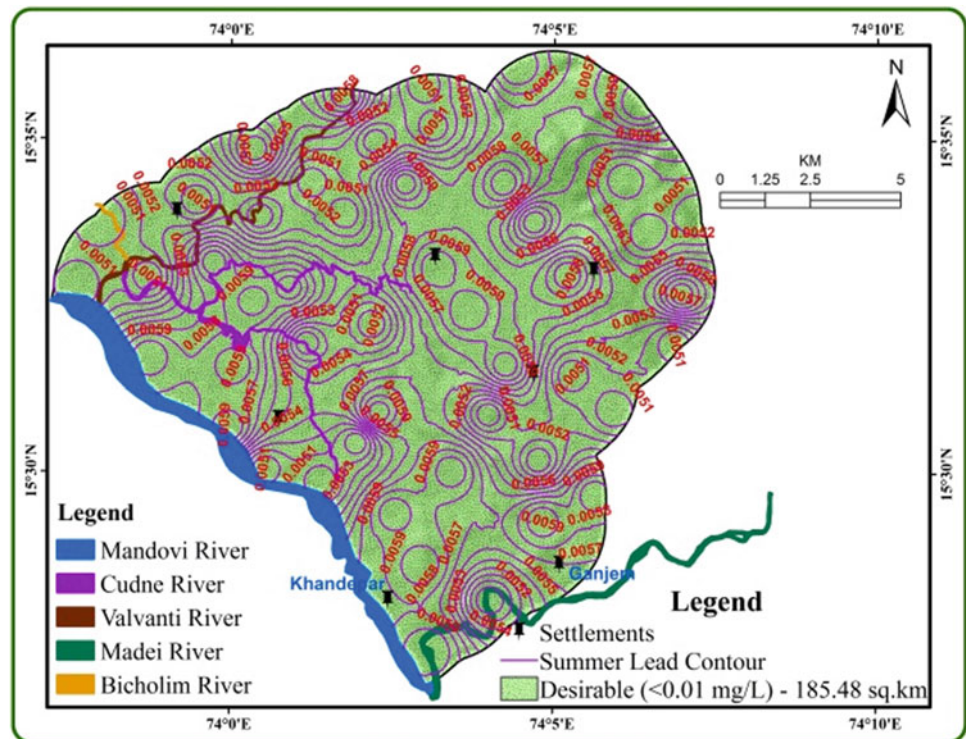




**Fig. 17** Summer season Pb spatial map



spatial maps show that in all the study area groundwater Pb is within the limit as per WHO 2011 standards. But small changes occur in contour values in the summer season.

## 2.9 Nickel (Ni)

Nickel is one of the common trace metals on the earth and is broadly disseminated in sandstone and shale. The element accumulates in sediments of biological cycles. It enters the groundwater from power plants and metal industrial waste. It enters the groundwater from the nickel–cadmium batteries’ wastewater and fly ashes. Nickel is a dietary metal required for many organisms. But excess amount of nickel is found to be carcinogenic in humans. It has very sensitive toxic effect of human beings. A higher nickel concentration is harmful to human health as this may lead to lung cancer (McNeely et al., 1979).

A maximum nickel concentration of 0.07 mg/L for drinking purpose is permissible (WHO, 2011). Based on this, the samples are under the desirable category in the study area. During winter season, groundwater nickel values start from 0.005 to 0.0095 mg/L. In the summer season, groundwater nickel values are from 0.006 to 0.011 mg/L. That values are characterized by desirable nature for drinking purpose of all the samples in both the seasons.

The spatial distribution maps of nickel during both the seasons are shown in Figs. 18 and 19. The significant values of nickel are in the lower part of the Cudnem River with a

portion of the Mandovi River. The nickel spatial maps show that in all the study area groundwater nickel is within the limit as per WHO 2011 standards. But small changes occur in contour values in the summer season.

## 2.10 Arsenic (As)

Arsenic is one of the naturally occurred trace elements on the earth. It does not have any smell and is a tasteless element but available in inorganic form. It enters the groundwater from soil, rocks and anthropogenic process. But, the excess amount of arsenic is found to cause cancer and neural disorders. A high arsenic concentration is harmful to human health as this may be carcinogenic and lead to anemia, leucopenia, eosinophilia and systemic health effects (Tchounwou et al., 1999; ATSDR, 2000; Yedjou et al., 2006). Recently, arsenic trioxide has been approved by the Food and Drug Administration as an anticancer agent in the treatment of acute promyelocytic leukemia (Rousselot et al., 1999).

A maximum arsenic concentration of 0.01 mg/L for drinking purpose is permissible (WHO, 2011). Based on this, the samples are under the desirable category in the study area. During winter season, groundwater arsenic values start from 0.001 to 0.002 mg/L. In the summer season, groundwater arsenic values are from 0.002 to 0.0022 mg/L. These values are characterized by a desirable nature for drinking purpose of all the samples in both the seasons.



**Fig. 18** Winter season Ni spatial map

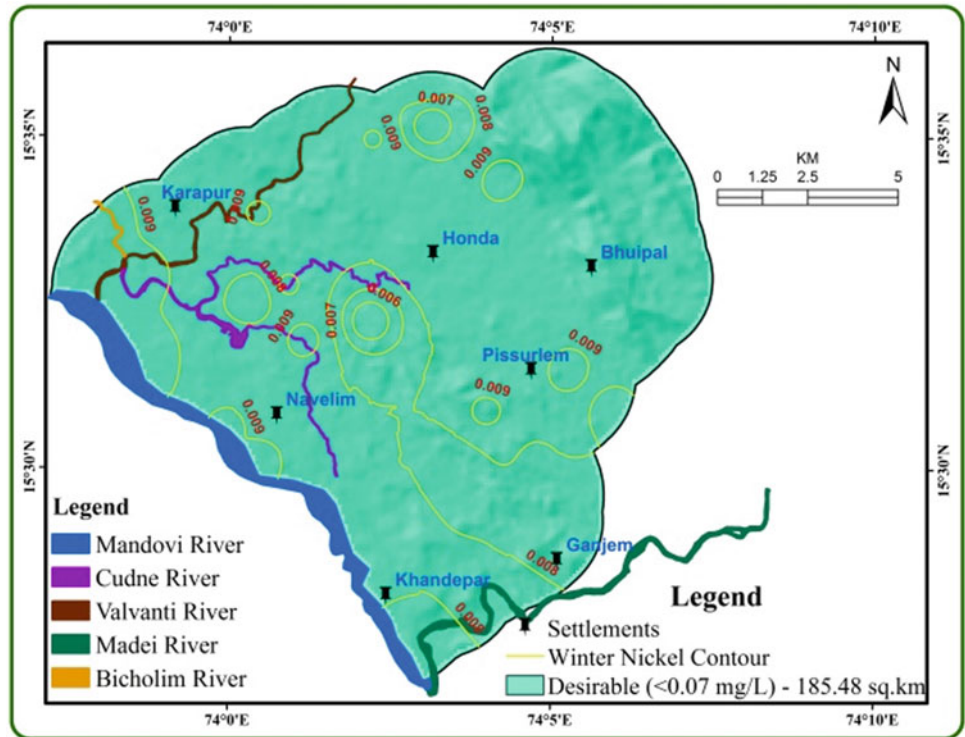
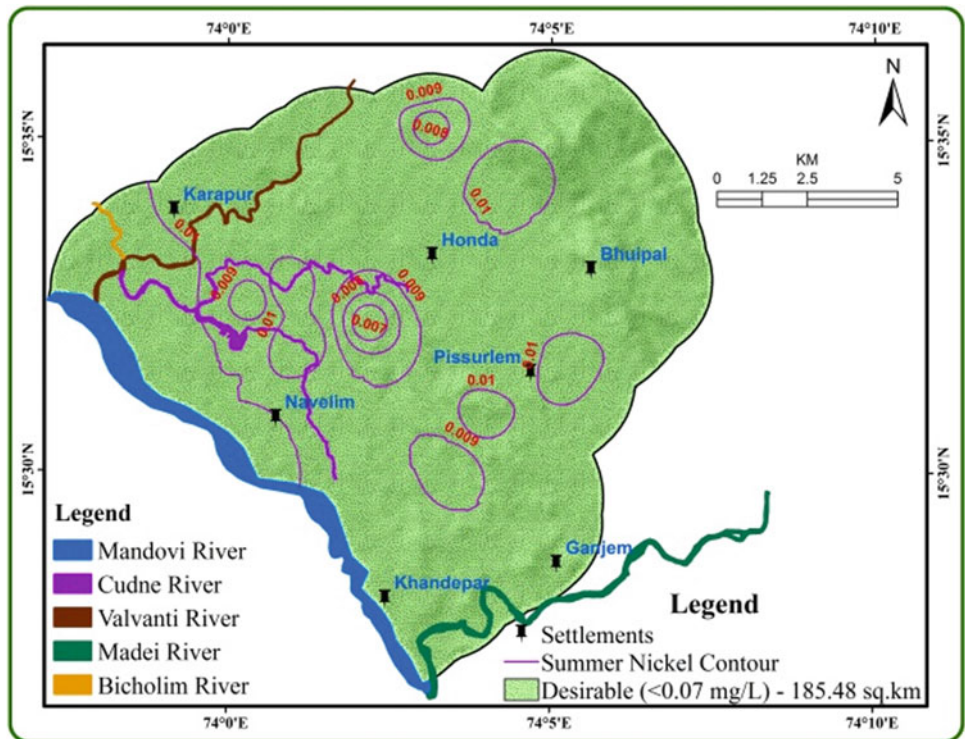


**Fig. 19** Summer season Ni spatial map



The spatial distribution maps of arsenic during both the seasons are shown in Figs. 20 and 21. The significant values of arsenic are recorded in the lower part of the Cudnem River meeting with a portion of the Mandovi River portion.

The arsenic spatial maps show that in all the study area groundwater arsenic is within the limit as per WHO 2011 standards. But small changes occur in contour values in the summer season.

**Fig. 20** Winter season As spatial map

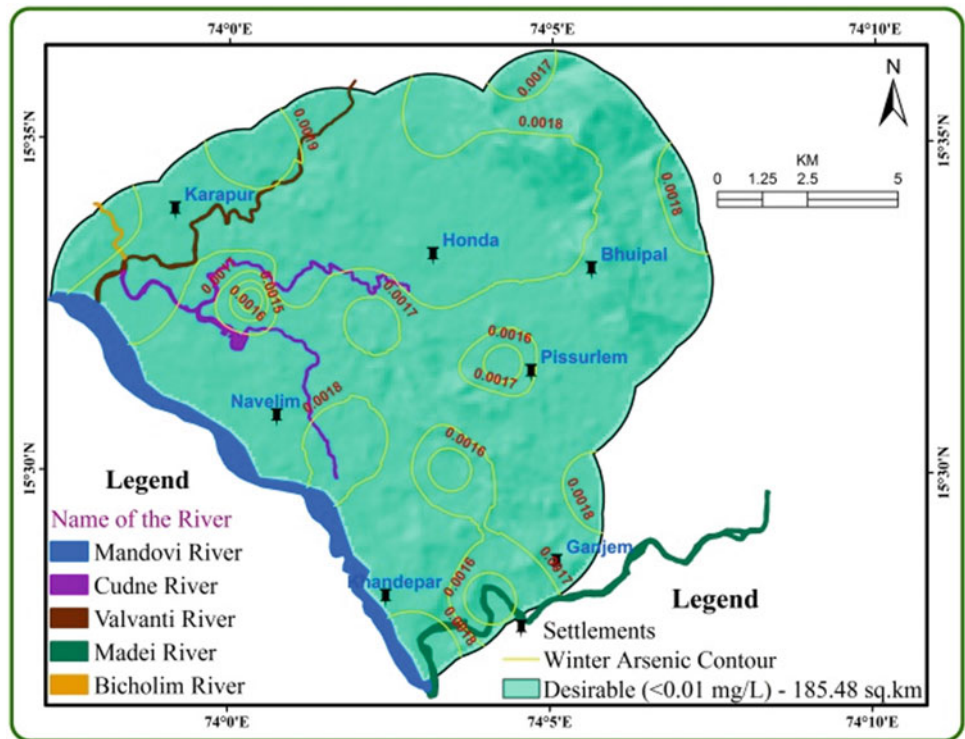


**Fig. 21** Summer season As spatial map

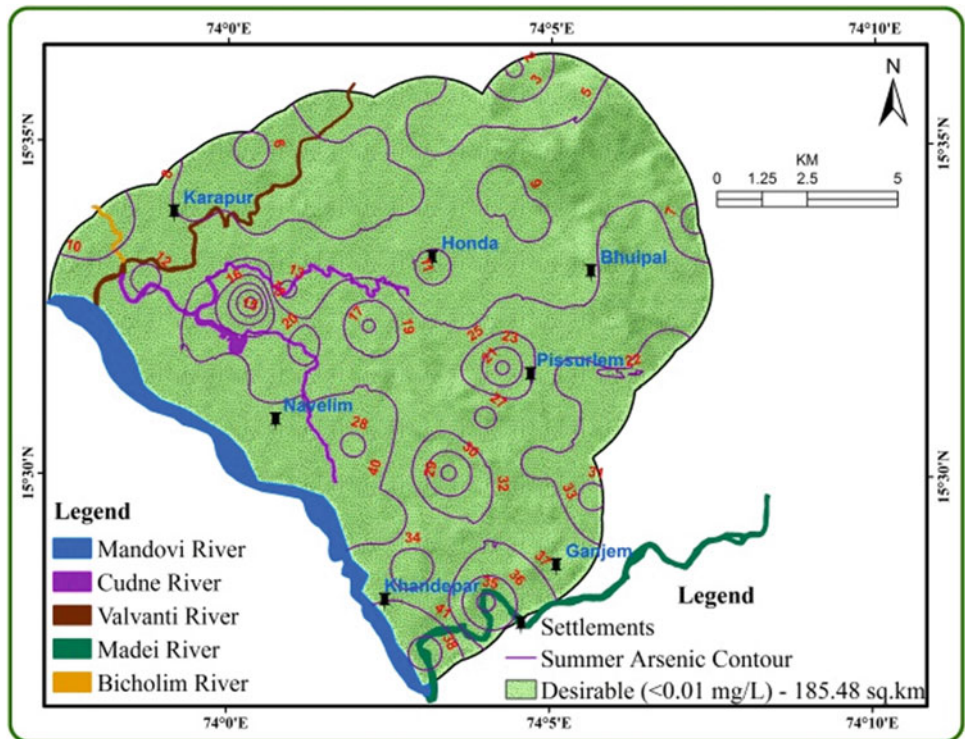
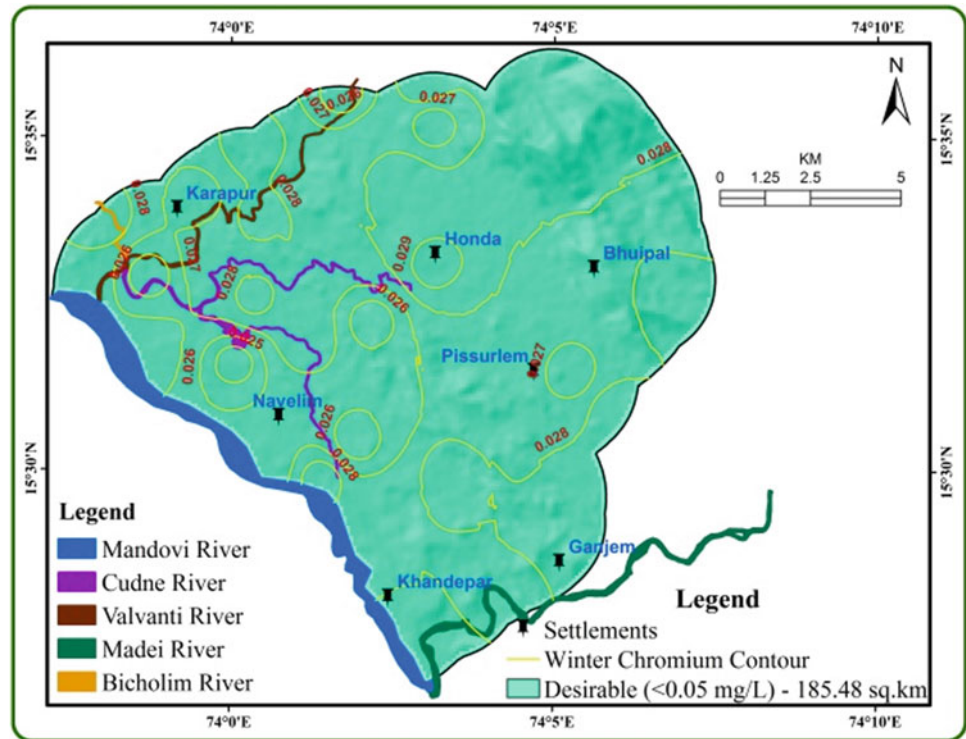


**Fig. 22** Winter season Cr spatial map



## 2.11 Chromium (Cr)

Chromium is one of the naturally occurred trace elements on the earth but occurs only in combined state. Traces of chromium are present in water. It enters the groundwater from metal refinery industries and alloy industries.  $\text{Cr}^{+3}$  form is an essential trace metal for human. Another stage of  $\text{Cr}^{+6}$  enters the water from wastewater of paint industry. It plays an important role in the removal of glucose from blood with the help of insulin. But, the excess amount of arsenic is found to cause cancer in the respiratory system. Chromium is present in small quantities in nature. It is present largely in rocks of silica type. The toxicity of chromium depends on its physicochemical shape; hexavalent salts are considered the most dangerous (Elhoussine, 2009).

A maximum chromium concentration of 0.05 mg/L for drinking purpose is permissible (WHO, 2011). Based on this, the samples are under the desirable category in the study area. During the winter season, groundwater chromium values start from 0.02 to 0.03 mg/L. In the summer season, groundwater chromium values are from 0.028 to 0.035 mg/L. These values are characterized by a desirable nature for drinking purpose of all the samples in both the seasons.

The spatial distribution maps of chromium during both the seasons are shown in Figs. 22 and 23. The significant values of chromium are recorded in the lower part of the Cudnem River meeting with a portion of the Mandovi River portion. The chromium spatial maps show that in all the study area groundwater chromium is within the limit as per WHO 2011 standards. But small changes occur in contour values in the summer season.

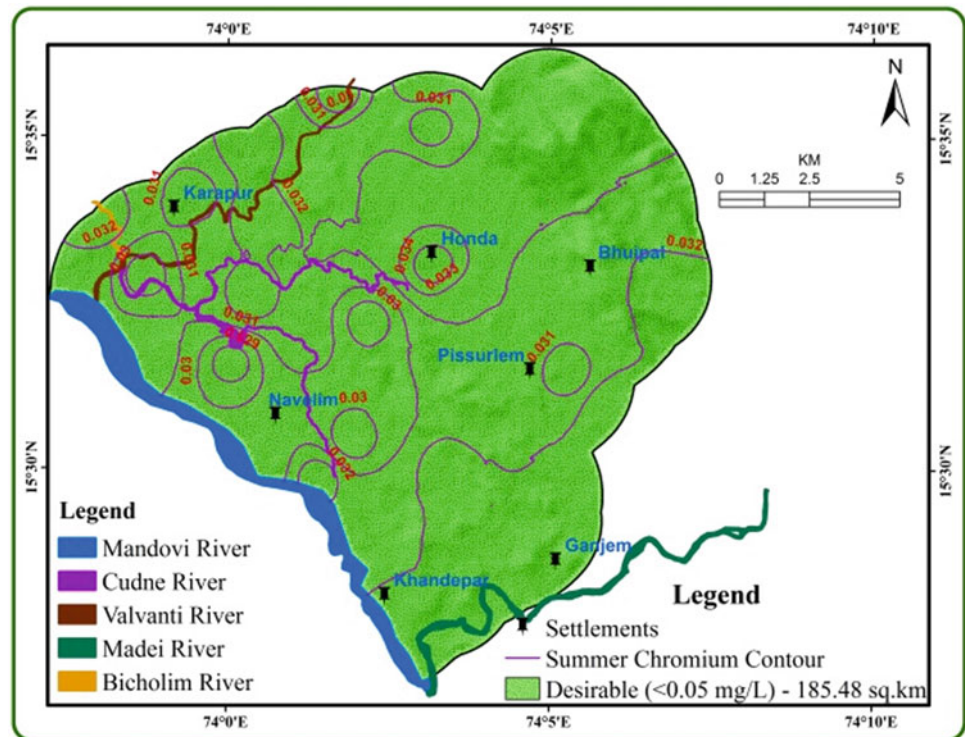
## 3 Conclusion

Trace metals in groundwater are characterized as chemical components dissolved in very small quantities in water. The levels of aluminum, barium, boron, copper, manganese, selenium, zinc, cadmium, lead, nickel, arsenic and chromium are well within the permissible limits and characterized by the favorable quality for drinking in both seasons for all the samples studied.

Iron levels in groundwater are distinguished by a favorable quality for the drinking of all samples, except for three test sites, such as Kumbharwada (S. No. 17), Vagheri (S. No. 22) and Morlem Colony (S. No. 40) in both seasons. The entire study area is widely distributed for the occurrence of iron ore and falls in the active mining belt.



**Fig. 23** Summer season Cr spatial map



## References

- Abdullah Khan, M., & Ahmad, S. (2010). Trace metal concentration in the water of rivers and ponds in valley field intermontane basin in the eastern Himalayas. *Journal of Applied Geochemistry*, 12(2), 242–252.
- Adaikpoh, E. O., Nwajei, G. E., & Ogala, J. E. (2005). Heavy metals concentrations in coal and sediments from river Ekulu in Enugu, Coal City of Nigeria. *Journal of Applied Science and Environmental Management*, 9(3), 5–8.
- Agency for Toxic Substances and Disease Registry. (2000). *Toxicological profile for chromium*. <https://www.atsdr.cdc.gov/toxprofiles/tp7.html>
- Elhoussine, D. (2009). Impact of urban waste waters on groundwater quality in the water shed of middle sebou. *Journal of Black Sea*, 15, 157–164.
- Goyal, P., Sharma, P., Srivastava, S., & Srivastava, M. M. (2008). Saracaindica leaf powder for decontamination of Pb: Removal, recovery, adsorbent characterization and equilibrium modeling. *International Journal of Environmental Science and Technology*, 5(1), 27–34.
- Haritash, A. K., & Garg, S. (2016). Assessment of water quality and suitability analysis of River Ganga in Rishikesh, India. *Applied Water Science*, 6(4), 383–392.
- Homady, M., Hussein, H., Jiries, A., Mahasneh, A., Al-Nasir, F., & Khleifat, K. (2002). Survey of some heavy metals in sediments from vehicular service stations in Jordan and their effects on social aggression in prepubertal male mice. *Environmental Research A*, 89, 43–49.
- Krasukopf, K., & Bird, D. K. (1994). *Textbook of introduction to geochemistry* (pp. 591). McGraw Hill Inc.
- Kumar, S. K., Bharani, R., Magesh, N. S., Godson, P. S., & Chandrasekar, N. (2014). Hydrogeochemistry and groundwater quality appraisal of part of south Chennai coastal aquifers, Tamil Nadu, India using WQI and Fuzzy logic method. *Applied Water Science*, 4(4), 341–350.
- Lakin, H. W. (1973). Selenium in our environment, in trace elements in the environment. In E. L. Kothy (Ed.), *Advances in chemistry series 123* (pp. 96–111). American Chemical Society.
- Mahato, M. K., Singh, P. K., & Tiwari, A. K. (2014). Evaluation of metals in mine water and assessment of heavy metal pollution index of East Bokaro Coalfield area, Jharkhand, India. *International Journal Earth Science and Engineering*, 7(04), 1611–1618.
- Marcovecchio, J. E., Botte, S. E., & Freije, R. H. (2007). Heavy metals, major metals, trace elements. In L. M. Nollet (Ed.), *Handbook of water analysis* (2nd Ed., pp. 275–311). CRC Press.
- Massadeh, A., Tahat, M., Jaradat, Q., & Al-Momani, L. (2004). Lead and cadmium contamination in roadside soils in Irbid city, Jordan: A case study. *Soil and Sediment Contamination (Formerly Journal of Soil Contamination)*, 13(4), 347–359.
- McNeely, R. N., Neimania, V. P., & Dwyer, L. (1979). Water quality source book. In *A guide to water quality parameter* (pp. 1–65). Inland water Directorate Water quality Branch.
- Mielke, H. W., Adams, J. L., Chaney, R. L., Mielke, P. W., & Ravikumar, V. C. (1991). The pattern of Cadmium in the environment of five Minnesota cities. *Environmental Geochemistry and Health*, 13, 29–34.
- Modassar, Y., Ibrampurkar, M. M., Virginkar, V. D., & Jyai, R. N. (2015). Geochemical assessment of groundwater quality in Mhadei River Watershed, Goa, India. *International Journal of Theoretical and Applied Sciences*, 7(1), 13–21.
- Momodu, M. A., & Anyakora, C. A. (2010). Heavy metal contamination of ground water: The surulere case study. *Research Journal Environmental and Earth Sciences*, 2(1), 39–43.
- Panigrahy, B. P., Singh, P. K., Tiwari, A. K., Kumar, B., & Kumar, A. (2015). Assessment of heavy metal pollution index for groundwater

- around Jharia Coalfield region, India. *Journal of Biodiversity and Environmental Sciences*, 6(3), 33–39.
- Robards, K., & Worsfold, P. (1991). Cadmium: Toxicology and analysis, a review. *The Analyst*, 116, 549–568.
- Rousselot, P., Labaume, S., Marolleau, J.-P., Larghero, J., Noguera, H., Brouet, M. C., & Femand, J. (1999). Arsenic trioxide and melarsoprol induce apoptosis in plasma cell lines and in plasma cells from myeloma patients. *Cancer Research*, 59, 1041–1048.
- Schroeder, H. A. (1965). Cadmium as a factor in hypertension. *Journal of Chronic Diseases*, 18, 647–656.
- Smirjakova, Ondrasovicova, O., Kaskova, A., & Lakticova, K. (2005). *Folia Veterinaria* 49, 3 Supplementum *The effect of cadmium and lead pollution on human health* (pp. 31–32).
- Taylor, M. C., & Demayo, A. (1980). Zinc. In *Guidelines for surface water quality. Vol. 1: Inorganic chemical substances*. Water Quality Branch, Inland Water Directorate, Environment.
- Tchounwou, P. B., Wilson, B., & Ishaque, A. (1999). Important considerations in the development of public health advisories for arsenic and arsenic-containing compounds in drinking water. *Reviews on Environmental Health*, 14(4), 211–229.
- Tiwari, A. K., & Sing, A. K. (2014). Hydrogeochemical investigation and groundwater quality assessment of Pratapgarh district, Uttar Pradesh. *Journal of the Geological Society of India*, 83(3), 329–343.
- U.S.G.S. (1993). National water Summary-1990–1991: Stream water quality U.S. Geology Survey Water Supply paper No. 2400 (p. 590).
- Vadiati, M., Asghari-Moghaddam, A., Nakhai, M., & Adamowski, J. (2016). A fuzzy-logic based decision-making approach for identification of groundwater quality based on groundwater quality indices. *Journal of Environment Management*. <https://doi.org/10.1016/j.jenvman.2016.09.082>.
- Verma, A. K., & Singh, T. N. (2013). Prediction of water quality from simple field parameters. *Environment and Earth Science*, 69(3), 821–829.
- WHO. (2011). *WHO guidelines for drinking-water quality*. World Health Organization.
- Yedjou, C. G., & Tchounwou, P. B. (2006). Oxidative stress in human leukemia (HL-60), human liver carcinoma (HepG2), and human (Jurkat-T) cells exposed to arsenic trioxide. In *Proceedings of the 9th International Symposium on Metal Ions in Biology and Medicine Held, Lisboa, Portugal* (pp. 298), May 21–24, 2006.



# The Impact of Different Design Approaches on Fine Sediment Transport in Gezira Scheme, Sudan

Awad M. Ali, Ishraga S. Osman, Hozafa Khalid, Maab Albager, and Amal Ibrahim

## Abstract

This study aims to understand the mechanism of cohesive sediment transport in irrigation canals when adopting different design approaches. This was achieved through developing a mathematical model to design unlined irrigation canals using three design approaches: regime theory, tractive force and maximum permissible velocity. The latter was modified by the authors to overcome some of its limitations. The model, named ICDesign, was developed using C Sharp language to design the irrigation canals and generate cross sections and a longitudinal profile. Then it was applied to design Zananda Major Canal in the Gezira scheme, Sudan, as a case study. HEC-RAS model was used to simulate the sediment transport based on different design approaches. It was found that the design obtained from the modified maximum permissible velocity gives the least amount and distribution of sediment accumulation along the canal. Thus, it was concluded that the developed software can be used in the design of a variety of irrigation canals. The extent of the applicability and use of the software shall be determined in the future studies.

## Keywords

Irrigation canals • Gezira scheme • Sediment deposition • HEC-RAS • Maximum permissible velocity • Tractive force

## 1 Introduction

Various techniques are used to deliver water from a source (river and reservoir) to an irrigation scheme such as sprinklers, drops, fallows and canals. Each system is based on different principles and theories, and the mobility of water through irrigation canals by gravity remains complex. Particularly, unlined canals are composed of natural materials which are erodible. Furthermore, the design of the canals should prevent the sediments from deposition throughout the canal which leads, when it happens, to serious problems on the entire system. The procedure for designing an irrigation system is not that obvious to be managed manually. So, a mathematical model will clarify the design process.

There are a large number of irrigation schemes in Africa, but the Gezira scheme is by far the most enormous one in the continent covering approximately an area of 880,000 ha. It accounts for 50% of Sudan's irrigated area and consumes 35% of its current allocation of the Nile water which represents 6.0–7.0 billion m<sup>3</sup>/year (Ahmed, 1984). The scheme has an irrigation network which consists of a series of earth canals minimized in capacity and geometry. Two main canals Gezira and Managil downstream the Sennar dam start to irrigate the Gezira scheme gravitationally and designed to carry up to 168 and 186 m<sup>3</sup>/s, respectively (Osman et al., 2011).

The water demand pattern could be forecasted if the canal design is based on a comprehensive assessment of the operation (Vanoni, 1975). Different studies have been carried out in the early years focusing on the sediment transport in the irrigation systems. It was demonstrated that every year Gezira system receives about 6 Mm<sup>3</sup> of silt, and most of it is fine silt and clay. The percentages of silt distribution along the main, major, minor canals and field are 4%, 23%, 35% and 38%, respectively (Gismalla, 2009). Both proper design and management of the irrigation system lead to a possible reduction in sediment accumulation problem (Paudel, 2010). Therefore, it was stated that during the design stage,

A. M. Ali (✉) · I. S. Osman · H. Khalid · M. Albager · A. Ibrahim  
Civil Engineering Department, University of Khartoum,  
Khartoum, Sudan

A. M. Ali · I. S. Osman · M. Albager · A. Ibrahim  
Water Research Center, University of Khartoum, Khartoum,  
Sudan

H. Khalid  
Regional Center for Water Harvesting, Khartoum, Sudan

controlling the sediment problem could be achieved by maintaining the continuity in sediment transport in the irrigation canals (Osman et al., 2017).

This study has been carried out taking the Gezira scheme as a study case. It is concerned with developing a software that assists in designing unlined irrigation canals with different design approaches. Moreover, the study aims to understand the mechanism of cohesive sediment transport in irrigation canals when adopting different design approaches. The software was applied in a selected major canal in the Gezira scheme, and the sediment transport was simulated using HEC-RAS model. The paper shows the differences in amount and distribution of the sediment deposition along the canal corresponding to each design theory.

## 2 Materials and Method

### 2.1 Study Area

In the Gezira scheme, the amount of sediment deposited in the main canals is considerably low when compared to the major and minor canals. The minor canals irrigate the field only during the first 12 h of the day and store water for the remaining 12 h; this process is called night storage system (NSS). Thus, the minor canals were designed using Manning equation. As a result, our study focuses on the major canals and the siltation in the first major canal that takes the water by gravity from the Gezira Main Canal called Zananda Major Canal. Figure 1 shows the Gezira scheme and the location of the study area illustrating its 3 reaches, 2 intermediate structures and 9 minor canals. The location of the offtake is at 14° 01' 42" N, 33° 32' 33" E with a total canal length of about 17 km and total command area of about 8520 ha (Osman, 2015).

### 2.2 Data Measurement

Osman (2015) performed field measurements in 2011 from June to October in order to handle the problem of sediment occurrence, because the largest amount of sediment deposited in the scheme takes place during this period. Figure 2 demonstrates the 14 monitoring points and measurement locations, one at the offtake of Gezira Main Canal, 3 along the Zananda Major Canal and 10 points at the lateral offtakes of the minor canals. Therefore, the required data to be used for the simulation using HEC-RAS model has been measured as follows:

1. **Flow data:** The water levels were measured manually on daily basis by using staff gauges and automatic monitoring instruments. Then, the discharges were computed.
2. **Sediment data:** The sediment concentrations were measured on daily basis, and the sediment load was computed based on the discharge and sediment concentrations.
3. **Cross sections:** Bathymetric surveys were carried along the canal every 200 m before and after the flood season in July and October in 2011.

## 2.3 Simulation Using HEC-RAS Model

### 2.3.1 General

The HEC-RAS modeling system was developed as a part of the Hydrologic Engineering Center's "Next Generation" (NexGen) of hydrologic engineering software. The NexGen project encompasses several aspects of hydrologic engineering, including: rainfall-runoff analysis (HEC-HMS); river hydraulics (HEC-RAS); reservoir system simulation (HEC-ResSim); flood damage analysis (HEC-FDA and HEC-FIA); and real-time river forecasting for reservoir operations (CWMS) (Brunner & CIWER-HEC, 2016).

### 2.3.2 Data Entering

The HEC-RAS model was set up and calibrated based on the measured data. The effects of different parameters on the deposition were investigated to detect the most effective ones. The main objective of the modeling and simulation of sediment transport in Gezira scheme is to analyze and investigate the responses of the system to sediment deposition under different design approaches. The required data to simulate the flow and sediment transport in the irrigation canals is geometric data, quasi-unsteady data of flow and sediment transport data. The inputs for each section are detailed below.

- (a) **Geometric data:** In order to simulate the canal, system schematic for the study area was uploaded. After that, the cross sections of the actual canal at the beginning of the simulation period, 1 July 2011, were entered based on the survey data as illustrated in Fig. 3.
- (b) **Quasi-unsteady data:** The quasi-unsteady hydrodynamic model simulates the flow series with a sequence of steady flow computation. HEC-RAS includes several quasi-unsteady boundary conditions, and for Zananda Major Canal the boundary conditions taken into account, based on the available information, are flow series and normal depth for the upstream and downstream of the canal, respectively. The flow series input of the measured flow data from 1 July to 28 October, during the flood season, was used with its duration of 24 h and computation increment.



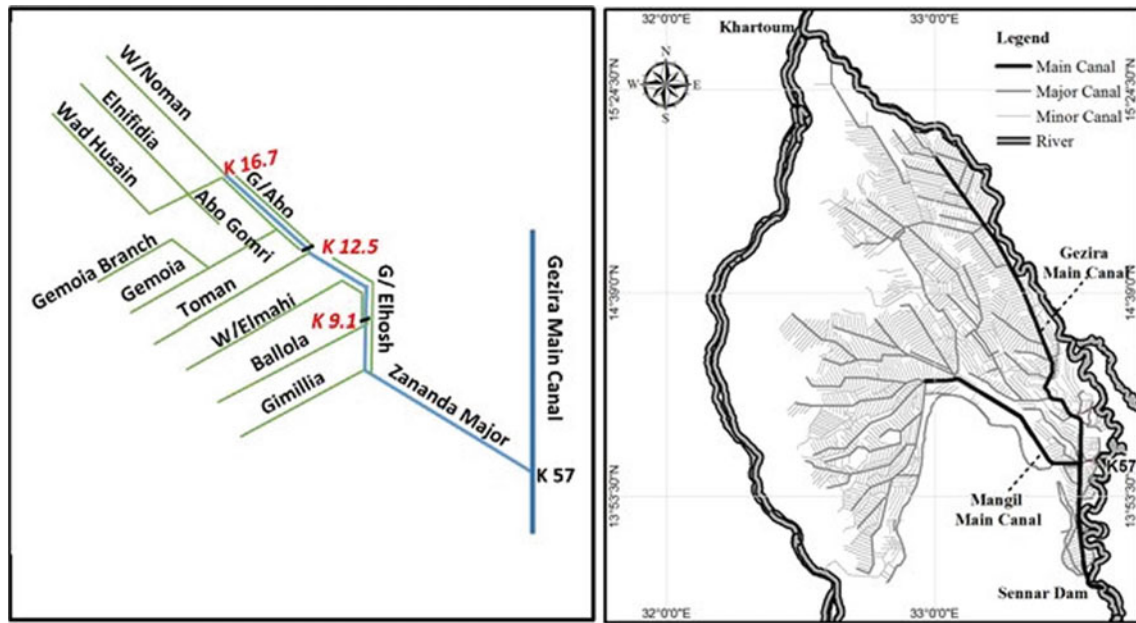


Fig. 1 Study area of Gezira scheme (Osman, 2015)

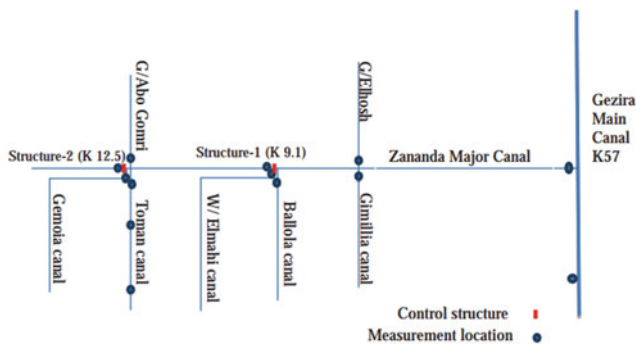


Fig. 2 Scheme of Zananda Major Canal and measurement locations (Osman, 2015)

(c) **Sediment transport data:** Based on the measured data, sediment load series is taken as sediment transport boundary condition during the study period.

### 2.3.3 Sensitivity Analysis

To identify the effect of the diversified input on the model’s output, an important step should be performed called sensitivity analysis that has two categories, namely the numerical and physical parameters. The numerical sensitivity is concerned with justifying the parameters that affect the numerical solution such as computational time step, while the physical parameter sensitivity considers the sensitivity of the hydraulic parameters such as Manning’s coefficient.

### 2.3.4 Calibration of the Model

The model was calibrated based on the most sensitive parameters as described in the following:

1. The sensitivity analysis shows the optimum value of Manning coefficient is 0.017 which found within the range of 0.015–0.025.
2. The model was run out on five different time steps which are locally far apart from each other [i.e., 24, 12, 6, 3, 1 h]. The result obtained from the simulation for 1 h computational increment gives the most accurate one. So, the hydrodynamic model has sensitivity to the computational increment.
3. After inputting the geometric, quasi-unsteady and sediment transport data, the sediment transport was simulated. Figure 4 shows the bed and water surface level.
4. The bed level predicted (simulated) by the model and measured bed levels based on field measurement are shown in Fig. 5. The measured and computed bed levels are compared to each other, and it was found that the  $R^2$  value is 0.9038.

## 2.4 Application of Different Design Approaches

### 2.4.1 General

At the irrigation schemes and throughout the irrigation season, the canals should meet the various requirements of irrigation. The design of the irrigation canals should preferably be based on capacity, command, sediment and/or erosion, and cost (Depeweg et al., 2014). A design of stable canals is needed to achieve the balance between the erosion and deposition that may take place during different phases of the irrigation season. Chow (1983), Raudkivi (1990), HR

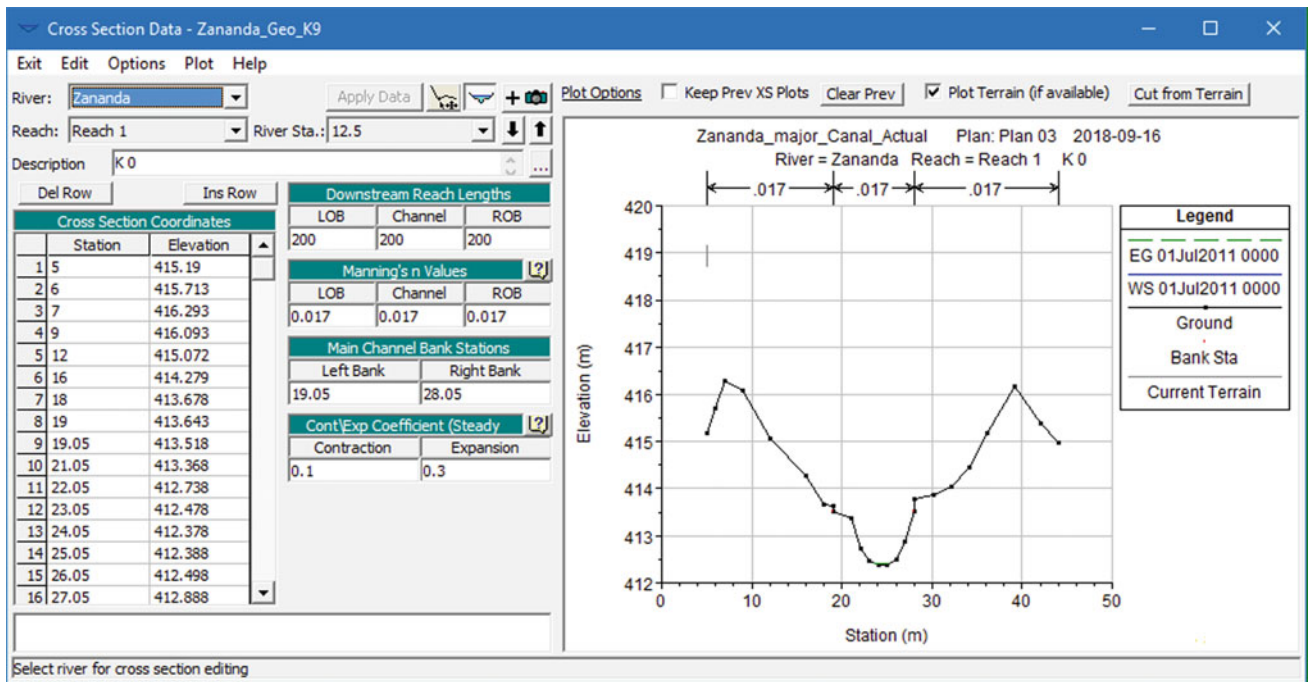
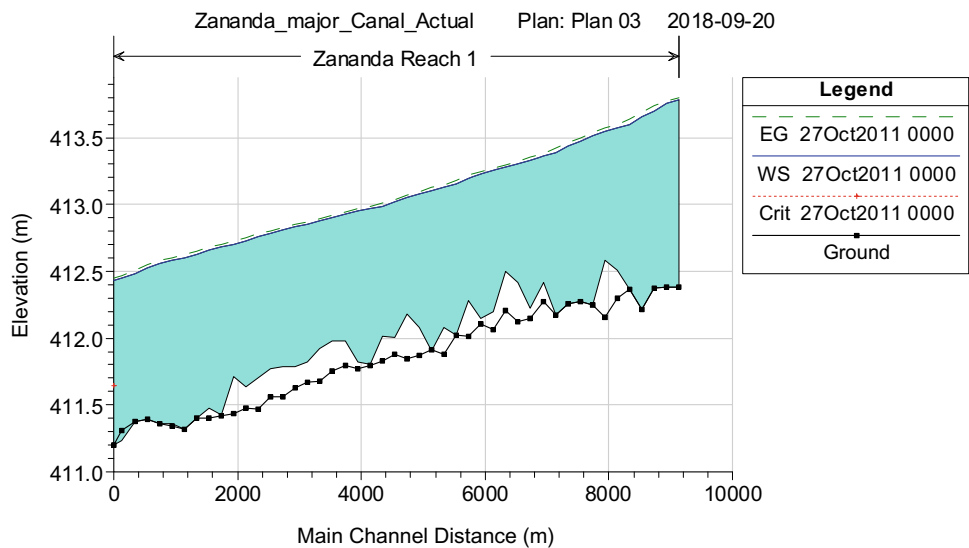


Fig. 3 Input cross-sectional data on July 1, 2011

Fig. 4 Water surface and bed-level elevation of Zananda actual canal



Wallingford (1992), and Simons and Sentürk (1992) mention four methods for the design of stable canals:

- The regime theory;
- The tractive force;
- The maximum permissible velocity;
- The rational method.

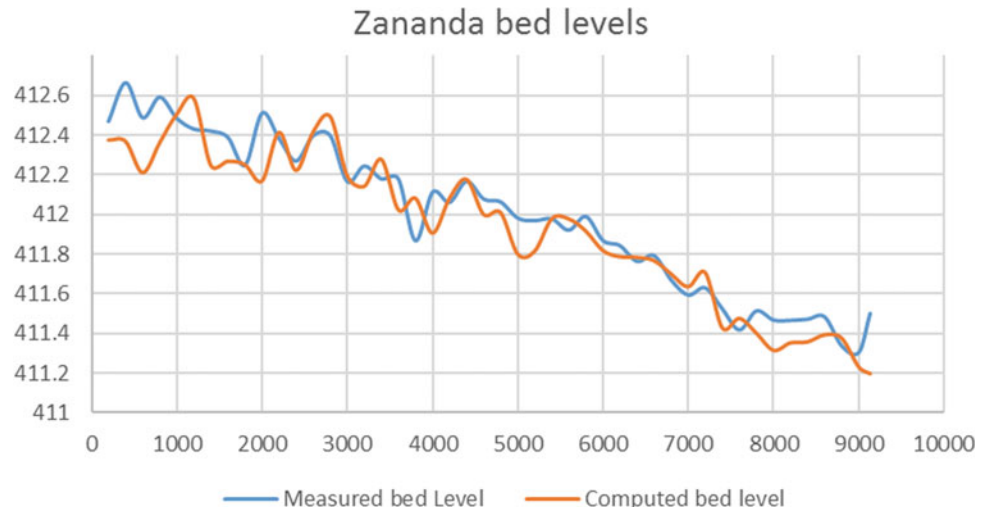
**2.4.2 The Regime Theory**

If the canals do not change over a period of one or more typical water years, the canals are described as being in

regime. In order to design regime canals, sets of empirical equations have been prepared based on observation of canals and rivers that have achieved the dynamic stability. This theory assumes that the discharge is the only needed factor to determine the wetting parameter, while the strength of the canal banks may also be an important factor. Following are the equations used for the design using Lacey’s regime theory:

$$P = K_P Q^{1/2} \tag{1}$$

**Fig. 5** Measured and computed bed profile



$$A = K_a Q^{5/6} \tag{2}$$

$$S_0 = K_s Q^{-1/6} \tag{3}$$

where

- $P$  = wetted perimeter (m)
- $Q$  = discharge ( $m^3/s$ )
- $A$  = cross-sectional area ( $m^2$ )
- $S_0$  = bed slope (cm/km)
- $K_p, K_a, K_s$  = constants.

In 1952, an investigation has been made to decide whether Lacey’s regime theory is applicable or not for designing the main and major canals in the Gezira canalization system. Therefore, 39 stable canal reaches have been investigated assuming that Lacey’s regime theory is applicable. Table 1 summarizes Lacey’s constants and the Manning coefficient ( $n$ ) for the design of stable canals in Gezira (Matthew, 1952).

### 2.4.3 Maximum Permissible Velocity

The maximum permissible velocity theory concerns with canal design using the maximum velocity that can be resisted by the canal’s material. Despite the erosion of the canals, the concept of the theory can be used for designing of stable canals.

The maximum permissible velocity is a velocity that does not cause erosion. This velocity is challenging to determine and is very changeable; it can only be evaluated with

experience and sound judgment. Moreover, the section of the canal will be designed to generate velocity corresponding to the maximum velocity that could be resisted by the canal materials. This velocity would not occur if the canal capacity is relatively small, which appears in the major canals of the Gezira scheme. So, the original theory has been modified by the authors to overcome this limitation of design. The modification states that “the design of an irrigation canal to be based on the maximum velocity could be produced by the canal capacity, but not greater than the maximum velocity that could be resisted by the canal material.”

Table 2 presents the maximum permissible velocities depending on the bed material. The United States Bureau of Reclamation (USBR) has derived from these velocities the corresponding tractive force values. The design steps, including the modification, are shown in Annex 1.

### 2.4.4 Tractive Force

The tractive force is in use for boundary shear stress and sediment transport relations. It uses the idea of static stability of a canal in which there is no movement of material (in both the bed and side slopes). For a given design discharge, the canal dimensions and bed slope are identified considering the flow velocity not exceeding a permissible velocity or boundary shear stress not exceeding its critical value of a bed and bank material (Paudel, 2009). A flowchart indicating the design steps is shown in Annex 2.

**Table 1** Different constants for the design of stable canals in Gezira

Parameters	Main canal 10 reaches	Major canal 29 reaches	All canals
$N$	0.021	0.017	0.018
$K_p$	4.55	5.51	5.26
$K_a$	2.75	2.6	2.64
$K_s$	14.57	13.9	14.5

Note:  $n$  = Manning roughness,  $K_p, K_a, K_s$  = constants

**Table 2** Maximum permissible velocities and the corresponding tractive force values (Depeweg et al., 2014)

Material	Manning $N$	Clear water		Silt-loaded water	
		$V$ (m/s)	$\tau$ (N/m <sup>2</sup> )	$V$ (m/s)	$\tau$ (N/m <sup>2</sup> )
Fine sand, colloidal	0.02	0.46	1.30	0.76	3.61
Sandy loam, non-colloidal	0.02	0.53	1.78	0.76	3.61
Silt loam, non-colloidal	0.02	0.61	2.31	0.91	5.29
Alluvial silts, non-colloidal	0.02	0.61	2.31	1.07	7.22
Ordinary firm load	0.02	0.76	3.61	1.07	7.22
Volcanic ash	0.02	0.76	3.61	1.07	7.22
Stiff clay, very colloidal	0.025	1.14	12.51	1.52	22.13
Alluvial silts, colloidal	0.025	1.14	12.51	1.52	22.13

### 2.4.5 Rational Method

The rational method includes, among others, the method of White et al. (1982) and Chang (1985). It is useful for the design of stable canals with very specific flow conditions. For canals with large variations in discharge and sediment load, the method is inadequate to describe accurately the sediment transport process and the conveyance of the sediment load through the whole canal network (Depeweg et al., 2014).

In the design of Zananda Major Canal, the rational method was not considered since both discharge and sediment load are highly fluctuated. Therefore, the software to be developed for the design of Zananda Major Canal will only adopt the first three design approaches.

## 2.5 ICDesign Software Development

### 2.5.1 Introduction

Irrigation Canals Design (ICDesign) software program was developed during this study using C Sharp language. The software has the capability to design the irrigation canals using three methods: regime theory, tractive force for both cohesive and non-cohesive soil and the modified maximum permissible velocity.

### 2.5.2 Input Data

The required data to design irrigation canals differs based on the design theory. Figures 6, 7, 8 and 9 show the input windows for ICDesign software highlighting the data needed for each theory of design.

### 2.5.3 Outputs

When designing a canal using one of the provided theories, the outputs are presented in three different forms:

(a) **Table tab:** This option displays the results in a table consisting of: discharge; length of reach; wetted

perimeter; cross-sectional area; bed width; depth of water; side slope; bed slope; and ground level at the upstream and the downstream with the headloss caused by the cross-structures as shown in Fig. 10, in addition to the final velocity in the maximum permissible velocity methods and design parameters of tractive force (i.e., unit tractive force on side and bottom  $C_s$ ,  $C_b$ ).

(b) **Cross-sectional tab:** This option displays the cross section for each reach of the designed canal as shown in Fig. 11.

(c) **Profile tab:** This option displays the longitudinal profile of the designed canal as shown Fig. 12.

## 3 Results

In the HEC-RAS model, the calibration was done by the actual cross section to determine the factors (e.g., Manning's  $n$ , computational increment, temperature, etc.) that reflect the real conditions of Zananda Major Canal. Once the factors were determined, the corresponding total sediment deposition during the period of study was calculated. Then, the same factors have been used to simulate the sediment deposition along the canal when applying the other three design approaches in addition to the original design which used earlier in the construction of the canal, but this time to determine the total sediment deposition corresponding to each design theory.

Figures 13, 14, 15 and 16 show the cross sections and profiles when applying the different design approaches in the HEC-RAS model. These profiles illustrate the distribution of the sediment along Zananda Major Canal. Finally, the total sediment deposition—mass bed change—quantities for each cross section and during the study period are shown in Fig. 17.

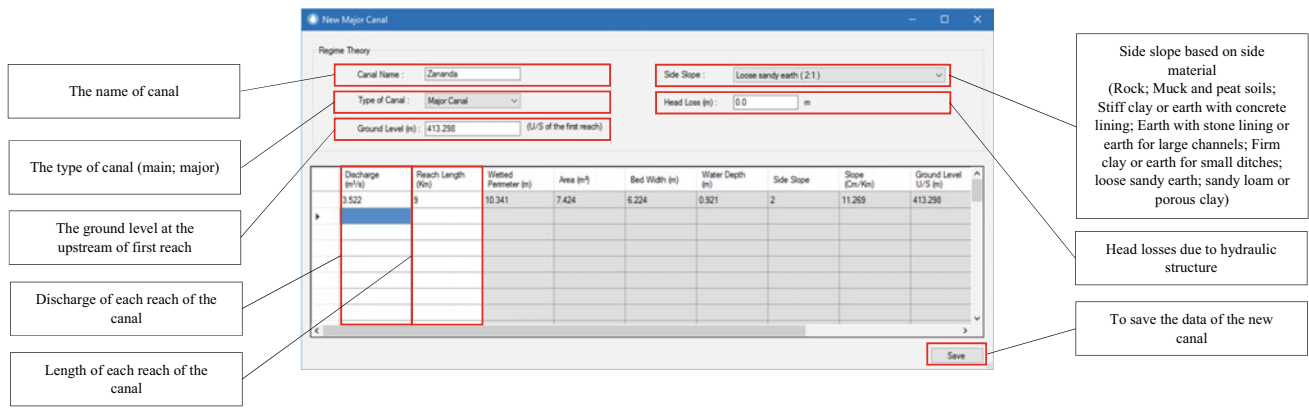


Fig. 6 Regime theory inputs

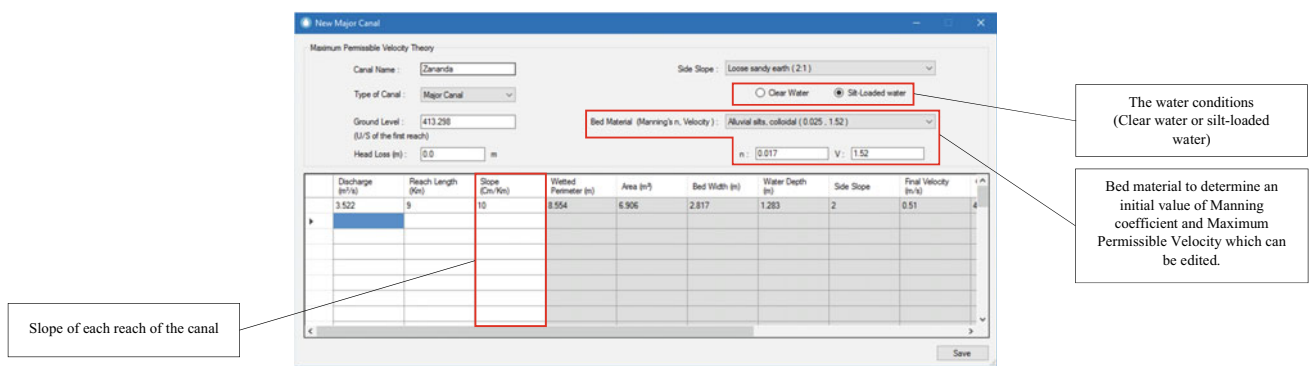


Fig. 7 Modified maximum permissible velocity inputs

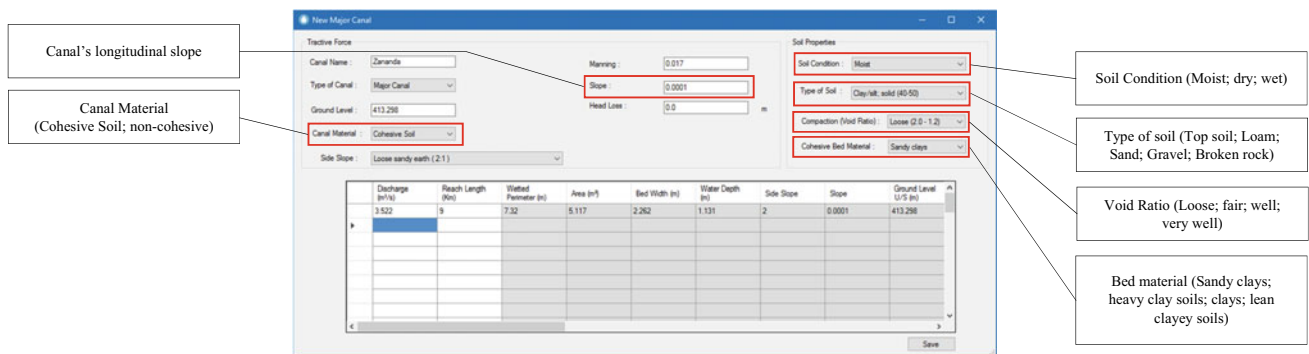


Fig. 8 Tractive force for cohesive soil inputs

### 3.1 Application of the Original Design

See Fig. 13.

### 3.2 Application of Regime Theory

See Fig. 14.

### 3.3 Application of the Modified Maximum Permissible Velocity

See Fig. 15.

### 3.4 Application of Tractive Force

See Figs. 16 and 17.

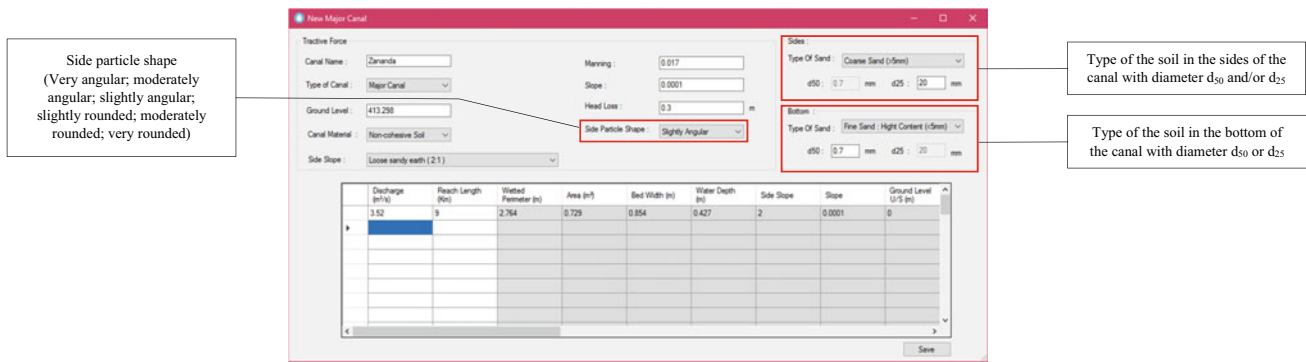


Fig. 9 Tractive force for non-cohesive soil inputs

Table	Cross-Section	Profile								
	Wetted Perimeter (m)	Area (m <sup>2</sup> )	Bed Width (m)	Water Depth (m)	Side Slope	Slope (Cm/Km)	Ground Level U/S (m)	Ground Level D/S (m)	Head Loss (m)	
▶	58.975	196.679	41.048	4.009	2	6.203	400	396.458	0.3	
	50.585	152.294	34.18	3.668	2	6.528	396.158	394.839	0.3	
	45.591	128.069	30.13	3.457	2	6.758	394.539	393.052	0.3	

Fig. 10 Outputs, table tab

## 4 Discussion and Conclusion

The simulation of Zananda Major Canal in HEC-RAS model showed that the total sediment deposition when applying the modified maximum permissible velocity is less than the other sections that were designed based on other design approaches. Thus, the sediment is reduced by 84.65% if compared to the current canal. Therefore, this method is recommended for the design of Zananda Major Canal.

The tractive force method is not applicable for major canals and especially for cohesive soils. It is widely used for non-cohesive soils, because the cohesive materials have different nature and depend on physiochemical properties. The design using tractive force produced the highest amount of sediment deposition that is distributed throughout the

whole reach. Furthermore, the canal experienced an over-bank issue when simulating this method.

Also, regime theory produced sediment deposition along the canal but lesser than tractive force. Moreover, regime theory has limitations for the discharge value ( $Q$ ) corresponding to each value of side slope ( $z$ ) as noticed throughout the study. The discharge should be greater than specific value  $Q_{\min}$  for main and major canals as specified in Table 3; otherwise, another method of design should be adopted.

The original design was considered in the investigation to study the suitability of the pre-designed section and to compare its appropriateness with respect to the other theories. The section was designed using regime theory but with different factors. The amount of sediment produced is lower than the two previous designs and almost distributed only in the first two-thirds of the canal length.



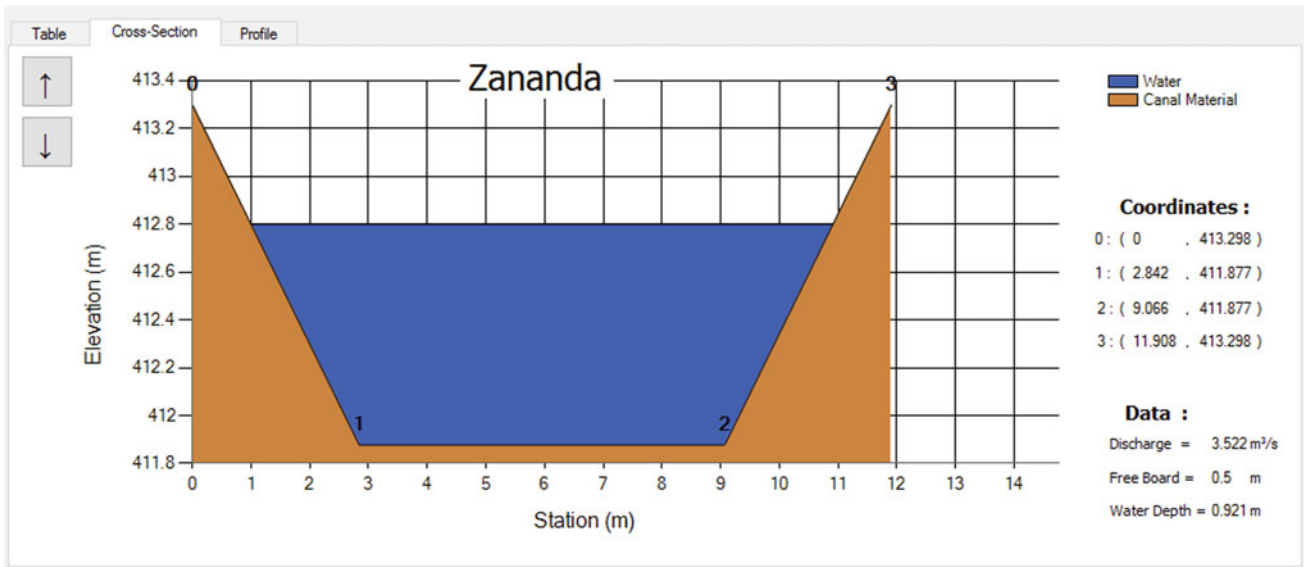


Fig. 11 Outputs, cross-sectional tab

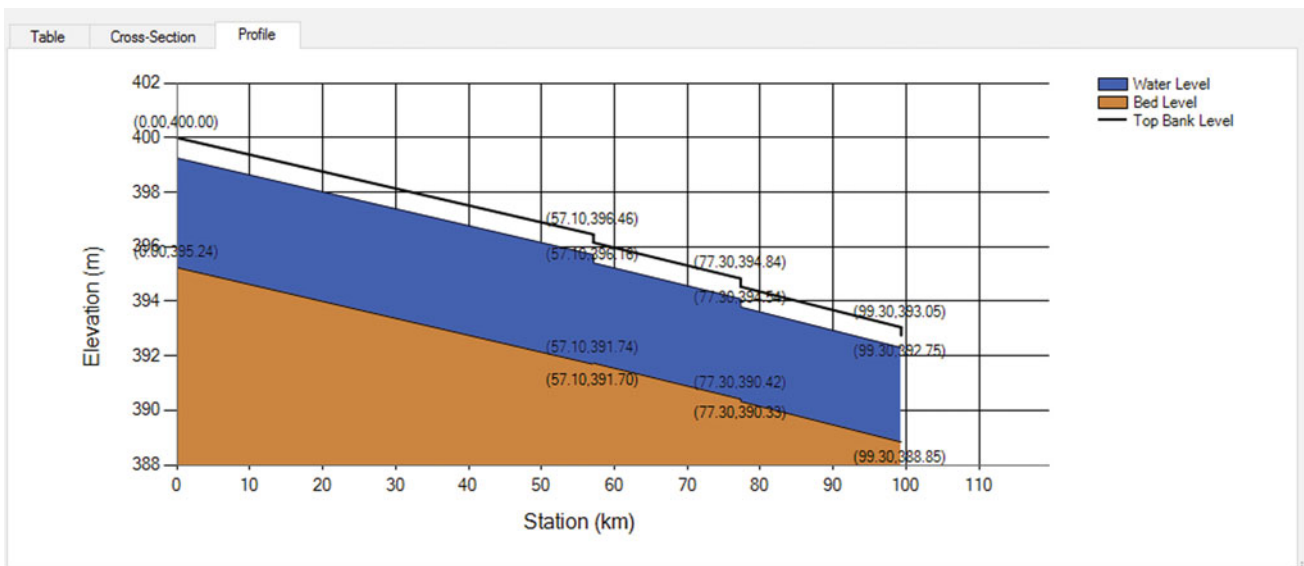


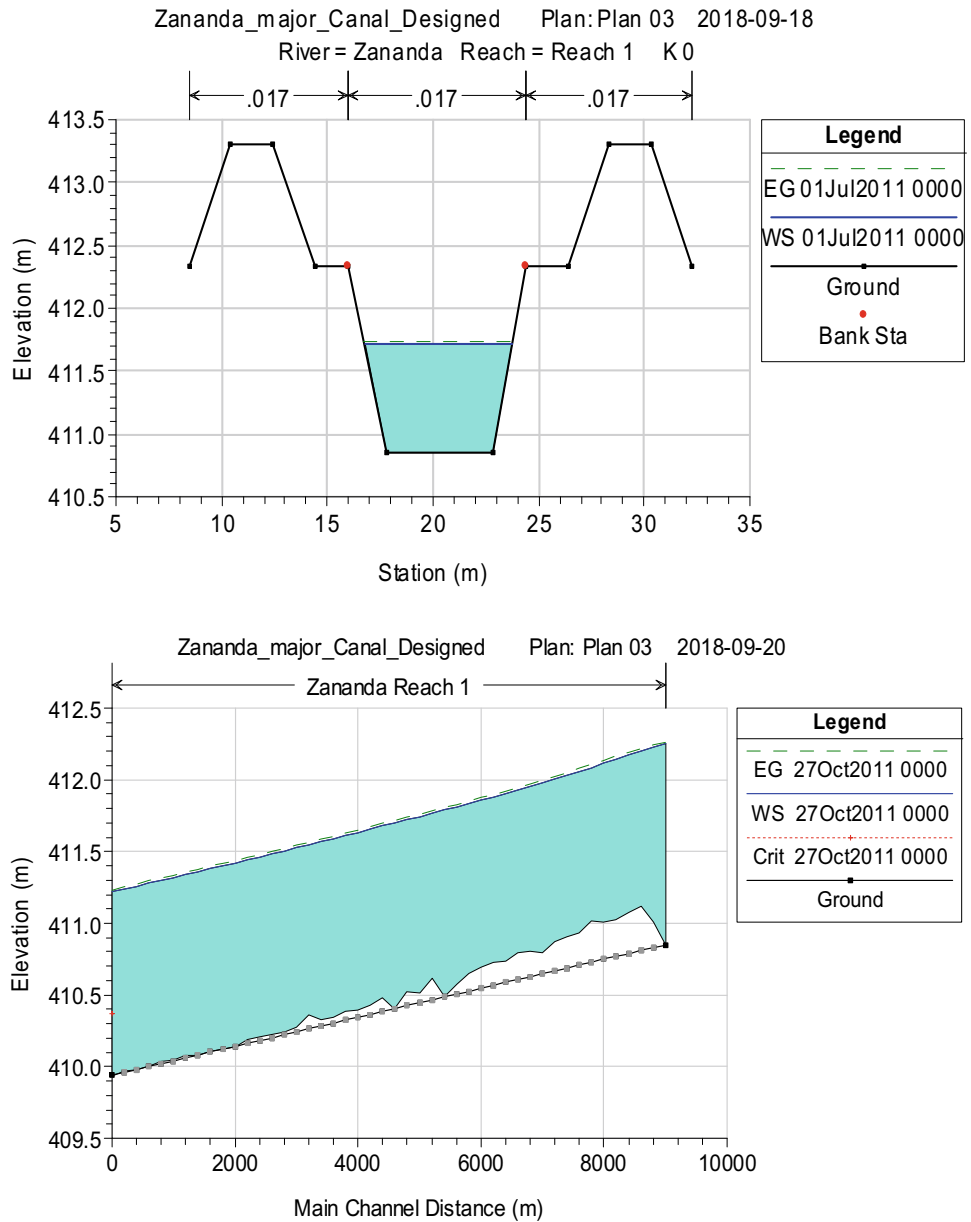
Fig. 12 Outputs, profile tab

The modified maximum permissible velocity comes with a new concept of design. It aims to overcome some of the maximum permissible velocity limitations. When the discharge is relatively small as in the major canals of Gezira scheme, it cannot flow as fast as to reach the permissible

velocity ( $V_{max}$ ) which is the maximum velocity that can be resisted by the canal material. The modification overcomes this limitation by using the maximum velocity that could be produced by a certain discharge ( $V_{new}$ ) which is lesser than ( $V_{max}$ ) and can also be resisted by the canal material. This



**Fig. 13** Simulation of Zananda Major Canal when applying the original design



theory produced the least amount of sediment deposition among the studied theories and concentrated on the one-third of the canal.

The ICDesign software gives the users the ability to design irrigation canals using the modified maximum

permissible velocity as well as regime theory and tractive force. Thus, it was concluded that the developed software may be used in the design of a variety of irrigation canals. The extent of the applicability and use of the software shall be determined in the future studies.

**Fig. 14** Simulation of Zananda Major Canal when applying regime theory

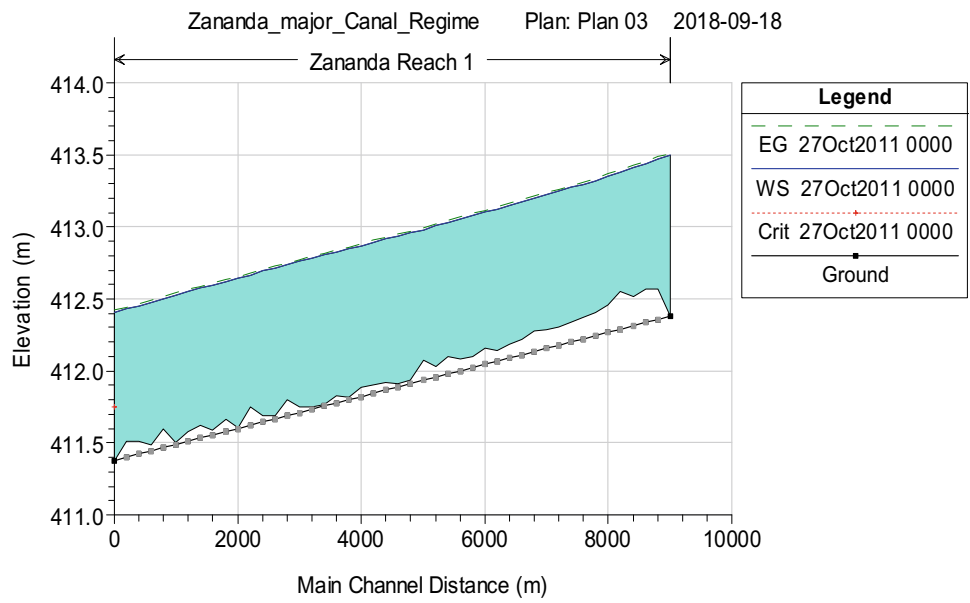
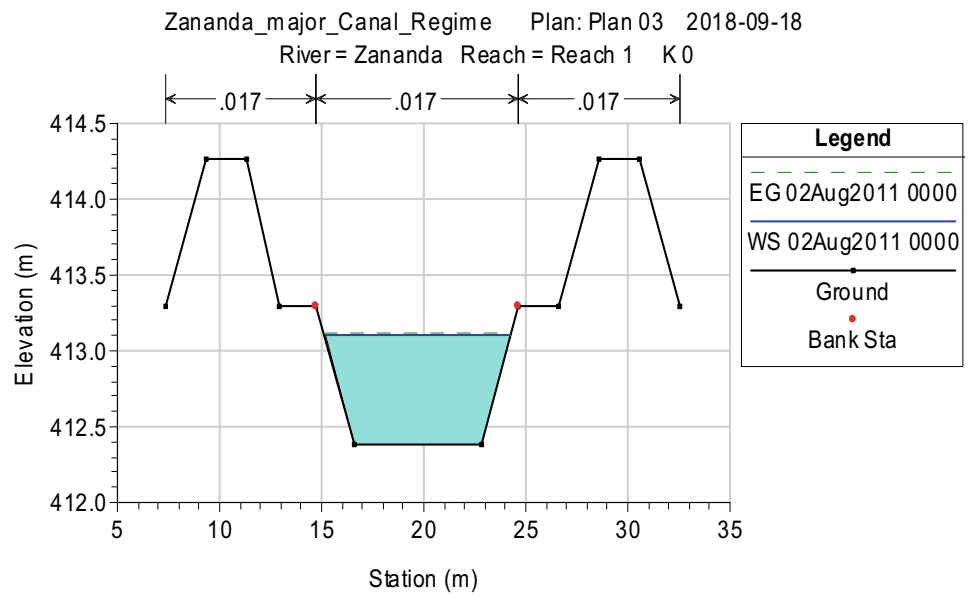


**Fig. 15** Simulation of Zananda Major Canal when applying the modified maximum permissible velocity

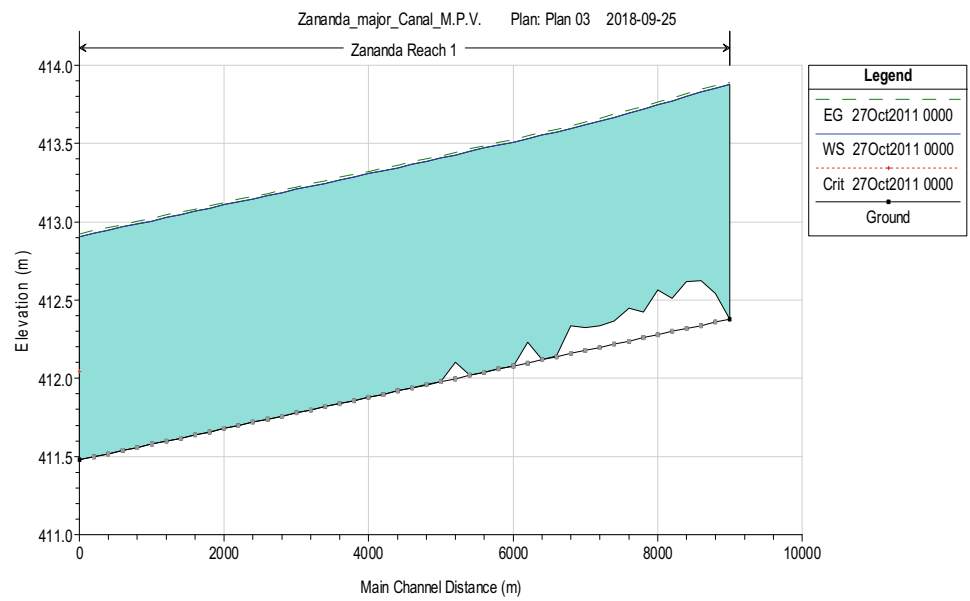
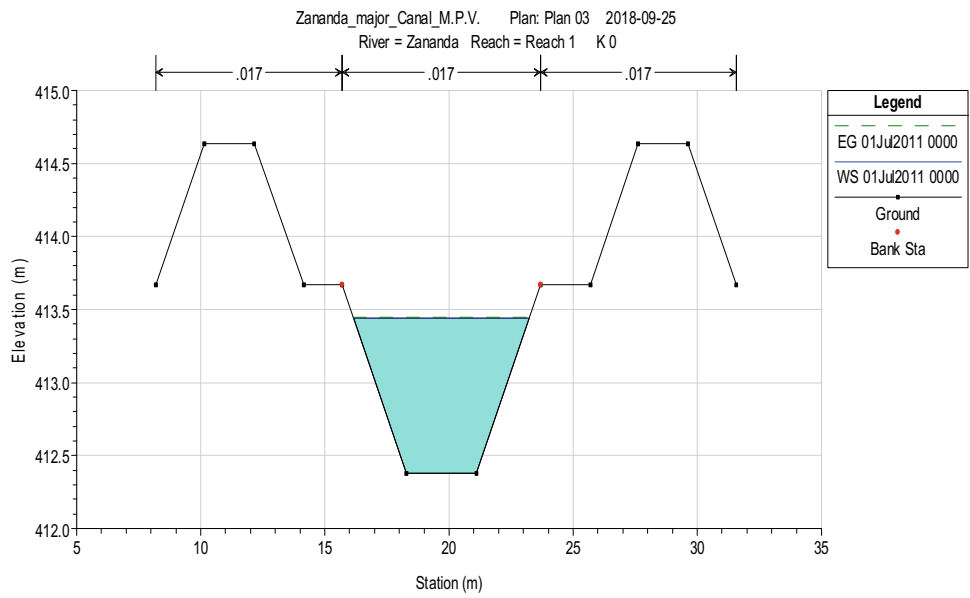


**Fig. 16** Simulation of Zananda Major Canal when applying tractive force method

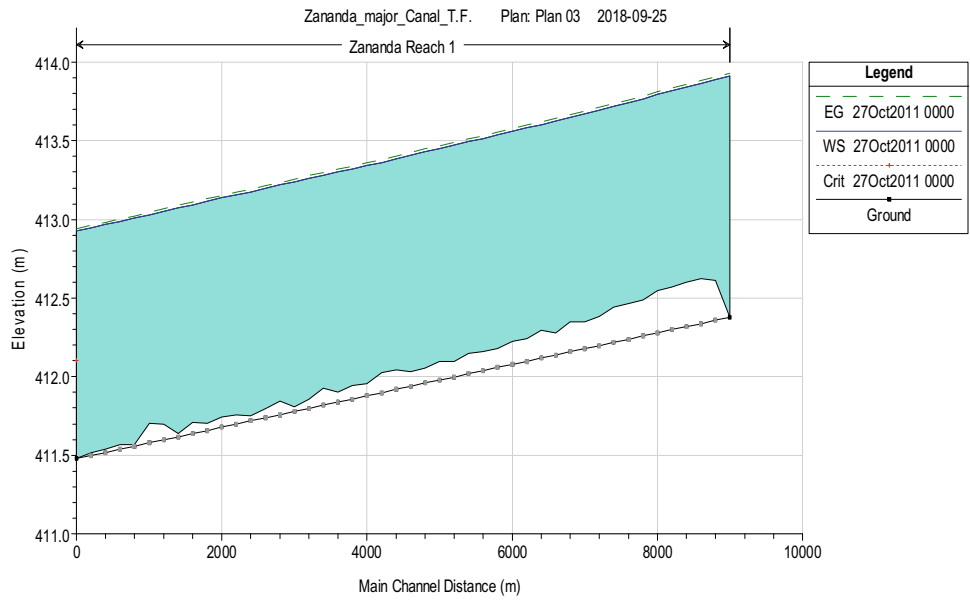
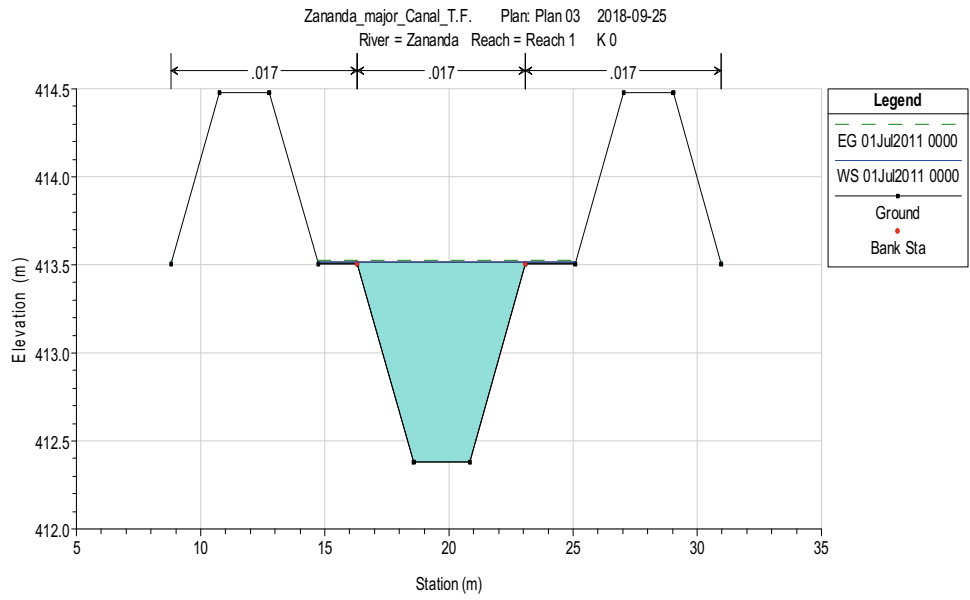


**Fig. 17** Total sediment deposition quantities along Zananda Major Canal during flood period of 2011

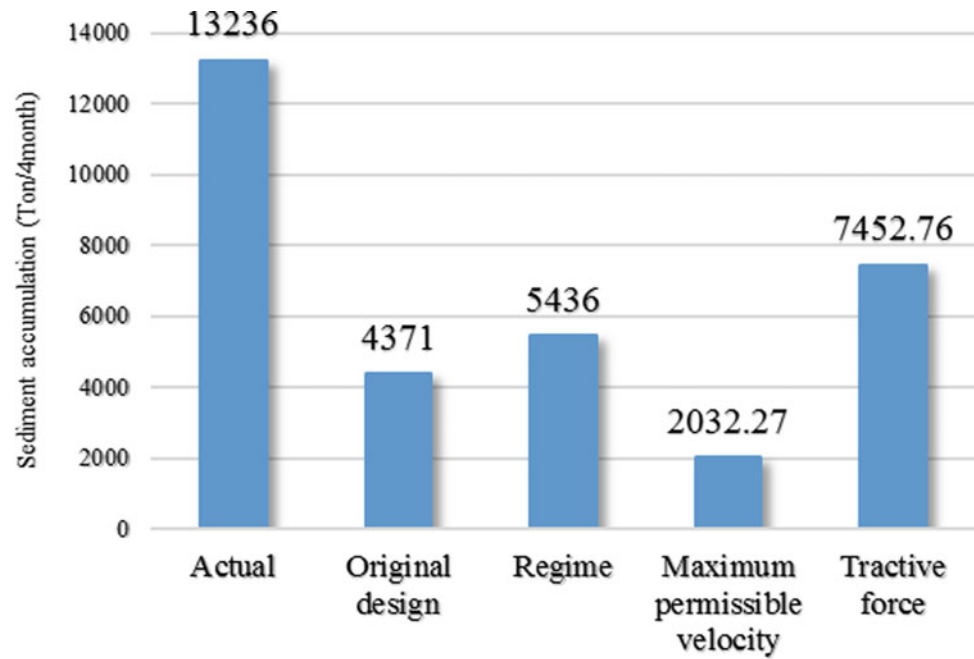


**Table 3**  $Q_{\min}$  values for main and major corresponding to each side slope for Gezira scheme

Side slope (z:1)	$Q_{\min}$ for main ( $\text{m}^3/\text{s}$ )	$Q_{\min}$ for major ( $\text{m}^3/\text{s}$ )
Nearly vertical	1.45	0.11
¼:1	0.62	0.05
½:1 to 1:1	0.65	0.05
1:1	0.85	0.07
1½:1	1.97	0.15
2:1	5.14	0.37
3:1	30.39	2.19

## Annexes

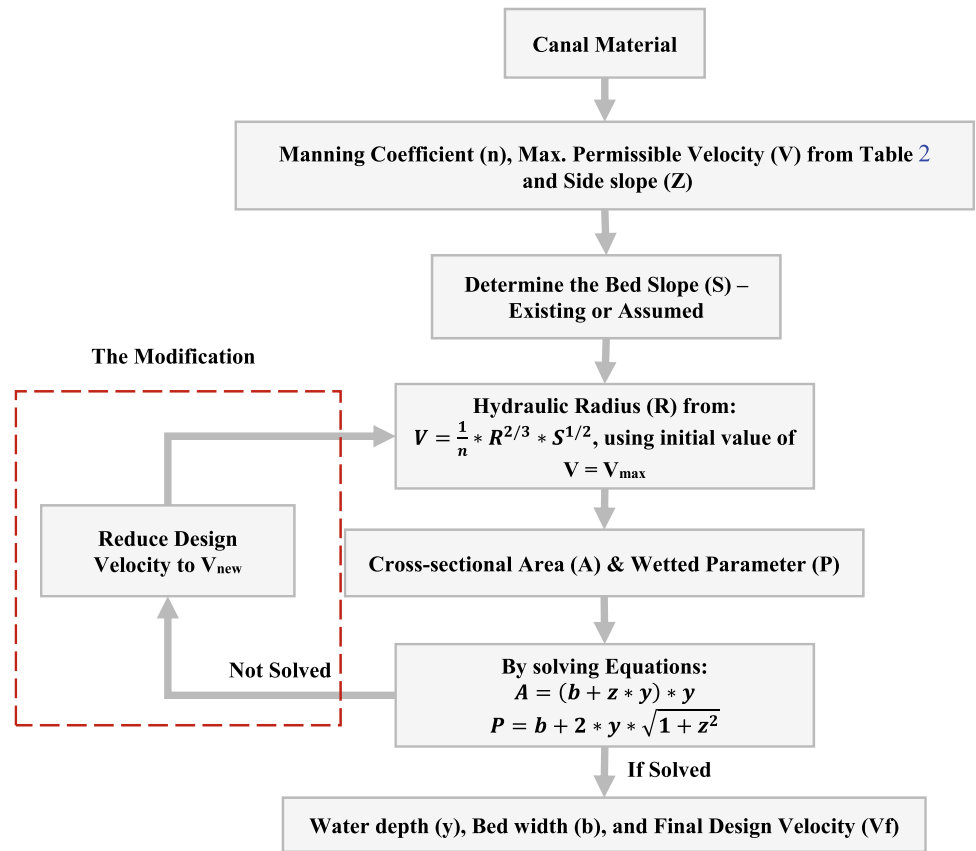
### Annex 1: Modified Maximum Permissible Velocity Design Steps

The design steps for designing the irrigation canals using the modified maximum permissible velocity are shown in Fig. 18.

### Annex 2: Tractive Force Design Steps

The design steps and charts used for designing the irrigation canals using tractive force method are shown in Figs. 19, 20, 21, 22 and 23 and Table 4.

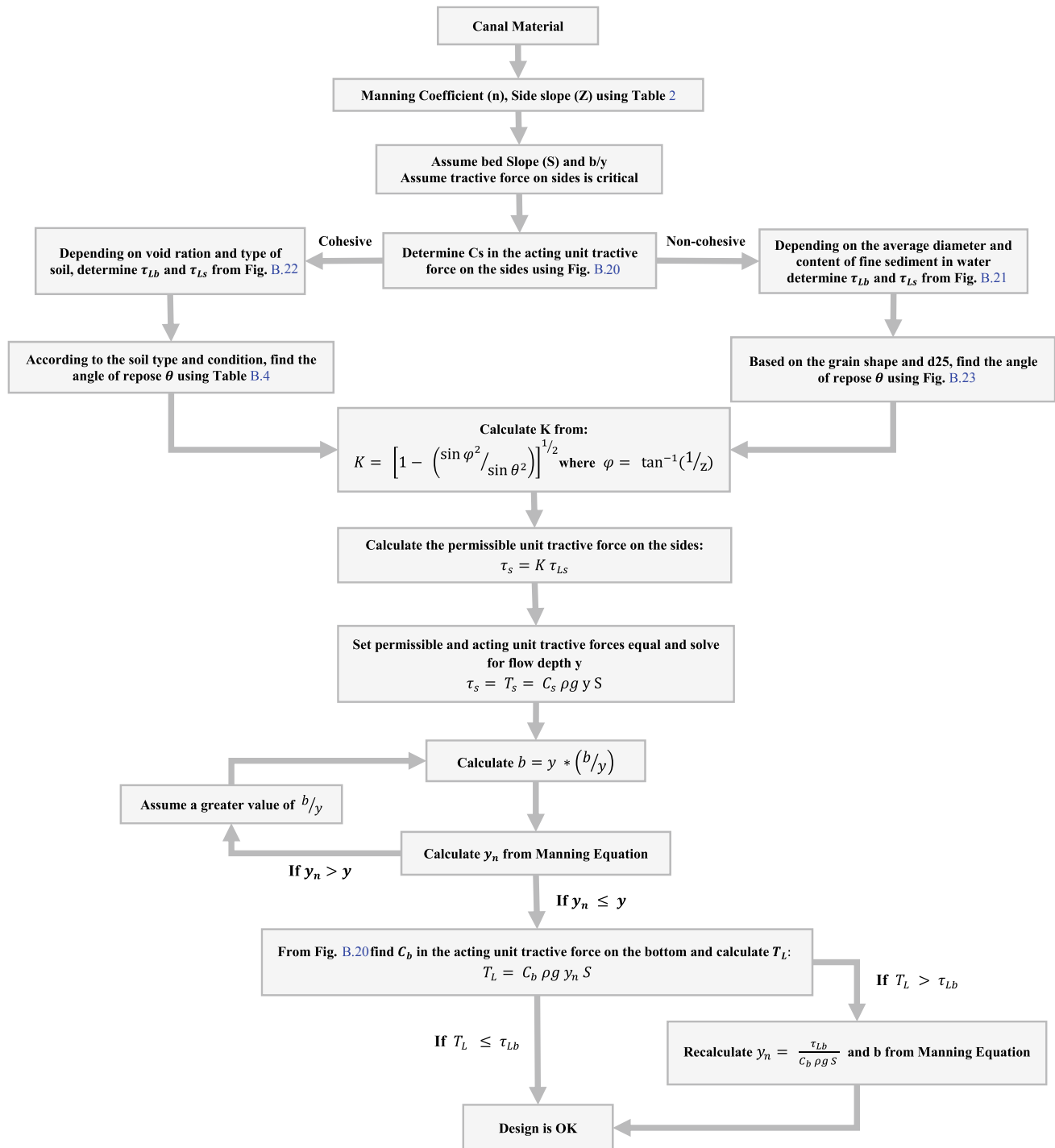
**Fig. 18** Design steps of the modified maximum permissible velocity



**Table 4** Angle of repose for cohesive materials (Anon, 2020)

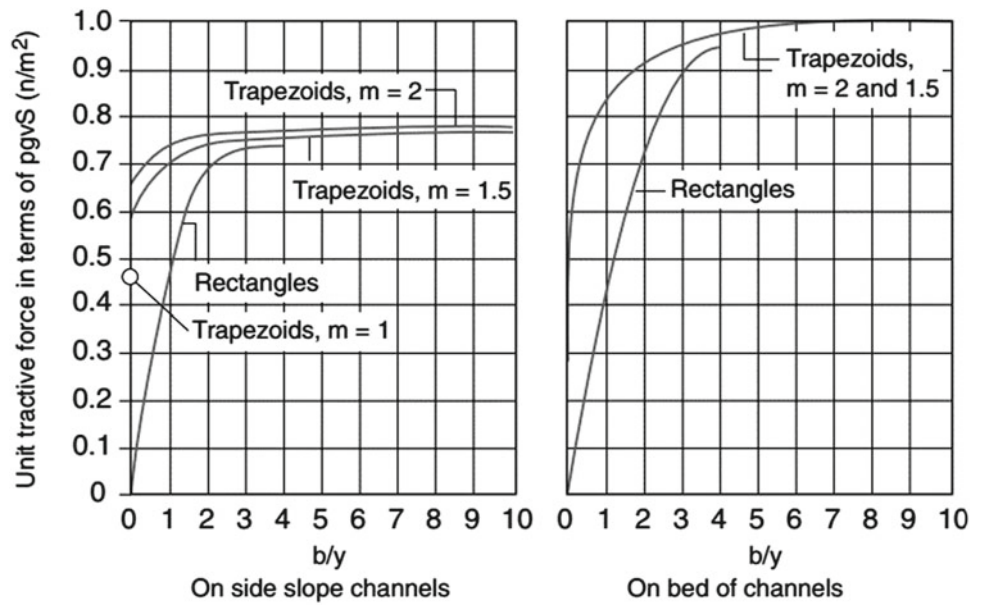
Soil type	Dry	Moist	Wet
Top soil; loose	35–40	–	45
Loam; loose	40–45	–	20–25
Clay/silt; solid	–	40–50	–
Clay/silt; firm	–	17–19	–
Clay/silt; loose	–	20–25	–
Puddle clay	–	–	15–19
Silt	–	19	–
Sandy clay	–	15	–
Sand; compact	–	35–40	–
Sand; loose	30–35	–	25
Sandy gravel; compact	–	40–45	–
Sandy gravel; loose	–	35–45	–
Sandy gravel; natural	–	25–30	–
Gravel; medium coarse	25–30	–	25–30
Shingle; loose	–	40	–
Shale; hard	–	19–22	–
Broken rock	35	–	45



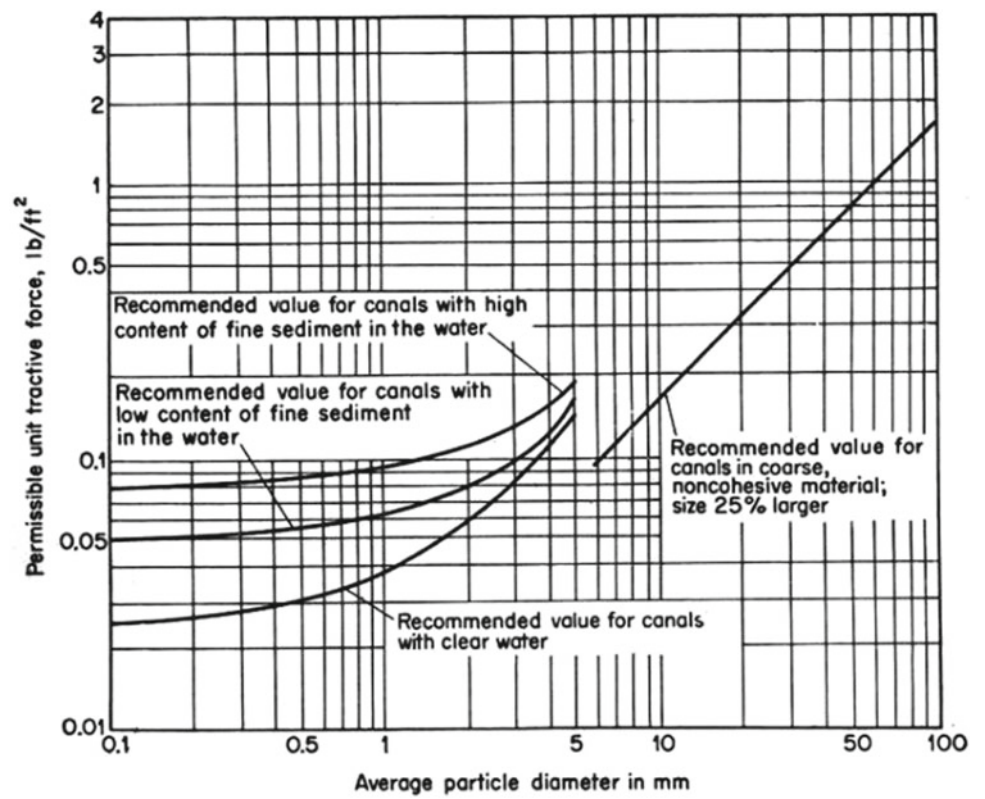


**Fig.19** Design steps of tractive force

**Fig. 20** Maximum unit tractive force in terms of  $\gamma_s S$  (Depeweg et al., 2014)



**Fig. 21** Recommended permissible unit tractive force for canals in non-cohesive material (Chow, 1959)



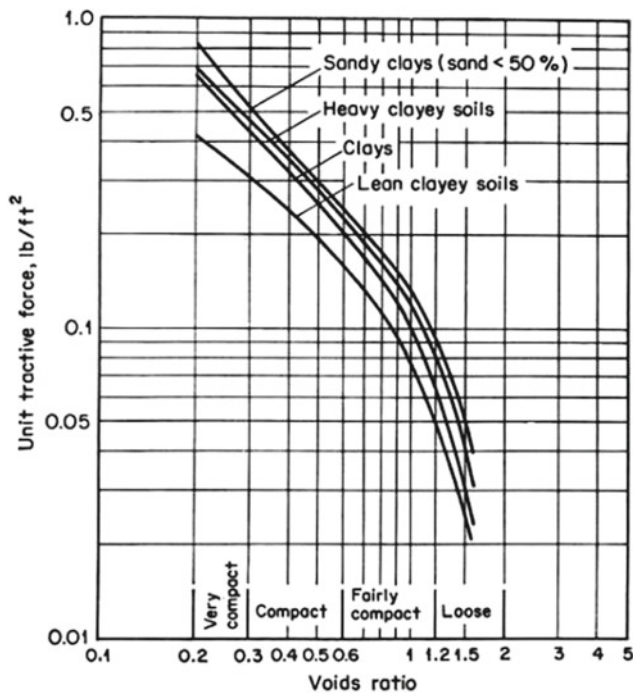


**Fig. 22** Permissible unit tractive forces for canals in cohesive material (Chow, 1959)

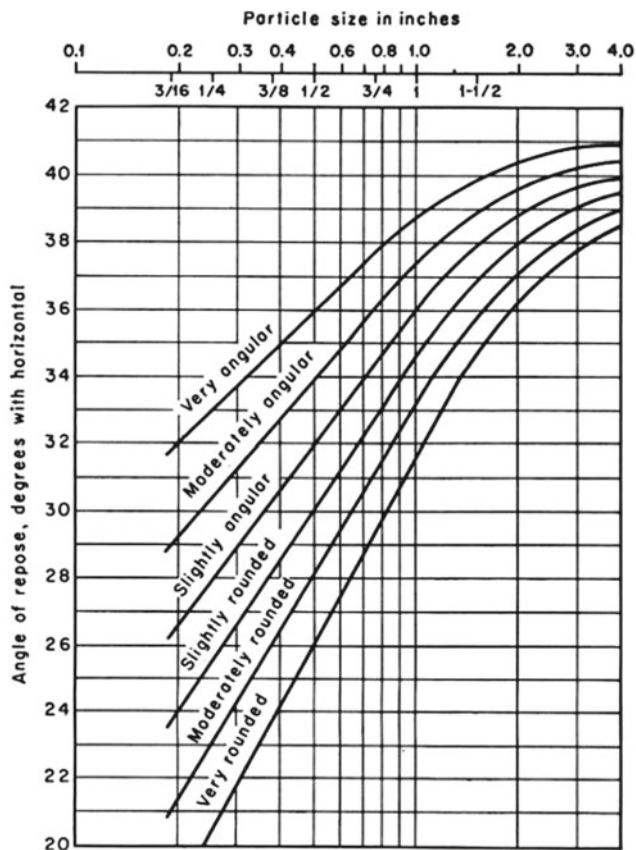


**Fig. 23** Angles of repose of non-cohesive material (Chow, 1959)

## References

- Ahmed, M. A. (1984). *Economic growth and water allocation in the Gezira*.
- Anon. (2020). *Angle of repose values for various soil types*. Retrieved August 17, 2020 [https://structx.com/Soil\\_Properties\\_005.html](https://structx.com/Soil_Properties_005.html)
- Brunner, G. W., & CIWER-HEC. (2016). *HEC-RAS, river analysis system hydraulic user's manual version 5.0*.
- Chang, H. (1985). Design of stable alluvial canals in a system. *Journal of Hydraulic Division*.
- Chow, V. T. (1959). *Open-channel hydraulics*. McGraw-Hill Book Company.
- Chow, V. T. (1983). *Open channel hydraulics*. McGraw Hill International Book Company.
- Depeweg, H., Paudel, K. P., & Néstor, M. V. (2014). *Sediment transport in irrigation canals: A new approach* (1st Ed.). CRC Press.
- Gismalla, Y. A. (2009). Sedimentation problems in the blue Nile reservoirs and Gezira scheme: A review. *Gezira Journal of Engineering and Applied Sciences*, 4(2), 1–19.
- Matthews, I. S. G. (1952). *Investigation of stable channels in the Gezira canalisation scheme*. SID, Tech. Note No.3/52.
- Osman, I. S. (2015). *Impact of improved operation and maintenance on cohesive sediment transport in Gezira scheme, Sudan*. CRC Press.
- Osman, I. S., Schultz, B., Osman, A., & Suryadi, F. X. (2017). *Effects of different operation scenarios on sedimentation of the Gezira scheme, Sudan* (pp. 82–89). Online 27 December 2016 in Wiley Online Library (Wileyonlinelibrary.Com).
- Osman, I. S., Schultz, B., Suryadi, F. X., & Mohamed, Y. (2011). Improving the operation and maintenance for better sediment and water management in Gezira scheme, Sudan. In *ICID 21st International Congress on Irrigation and Drainage* (pp. 51–62).
- Paudel, K. P. (2009). *Role of sediment in the design and management of irrigation canals*. CRC Press.
- Paudel, K. P. (2010). *Role of sediment in the design and management of irrigation canals*. CRC Press.
- Raudkivi, A. J. (1990). *Loose boundary hydraulics* (3rd Ed.). Pergamon Press.
- Simons, D., & Senturk, F. (1992). *Sediment transport technology*. Water Resources Publications.
- Vanoni, V. A. (1975). *Sedimentation engineering practice. American Society of Civil Engineers, Manuals and Reports on Engineering Practice*, 54, 745.
- Wallingford, H. R. (1992). *DORC: User manual*. HR Wallingford.
- White, W. R., Bettes, R., & Paris, E. (1982). Analytical approach to river regime. *Journal of the Hydraulics Division, ASCE*, 108(10), 1179–1193.



# Remote Sensing Approach for Estimating Evapotranspiration Using Satellite-Based Energy Balance Models in Al Hamra, Oman

Ahsan Ali, Yaseen Al-Mulla, Yassin Charabi, Ghazi Al-Rawas, and Malik Al-Wardy

## Abstract

The conventional physical- and climatological-based models estimating actual evapotranspiration (ET<sub>a</sub>) do not provide accurate ET<sub>a</sub>, especially for regional-scale which is a challenge that needs to be tackled for the accurate assessment of irrigation practices. In this study, two energy balance models (1) Surface Energy Balance Algorithm for Land (SEBAL) and (2) Mapping Evapotranspiration at High Resolution with Internalized Calibration (METRIC) were applied in the Al Hamra region of Oman to estimate ET<sub>a</sub> using Landsat 8 satellite imagery. The aim of the study was to estimate ET<sub>a</sub> using the SEBAL and METRIC model for the period of two years and validate the outcome against modified Penman–Monteith (PM) model. In addition, this study highlighted procedural differences between METRIC and SEBAL models. The results showed that METRIC model estimated ET<sub>a</sub> successfully with a  $R^2$  value of 0.81 as compared to SEBAL model ( $R^2 = 0.17$ ). Study validated against PM model showed that the METRIC model outperformed the SEBAL with MAE and RMSE values of 0.30 and 0.36 mm as compared to 2.67 and 1.42 mm, respectively. Study concluded that the SEBAL model used cumulative daily net radiation, while METRIC used cumulative reference evapotranspiration to extrapolate ET<sub>a</sub> on daily basis. Although METRIC performed well

than SEBAL, the manual selection of hot and cold pixel in METRIC was a difficult process and it creates vulnerability of inaccurate estimates of ET<sub>a</sub>. However, from this study, we can conclude that the METRIC model can be useful in providing high spatial and temporal ET<sub>a</sub> estimates. Furthermore, the approach used in this paper can be generalized and pave the way for further developments of the studied models.

## Keywords

Remote sensing • SEBAL • METRIC • Landsat 8 • Energy balance

## 1 Introduction

Water scarcity leads to groundwater depletion and decline in agricultural area reduction as Arab region stands with a yearly total of 763 m<sup>3</sup> per capita renewable water resources (WWAP, 2019). Agriculture stands as one of the many water uses including domestic and industrial usage. In the past 40 years, increment in water productivity by agriculture played an important role to increase in food production (OECD, 2010). Evapotranspiration (ET<sub>a</sub>) plays an important role in the local and global water budget (Chen et al., 2018). There is a dire need to observe the distribution of ET<sub>a</sub> on both temporal and spatial scales as ET<sub>a</sub>, especially for hot hyper-arid regions. Many research had already been done in order to estimate the amount of water required for different crops. However, accurate estimation of crop water requirement is still an immense challenge. Many researchers have proposed models to estimate ET<sub>a</sub> for different crops. FAO Penman–Monteith equation is one most widely used models requiring many weather parameters (Djaman et al., 2016). An agro-hydrological simulation model was applied by Droogers (2000) to access the ET<sub>a</sub>. Traditional methods like lysimeters, Bowen ratio (Bowen, 1926), Eddy correlation,

A. Ali (✉) · Y. Al-Mulla · M. Al-Wardy  
Department of Soils, Water and Ag Engineering, Sultan Qaboos University, Al-Khoud 123, PO Box 34 Muscat, Sultanate of Oman

Y. Al-Mulla  
Remote Sensing and GIS Research Center, Sultan Qaboos University, Al-Khoud 123, PO Box 33 Muscat, Sultanate of Oman

Y. Charabi  
Center of Environmental Studies and Research, Sultan Qaboos University, Al-Khoud 123, PO Box 33 Muscat, Sultanate of Oman

G. Al-Rawas  
Department of Civil and Architectural Engineering, Sultan Qaboos University, Al-Khoud 123, PO Box 33 Muscat, Sultanate of Oman

and scintillometry methods were also used in many studies, providing point-based ETa estimates (Sun et al., 2011). Although traditional methods provided an accurate estimation of ETa on the local scale, these models cannot be applied on the large areas/scale to observe spatial-temporal distribution of ETa. In this aspect, remote sensing techniques are vital to provide an accurate estimation of ETa on both local and regional scales (Ali & Al-Mulla, 2019). Many studies were carried out in the field of remotely assessed ETa using algorithms. A review study on the traditional and remotely sensed algorithm was highlighted providing a result that each model was designed and applied for a specific condition and land cover type (Jovanovic & Israel, 2012). In the last 2 decades, many single/multiple source algorithms were suggested by the different researchers. But Surface Energy Balance Algorithm for Land (SEBAL) by Bastiaanssen et al. (1998) and Mapping Evapotranspiration using Internalized Calibration (METRIC) by Allen et al. (2005) are the two widely one-source models. SEBAL model has been widely used and validated in different conditions around the globe, including Idaho (Allen et al., 2003), southern California (Suleiman et al., 2009) Kimberly, Idaho (Allen et al., 2011), Turkey (Bastiaanssen, 2000), Brazil (Santos et al., 2010), Florida (Bhattarai et al., 2017) and Jordan (Owaneh and Suleiman, 2018). On the other hand, METRIC model was also validated in Brazil (Oliveira et al., 2018), Idaho (Allen et al., 2011), Saudi Arabia (Madugundu et al., 2017), Florida (Bhattarai et al., 2017), Arizona (French et al., 2015), Brazilian Amazon (Numata et al., 2017), central Ireland (Spiliotopoulos et al., 2017) and south Portugal (PÓças et al., 2014).

However, SEBAL and METRIC models have been applied successfully in many conditions all around the globe. But very limited studies were done in the hot and hyper-arid regions like Oman. Hence, there is a dire need to apply SEBAL and METRIC models in the harsh conditions of the selected study area to evaluate the ETa estimates of both models. The results of the model will be validated against the PM model followed by Allen et al. (1998).

## 2 Materials and Methods

### 2.1 Study Area and Satellite Imagery

Omani civilization is greatly influenced by the traditional agriculture, providing a path to live under harsh conditions (Al-Marshudi, 2001). Old Aflaj irrigation system that consists of open water channels conveying water from the mountain to the crop is the main sources of irrigation. For the study, date palm tree was selected as it stands as one of the most cultivated crop types in Oman; being the eighth largest date-producing country in the world (Al-Khayri et al.,

2015). Study area was selected in the region of Al Hamra, Al Dakhiliyah, in the northeast of Oman. Figure 1 shows the geographical location of study area.

Landsat 8 (OLI and TIRS) satellite imagery was used as an input for the SEBAL and METRIC model for the year 2015. Figure 2 shows metrological data was recorded from a weather station installed near study area.

### 2.2 Model Description

SEBAL and METRIC models use same surface energy balance equation (Eq. 1) to estimate ETa flux.

$$\lambda ET = R_n - G - H \quad (1)$$

where  $\lambda ET$  is amount of energy ( $W m^{-2}$ ) that is required to convert water into vapors either from soil/plant or both. " $R_n$ " is amount of available net radiation ( $W m^{-2}$ ) after reflecting from the sun or atmosphere,  $G$  is the amount of energy ( $W m^{-2}$ ) that is available on the soil surface after radiations absorbed the soil from the atmosphere, and  $H$  is the amount of energy ( $W m^{-2}$ ) that is required to transfer heat through advection to increase the temperature of a body.

In SEBAL and METRIC, procedural steps to estimate  $R_n$  and  $G$  are the same. Hence, same values of  $R_n$  and  $G$  were used by SEBAL and METRIC. Procedural steps for  $R_n$  and  $G$  can be found in Bastiaanssen (2000). The difference between the two models was observed in required calibration of values of  $H$  using Eq. (2)

$$H = \frac{P_{air} \times C_p \times dT}{R_{ah}} \quad (2)$$

The difference between the two models occurs in the  $dT$  values as it is the temperature difference between two reference heights. Both models use a linear equation to estimate  $dT$  by selecting two extreme conditions within the study area that can show two extreme conditions (hot and cold). The selection of these extreme conditions is the step differentiating the two models. The hot pixel in SEBAL and METRIC model is selected from an area with no vegetation. Cold pixel in SEBAL is recommended to be selected from a wellirrigated or water body. But in METRIC, cold pixel is selected from a well-vegetated area.

In Eq. (2), there were two unknowns  $R_{ah}$  and  $H$ . Hence, using  $dT$  values an iteration process is initialized as recommended by the SEBAL and METRIC model by using an ideal situation for the first iteration. After the first estimation of  $H$ , a correction factor is introduced providing the correct values of  $R_{ah}$  and  $H$ . More details of the iteration process can be found in Allen et al. (2011). Once the value of  $H$  is calculated, then ET flux is estimated using Eq. (1).



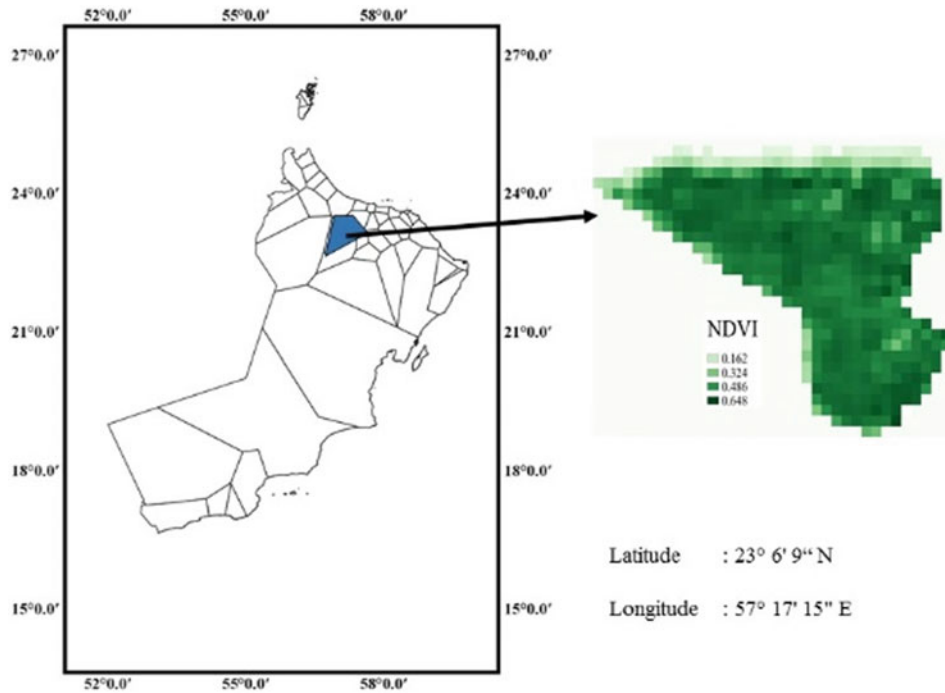


**Fig. 1** Location of study area in Al Hamra, Al Dakhiliyah, Oman

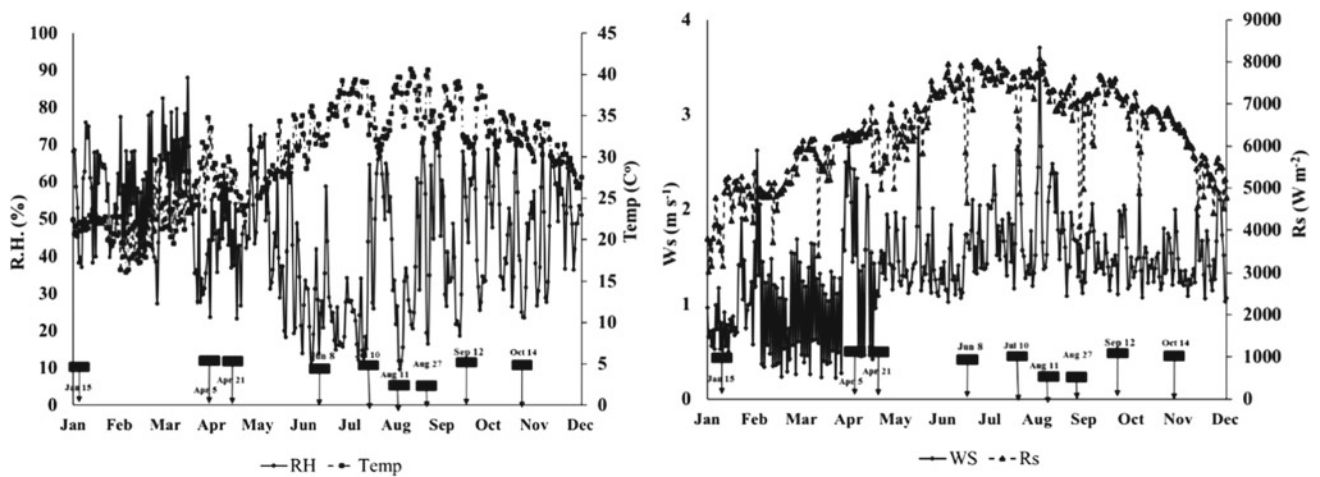


**Fig. 2** Meteorological data recorded from a weather station installed near study area. Here, “Ws” is wind speed ( $\text{m s}^{-1}$ ), “Rs” is cumulative daily solar radiation ( $\text{W m}^{-2}$ ), “RH” is relative humidity (%), “Temp” is the temperature of air ( $^{\circ}\text{C}$ ), and “-” shows the satellite imagery acquisition date

The values of  $R_n$ ,  $G$ , and  $H$  are instantaneous values at the time of satellite-overpass, that are used to estimate the instantaneous amount of evapotranspiration ( $ET_{\text{inst}}$ ). Hence, SEBAL and METRIC models use different formulations to extrapolate instantaneous  $\lambda ET$  value for the day. SEBAL model uses evaporative fraction (EF), and METRIC uses reference evapotranspirative fraction (ETrF) by using Eqs. (3) and (4), respectively.

$$EF = \frac{R_n - G - H}{R_n - G} \quad (3)$$

$$ETrF = \frac{ET_{\text{inst}}}{ET_r} \quad (4)$$

METRIC model uses ETrF values that are estimated using reference evapotranspiration equation as recommended by Allen et al. (2005). SEBAL and METRIC model suggested that EF and ETrF values are kept the same throughout the day. SEBAL model uses EF in cooperation with Eq. (5), while METRIC model uses Eq. (6) to estimate  $ET_a$  values.

$$ET_a = ET_{p_{24}} \times EF \quad (5)$$

$$ET_a = E_{r_{-24}} \times E_{TrF} \quad (6)$$

Here,  $ET_{p24}$  is cumulative potential evapotranspiration that is formulated by Bastiaanssen (2000) and  $ET_{r_{-24}}$  is cumulative reference evapotranspiration followed by Allen et al. (2005).

### 2.3 Validation

To validate the application of SEBAL and METRIC, Penman–Monteith (PM) equation was used that is formulated in Eq. (7). PM model is considered in many researches as a benchmark in the estimation of crop evapotranspiration (Costa et al., 2019).

$$ET_o = Kc \times \frac{0.408\Delta(R_n - G) + \gamma \frac{900}{T+273} u_2 (e_s - e_a)}{\Delta + \gamma(1 + 0.34u_2)} \quad (7)$$

where  $ET_o$  is reference evapotranspiration ( $\text{mm day}^{-1}$ ),  $R_n$  is net radiation at the crop surface ( $\text{MJ m}^{-2} \text{day}^{-1}$ ),  $G$  is soil heat flux density in ( $\text{MJ m}^{-2} \text{day}^{-1}$ ),  $T$  is mean daily air temperature at 2 m height ( $^{\circ}\text{C}$ ),  $u_2$  is the wind speed at 2 m height ( $\text{m s}^{-1}$ ),  $e_s$  is saturation vapor pressure [kPa],  $e_a$  expresses actual vapor pressure (kPa),  $e_s - e_a$  is saturation vapor pressure deficit (kPa),  $\Delta$  denotes slope vapor pressure curve ( $\text{kPa } ^{\circ}\text{C}^{-1}$ ) and  $\gamma$  is psychrometric constant ( $\text{kPa } ^{\circ}\text{C}^{-1}$ ).

## 3 Results and Discussion

Firstly, satellite imagery was downloaded, and then digital numbers were converted to both radiance and reflectance values. Then, the reflectance or radiance values were converted into NDVI, emissivity, albedo, and LST values. These estimated factors were then used in the calculation of three basic parameters ( $R_n$ ,  $G$ , and  $H$ ) used in Eq. (1). As discussed in the previous sections, SEBAL and METRIC models use same formulation for  $R_n$  and  $G$ . Hence, values of  $R_n$  and  $G$  as shown in Fig. 3 were kept the same in both SEBAL and METRIC to see the effect of  $H$  on the estimation of  $ET_a$  by both models.

The study resulted in a strong correlation between land surface temperature (LST) and  $R_n$ . The slope between LST and  $R_n$  was low in the winter as compared to the summer season. A minimum slope value was observed in the month of April as the LST values started to increase. The trend between LST and  $R_n$  observed steep slopes, especially in the month of June as LST values increased while reaching to its maximum values.

The study also resulted that even  $R_n$  and  $G$  were kept the same for both models, values of  $H$  for both models were

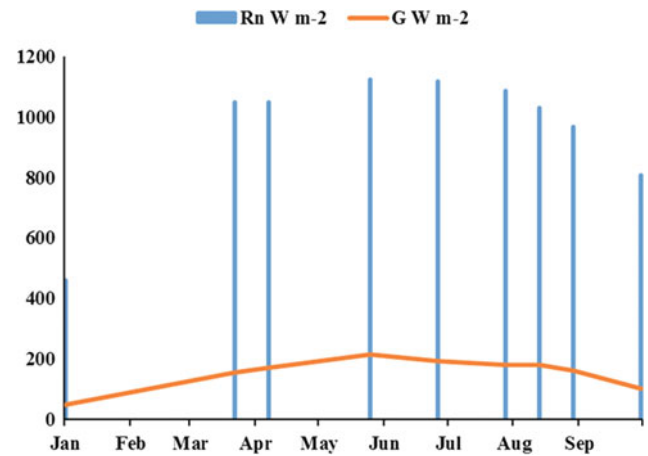


**Fig. 3** Values of  $R_n$  and  $G$  estimated in study area ( $\text{W m}^{-2}$ ) for SEBAL and METRIC

different from each other. The study resulted that the difference between SEBAL and METRIC was observed because of the difference in the estimation of extreme conditions in each model. The selection of these extreme conditions paved the way for the correct estimation of  $H$ . For SEBAL, hot pixel was selected from a bare soil with highest land surface temperature, while the extreme conditions (hot and cold pixel) were selected from an area of dense vegetation with high NDVI values. On the other hand, in METRIC, the hot pixel was selected from an area with the lowest NDVI value and cold pixel was selected with the dense vegetation, by which more than 90% of the pixel was selected from the area. Figure 4 shows the NDVI values and LST values of pixels selected for the study.

Figure 5 clearly shows the difference between METRIC and SEBAL models. Results from the study showed that the SEBAL model was overestimating values of  $H$  as compared

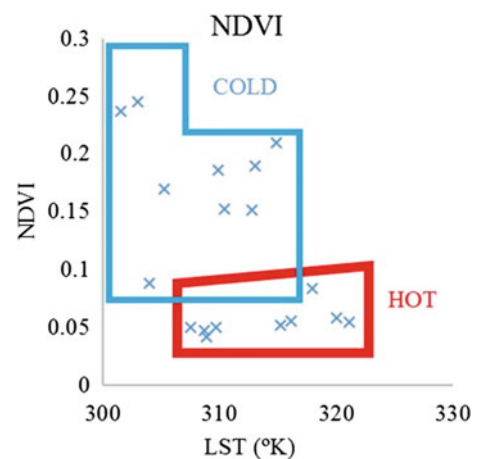


**Fig. 4** NDVI versus LST values of pixels selected in the study

to the METRIC model. The difference of  $H$  between SEBAL and METRIC was increasing in hot summer and became equal at the end of the study period. The overestimation of SEBAL ranged to a maximum value of  $150 \text{ W m}^{-2}$ .

The difference between SEBAL and METRIC in the estimation of  $H$  affected the  $\text{ET}_a$  values of both models as shown in Fig. 6. Results showed that SEBAL and METRIC models were overestimating at the start of the study period. But SEBAL model was underestimating  $\text{ET}_a$  values with a difference of  $2 \text{ mm d}^{-1}$  and  $2.3 \text{ mm d}^{-1}$  with METRIC and PM model, respectively. The study resulted that the difference between SEBAL and METRIC models was observed to be higher in the month of April as difference in values of  $H$  estimated by SEBAL was higher than  $100 \text{ W m}^{-2}$ . Figure 5 also shows that overall SEBAL model resulted in a high value of  $H$  as compared to METRIC model, especially in the summer season. The study also resulted that the SEBAL model over estimated  $H$  as compared to METRIC model, that lead SEBAL to underestimate  $\text{ET}_a$  in the summer seasons. Figure 5 shows that in the winter season, METRIC and SEBAL models were very close to each other in estimation of  $H$ , but the difference between  $\text{ET}_a$  values of both models was high. One of the reasons might be the difference in the extrapolation of 24-h daily values of  $\text{ET}_a$  (Eqs. 5 and 6) as METRIC and SEBAL models use different methods to extrapolate  $\text{ET}_a$  from hourly value to daily values.

Results from Fig. 6 show that SEBAL model was underestimating  $\text{ET}_a$  in summer season as compared to both METRIC and PM with the lowest value of  $4.753 \text{ mm d}^{-1}$ . Figure 7 resulted that no strong correlation was found between SEBAL and PM as the regression coefficient resulted in a value of 0.17. On the other hand, METRIC model shows good correlation with PM model as the

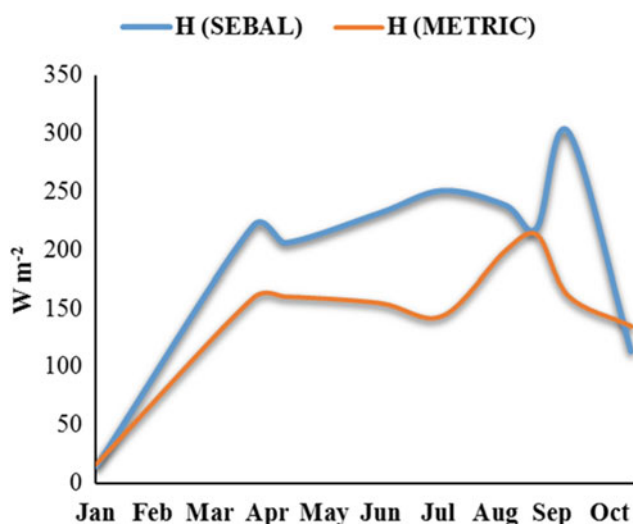


**Fig. 5** Variation of  $H$  ( $\text{W m}^{-2}$ ) in SEBAL and METRIC for the study area

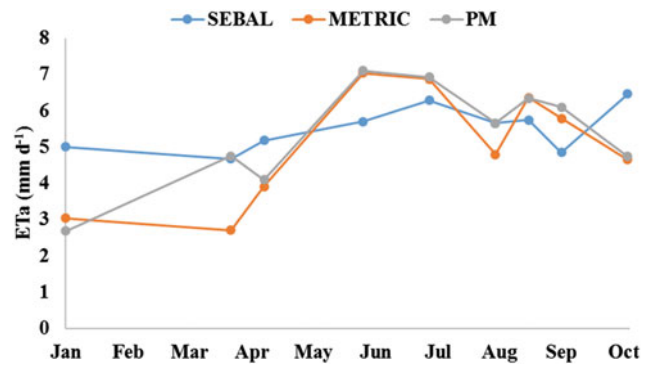


**Fig. 6** Trend of  $\text{ET}_a$  estimates from SEBAL, METRIC and PM models

regression coefficient resulted in a value of 0.81. Statistical analysis (Table 1) also shows that METRIC model resulted in low value of root-mean-square error (RMSE) of 0.36 as compared to 1.42 resulted by SEBAL model. Statistical analysis also resulted that the mean absolute error (MAE) of METRIC model was also lower ( $0.30 \text{ mm d}^{-1}$ ) as compared to SEBAL ( $2.67 \text{ mm d}^{-1}$ ) model.

The study resulted that SEBAL model was overestimating  $\text{ET}_a$  in the winter season with an average difference of  $2.33 \text{ mm d}^{-1}$  as compared to METRIC and  $2.7 \text{ mm d}^{-1}$  as compared to PM model. SEBAL model was underestimating  $\text{ET}_a$  as the temperature went high while compared with PM and METRIC. Based on statistical results, study concluded that METRIC model outperformed SEBAL model for the estimation of  $\text{ET}_a$  in Al Hamra region, Oman.

## 4 Conclusions

SEBAL and METRIC models were applied in the Al Hamra region of Oman to evaluate the performance of  $\text{ET}_a$  estimates in the region. Study explained the difference of selection of extreme conditions in both the models. The study resulted that even  $R_n$  and  $G$  were kept the same for both the models, and the difference in the estimation of  $H$  causes both the models to act differently in the same conditions. It was resulted that SEBAL model was overestimating  $\text{ET}_a$  with an average value of  $2.3 \text{ mm d}^{-1}$  as compared to METRIC and PM models. It was also observed that SEBAL model was underestimating  $\text{ET}_a$  in the peak summer days as compared with PM and METRIC. The study validated against the PM model showed that the METRIC model outperformed the SEBAL with MAE and RMSE value of 0.30 mm and 0.36 mm as compared to 2.67 mm and 1.42 mm, respectively. Although METRIC performed well than SEBAL, the manual selection of hot and cold pixel in METRIC was a difficult process and it creates vulnerability of inaccurate estimates of  $\text{ET}_a$ . However, from this study we

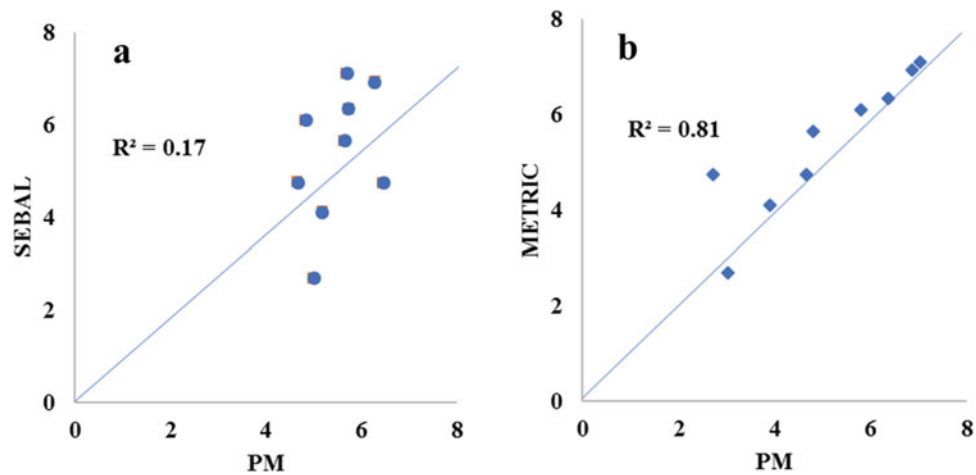


**Fig. 7** Comparison between **a** SEBAL versus PM and **b** METRIC versus PM

**Table 1** Results of statistical parameters

Parameters	SEBAL	METRIC
$R^2$	0.17	0.81
MAE (mm)	2.67	0.30
RMSE (mm)	1.42	0.36

Note MAE is mean absolute error (mm), and RMSE is root-mean-square error in (mm)

can conclude that METRIC model can be useful in providing high spatial and temporal ETa estimates. Furthermore, the approach used in this paper can be generalized and pave the way for further developments of the studied models.

## References

- Ali, A., & Al-Mulla, Y. (2019). Evaluation of sebal and metric based evapotranspiration in arid region of Samail, Oman. In *The 40th Asian Conference on Remote Sensing (ACRS 2019)*. Daejeon Convention Center(DCC), Daejeon, Korea, (pp. 1–7).
- Al-Khayri, J. M., Jain, S. M., & Johnson, D. V. (2015). Date palm genetic resources and utilization: Volume 2: Asia and Europe. Date Palm Genetic Resources and Utilization: Volume 2: Asia and Europe, 1–566. <https://doi.org/https://doi.org/10.1007/978-94-017-9707-8>.
- Allen, R., Irmak, A., Trezza, R., Hendrickx, J. M. H., Bastiaanssen, W., & Kjaersgaard, J. (2011). Satellite-based ET estimation in agriculture using SEBAL and METRIC. *Hydrological Processes*, 25, 4011–4027. <https://doi.org/10.1002/hyp.8408>.
- Allen, R. G., Luis, S. P., Raes, D., & Smith, M. (1998). FAO irrigation and drainage paper No. 56. crop evapotranspiration (guidelines for computing crop water requirements). *Irrigation and Drainage* 300, 300. <https://doi.org/https://doi.org/10.1016/j.eja.2010.12.001>
- Allen, R. G., Morse, A., & Tasumi, M. (2003). Application of SEBAL for Western US water rights regulation and planning, ICID Workshop on Remote Sensing of ET for Large Regions.
- Allen, R. G., Tasumi, M., Morse, A., & Trezza, R. (2005). A landsat-based energy balance and evapotranspiration model in Western US water rights regulation and planning. *Irrigation and Drainage Systems*, 19, 251–268. <https://doi.org/10.1007/s10795-005-5187-z>.
- Al-Marshudi, A. S. (2001). Traditional irrigated agriculture in Oman: Operation and management of the Aflaj system. *Water International*, 26, 259–264.
- Bastiaanssen, W. G. M. (2000). SEBAL-based sensible and latent heat fluxes in the irrigated Gediz Basin, Turkey. *Journal of Hydrology*, 229, 87–100.
- Bastiaanssen, W. G. M., Menenti, M., Feddes, R. A., & Holtslag, A. A. M. (1998). A remote sensing surface energy balance algorithm for land (SEBAL). 1. Formulation. *Journal of Hydrology*, 212, 198–212.
- Bhattarai, N., Quackenbush, L. J., Im, J., & Shaw, S. B. (2017). A new optimized algorithm for automating endmember pixel selection in the SEBAL and METRIC models. *Remote Sensing of Environment*, 196, 178–192. <https://doi.org/10.1016/j.rse.2017.05.009>.
- Bowen, I. S. (1926). The ratio of heat losses by conduction and by evaporation from any water surface. *Physical Review*, 27, 779.
- Chen, H., Huo, Z., Dai, X., Ma, S., Xu, X., & Huang, G. (2018). Impact of agricultural water-saving practices on regional evapotranspiration: The role of groundwater in sustainable agriculture in arid and semi-arid areas. *Agricultural and Forest Meteorology*, 263, 156–168. <https://doi.org/10.1016/j.agrformet.2018.08.013>.
- Costa, O., Coelho, R. T., Wolff, W., et al. (2019). Spatial variability of coffee plant water consumption based on the SEBAL algorithm. *Scientia Agricola*, 76(2), 93–101. <https://doi.org/10.1590/1678-992x-2017-0158>.
- Djaman, K., Irmak, S., Kabenge, I., & Futakuchi, K. (2016). Evaluation of FAO-56 penman-monteith model with limited data and the valiantzas models for estimating grass-reference evapotranspiration in Sahelian conditions. *Journal of Irrigation and Drainage Engineering*, 142, 4016044.
- dos Santos, C. A. C., Bezerra, B. G., da Silva, B. B., & Rao, T. V. R. (2010). Assessment of daily actual evapotranspiration with SEBAL

- and S-SEBI algorithms in cotton crop. *Revista Brasileira De Meteorologia*, 25, 383–392. <https://doi.org/10.1590/s0102-77862010000300010>.
- Droogers, P. (2000). Estimating actual evapotranspiration using a detailed.pdf. 229, 50–58.
- French, A. N., Hunsaker, D. J., & Thorp, K. R. (2015). Remote sensing of evapotranspiration over cotton using the TSEB and METRIC energy balance models. *Remote Sensing of Environment*, 158, 281–294. <https://doi.org/10.1016/j.rse.2014.11.003>.
- Jovanovic, N., & Israel, S. (2012). Critical review of methods for the estimation of actual evapotranspiration in hydrological models. *Evapotranspiration Remote Sensing and Modeling*. <https://doi.org/10.5772/21279>.
- Madugundu, R., Al-Gaadi, K. A., Tola, E., Hassaballa, A. A., & Patil, V. C. (2017). Performance of METRIC in estimating hourly and daily evapotranspiration fluxes over an irrigated field in Saudi Arabia. *Hydrology and Earth System Sciences Discussions*, 1–23 <https://doi.org/10.5194/hess-2017-206>.
- Numata, I., Khand, K., Kjaersgaard, J., Cochrane, M.A., & Silva, S. S. (2017). Evaluation of landsat-based metric modeling to provide high-spatial resolution evapotranspiration estimates for amazonian forests. *Remote Sensing*, 9 <https://doi.org/10.3390/rs9010046>
- OECD. (2010). Sustainable management of water in agriculture. *Sustainable Management of Water in Agriculture*. <https://doi.org/10.1787/9789264163225-en>.
- Oliveira, B. S., Moraes, E. C., Carrasco-Benavides, M., Bertani, G., Mataveli, G. A. V. (2018). Improved albedo estimates implemented in the METRIC model for modeling energy balance fluxes and evapotranspiration over agricultural and natural areas in the Brazilian Cerrado. *Remote Sensing*, 10 <https://doi.org/10.3390/rs10081181>
- Owaneh, O. M., & Suleiman, A. A. (2018). Comparison of the performance of ALARM and SEBAL in estimating the actual daily ET from satellite data. *Journal of Irrigation and Drainage Engineering*, 144, 04018024. [https://doi.org/10.1061/\(asce\)ir.1943-4774.0001335](https://doi.org/10.1061/(asce)ir.1943-4774.0001335).
- PÔças, I., Paço, T. A., Cunha, M., Andrade, J. A., Silvestre, J., Sousa, A., Santos, F. L., Pereira, L. S., Allen, R. G. (2014). Satellite-based evapotranspiration of a super-intensive olive orchard: Application of METRIC algorithms. *Biosystems Engineering*, 128, 69–81. <https://doi.org/10.1016/j.biosystemseng.2014.06.019>
- Spiliotopoulos, M., Holden, N. M., & Loukas, A. (2017). Mapping evapotranspiration coefficients in a temperate maritime climate using the metric model and landsat TM. *Water* (Switzerland), 9 <https://doi.org/10.3390/w9010023>
- Suleiman, A. A., Bali, K. M., & Kleissl, J. (2009). Comparison of ALARM and SEBAL evapotranspiration of Irrigated Alfalfa. In ASABE (Ed.), *ASABE Annual International Meeting*. ASABE, Reno, Nevada.
- Sun, Z., Wei, B., Su, W., Shen, W., Wang, C., You, D., & Liu, Z. (2011). Evapotranspiration estimation based on the SEBAL model in the Nansi Lake Wetland of China. *Mathematical and Computer Modelling*, 54, 1086–1092. <https://doi.org/10.1016/j.mcm.2010.11.039>WWAP,20.





# Application of Dipole–Dipole, Schlumberger, and Wenner–Schlumberger Arrays in Groundwater Exploration in Karst Areas Using Electrical Resistivity and IP Methods in a Semi-arid Area, Southwest Iran

Leila Mirzaei, Mohammad Kazem Hafizi, and Mohammad Ali Riahi

## Abstract

Cost-effective and efficient techniques of geoelectrics for groundwater exploration, especially in karstic regions, can be used to as an appropriate tool to recognition of karst hydrogeological potential. This paper provides a method based on the geoelectrical tomography to precise determination of the water well drilling location in karstic limestones of Izeh, southwest Iran. The geoelectrical operation done in 98 VES of Schlumberger and two profiles using dipole–dipole and Wenner–Shlumberger arrays. The 1D interpretation of VES using IPI2win followed by 2D electrical resistivity and induced polarization (IP) tomography using Res2Dinv in two sites, Naale Asbi syncline and the west of Izeh limestones, is carried out in order to propose the best locations for drilling of water wells. The results of the geoelectrical study of Asmari limestone of Izeh show the high electrical resistivity (between 200 and 1000 ohms-m) and low IP (lower than 3 Mv%V) indicates dry limestone, which decreases electrical resistivity (between 50 and 150 ohms-m) and stability in IP values, while the layers become water bearing. The dry cavities are characterized by very high electrical resistivity anomalies (ranging from 1500 to higher than 2000 ohms-m) with low IP values in the matrix of limestone with medium high electrical resistivity. The marl and marly limestone layers with low permeability can be detected by very low electrical resistivity (lover than 20 ohms-m) and high IP (higher than 10 Mv%V). The tomography of electrical resistivity and IP have strongly confirmed each other especially in the dipole–dipole array, and however, in some cases of

Schlumberger array, the deviations are seen in the depth that can arise due to the high sensitivity of the IP data in high depths.

## Keywords

Karst groundwater exploration • Electrical resistivity tomography • Induced polarization • Southwest Iran

## 1 Introduction

Groundwater is the largest available freshwater resource in the world. Groundwater resources can be expected to be increasingly relied upon in the near future, as a consequence of rapid population growth and global environmental change, especially on arid regions. Cost-effective and efficient geoelectrical methods for groundwater exploration, especially in karstic regions, can be used to as an appropriate tool to recognition of karst hydrogeological potential. Karst is a type of landscape and also an aquifer type. Karst comprises terrain with distinctive hydrology and landforms that arise from a combination of high rock solubility and well-developed secondary (fracture) porosity.

The Zagros karst system is mainly comprised of the limestone of Asmari and Ilam-Sarvak Formations. There are no surface streams in the outcrops or in contact with limestones in the study area. The karst aquifers in Izeh area, southwest Iran, are the only source of drinking water supply of the city. Hence, the exploration, production, and quantitative and qualitative protection of karst aquifers are of essential importance in these areas. During the last two decades, 20 water wells have been drilled in different areas of Izeh karstic area for the supply of Izeh drinking water. Since 2015, the discharge of some drinking water wells in Izeh area has decreased, due to continuous droughts, and the drilling of new alternative water wells in the Asmari Formation has become more necessary. However, the lack of

L. Mirzaei (✉) · M. K. Hafizi · M. A. Riahi  
Institute of Geophysics, University of Tehran, Tehran, Iran  
e-mail: [leila.mirzaei@ut.ac.ir](mailto:leila.mirzaei@ut.ac.ir)

M. K. Hafizi  
e-mail: [hafizi@ut.ac.ir](mailto:hafizi@ut.ac.ir)

M. A. Riahi  
e-mail: [mariahi@ut.ac.ir](mailto:mariahi@ut.ac.ir)

appropriate studies in recent years has led to the failure of the drilling wells and wasting costs.

The fractured limestone of Asmari formation and cavities serve as major resource for groundwater in the Izeh area. A water-filled underground void of Asmari limestone has lower resistivity than most of the surrounding rocks, in principle it can be detected using the electrical resistivity tomography. Electrical resistivity is based on the injection of an electric current into the ground through electrodes. Bulk electrical resistivities in the shallow subsurface are controlled largely by electrolytic conduction in aqueous fluids that are either distributed across grain boundaries or contained in pores, fractures, and faults (Stummer et al., 2004). Since each electrical resistivity image is limited to a few meters in depth and length, here an approach based on an integrated method of electrical resistivity and induced polarization (IP) with three common arrays proposed for tomography to characterize the karst aquifer and detection of best location for drilling of new water wells. Conventional geoelectric arrays used to explorations in karst environments, each with its own advantages and limitations. The main purpose of this article is to determine which array and by which method electrical resistivity or IP can be better suited for detecting of water bearing karstic cavities, especially in the sloping carbonate layers.

In recent years, many advances have been made in computer systems for data exploration and 2D and 3D inverse modeling software. Imaging or electrical resistivity tomography (ERT) and induction polarization are increasingly used in the electrical exploration of karst zones with subsurface cavities, water bearing limestones, and marly limestones (Aizebeokhai and Oyeyemi, 2014; Dahlin, 1996; Loke & Barker, 1995; Oldenberg & Li, 1999; Samanovac & Alvanja, 2007). The electrical resistivity sections derived from inverse modeling and their interpretation could be used to identification of groundwater potential (Alile et al., 2010), groundwater level (Ranjy Roodposhti et al., 2019), depth bed rock and aquifer thickness (Gupta et al., 2015), separation of water bearing and dry karstic structures and sink-holes, and identification of faulted and fractured zones (Saribudak & Hawkins, 2019), and karstic anomalies (Bharti, 2016; Prins et al., 2018).

## 2 Material and Methods

### 2.1 Geological Setting

The study area is located in the surroundings of Izeh area, in Khuzestan Province, southwest Iran (Fig. 1), within Zagros Ranges. The area consists of a very gently dipping Oligocene–Miocene age limestone and marly limestone, Asmari Formation in Chal Khoshk Anticline and Naale Asbi

syncline (Fig. 2). The elevation of Asmari formation in contact with alluvium ranges from 850 to 900 m absolute sea level (ASL), and the depth of karst water table is 50–100 m, respectively. The Asmari Formation in Izeh polje consisting of limestone, dolomites, and marly limestone, reaching thicknesses of greater than 250 m. Based on the results obtained by time series analysis of karst aquifers in Izeh area (Nassery et al., 2013), Asmari karst was identified as an aquifer with high storage capacity as well as a dominated baseflow and the karstification of Asmari Formation bring about a dual porosity karst aquifer, where fracture and conduit porosity coexist. Although the existence of cavities in unsaturated zone of the Asmari limestone is evident, the conduit network in the lower part of the karst aquifer is poorly developed, and groundwater is stored in a matrix with a high storage capacity (Nassery et al., 2013). The average annual precipitation at Izeh area is 420 mm in the 30-years period, which is considered as a semi-arid climate in the Middle East.

In hydrogeological terms, the aquifer consists of a mature karstic system with a low high hydraulic gradient, suggesting very high permeabilities. Dissolution of the carbonate rocks of the Asmari Formation has resulted in a presence of unconfined aquifers. Over 20 boreholes have been drilled in karstic aquifer of Izeh for supplying the residence with drinking water. Despite the common use of geology for improving the siting of boreholes, some of the drilled holes does not deliver enough water to be equipped.

### 2.2 Data Collection

In order to exact determination of the water well drilling locations in high groundwater potential areas, the geoelectrical operation done in 98 VES of Schlumberger and two profiles using dipole–dipole and Wenner–Schlumberger arrays (Fig. 2). The arrays were chosen based on the previous works indicating good resolution of epikarst fracture and caves with these configurations. Although any available electrode array can be applied in measurements, the most frequently used are: the Wenner, Wenner–Schlumberger, dipole–dipole, and pole–pole arrays. The Wenner array must be used for the shallowest depth in a multielectrode system, and the Schlumberger array is used for all other depths. Therefore, the Schlumberger array is usually used in combination with the Wenner array. In particular, the Schlumberger array and the dipole–dipole arrays, can achieve a better lateral coverage for deeper targets, and they can penetrate to greater depths in the same multielectrode system. The Schlumberger array and the dipole–dipole array are significantly more sensitive to noises and surface heterogeneities due to a short spacing between potential electrodes. Resistivity data were gathered in two lines with different



**Fig. 1** Location of study area, southwest Iran

electrode spacing of dipole–dipole configuration 20 and 40 m for Jamushi and Tasisat sites (Fig. 2), respectively.

The data were collected using the IP-RS geoelectric instrument of ARES mark, manufactured by GF Instruments of Czech Republic, with a power of 850 W. In order to obtain accurate induced polarization data, a costrel was used which filled with  $\text{CuSO}_4$  solution containing an electrode. In order to measure IP, the instrument setting was defined by for 10 windows and increments of 0.02, 0.04, 0.08, 0.16, and 0.32 s (each interval for two windows). However, the presence of industrial and telecommunication noises could have a significant impact on IP. With increasing depth, IP measurement is problematic due to its sensitivity.

### 2.3 Methodology

The interpretation result of a resistivity sounding dataset is demonstrated in one-dimensional (1-D) using IPI2win, form that includes resistivities and thicknesses of the subsurface layers. To interpret the data from such a survey, it is normally assumed that the subsurface consists of horizontal layers and it does not take into account lateral changes in the layer resistivity (Fig. 3). The pattern of the curves changes suddenly in terms of the karstification degrees which generally are associated with lithologic changes of limestones and tectonic structures like fractures. VES apparent resistivity data were inverted assuming layered earth models to



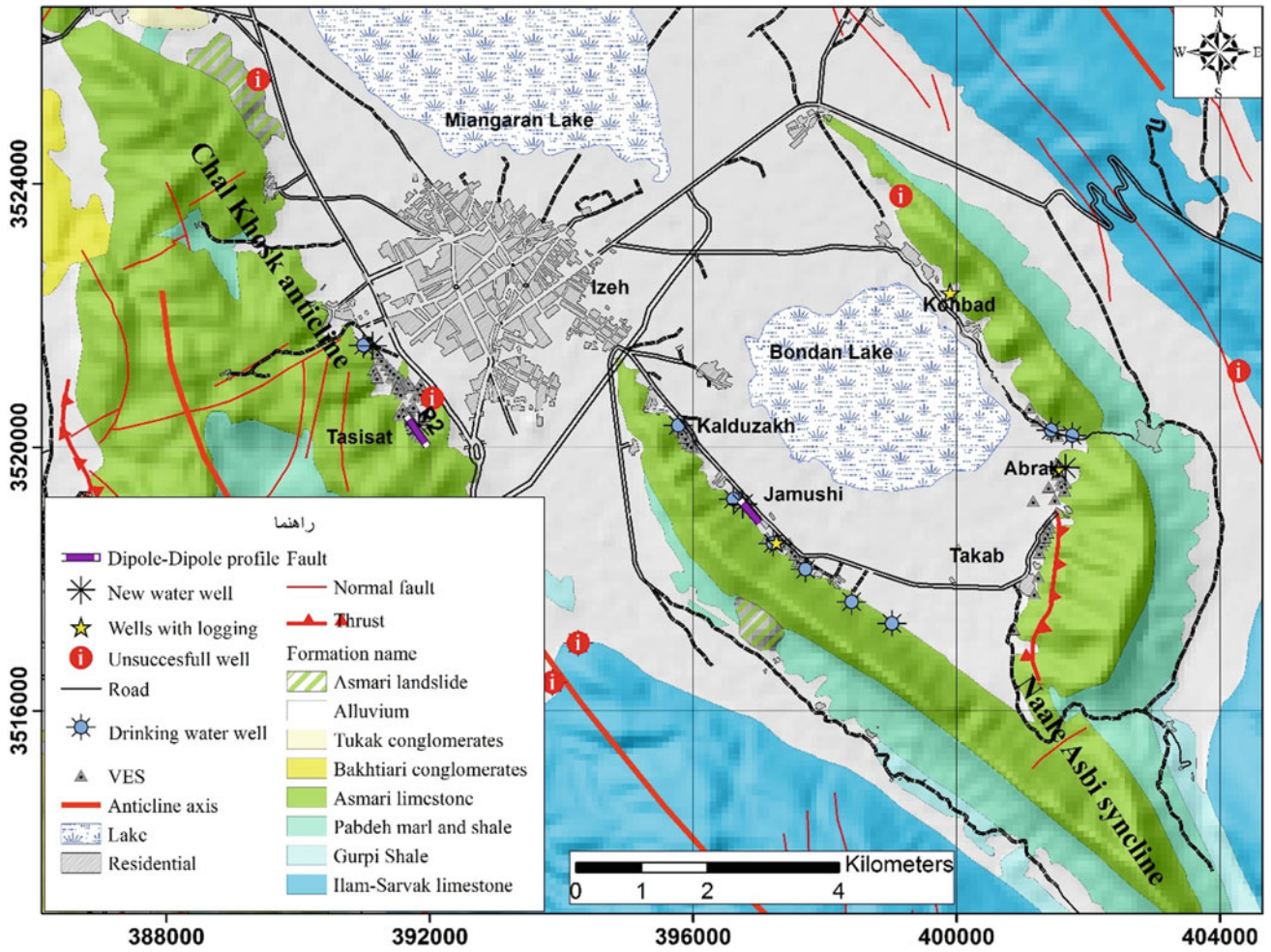
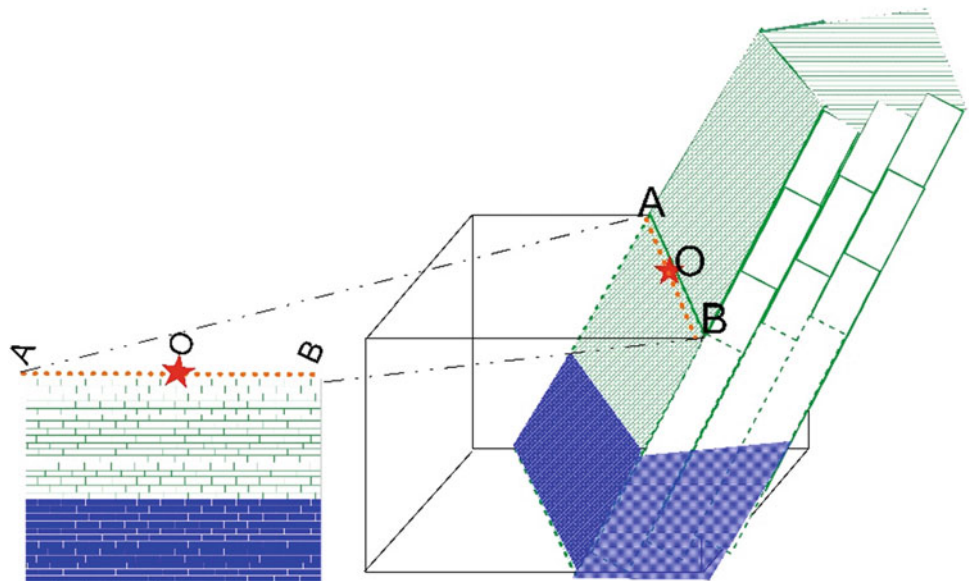


Fig. 2 Geological map of study area

Fig. 3 Schematic model explanation using one-dimensional inverse modeling of electrical resistivity sounding for sloping carbonate layers by expanding the electrode array parallel to the direction of bedding plane of limestone layers



determine the thicknesses and true resistivities of the successive strata below each VES site.

The ERT method is used to determine the electrical resistivity distribution of the subsurface. Resistivity of the limestone rocks is linked to several parameters including type of limestone, cavity, water content, marl layers, electrical conductivity of water, and thickness. Because of different respective electrical resistivities in karstic areas, the ERT method provides useful results on the geometry of bedrock and aquifer. In this ERT survey, after inversion of the field data, the method provided a two-dimensional (2D) resistivity model of a section of the underground. Field data processing was performed with Res2DInv software. The parameters used in the inversion were the same for both of profiles, and topography was taken to normalize profile elevations to the actual ground surface. A robust algorithm was chosen for inversion, because it provides more net changes in resistivity between different parts of the section. However, care must be taken when studying the final sections, because the geometry and boundaries of the structures are not always clearly identified and may be influenced by changes in resistivity due to rocks outside the plane of the section. The interpreted sections must be understood as an indication of the approximate location of the lithological boundaries, and not as its true geometry. The interpretation of the resistivity sections for all the ERT profiles has been drawn with the help of the correlation between the resistivity and IP with the lithology along with the hydrogeologic data, and taking into account the continuity of the resistivity values at the crossing of the profiles. Overall, a very complicated structure is interpreted with the presence of dry and wet limestones, cavities, and marly layers interbedded with carbonates. Finally, three locations were proposed for drilling of water wells in the Izeh karst area.

### 3 Results

The VES surveys have been carried out in 98 resistivity sounding using the Schlumberger array with the current electrode separations of maximum 1000 m. In addition, the resistivity profiling surveys were carried out along 2 lines using dipole–dipole with 20 and 40 m electrode spacing and maximum  $n = 12$  for Jamushi and Tasisat sites, respectively, and Schlumberger and Wenner–Schlumberger arrays with horizontal distance between VES ranges from 40 to 80 m.

1D modeling and interpretation of the VES data were made using IPI2win software. The depth of water table, thickness of the layers, and the true resistivity of the dry and water bearing limestones, marly limestones, and fractured limestones were determined based on the VES curves and the interpretation. Then the interpretation results of all sounding points have been summarized to selection of best

sites for 2D profiling and determination of best location of drilling of water wells. For example, the VES interpretation of Abrak water well in the southeast Naale Asbi syncline (Fig. 2) is compared with the gamma, SP, and resistivity logs (Fig. 4). Interpretation and translation of the Logging of Abrak water well has been carried out in order to distinguish marly limestones from water bearing limestones, fractured zones, and identify high-yield cavities. The videometry operation from different depths of the open borehole has been used to validate the interpretation of logs. An interpretation of the Schlumberger VES adjacent to the Abrak well is also provided alongside the various logs (Fig. 4f). The electrical resistivity in the logs of Abrak borehole varies from 73 to 283 ohms-m, while the apparent electrical resistivity in the VES ranges from 50 to 227 ohms-m. The water level is at a depth of 50 m in the Abrak well, while the IPI2win interpretation indicates the depth of the water at 79 m. In the interpretation of the VES, the resistivity of dry and water bearing limestone is 425 and 93 ohms-m, respectively. Of course, during the drilling, the well encounters the water at a depth of 72 m and then the water table rises to a depth of 50 m after termination of drilling, which indicates the karst aquifer is confined. According to borehole videometry, there is a fully open karst cavity at 110–113 m in which a large volume of water flows, it is not detectable in the logs and VES curve. Based on the well logging, three zones with high yield were identified at depths of 58–61 m, 90–93 m, and 98–105 m. The continuous decrease in gamma and electrical resistivity indicates the presence of fractured limestone zone and the increase in SP indicates a rapid groundwater flow in the cavities and fractures from 110 to 130 m depth of the Abrak water well, which has an indicators of a high-yield well.

The inversion modeling results of the resistivity and IP profiling data along two lines, Jamushi in Naale Asbi syncline and Tasisat in Chal Khoshk anticline (Fig. 2), represented by tomography sections (Figs. 5 and 6), imply various resistive and conductive zones in the subsurface. The various lithological zones marked in the resistivity and IP sections represent the subsurface complexity of the Izeh karstic limestones. 2D resistivity and IP surveys clearly show the dry voids in Asmari formation as well as resistivity contrasts between the matrix limestones and the cavity. In the resistivity images, cavities are represented as high resistivity zones. As all of these cavities are above the water table, the high resistivities may be due to the lack of infilling sediments.

The results of the geoelectrical tomography of Asmari limestone in Izeh study area show the dry limestones have high electrical resistivity (between 200 and 1000 ohms-m) and low IP (lower than 3 Mv%V), while the layers become water bearing, the electrical resistivity decreases (between 50 and 150 ohms-m) and IP values reside in a stable condition.

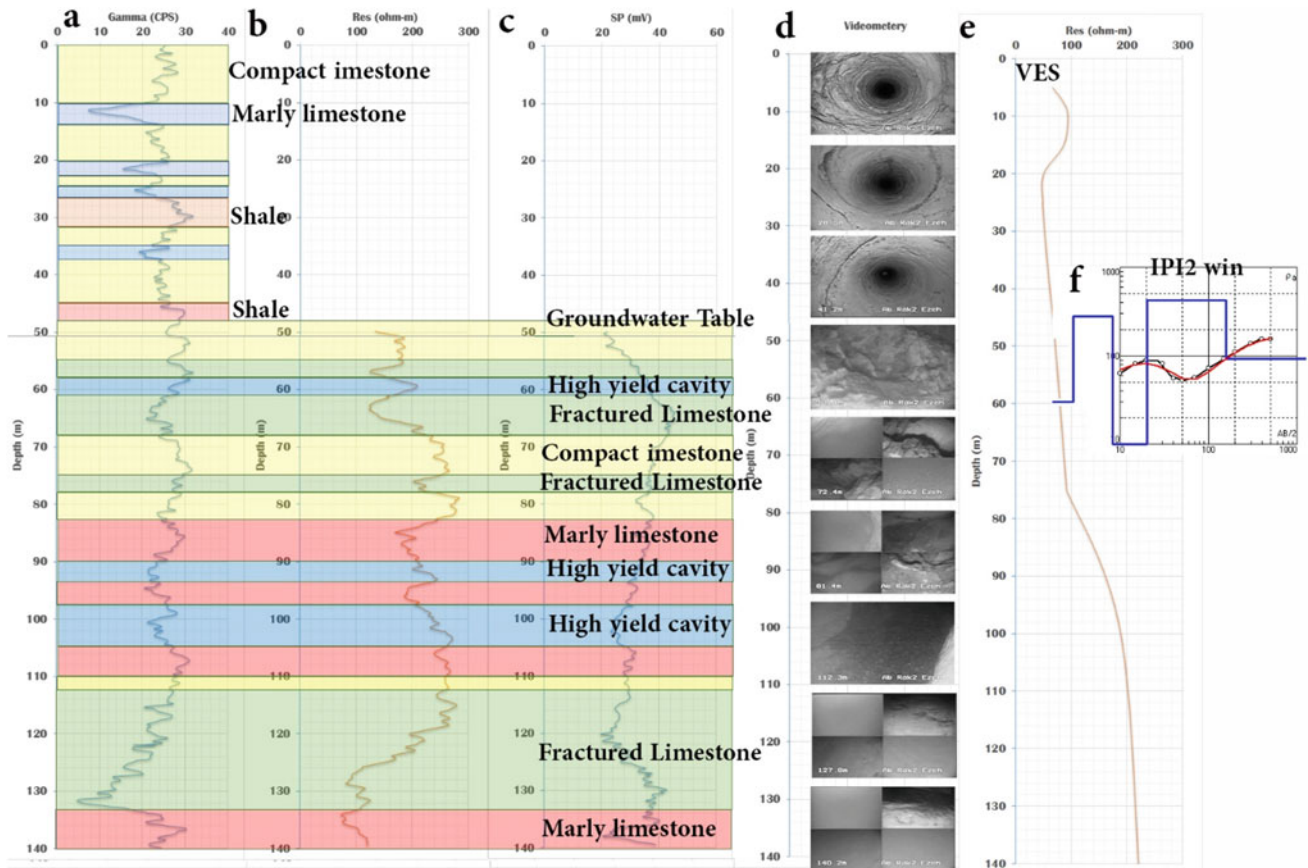


**Fig. 4** Comparison of well logging of **a** gamma, **b** resistivity, and **c** SP, **d** borehole videometry images, **e** VES curve of Schlumberger array, and **f** 1D interpretation of VES using IPI2win of Abrak water well, southeast Naale Asbi syncline

The dry cavities are characterized by very high electrical resistivity anomalies (ranging from 1500 to higher than 2000 ohms-m) with low IP values in the matrix of limestone with medium high electrical resistivity. The marl and marly limestone layers with low permeability can be detected by very low electrical resistivity (lower than 20 ohms-m) and high IP (higher than 10 Mv%V).

The results show Asmari formation has a developed karst with high yield. The results in the 2D geoelectrical tomography using a dipole–dipole array delineate the karst voids filled water to 70 m depth. The drilling of three high-yield water well (discharge between 60 and 100 l/s) and the low drawdown (0.5–1.5 m) in the karst of Izeh indicates the effectiveness of the integration of the applied exploration methods (Fig. 7).

## 4 Discussion

The tomography of electrical resistivity and IP have strongly confirmed each other especially in the dipole–dipole array, however, in some cases of Schlumberger array, the

deviations are seen in the depth that can arise due to the high sensitivity of the IP data in high depths. The Schlumberger and Wenner–Schlumberger tomography with high investigation depth (about 200 m) may show the different zones of karst aquifer but because of 50 m of VES spacing has not the detectability of cavities with lower than 10 m diameter.

According to Schrott and Sass (2008), geophysics methods could provide a continuous cover of subsurface information of the study area, the information which in turn could connect the data obtained from the bores to the neighboring areas in order to develop geological models.

ERT surveys may be performed applying different electrode configurations (dipole–dipole, Schlumberger, Wenner, etc.) depending on the subsurface, the depth of investigation, the sensitivity to vertical and horizontal changes in the subsurface resistivity, the horizontal data coverage and the signal strength (Loke and Barker, 1995). Resistivity data are usually interpreted assuming one-dimensional (1D) or two-dimensional (2D) models.

As a usual difficulty of ERT, we often need to determine which of the many existing electrode configurations would respond best to the material changes in karst features. Each



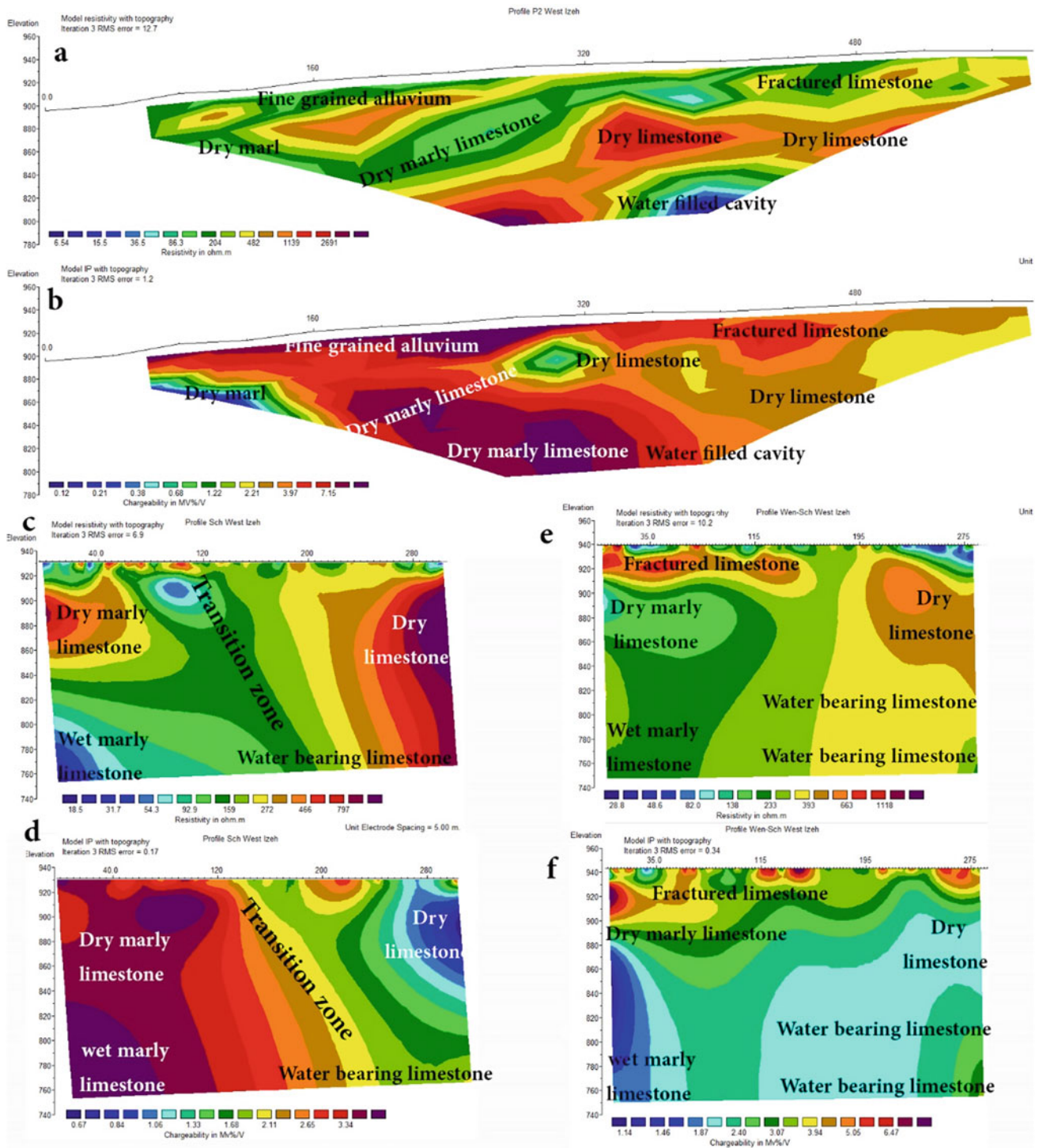


**Fig. 5** 2D modeling and interpretation results of the resistivity profiling data along tomograms of **a** electrical resistivity and **b** IP of dipole–dipole array; **c** electrical resistivity IP of Wenner–

Schlumberger; **d** electrical resistivity and **e** IP of array of Schlumberger array in Asmari limestones of Chal Khoshk anticline (site of Tasisat)

array has distinctive advantages and disadvantages in terms of depth of investigation, sensitivity to horizontal or vertical variations, and signal strength. Setting aside the effects of “noise” (i.e., the effects of near surface local variations in

resistivity which in themselves may place a limit on the detect ability and resolution of karst features), application of an inappropriate array type will affect their recognition in the pseudosections.

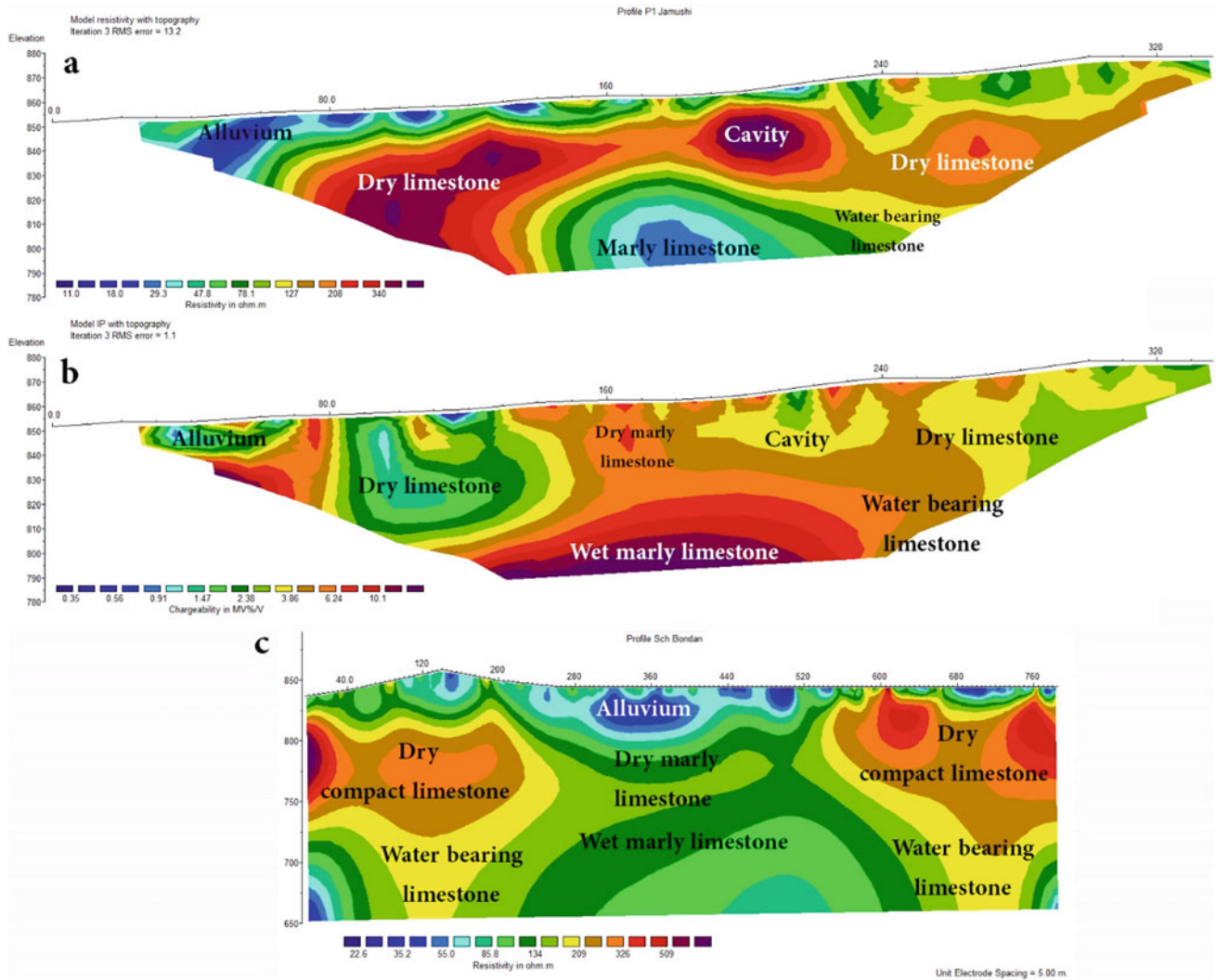


**Fig. 6** 2D modeling and interpretation results of the resistivity profiling data along tomograms of **a** electrical resistivity and **b** IP of dipole–dipole array; **c** electrical resistivity of Schlumberger array in Asmari limestones of Naale Asbi syncline (site of Jamushi)



**Fig. 7** Photograph of the pumping test of the new drilled water wells in Izeh areas at December 2019 (the sites were determined using the ERT of dipole–dipole array)

The dipole–dipole array is very sensitive to horizontal changes in resistivity, but relatively insensitive to vertical changes in the resistivity and IP. The dipole–dipole array is convenient in detection vertical structures, e.g., shafts and cavities, but relatively inefficient in depicting horizontal structures, e.g., limestone and marly limestone layers. The median depth of investigation of this array depends on both the dipole spacing and the dipole separation factor that are normally defined by “*a*” and “*n*” symbols, respectively. In the study area due to the existence of bedding with a high dip, the water table can be detected by performing VES surveys using Schlumberger and Wenner–Schlumberger arrays. Due to low sensitivity of the Schlumberger and Wenner–Schlumberger arrays to lateral heterogeneities, and also high efficiency of the dipole–dipole array, especially its moderate depth of penetration, low EM coupling between the current and potential circuits and high sensitivity to horizontal changes in resistivity (Sharifi et al., 2014), the combination of these arrays for VES and electrical resistivity and IP profiling, respectively, can lead to an intelligence for subsurface in the study area.

## 5 Conclusion

To achieve the desired results of groundwater explorations in the karstic areas and determination of exact location for the drilling of water wells, the geoelectrical field work using the combination of the arrays and methods (especially electrical resistivity and IP) can be used with low cost. IP method can assist in complying with the electrical resistivity method in the separation of water bearing limestone and marly limestone layers, one of the reasons for ambiguity in the interpretation of electrical resistivity tomography. The methodology proposed in this study is potentially a very powerful tool for investigating karst aquifers where conventional hydrogeological methods (e.g., pumping tests and groundwater potential mapping using RS/GIS) are not available or difficult to perform. The combination of a proved geoelectrical techniques (i.e., ERT and IP) to investigate the underground geological structure, with powerful arrays such as dipole–dipole and Wenner–Schlumberger, allows us to detect best location for drilling of water wells.

In the study area, we applied our proposed methodology to the Izeh karst area where there were no reliable hydrogeological information, such as information on the groundwater table, and it provides us three sites for drilling of water

wells, which drilling results are in accordance with our findings.

## References

- Aizebeokhai, A. P., & Oyeyemi, K. D. (2014). The use of the multiple-gradient array for geoelectrical resistivity and induced polarization imaging. *Journal of Applied Geophysics*, *111*, 364–376.
- Alile, O. M., Ujuanbi, O., & Evbuomwan, I. A. (2010). Geoelectric investigation of groundwater in Obaretin Iyanomon Locality, Edostate. *Nigeria. Geology and Mining Research*, *3*(1), 13–20.
- Bharti, R. (2016). The vertical electrical sounding (VES) procedure to delineate potential groundwater aquifer in Guna Madhya Pradesh. *Imperial Journal of Interdisciplinary Research*, *24*, 253–256.
- Dahlin, T. (1996). 2D resistivity surveying for environmental and engineering application. *First Break*, *14*, 275–283.
- Gupta, G., Patil, J. D., Maiti, S., Erram, V. C., Pawar, N. J., Mahajan, S. H., & Suryawanshi, R. A. (2015). Electrical resistivity imaging for aquifer mapping over Chikotra basin, Kolhapur district. *Maharashtra. Environmental Earth Sciences*, *73*(12), 8125–8143.
- Loke, M. H., & Barker, R. D. (1995). Least-squares deconvolution of apparent resistivity pseudosections. *Geophysics*, *60*(6), 1682–1690.
- Nassery, H. R., Alijani, F., & Nakhaei, M. (2013). The comparison of hydrodynamic characteristics of karst aquifers: Application on two karst formations in Zagros (Asmari and Ilam-Sarvak), southwest Iran. *Arabian Journal of Geosciences*, *7*(11), 4809–4818.
- Oldenburg, D. W., & Li, Y. G. (1999). Estimating depth of investigation in DC resistivity and IP surveys. *Geophysics*, *64*, 403–416.
- Prins, C., Thuro, K., & Krautblatter, M., (2018). The effectiveness of an inverse Wenner-Schlumberger array for geoelectrical karst reconnaissance, on the Swabian Alb high plain, new line Wendlingen-Ulm, Southwestern Germany. In *IAEG/AEG Annual Meeting Proceedings*, San Francisco, California, vol 3, 115–122.
- Ranjy Roodposhti, H., Hafizi, M. K., Soleymani Kermani, M. R., & Ghorbani Nik, M. R., (2019). Electrical resistivity method for water content and compaction evaluation, a laboratory test on construction material. *Journal of Applied Geophysics*, *168*, 49–58.
- Samanovac, F., & Alvanja, S. D. (2007). Determination of resolution limits of electrical tomography on the block model in a homogenous environment by means of electrical modeling. *Rudarsko Geološko Naftni Zbornik*, *19*(1), 47–56.
- Saribudaka, M., & Hawkins, A. (2019). Hydrogeophysical characterization of the Haby Crossing fault, San Antonio, Texas, USA. *Journal of Applied Geophysics*. <https://doi.org/org/10.1016/j.jappgeo.2019.01.009>
- Schrott, L., & Sass, O. (2008). Application of field geophysics in geomorphology: Advances and limitations exemplified by case studies. *Geomorphology*, *93*, 55–73.
- Sharifi, F., Arab-Amiri, A. R., & Kamkar-Rouhani, A., (2014). Karstic water exploration using the Schlumberger VES and dipole–dipole resistivity profiling surveys in the Tepal area, west of Shahrood, Iran. *Journal of Mining & Environment*, *5*(1), 1–12.
- Stummer, P., Maurer, H., & Green, A. G. (2004). Experimental design: Electrical resistivity data sets that provide optimum subsurface information. *Geophysics*, *69*(1), 120–139.





# A Comparative Study on Regional Drought Characterization Using Estimated Drought Indices in Conjunction with Trend Analysis in Peninsular India

M. P. Akhtar , L. B. Roy, and Abhishek Sinha

## Abstract

The objective of the present study is the characterization of drought conditions in two important peninsular states of India namely Tamil Nadu and Karnataka through assessment of meteorological drought indices namely drought index (DI), Palmer index (PI), and standardized precipitation index (SPI). For this, monthly and yearly data of precipitation and temperature have been considered for 110 years (1901–2010). Precipitation deficit conditions have been estimated and compared for both regions using annual rainfall classification thresholds. The annual variability of rainfall and associated trend were estimated using Mann-Kendall test and comparative analysis was done to assess the regional variation during the last 110 years. Comparative study on results implied that drought characterization using SPI may amply facilitate the standardization of threshold classification for severity and frequency that was good agreement with observed events. The application of trend detection framework resulted in the identification of significant trends in those districts which were reported to be drought prone regions. Study amply suggested that drought vulnerability in Tamil Nadu was relatively more than that of Karnataka region depending upon the number of dry and wet years in terms of SPI threshold values and areal extend within 110 years of study period however in terms of severity and number of occurrence, Karnataka was more vulnerable. Analysis based on droughts indices suggests that SPI is simple to evaluate and may relatively more meaningful and conclusive in terms of decision

making for the study region if compared with other indices.

## Keywords

Trend analysis • Drought • Drought characterization • Drought indices • Standard precipitation index • Vulnerability map

## 1 Introduction

Drought may be defined as deficient precipitation for long period inducing negative or adverse impact on socioeconomic activities in a region (Warrick, 1975). Drought in different regions may have classifications according to their precipitation pattern. As per Indian Meteorological Department (IMD), drought in region may be defined as the rainfall shortfall greater than 26% of its long term normal in that region. Furthermore, it can be classified as moderate drought if the rainfall deficiency varies between 26 and 50% of long term normal in that area. Similarly, 50% or less than long term normal is considered as *severe* drought condition. Drought may be considered one of the major reasons for desertification. Rainfall is one of the most important climatic indicators that primarily determines different drought condition depending upon its long-term intensities, distribution, and frequency. Any shortage of rainfall directly influences the agriculture and running economy (Mooley & Parthasarathy, 1984).

Numerous studies have been carried out and reported for analysis of rainfall trend and drought indices using different methodologies for regions with distinct climatic variability. De et al. (2005) presented a factual and a brief review of the extreme weather events that occurred in India during the 100 years (1991–2004). Severe drought conditions were also included under extreme condition for analyzing socioeconomic impact on human society. Pai et al. (2011) compiled

M. P. Akhtar (✉)  
Department of Civil Engineering, School of Civil & Chemical  
Engineering (SCCE), Manipal University, Jaipur, 303007, India  
e-mail: [parwez.akhtar@jaipur.manipal.edu](mailto:parwez.akhtar@jaipur.manipal.edu)

L. B. Roy · A. Sinha  
Department of Civil Engineering, National Institute of Technology  
Patna, Patna, 800015, India

districtwide drought climatology of the southwest monsoon season over India based on drought indicator estimation namely standardized precipitation index (SPI). Yosuf et al. (2013) attempted characterization of drought properties with bivariate copula analysis. Shah et al. (2015) have reported drought index computation using standard precipitation index method for Surat District in Gujrat (India). Pathak and Dodamani (2016) reported study on comparison of two chosen hydrological drought indices namely stream flow drought index (SDI) and standardized runoff index (SRI). To obtain these indices, 36 years (1972–2007) of daily discharge data measured in Ghataprabha river basin (a sub-basin of Krishna river) were considered. Huang et al. (2016) worked out on drought forecasting using SPI and effective drought index (EDI) under Representative Concentration Pathway (RCP) –8.5 Climate Change Scenarios for Langat River Basin, Malaysia. Langat et al. (2017) investigated temporal variabilities and rainfall trend and discharges of Tana River Basin in Kenya using Mann-Kandell nonparametric tests. Numerous analytical works related to trend analysis for climatic parameters of regional hydrological time series were presented in past such as Hirsch et al. (1982), Coles (2001), Yue et al. (2002), Yue and Hashino (2003), Modarres and Da Silva (2007), Longobardi and Villani (2010), Ghanem (2011), Jain and Kumar (2012), Duhan and Pandey (2013) Da Silva et al. (2015), and Mohorji et al. (2017).

Similarly, drought assessment for arid and semi-arid regions across the Globe has been carried out continuously to develop efficient decision support systems for regional ground and surface water management and planning. Palmer (1965) evolved index to identify drought condition with a statistical correlation with mean and standard deviation of mean. Gibbs and Mehar (1967) worked out on rainfall decile as drought indicator. Subsequently McKee et al. (1993) devised more meaningful indicator namely standard precipitation indicator to analyze and prediction regional drought conditions derived from meteorological data. Hammori and El Naqa (2007) deployed remote sensing data and GIS tools to assess drought condition in Amman-Zarqa Basin of Jordan. Kumar et al. (2018) analyzed regional drought characteristics namely frequency, severity, and occurrence of meteorological droughts in arid and semi-arid regions of northwestern India and identified region-specific event years with extreme drought severity. Mallya et al. (2016) findings amply facilitated insight, looking into detailed investigation on drought severity and recurrence with estimated drought indices with apparent drought vulnerability in peninsular India. Such studies need to be considered to get more meaningful results for planning regional drought mitigation measures. Many works have been reported on drought analysis for regions with distinct climatic variability. More recently, numerous related works have been reported. Some

of them are Oguntunde et al. (2017a), (2017b), Musafa and Rehaman (2018), Quenum et al. (2019), Al Bakri et al. (2019), and Al adaileh et al. (2019). Al adaileh et al. (2019) attempted evolvement of a drought adaption management system for ground water resources based on combined drought index and vulnerability analysis. Furthermore, several studies have also been reported on comparative analysis of drought indices with an objective to get better insight into their suitability and accuracy of assessment for chosen study areas, such as Gutmann (1998), Sims et al. (2002), Dubrovsky et al. (2006), Bonsal and Regier (2007), Krysanova et al. (2008), Paulo and Pereira (2006), Zhai et al. (2009), Paulo et al. (2012), Hughes and Saunders (2002), Liu et al. (2013), Jacobi et al. (2013), and Al adaileh et al. (2019). These reported works were carried out exclusively for chosen study areas. It can be inferred that performance and efficiency of drought indicators depend on many factors such as climatic variability, geography and initial soil moisture conditions. It can further be inferred that a drought assessment or quantification should not rely on a single drought indicator rather it should preferably be done with multiple indicators to get better insight and realistic drought assessment and suitability. Bonsal and Regier (2009) and many others pointed out that no universally accepted definition for drought exists. Numerous indices have been deployed to quantify its severity. Meteorological approaches range from indices that only consider precipitation e.g., SPI, (Mackee, 1993, World Meteorological Organization, 2012) to more complex methods that incorporate a water balance approach using precipitation and potential evapotranspiration such as PDI (Palmer, 1965).

Two most water stressed states of southern India are Tamil Nadu and Karnataka. Tamil Nadu is the eleventh largest state of India whereas Karnataka has the second largest rain-fed area in India after state of Rajasthan. Only 35–45% of rainwater is presently used to grow dryland crops in the Karnataka. Hence, there is huge scope for improving rainwater harvesting and efficient use of it for rain-fed crops to tackle drought condition in such arid regions, provided an adequate assessing severity and recurrence of drought condition with spatial distribution is done through estimating and analyzing appropriate metrological drought indicators in conjunction with trend analysis of historical precipitation data.

Furthermore, both regions of Indian peninsula were chosen for comparative analysis of drought situations keeping in view of the prevailing water crisis between them. Tamil Nadu is facing acute water shortage due to erratic rainfall and depleting reservoir levels. The main source of water is Cauvery River Basin which lies mostly in Karnataka region. Both states have been locked—long dispute over sharing of Cauvery Water. The conflict has continued since long and impasse is persisted (Anand, 2007, Gebert, 1983; Pani, 2009). A lack of multilevel, intersectoral, and



participative approaches, on the one hand, has led to inadequate conditions in water management and water use in both states (Ferdin et al., 2010). This study will facilitate a better scientific insight into prevailing issue with respect to meteorological drought situation and relative regional water scarcity for comparison and help decisionmakers to arrive at consensus solution that may lead to equitable share of Kaveri Water among both states.

In view of the above, the objectives of the present work are set as follows.

1. To investigate the monotonic trend of rainfall and comparison thereof for Tamil Nadu and Karnataka regions with a period of 110 years using nonparametric methods such as Mann-Kendall and Sen's Slope tests.
2. To analyze the annual series of the available historical climatic data and assessment of severity distribution with comparison in both states using estimated drought indices namely drought index (DI), Palmer drought index (PDI) and standard precipitation index (SPI) and development of vulnerability map-based chosen drought indicator.

To begin with, this paper first discusses indicators and methodology those used and adopted for assessing severity and trend analysis of climate parameters.

## 2 Material and Methodology

### 2.1 Trend Analysis of Annual Rainfall by Using Mann-Kendall's Test (Mann, 1945; Kendall, 1975)

The Mann-Kendall test is applied where the data values  $x_i$  of a time series can be assumed to obey the model as enumerated below (Eq. 1) (Alexander et al., 2006; Mann, 1945; Kendall, 1975)

$$x = f(t) + \varepsilon_i \quad (1)$$

where  $f(t)$  is a continuous monotonic increasing or decreasing function of time and the residuals  $\varepsilon_i$  is assumed to be from the identical distribution with zero mean. Hence, it is assumed that the variance of the distribution is temporally constant. The Mann-Kendall test statistic  $S$  is computed using the following formula (Eq. 2)

$$S = \sum_{k=1}^{n-1} \sum_{j=k+1}^n \text{sgn}(x_i - x_k) \quad (2)$$

where  $x_j$  and  $x_k$  are the annual values in years  $j$  and  $k$ ,  $j > k$ , respectively,  $\text{sgn}(x_i - x_k)$  can be given as shown in Eq. (3),

$$\text{sgn}(x_j - x_k) = \begin{cases} 1 & \text{if } x_j - x_k > 0 \\ 0 & \text{if } x_j - x_k = 0 \\ -1 & \text{if } x_j - x_k < 0 \end{cases} \quad (3)$$

If  $n \leq 9$ , the absolute value of  $S$  is compared directly to the theoretical distribution of  $S$  derived by Mann and Kendall (Gilbert 1987). A positive and negative value of  $S$  suggests an upward and downward trend, respectively. The minimum values of  $n$  with which these four significance levels may be arrived at are obtained from the probability Table 1 for  $S$ .

If  $n \geq 10$ , the normal approximation test is used. However, if there are several equal values in the time series, it may reduce the validity of the normal approximation when the number of data values is close to 10. At first, the variance of  $S$  is computed using Eq. (4) presented below, which takes into consideration of equals,

$$\text{VAR}(S) = \frac{1}{18} \left[ n(n-1)(2n+5) - \sum_{p=1}^q t_p(t_p-1)(2t_p+5) \right] \quad (4)$$

Here,  $q$  is the number of groups with equal values and  $t_p$  is the number of data values in the  $p$ th group. The values of  $S$  and  $\text{VAR}(S)$  are used to compute the test statistic  $Z$  as shown in Eq. (5)

$$Z = \begin{cases} \frac{S-1}{\sqrt{\text{VAR}}} & \text{if } S > 1 \\ 0 & \text{if } S = 1 \\ \frac{S+1}{\sqrt{\text{VAR}}} & \text{if } S < 1 \end{cases} \quad (5)$$

The presence of statistically significant trend is evaluated using the  $Z$  value. A positive or negative value of  $Z$  indicates an upward or downward trend, respectively. The statistic  $Z$  has a normal distribution. To test for an upward or downward monotone trend (a two-tailed test) at  $\alpha$  level of significance,  $H_0$  is rejected if the absolute value of  $Z$  is greater than  $Z_{1-\alpha/2}$ , where  $Z_{1-\alpha/2}$  is obtained from the standard normal cumulative distribution tables. Here, the tested significance levels  $\alpha$  are 0.001, 0.01, 0.05, and 0.1.

To estimate the true slope of an existing trend (as a change per year), the Sen's nonparametric method (Sen, 1968) is used. The Sen's method can be used in cases where the trend can be assumed to be linear.

**Table 1** Significance level verses required  $n$ 

Significance level $\alpha$	Required $n$
0.1	$\geq 4$
0.05	$\geq 5$
0.01	$\geq 6$
0.001	$\geq 7$

## 2.2 Drought Index

Numerous methods are applied to compute the drought events in terms of severity and occurrence drought. Drought index can be defined as shown in the following equation (IMD 1971 and NCA 1976)

$$DI = \frac{P - X}{SD} \times 100 \quad (6)$$

where  $P$  is annual precipitation,  $X$  is long-term mean and  $SD$  is standard deviation. The DI values may be categorized into four conditions namely *no drought*, *mild drought*, *moderate drought*, and *severe drought* conditions as shown in Table 2.

## 2.3 Palmer Drought Index (Palmer, 1965)

One of the most common indicators to assess drought is Palmer drought index (PDI) introduced by Palmer (1965) to simulate moisture content month by month and to compare its monthly anomalies at regions with different climatic conditions and seasons. PDI indicates the severity of wet or dry spell, the greater the absolute value more severe the dry or wet period. In this paper, the methodology adopted is based on Guttman (1998).

The PDI was designed to quantify metrological drought. It is a prolonged and abnormal moisture deficiency rather than an indicator of the affect of a prolonged weather anomaly.

The index is computed by carrying out monthly hydrological accounting for prolong time series. Then the coefficients depending upon the climatic condition of the study area were obtained. The monthly departures from normal conditions are converted to determine the amount of moisture required for normal weather during each month.

Climatically appropriate precipitation  $P_c$  for individual time scale (month) is,

$$P_c = \alpha P_{et} + \beta P_r + \gamma P_{ro} - \delta P_l \quad (7)$$

where

$P_{et}$  = Potential evapotranspiration

$P_r$  = Potential recharge

$P_{ro}$  = Potential runoff

$P_l$  = Potential loss.

And coefficients  $\alpha, \beta, \gamma, \delta$  are ratios of long-term mean quantities for evapotranspiration, recharge to potential recharge, runoff to potential runoff, and loss to potential loss, respectively.

The difference between the observed precipitation and  $P_c$  is monthly moisture anomaly. It is then multiplied by standardizing factor at different size (can be designed to account the variations in climate (using climatic parameters such as long-term mean precipitation and temperature in this case) and the product is called the moisture anomaly index  $Z$ .

Thus, Palmer drought index (PDI) for month  $t$  is then computed by,

$$PDI = 0.897PDI_{t-1} + 0.333Z_t \quad (8)$$

The values of the coefficients show that a current month's PDI is comprised of only one-third of the current month's precipitation deficit and almost nine-tenth of the previous month's PDI. In other words, the PDI for a given month contains a long-term memory of previous moisture content. The PDI calculation requires both precipitation and temperatures data as evapotranspiration estimation is also involved. Separate indices are calculated for wet and dry spells. The final PDI is either the wet or dry index.

The PDI has several advantages when compared with other drought indices. It considers soil moisture content at a monthly time interval along with meteorological data. It allows also spatial and temporal representation of historical

**Table 2** IMD classification of drought

Intensity of meteorological drought	% of departure from normal rainfall	Code
No drought	0.0 or above	M0
Mild drought	0.0 to -25.0	M1
Moderate drought	-25.0 to -50.0	M2
Severe drought	-50.0 or above	M3

Source (IMD, 1971 and NCA 1976)

droughts. There are some limitation also such that it: (a) simplifies soil representation (b) uses the simplified Thornthwaite method (Thornthwaite, 1978) for estimating potential evapotranspiration, and (c) does not take into account precipitation that falls as snow and snow cover (Krysanova et al., 2008) (Table 3).

The SPI values may be classified into seven categories namely extremely wet, very wet, moderately wet, near normal, moderately dry, severely dry, and extremely dry as shown in Table 4

### 2.4 Standardized Precipitation Index (SPI)

Standardized precipitation index (SPI), a tool derived by McKee et al. (1993), is a measure of meteorological drought. It is computed from the available rainfall data for a given duration. For transforming precipitation values to SPI values, following steps have been adopted (Guttman, 1999).

1. Transforming the mean of the precipitation values adjusted to 0.
2. Standard deviation of the precipitation is adjusted to 1.0.
3. Skewness of the existing data readjusted to zero.
4. SPI values now may be interpreted with mean as 0 with standard deviation 1.0.
5. Mean of precipitations can be computed as follows

$$\text{Mean}(\bar{X}_{im}) = \frac{\sum(X_{ij})}{N} \tag{9a}$$

where  $N$  = Number of precipitation observations, where  $X_{ij}$  is seasonal precipitation at the  $i$ th rain gauge station and the  $j$ th observation,  $\bar{X}_{im}$  is long-term seasonal mean and  $s$  is the standard deviation for precipitation dataset is computed as,

$$s = \sqrt{\frac{\sum(X_{ij} - \bar{X}_{im})^2}{N}} \tag{9b}$$

6. The skewness of the given dataset is computed as

$$\text{Skew} = \frac{1}{(N - 1)(N - 2)} \sum \frac{(X_{ij} - \bar{X}_{im})^3}{s} \tag{9c}$$

7. The precipitation values are converted to lognormal values in terms of statistical value  $U$  as

$$\text{Long term mean} = \ln(\bar{X}_{im}) \tag{9d}$$

$$U = \bar{X}_{im} - \frac{\sum \ln(\bar{X}_{im})}{N}$$

$$\text{Shape parameter} = \beta = \frac{1 + \sqrt{1 + \frac{4U}{3}}}{4U} \tag{9e}$$

$$\text{Scale parameter} = \alpha = \frac{\bar{X}_{im}}{\beta} \tag{9f}$$

10. Equations (9a)–(9f) are computed using built-in functions in Excel software. The resulting parameters are then used to find the cumulative probability of observed precipitation events. The cumulative probability is given by

$$G(x) = \frac{\int_0^x t^{\alpha-1} e^{-\frac{t}{\beta}} dt}{\beta^\alpha \Gamma(\alpha)} \tag{10}$$

**Table 3** Drought classification based on SPI values

Classification	Extremely wet (EW)	Very wet (VW)	Moderately wet (MW)	Near normal (NN)	Moderately dry (MD)	Severely dry (SD)	Extremely dry (ED)
SPI value	$\geq 2$	1.5–1.99	1–1.49	–0.99 to 0.99	–1.0 to –1.49	–1.5 to –1.99	$\leq -2$

Source (Shah et al., 2015; Zhai et al., 2009; Paulo Ana & Pereira, 2006)

**Table 4** Drought classification based on PDI values

Classification	Extremely wet (EW)	Very wet (VW)	Moderately wet (MW)	Slightly wet (SW)	Incipient wet spell (IWS)	Near normal (NN)	Incipient dry spell (IDS)	Mild drought (MiD)	Moderate drought (MoD)	Severe drought (SD)	Extreme drought (ED)
PDI value	4.0 or more	3.0–3.99	2.0–2.99	1.0–1.99	0.5–0.99	0.49 to –0.49	–0.5 to –0.99	–1.0 to –1.99	–2.0 to –2.99	–3.0 to –3.99	–4.0 or less

Source (Paulo and Pereira, 2006; Zhai et al., 2009)

Since the gamma function is undefined for  $x = 0$  and a precipitation distribution may contain zeroes, the cumulative probability may be considered as

$$H(x) = q + (1 - q)G(x) \quad (11)$$

The cumulative probability  $H(x)$  is then transformed to standard normal random variable  $Z$  (mean = 0, standard deviation: 1) values and considered the SPI values as suggested by Edward and McKee (1997).

10. The approximate conversion as per Abromowitz and Stegun (1965) is adopted as

$$Z = \text{SPI} = - \left[ t - \frac{C_0 + C_1 t + C_2 t^2}{1 + d_1 t + d_2 t^2 + d_3 t^3} \right] \quad (12a)$$

for  $0 < H(x) \leq 0.50$  and

$$Z = \text{SPI} = + \left[ t - \frac{C_0 + C_1 t + C_2 t^2}{1 + d_1 t + d_2 t^2 + d_3 t^3} \right] \quad (12b)$$

for  $0.5 < H(x) \leq 1.00$  and  
where,

$$t = \sqrt{\ln \left( \frac{1}{H(x)^2} \right)} \text{ for } 0 < H(x) \quad (13a)$$

$$t = \sqrt{\ln \left( \frac{1}{H(x)^2} \right)} \text{ for } 0 < H(x) \leq 1 \quad (13b)$$

where  $C_0 = 2.515517$ ,  $C_1 = 0.802583$ ,  $C_2 = 0.010328$ ,  $D_1 = 1.432788$ ,  $D_2 = 0.189269$ ,  $D_3 = 0.001308$ .

The SPI values may be classified into eleven categories namely *extremely wet (EW)*, *very wet (VW)*, *moderately wet, slightly wet (SW)*, *incipient wet spell (IWS)*, *near normal (NN)*, *incipient dry spell (IDS)*, *mild drought (MiD)*, *moderate dry (MoD)*, *severely dr (SD)*y, and *extremely dry (ED)* as shown in Table 3.

### 3 Study Area and Data Used

Tamil Nadu in southeastern region of India and is the eleventh largest state of India with having geographical area of 130,058 km<sup>2</sup> (<https://www.walkthroughindia.com/offbeat/top-15-largest-states-india-geographical-area/>) extending its length and breadth approximately between 8° N-14° N, 76° E-81°E. Tamil Nadu is having the third largest costal line of 940 km after Gujarat and Andhra Pradesh ([https://en.wikipedia.org/wiki/Coastline\\_of\\_Tamil\\_Nadu](https://en.wikipedia.org/wiki/Coastline_of_Tamil_Nadu)). It is located

on the inward side of the Western Ghats resulting in relatively low rainfall compared to outward coastline of Western Ghats of Kerala state. Hence, drought-like situation is prevalent on the part of Western Ghats which lies in western Tamil Nadu, whereas Karnataka is a landlocked state situated in southern India. It is having longitudinal extent of 74°E to 78°30'E and latitudinal extent of 11°30'N to 18°30'N. It is the seventh largest state of India approximately 191,791 km<sup>2</sup> (<https://www.walkthroughindia.com/offbeat/top-15-largest-states-india-geographical-area/>).

The southernmost point of India (Indira Point) in Kanyakumari is also located in Tamil Nadu. Figure 2 representing mean annual rainfall and temperature suggests that Karnataka has relative higher annual rainfall in comparison of Tamil Nadu with respect to districtwise distribution (Fig. 2) but temperature pattern for those districts is distinct. The location map of study region that contains both states is represented as Fig. 1.

Monthly precipitation and temperature data of all districts covering a period of 110 years (1901–2010) for Tamil Nadu and Karnataka were obtained from India Water Portal (<https://www.indiawaterportal.org/metdata/>). A prewhitening procedure is done before applying these data for further statistical analysis namely Mann-Kendall's test.

## 4 Results and Discussion

### 4.1 Rainfall Trend Analysis

#### 4.1.1 Annual Rainfall Classification

Data analysis was worked out in steps to get better insight into drought conditions considering rainfall data for 110 year for both regions. Monthly rainfall gauge data for each district or climatic division of both regions were acquired and annual rainfall were computed for 110 years. Rainfall dataset for 110 years for Tamil Nadu and Karnataka was segregated according to regional rainfall classification suggested by Subramanya (2013) and presented in Table 5 in order to understand the relative wetness status of two study regions. A number of years within study time of 110 years for annual rainfall under low, medium, high, and very high ranges for both states were counted, statistically analyzed and presented in graphical form in Fig. 3a and corresponding distribution shown in map represented in Fig. 3b.

It is readily inferred from Fig. 3a, b that relative wetness in Karnataka region was higher if compared with Tamil Nadu. In Karnataka region, three district stations were exhibiting high annual rainfall status whereas Tamil Nadu had majority of district having medium annual rainfall for the last 110 years of time span. This is due to the fact that Tamil Nadu lies in eastern zone of Western Ghats. The Eastern Ghats lying in Tamil Nadu, is irregular, broken, and

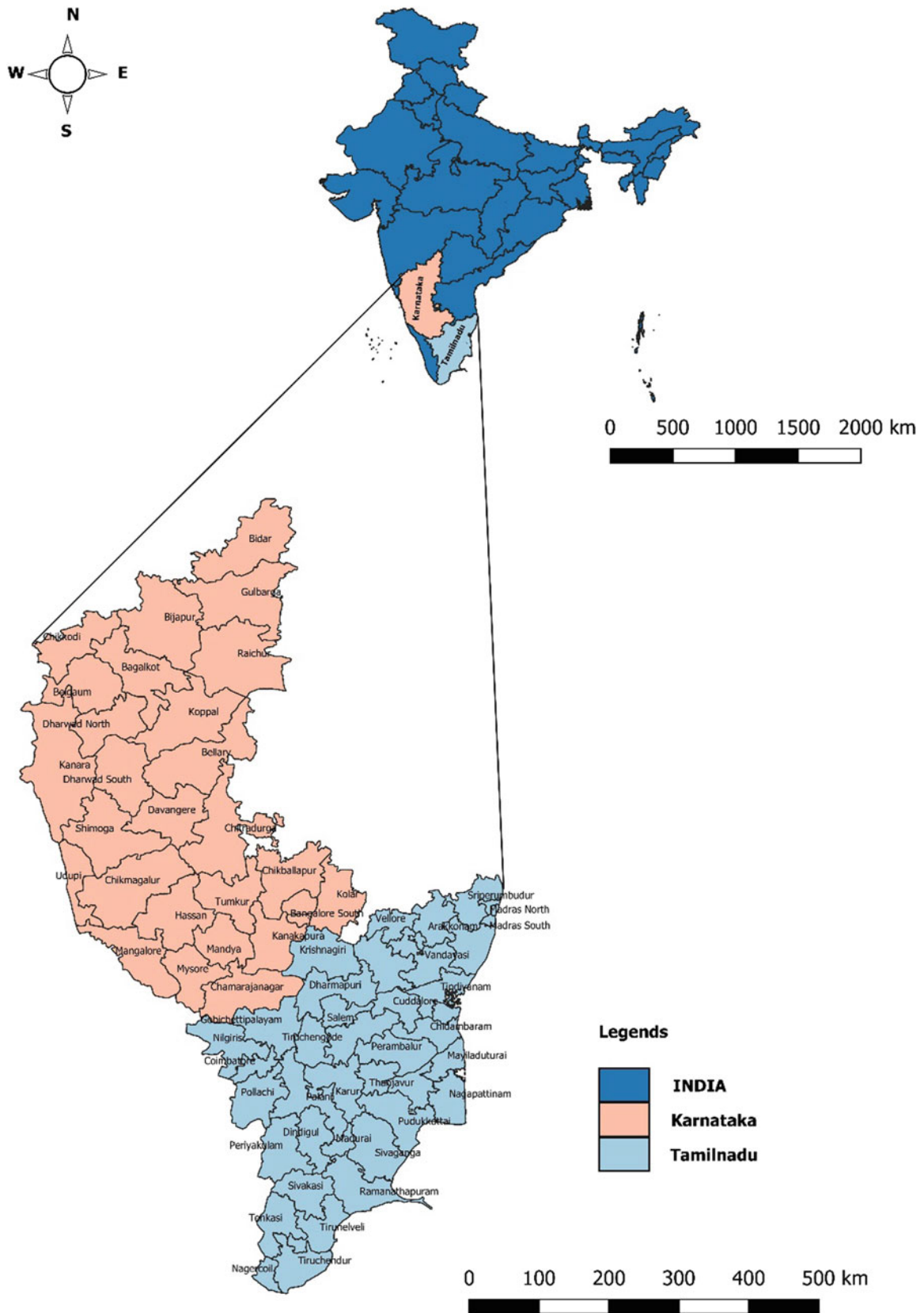
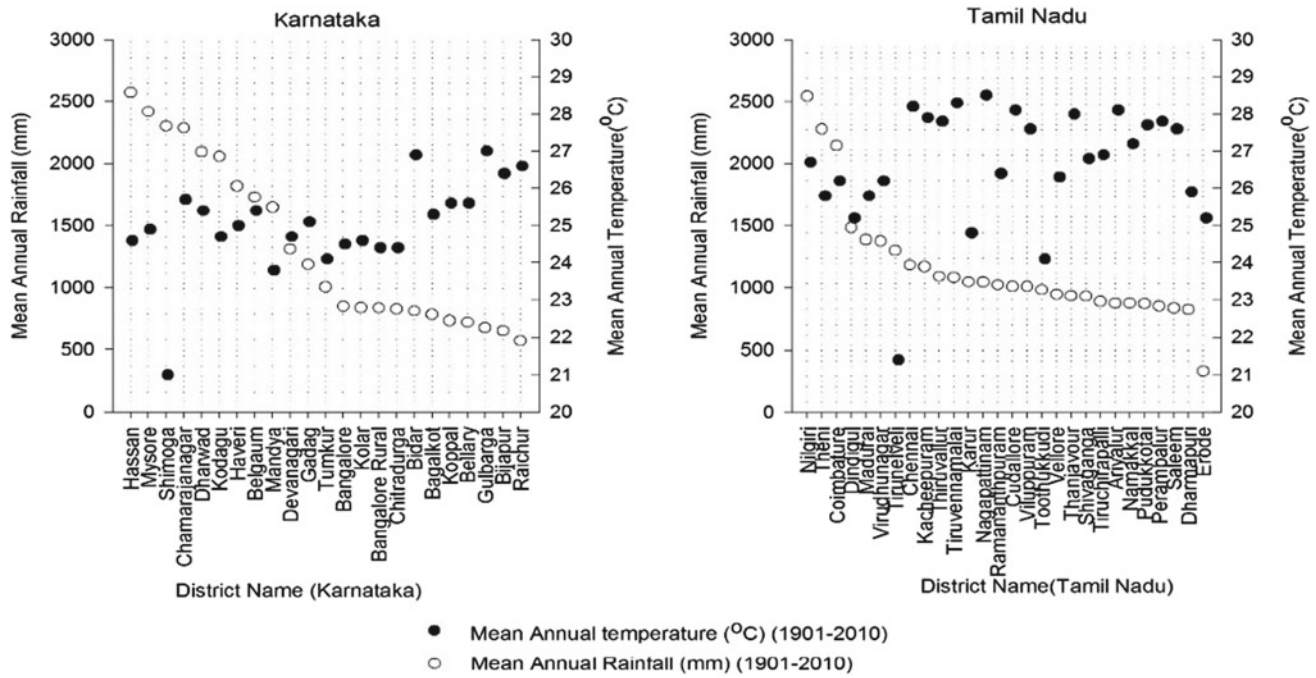


Fig. 1 Location map representing Karnataka and Tamil Nadu states of India





**Fig. 2** Districtwise mean annual rainfall and mean annual temperature for two states

**Table 5** Ranges of rainfall distribution

Classification	Range (in mm)
Low rainfall	<750
Medium rainfall	750–1125
High rainfall	1125–2000
Very high rainfall	>2000

Source (Subramanya, 2013)

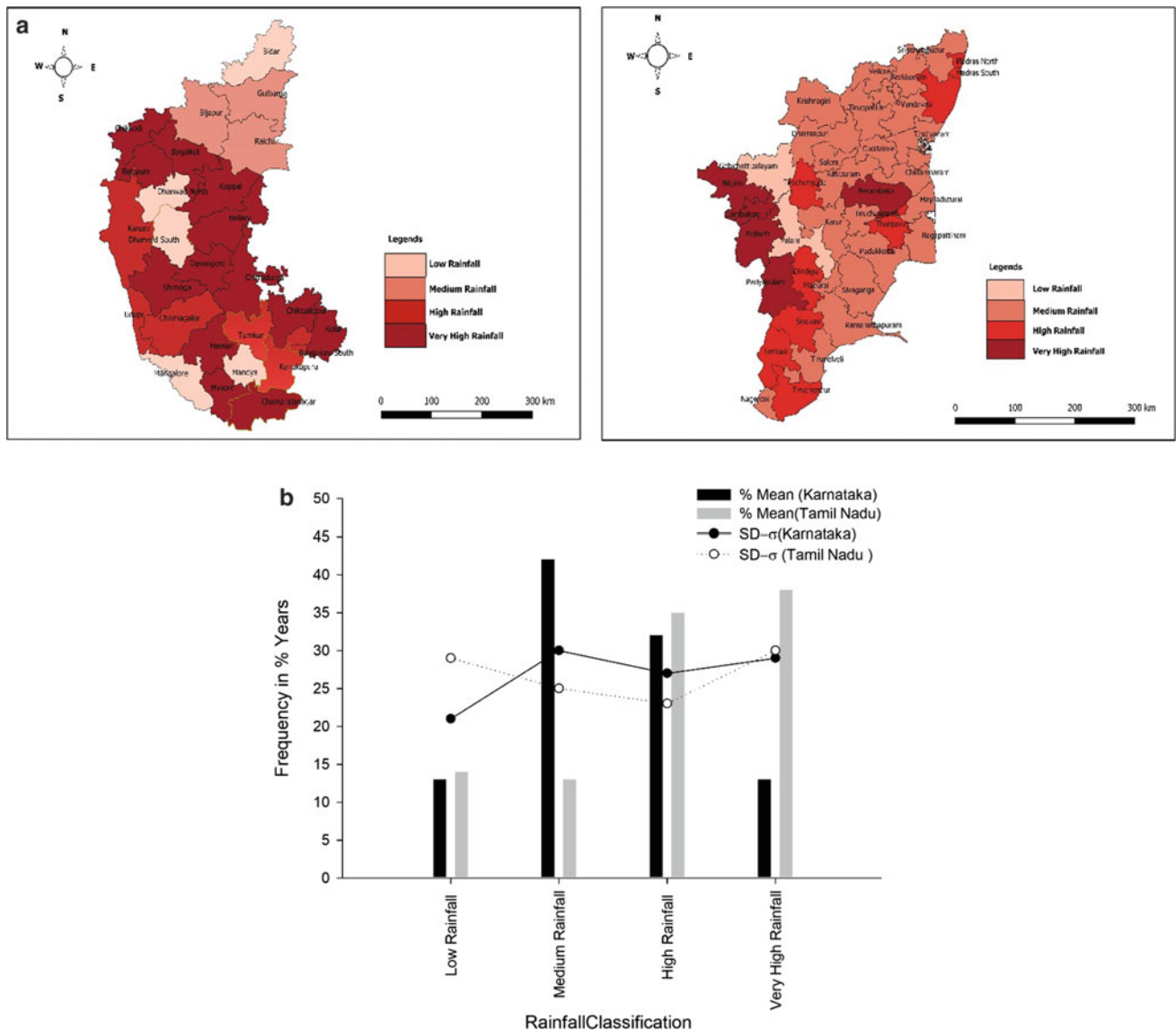
smaller in heights compare to Western Ghats. However, moisture laden winds reach on the eastern part leading to moderately good rainfall condition in this region. Hence, one can even find large variation in rainfall intensities between eastern and western Tamil Nadu.

### 4.1.2 Rainfall Trend Analysis Using Mann-Kendall’s Test

Rainfall data all district gauge stations for two states were further analyzed using Mann-Kendall’s test and trend of rainfall variation using linear regression techniques had been worked out. All the district stations those registered decreasing trends were identified and corresponding trends with data points were graphically represented in Fig. 4a, b for Karnataka and Tamil Nadu, respectively. The district gauge stations with decreasing trends were segregated after performing Mann-Kendall’s test and represented in tabular form in Table 6 with all its indicators and parameters. Further districts with decreasing trends are vividly depicted in

map showing two states in Fig. 5. From all the results shown, it can be inferred that number of districts with decreasing rainfall trend was 14 whereas in Tamil Nadu districts with rainfall decrease is 8. In Karnataka, the trend lines of districts with rainfall decrease were considerably higher with respect to that of Tamil Nadu. This behavior is natural as the average annual rainfall in Karnataka was relatively higher side with respect to Tamil Nadu and may not necessarily indicate meteorological drought condition in Karnataka. However, insignificant or slight rainfall decrease in regions with low annual rainfall may come under meteorological drought condition as region is already water scarce in character.

From the obtained result, it may be inferred that Karnataka as being rain-fed region may have decreased rainfall trends in many districts, however, with respect to drought conditions, Tamil Nadu has more vulnerability with areal extends. It can be easily inferred from Fig. 4a, b that Tirunelveli, Dindigul, Madurai, Vidyut Nagar are reported to



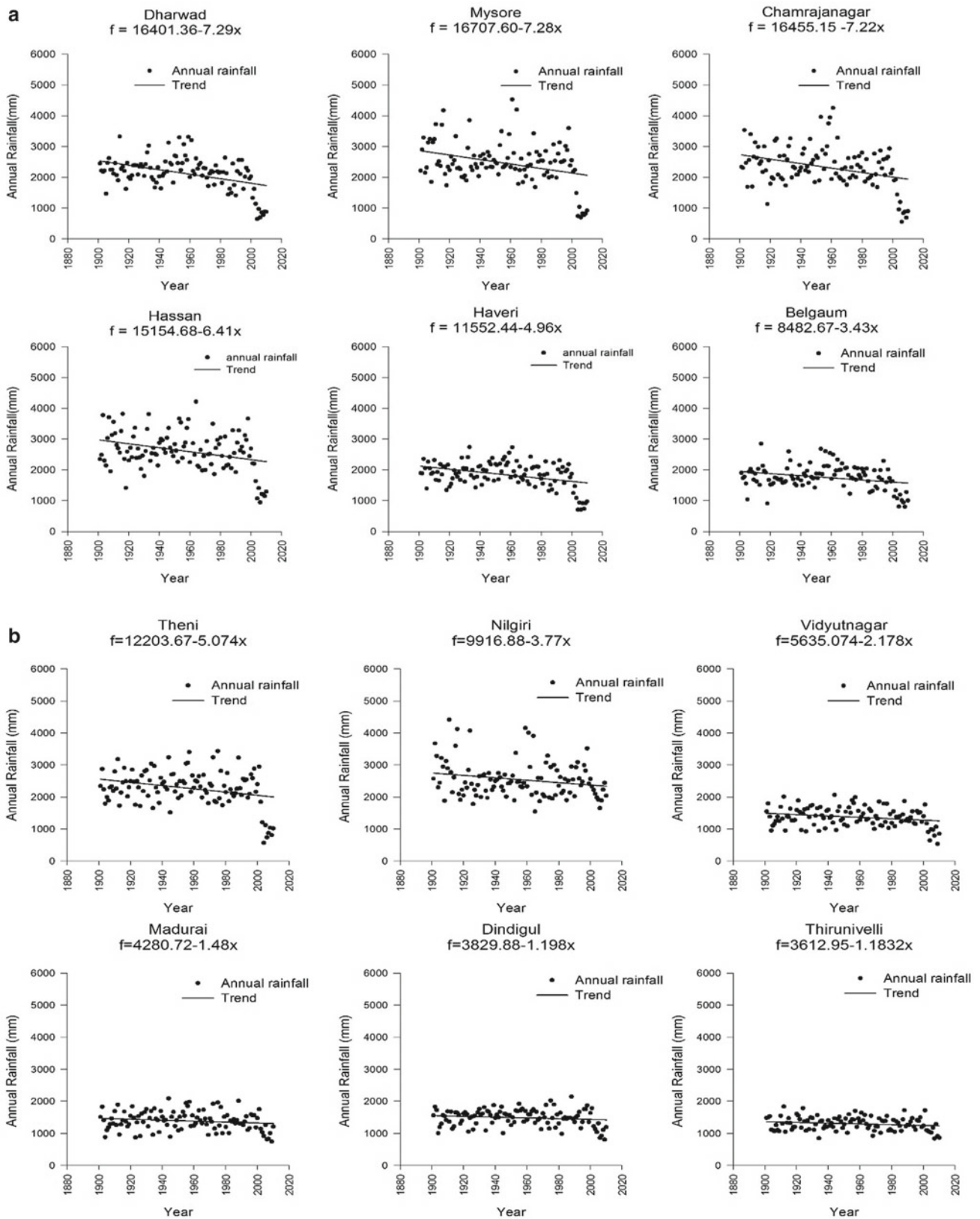
**Fig. 3** Rainfall distribution of study area based on annual rainfall classification. **b** Number of year verses rainfall classification for all districts

exhibit more water scarce situation than any of the districts of Karnataka with decreasing rainfall trends. Situation could be further analyzed in the subsequent section where decadal percentage departures from the normal have been analyzed for both states to get more vivid findings.

The nonparametric trend of annual rainfall of districts of Karnataka with decreasing trends is also presented in Table 6. Only Karur district in Tamil Nadu state lies under the lowest decrease rainfall interval of less than 1.0 mm. None of the districts are having decreasing rainfall less than 0.5 mm. Study also suggests that Ariyalur, Namakkal, Ramanathapuram, Thoothukudi, Vellore are the districts which lies under the lowest increase rainfall interval of less than 0.5 mm while Cuddalore and Nagapattinam districts lie under the highest rainfall increase interval between 2 and

3 mm. None of the districts are having rainfall increasing value more than 3 mm. Similarly, Bellary and Koppal are the districts in Karnataka which lie under the lowest decrease rainfall interval of less than 0.5 mm while Dharwad, Mysore, Hassan, and Chamarajanagar districts lie under the highest rainfall decrease interval of above 5 mm. Trend analysis also suggests that Bagalkot and Kolar are the districts which lie under the lowest increase rainfall interval of less than 0.5 mm while Bangalore, Bijapur, Gulbarga, and Kodagu districts lie under the highest rainfall increase interval between 1 and 2 mm. None of the districts were having rainfall increase value more than 2 mm

Figure 5 shows a map of Karnataka and Tamil Nadu, where all the districts are with decreasing rainfall trend and increasing rainfall trend for the study period (1901–2010). It



**Fig. 4** District with higher decreasing rainfall trends in Karnataka. **b** Districts with higher decreasing rainfall trends in Tamil Nadu

**Table 6** Consolidated Mann-Kendall test results (of decreasing rainfall trends) for study regions for 110 years

District	Kendall's Tau	Mann-Kendall statistics (S)	P-district two value (two-tailed)	Alpha	Trend
<i>Karnataka</i>					
Bangalore Rural	0.09	531	0.17	0.05	Decreasing
Belgaum	-0.15	-911	0.02	0.05	Decreasing
Bellary	-0.03	-191	0.62	0.05	Decreasing
Chamarajanagar	-0.20	-1219	0.00	0.05	Decreasing
Chitradurga	-0.08	-493	0.20	0.05	Decreasing
Devanagari	-0.19	-1147	0.00	0.05	Decreasing
Dharwad	-0.26	-1543	0.00	0.05	Decreasing
Gadag	-0.21	-1231	0.00	0.05	Decreasing
Hassan	-0.17	-1025	0.01	0.05	Decreasing
Haveri	-0.20	-1181	0.00	0.05	Decreasing
Koppal	0.01	83	0.83	0.05	Decreasing
Mandya	-0.10	-601	0.12	0.05	Decreasing
Mysore	-0.14	-839	0.03	0.05	Decreasing
Shimoga	-0.12	-725	0.06	0.05	Decreasing
Tumkur	-0.05	-325	0.40	0.05	Decreasing
<i>Tamil Nadu</i>					
Coimbatore	-0.138	-825	0.033	0.05	Decreasing
Dindigul	-0.090	-539	0.165	0.05	Decreasing
Karur	-0.057	-339	0.383	0.05	Decreasing
Madurai	-0.104	-621	0.109	0.05	Decreasing
Nilgiri	-0.127	-761	0.050	0.05	Decreasing
Tirunelveli	-0.118	-707	0.068	0.05	Decreasing
Virudhunagar	-0.141	-847	0.029	0.05	Decreasing

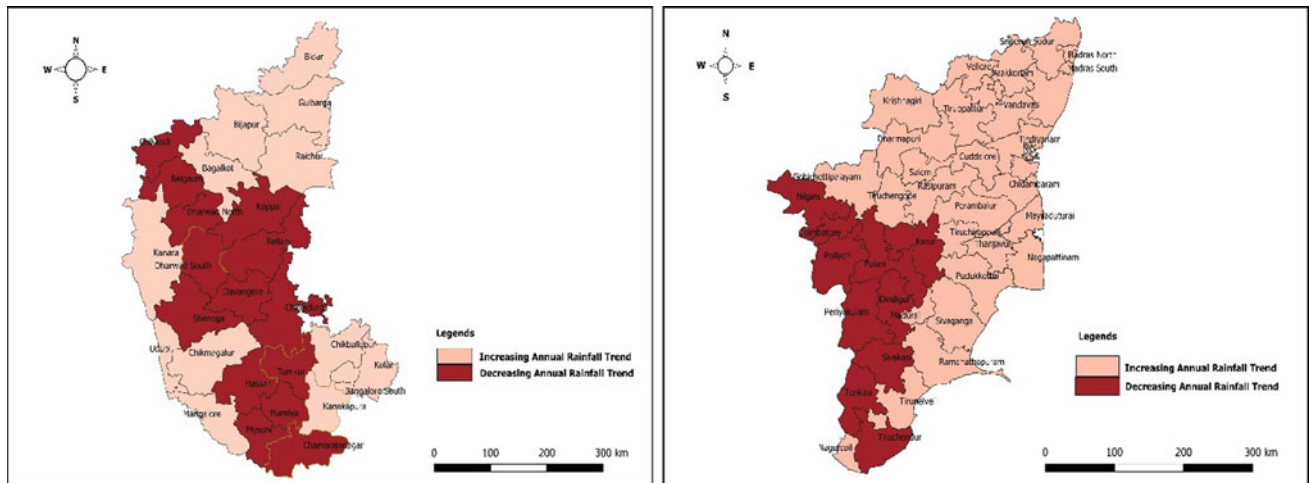


**Fig. 5** Districtwise annual rainfall trend for both states

is noticeable that slight decrease or insignificant increase in rainfall in most districts of Tamil Nadu would have larger impact on drought vulnerability with respect to that of Karnataka and the mean annual rainfall in Tamil Nadu

region comparatively lower than that of Karnataka region. It is pertinent to mention that, for the period of study (1901–2010) based on annual rainfall classification, there were either high rainfalls in 38 years or medium rainfalls in



15 years. However, there were low rainfalls only for 15 years in some of the districts of Karnataka. Very high rainfalls were recorded in 42 years for some districts of Karnataka.

On the basis of annual rainfall classification, it was found that four districts were having low rainfall (high risk of drought), seven districts were having medium rainfall (high risk of drought), five districts were having high rainfall (low risk of drought), and six districts were having very high rainfall (very low risk of drought), whereas in Tamil Nadu region, for the period of study (1901–2010) in general, there were either high rainfalls in 35 years or medium rainfalls in 45 years. However, in 16 years, there were low rainfalls in some of the districts of Tamil Nadu. Very high rainfalls were recorded in 14 years for the districts of Tamil Nadu. On the basis of annual rainfall classification, it was found that one district was having low rainfall (very high risk of drought), 18 districts were having medium rainfall (high risk of drought), six districts were having high rainfall (low risk of drought), and only three districts were having very high rainfall (very low risk of drought). Precipitation data analysis using annual rainfall classification in conjunction with trend analysis can depict a qualitative indication of meteorological processes however adequate metrological drought characterization requires further in-depth analysis.

## 4.2 Drought Analysis

### 4.2.1 Drought Index (DI) Analysis

It can be readily inferred from the previous section, that based on annual rainfall classification (Fig. 3a), there were 11–12 districts with high/very rainfall (low risk of drought) for many of the years in Karnataka whereas almost 19 districts of Tamil Nadu had medium or low rainfall in most of the years (high risk of drought) of the study period of 110 years (1901–2010).

However, one can observe that a relatively qualitative idea can possibly be established from this analysis. Districts namely Dharwad, Mysore, Begaum, Devnagri, and Bagalkot were representing considerable numbers of years under high rainfall if one considers only the classification. Similarly, Nilgiri and Vidyut Nagar in Tamil Nadu came under high rainfall category. However, looking at the statistical trend analysis as described in last section, rainfall was on decreasing trend in these districts leading to meteorological drought condition which supported realistic scenario of those districts. Hence, it is apparent that annual rainfall classification has limitation and cease to suggest concrete drought situation in the study region. To get a deeper insight into drought situation, one can appropriately choose a drought indicator that possibly incorporate the cumulative impact of

rainfall decrease or increase for a longer span of time with possible data analysis for further in-depth study.

Keeping in view of the fact, drought index (IMD, 1971) was computed using Eq. (6) considering 110 years of monthly rainfall data. It was found that out of 110 years and out of 23 districts of Karnataka, 14 districts were found with average 44 event years of mild drought, 10 event years of moderate drought and 2 event years of severe drought condition during the year 1901 to 2010 as per the threshold values presented in Table 2. Similarly, in Tamil Nadu too, average 46 times mild drought, 6 times moderate drought, and 1 times severe drought in 28 districts were found during the study period (1901 to 2010). The only difference that can be readily inferred is that % areal extend of drought condition was more in Tamil Nadu than that of Karnataka due to low-to-medium annual rainfall recorded in Tamil Nadu. The areal extend of drought affected of Karnataka and Tamil Nadu as per DI values is shown in Fig. 6.

The graphical comparison based on no drought, mild drought, moderate drought, and severe drought based on DI values for both states are vividly depicted in Fig. 7 for illustration. It can be found that so far drought recurrence is concerned (mostly mild drought cases), Tamil Nadu is predominating however in terms of severity (Moderate or severe drought situation) Karnataka is ahead of Tamil Nadu. However, to get better insight another drought index namely Palmer drought index as described in previous Sect. 2.3 was evaluated for all meteorological district stations for both study regions in subsequent section.

### 4.2.2 Palmer Drought Index (PDI) Analysis

Palmer index values were computed using climatic data, i.e., precipitation and temperature (Palmer, 1965) using the relation presented in Eqs. (7) and (8) and methodology presented in Sect. 2.3. The practical calculation illustrates the complexity of the PDI (Gutmann, 1998). To reduce the complexity, Eq. (7) was simplified with considering the evapotranspiration term only. The simplified Thornthwaite method (Thornthwaite, 1978) was used for estimating potential evapotranspiration. Thus, PDI is calculated from precipitation deficits for monitoring long-term drought conditions with 12-month intervals to compare it with twelve-month SPI values. Event years including different intensities of meteorological drought, wet and near normal (NN) condition (based on threshold values presented in Table 3) based on computed PI values for precipitation for both study regions are presented in graphical form in Fig. 8, respectively.

It was found that incipient dry spell (IDS) condition was predominant in all most all district gauge stations of Karnataka for considerable number of years during the study period. However, moderate-to-severe drought was observed



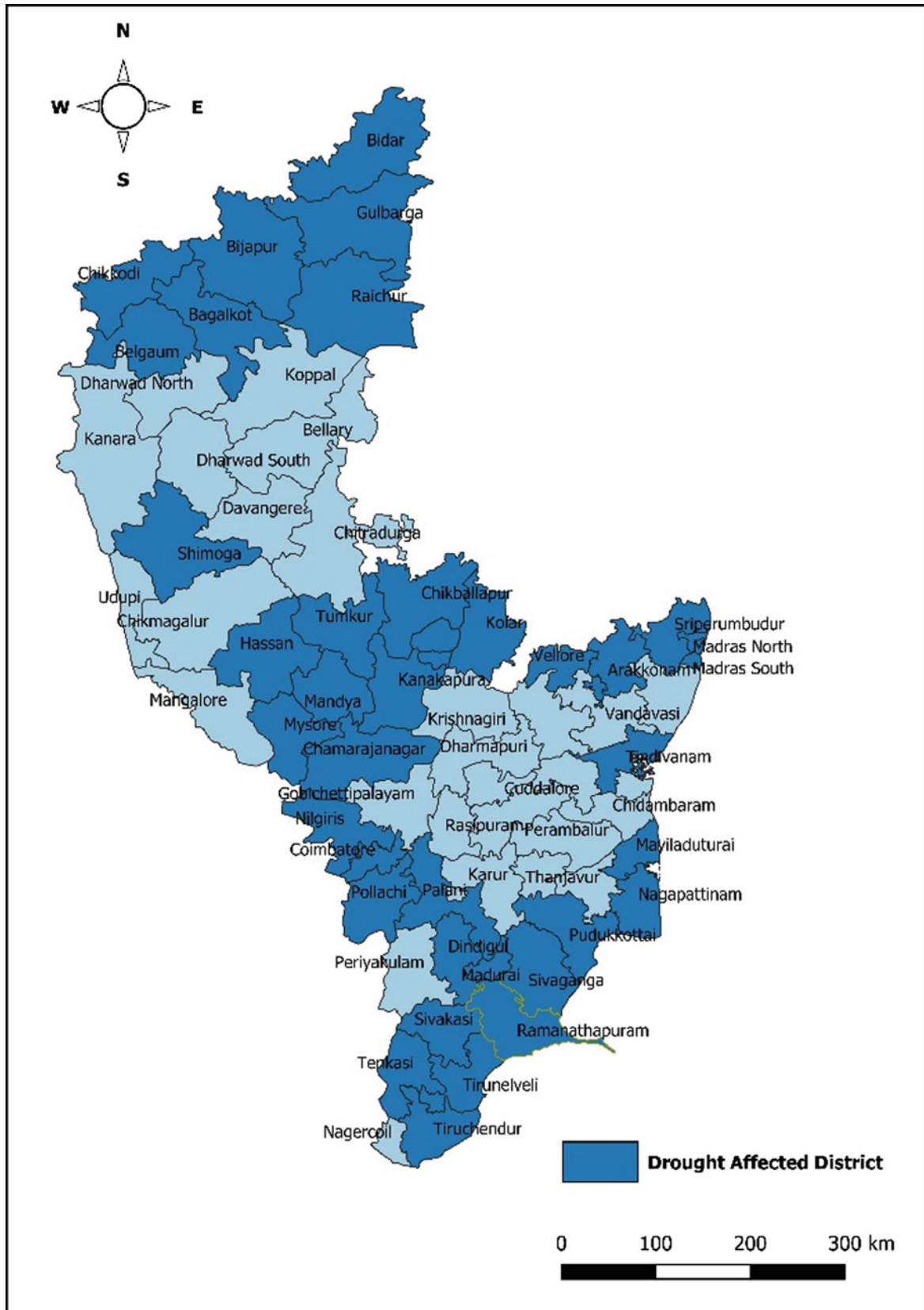


Fig. 6 Drought-affected districts of study region as per DI values

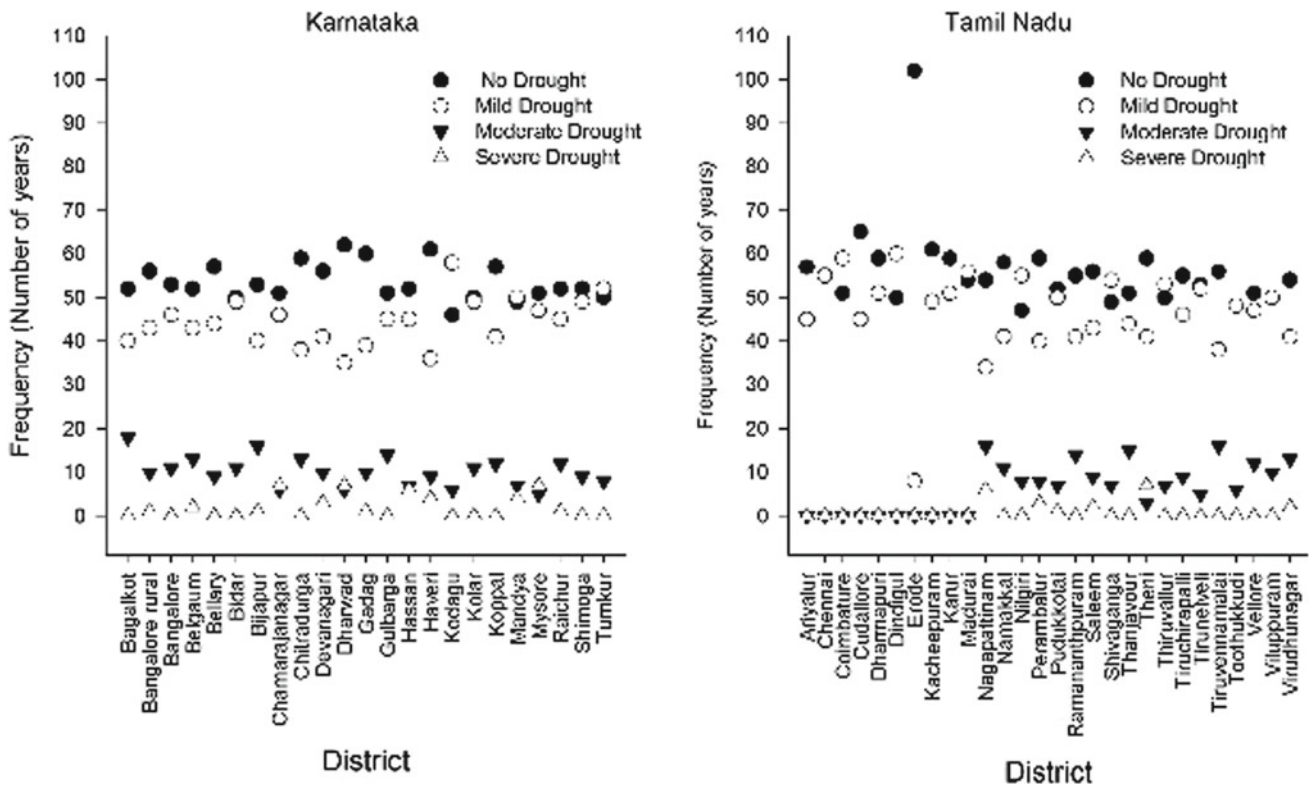


Fig. 7 Drought intensity based on DI values

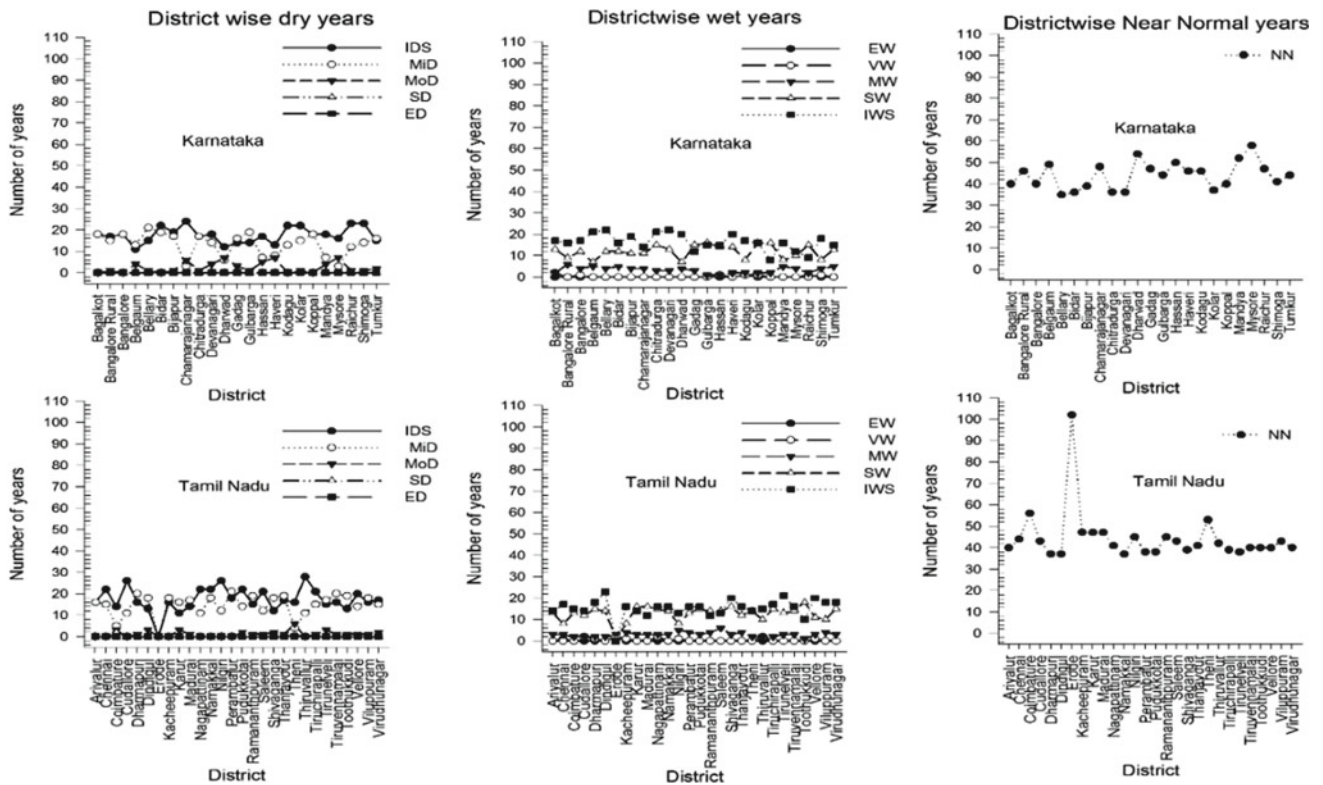


Fig. 8 Drought intensity based on PDI values

**Table 7** Number of drought event years with respect to SPI values for districts of Tamil Nadu and Karnataka region

Sl. no.	Tamil Nadu				Karnataka			
	District	MD (event years)	SD (event years)	ED (event years)	District	MD (event years)	SD (event years)	ED (event years)
1	Ariyalur	12	5	0	Bagalkot	14	4	0
2	Chennai	11	5	0	Bangalore rural	8	7	1
3	Coimbatore	2	3	5	Bangalore	9	9	0
4	Cuddalore	8	4	0	Belgaum	8	5	4
5	Dharmapuri	17	3	1	Bellary	18	4	1
6	Dindigul	12	6	3	Bidar	16	4	0
7	Erode	0	0	0	Bijapur	14	4	1
8	Kanchipuram	12	6	0	Chamarajanagar	1	2	6
9	Karur	11	5	3	Chitradurga	11	7	1
10	Madurai	10	7	1	Devanagari	12	3	4
11	Nagapattinam	16	2	0	Dharwad	4	2	7
12	Namakkal	13	5	0	Gadag	11	5	3
13	Nilgiri	10	2	0	Gulbarga	14	5	2
14	Perambalur	16	5	0	Hassan	4	3	5
15	Pudukkottai	9	5	2	Haveri	7	1	7
16	Ramanathapuram	11	8	1	Kodagu	12	2	0
17	Salem	16	3	1	Kolar	9	6	1
18	Sivaganga	11	7	2	Koppal	14	4	2
19	Thanjavur	16	3	1	Mandya	5	2	4
20	Theni	3	1	7	Mysore	0	0	0
21	Thiruvallur	5	6	0	Raichur	10	3	1
22	Tiruchirappalli	9	5	1	Shimoga	12	3	1
23	Tirunelveli	15	2	3	Tumkur	11	5	2
24	Tiruvannamalai	15	5	1				
25	Thoothukudi	14	6	1				
26	Vellore	9	5	1				
27	Viluppuram	13	5	1				
28	Virudhunagar	12	3	2				
Mean		11	4.36	1.32		9.74	3.91	2.30
Standard deviation		4.28	1.87	1.63		4.54	2.04	2.21

in at least 5–10-year counts in several districts namely Chamarajanagar, Dharwad, Belgaum, Haveri, and Mysore. Similarly, Palmer index values were also computed for temperature parameter. It was found that there was no cases of extreme drought (ED) nor severe drought (SD) events in any of 23 districts of study region. Apart from drought event years, in an average 3 event years of moderately wet (MW), 31 events of near normal (NN), 14 events of slightly wet (SW) and 12 events of incipient wet spell (IWS) climatic situations could be identified in different districts. In three districts, one event year with very wet climate was found along with two event year of very wet condition (in Shimoga district). None of the districts have indicative of extremely

wet (EW) climate condition as in case of Palmer drought index values.

Similarly, in case of Tamil Nadu, incipient dry spell (IDS) was prevalent in all most all districts of Tamil Nadu. At least 15–17 event years of mild drought-to-moderate droughts, 18 event years of incipient dry spell were inferred in Tamil Nadu, mostly in districts of Nilgiri, Vidyut Nagar, Dindigul, and Theni in past 110 years. It is pertinent to mention that for both states almost identical event years (44 times) were under near normal (NN) condition with 12–13 event years as slightly wet and 3 event years as moderately wet conditions. Furthermore, no extremely wet or very wet conditions were observed during the period of study for all district of both

states. The finding suggests that mild-to-moderate drought was predominating (with higher event years) in Tamil Nadu whereas moderate-to-severe drought were existed but for lesser number of years (10–11 years) in Karnataka.

#### 4.2.3 Standardized Precipitation Index (SPI) Analysis

Standardized precipitation index (SPI) as suggested by McKee et al. (1993, 1995) incorporates the seasonal variation of rainfall and may be analyzed statistically through fitting to gamma distribution function (Rahmat et al., 2015), computed using methodology presented in Sect. 2.4 for available precipitation data. Twelve-month SPI values were chosen considering the suitability for water resources studies (Bonaccorso et al., 2003; Raziqi et al., 2009). A number of event years were found to be under drought situation in categories such as moderately dry, severely dry, and extremely dry for all meteorological district stations of both states. It is presented in Table 7 with statistical mean and standard deviations and is graphically represented in Fig. 9.

One can observe that mean event years for moderately dry and severely dry were considerably higher in case of Tamil Nadu whereas for extremely dry condition, Karnataka was registering higher value. Similarly, for statistical spread of the distribution, Tamil Nadu landed up with lower values than that of Karnataka. It means that higher numbers of event years were nearer to peak events values. That is also suggestive of relatively higher vulnerability of drought situations in Tamil Nadu. In conclusion, Tamil Nadu had more vulnerability of moderate-to-severe drought situation with larger areal extend whereas Karnataka had more localized drought vulnerability with severity on higher side.

#### 4.2.4 Comparison of Three Drought Indices for Two Study Regions.

Districtwide computed drought indicators namely DI, PI (precipitation), PI (temperature), and SPI for both states for the study period were compared with percentage mean frequency of occurrence with their indicatorwise threshold values and presented in Fig. 10. Near normal (NN) condition was prevailing more than 50 percent of the study period for all considered indices. However, there were visible difference of estimated frequencies of occurrence for mild-to-severe drought conditions for each index analysis of two study regions. Noticeably, pattern is coherent in case of DI, PDI, and SPI for the with small variations. Furthermore, it is interesting to note that for extreme drought condition all indicators are registering more vulnerability for Karnataka if compared with that of Tamil Nadu. Corresponding standard deviation (SD— $\sigma$ ) values are also plotted in order to have insight into the spread of the variation of severity for all districts of each state (Fig. 10).

From the above analysis, it can be concluded that drought characterization using three drought indicators namely DI, PDI, and the SPI produced somehow coherent information, but the use of PDI is limited and complex to assess with respect to DI and SPI, as it requires huge additional data and computations to perform an adequate and accurate soil water balance while the DI and SPI need only precipitation data, which are more easily available in numerous location of the study areas. It is also concluded that using SPI is more meaningful relative to DI as it incorporates seasonal variation also and better statistical information can be obtained for further in-depth analysis.

#### 4.2.5 Identification of Drought Events Using Log Pearson Type—III Distribution Technique for Karnataka

As the meteorological drought indicator values involves precipitation and computed indicators were based on rainfall data in this study, Log Pearson type III distribution presumed (Rahmat et al., 2015) to be fit nicely to get more meaningful analysis. The statistical parameters for implementing Pearson III are the obvious way using the mean, standard deviation, and skewness of the sample. A popular approach is to sort the sample and assign rough probability estimates to each point according to its rank (Hovey and DeFiore, 2003). The computed SPI data for Karnataka were further analyzed to compute the probability of exceedance for threshold values of SPI with respect to severity.

The Log Pearson Type III distribution on the modified nonzero drought deficit in terms of SPI (namely ‘Scaled SPI’ using a nonzero drought deficit parameter = SPI threshold value plus five as presented in Table 8) for 110 years (1901–2010) were computed. Further, percentage exceedance of drought deficit hence return period of all 23 districts of Karnataka was computed using analytical method with probability estimates using skewness functions as per equations presented in Eqs. (14a)–(14c). The Microsoft Excel spreadsheet has skewness functions (Hovey and DeFiore, 2003) that return estimates of  $\gamma_1$  as follows.

$$PIII(x) = \Gamma D(x - \Upsilon, \alpha, \beta); \gamma_1 > 0 \quad (14a)$$

$$PIII(x) = \Gamma D(\Upsilon - x, \alpha, \beta); \gamma_1 < 0$$

One can write combining the above two expression as,

$$PIII(x) = \Gamma D\left((x - \Upsilon) \cdot \frac{\gamma_1}{|\gamma_1|}, \alpha, \beta\right) \quad (14b)$$

where  $\Gamma D$  is the standard gamma distribution function and ‘shape’  $\alpha = 4/\gamma_1^2$ ; ‘scale’  $\beta = |\sigma\gamma_1/2|$  ( $\beta = \sigma/\sqrt{\alpha}$ ); ‘shift’  $\gamma = \mu - 2\sigma/\gamma_1$  ( $\gamma = \mu \pm \alpha\beta$ , depending upon the sign of  $\gamma_1$ ).



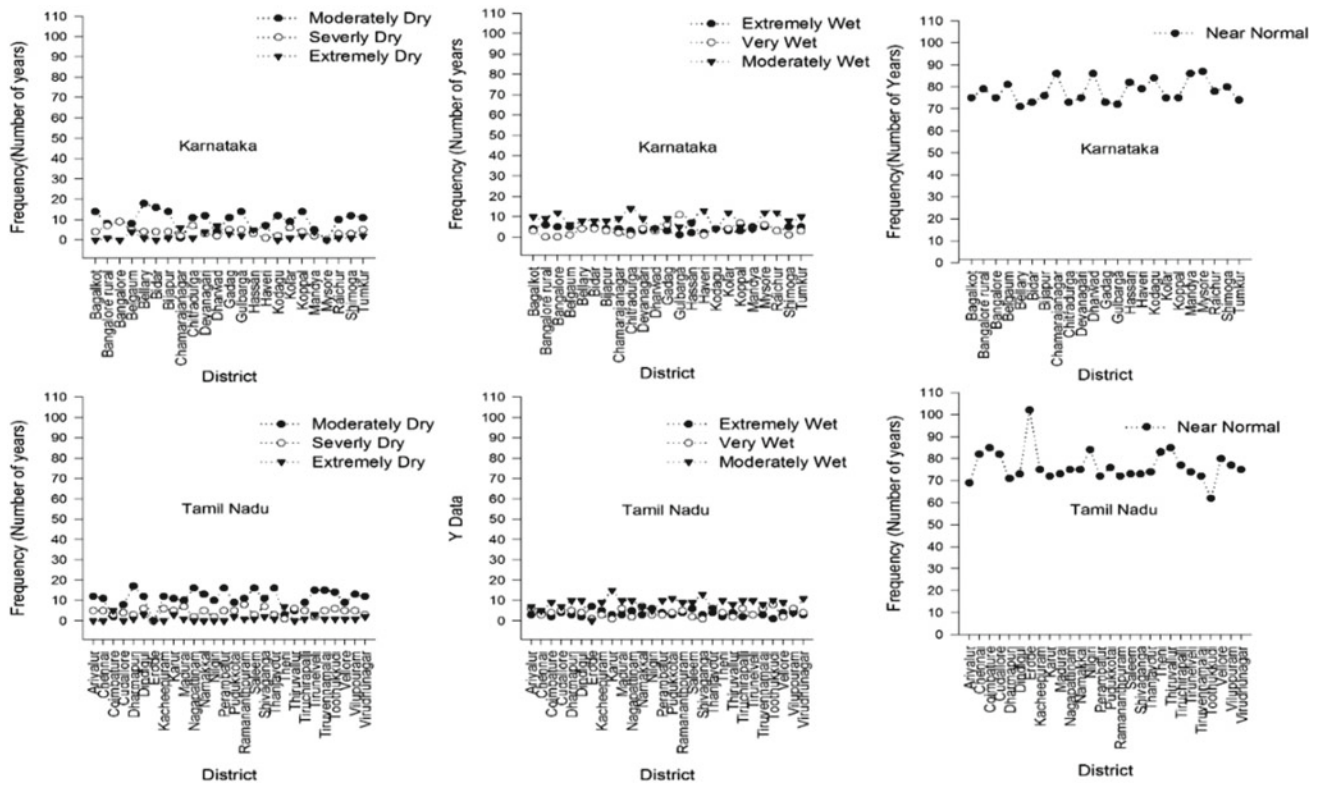


Fig. 9 Drought intensity based on SPI values

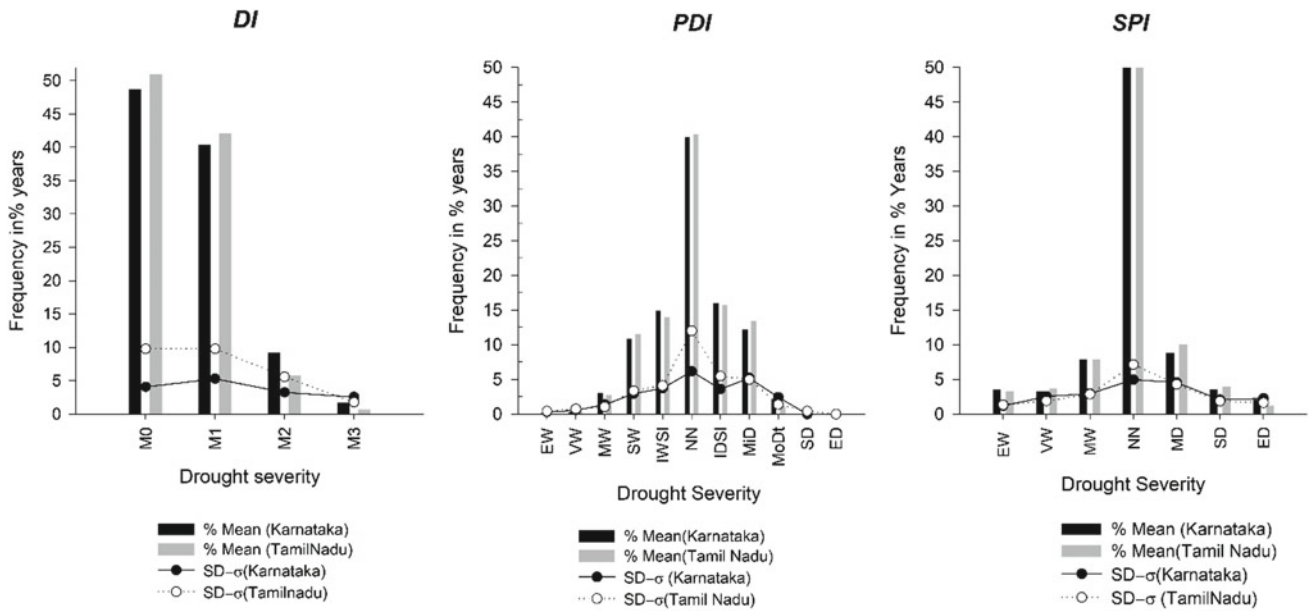
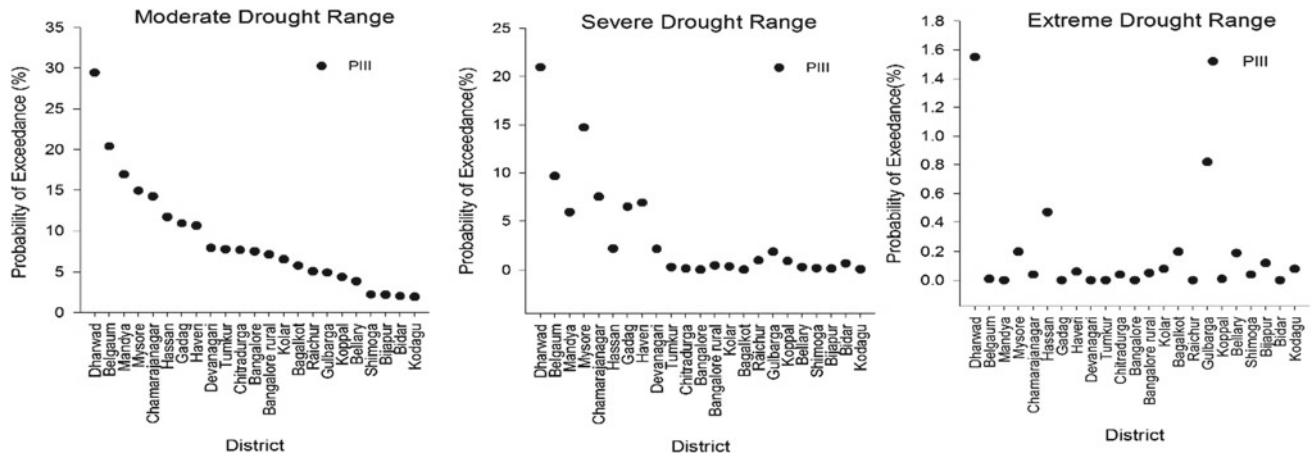


Fig. 10 Yearly drought intensity for 110 years based on PI with respect to precipitation values

Table 8 Threshold values of Scaled SPI (drought deficit)

Classification	EW	VW	MW	NN	MD	SD	ED
Scaled SPI value	$\geq 7$	6.5–6.99	6–6.49	4.01–5.99	4.0–3.51	3.5 to –3.01	$\leq 3$





**Fig. 11** Percentage exceedance probabilities for drought events using analytical LPIII technique for 110 years on with scaled *SPI* values for Karnataka

where  $\mu$ ,  $\sigma$ , and  $\gamma_1$  are mean, standard deviation, and skewness of the distribution.

The logarithmic transformation will be written as follows,

$$PIII(x) = \Gamma D \left( \log(x - \Upsilon) \cdot \frac{\gamma_1}{|\gamma_1|}, \alpha, \beta \right) \quad (14c)$$

where  $\alpha$ ,  $\beta$ ,  $\Upsilon$  and  $\mu$ ,  $\sigma$ ,  $\gamma_1$  are defined in terms of  $\log(x)$  instead of  $x$  (base is 10). The distribution is not defined for  $x$  beyond the shift, which is the lower bound for the positive skew case and the upper bound for the negative, if  $\gamma_1$  is exactly zero. The in-built functions are available in Excel software. Accordingly, the Log Pearson Type III distribution on the modified nonzero drought deficit in terms of *SPI* (namely ‘Scaled *SPI*’ using a nonzero drought deficit parameter = *SPI* threshold value plus five as presented in Table 8) for 110 years (1901–2010) has been computed.

The derived dataset for all 23 districts of Karnataka region in Indian Peninsula is graphically represented in Fig. 11 for moderate, severe, and extreme drought events based on the threshold values (presented in Table 8).

Analyzing Fig. 11, it is found that under moderate drought condition, Dharwad district is having maximum percentage probability of exceedance of drought, followed by Belgaum district. On the other hand, Kodagu district is having minimum percentage of probability of exceedance, i.e., 2.3%. Similarly, for severe drought condition, again Dharwad district is having maximum exceedance probability followed by Mysore, while Bangalore and Bagalkot are having least exceedance probabilities. In case of extreme drought condition, again Dharwad district is found to be having largest exceedance probability followed by Gulbarga district. However, Mandya, Gadag, Devnagri, Tumkur, Bangalore, Raichur, and Bider are found to be having least exceedance probabilities.

## 5 Conclusion

1. The present study to predict meteorological drought condition of classified thresholds namely moderate, severe, and extreme drought conditions using standard precipitation index with assessment of twelve-month *SPI* along with other two indices namely Palmer index and drought index for two southern Indian states and compared.
2. Results from climatic divisions of two states under study show that drought characterization using three drought indicators namely *DI*, *PDI*, and the *SPI* produce somehow coherent information, but the use of *PDI* is limited and complex to assess with respect to *DI* and *SPI*, as it requires huge additional data and computations to perform an adequate and accurate soil water balance while the *DI* and *SPI* need only precipitation data, which are more easily available in numerous location of the study areas. It is also concluded that using *SPI* is more meaningful relative to *DI* as it incorporates seasonal variation also and better statistical information can be obtained for further in-depth analysis.
3. Tamil Nadu was found to be more vulnerable to moderate-to-severe drought situation with larger areal extend whereas Karnataka had more localized drought vulnerability with severity on higher side.
4. The monotonic trend of rainfall of the districts of Karnataka and Tamil Nadu in the past 110 years using nonparametric methods namely Mann-Kendall and Sen’s Slope tests were investigated and six districts of each state with decreasing rainfall trends have been critically analyzed. It was found that decreasing trend in Karnataka is more significant as compared to that of Tamil Nadu.

5. Log Pearson probability distribution technique using SPI is attempted to assess exceedance probabilities of meteorological drought condition of classified thresholds for Karnataka region. It was found that Dharwad district in Karnataka is the most vulnerable among 23 districts, with respect to severity and recurrence of drought conditions.

## 6 Conflict of Interest/Competing Interests

On behalf of all authors, the corresponding author states that there is no conflict of interest.

## 7 Availability of Data and Materials

The online version of this article contains supplementary material, which is available to authorized users.

**Code availability:** custom code part is absent.

**Acknowledgements** For the present study, data are provided by India Water Portal, Government of India, and Indian Meteorological Department, Govt. of India which is gratefully acknowledged here.

### Declarations

### Funding

Data used for this study were procured from Governmental data base which has been duly acknowledged in the manuscript text. As this work is part of field specific research conducted within the Institutional resources hence external funding resource part is absent.

## References

- Alexander, L. V., Zhang, X., Peterson, T. C., Caesar, J., Gleason, B., Klein Tank, A. M. G., Haylock, M., Collins, D., Trewin, B., Rahim, F., Tagipour, A., Rupa Kumar, K., Revadekar, J., Griffiths, G., Vincent, L., Stephenson, D. B., Burn, J., Aguilar, E., Brunet, M., Taylor, M., ..., Vazquez-Aguirre, J. L. (2006). Global observed changes in daily climate extremes of temperature and precipitation. *Journal of Geophysical Research Atmosphere*, *111*, 105–109.
- Al Adaileh, H., Al Qinna, M., & Barta, K. (2019). A drought adaptation management system for groundwater resources based on combined drought index and vulnerability analysis. *Earth System Environment*, *3*, 445–461. <https://doi.org/10.1007/s41748-019-00118-9>.
- Al-Bakri, J. T., Alnaimat, M. J., Al-Karablieh, E., & Qaryouti, E. A. (2019). Assessment of combined drought index and mapping of drought vulnerability in Jordan. *International Journal of Engineering Research and Applications*, *9*(3), 59–68.
- Bonaccorso, B., Cancelliere, A., Rossi, G. (2003). An analytical formulation of return period of drought severity. *Stochastic Environment Research Risk Assessment*, *17*, 157–174.
- Bonsal, B., & Regier, M. (2007). Historical comparison of the 2001/2002 drought in the Canadian Prairies. *Climate Research*, *33*, 229–242.
- Coles, S (2001). *An introduction to statistical modeling of extreme values*. New York, Springer.
- Da Silva, R. M., Santos, C. A. G., Moreira, M., Corte-Real, J., Silva, V. C. L., & Medeiros, I. C. (2015). Rainfall and river flow trends using Mann-Kendall and Sen's slope estimator statistical tests in the Cobre River basin. *Natural Hazards*, *77*, 1205–1221.
- Dubrovsky, M., Svoboda, M. D., Hayes, T. M., Wilhite, D. A., Zalud, Z., & Hlavinka, P. (2006). Application of relative drought indices in assessing climate-change impacts on drought conditions in Czechia (2006) Drought Mitigation Center Faculty Publications. 41. <https://digitalcommons.unl.edu/droughtfacpub/41>.
- Duhan, D., & Pandey, A. (2013). Statistical analysis of long term spatial and temporal trends of precipitation during 1901–2002 at Madhya Pradesh India. *Atmospheric Research*, *122*, 136–149.
- Ferdin, M., Görlitz, S., & Schwörer, S. (2010). Water stress in the Cauvery Basin, South India-how current water management approaches and allocation conflict constrain reform. *ASIEN*, *117*, S. 27–44, Retrieved from M Ferdin, S Görlitz, S Schwörer - ASIEN, 2010 - asien.asienforschung.de.
- Gebert, R. I. (1983). The Cauvery River dispute: hydrological politics in Indian federalism (T). Retrieved from <https://open.library.ubc.ca/collections/ubctheses/831/items/1.0095680>
- Gibbs, W. J., & Maher, J. V. (1967). *Rainfall deciles as drought indicators*. Melbourne: Bureau of Meteorology.
- Ghanem, A. (2011). Trends in mean seasonal and annual rainfall amounts over Jordan Human. *Social Science*, *38*, 1041–1049.
- Gilbert, R. O. (1987). *Statistical methods for environmental pollution monitoring* (p. 320). NY: Van Nostr Reinhold Co.
- Guttman, N. B. (1998). Comparing the Palmer drought index and the standardized precipitation index. *Journal of the American Water Resources Association*, *34*, 113–121. <https://doi.org/10.1111/j.1752-1688.1998.tb05964.x>.
- Guttman, N. B. (1999). Accepting the standardized precipitation index: A calculation algorithm. *Journal of American Water Resource Association*, *35*(2), 311–322.
- Hammouri, N., & El-Naqa, A. (2007). Drought assessment using GIS and remote sensing in Amman-Zarqa Basin Jordan. *Jordan Journal of Civil Engineering*, *1*(2), 142–152.
- Hirsch, R. M., Slack, J. R., & Smith, R. A. (1982). Techniques of trend analysis for monthly water quality data. *Water Resources Research*, *18*, 107–121.
- Hovey, P., & DeFoire, T. (2003). Final report on fit the Pearson Type III distribution to aviation loads data. US Department of Transportation Federal Aviation Administration Washington DC 205901 Rep No DOT/FAA/AR-03/62 (Unclassified).
- Huang, Y. F., Jong, T. A., Yong, J. T., Mirzaei, M., & Amin, M. Z. M. (2016). Drought Forecasting using SPI and EDI under RCP-8.5 Climate Change Scenarios for Langat River Basin. In: *Malaysia 12th International Conference on Hydroinformatics HIC 2016 Proceedings Engineering* (Vol. 154, pp. 710–717).
- IMD. (1971). Rainfall and drought in India: A report Indian Meteorological Department Govt. of India & NCA, 1976 Agri Comm Rep Nat Comm on Agri Min of Agri GoI New Delhi.
- IPCC. (2007). The physical science basis. *Working Group I Contribution to the Fourth Assessment Report of the IPCC Cambridge University Press*.
- Jain, S. K., & Kumar, V. (2012). Trend analysis of rainfall and temperature data for India. *Current Science*, *102*, 37–49.
- Jacobi, J., Perrone, D., Duncan, L. L., & Hornberger, G. (2013). A tool for calculating the Palmer drought indices Water Resour. *Philosophy and Phenomenological Research*, *49*, 6086–6089. <https://doi.org/10.1002/wrcr.20342>.
- Kumar, A., Pandey, R. P., Mishra S. K. (2018). Characteristics of meteorological droughts in north western India. *Natural Hazard Journal of International Society of Prevention and Mitigation of Natural Hazard Springer International Society for Prevention and Mitigation of Natural Hazard*, *94*(2), 561–582.
- Kendall, M. (1975). *Rank correlation methods* (4th ed.). London: Charles Griffin.

- Krysanova, V., Tobias, V., & Fred, H. (2008). Detection of change in drought frequency in the Elbe basin: Comparison of three methods. *Hydrological Sciences Journal*, 53(3), 519–537. <https://doi.org/10.1623/hysj.53.3.519>.
- Langat, P. K., Kumar, L., & Koech, R. (2017). Temporal variability and trends of rainfall and streamflow in Tana River Basin. *Kenya Sustainability*, 9(1963), 1–18.
- Liu, L., Hong, Y., Looper, J., Riley, R., Yong, B., Zhang, Z., Hocker, J., & Shafer, M. (2013). Climatological drought analyses and projection using SPI. *Journal of Hydrologic Engineering*, 18(7).
- Lloyd-Hughes, B., Saunderson, A. (2002). A drought climatology for Europe. *International Journal of Climatology*, 22, 1571–1592.
- Longobardi, A., & Villani, P. (2010). Trend analysis of annual and seasonal rainfall time series in the Mediterranean area. *International Journal of Climatology*, 30, 1538–1546.
- Mallya, G., Mishra, V., Niyogi, D., Tripathi, S., Govindaraju, R. S. (2016). Trends and variability of droughts over the Indian monsoon region. *Weather and Climate Extremes*, 12, 43–68.
- Mann, H. (1945). Non-parametric tests against trend. *Econometrica*, 13, 245–259.
- McKee, T. B., Doesken, N. J., & Kliest, J. (1993). The relationship of drought frequency and duration to time scales. In *Proceedings of the 8th Conference of Applied Climatology* (pp. 179–184), 17–22 January, Anaheim, CA. American Meteorological Society, Boston, MA.
- McKee, T. B., Doesken, N. J., & Kleist, J. (1995). Drought monitoring with multiple time scales. In *Proceedings of the ninth conference on applied climatology* (pp. 233–236). American Meteorology Society, Boston.
- Modarres, R., & da Silva, V. D. P. R. (2007). Rainfall trends in arid and semi-arid regions of Iran. *Journal of Arid Environments*, 70, 344–355.
- Mohorji, A. M., Şen, Z., & Almazroui, M. (2017). Trend analyses revision and global monthly temperature innovative multi-duration analysis. *Earth System Environment*, 1, 9. <https://doi.org/10.1007/s41748-017-0014-x>.
- Mooley, D. A., & Parthasarathy, B. (1984). Large scale drought over India and their impact on agricultural production. *Mausam*, 35, 26.
- Mustafa, A., & Rahman, G. (2018). Assessing the spatio-temporal variability of meteorological drought in Jordan. *Earth System Environment*, 2, 247–264.
- Oguntunde, P. G., Abiodun, B. J., Lischeid, G. (2017a). Impacts of climate change on hydro-meteorological drought over the Volta Basin, West Africa. *Glob Planet Change*, 155(March), 121–132. <https://doi.org/https://doi.org/10.1016/j.gloplacha.2017.07.003>
- Oguntunde, P. G., Lischeid, G., & Abiodun, B. J. (2017). Impacts of climate variability and change on drought characteristics in the Niger River Basin. *Stochastic Environment Research Risk Assessment, West Africa*. <https://doi.org/10.1007/s00477-017-1484-y>.
- Pai, D. S., Sridhar, L., Guhathakurta, P., & Hatwar, H. R. (2011). District-wide drought climatology of the southwest monsoon season over India based on standardized precipitation index (SPI) *Natural Hazard*, 59(3), 1797–1813.
- Palmer, W. C. (1965). Meteorological drought. Research Paper No 45 US Department of Commerce Weather Bureau, Washington DC.
- Pani, N. (2009). Institutions that cannot manage change: A Gandhian perspective on the Cauvery dispute in South India. *Water Alternatives*, 2(3), 315–327.
- Paulo, A. A., Rosa, R. D., & Pereira, L. S. (2012). Climate trends and behaviour of drought indices based on precipitation and evapotranspiration in Portugal. *Nat. Hazards Earth System Science*, 12, 1481–1491.
- Paulo, A. A., & Pereira, L. S. (2006). Drought concepts and characterization: Comparing drought indices applied at local and regional scales. International water resources association. *Water International*, 31(1), 37–49.
- Pathak Abhishek, A., & Dodamani Channaveerappa, B. M. (2016). *Comparison of two hydrological drought indices Perspectives in Science*, 8, 626–628.
- Quenum, G. M. L. D., Klutse, N. A. B., & Dieng, D. (2019). Identification of potential drought areas in West Africa under climate change and variability. *Earth System Environment*, 3, 429–444. <https://doi.org/https://doi.org/10.1007/s41748-019-00133-w>
- Rahmat SN, Jayasuria N, Bhuiyan M (2015) Development of Drought Severity-Duration-Frequency Curves in Victoria Australia. *Australian J of Wat Res* 19(1): 31–42
- Sims Aaron, P., Niyogi, Dev dutta, S., & Raman, S. (2002). Adopting drought indices for estimating soil moisture. *A North Carolina case study Geophysical Research Letters*, 29(8), 1183. <https://doi.org/10.1029/2001GL013343>.
- Shah, R., Bharadiya, N., & Manekar, V. (2015). Drought index computation using standardized precipitation index (SPI) Method for Surat District Gujarat. *Aquatic Procedia*, 4, 1243–1249.
- Subramanya, K. (2013). *Engineering hydrology* (3rd edn., Vol 217) TMH New Delhi India.
- Thornthwaite, C. (1948). W (1978) An approach toward a rational classification of climate. *Geographical Review*, 38, 55–94.
- Warrick, R. A. (1975). Drought hazards in United States: A research assessment NSF/RA/E-75/004. National Technical Information Services Springfield Virginia.
- World Meteorological Organization. (2012). Standardized precipitation index user guide M Svoboda M. Hayes and D. Wood WMO-No 1173 Geneva.
- Yue, S., & Hashino, M. (2003). *Long term trends of annual and monthly precipitation in Japan Journal of American Water Resource Association*, 39, 587–596.
- Yue, S., Pilon, P., & Cavadias, G. (2002). Power of the Mann-Kendall and Spearman's rho tests for detecting monotonic trends in hydrological series. *Journal of Hydrology*, 259, 254–271.
- Yusof, F., Hui-Mean, F., Suhaila, J., & Yousof, Z. (2013). Characterisation of drought properties with bivariate copula analysis. *Water Resources Management*, 27(12), 4183–4207.
- Zhai, J., Su, B., Krysanova, V., Vetter, T., Gao, C., & Jiang, T. (2009). Spatial variation and trends in PDSI and SPI indices and their relation to streamflow in 10 large regions of China. *Journal of Climate*, 23, 649–663. <https://doi.org/https://doi.org/10.1175/2009JCLI2968.1>



# An Investigation Standardized Precipitation Index Trend in Arid and Semi-arid Region of Pakistan Applying the Innovative Trend Analysis (ITA) Technique

Kashif Hussain and Muhammad Shahab

## Abstract

In the arid and Semi-arid regions of Pakistan uncertainties in rainfall, projections are high due to the large fluctuation of climate and lack of observed quality of rainfall data. An extremely dry and wet event of rainfall directly impacts water resources, soil, agricultural yields, and human activities, especially in the arid region. In this study, a short- and long-term wet and dry period in the selected region of Pakistan was expressed using the standardized precipitation index (SPI) based on the 35 years of monthly rainfall data collected from six meteorological stations. In the first step, the short term (SPI-3 and SPI-6) and the long term (SPI-12 and SPI-24) were computed. Results of the study investigated that extreme drought occurred 0–3%, a severe drought occurred 2–7%, and moderate drought occurred 6–15% for the period 3- to 24-month SPI within the study area. Then SPI values trends were detected using a new graphical approach innovative trend analysis (ITA). ITA test shows that in five stations subject to wet conditions trend decrease and severe drought at three stations increase for the period 3-month SPI. Overall results show that the drought trend especially in Lahore, Multan, and Mianwali stations were detected negative (heavier drought) under 3- to 24-month SPI. This study assessment showing that policymaker is required to launch a monitoring program to find out the local or national drought impacts on wheat, rice, and cotton agriculture land as well as on many other sectors, especially in this study region of the country. The general reduction in SPI

values is at some stations that is, a propensity toward heavier dry seasons. These investigated results would also be significant and beneficial for rural agriculture zone where no observed data information exists.

## Keywords

Arid • Drought • ITA • Semi-arid • SPI • Pakistan

## 1 Introduction

The arid regions of the world are characterized by the limited availability of water, the uncertainty of available quantities, and the low natural replenishment of water resources. In recent climate change, water shortage is a crucial problem in arid or semi-arid regions especially that have extensive cash crop agricultural areas and required a solid investigation for prediction of future water demands and water utilization (Shadeed, 2013). The increase in flood's extreme event threats, heat waves, drought, and forest fire due to the influence of climate change has attracted the attention of the international scientist (Caloiero, 2018; Estrela & Vargas, 2012; Kreibich et al., 2017) to work out the possible solution for controlling or mitigation such disasters. Extreme flood and drought are the most complex and least-understood natural disasters (Güner Bacanlı, 2017; Kvočka et al., 2016) expected to occur even more frequently in the future as a result of the influence of climate change. Moreover, understanding drought phenomena, especially in an arid and semi-arid region, is essential for the appropriate planning, policymaking and management of water resources (Caloiero, 2018). Agricultural drought in that region is directly connected to crop failure as a consequence of decreases in soil moisture and has no reference to stream flow (Shadeed, 2013). In many parts of the world, the most important variable of climate is precipitation which can cause the occurrence of drought or flood. To improve water

---

K. Hussain (✉)  
National Development Consultants, 114, Sector-A, Commercial  
Broadway, Phase-VIII, Lahore, 54000, Pakistan

M. Shahab  
Department of Civil Engineering, University of Engineering  
and Technology Peshawar, Peshawar, 25000, Pakistan



management policy for agricultural production, certain regions required important information about precipitation intensities and drought yields (Gocic & Trajkovic, 2013; Jemai et al., 2016). Drought researcher and planners usually depend on some statistical indices, which vary in data requirement and complexity, to decide when to execute water preservation or relief measures against drought (Awchi & Kalyana, 2017; Lloyd-Hughes, 2014) because the drought is a fundamental phenomenon which seriously affects the majority of the world population in different ways such as socially, economically, and environmentally (Cavus & Aksoy, 2019). The evaluation of drought trends and future scenarios is significant for some parts of the national economy including water management sectors, hydropower, forestry, health, biodiversity, and agriculture (Jenkins & Warren, 2015; Osuch et al., 2016). A well-known index, for assessment of the meteorological drought trend in an arid and semi-arid region of Pakistan, standardized precipitation index (SPI) was selected due to its extensive applicability in the world's different climatic zones, e.g., South Africa (Rouault & Richard, 2003), USA (Manatsa et al., 2008), India (He et al., 2009), China (He et al., 2011), Greece (Karavitis et al., 2011), Jordan (Al-Qinna et al., 2011; Saada & Abu-Romman, 2017), Turkey (Karabulut, 2015), UK (Barker et al., 2016), Australia (Halwatura et al., 2015; Rahmat et al., 2012; Rashid & Beecham, 2019) and SPI have innate probabilistic nature and a perfect possibility for carrying out a drought risk assessment (Cancelliere et al., 2007). A trend in the SPI time series was investigated based on the nonparametric Mann-Kendall trend test and innovative trend analysis (ITA). The ITA, a graphical trend evaluation technique, was proposed by Şen (2012) and widely used to the trend detection of hydrometeorological variables. Caloiero (2018) detected the trend in SPI data series employing the ITA method, Wu and Qiana (2017) assessed trends in annual and seasonal rainfall and extreme values by means of the ITA. Zarei (2019) studied trend in spatial and temporal pattern of drought based on Mann-Kendall test. Lee et al. (2016) used the Mann-Kendall method to identify drought trends under extreme climate change over South Korea. Ali et al. (2019) studied long-term and seasonality trends for the Yangtze River flows by means of the ITA and the MK. Gedefaw et al. (2018) detected trend in annual and seasonal rainfall variability by using ITA and MK. The main objectives of this article to investigate the drought in the arid and semi-arid region of Pakistan by applying the SPI at various time scales (3, 6, 12, and 24 months) for rainfall series for the period 1981–2015. To investigate drought trend with the innovative trend analysis (ITA) method in the 3, 6, 12, and 24 monthly SPI.

## 2 Materials and Methods

### 2.1 Study Area

The study focused on six meteorological stations located in the central, eastern, western, and southern parts of province Punjab and one of them located in district D.I. Khan (Khyber Pakhtunkhwa) illustrated in Fig. 1 and the salient characteristics of the meteorological stations are shown in Table 1. Geographically north part of the study area contains steep mountains, the western part contains medium–high mountains and massive deserts are located in the southern of a region. The altitude ranges of selected meteorological stations vary between 122 and 216 m above sea level. The landscape of this region mostly covered the largest part of fertile alluvial plains due to the Indus basin and its four major tributaries. Agriculture is one of the largest sectors of the economy, and it is a principal occupation of the rural population especially living in this region. The climate of the study area is semi-arid to arid, characterized by moderately dry, hot summers, and mild winters. The mean annual minimum temperature changes from 16.3 to 18.2 °C and mean annual maximum temperature varies from 29.3 to 31.3 °C (Abid et al., 2016). The rainfall data from the year 1981 to 2015 that were processed in this analysis were collected from the Pakistan Meteorological Department (PMD). Rainfall events normally occur in monsoon season to account for 70% of the total annual Rainfall.

### 2.2 Standardized Precipitation Index (SPI)

The aim of study is to quantify the precipitation deficit using SPI at different time scales (3, 6, 12, and 24 months) most widely accepted technique based on probability concept and not affected adversely by topography. The SPI versatility allows the researcher to monitor soil moisture/short-term water supplies which are essential for vegetation/agricultural production and as well as to quantify long-term water resources. The SPI index computation for a certain period in any place is based on the long-term rainfall by fitting a probability distribution function to the aggregated data and then transformed to the standard normal distribution with a mean of zero and a standard deviation equal to one (Barker et al., 2016). The SPI is a dimensionless index, positive and negative index values are indicator's wet and drought conditions. The SPI is a relatively simple statistical tool first design by Mckee (1993) used to quantify drought. The standardized precipitation index used in this study was calculated by using R statistic software package `precintcon`,



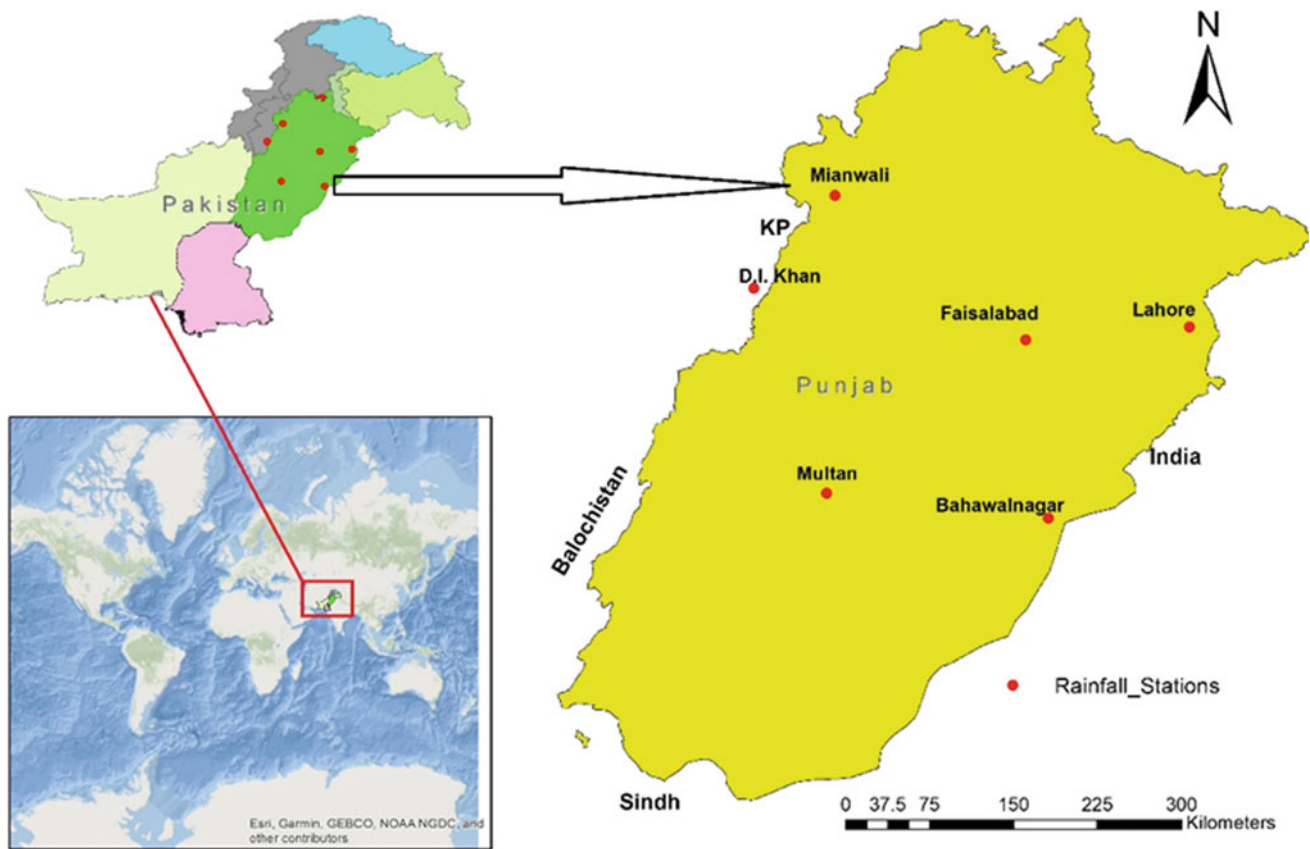


**Fig. 1** Location of the study area showing selected six climate stations

**Table 1** Salient characteristics of the meteorological station in the study area

Sr.#	Station	Elevation (m)	Latitude	Longitude	Record (year)	Period	Max. annual rainfall (mm)	Min. annual rainfall (mm)	Annual rainfall (mm)	Annual standard deviation
1	Bahawalnagar	161.05	29° 20'	73° 51'	35	1981–2015	543.23	57.90	264.4	130.8
2	Faisalabad	185.60	31° 26'	73° 08'	35	1981–2015	807.30	155.80	387.3	137.4
3	Lahore	214.00	31° 33'	74° 20'	35	1981–2015	1231.70	372.20	680.5	205.4
4	Mianwali	203.00	32° 32'	71° 32'	35	1981–2015	1083.40	148.70	508.4	210.4
5	Multan	121.95	30° 12'	71° 26'	35	1981–2015	514.40	83.20	213.5	89.6
6	D. I. Khan	171.20	31° 49'	70° 56'	35	1981–2015	628.70	117.11	322.4	120.4

a detailed SPI index calculation description for different time scale is available in user manual (Povoa & Teixeira, 2016). A classification of the drought is considered in this study according to the values of the SPI illustrate in Table 2.

### 2.3 Innovative Trend Analysis (ITA)

Innovative trend analysis method (ITAM), in recent, is considered one of the most famous trends detection method,

was first proposed by Şen (2012), and has been used in many research studies to assess the trend in the hydrometeorological observations and simulated results accuracy was compared with the MK method (Gedefaw et al., 2018). Drought trend assessment in proposed areas by the ITA method is generally based on graphical representation, a simulated time series before plotting was classified into two equal parts and then arranged independently in ascending order. The first half portion of the simulated results is graphed on the X-axis and the second half portion of the

**Table 2** Classification of drought/wet according to SPI values

SPI value	Class
$SPI \geq 2$	Extremely wet
$1.5 \leq SPI < 2$	Severely wet
$SPI < 1.5$	Moderately wet
$SPI < 1$	Mildly wet
$-1 \leq SPI < 0$	Mild drought
$-1.5 \leq SPI < -1$	Moderate drought
$-2 \leq SPI < -1.5$	Severe drought
$SPI < -2$	Extreme drought

simulated time series is graphed on *Y*-axis, respectively. If the time series data plot shows a scatter of points along a 1:1 (45°) straight line, it indicates no trend in the time series. However, if the scatter of points accumulates above the 1:1 line indicates the trend is increasing and if data points accumulate below the 1:1 indicates the decreasing trend. The ITA has some significant advantage, that it does not require any sample length, serial relationship, and non-normality, etc. ITA can easily detect the trend in the lower, medium, or higher hydrological processes (Kışı et al., 2018; Zekâi Şen; Kisi 2015).

### 3 Results and Discussion

A six-climate station at the district scale of Pakistan has been used in this study to analyze the drought and wet conditions for the period 1981–2015. Before applying the trend method such as MK and ITA, a percent of the month showing extremely wet, severely wet, moderately wet, mild wet, mild drought, moderately drought, severe drought, and extremely drought was evaluated particularly based on the SPI method. As a simulated result, different drought or wet conditions have been detected for each meteorology station considering the 3-, 6-, 12-, and 24-time scales and shown in Fig. 2. It is noticed that severely drought is estimated at 6% by 3-month SPI in Mianwali which is higher than in other regions. In particular, in the Multan and Lahore areas, 37 and 36% mild drought have been detected, while extremely drought condition 3% was estimated in D.I. Khan. From (Fig. 2), a simulated result for 6-month SPI showed comparatively different behavior in some areas concerning the 3-month SPI. In the Bahawalnagar region, mild drought 31%, moderately drought 8%, and severely drought 6% were detected while the percentage of mild wet condition was estimated 37% which is the highest relatively other regions. Considering the 12-month SPI showed that dry conditions of three regions such as Multan, Lahore, and Faisalabad were detected 51, 55, and 51% so the rate of the dry condition in Lahore was found highest under this scenario, and therefore,

dry and wet conditions of Bahawalnagar were detected equal. Conversely, Mianwali and D.I. Khan wet conditions (51 & 52%) are higher than the one showing dry conditions. Finally, the wet and dry conditions of six stations located in the arid or semi-arid region were computed by 24-month SPI that showed a clear difference. A dry condition in Multan was estimated at 56% and the wet condition has been detected 44%. Therefore, dry conditions in Mianwali and Bahawalnagar have also been detected higher than other regions while wet conditions at D.I. Khan were estimated at 54%. Overall the moderate, severe, and extreme drought distribution for the six stations varies between 6–15%, 2–7%, and 0–3% for the period 3–24 months.

The applications of ITA method were applied for possible trend detections in the 3-, 6-, 12-, and 24-month SPI estimated based on the fitted gamma distribution for six stations located in arid and semi-arid region, because it is a vital technique to evaluate climate changes impacts and propose suitable water management policy for the future. As a result, investigated trend by ITA method, for the 3-, 6-, 12-, and 24-month SPI, respectively, from 1981 to 2015, plotted with the ArcGIS were shown in Figs. 3, 4, 5 and 6. To better understanding the tendency of the severe dry and wet conditions of each climate station two vertical line has been added in each trend graph. A red vertical line represents the limit of severe drought ( $SPI = -1.5$ ), and blue vertical line represents the severe wet limit ( $SPI = 1.5$ ). The frequency of severe droughts and severe wet condition in each station under 3-SPI was evaluated based on ITA graphical representations (Fig. 3). The decreasing tendency of the highest values of the index has been detected in four out of 6 stations, which indicated the weaker wet periods in these regions. In Mianwali station, a negative trend of the lowest and positive trend of the highest values of the index have been detected, which mean that extremely drought and weaker wet periods. A positive trend in the lowest value of the index has been detected in D.I. Khan station, thus evidencing weaker droughts. Therefore, in Bahawalnagar and Lahore trend of lowest value of index found positive and trend of highest value of index detected negative, which

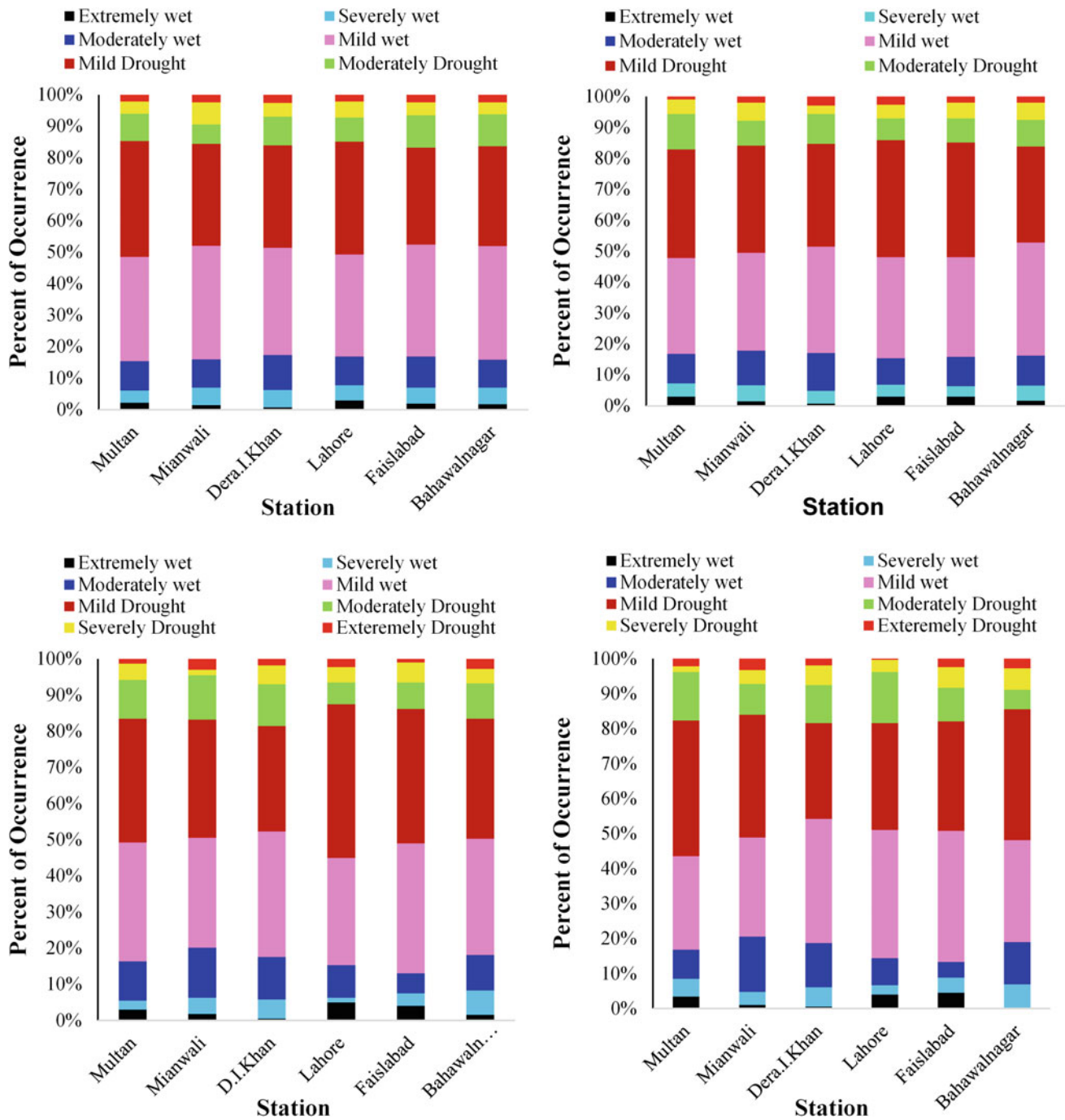


**Fig. 2** Percent of occurrence for SPI-3, -6, -12, and -24 classes for the considered stations through the study period

indicated that in these regions both drought and wet period were weaker. In Multan and Faisalabad, heavier droughts and weaker wet period have been detected according to the ITA method for 3-SPI.

The 6-month SPI results at Bahawalnagar station showed similar trend as detected in 3-month SPI. In both cases, it was investigated that the improvement of plant life and farming in that area required specially strategies. In D.I.

Khan station, a different trend result is obtained for the 6-SPI as comparatively 3-SPI. A Fig. 4, indicated that a trend of lowest and highest value of index has been detected positive at D.I. Khan stations, which are representing the weaker drought and stronger wet period. In fact, trend results obtained by ITA method in Lahore station for 6-SPI also different to the 3-SPI. In this station, trend of lowest and highest value of index has been detected negative under

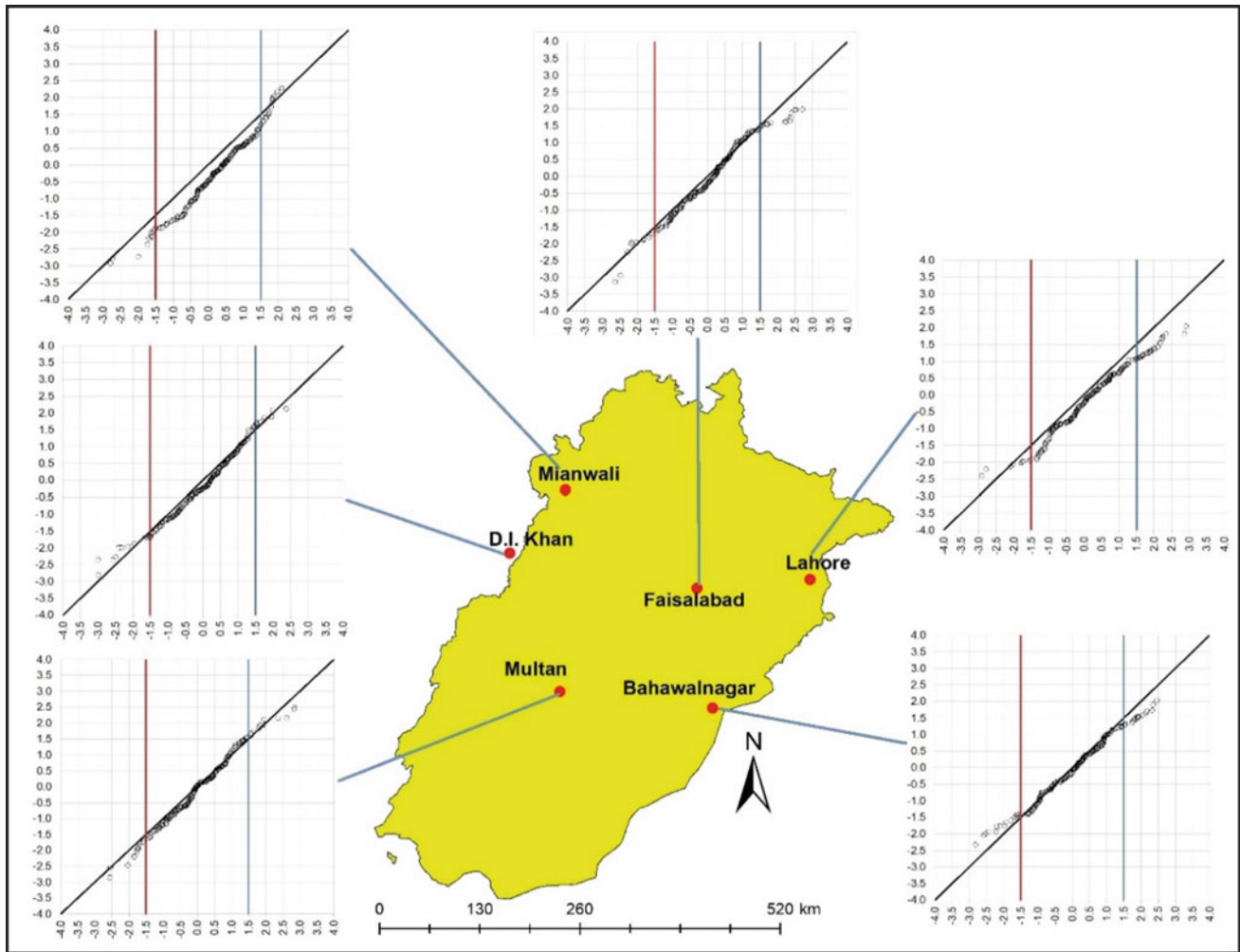


**Fig. 3** Six rainfall station results of the innovative trend analysis (ITA) method for 3-SPI

6-SPI. In the Multan and Faisalabad stations, trend of lowest and highest value of index has been detected negative. Finally, the Mianwali station has negative trend in lowest value of index and positive has been trend detected in highest value of index.

The trends of 3-SPI and 6-SPI series of index value computed to check drought or wet conditions impacts on vegetation and crop farming practice, because agriculture in these areas is one of the major sources of earning especially population living in rural area. As trend detected results based on these two time scales, a positive wet condition was quantified in Mianwali, but majority of the station indicated negative trend of the highest SPI value, which dominating the weaker wet periods. These evaluations reflect a broader change in climate change. The 12-month SPI estimated data

series for the six stations of this study is shown in Fig. 5. The 12-SPI index is commonly used to define the excess of rainfall or to identify hydrological extremes in the study areas. Considering the medium time scales, the 12-month SPI computed data series trend showed relatively similar results than the 6-month SPI in most of the stations but with an increase in the negative trend of both lower and highest value of index. The Lahore and Multan stations' 12-SPI lowest and highest index value trend detected negative, while in D.I. Khan a positive trend was detected in both lowest and highest index values.

A long-term water resources management used for agriculture production in arid and semi-arid region required special policy and technique. The computation of 24-SPI directly connected to describe the water resources condition

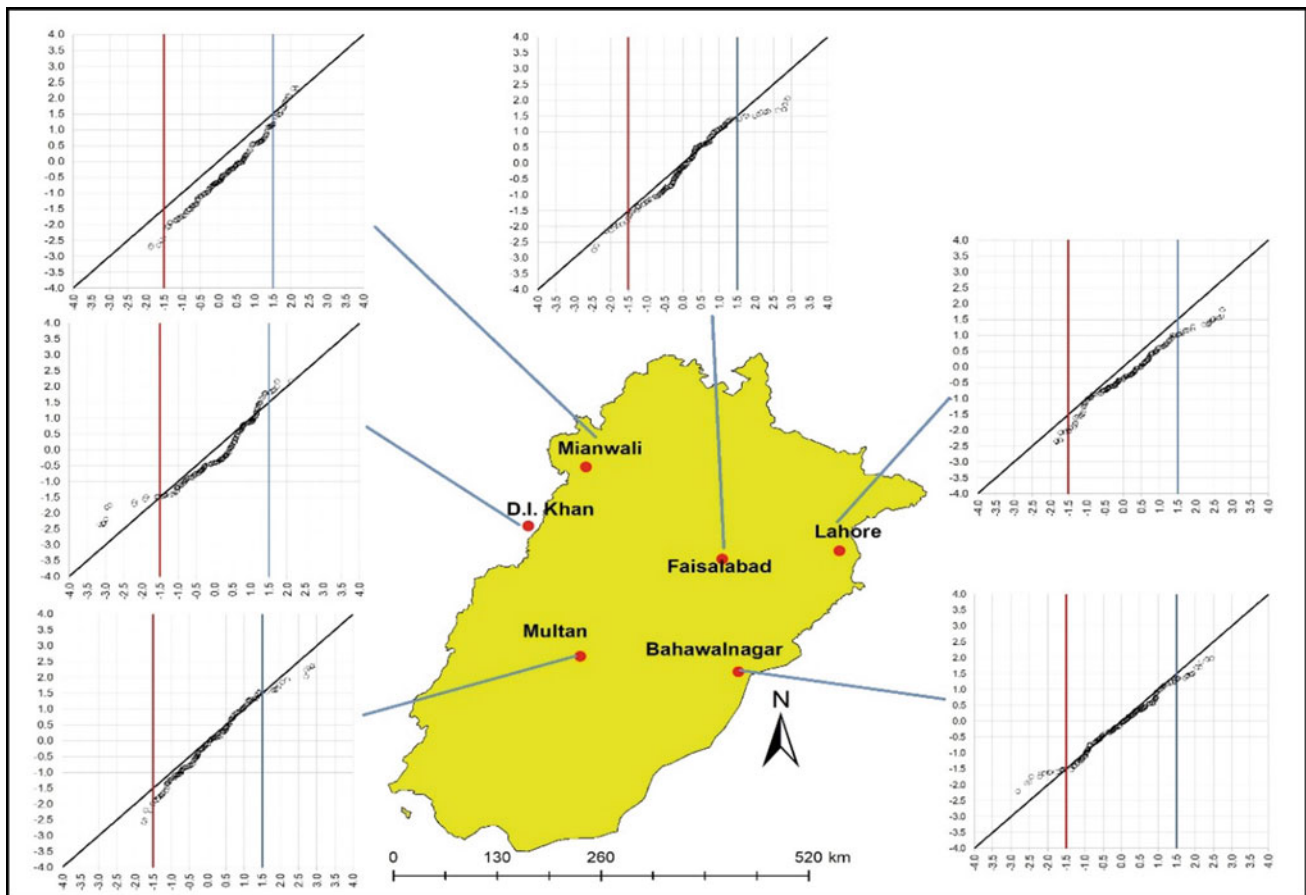


**Fig. 4** Six rainfall station results of the innovative trend analysis (ITA) method for 6-SPI

in the study area can be helpful for planning and management strategy. The trend investigated by ITA graphical technique for 24-month SPI within the study area was shown in Fig. 6. The results of three rainfall station (Mianwali, D.I Khan & Faisalabad) indicated the positive trend for highest index value. The trend of lowest index value at Mianwali and Faisalabad has been detected negative, while trend of lowest index value at D. I. Khan has been detected positive which showed the drought reduction. The trend of lowest and highest index value at Lahore and Multan station was investigated negative, which indicated the heavier drought and weaker wet conditions. At Bahawalnagar station, trend of lowest index value was also detected positive, while no trend of highest index value has been detected.

## 4 Conclusions

Drought and extreme wet events are one of the most drastic natural disasters that impact agriculture production, soil quality, society's environment, economy, and life of living organisms throughout the world. The assessment of the meteorological drought in six climate stations located in the arid and semi-arid region of Pakistan during the years 1981–2015 has been investigated by using the standardized precipitation index (SPI) for multiple timescales 3-, 6-, 12-, and 24-month. Results of the study show that extreme drought occurred 0–3%, a severe drought occurred 2–7%, and moderate drought occurred 6–15% for the period 3- to



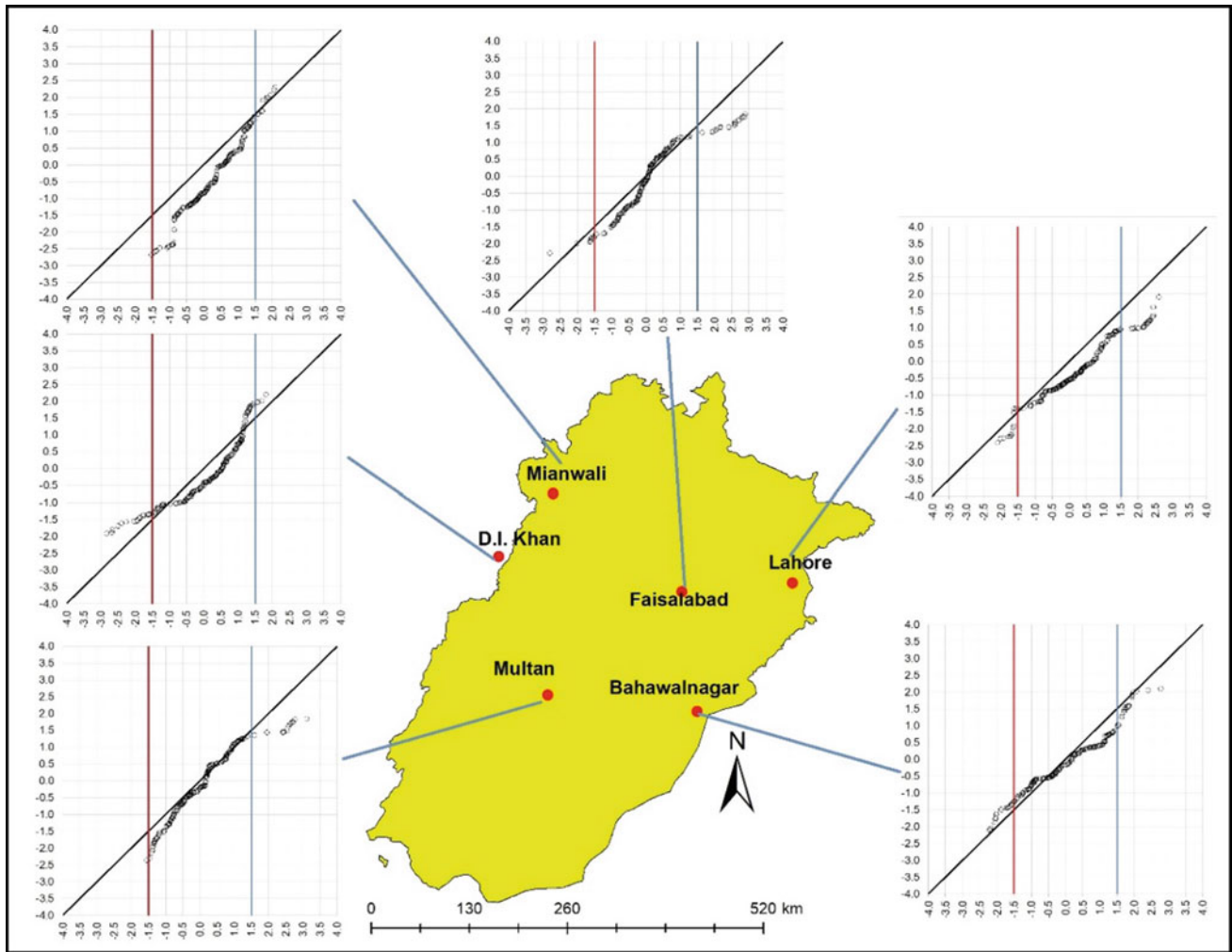


**Fig. 5** Six rainfall station results of the innovative trend analysis (ITA) method for 12-SPI

24-month SPI within the study area. Consequently, rainfall deficiency at Lahore station has been investigated higher and 42% mild drought detected for the period 12-month SPI. A dry condition in Multan was estimated at 56%, and wet conditions have been detected 44%. Innovative trend analysis (ITA), a graphical technique, was used to assess the trend for the standardized precipitation index (SPI) values. ITA test shows that in five stations (Multan, Lahore,

Faisalabad, Bahawalnagar, D.I. Khan) subject to wet conditions, trend decreases and severe drought at three stations increases for the period 3-month SPI. Overall results show that drought trends especially in Lahore, Multan, and Mianwali stations were detected negative (heavier drought) under 3- to 24-month SPI. This spatial trend analysis of drought might help policymakers to achieve better planning for natural resources management.

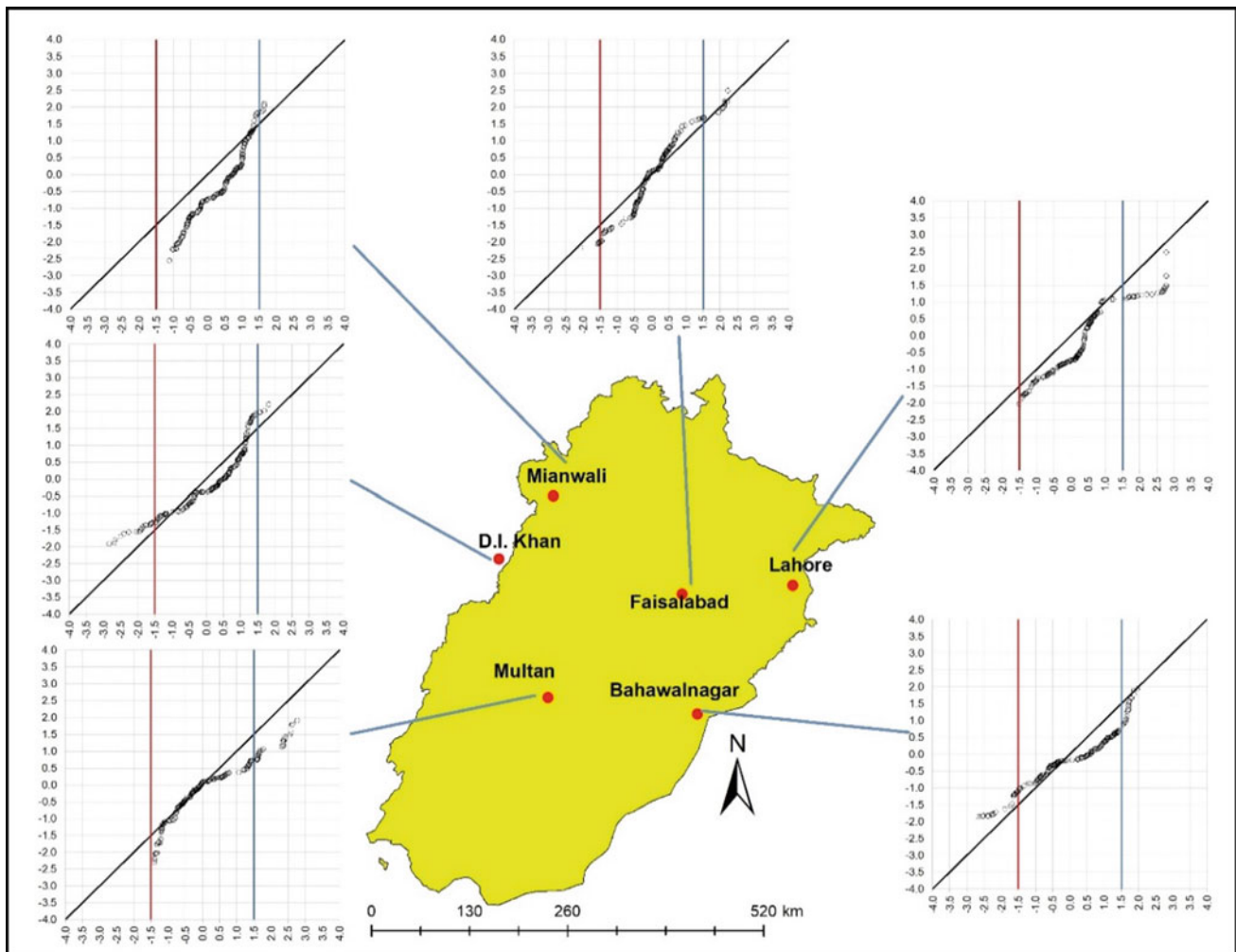


**Fig. 6** Six rainfall station results of the innovative trend analysis (ITA) method for 24-SPI

**Acknowledgements** The data for the study was provided by the Pakistan Meteorological Department (PMD). We appreciate their help and cooperation.

## References

- Abid, M., Schilling, J., Scheffran, J., & Zulfiqar, F. (2016). Climate change vulnerability, adaptation and risk perception at farm level in Punjab, Pakistan. *Science of Total Environment*, 547, 447–460.
- Al-Qinna, M. I., Hammouri, N. A., Obeidat, M. M., & Ahmad, F. Y. (2011). Drought analysis in Jordan under current and future climates. *Climatic Change*, 106(3), 421–440.
- Ali, R., Kuriqi, A., Abubaker, S., & Kisi, O. (2019). Long-term trends and seasonality detection of the observed flow in Yangtze River using Mann-Kendall and Sen's innovative trend method. *Water (Switzerland)*, 11(9), 1855.
- Awchi, T. A., & Kalyana, M. M. (2017). Meteorological drought analysis in Northern Iraq using SPI and GIS. *Sustainable Water Resources Management*, 3(4), 451–463.
- Barker, L. J., Hannaford, J., Chiverton, A., & Svensson, C. (2016). From Meteorological to hydrological drought using standardised indicators. *Hydrology and Earth System Sciences*, 20(6), 2483–2505.
- Caloiero, T. (2018). SPI Trend analysis of New Zealand applying the ITA technique. *Geosciences (Switzerland)*, 8(3), 101.
- Cancelliere, A., Di Mauro, G., Bonaccorso, B., & Rossi, G. (2007). Drought forecasting using the standardized precipitation index. *Water Resources Management*, 21(5), 801–819.
- Cavus, Y., & Aksoy, H. (2019). Spatial drought characterization for Seyhan River basin in the mediterranean region of Turkey. *Water (Switzerland)*, 11(7), 1331.
- Estrela, T., & Vargas, E. (2012). Drought management plans in the European Union. The case of Spain. *Water Resources Management*, 26(6), 1537–1553.
- Gedefaw, M., et al. (2018). Innovative trend analysis of annual and seasonal rainfall variability in Amhara Regional State, Ethiopia. *Atmosphere*, 9(9).
- Gocic, M., & Trajkovic, S. (2013). Analysis of precipitation and drought data in Serbia over the period 1980–2010. *Journal of Hydrology*, 494, 32–42.
- Bacanli, G., & Ülker, . (2017). Trend analysis of precipitation and drought in the Aegean region, Turkey. *Meteorological Applications*, 24(2), 239–249.
- Halwatura, D., Lechner, A. M., & Arnold, S. (2015). Drought severity-duration-frequency curves: A foundation for risk

- assessment and planning tool for ecosystem establishment in post-mining landscapes. *Hydrology and Earth System Sciences*, 19(2), 1069–1091.
- He, B., et al. (2011). Drought hazard assessment and spatial characteristics analysis in China. *Journal of Geographical Sciences*, 21(2), 235–249.
- He, Y., et al. (2009). Tracking the uncertainty in flood alerts driven by grand. *Meteorological Applications*, 16(1), 91–101.
- Jemai, S., Ellouze, M., Agoubi, B., & Abida, H. (2016). Drought intensity and spatial variability in Gabes watershed, South-Eastern Tunisia. *Journal of Water and Land Development*, 31(1), 63–72.
- Jenkins, K., & Warren, R. (2015). Quantifying the impact of climate change on drought regimes using the standardised precipitation index. *Theoretical and Applied Climatology*, 120(1–2), 41–54.
- Karabulut, M. (2015). Drought analysis in Antakya-Kahramanmaraş Graben, Turkey. *Journal of Arid Land*, 7(6), 741–754.
- Karavitis, C. A., Alexandris, S., Tsesmelis, D. E., & Athanasopoulos, G. (2011). Application of the standardized precipitation index (SPI) in Greece. *Water (Switzerland)*, 3(3), 787–805.
- Kisi, O. (2015). An innovative method for trend analysis of monthly pan evaporations. *Journal of Hydrology*, 527, 1123–1129.
- Kişi, Ö., Guimarães Santos, C. A. R., Marques da Silva, R., & Zounemat-Kermani, M. (2018). Trend analysis of monthly streamflows using Şen's innovative trend method. *Geofizika*, 35(1), 53–68.
- Kreibich, H. et al. 2017. "Adaptation to Flood Risk: Results of International Paired Flood Event Studies." *Earth's Future* 5(10).
- Kvočka, D., Falconer, R. A., & Bray, M. (2016). Flood hazard assessment for extreme flood events. *Natural Hazards*, 84(3), 1569–1599.
- Lee, J. H., Kwon, H. H., Jang, H. W., & Kim, T. W. (2016). Future changes in drought characteristics under extreme climate change over South Korea. *Advances in Meteorology* (1).
- Lloyd-Hughes, B. (2014). The impracticality of a universal drought definition. *Theoretical and Applied Climatology*, 117(3–4), 607–611.
- Manatsa, D., Chingombe, W., & Matarira, C. H. (2008). The impact of the positive Indian Ocean dipole on Zimbabwe droughts. *International Journal of Climatology*, 28, 2011–2029.
- McKee, T. B., Doesken, N. J., & Kleist, J. (1993). The relationship of drought frequency and duration to time scales. In: *Eighth Conference on Applied Climatology*, Anaheim, California.
- Osuch, M., Romanowicz, R. J., Lawrence, D., & Wong, W. K. (2016). Trends in projections of standardized precipitation indices in a future climate in Poland. *Hydrology and Earth System Sciences*, 20(5), 1947–1969.
- Povoa, L. V., & Teixeira, J. (2016). Package 'Precintcon.' <https://cran.r-project.org/web/packages/precintcon/precintcon.pdf>.
- Rahmat, S. N., Jayasuriya, N., & Bhuiyan, M. (2012). Trend analysis of drought using standardised precipitation index (SPI) in Victoria, Australia. In *Proceedings of the 34th Hydrology and Water Resources Symposium, HWRS 2012* (pp. 441–448).
- Mamunur, R. M., & Beecham, S. (2019). Characterization of meteorological droughts across South Australia. *Meteorological Applications*, 26(4), 556–568.
- Rouault, M., & Richard, Y. (2003). Intensity and spatial extension of drought in South Africa at different time scales. *Water SA*, 29(4), 489–500.
- Saada, N., & Abu-Romman, A. (2017). Multi-site modeling and simulation of the standardized precipitation index (SPI) in Jordan. *Journal of Hydrology: Regional Studies*, 14(October), 83–91.
- Şen, Z. (2012). Innovative trend analysis methodology. *Journal of Hydrologic Engineering*, 17(9), 1042–1046.
- Şen, Z. (2013). Trend identification simulation and application. *Journal of Hydrologic Engineering*, 19(3), 635–642.
- Shadeed, S. (2013). Spatio-temporal drought analysis in arid and semi-arid regions: A case study from Palestine. *Arabian Journal for Science and Engineering*, 38(9), 2303–2313.
- Wu, H., & Qian, H. (2017). Innovative trend analysis of annual and seasonal rainfall and extreme values in Shaanxi, China, since the 1950s. *International Journal of Climatology*, 37(5), 2582–2592.
- Zarei, A. R. (2019). Analysis of changes trend in spatial and temporal pattern of drought over South of Iran using standardized precipitation index (SPI). *SN Applied Sciences*, 1(5), 1–14.



# The Impacts of Land-Use Change on the Runoff Characteristics Using HEC-HMS Model: A Case Study in Wadi Al-Mulaikhy Sub-Watershed in Sana'a Basin, Yemen

Ibrahim Al-Samawi, Abdullah Noman, Khaled Khanbari, Hadi Quriaa, Nabil Al-Areeq, and Musaed Aklan

## Abstract

Runoff is affected by several parameters such as soil type, and Land-use/cover changes, which include vegetation cover and level of urbanization. The current study assesses the impact of Land-use/cover change between 1994 and 2018, on the runoff characteristics of Wadi Al-Mulaikhy Sub-watershed in the Sana'a basin, Yemen by integrated GIS, HEC-GeoHMS extension, and HEC-HMS model. Remote sensing data, land-use/cover, soil type, and rainfall are the main input data. The study results show that the agricultural area was reduced by 5.67%. Conversely, the surface runoff for the overall study area has been increased by 1.65%. It was found that there is no significant change in runoff volume relative to Land-use/cover change due to some agricultural general class changes to other classes (shrubs/brush), which have similar runoff characteristics. The second change, agricultural general class changes to urban classes (urban high density, urban medium to low density and roads) which occurred at the north of the study area near the boundary of the city of Sana'a which has an urban expansion. The changes in runoff parameters were found in the sub-basin (W300, W310, and W320) which are located in the north of the study area due to the changes of agricultural general class to urban classes (urban high density, urban medium to low density, and roads).

## Keywords

Runoff • Land-use/cover • GIS • HEC-HMS • Agriculture • Runoff • Sanaa basin • Yemen

## 1 Introduction

Water is the most essential natural resource for living species. Since the available amount of water is limited, scarce, and not spatially distributed in relation to the population needs, proper management of water resources is essential to satisfy the current demands as well as to maintain sustainability (Geremew, 2013).

Water availability in Sana'a City, capital of Yemen, is one of the scarcest in the world. The region has no perennial surface water runoff, and is practically dependent on the use of groundwater. Over-exploitation is causing the groundwater table to deplete at an alarming rate and Sana'a Basin, with a water table drawdown of about 3 m per annum, is amongst the worst affected areas in the country (Al-Derwish, 2014).

Change in runoff characteristics that induced by urbanization, is important for understanding the effects of Land-use/cover change on earth surface hydrological processes. With urban land development, the impervious land surfaces expand rapidly, and the capability of rainfall detention declines sharply and runoff coefficient increases. Usually, urbanized land leads to a decrease in surface roughness; hard road and drainage system can greatly shorten the time of runoff confluences (Shi et al., 2007).

Remote Sensing and Geographic Information System (GIS) provide effective tools for Land-use/cover planning and modeling. Land-use/cover change is an indicator of human interaction with nature. Therefore, it is necessary to discover and monitor Land-use/cover changes in order to either protect the environment or ensure sustainable development (Mousazadeh et al., 2015).

I. Al-Samawi (✉) · H. Quriaa · N. Al-Areeq  
National Water Resource Authority (NWRA), Sana'a, Yemen

A. Noman · M. Aklan  
Water and Environment Center, Sana'a University, Sana'a,  
Yemen

K. Khanbari  
Department of Earth and Environmental Sciences, Sana'a  
University, Sana'a, Yemen

I. Al-Samawi · K. Khanbari  
Yemen Remote Sensing and GIS Center, Sana'a, Yemen

Hydrological modeling is a commonly used tool to estimate the basin's hydrological response due to precipitation. It allows to predict the hydrologic response to various watershed management and to have a better understanding of the impacts of these practices (Choudhari et al., 2014).

Several studies have been conducted using the HEC-HMS model in different regions under different soil and climatic conditions. The model was precisely obtained in spatially and temporally predicting watershed response in event-based and continuous simulation as well as simulating various scenarios in flood forecasting and early warnings (Choudhari et al., 2014). From regional perspective, there have been abundant researches on the impact of land-use change on runoff. Some of them used lumped models and others used distributed and semi-distributed models to estimate the runoff characteristics, and each of these models has its own merits and demerits. (Mistry et al., 2017; Köylü & Geymen, 2016; Nachshon et al., 2016; Ajmal et al., 2015; Tiwari et al., 2014; Ramakrishnan et al., 2009; Shi et al., 2007; Noman, 2016) calculated the surface runoff by using SCS-CN method. Other studies calculated runoff volume by using semi-distributed models (Maisa'a et al., 2017; Sajikumar & Remya, 2015; Ngo et al., 2015; Maalim et al., 2013; Hundecha & Bárdossy, 2004).

The objectives of this study can be summarized as flowing: (1) Produce Land-use/cover maps of the Wadi Al Mulaikhy sub-watershed in Sana'a basin, (2) Assess the change in land-use between 1994 and 2018, (3) Assess the change in surface runoff volume between 1994 and 2018 by using HEC-HMS model.

## 2 Data and Methods

### 2.1 Study Area and Data Acquisition

The study area is located in Wadi Al Mulaikhy in the southern part of the Sana'a Basin as showing in (Fig. 1). The total area of Wadi is 63.2 km<sup>2</sup> and located in the upstream of Sana'a Basin and it has one major stream that extends from south to north. Its coordinate is between (1,687,890 to 1,675,760 N) longitude and (407,908 to 418,001 E) latitude. The average monthly temperature from National Water Resource Authority (NWRA) records 1989–1997 ranges between about 15 and 25. The annual rainfall is 249 mm (JICA, 2007). The data analysis of the present study was carried out using the available data:

- Aerial photo (1994) with spatial resolution one meter which have been supplied by the General Authority of Land, Survey and Urban Planning. The satellite image (2018) with spatial resolution 60 cm which was obtained from Google Earth.

- Digital Elevation Model (DEM) with a resolution of 20 m which has been supplied by Yemen Remote Sensing and GIS Center.
- Soil map with spatial resolution 30 s which was obtained from Harmonized World Soil Database (HWSD).
- The processing of images was made by using ArcGIS version 10.4.1 software and HEC-GeoHMS extension which was used to create the basic model.

### 2.2 Land-Use/Cover Classification and Mapping

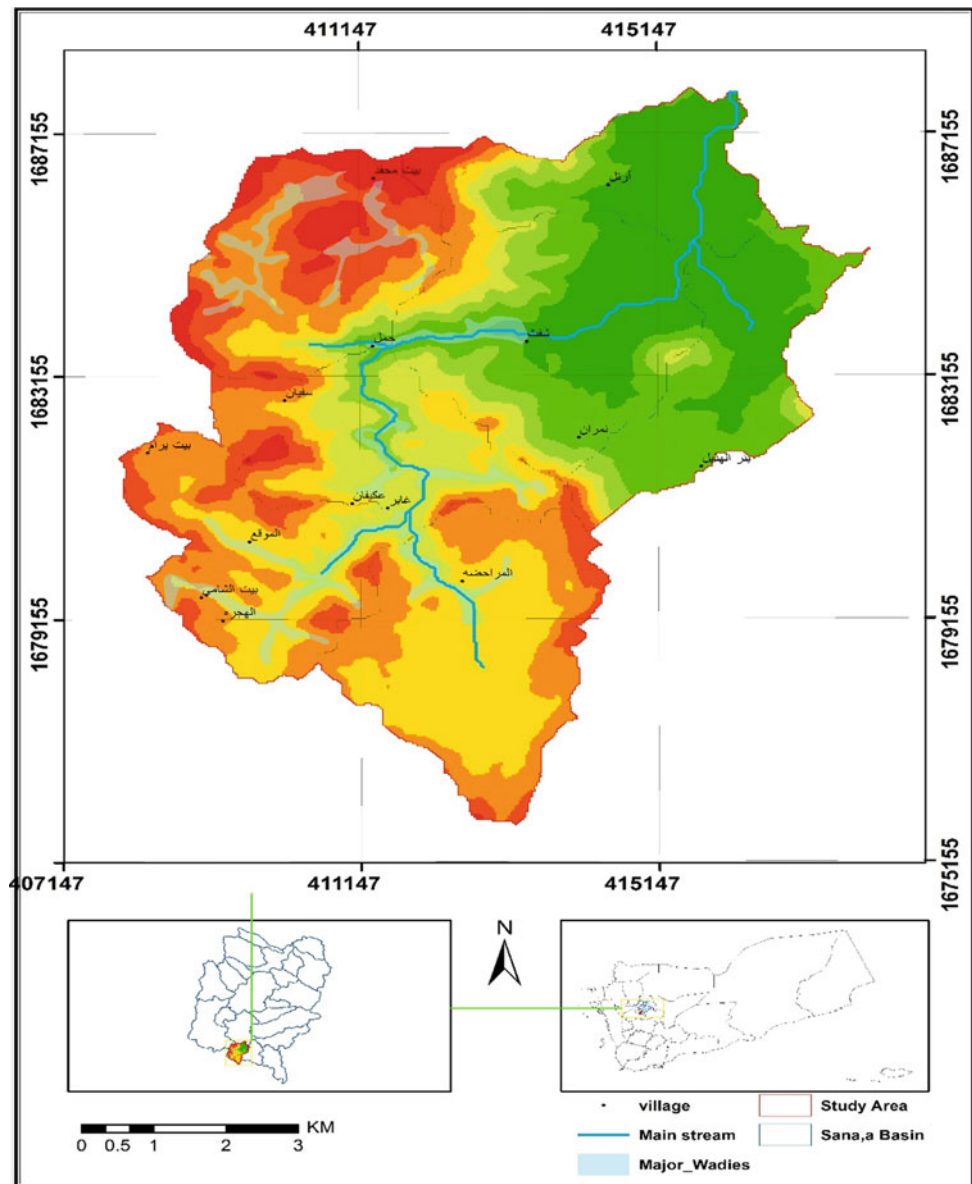
The geo-referencing operation of the aerial photo (1994) and satellite image (2018) of the study area was performed based on the digital map of the Republic of Yemen. The coordinate system was set on Universal Transverse Mercator (UTM) zone 38 north WGS84. Land-use classification was digitizing manually. The study area was classified into six Land-use/cover classes including: Urban High Density, Urban Medium to Low Density, Agriculture General, Barren/Minimal Vegetation, Shrub/Scrub, and Roads. The total area of Land-use/cover category for the years 1994 and 2018 were calculated.

### 2.3 Creation The Basin Model

The basin model was created by using HEC-GeoHMS GIS extension in ArcMap. The first step was delineating the stream network and watershed boundaries of the study area. This process is commonly referred to as terrain preprocessing and is entirely based on the input digital elevation model (DEM). The GRID files were derived from the DEM are fill sink grid, flow direction grid, flow accumulation grid, stream definition grid, stream segmentation grid, and catchment grid. The vector layers were created based on the previous computational steps which divided Wadi Al-Mulaikhy into seven sub-basins catchment polygons, drainage line, and adjoint catchment (Fig. 2). The hydrologic modeling was based on the SCS Curve Number Loss Model. This method only requires the definition of a single input parameter curve number (CN). The CN depends on the land-use, the hydrologic soil group, and the hydrologic condition of the top soil. The Land-use/cover classification, the semi-arid climatic characteristics of the area, the CN table for arid and semi-arid rangeland were used with hydrologic soil group map for creating CN grid numbers. The basin model file contains the hydrological data structure which includes the hydrologic elements, their connectivity, and related parameters. HEC-GeoHMS can be exported some of the hydrologic parameters to HMS basin model file. Background map, basin file, and meteorological model file were created by



**Fig. 1** Location map of the Wadi Al Mulaikhy sub-watershed in Sana'a Basin, Yemen



generate rainfall gage grid layers and import it to HEC-GeoHMS geo-database.

### 2.4 Model Completion in HEC-HMS Model

The basin model was imported into a HEC-HMS project by using the HEC-GeoHMS data export to HMS function. The model consists of 7 basin, 8 junctions, 4 reaches, and the basin outlet. In addition to the basin model and the meteorological model, the simulation of runoff volume for the years 1994 and 2018 was calculated in HEC-HMS by using SCS-CN curve number losses method. The basic runoff equation of the CN method is shown in Eq. (1).

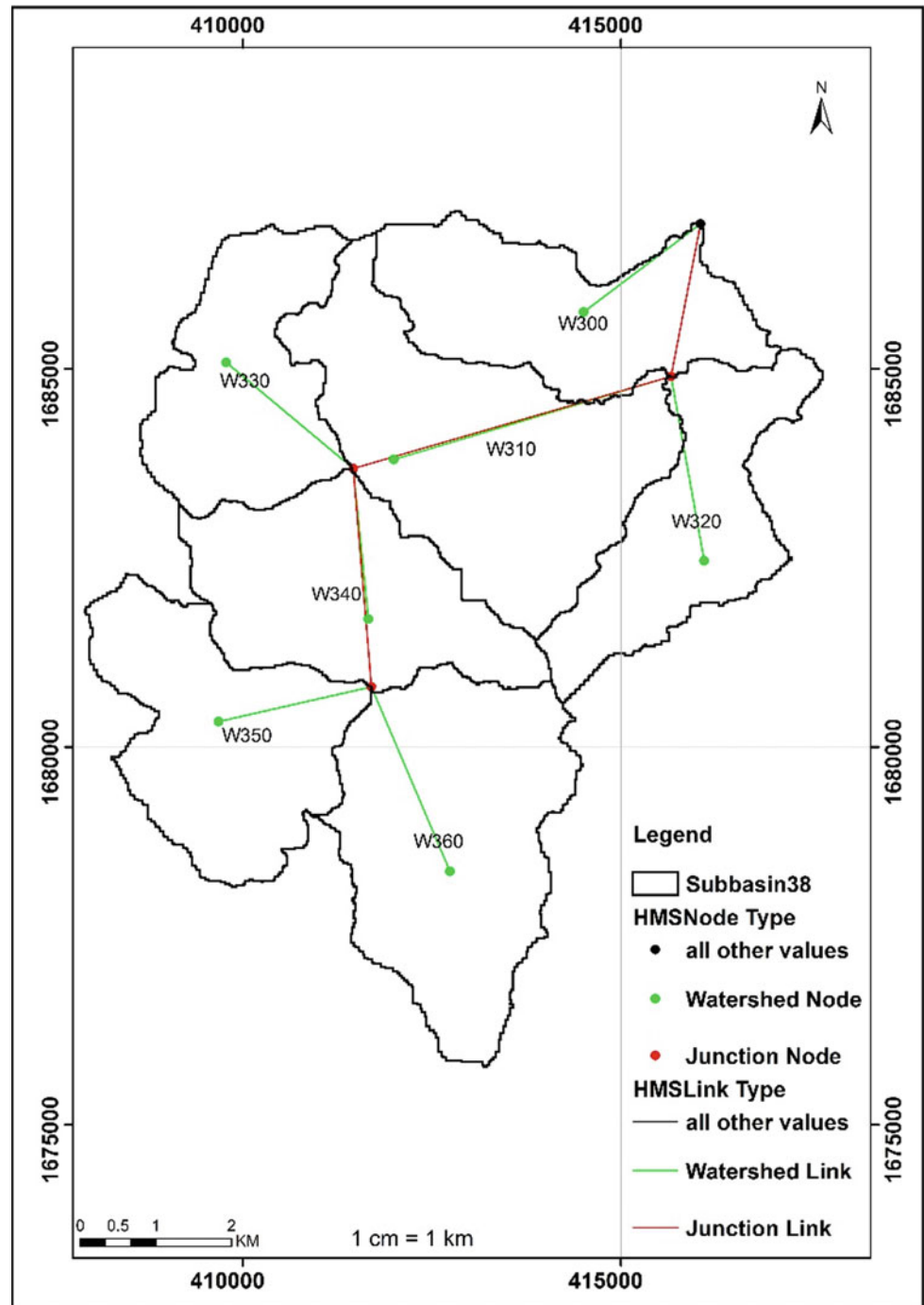
$$Q = \frac{(P - I_a)^2}{(P - I_a) + S} \tag{1}$$

where,  $Q$  = runoff (mm),  $P$  = rainfall (mm),  $S$  = potential maximum retention after runoff begins (mm),  $I_a$  = initial abstraction.

The initial abstraction includes all the losses that occur before surface runoff begins. According to the NRCS (2004), it contains water retained in surface depressions as well as water intercepted by vegetation, evaporation, and infiltration. In the CN model,  $I_a$  is assumed to be correlated to  $S$  through Eq. (2).

$$I_a = 0.2 S \tag{2}$$

**Fig. 2** Model representation of Wadi Al-Mulaikhy Watershed in HEC-GeoHMS



The maximum retention  $S$  is further related to the soil and cover conditions of the analyzed watershed through the CN by Eq. (3).

$$S = \frac{25,400}{CN} - 254 \quad (3)$$

In the HEC-HMS modeling process, the incremental excess rainfall for each computation time interval is calculated as the difference between the accumulated excess at the end of and the beginning of the period. The cumulative excess  $P_e$  is computed with Eq. (4).

$$P_e = \frac{(P - 0.25S)^2}{P + 0.8S} \quad (4)$$

### 3 Results and Discussion

#### 3.1 Land-Use/Cover Changes

Land-use/cover maps of the study area in 1994, and 2018 which were generated manually, include land-use categories for agriculture general, barren/minimal vegetation, shrub/scrub, roads, urban high density, and urban medium to low density. The area of each Land-use/cover type of different years and the changes procedures over 24 years are shown in (Table 1). Most of the area of Wadi Al-Mulaikhy is covered by barren/minimal vegetation distributed throughout the basin for the two periods of time 1994 and 2018, also agriculture general distributed throughout the study area. Shrub/Scrub areas are covering a small area and spread in the north and middle of the basin. The low, medium, and high density of urban areas are located in the northeast of the study area. The land-use/cover classification of 1994 (Fig. 3) was compared to the Land-use/cover classification of 2018 (Fig. 4) to identify the area where the main changes between 1994 and 2018 occurred. The results of land-use changes show a decrease in the agriculture general Land-use/cover category. (Table 1) shows that the area of Wadi Al Mulaikhy sub-watershed with the land-use classes Urban High Density, Urban Medium to Low Density, Barren/Minimal Vegetation, Shrub/Scrub and roads increased (1.5%, 0.22%, 0.53%, 2.84%, 0.55%), respectively, with increasing of total area 5.65 km<sup>2</sup> about 8.96%. Whereas the agriculture general has decreased by about 5.65% over 24 years period. The major change in agriculture general class is the conversion to Shrub/Scrub and urban with high and medium to low-density classes (2.8% and 1.7%) respectively. The

major increase of the urban area occurred on the north at the boundary of the study area due to urban expansion of Sana, a city in addition to the simple conversion of agricultural general class to roads, shrub/scrub, and Barren/Minimal Vegetation.

#### 3.2 Runoff Changes

As previously mentioned, the HEC-HMS model was used to calculate runoff volume for the two Land-use/cover periods (1994, 2018). The results of runoff changes are related to Land-use/cover changes for the periods 1994, 2018 are presented in (Table 2). Modeling results indicated that the largest volume of runoff in 2018 ( $1291.9 \times 10^3$  m<sup>3</sup>/year), and the volume of runoff in 1994 ( $1270.9 \times 10^3$  m<sup>3</sup>/year). Thus, it increased by 2100 cubic meter about 1.652% over 24 years (Fig. 6). The results of land-use changes between the two periods are indicating that the total change in Land-use/cover categories increased by 5.66% in the categories (urban high density, urban medium to low density, barren/minimal vegetation, shrub/scrub, and roads) by (1.5%, 0.22%, 0.53%, 2.84%, and 0.55%) respectively, and 5.66% decreased from agriculture general. Since the increase in urban high density and urban medium to low density 1.7%, the increasing in roads 0.5% and the increasing in barren/minimal vegetation and shrub/scrub 3.6%. The decrease in agriculture general 5.66% means an increase in the volume of runoff 1.652% and peak discharge 1.27% due to the increase in Urban High density and urban medium to Low density 1.73.

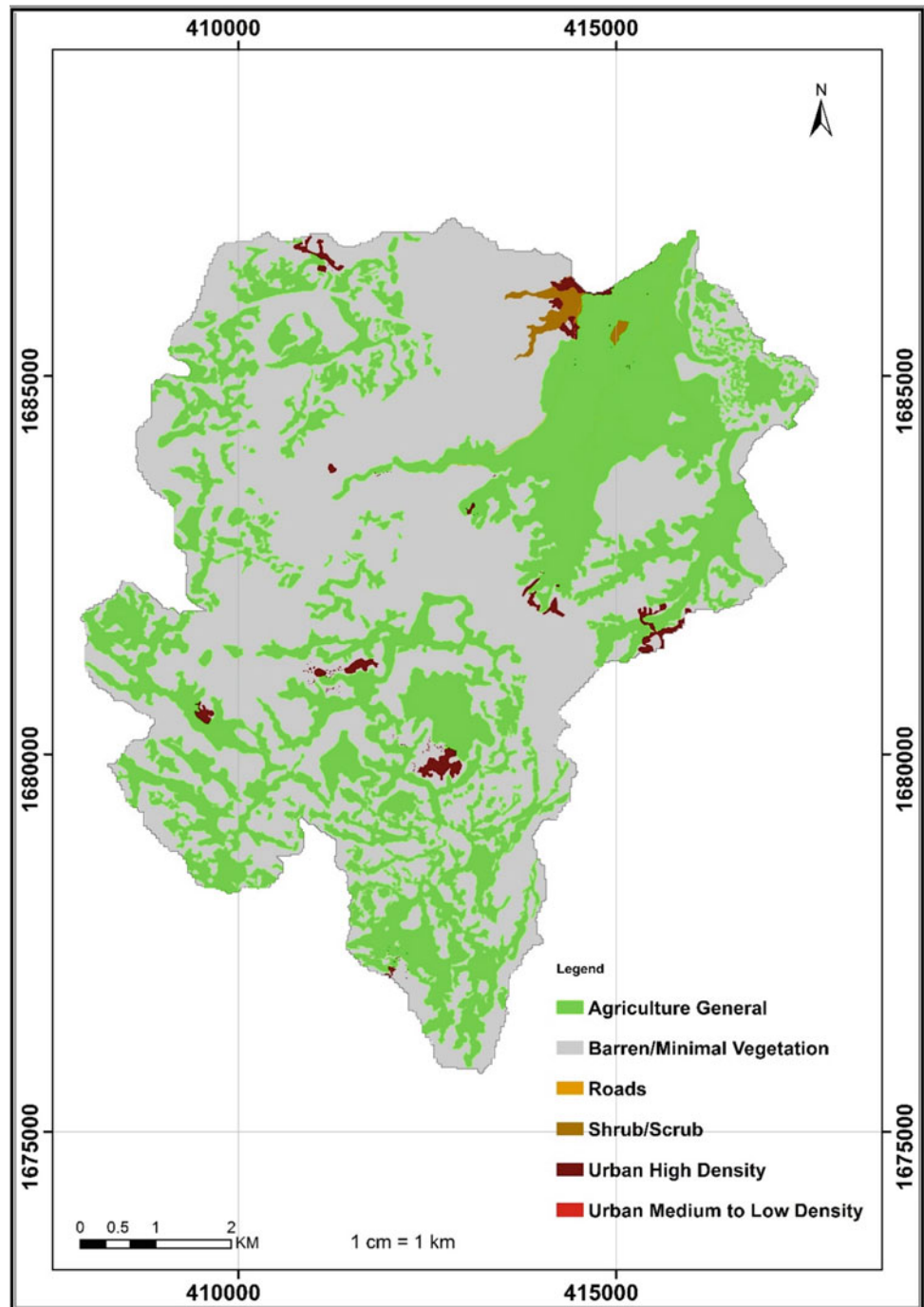
#### 3.3 CN Values

The average of the curve number (CN) values for Land-use/cover in the years 1994, 2018 is (88.69, 89.46)

**Table 1** Total estimated area of land-use/cover classes in Wadi Al-Mulaikhy sub-watershed in 1994 and 2018

No.	Land-use classes	Land-use classes	Area 1994 (%)	Area 2018 in (km <sup>2</sup> )	Area 2018 (%)	Change percent (%)
1	Urban high density	0.62	0.98	1.57	2.49	1.51
2	Urban medium to low density	0	0	0.13	0.22	0.22
3	Agriculture general	24.14	38.32	20.57	32.65	-5.67
4	Barren/minimal vegetation	37.86	60.09	38.19	60.62	0.53
5	Shrub/scrub	0.32	0.50	2.11	3.35	2.84
6	Roads	0.05	0.089	0.40	0.63	0.55
Sum		<b>63.00</b>	100	<b>63.00</b>	100	

**Fig. 3** Land use map of Wadi Al-Mulaikhy sub-watershed in 1994

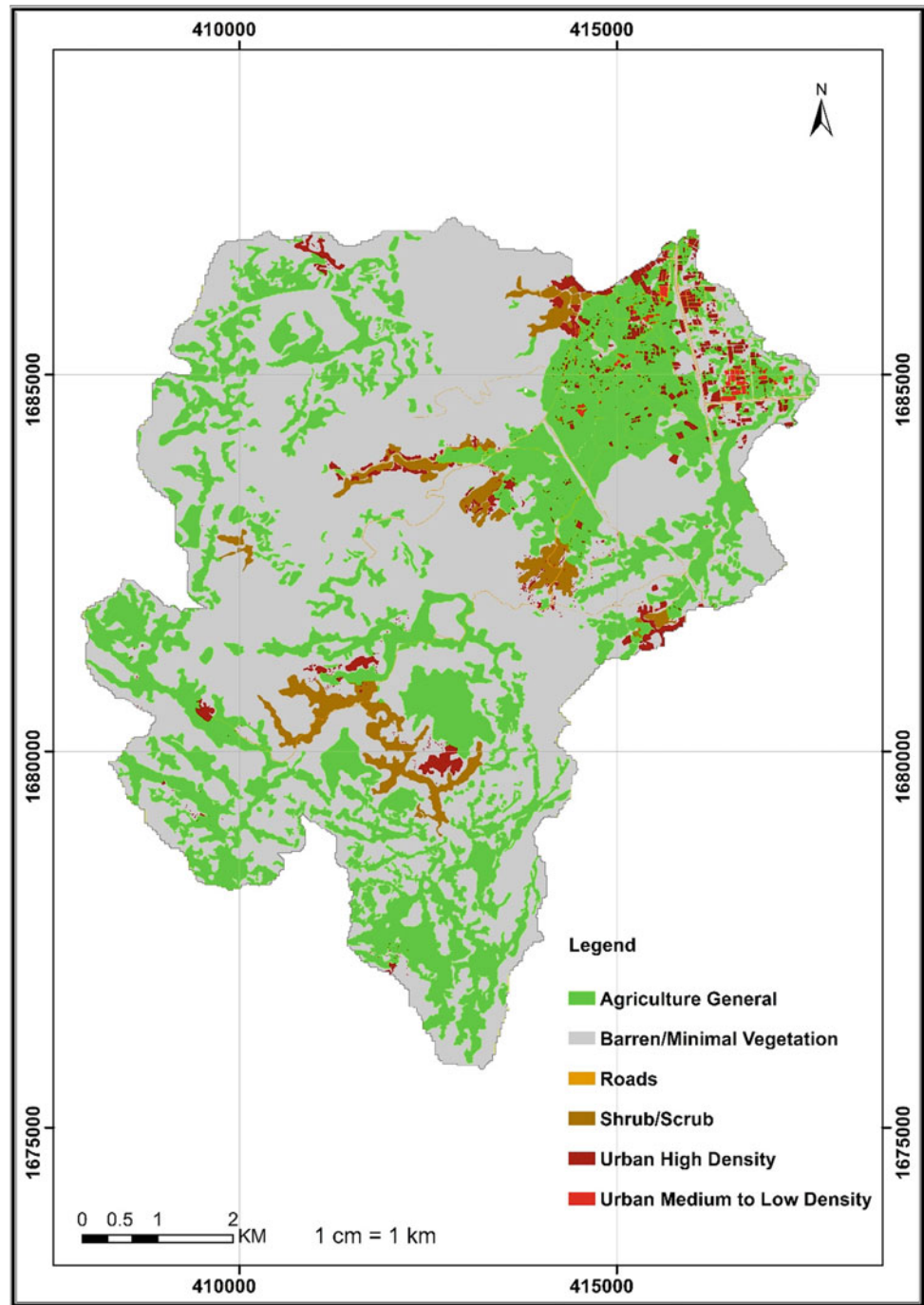


respectively as showing in (Table 3). The increase in CN values from 88.69 in 1994 to 89.46 in 2018 lead to increase in surface runoff values (Table 3). the comparison of CN values for each sub-basin showed that there is an increase in CN values in sub-basins W300, W310, and W320 which were agricultural general area converted to the urban area due to the urbanization of Sana'a city and its location at the boundary of the study area.

### 3.4 S Values

This parameter describes the state of water-saturated soil after runoff begins. Therefore, the factor S is related to soil type and LU, which was reflected in the CN values. S values near-zero indicate that the low potential for soil water retention after the surface runoff, and increasing the surface runoff (Table 4) shows that S values were decreased from

**Fig. 4** Land-use/cover map of Wadi Al-Mulaikhy sub-watershed in 2018



32.5 in 1994 to 29.94 in 2018. The decrease in S values led to a decrease in the water retention potential of soil after surface runoff. When comparing the S values in the sub-basins, a decrease in the S values was observed in the sub-basin W300, W310, and W320, which were converted from agriculture general to urbanization.

### 3.5 $I_a$ Values

The initial abstraction ( $I_a$ ) reflects the water loss by evaporation, plants, and infiltration. The low value of initial abstraction ( $I_a$ ) which is close to zero indicates low water losses before surface runoff, and leading to generate the



**Fig. 5** Comparison of land use classes area in Wadi Al-Mulaikhy sub-watershed between 1994 and 2018

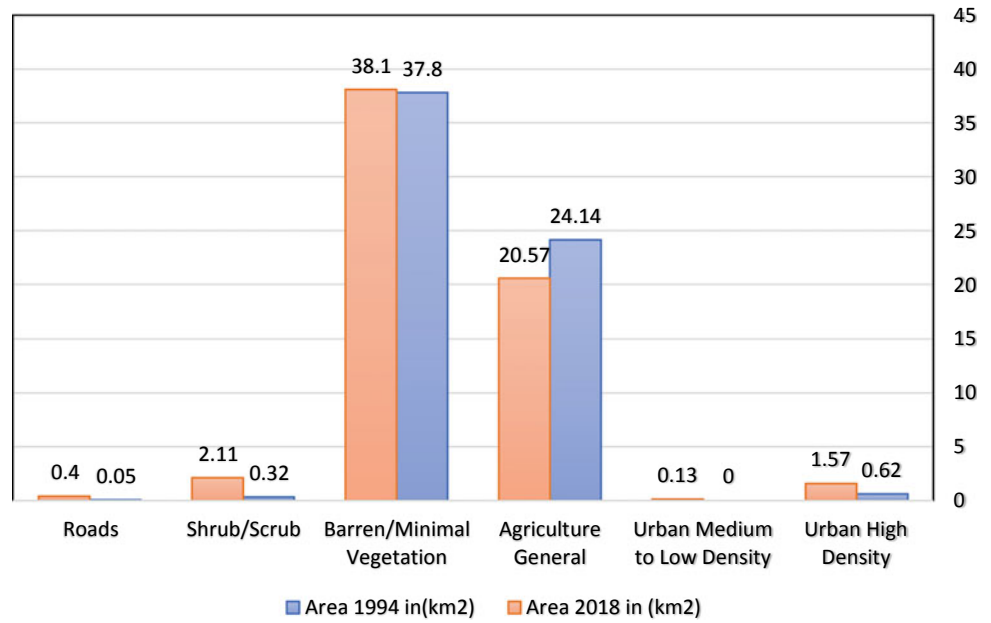


**Table 2** Total runoff volume Wadi Al-Mulaikhy sub-watershed in 1994 and 2018

S. No.	Sub-Basin	Drainage area (km <sup>2</sup> )	Runoff volume (1000 m <sup>3</sup> ) 1994	Volume (mm)	Runoff volume (1000 m <sup>3</sup> ) 2018	Volume (mm)
1	W300	7.9154	138.5	17.42	153.1	19.24
2	W310	12.6014	240.6	19.10	241.7	19.18
3	W320	6.9156	118.3	17.11	126.5	18.29
4	W330	6.9256	152.2	21.85	151.9	21.81
5	W340	8.4888	189.5	22.32	188.8	22.24
6	W350	8.5128	191.0	22.44	190.3	22.35
7	W360	11.6458	240.7	20.67	239.6	20.58
Outlet			1270.9	20.15	1291.9	20.48

**Fig. 6** Comparing of Runoff Volume in Wadi Al-Mulaikhy Sub-watershed in 1994 and 2018

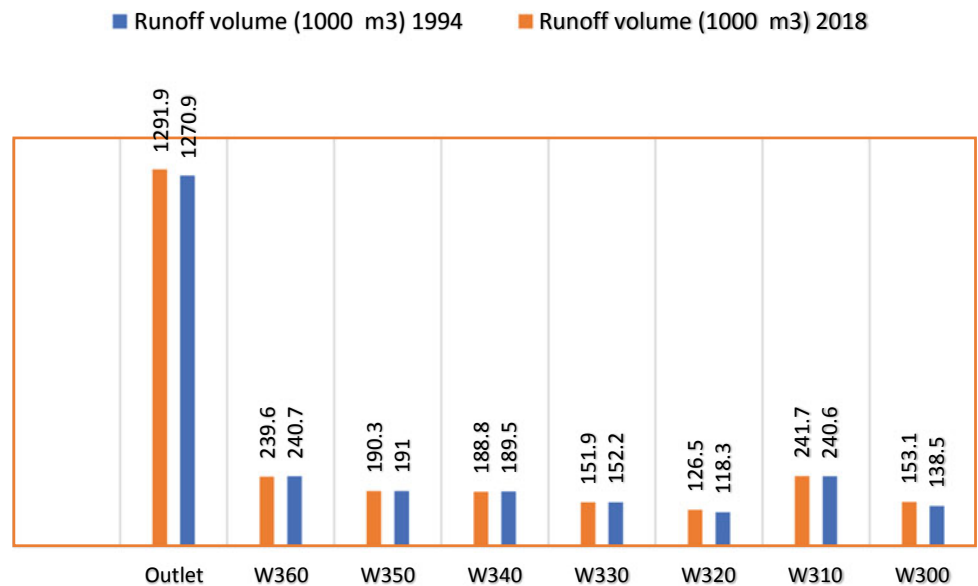


**Table 3** Comparing of CN values for Land-use/cover classes in Wadi Al-Mulaikhy Sub-watershed in 1994 and 2018

S. No	Sub-basin	Area (km <sup>2</sup> )	CN (1994)	CN (2018)
1	W300	7.9154	86.17	89.56
2	W310	12.6014	89.02	89.19
3	W320	6.9156	86.11	88.37
4	W330	6.9256	90.97	90.92
5	W340	8.4888	91.13	91.01
6	W350	8.5128	89.02	88.90
7	W360	11.6458	88.43	88.30
Average			88.69	89.46

**Table 4** Comparing the maximum retention (*S*) for land-use/cover classes in Wadi Al-Mulaikhy Sub-watershed in 1994 and 2018

S. No.	Sub-Basin	Area (km <sup>2</sup> )	<i>S</i> (1994)	<i>S</i> (2018)
1	W300	7.91	40.76	29.60
2	W310	12.60	31.32	30.78
3	W320	6.91	40.97	33.42
4	W330	6.92	25.21	25.36
5	W340	8.48	24.72	25.09
6	W350	8.51	31.32	31.71
7	W360	11.64	33.23	33.65
Average			32.50	29.94

**Table 5** Comparing the Initial Abstraction (*I<sub>a</sub>*) for Land-use/cover classes in Wadi Al-Mulaikhy Sub-watershed in 1994 and 2018

S. No.	Sub-Basin	Area (km <sup>2</sup> )	<i>I<sub>a</sub></i> (1994)	<i>I<sub>a</sub></i> (2018)
1	W300	7.9154	8.15	5.92
2	W310	12.6014	6.26	6.15
3	W320	6.9156	8.19	6.68
4	W330	6.9256	5.04	5.07
5	W340	8.4888	4.94	5.01
6	W350	8.5128	6.26	6.34
7	W360	11.6458	6.64	6.73
Average			6.49	5.98

surface runoff quickly. Table 5 shows that the average value of *I<sub>a</sub>* decreased from 6.49 in 1994 to 5.98 in 2018, which led to a decrease in water loss and an increase in surface runoff.

#### 4 Conclusions

local Land-use maps for Wadi Al Mulaikhy sub-watershed in Sana'a basin were used to simulate surface runoff by using HEC-HMS model to assess the impact of Land-use changes on runoff characteristics, the runoff was simulated with the Land-use maps of the years 1994, and 2018.

1. The major change in Land-use/cover classes was identified agricultural general class converted to other classes (urban high density, urban medium to low density, barren/minimal vegetation, shrub/scrub, and roads)
2. The impact of Land-use/cover change on runoff characteristics only exists through the conversion of 5.65% from agricultural general class to the classes (urban high density, urban medium to low density, barren/minimal vegetation, shrub/scrub, and roads) by (1.5%, 0.22%, 0.53%, 2.84%, and 0.55%), respectively.
3. The runoff volume increased from 1,270,900 cubic meters of the year 1994 to 1,291,900 cubic meters in the year 2018 about 1.625% over 24 years period

4. It was found that there is no big change in runoff volume comparing with the change in Land-use/cover due to some of agricultural general class changes to other classes (Shrub/Scrub), which has the similar runoff characteristics. The second changes from agricultural general class changes to urban classes (urban high density, urban medium to low density and roads) which occurred in the north of the study area at the boundary of Sana'a City which has urban expansion.
5. The average of CN values increased from 88.69 in the year 1994 to 89.46 in the year 2018. The average of  $S$  values decreased from 32.5 in the year 1994 to 29.94 in the year 2018. While, the average of  $I_a$  values decreased from 13 in the year 1994 to 11.97 in the year 2018.
6. The changes in runoff parameters were found in the sub basin (W300, W310 and W320), which are located in the north of the study area due to the changes of agricultural general class changes to urban classes (urban high density, urban medium to low density and roads).

**Acknowledgements** The authors are grateful to the National Water Resource Authority (NWRA) and Yemen Remote Sensing and GIS Center for providing the data for this study.

## References

- Ajmal, M., Moon, G.-W., Ahn, J.-H., & Kim, T.-W. (2015). Investigation of SCS-CN and its inspired modified models for runoff estimation in South Korean watersheds. *Journal of Hydro-Environment Research*, 9(4), 592–603.
- Al-Derwish. (2014). *Integrated watershed management for small catchments within Sana'a Basin, Yemen*.
- Choudhari, K., Panigrahi, B., & Paul, J. C. (2014). Simulation of rainfall-runoff process using HEC-HMS model for Balijore Nala watershed, Odisha, India. *International Journal of Geomatics and Geosciences*, 5(2), 253.
- Geremew, A. A. (2013). *Assessing the impacts of land use and land cover change on hydrology of watershed: a case study on Gigel-Abbay Watershed, Lake Tana Basin, Ethiopia*.
- Hundecha, Y., & Bárdossy, A. (2004). Modeling of the effect of land use changes on the runoff generation of a river basin through parameter regionalization of a watershed model. *Journal of Hydrology*, 292(1–4), 281–295.
- JICA. (2007). The study for the water resources management and rural water supply improvement in the republic of Yemen water resources management action plan for Sana'a basin.
- Köylü, Ü., & Geymen, A. (2016). GIS and remote sensing techniques for the assessment of the impact of land use change on runoff. *Arabian Journal of Geosciences*, 9(7), 484.
- Maalim, F. K., Melesse, A. M., Belmont, P. & Gran, K. B. (2013). Modeling the impact of land use changes on runoff and sediment yield in the Le Sueur watershed, Minnesota using GeoWEPP. *Catena*, 107(35–45).
- Maisa'a, W. S., Shatanawi, M. & Nelson, J. (2017). Curve number applications for restoration the Zarqa River Basin.
- Mistry, A., Lodha, P., Prakash, I. & Mehmood, K. (2017). Estimation of direct runoff for Purna river sub-basin, using SCS-CN method, dangs district, Gujarat. *Development*, 4(4).
- Mousazadeh, R., Ghaffarzadeh, H., Nouri, J., Gharagozlou, A., & Farahpour, M. (2015). Land use change detection and impact assessment in Anzali international coastal wetland using multi-temporal satellite images. *Environmental Monitoring and Assessment*, 187(12), 776.
- Nachshon, U., Netzer, L. & Livshitz, Y. (2016). Land cover properties and rain water harvesting in urban environments. *Sustainable Cities and Society*, 27(398–406).
- Ngo, T. S., Nguyen, D. B., & Rajendra, P. S. (2015). Effect of land use change on runoff and sediment yield in Da River Basin of Hoa Binh province, Northwest Vietnam. *Journal of Mountain Science*, 12(4), 1051–1064.
- Noman, A. A. (2016). Water resources V&A study third national communication biennial update.
- NRCS, U. (2004). National engineering handbook: Part 630—hydrology. USDA Soil Conservation Service: Washington, DC, USA.

## Report Rapid

- Ramakrishnan, D., Bandyopadhyay, A., & Kusuma, K. (2009). SCS-CN and GIS-based approach for identifying potential water harvesting sites in the Kali Watershed, Mahi River Basin, India. *Journal of Earth System Science*, 118(4), 355–368.
- Sajikumar, N. & Remya, R. (2015). Impact of land cover and land use change on runoff characteristics. *Journal of environmental management*, 161(460–468).
- Shi, P.-J., Yuan, Y., Zheng, J., Wang, J.-A., Ge, Y., & Qiu, G.-Y. (2007). The effect of land use/cover change on surface runoff in Shenzhen region, China. *CATENA*, 69(1), 31–35.
- Tiwari, M. K., Gaur, M., Siyag, P. R. & Kumar, A. (2014). Impact assessment of land use change on runoff generation using remote sensing & geographical information system (GIS).



# Evaluation of Groundwater Quality Variations Using Geographical Information System (GIS) and Multivariate Statistical Techniques: A Case Study from Qa'Jahran Basin, Dhamar, Yemen

Nabil M. AL-Areeq, Hadi A. Quriaa, Ahmed M. AL-Areeq, and Amer M. Al-Sabri

## Abstract

The current study investigates the water quality of the water resources in Qa'Jahran basin, Dhamar, Yemen. Thirty water wells with a depth ranging from 100 to 600 m below ground level were used to collect water samples. A total of seventeen water quality parameters were measured during 2019, allowing investigation of spatial variation and indication of potential pollution sources. It is essential to have adequate understanding on the interaction effect, trends, and the correlation structure of these parameters to control water quality. Geographical Information System (GIS) and multivariate statistics techniques were used to understand the water resource quality and generate a water quality index map of Qa'Jahran basin. Based on multivariate statistical analysis, strong correlations were observed between total dissolved solids (TDS), conductivity, chloride, total alkalinity, bicarbonate, sodium, and chloride. Sodium has strong correlation with total alkalinity, chloride, and bicarbonate, while it has moderate correlation with fluoride. On the other side, principal component analysis shows that 85.22% of the overall variances were explained by four major principal components. Accordingly, 52% of the data were required to explain 85.22% of total variances as shown by the factor analysis indicating significant data reduction was resulted in this study. According to the water quality index (WQI), most of the water samples were classified as excellent to good for drinking purpose.

## Keywords

Water quality parameters • Multivariate statistical analysis • GIS • Water quality index • Qa'Jahran basin • Yemen

## 1 Introduction

A great increase in the demand in Yemen for the freshwater in the last few decades due to the rapid growth of the population leads to imbalance in available water resource and demand. Hence, the gap between water supply and demand is increasing with time. The groundwater resources are considered as the main source of freshwater in Yemen. This resource is depleted at high rates, and many of groundwater basins in Yemen such as Sana'a are showing decline in the groundwater levels and increase in the salinity which is a strong sign of depletion. The expansions of urbanization, irrigation activities, and industrialization have a significant effect on the groundwater resources. Accordingly, conserving and monitoring this important resource is essential. The aquifer in Qa'Jahran basin consists of two layers (sedimentary unit and volcanic fractures unit), and as a result of this weakness, the probability of water contamination by human or nature is very high. There are many sources of water contamination in the study area which disposed randomly such as wastewater, oils, structures waste, and municipal solid waste. Large quantities of human and industrial waste disposals pose a serious threat to this valuable resource. The sources of these contaminants are the study area itself. These contamination sources will affect the quality of water resources which are used by about 137,804 persons. According to the report of WHO, water is the main reason for 80% of all human diseases. Regular monitoring of the groundwater is required to protect it where it is impossible in most of the cases to stop the pollutants from the source (Al-hadithi, 2012).

N. M. AL-Areeq (✉) · H. A. Quriaa · A. M. Al-Sabri  
National Water Resource Authority (NWRA), Sanaa, Yemen

N. M. AL-Areeq · A. M. Al-Sabri  
Department of Geology and Environment, Faculty of Applied Sciences, Thamar University, Dhamar, Yemen

A. M. AL-Areeq  
Civil and Environmental Engineering Department King, Fahd University of Petroleum & Minerals, Dhahran, 31261, Saudi Arabia

Manual, tube wells, and springs constitute the main resources for domestic, industrial, and irrigation uses in many areas. But, few of them are maintained in their original condition due to intensive human activities (Zhao et al., 2011). Today, the shortage of freshwater sources in many countries is a great concern (Alberto et al., 2001; Singh et al., 2004; Qadir et al., 2008). A constant polluting source due to municipal and industrial wastewater discharge and a seasonal phenomenon due to surface runoff can be most affected by climate (Singh et al., 2004). Decision-makers and water quality specialists often face significant challenges to control water contamination due to these complexities (Elhatip et al., 2008). To keep water sources useable, protecting water quality is essential to minimize water treatment cost and to satisfy regulatory limitations (Chowdhury et al., 2007; WHO, 2017; Canada, 2017).

Statistical analyses of water chemistry data are widely used in water analysis interpretation. Complex data matrices of water quality can be better interpreted and understood by applying different multivariate statistical techniques, such as factor analysis (FA) and principal component analysis (PCA). Rapid solution to pollution problems and the reliable management of water resources can be done using such statistical techniques which facilitate the identification of possible factors that influence water quality (Lee et al., 2001; Reghunath et al., 2002). Voza et al. (2015) proved the utility of multivariate statistical methods, factor analysis (FA), principal component analysis (PCA), and cluster analysis (CA) for the analysis and interpretation of the complex water quality data sets. Many studies demonstrated that multivariate statistical analysis is useful to assess the spatial water quality variations (Simeonov et al., 2003; Zeilhofer et al., 2006; Zhang et al., 2009a, 2009b; Olsen et al., 2012; Marinović & Ružđjak, 2015; Phung et al., 2015; Muangthong & Shrestha, 2015). Freshwater quality can be characterized and evaluated using multivariate statistical techniques which are also useful in verifying temporal and spatial variations (Singh et al., 2005; Chowdhury & Al-Zahrani, 2014).

Environmental data management is one of the important applications of Geographic Information System (GIS). To avoid possible environmental crisis, managers and scientists can be provided with different scenarios using GIS for predicting future trends and spatial distribution of the data. GIS is widely used in pollution and water resource management due to its importance in playing a critical role in these fields (Zeilhofer et al., 2007; Igboekwe & Akankpo, 2011; Yan et al., 2015). Nasher and El-Sagheer (2012) studied bacteriological, chemical, and physical parameters of water resources in Bura'a natural protected area, Hodeidah, Yemen, to evaluate the water quality for agricultural and drinking purpose. They found that the water is suitable for irrigation purposes, but it is unsuitable for drinking. Saleh

et al. (2018) assessed the suitability of groundwater quality of rural areas (Zabid, Hodeidah) for drinking purpose using water quality index (WQI). They found that the groundwater quality is generally good–poor water quality status. Aqeel et al. (2017) used GIS to create a geospatial distribution map of fluoride concentrations and identified three risky zones in the Al-Howban Basin, Taiz-Yemen. Mohamed and Hassane (2016) studied the impact of urbanization on groundwater resources in Al Ain city, UAE, by performing hydrochemistry assessment of the quality of groundwater. Nasher et al. (2013) identified and evaluated the hydrogeochemical processes for the management of the groundwater resources of the lower part of Wadi Siham, Tihama plain, Yemen. Nazzal et al. (2015) investigated Saq aquifer, northwestern part of KSA by conducting a combined hydrochemical–statistical analysis to assess groundwater resources. Toumi et al. (2015) studied the water quality and the hydrochemical characteristics in Al-Ula Region, Saudi Arabia, and they found that the lithological influences are the guide of water chemistry. Gebrehiwot et al. (2011) evaluated the suitability of groundwater quality in El Khairat aquifer, Enfidha, Tunisia, for drinking purposes. They conclude that GIS is an effective tool for creating maps showing the spatial distribution of water quality parameters. Eslami et al. (2013) used GIS interpolation techniques to evaluate the groundwater quality of Mianab plain, Iran, and they found that groundwater quality in their study area is not suitable for drink and agricultural uses. They also confirm the importance of selecting an appropriate interpolation technique and illustrated the effective of geostatistical technique in groundwater management system. Al-Omran et al. (2018) used different techniques such as water quality index (WQI) and Durov diagrams to assess the groundwater quality of Al-Hasa region, Saudi Arabia, for drinking and irrigation purposes, and they found that the water is excellent for irrigation and poor to unsuitable for drinking purposes.

The main objective of this study is for evaluation of groundwater quality variations in Qa'Jahran basin in Yemen. This study focuses on using the Geographical Information System (GIS) and multivariate statistics to understand the water resource quality and generate a water quality index map for the first time in this area.

---

## 2 Study Area and Data Acquisition

The Qa'Jahran basin is located in the middle western part of Yemen, at the Central Highland Plains in Jahran district. It represents the main catchments of Jahran plain (Fig. 1). The geographic extent of the basin area lies between longitudes 44° 12' 20" and 44° 22' 30" E and latitudes 14° 38' 11" and 14° 57' 30" N with total area extent 406 km<sup>2</sup>, and it is about 25 kma distance toward the north of Dhamar city. The



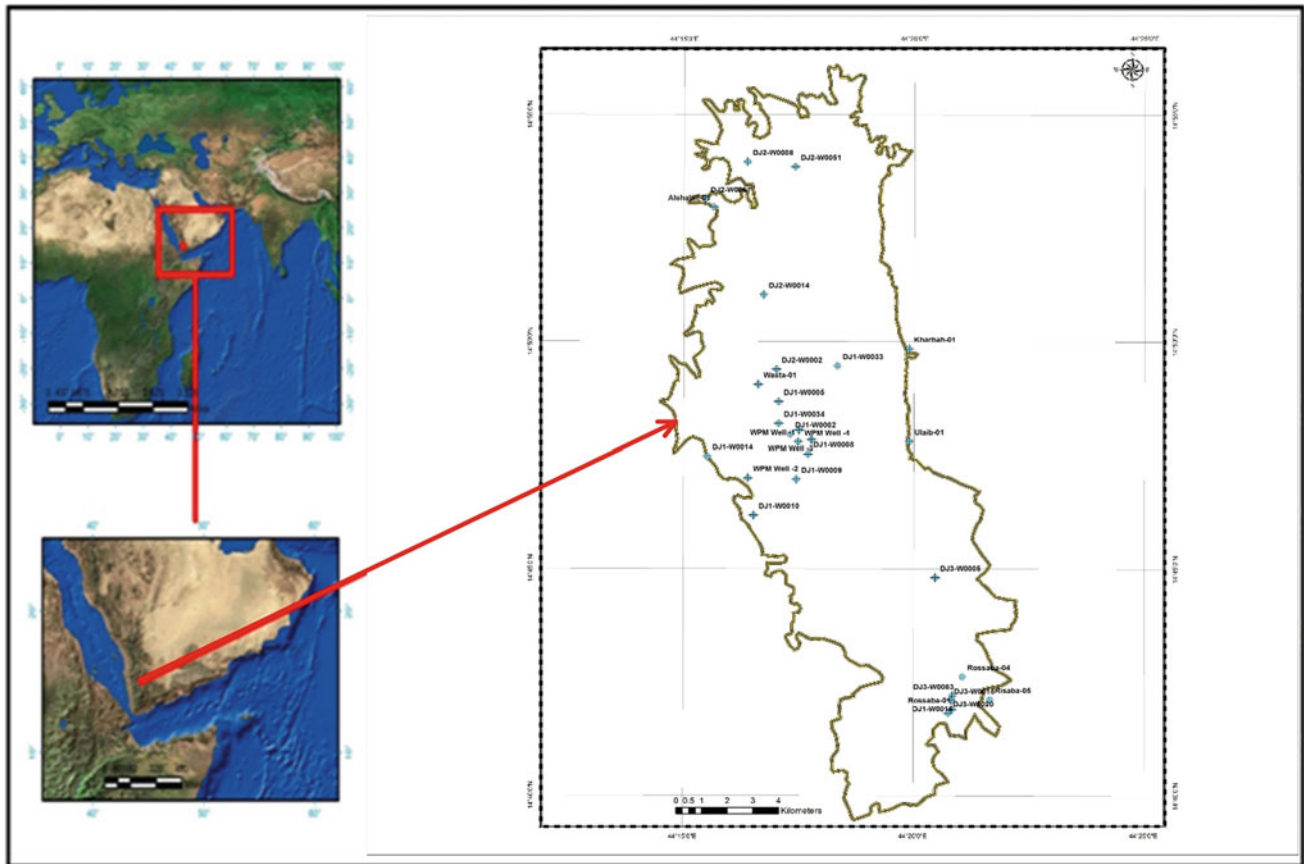


**Fig. 1** Location map of the groundwater samples from the Qa'Jahran basin, Dhamar, Yemen

Qa'Jahran basin is one of the largest and most completely flat areas of its size in the Highland Plains of Yemen. The catchment area of the basin is affected by soil erosion. The intensive drilling activity for water quest in the catchment and water scarcity related to human interface with water storage has resulted in groundwater to sink down and the basin threatened by drought due to groundwater depletion. The manual and tube wells are the main resource of the water in Qa'Jahran basin. The people in the area depend mainly on these resources for their water requirements. Thirty water wells were selected from Qa'Jahran basin from different locations for the study taking into consideration the hydrologic, social, and economic variation. All statistical and mathematical computations were made using JMP, MINITAB™, SPSS Statistics, XLSAT, and Microsoft Office Excel 2016.

## 2.1 Scatterplots and Pairwise Correlations

The indication of linear or nonlinear relationships and possible correlations were represented by scatterplots and pairwise correlations. Scatterplots and pairwise correlations of

Qa'Jahran basin data were investigated by this study using JMP and the MINITAB™ statistical package.

## 2.2 Principle Component Analysis (PCA)

PCA is designed to convert the original variables (correlated variables) into new, linearly uncorrelated variables, called principal components. The majority of the data set can be described by the most meaningful parameter information which is provided by PCA (Helena et al., 2000). As a result of the reduction in the dimensionality of data by PCA, a smaller number of transformed variables can be used to represent the bulk of the variation in the data (Jackson & John Wiley & Sons, 1991; Wold et al., 1987). The following equation can represent the principal component (PC):

$$Z_{ji} = a_{i1}x_{1j} + a_{i2}x_{2j} + a_{i3}x_{3j} + \dots + a_{im}x_{mj}$$

where  $Z$  is the component score,  $i$  is the component number,  $j$  is the sample number,  $a$  is the component loading,  $x$  is the measured value of variable, and  $m$  is the total number of variables.

The transformed data coming from the PCA can be simplified even more with the benefit of the factor analysis (FA) which construct new variables, called varifactors (VFs) by reducing the contribution of less significant variables. VF includes hypothetical, unobservable, latent variables, while PC is a linear combination of observed water quality variables (Helena et al., 2000; Vega et al., 1998). Normalized variables are used in PCA to extract PCs with major significance and reduce that have minor significance (Zhang et al., 2009a,2009b; Bu et al. 2010). As a result, the amount of information obtained from a less number of variables will be similar to that resulted from the much larger set of original variables. The following equation can represent the factor analysis (FA):

$$Z_{ji} = a_{f1}f_{1i} + a_{f2}f_{2i} + a_{f3}f_{3i} + \dots + a_{fm}f_{mi} + e_{ji}$$

where  $Z$  is the measured variable,  $i$  is the sample number,  $a$  is the factor loading,  $f$  is the factor score,  $m$  is the total number of factors, and  $e$  is the residual term accounting for errors or other source of variation. In this study, fifteen of Qa'Jahran water quality data set was subjected to FA/PCA.

### 2.3 Water Quality Index (WQI)

It is a rating that can be used to reflect the composite influence of different water quality parameters on the overall water quality. The main objective of computing water quality index (WQI) is to obtain usable and understandable information from the complex water quality data. A parameter is selected based on its impact on health and the overall quality of water. The WQI can be computed by the following three steps.

First step: Assign weight ( $w_i$ ) to the selected water parameters (e.g., TDS, pH, TH,  $\text{HCO}_3$ ,  $\text{SO}_4$ , Cl,  $\text{NO}_3$ , Fe, etc.) according to their relative importance in the overall water quality for drinking purposes (weight may be from 1 to 5).

Second step: Compute a relative weight ( $W_i$ ) of the chemical parameter using the following equation:

$$W_i = w_i / \sum_{i=1}^n w_i$$

where  $W_i$  is the relative weight, ' $n$ ' is the number of parameters, and  $w_i$  is the weight of each parameter.

Third step: Assign a quality rating scale ( $q_i$ ) for each parameter, as below:

$$q_i = (C_i / S_i) \times 100$$

where  $q_i$  is the quality rating,  $S_i$  is the guideline value/desirable limit as given in Yemeni drinking water

standard, and  $C_i$  is the concentration of each chemical parameter in mg/l. For the computation of WQI, firstly the subindex (SI) is determined for each water quality parameter, as given below:

$$\begin{aligned} \text{SI} &= W_i \times q_i \\ \text{WQI} &= \sum \text{SI}_i \end{aligned}$$

where  $W_i$  is relative weight of the parameter,  $\text{SI}_i$  is the subindex of the parameter, and  $q_i$  is the rating based on concentration of the parameter.

### 2.4 Classification of Water

The water can be classified into five types based on computed WQI, as given below:

Excellent water (<50); good water (50–100); poor water (100–200); very poor water (200–300); and water unsuitable for drinking (>300).

## 3 Results and Discussion

The statistical analysis of water quality parameters (WQPs) is calculated for 30 (WQP) in Qa'Jahran wells as shown in Table 1. Distribution fitting was examined using maximum likelihood as an estimation method and tested using Kolmogorov–Smirnov and chi-square method. The gamma (2) distribution is the distribution that fits best the data as shown in Table 2. The water quality data sets of Qa'Jahran basin were subjected to multivariate statistical techniques: FA and PCA.

### 3.1 Correlation and Scatterplots

The correlations between different water quality parameters are carried out as shown in Table 3. The pH has strong correlation with carbonate ( $r = 0.857$ ) and negative strong correlation with hardness ( $r = -0.632$ ) and calcium ( $-0.639$ ). Total dissolved solids is perfectly correlated with conductivity ( $r = 1$ ). Total dissolved solids and conductivity show strong correlation with chloride and bicarbonate ( $r = 0.881$ ), total alkalinity ( $r = 0.868$ ), sodium ( $r = 0.803$ ), and sulfate ( $r = 0.743$ ), and moderate correlations with magnesium ( $r = 0.597$ ) and potassium ( $r = 0.475$ ). Sodium has strong correlation with total alkalinity, bicarbonate, and chloride ( $r = 0.845$ ,  $0.822$ , and  $0.628$ , respectively), and moderately correlated with fluoride ( $r = 0.484$ ). The strong positive correlation of sodium with chloride and between them with conductivity reflects a common source of these

**Table 1** Statistical analysis of water quality parameters (WQPs) of Qa'Jahran wells

Statistic	Minimum	Maximum	Median	Mean	Variance	Standard deviation	WHO	G.Y.L
Turbidity	0.040	4.800	0.290	1.073	2.162	1.470		
PH (9–6.5)	7.960	9.260	8.385	8.473	0.112	0.335	6.5–8.5	6.5–8.5
EC	117.800	1006.000	435.250	462.461	41,484.80	203.678	400–1500	450–2500
TDS	76.570	653.900	282.913	300.600	17,527.33	132.391	1000.00	650–1000
TH	0.000	192.200	72.300	77.737	3287.23	57.334	100–500	100–500
TA	38.800	272.570	146.470	148.238	3256.08	57.062		
HCO <sub>3</sub>	42.600	332.500	178.100	177.038	4799.40	69.278	150–500	150–500
CO <sub>3</sub>	0.000	17.500	0.000	3.128	28.01	5.293		
Cl	7.800	110.600	25.500	32.472	555.70	23.573	250.00	200–600
SO <sub>4</sub>	1.000	102.000	21.500	30.111	734.45	27.101	25–400	200–400
F	0.220	3.700	0.580	0.973	0.97	0.986	0.5–1.5	0.5–1.5
Ca	0.000	54.600	18.650	21.622	296.80	17.228	75–200	75–200
Mg	0.000	20.600	3.300	5.728	28.00	5.292	30–50	30–150
Na	7.500	190.600	71.500	82.200	2560.48	50.601	20–175	200–400
K	0.400	5.400	0.950	1.611	2.06	1.436	8–12	8–12
NO <sub>3</sub>	2.200	34.500	7.700	9.244	49.25	7.018	25–50	10–50
Fe	0.010	0.340	0.035	0.053	0.006	0.076	0.3–1	0.3–1

**Table 2** Distribution fitting of the data analysis

Distribution	<i>p</i> -value	Distribution	<i>p</i> -value	Distribution	<i>p</i> -value
Beta4	0.181	Gamma (1)	0.044	Normal	0.096
Chi-square	0.733	Gamma (2)	<b>0.745</b>	Normal (Standard)	<0.0001
Erlang	0.002	GEV	0.014	Student	<0.0001
Exponential	0.063	Gumbel	0.007	Weibull (1)	0.318
Fisher–Tippett (1)	<0.0001	Log-normal	0.683	Weibull (2)	0.496
Fisher–Tippett (2)	<0.0001	Logistic	0.147	Weibull (3)	0.366

ions. Potassium is moderately correlated with chloride ( $r = 0.52$ ). Hardness shows strong correlation with calcium ( $r = 0.945$ ) and magnesium ( $r = 0.76$ ) and moderate correlation with chloride, sulfate, and nitrate ( $r = 0.474$ ,  $0.533$ , and  $0.494$ , respectively), while it has negative moderate correlation with carbonate ( $r = -0.534$ ). Magnesium has strong correlations with chloride ( $r = 0.705$ ) and moderate correlations with sulfate and calcium ( $r = 0.544$  and  $0.51$ , respectively). Total alkalinity is strongly correlated with bicarbonate ( $r = 0.996$ ) and shows moderate correlation with chloride ( $r = 0.598$ ). Bicarbonate has strong correlation with chloride ( $r = 0.624$ ) and moderate correlation with sulfate ( $r = 0.473$ ). Carbonate shows moderate correlation with calcium ( $r = 0.575$ ) and same correlation between calcium and nitrate ( $r = 0.503$ ). Strong correlations were

shown between chloride and sulfate ( $r = 0.632$ ) and between nitrate and fluoride ( $r = 0.851$ ).

### 3.2 Principal Component Analysis (PCA)

PCA was performed for Qa'Jahran basin data. Based on the eigenvalue–one and scree plot (Fig. 2 and Table 4), the number of significant principal components (PCs) was determined. PCs are regarded as significant if eigenvalues are greater than one. Four significant PCs with eigenvalues  $> 1$  were extracted in this study and explained 40.137%, 26.277%, 11.943%, and 6.863% of the variance, respectively. The findings indicate that 85.22% of total variance associated with WQP in Qa'Jahran basin can be explained by the first four PCs.

**Table 3** Correlation of different parameters of chemical analysis for water samples in Qa'Jahran basin

Variables	Turbidity NTU (5)	PH (9– 6.5)	EC µS/cm (2500)	TDS mg/L (1500)	TH mg/L (500)	TA mg/L (–)	HCO <sub>3</sub> mg/L (500)	CO <sub>3</sub> mg/L (–)	Cl mg/L (600)	SO <sub>4</sub> mg/L (400)	F mg/L (1.5)	Ca mg/L (200)	Mg mg/L (150)	Na mg/L (400)	K mg/L (12)	NO <sub>3</sub> mg/L (50)	Fe mg/L (1)		
Turbidity NTU (5)	<b>1</b>																		
PH (9– 6.5)	0.030	<b>1</b>																	
EC µS/cm (2500)	-0.322	-0.242	<b>1</b>																
TDS mg/L (1500)	-0.322	-0.242	<b>1.000</b>	<b>1</b>															
TH mg/L (500)	0.100	-0.632	0.443	0.443	<b>1</b>														
TA mg/L (–)	-0.558	0.008	<b>0.868</b>	<b>0.868</b>	0.205	<b>1</b>													
HCO <sub>3</sub> mg/L (500)	-0.556	-0.072	<b>0.881</b>	<b>0.881</b>	0.256	<b>0.996</b>	<b>1</b>												
CO <sub>3</sub> mg/L (–)	-0.050	<b>0.857</b>	-0.086	-0.086	-0.534	0.099	0.006	<b>1</b>											
Cl mg/L (600)	-0.089	-0.354	<b>0.881</b>	<b>0.881</b>	<b>0.474</b>	<b>0.598</b>	<b>0.624</b>	-0.243	<b>1</b>										
SO <sub>4</sub> mg/L (400)	-0.057	-0.377	<b>0.743</b>	<b>0.743</b>	<b>0.533</b>	0.455	<b>0.473</b>	-0.173	<b>0.632</b>	<b>1</b>									
F mg/L (1.5)	-0.326	0.117	0.355	0.355	-0.160	0.318	0.302	0.187	0.141	<b>0.557</b>	<b>1</b>								
Ca mg/L (200)	0.048	-0.639	0.288	0.288	<b>0.945</b>	0.097	0.151	-0.575	0.274	0.433	-0.147	<b>1</b>							
Mg mg/L (150)	0.166	-0.398	<b>0.597</b>	<b>0.597</b>	<b>0.764</b>	0.348	0.375	-0.268	<b>0.705</b>	<b>0.544</b>	-0.131	<b>0.510</b>	<b>1</b>						
Na mg/L (400)	-0.406	0.180	<b>0.803</b>	<b>0.803</b>	-0.160	<b>0.845</b>	<b>0.822</b>	0.292	<b>0.628</b>	0.454	<b>0.484</b>	-0.312	0.195	<b>1</b>					
K mg/L (12)	-0.334	-0.242	<b>0.475</b>	<b>0.475</b>	0.183	0.365	0.393	-0.284	<b>0.521</b>	0.245	0.000	0.146	0.196	0.327	<b>1</b>				
NO <sub>3</sub> mg/L (50)	<b>0.630</b>	-0.341	0.033	0.033	<b>0.494</b>	-0.209	-0.180	-0.316	0.161	0.125	-0.413	<b>0.503</b>	0.304	-0.302	-0.189	<b>1</b>			
Fe mg/L (1)	<b>0.796</b>	-0.113	0.003	0.003	0.332	-0.317	-0.311	-0.070	0.166	0.246	-0.090	0.292	0.294	-0.218	-0.340	<b>0.851</b>	<b>1</b>		

Values in bold are different from 0 with a significance level alpha = 0.05

**Fig. 2** Scree plot of water samples in Qa’Jahran basin

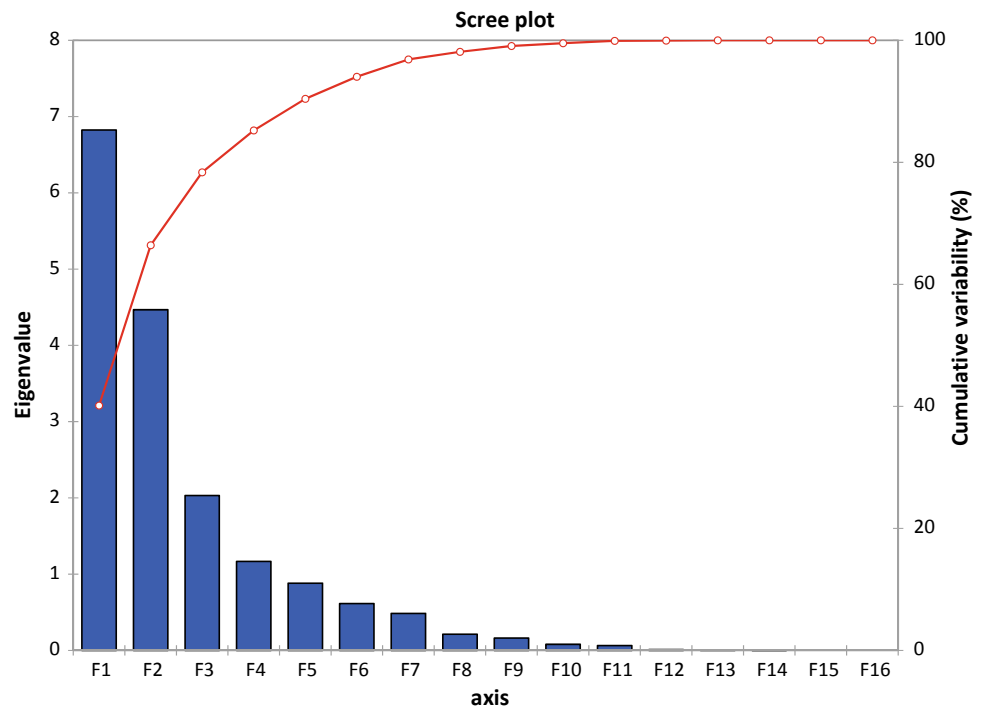


**Table 4** Total variance explained of water samples in Qa’Jahran wells

Component	Initial eigenvalues			Extraction sums of squared loadings		
	Total	% of variance	Cumulative %	Total	% of variance	Cumulative %
1	6.823	40.137	40.137	6.823	40.137	40.137
2	4.467	26.277	66.414	4.467	26.277	66.414
3	2.03	11.943	78.357	2.03	11.943	78.357
4	1.167	6.863	85.22	1.167	6.863	85.22
5	0.882	5.186	90.406			
6	0.614	3.615	94.021			
7	0.485	2.853	96.874			
8	0.211	1.242	98.116			
9	0.161	0.945	99.061			
10	0.08	0.469	99.53			
11	0.063	0.373	99.903			
12	0.009	0.054	99.957			
13	0.007	0.039	99.996			
14	0.001	0.004	100			
15	7.61E-07	4.48E-06	100			
16	2.96E-08	1.74E-07	100			
17	1.01E-16	5.91E-16	100			



### 3.3 Loading and Scatterplots

Understanding the contribution of original WQP to the major PCs is essential to decide which parameter is important and which is not. Figures 3 and 4 show the scatterplots and loading on the major PCs for Qa’Jahran basin. The WQPs, EC, TDS, TA, HCO<sub>3</sub>, Cl, SO<sub>4</sub>, Mg, and Na exceeded the threshold limit of 0.55 on PC1 (Fig. 3). Therefore, they had significant loadings in PC1 and PC2 and have significant loadings from turbidity, pH, TH, CO<sub>3</sub>, Ca, Na, NO<sub>3</sub>, and Fe. In PC3, significant loadings were assigned from iron turbidity, CO<sub>3</sub>, and Fe. The PC4 obtained significant loading from fluoride (F) (Table 5). Figure 4 shows the scatterplots of the loadings. The plot of PC1 × PC2 shows that nitrate and iron were significantly associated with PC2 only, while conductivity, TDS, alkalinity, chloride, bicarbonate, magnesium, sulfate, and sodium were significantly associated with PC1. To represent water quality, it may be required one or two parameters from each cluster. In general, the four PCs were mainly associated with conductivity, TDS, alkalinity, chloride, bicarbonate, magnesium, sulfate, sodium, nitrate, and iron.

The corresponding VFs were obtained for Qa’Jahran basin (Table 5). The factor loadings were classified

according to absolute loading values as strong > 0.75, moderate, 0.75–0.50, and weak 0.50–0.30 (Liu et al., 2003). The percent (40.137%) of total variance was explained by VF1 and had strong positive loadings from alkalinity, bicarbonate, sulfate, chloride, total dissolved solids, and conductivity, while hardness, sodium, manganese, and potassium had a medium loading on VF1. The percent (26.277%) of total variance was explained by VF2, had strong positive loadings from nitrate, and had medium loading from turbidity, hardness, and calcium. The percent (11.943%) of total variance was explained by VF3 which had medium loadings from iron, turbidity, and carbonate. The VF4 explained 6.863% of the total variance and had weak negative loading from sulfate.

### 3.4 Data Reduction

The original parameters on the major VFs were assessed to investigate the possibility of reduction of data. It was reported by the past studies that the original parameters have the greatest contribution to temporal variation if they have loadings greater than 0.7 or 0.75 in the major VFs (Liu et al., 2003; Varol et al., 2012). The value (85.22%) of variance is

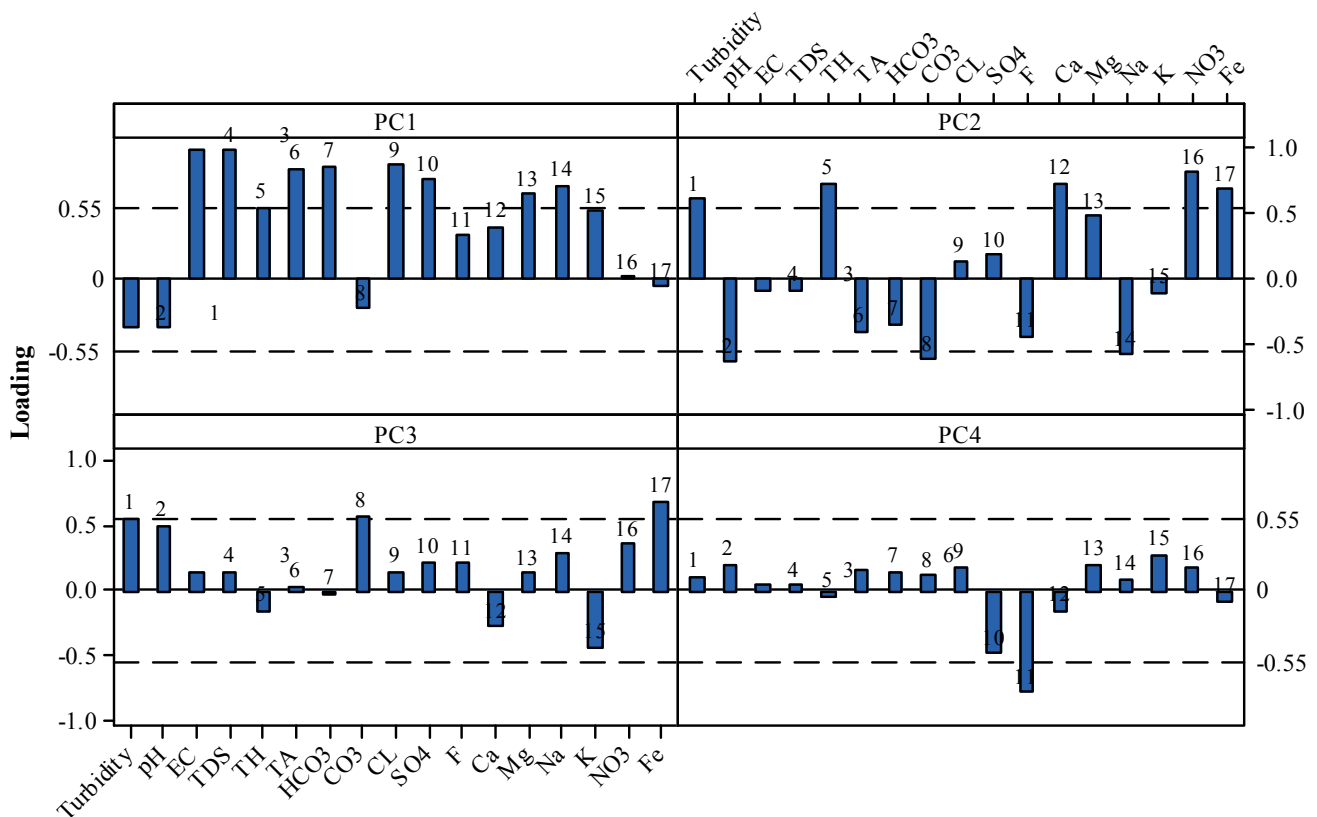
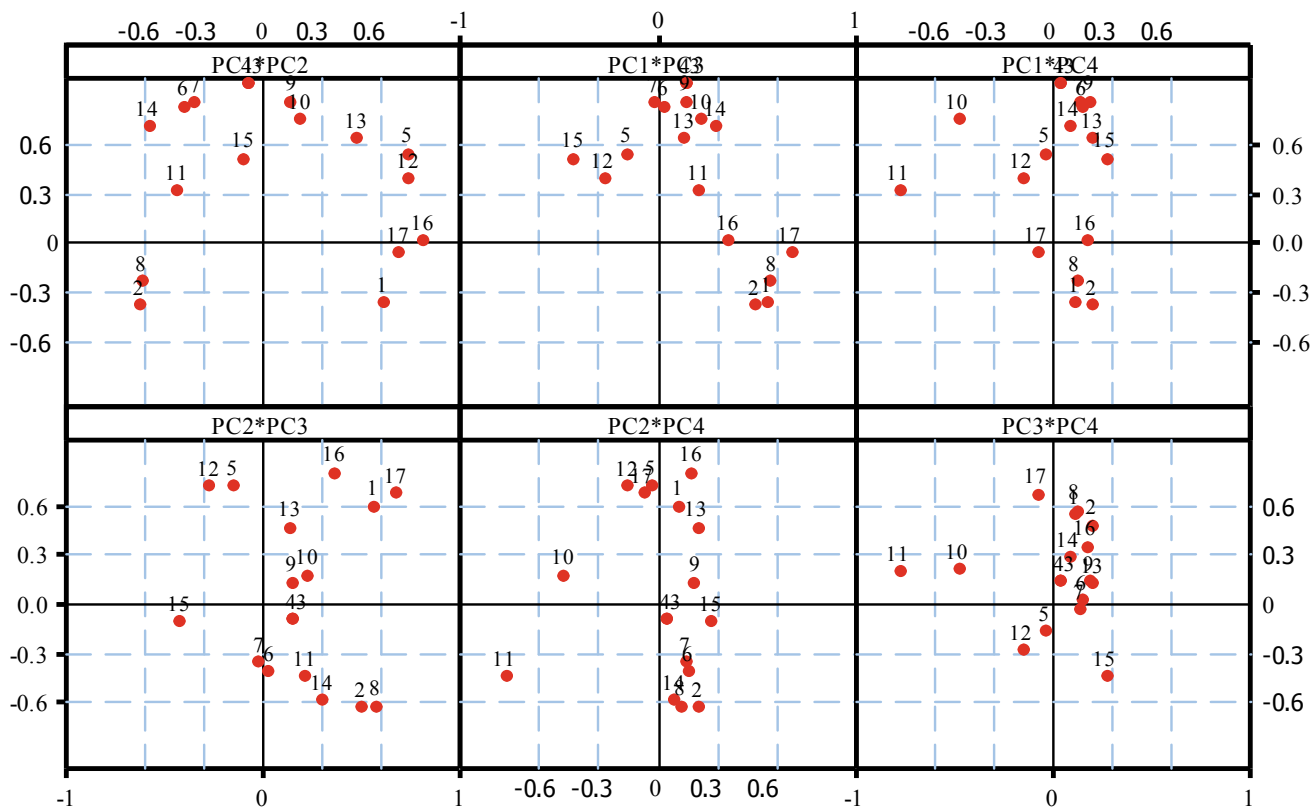


Fig. 3 Scatterplots and loading on the major PCs for Qa’Jahran basin



**Fig. 4** Scatterplots of the (1) turbidity, (2) pH, (3) conductivity, (4) TDS, (5) hardness, (6) alkalinity, (7) bicarbonate, (8) carbonate, (9) chloride, (10) sulfate, (11) fluoride, (12) calcium, (13) magnesium, (14) sodium, (15) potassium, (16) nitrate, and (17) iron

explained by the major four VFs which had strong loadings from sulfate, sodium, chloride, manganese, calcium, total dissolved solids, hardness, bicarbonate, conductivity, iron, total alkalinity, and nitrate as shown in Table 7. As TDS, conductivity, chloride, hardness, magnesium, sodium, and sulfate are strongly correlated as shown in Table 5, TDS can be selected to be significant. Accordingly, a total of twelve parameters (sulfate, chloride, sodium, manganese, calcium, hardness, total dissolved solids, conductivity, bicarbonate, total alkalinity, nitrate, and iron) are needed (approximately 80% of the 15 parameters) to explain 85.22% of the data variance (Table 5).

### 3.5 Water Quality Parameters

The minimum and maximum values of each parameter were identified, and the spatial distributions for sixteen parameters were determined for the study area. The value of iron (Fe) varies from 0.01 to 1.08 mg/l, and the highest concentration is in the Al-ulaib well east part of the study area (Fig. 5a). The spatial distribution of nitrate (NO<sub>3</sub>) is shown in Fig. 5b which shows the concentration variation range from 0.8 to 101 with highest concentration only in DJ2-W-9

well. The concentration of potassium is low in the whole study area with values between 0.4 and 5.4 mg/l (Fig. 5c). The spatial distribution of sodium varies from 7.5 to 190.6, and the highest concentration is in the DJ1-W8 (Fig. 5d). Figure 5e shows that spatial distribution of magnesium which varies from 0.0 to 37 mg/l. The spatial distribution of calcium varies from 0.0 to 150, and the highest concentration of calcium is in the DJ2-W-9 well. Fluoride varies from 0.2 to 3.7 with high concentration in the northern part and low concentration only in the central part of the study area (Fig. 5f). The value of sulfate (SO<sub>4</sub>) varies from 1 to 102 mg/l, and the low concentration is in the northern and southern parts of the study area (Fig. 5g). The spatial distribution of chloride is shown in Fig. 5h which shows the concentration variation is from 7.8 to 110.6. The concentration of bicarbonate varies from 42.6 to 332.5 and is low in the whole study area except DJ1-W33 within the permissible range (Fig. 5i). The value of pH range between 7.9 and 9.2 mg/l is shown in Fig. 5k, which shows that the water is alkaline in most of the study area. TDS varies from 76.5 to 653.9 mg/l which proved that the TDS in groundwater is low (Fig. 5l). That spatial distribution of total hardness of water varies from 0 to 192, and most of the study area has low concentration of TH as shown in Fig. 5n. Figure 5o

**Table 5** Factor loadings on the major PCs for Qa'Jahran basin

Variable	Factor				Communalities
	VF1	VF2	VF3	VF4	
Turbidity	-0.364	<b>0.61</b>	0.559	0.111	0.83
pH	-0.369	-0.627	0.494	0.206	0.817
EC	<b>0.982</b>	-0.08	0.148	0.043	0.995
TDS	<b>0.982</b>	-0.08	0.148	0.043	0.995
TH	0.549	<b>0.733</b>	-0.156	-0.035	0.865
TA	<b>0.842</b>	-0.4	0.03	0.153	0.892
HCO <sub>3</sub>	<b>0.867</b>	-0.344	-0.023	0.143	0.89
CO <sub>3</sub>	-0.224	-0.614	0.575	0.119	0.772
CL	<b>0.87</b>	0.142	0.145	0.188	0.833
SO <sub>4</sub>	<b>0.763</b>	0.185	0.22	-0.479	0.895
F	0.329	-0.438	0.21	-0.777	0.948
Ca	0.403	<b>0.733</b>	-0.276	-0.151	0.799
Mg	<b>0.649</b>	0.479	0.135	0.206	0.711
Na	0.714	-0.58	0.298	0.085	0.941
K	0.52	-0.103	-0.429	0.272	0.539
NO <sub>3</sub>	0.02	<b>0.812</b>	0.359	0.172	0.819
Fe	-0.049	<b>0.69</b>	<b>0.68</b>	-0.074	0.947
% variance	40.137	26.277	11.943	6.863	
Cumulative (%)	40.137	66.414	78.357	85.22	

shows that spatial distribution of total alkalinity varies from 38 to 278. Figure 5p shows that spatial distribution of turbidity which varies from 0.04 to 4.8.

### 3.6 Water Quality Index (WQI)

WQI is widely used tool to assess the water quality. According to the relative importance of each water quality parameter, the relative weight was determined as shown in Table 6. Water quality index was calculated for each parameter as shown in Table 7 and Fig. 6. It can be noticed that 72% of the samples fall in excellent water category and 28% of the samples fall in good water category that reflect good-quality water in Qa'Jahran basin.

## 4 Conclusions

Spatial variability of water quality parameter (WQP) in Qa'Jahran basin was evaluated in this study. Several techniques, including pairwise correlations, FA, and PCA, were performed on the data collected in 2019. Data reduction was also investigated based on assessing their loadings and correlation structure on the major PCs and VFs. The possibility of data reduction was investigated in this study. About 80% of data in Qa'Jahran basin can be reduced in expense of 20% of overall variance. This research points out that the data reduction can be possible in the monitoring program. Approximately 48% can be reduced in expense of 14.78% of the overall variance. A total of nine parameters out of 17

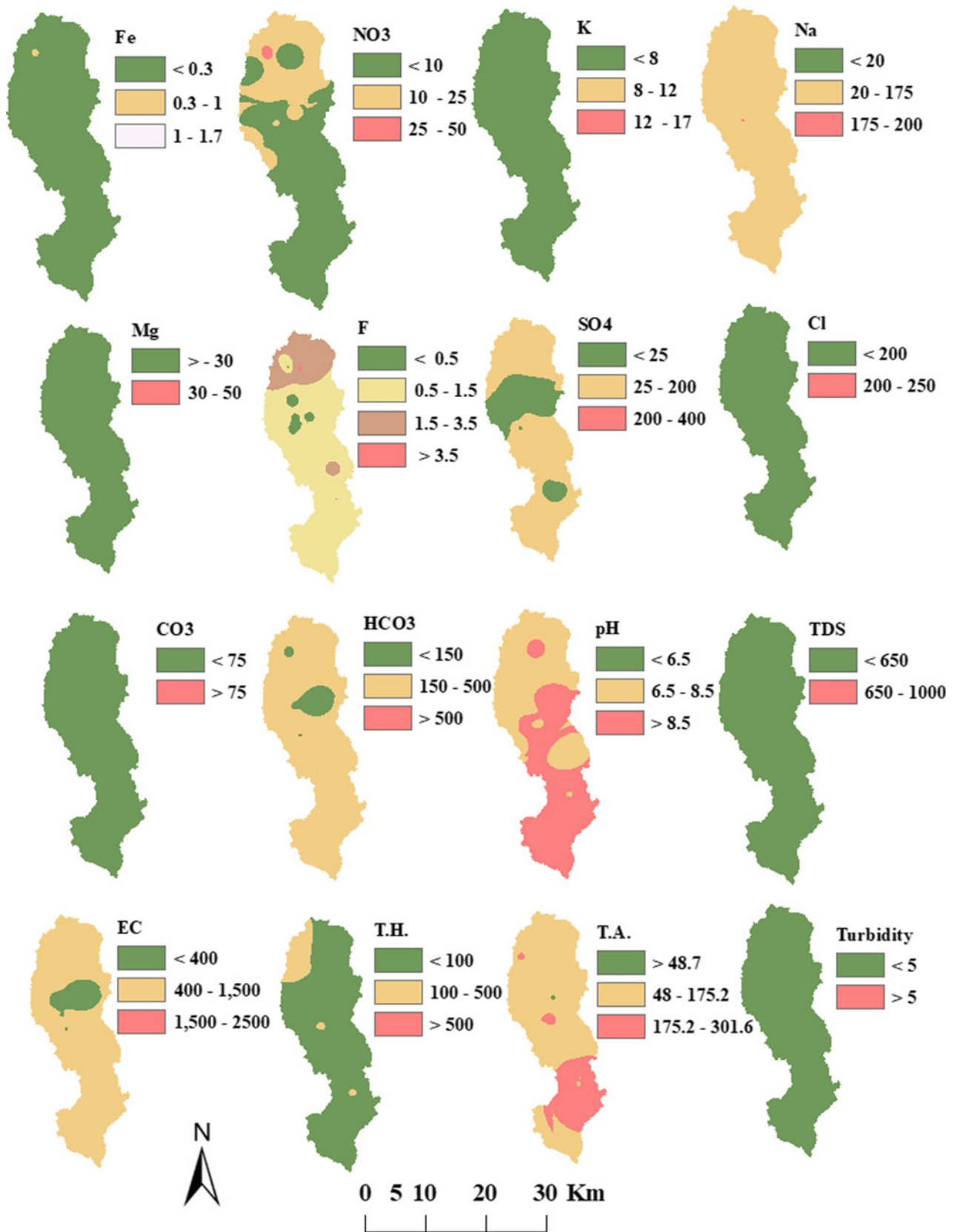


Fig. 5 Water quality parameters (spatial distribution maps) of Qa'Jahran basin

**Table 6** Relative weight for each water quality parameter (Gebrehiwot et al., 2011)

Chemical parameters	G.Y.L	WHO (2011)	Weight ( $w_i$ )	Relative weight $W_i = w_i / \sum n w_i$
Turbidity		5	2	0.03922
pH	6.5–8.5	8.5	4	0.07843
EC ( $\mu\text{S}/\text{cm}$ )	450–2500	500	4	0.07843
TDS (mg/L)	650–1000	500	5	0.09804
TH (mg/L)	100–500	–	3	0.05882
TA		100	2	0.03922
HCO <sub>3</sub> <sup>–</sup> (mg/L)	150–500	500	3	0.05882
Cl <sup>–</sup> (mg/L)	200–600	250	3	0.05882
SO <sub>4</sub> <sup>2–</sup> (mg/L)	200–400	250	4	0.07843
F <sup>–</sup> (mg/L)	0.5–1.5	1	4	0.07843
Ca <sup>2+</sup> (mg/L)	75–200	75	2	0.03922
Mg <sup>2+</sup> (mg/L)	30–150	50	2	0.03922
Na <sup>+</sup> (mg/L)	200–400	200	2	0.03922
K <sup>+</sup> (mg/L)	8–12	12	2	0.03922
NO <sub>3</sub> <sup>–</sup> N (mg/L)	10–50	45	5	0.09804
Fe <sup>2+</sup> (mg/L)	0.3–1	0.3	4	0.07843

**Table 7** Water quality index for the Qa'Jahran wells

ID	WQI	Water classification
DJ1-W0005	38.243843	Excellent water
DJ1-W0015	64.904057	Good water
DJ1-W0002	39.601739	Excellent water
DJ1-W0008	73.76476	Good water
DJ1-W0014	43.2662	Excellent water
DJ1-W0034	35.64832	Excellent water
DJ1-W0010	43.719578	Excellent water
DJ2-W0051	64.260741	Good water
DJ3-W0020	42.006772	Excellent water
DJ2-W0002	34.78738	Excellent water
DJ3-W0005	61.615663	Good water
DJ3-W0083	41.377107	Excellent water
DJ2-W0014	37.560144	Excellent water
DJ2-W0067	45.272093	Excellent water
DJ2-W0008	58.925567	Good water
DJ1-W0009	34.209919	Excellent water
DJ1-W0033	23.970572	Excellent water
DJ3-W0015	19.979173	Excellent water

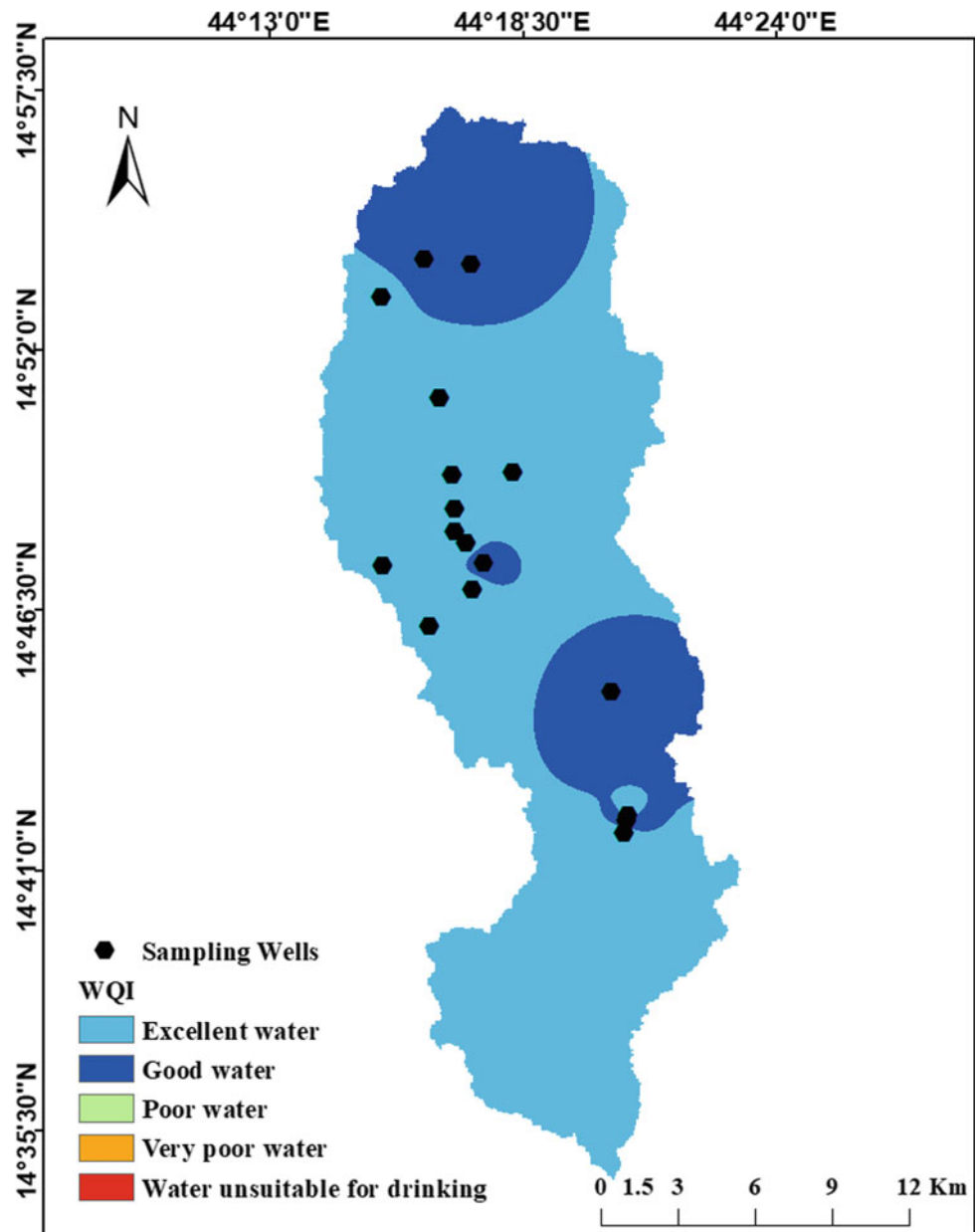
(conductivity, TDS, hardness, total alkalinity, bicarbonate, chloride, sulfate, calcium, nitrate) explained 85.22% of the data variance.

According to WHO and G.Y.L., most of the chemical elements in the study area fall in the permissible limits. WQI and GIS approach were integrated to evaluate water quality

in the study area and identify the potential risky zones. This water quality index map shows that the water in the study area is mostly excellent to good water, and based on that, this water is recommended for domestic use and human drinking.



**Fig. 6** Spatial distribution of water quality index in Qa'Jahran basin



**Acknowledgements** The authors are grateful to the National Water Resources Authority (NWRA) of Yemen for providing the facilities to analysis water samples for this research.

## References

- Al-hadithi, M. (2012). Application of water quality index to assess suitability of groundwater quality for drinking purposes in Ratmao-Pathri Rao watershed, Haridwar District, India. *American Journal of Scientific and Industrial Research*, 3(6), 396–402. <https://doi.org/10.5251/ajsir.2012.3.6.395.402>.
- Al-Omran, A. M., Mousa, M. A., AlHarbi, M. M., & Nadeem, M. E. A. (2018). Hydrogeochemical characterization and groundwater quality assessment in Al-Hasa, Saudi Arabia. *Arabian Journal of Geosciences*, 11(4). <https://doi.org/10.1007/s12517-018-3420-y>
- Alberto, W. D., María del Pilar, D., María Valeria, A., Fabiana, P. S., Cecilia, H. A., & María de los Ángeles, B. (2001). Pattern recognition techniques for the evaluation of spatial and temporal variations in water quality. A case study: Suquia River Basin (Córdoba-Argentina). *Water Research*, 35(12), 2881–2894. [https://doi.org/10.1016/S0043-1354\(00\)00592-3](https://doi.org/10.1016/S0043-1354(00)00592-3)
- Aqeel, A., Al-Amry, A., & Alharbi, O. (2017). Assessment and geospatial distribution mapping of fluoride concentrations in the groundwater of Al-Howban Basin, Taiz-Yemen. *Arabian Journal of Geosciences*, 10(14). <https://doi.org/10.1007/s12517-017-3069-y>
- Bu, H., Tan, X., Li, S., & Safety, Q. Z.-E. (2010). Temporal and spatial variations of water quality in the Jinshui River of the South Qinling Mts., China. *Elsevier*. Retrieved from <https://www.sciencedirect.com/science/article/pii/S0147651309002735>
- Canada, H. (2017). Guidelines for Canadian drinking water quality summary table. Retrieved from <https://www.canada.ca/content/dam/>

- [hc-sc/migration/hc-sc/ewh-semt/alt\\_formats/pdf/pubs/water-eau/sum\\_guide-res\\_recom/sum\\_guide-res\\_recom-eng.pdf](https://doi.org/10.1007/s10661-014-3844-0)
- Chowdhury, S., & Al-Zahrani, M. (2014). Water quality change in dam reservoir and shallow aquifer: Analysis on trend, seasonal variability, and data reduction. *Environmental Monitoring and Assessment*, 186(10), 6127–6143. <https://doi.org/10.1007/s10661-014-3844-0>.
- Chowdhury, S., Champagne, P., & Husain, T. (2007). Fuzzy risk-based decision-making approach for selection of drinking water disinfectants. *Water Supply*. <https://doi.org/10.2166/aqua.2007.090>.
- Elhatip, H., Himis, M. A., & Gülbahar, N. (2008). Evaluation of the water quality at Tahtali dam watershed in Izmir-Turkey by means of statistical methodology. *Stochastic Environmental Research and Risk Assessment*, 22(3), 391–400. <https://doi.org/10.1007/s00477-007-0127-0>.
- Eslami, H., Dastorani, J., Javadi, M. R., & Chamheidar, H. (2013). Geostatistical evaluation of ground water quality distribution with GIS (case study: Mianab-Shoushtar plain. *BEPLS Bulletin Environment, Pharmacology and Life Science*, 3(31), 78–82. Retrieved from <https://www.bepls.com/dec2013/15.pdf>
- Gebrehiwot, A. B., Tadesse, N., & Jigar, E. (2011). Application of water quality index to assess suitability of groundwater quality for drinking purposes in Hantebet watershed, Tigray, Northern Ethiopia. *ISABB Journal of Food and Agriculture Science*, 1(1), 22–30. Retrieved from <https://www.isabb.academicjournals.org/JFAS>
- Helena, B., Pardo, R., Vega, M., Barrado, E., & Research, J. F.-W. (2000). Temporal evolution of groundwater composition in an alluvial aquifer (Pisuerga River, Spain) by principal component analysis. *Elsevier*. Retrieved from <https://www.sciencedirect.com/science/article/pii/S0043135499002250>
- Igboekwe, M. U., & Akankpo, A. O. (2011). Application of Geographic Information System (GIS) in Mapping Groundwater Quality in Uyo, Nigeria. *International Journal of Geosciences*, 02(04), 394–397. <https://doi.org/10.4236/ijg.2011.24042>.
- Jackson, J. E., & John Wiley & Sons. (1991). *A user's guide to principal components*. Wiley. Retrieved from [https://books.google.com.sa/books?hl=ar&lr=&id=f9s6g6cmUTUC&oi=fnd&pg=PR7&dq=A+user+guide+to+principal+components&ots=Lcl7kJWoP4&sig=PBRTmtL0IFqY-\\_xluYIrCLLLKw4&redir\\_esc=y#v=onepage&q=Auserguidetoprincipalcomponents&f=false](https://books.google.com.sa/books?hl=ar&lr=&id=f9s6g6cmUTUC&oi=fnd&pg=PR7&dq=A+user+guide+to+principal+components&ots=Lcl7kJWoP4&sig=PBRTmtL0IFqY-_xluYIrCLLLKw4&redir_esc=y#v=onepage&q=Auserguidetoprincipalcomponents&f=false)
- Lee, J. Y., Cheon, J. Y., Lee, K. K., Lee, S. Y., & Lee, M. H. (2001). Statistical evaluation of geochemical parameter distribution in a groundwater system contaminated with petroleum hydrocarbons. *Journal of Environmental Quality*, 30(5), 1548–1563. Retrieved from <https://www.ncbi.nlm.nih.gov/pubmed/11577860>
- Liu, C.-W., Kao-Hung Lin, Y.-M. K. (2003). Application of factor analysis in the assessment of groundwater quality in a Blackfoot disease area in Taiwan. *The Science of the Total Environment*, 313(77–89). Retrieved from [https://ac.els-cdn.com/S0048969702006836/1-s2.0-S0048969702006836-main.pdf?\\_tid=1aed8f8e-e69b-11e7-a470-00000aabb0f02&acdnat=1513894139\\_fbe8c3f1459c9905ba53e96ed9587261](https://ac.els-cdn.com/S0048969702006836/1-s2.0-S0048969702006836-main.pdf?_tid=1aed8f8e-e69b-11e7-a470-00000aabb0f02&acdnat=1513894139_fbe8c3f1459c9905ba53e96ed9587261)
- Marinović Ruždjak, A., & Ruždjak, D. (2015). Evaluation of river water quality variations using multivariate statistical techniques. *Environmental Monitoring and Assessment*, 187(4), 215. <https://doi.org/10.1007/s10661-015-4393-x>.
- Mohamed, M. M. A., & Hassane, A. B. (2016). Hydrochemistry assessment of groundwater quality in Al-Ain city, UAE. *Environmental Earth Sciences*, 75(4), 1–17. <https://doi.org/10.1007/s12665-015-4942-1>.
- Muangthong, S., & Shrestha, S. (2015). Assessment of surface water quality using multivariate statistical techniques: Case study of the Nampong River and Songkhram River. *Thailand. Environmental Monitoring and Assessment*, 187(9), 548. <https://doi.org/10.1007/s10661-015-4774-1>.
- Nair, H. C., Padmalal, D., Joseph, A., & Gopinthan, V. P. (2018). Hydrogeochemistry and water quality assessment of shallow aquifers in the western flanks of Southern Western Ghats, SW India.
- Nasher, G., Al-Sayyaghi, A., & Al-Matary, A. (2013). Identification and evaluation of the hydrogeochemical processes of the lower part of Wadi Siham catchment area, Tihama plain, Yemen. *Arabian Journal of Geosciences*, 6(6), 2131–2146. <https://doi.org/10.1007/s12517-011-0471-8>.
- Nazzal, Y., Ahmed, I., Al-Arifi, N. S. N., Ghrefat, H., Batayneh, A., Abuamarah, B. A., & Zaidi, F. K. (2015). A combined hydrochemical-statistical analysis of Saq aquifer, northwestern part of the Kingdom of Saudi Arabia. *Geosciences Journal*, 19(1), 145–155. <https://doi.org/10.1007/s12303-014-0016-8>.
- Olsen, R. L., Chappell, R. W., & Loftis, J. C. (2012). Water quality sample collection, data treatment and results presentation for principal components analysis—literature review and Illinois River watershed case study. *Water Research*, 46(9), 3110–3122. <https://doi.org/10.1016/j.watres.2012.03.028>.
- Phung, D., Huang, C., Rutherford, S., Dwirahmadi, F., Chu, C., Wang, X., ... Dinh, T. A. D. (2015). Temporal and spatial assessment of river surface water quality using multivariate statistical techniques: a study in Can Tho City, a Mekong Delta area, Vietnam. *Environmental Monitoring and Assessment*, 187(5), 229. <https://doi.org/10.1007/s10661-015-4474-x>
- Qadir, A., Malik, R., Assessment, S. H.-E. M. (2008). Spatio-temporal variations in water quality of Nullah Aik-tributary of the river Chenab, Pakistan. *Springer*. Retrieved from <https://www.springerlink.com/index/E13326127137RKR4.pdf>
- Reghunath, R., Murthy, T. R. S., & Raghavan, B. R. (2002). The utility of multivariate statistical techniques in hydrogeochemical studies: an example from Karnataka, India. *Water Research*, 36, 2437–2442. Retrieved from [https://ac.els-cdn.com/S0043135401004900/1-s2.0-S0043135401004900-main.pdf?\\_tid=9fa18c4c-e8f5-11e7-ae81-00000aabb0f26&acdnat=1514152910\\_f7dce303e1c01b0339b9b99040034200](https://ac.els-cdn.com/S0043135401004900/1-s2.0-S0043135401004900-main.pdf?_tid=9fa18c4c-e8f5-11e7-ae81-00000aabb0f26&acdnat=1514152910_f7dce303e1c01b0339b9b99040034200)
- Rice, E. W., Baird, R. B., & Eaton, A.D. (Eds.) (2017). *Standard methods for the examination of water and wastewater* (23rd ed). Retrieved May 6, 2018, from <https://www.awwa.org/store/productdetail.aspx?productid=65266295>
- Saleh, S. M. K., Al-alaiy, S. H. G., & Abdul-razzak, B. (2018). Application of water quality index to assessment of groundwater quality Application of water quality index to assessment of groundwater quality (April 2017).
- Sh Nasher, G. A., & A El-Sagheer, A. A. (2012). Water quality evaluation of Bura'a natural protected area, Hodeidah, Yemen. *Academic & Scholarly Research Journal*, 4. Retrieved from [www.aasrc.org/aasrj](http://www.aasrc.org/aasrj)
- Simeonov, V., Stratis, J., Samara, C., Rresearch, G. Z.-W. (2003). Assessment of the surface water quality in Northern Greece. *Elsevier*. Retrieved from <https://www.sciencedirect.com/science/article/pii/S0043135403003981>
- Singh, A. K., Tewary, B. K., & Sinha, A. (2011). Hydrochemistry and quality assessment of groundwater in part of NOIDA metropolitan city, Uttar Pradesh. *Journal of the Geological Society of India*, 78(6), 523–540. <https://doi.org/10.1007/s12594-011-0124-2>.
- Singh, K. P., Malik, A., Mohan, D., & Sinha, S. (2004). Multivariate statistical techniques for the evaluation of spatial and temporal variations in water quality of Gomti River (India)—A case study. *Water Research*, 38(18), 3980–3992. <https://doi.org/10.1016/j.watres.2004.06.011>.
- Singh, K. P., Malik, A., & Sinha, S. (2005). Water quality assessment and apportionment of pollution sources of Gomti river (India) using multivariate statistical techniques— A case study. *Analytica Chimica Acta*, 538, 355–374. <https://doi.org/10.1016/j.aca.2005.02.006>.

- Toumi, N., Hussein, B. H. M., Rafrafi, S., & El kassas, N. (2015). Groundwater quality and hydrochemical properties of Al-Ula Region, Saudi Arabia. *Environmental Monitoring and Assessment*, 187(3), 1–16. <https://doi.org/10.1007/s10661-014-4241-4>
- Varol, M., Gökot, B., Bekleyen, A., & Şen, B. (2012). Spatial and temporal variations in surface water quality of the dam reservoirs in the Tigris River basin, Turkey. *CATENA*, 92, 11–21. <https://doi.org/10.1016/J.CATENA.2011.11.013>.
- Vega, M., Pardo, R., Barrado, E., & Research, L. D.-W. (1998). Assessment of seasonal and polluting effects on the quality of river water by exploratory data analysis. *Elsevier*. Retrieved from <https://www.sciencedirect.com/science/article/pii/S0043135498001389>
- Voza1\*, D., Ljiljana Takic2, M. V., Nikolic1, D., & Mladenovic-Ranisavljevic2. I. (2015). Application of multivariate statistical techniques in the water quality assessment of Danube river, Serbia. *Archives of Environmental Protection*, 41, 96–103. <https://doi.org/10.1515/aep-2015-0044>
- Wold, S., Esbensen, K., & Geladi, P. (1987). Principal component analysis. *Tutorial n Chemometrics and Intelligent Laboratory Systems Elsevier Science Publishers B.V*, 2, 37–52. Retrieved from [https://ac.els-cdn.com/0169743987800849/1-s2.0-0169743987800849-main.pdf?\\_tid=5be82b5a-dd10-11e7-a4d8-00000aacb362&acdnat=1512844979\\_52f5a071600a5e73564aabe03448d36f](https://ac.els-cdn.com/0169743987800849/1-s2.0-0169743987800849-main.pdf?_tid=5be82b5a-dd10-11e7-a4d8-00000aacb362&acdnat=1512844979_52f5a071600a5e73564aabe03448d36f)
- WHO. (2017). *Guidelines for Drinking-Water Quality: Fourth Edition Incorporating the First Addendum*. World Health Organization. Geneva, Switzerland. License: CC BY-NC-SA 3.0 IGO.
- Yan, C. A., Zhang, W., Zhang, Z., Liu, Y., Deng, C., & Nie, N. (2015). Assessment of water quality and identification of polluted risky regions based on field observations & GIS in the Honghe River Watershed. *China. PLoS ONE*, 10(3), 1–13. <https://doi.org/10.1371/journal.pone.0119130>.
- Zeilhofer, P., Lima, E. B. N. R., & Lima, G. A. R. (2006). Spatial Patterns of Water Quality in the Cuiabá River Basin. *Central Brazil. Environmental Monitoring and Assessment*, 123(1–3), 41–62. <https://doi.org/10.1007/s10661-005-9114-4>.
- Zeilhofer, P., Zeilhofer, L. V. A. C., Hardoim, E. L., de Lima, Z. M., & Oliveira, C. S. (2007). GIS applications for mapping and spatial modeling of urban-use water quality: A case study in District of Cuiabá, Mato Grosso. *Brazil. Cadernos De Saúde Pública*, 23(4), 875–884. <https://doi.org/10.1590/S0102-311X2007000400015>.
- Zhang, Q., Li, Z., Zeng, G., Li, J., Fang, Y., Yuan, Q., ... Ye, F. (2009a). Assessment of surface water quality using multivariate statistical techniques in red soil hilly region: a case study of Xiangjiang watershed, China. *Environmental Monitoring and Assessment*, 152(1–4), 123–131. <https://doi.org/https://doi.org/10.1007/s10661-008-0301-y>
- Zhang, Y., Guo, F., Meng, W., & Wang, X.-Q. (2009). Water quality assessment and source identification of Daliao river basin using multivariate statistical methods. *Environmental Monitoring and Assessment*, 152(1–4), 105–121. <https://doi.org/10.1007/s10661-008-0300-z>.
- Zhao, J., Fu, G., Lei, K., Li, Y., Li, X., Li, J., & Zheng, Y. (2011). Assessment of spatial-temporal patterns of surface water quality in the Min River (China) and implications for management. In *Proceedings—International Conference on Computer Distributed Control and Intelligent Environmental Monitoring, CDCIEM 2011*, 1983–1989. <https://doi.org/10.1109/CDCIEM.2011.499>



# Development and Calibration of Transient Groundwater Flow Model for Al Kufrah Region, Southeast Libya

Abdalraheem M. Huwaysh and Zuhair B. Hafi

## Abstract

Al Kufrah basin, which is a part of the huge trans-boundary Nubian Sandstone Aquifer System (NSAS) shared by Libya, Egypt, Sudan and Chad, is a major water resource in North Africa. The NSAS consists of a number of aquifers laterally and /or vertically interconnected, extending over more than  $2 \times 10^6$  km<sup>2</sup>. In recent years, the demand in some areas has resulted in withdrawals that substantially exceed replenishment of the aquifers. A 3-D groundwater flow model was constructed and calibrated to simulate the subregional groundwater flow during the pre- and post-development periods in response to stresses within Al Kufrah Region. The developed model utilized PMWIN<sup>®</sup> software, a fully integrated modeling platform that uses the USGS Modular MODFLOW2000<sup>®</sup>. The entire simulated thickness of 300 m was modeled as three hydraulically connected horizontal layers; each layer consists of 181 rows and 181 columns with grid spacing of 500 m by 500 m to cover a total area of 8190 km<sup>2</sup>. General head boundaries (GHBs) were assigned to the southern and eastern nodes to simulate the groundwater inflow and outflow. Evapotranspiration was assigned to the upper model layer, with a maximum rate of 2750 mm/yr and an extinction depth of 2 m below the ground surface. Groundwater flow parameters (principally hydraulic conductivities, boundary conditions and recharge) were set during the steady-state calibration process. Calibration proceeded by varying these input parameters until the model results in most closely matched field measurements. In addition, the simulated

hydraulic heads were consistent within the model domain with the actual field measurements (before the year 1968). Five stress periods—transient-state flow model, were constructed and calibrated using all available data from 1968 to 2010. Specific storage values range from  $10^{-5}$  to  $10^{-2}$  for the middle and the lower layers, and specific yield range between  $2 \times 10^{-3}$  and  $2 \times 10^{-1}$  for the upper layer was initially assigned based on the previous hydrogeological studies of Al Kufrah basin; these values were repeatedly adjusted for the three layers during the calibration of the first period until satisfactorily calibrated hydraulic heads were reached. A value of about 10% of the total applied water was assigned to layer 1 as a surface recharge. Analysis of the residual statistics and spatial distribution of residuals as well as the visual comparison between simulated and observed hydrographs and potentiometric surfaces were used to analyze the ability of the calibrated model to simulate aquifer conditions within acceptable error. The root of mean square errors ranges from 0.8 m to 2.34 m for the 33 observation wells. Calibrated model output includes a 43-year estimate of the water budget by the end of each stress period at the shallow and deep layers. The historical calibration of this transient-state model indicated a very close matching between the calculated and the observed drawdown values that have exceeded 40 m during some periods.

## Keywords

Nubian aquifer system • Al Kufrah region • Transient-state flow model • Stress periods

A. M. Huwaysh (✉)

Joint Authority for the Study and Development of the Nubian Sandstone Aquifer System., Tripoli, Libya  
e-mail: [Ahweesh@yahoo.co.uk](mailto:Ahweesh@yahoo.co.uk)

A. M. Huwaysh · Z. B. Hafi

Department of Geology, Faculty of Science, University of Tripoli,  
P.O. Box 13258 Tripoli, Libya

## 1 Introduction

Libya, in spite of its vast area, more than 90% of its territories receive an annual rainfall less than 100 mm, which makes the country to be classified as a water-scarce country.

Al Kufrah basin is one of the main groundwater resources in Libya (Pallas, 1980). It covers the southeastern corner of the country, with fast-growing Al Kufrah settlement cluster in its center. The rest of the basin is deserted with some operational agricultural projects. To meet this growing water demand, the development and calibration of computer-based numerical models to simulate the movement of groundwater in the shallow and deep aquifers under transient flow conditions are vital for future modeling of groundwater contamination.

## 2 Description and Location of the Modeled Area

The targeted area is a part of Al Kufrah basin. It is also a part of the huge Nubian Sandstone Aquifer System (NSAS) which represents a huge trans-boundary groundwater system consists of a number of aquifers laterally and/or vertically interconnected, extending over more than  $2.2 \times 10^6$  km<sup>2</sup>, shared by Libya, Egypt, Sudan and Chad (CEDARE, 2001). Several water well fields as well as hundreds of private water wells have been drilled for the agricultural and domestic purposes in the urbanized and rural areas. The piezometric network was the main source of data about the periodical water-level measurements recorded from several shallow and deep piezometers (Fig. 1).

## 3 Model Development

A three-dimensional (3-D) steady-state groundwater flow model of the Kufrah aquifers has been previously developed and calibrated by the authors, and the results were published in Water Resources of Libya (Hweesh & Hafi, 2015). This paper deals with the results obtained from the model simulation of groundwater under **transient-state flow conditions** during the post-development period (1968–2010).

### 3.1 Conceptual Model

The conceptual groundwater model upon which this transient-state flow model was based has been developed to provide a description of the hydrogeologic conditions and processes within the modeled area (Hweesh & Hafi, 2015). The components of the conceptual model included (1) descriptions of the hydrogeologic framework and hydraulic properties of the media; (2) descriptions of the spatial and temporal characteristics of the model boundaries; (3) estimates of inflows, outflows and fluxes across model boundaries; (4) descriptions of the approaches used to estimate the

components of the steady-state water budget and the possible effects of transient influences on groundwater flow directions; and (6) descriptions of the stratigraphic and hydrologic controls on groundwater flow.

Because the existing pumping wells have been drilled during different periods of time and penetrating the aquifer at various depths (Eddib, 1973), the entire simulated thickness of 300 m was modeled as three horizontal layers; layer 1, layer 2 and layer 3 of thicknesses 70 m, 80 m and 150 m, respectively, and with vertical upward and downward flow between them (Fig. 2).

### 3.2 Transient-State Model Setup

The excessive use of groundwater in Al Kufrah region for irrigation practices has disturbed the primordial equilibrium in the aquifer system, ever since the net extraction of groundwater exceeded the net natural recharge. Consequently, the overall groundwater storage in the region is under ongoing decrease (General Water Authority, 2014). For a period of thirty years (from 1976 to 2006), the data collected from the deep piezometer (Pz. 19), for example, which is located at the center of the pumping area of Al Kufrah Production Project (KPP), indicated that the measured water level in the deep aquifer declined as much as 23 m in average, with a rate of 0.76 m/y (Fig. 3).

The transient simulation phase of groundwater flow in the targeted area is intended to represent temporal changes of water levels in the shallow and deep aquifers for water extraction period of 43 years (from 1968 to 2010). The model input consists of two parts; the first part includes the results (outputs) obtained during the steady-state calibration phase which are hydraulic heads, hydraulic conductivity values (horizontal and vertical), boundary conditions and the evapotranspiration parameters. The second part of the input package contains stress periods, length (time), groundwater pumpage, recharge from irrigation return and the initial estimate of aquifer storativities for the shallow and deep layers.

#### 3.2.1 Time Discretization

The model simulates total of 43 years (from 1968 up to 2010) of continuous pumping of variable rates and locations. Consequently, the total modeled pumping duration was divided into five stress periods as shown in Table 1, based on the number of operated wells and the availability of historical hydraulic head measurements required for the model calibration at each period. Time-dependent hydrogeological variables, such as the field-measured hydraulic heads and the quantities of the extracted and irrigation return water, were assigned specifically to each period.



**Fig. 1** Location map of the modeled area

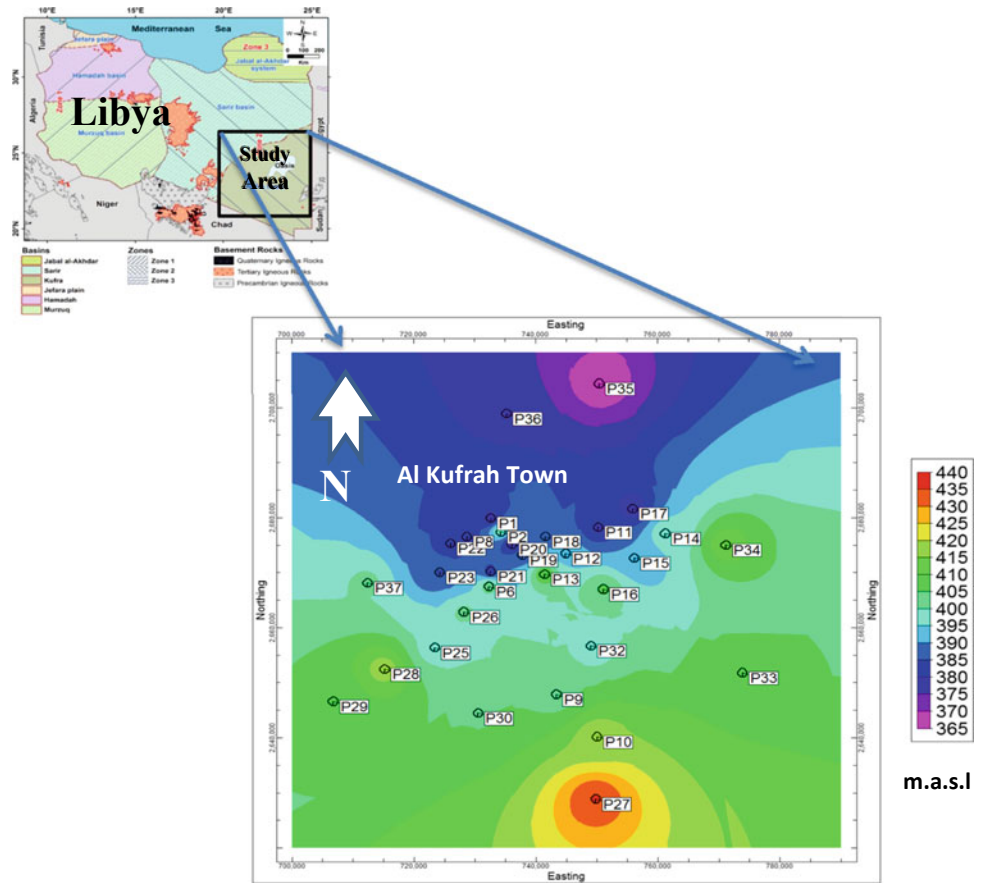


**Fig. 2** Schematic conceptual model of the study area

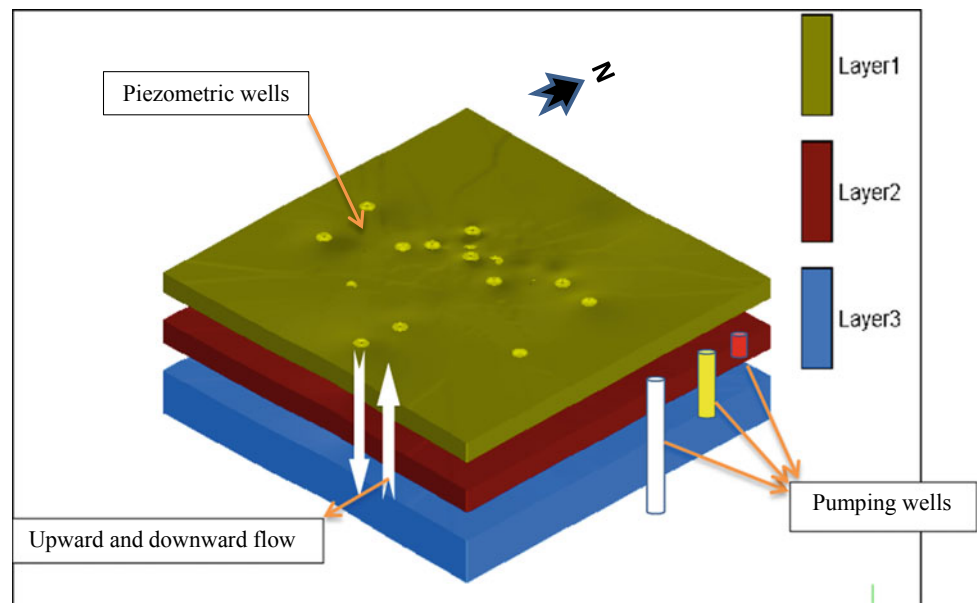


**Fig. 3** Sample of measured water levels from one of the deep piezometers (piezometer 19) at the center of the pumping area

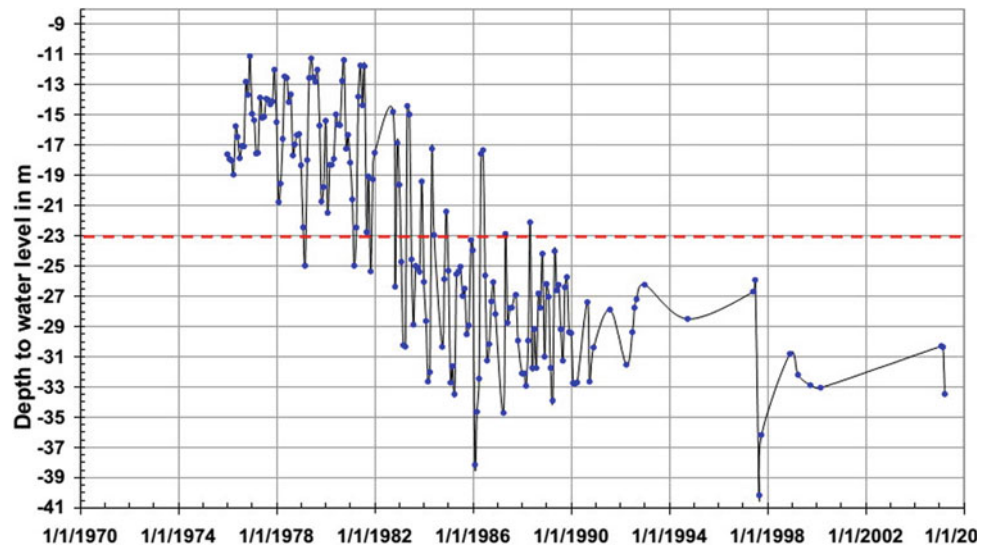


**Table 1** Stress periods for the model simulation

Stress period	Years	Length (year)	Length (days)	Accumulative time (days)
I	1968–1976	9	3285	3285
II	1977–1986	10	3650	6395
III	1987–1998	12	4380	11,315
IV	1999–2004	6	2190	13,505
V	2005–2010	6	2190	15,695

### 3.2.2 Groundwater Withdrawal

Abstraction rates are rarely documented, especially for the private farms, and the expansion of the irrigated areas with increase of the number of wells led to discretize the total simulation time into five pumping periods. Quantification of the modeled abstraction rate for individual wells was estimated according to the average daily irrigation hours and pumping rates as reported by Kufrah Production Project (KPP) and Kufrah Date Palms Project (KDP).

In Al Kufrah region, the major exploitation of groundwater for agricultural purposes began in 1968 when the KPP was started by the drilling of about 20 deep wells' tapping layer 3. By the year of 1974, the total number of drilled wells had been reached up to 100 wells. Data presented by General Water Authority (GWA) in Libya indicate a rapid increase in the number of wells penetrating both the shallow and deep aquifers through the past 40 years in and around Al Kufrah Town. This is evidently recognized from the historical satellite images that cover the study area.

### 3.2.3 Surface Recharge

Because of the aridity of the study area, the only direct surface recharge is limited to irrigation return water at cultivated fields. Based on the literature review and internal reports, a value of about 10 percent of the total applied water

was assigned to layer 1 as a surface recharge. It is variable from pumping period to another.

## 4 Transient-State Model Calibration

Transient-state model calibration has been carried out by manual trial-and-error adjustments of the storativity parameters (specific yield and specific storage), while the steady-state hydraulic conductivities ( $K_h$  and  $K_v$ ) kept unchanged. In order to achieve the reasonable match between the field-measured and simulated hydraulic heads, hundreds of computer runs was done.

The model was calibrated for transient conditions starting from 1968 to 2010 (43 years) simulating five stress periods of different lengths. A total of 315 hydraulic head measurements recorded from 31 shallow piezometers' monitoring layer 1 and 32 deep piezometers' monitoring layer 3 were used to validate the matching between the simulated and the measured heads over the whole simulation time.

### 4.1 Storativity

Specific storage values range from  $10^{-5}$  to  $10^{-2}$  for the middle and the lower layers, and specific yield range

between  $2 \times 10^{-3}$  and  $2 \times 10^{-1}$  for the upper layer was initially assigned based on the previous hydrogeological studies of Al Kufrah basin (Fisk & Pennigton, 1976). As mentioned above, these values were repeatedly adjusted for the three layers during the calibration of the first period until satisfactorily calibrated hydraulic heads were reached (Fig. 4).

### 4.2 Pumpage

The various time-related uses of the groundwater for irrigation induced significant transient changes in hydraulic

heads as noted in the field-measured heads. Therefore, the hydrogeologic history of the aquifer was simulated by five successive transient stress periods, based on the growing water demand which led to dramatic increase of new drilled wells as shown in Table 1 (General Water Authority, 2006). During the calibration stage, pumping rates and the total number of working wells from the deep and shallow layers have been modified from one period to the next according to the number of operated wells and their pumping rates during each stress period. As shown in Table 2 and Fig. 5, the most significant quantities of water were extracted from KPP wells (layer 3). Even though the extracted quantities from the private farm wells are much smaller than that of the KPP

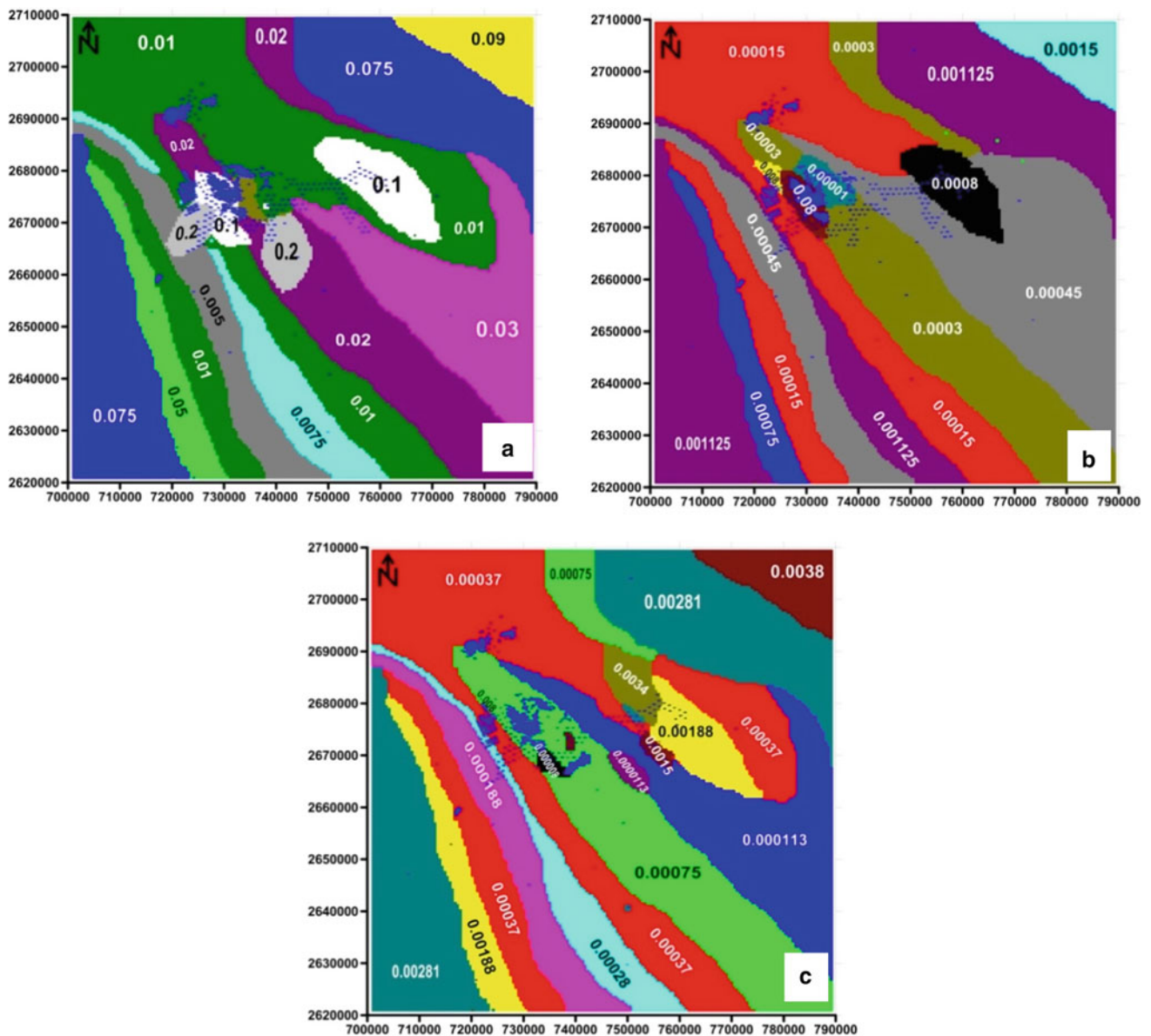


**Fig. 4** Specific yield and specific storage values used for calibration; **a** specific yield for layer 1, **b** specific storage for layer 2 and **c** specific storage for layer 3

wells, they played major effect on the calibration of the upper layer.

## 5 Calibration Results and Statistical Analysis of Residuals

The results of transient calibration phase are the spatial and temporal hydraulic head distribution and the water balance within the modeled area in response to the variable pumping stresses. The reliability of these results has been verified at the end of every simulation period using the following three different approaches:

- Visual matching between the simulated and observed hydraulic heads.
- Statistical analyses of residuals between the simulated and observed hydraulic heads.
- Comparison between the simulated and observed hydrographs at most of the deep and shallow piezometers.

### 5.1 Stress Period I

The simulated duration of this period had lasted for nine consecutive years (1968–1976). The input data for this period include the initial estimate of storativities and the time-dependent variables which are surface recharge from irrigation return, initial head distribution and the estimated groundwater withdrawal rates. As previously indicated, these parameters have been repeatedly revised until a satisfactorily calibration was accomplished.

For the upper model layer (layer 1), 315 private farm wells with average pumping rate of 18 m<sup>3</sup>/h and about 10% of the pumped water were implemented to represent the surface recharge from the irrigation water return. For the lower model layer (layer 3), 95 deep production wells for the KPP and 4 public wells with average pumping rate of 273 m<sup>3</sup>/h were applied. Model calibration can be assessed qualitatively by visually comparing simulated hydraulic heads with measured values. Figures 6 and 7 show a

reasonable match between the simulated heads at the end of the period and the interpolated field observed heads in December 1976 for the model layer 1 and model layer 3, respectively. The slight discrepancy between simulated and observed contours at the northeastern corner of the study area can be attributed to the lack of piezometers.

The simulated head values of the thirty-two piezometers were plotted against their standardized residuals for each layer to check the degree of linearity between the simulated and the observed hydraulic head values. The closer the points to the zero line, the less the model bias, where a negative value indicates the model tends to overprediction (simulated hydraulic heads greater than observed) and a positive value indicates underprediction (simulated hydraulic heads less than observed). Out of 31 observations in layer 1, only 3 simulated head points showed residuals greater than one (slightly underestimated) and 6 simulated head points showed residuals less than one (slightly overestimated), and out of 32 observations in layer 3, only 6 simulated head points are slightly underestimated, whereas 5 simulated head points are slightly overestimated (Fig. 8). Figure 8 shows also the linear correlation between the simulated and the observed head points for both shallow and deep layers with a confidence interval of 95%.

### 5.2 Stress Period II

The last (fifth) simulated period continued for 6 years (2005–2010), where the total number of KPP production wells reduced to 37 wells only because several difficulties encountered the project. On the other hand, new additional wells were implemented; they include 100 production wells for the KDP, 2 public wells and 486 private farm wells. The simulated and observed hydraulic head distributions are more or less matched in the most of the study area with minor differences at close to the center of the KPP well field (Figs. 9 and 10).

The standardized residuals versus simulated heads as well as the linear regression plots with 95% confidence of observed heads versus simulated heads for the layer 1 and layer 3 are displayed in Fig. 11. Six simulated head points in the layer 1 are slightly underestimated, and 5 simulated head points are slightly overestimated; for the lower layer, the

**Table 2** Simulated discharge and the number of wells for each stress period

Period	Total discharge (m <sup>3</sup> )				Number of wells			
	Public wells	Private farms	KPP	KDP	Public wells	Private farms	KPP	KDP
I	6,898,500	43,299,585	360,190,395	0	4	315	100	0
II	52,100,100	78,734,150	798,828,050	66,685,500	13	393	95	9
III	104,143,260	94,853,280	1,112,169,600	107,222,400	13	456	86	9
IV	70,301,190	64,618,140	256,617,630	33,774,180	14	603	55	7
V	86,356,080	112,143,330	83,095,170	57,489,690	16	1089	37	106



**Fig. 5** Total simulated groundwater volumes pumped for different uses during each period

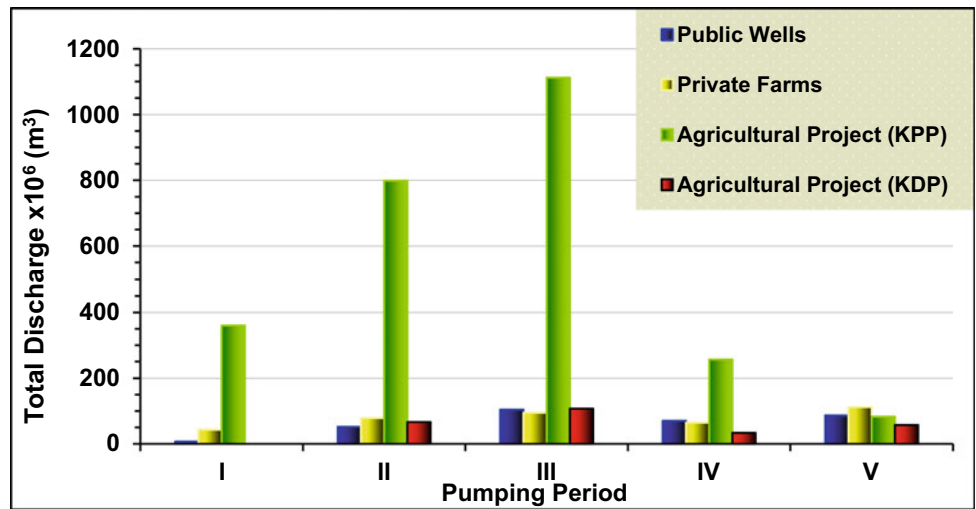


**Fig. 6** Contour maps of observed (a) and simulated (b) hydraulic heads of the layer 1 during the period I (m.a.s.l)

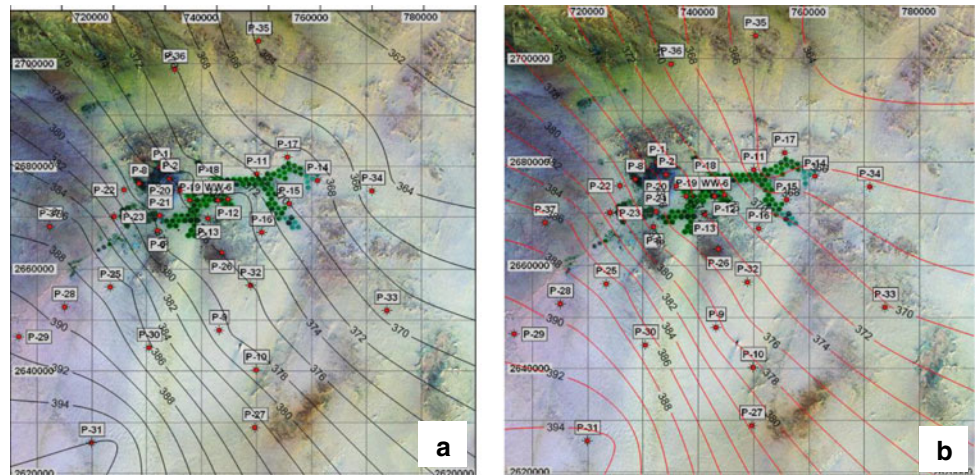
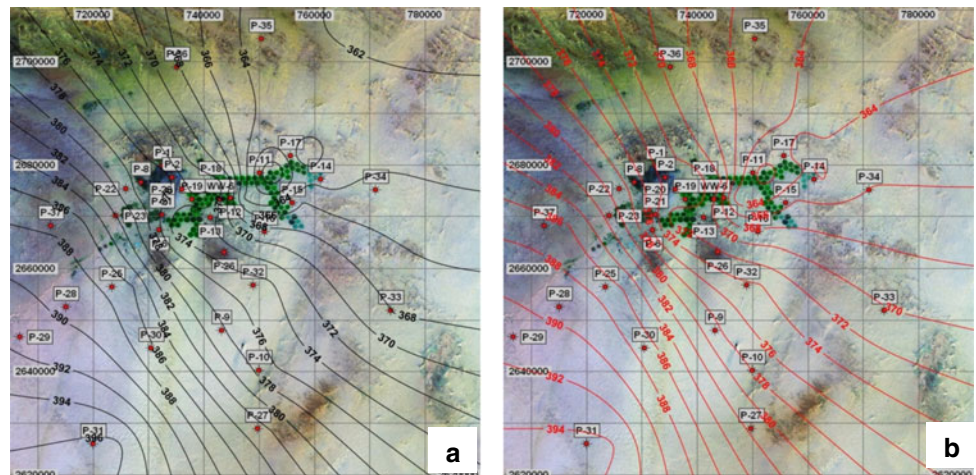


**Fig. 7** Contour maps of observed (a) and simulated (b) hydraulic heads of the layer 3 during the period I (m.a.s.l)



number of the overestimated and underestimated simulated head points found to be 5 points.

RMSE's for the model range from 1.15 to 2.34 m for all time periods for layer 1 and from 0.81 to 2.34 m for the

layer 3, with slightly flat increasing trend throughout simulation time for both layers. The RMSE parameters presented in Table 3 confirm the ability of the model to simulate observed hydraulic heads under different sets of



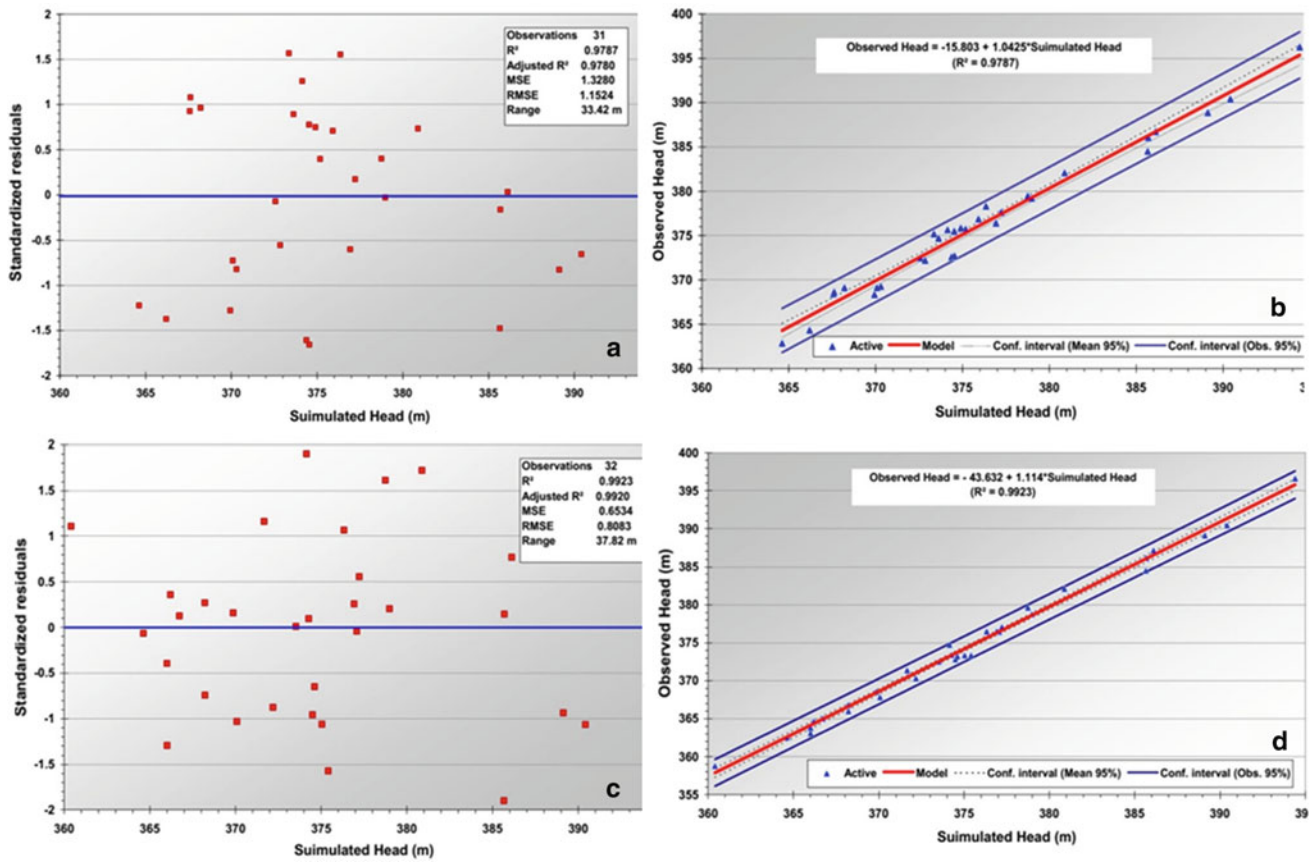
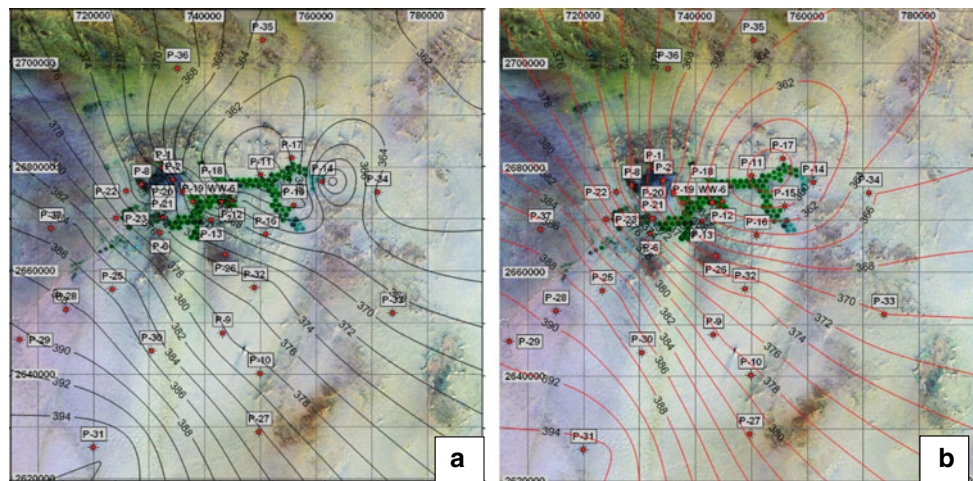


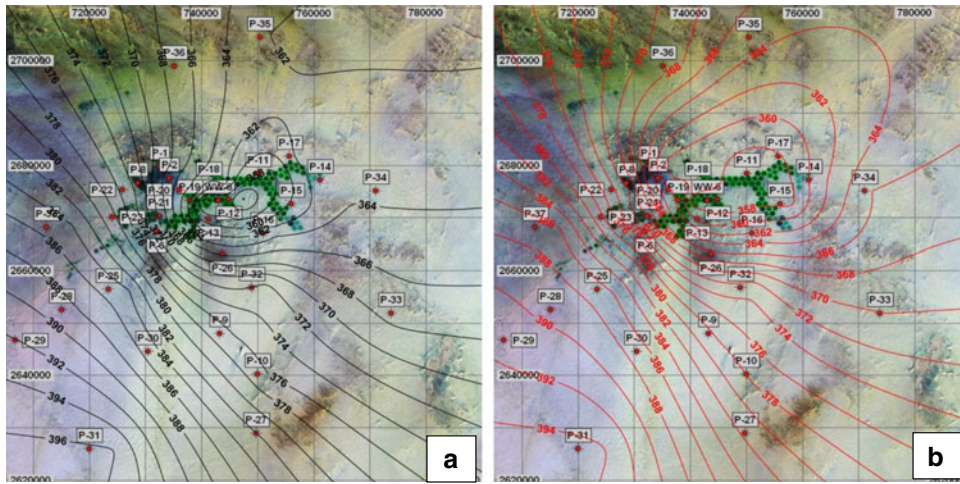
Fig. 8 Standardized residuals and regression lines versus simulated heads for period I: a, b layer 1; c, d layer 3

Fig. 9 Contour maps of observed (a) and simulated (b) hydraulic heads of the layer 1 during the period V (m.a.s.l)



pumping stress and strengthen the prediction confidence for future pumping scenarios. These RMSE flat trends are probably attributed to the implicit error in the estimated pumping rates and number of private wells.

From the above presented standardized residuals versus simulated head plots, it can be noticed that, for all stress periods, the number of underestimated heads for layer 1 ranges from 3 to 6 and from 4 to 6 for layer 3.



**Fig. 10** Contour maps of observed (a) and simulated (b) hydraulic heads of the layer 3 during the period V (m.a.s.l)

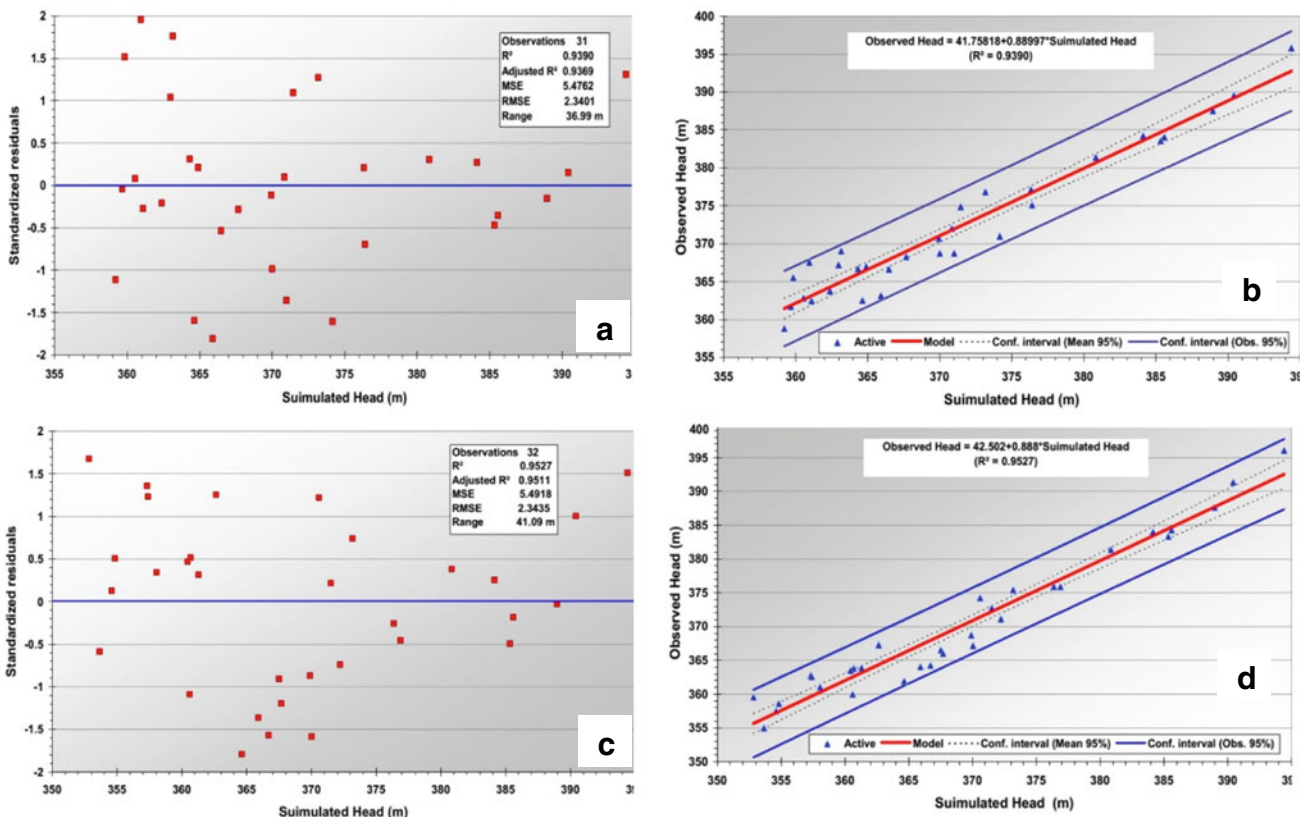


**Fig. 11** Standardized residuals and regression lines versus simulated heads for period V: a, b layer 1; c, d layer 3

### 5.3 Simulated and Observed Hydrographs

As model calibration and parameter estimation are keyed to a set of historical data, the confidence in and reliability of the calibration process is proportional to the quality and comprehensiveness of the historical record (Konikow & Reilly, 1998).

Hydrograph is an important graphical representation of periodic measurements of groundwater levels as displayed versus time. In this study, the simulated and observed hydraulic heads of both shallow and deep piezometers were plotted against the five modeled stress periods in order to validate the model calibration results. Deep piezometer

**Table 3** Summary of the model residual statistics

Period		RMSE	Minimum (m)	Maximum (m)	Range (m)	SD/range (%)
I	Layer 1	1.15	362.89	396.31	33.42	3.45
	Layer 3	0.81	358.80	396.62	37.82	2.14
II	Layer 1	1.43	362.75	396.19	33.44	4.27
	Layer 3	1.08	355.94	396.19	40.25	2.69
III	Layer 1	1.69	358.20	396.24	38.04	4.45
	Layer 3	1.18	348.36	396.01	47.65	2.47
IV	Layer 1	1.98	357.73	395.96	38.23	5.17
	Layer 3	1.42	353.59	396.21	42.62	3.34
V	Layer 1	2.34	358.84	395.83	36.99	6.33
	Layer 3	2.34	355.01	396.10	41.09	5.70

RMSE = Root of mean square error (= SD), range = maximum observed head—minimum observed head

hydrographs can be classified into three distinctive categories taking into account the general trends and matching of the simulated and observed heads; these categories reflect the location of the piezometer with respect to the KPP irrigation pivots. Even though the nearby piezometers show good trends, little discrepancies between the two heads are prominent for some periods which could be related to the effect of pumping during the water-level measurements (Fig. 12).

Those piezometers which are located in KPP well field but not very close to certain irrigation pivot or a little bit farther show excellent trend and minimal discrepancy between the two hydrographs as well (Figs. 13 and 14).

In the far southern and northern parts of the study area, where no discharge is taking place, the observed hydraulic head fluctuations are minimal, varying by less than 1 m, while the trend of the simulated head almost flats all over the five simulated periods (Figs. 15 and 16).

## 6 Simulated Drawdown

The model has been used to simulate historical drawdown effects from pumping for the three model layers. During the development periods (1968–2010), a considerable drawdown has occurred in the potentiometric surface forming local cones of depression as water is removed from storage by withdrawals. **The maximum simulated drawdown that to be mentioned in the following sections represents spot value within the center of model active cell.**

### 6.1 Stress Period I (1968–1976)

After 9 years of continuous pumping since the post-development stage started, a remarkable drawdown in the model layer 1 occurred at the center of the KPP well field with a maximum value of 9 m. The effect of extraction of

groundwater from the private farms is evident at the north-western part of the study area (Al Hawari village), where it reached up to 6 m (Fig. 17). In layer 2, almost the same pattern of drawdown distribution had occurred at the KPP well field with a maximum value of 9 m; however, the groundwater extraction from the private farms had no significant effect in this layer. Due to the extensive pumping of groundwater from layer 3 where the KPP wells are tapped, two major spots of drawdown were resulted with maximum values of 16 m at the center and 10 m at the southwestern part of the well field (Fig. 17).

### 6.2 Stress Period II (1977–1986)

As the number of wells' tapping layer 1 for irrigation use in the private farms has expanded, the drawdown pattern had widened toward the west. The maximum drawdown has increased by 4 m compared to the period I at the KPP well field. The drawdown pattern during this period in layer 2 covers wider area with values higher than period I, and these can be attributed to the implementation of the KDP wells tapping this layer as well as to the continuous pumping from the KPP. In comparison with stress period I, the drawdown in this layer had higher values and wider spread than the previous stress period. In layer 3, maximum drawdown of more than 29 m was located at the southwestern part of the KPP well field and 15 m of drawdown was recorded at the center of the field; these could be attributed to the redistribution of the pumping rates as documented in the KPP reports (Fig. 18).

### 6.3 Stress Period III (1987–1998)

The simulated drawdown at the layer 1 over 12 years from the previous period had laterally expanded, and the three distinctive separated cones of depression at the KPP and the



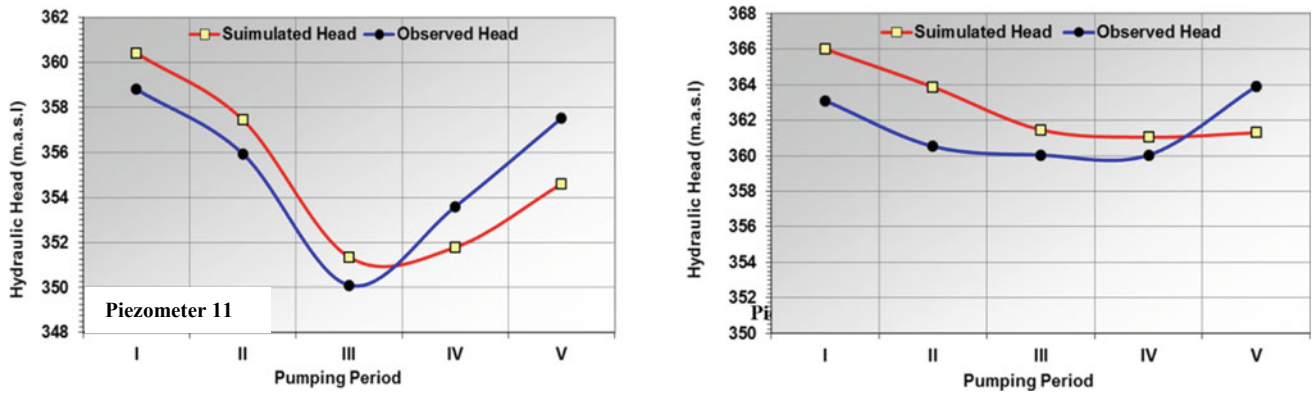


Fig. 12 Simulated and observed hydrographs for piezometers 11 and 14

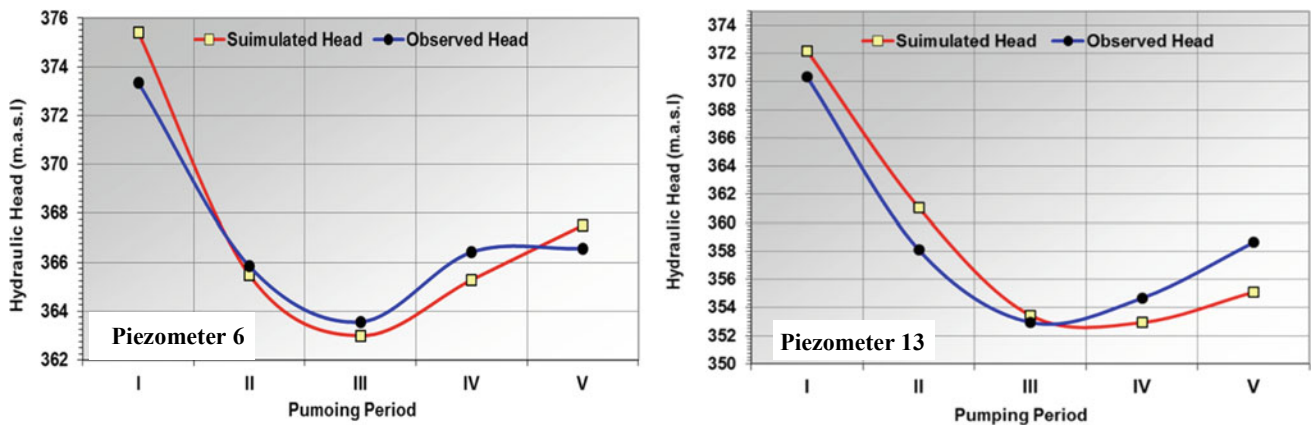


Fig. 13 Simulated and observed hydrographs for piezometers 6 and 13

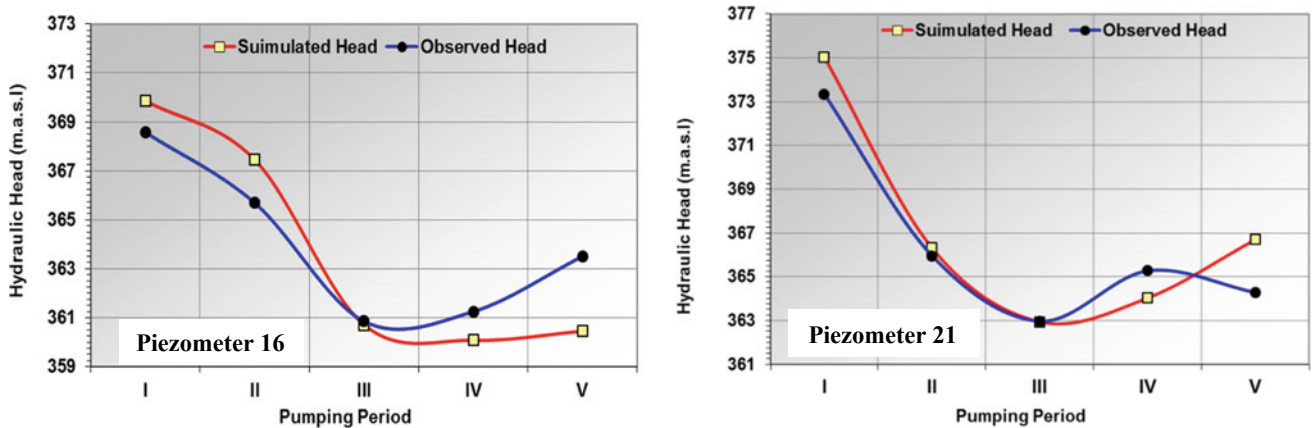


Fig. 14 Simulated and observed hydrographs for piezometers 16 and 21

KDP well fields as well as Al Hawari private farms were combined which could be related to the length of the stress period. The simulated drawdown at the center of the KPP well field had reached up to 21 m whereas at Al Hawari village did not exceed 15 m. Concerning the layer 2, the

simulated drawdown configuration behaves more or less similar to that in layer 1, except at Al Hawari village where it shows a lower value (Fig. 19). Because all the KPP wells tapped the third layer with extensive pumping for longer duration, the drawdown in this layer had reached its highest

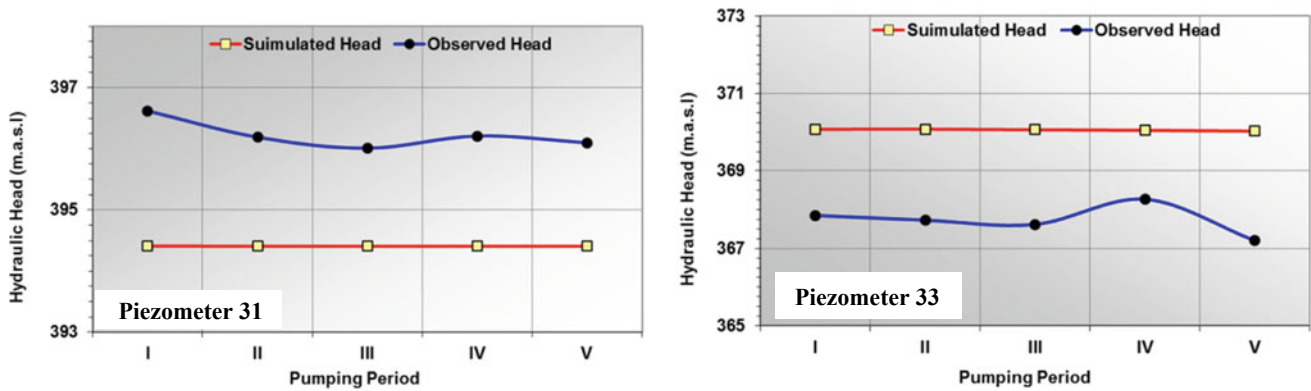


Fig. 15 Simulated and observed hydrographs for piezometers 31 and 33

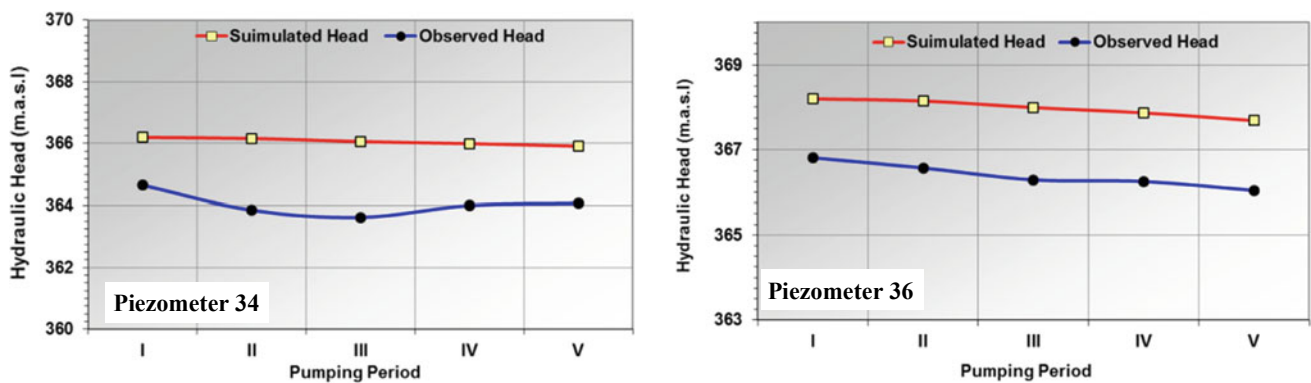


Fig. 16 Simulated and observed hydrographs for piezometers 34 and 36

value from 40 to 45 m that covers an area of 235 hectare at the center of the KPP well field (Fig. 19).

#### 6.4 Stress Period IV (1999–2004)

After 37 years of continuous groundwater pumping, the affected area by drawdown was expanded laterally wider than that in the previous periods for the three simulated layers. The most significant drawdown was recognized in layer 3 (45 m) at the KDP well field, where previously located at the center of the KPP well field. This shift is evidently related to two reasons: the decline of the number of pumping wells at the KPP well field and the resuming of pumping from the KDP wells (Fig. 20).

#### 6.5 Stress Period V (2005–2010)

The modeled area during the last pumping period is characterized by decrease of the maximum simulated drawdown

compared to the last two stress periods (III and IV), where it reached up to 27 m, even though the affected area due to water extraction was continuously increased in the three layers (Fig. 21). This can be attributed to the shutdown of most of the KPP wells due to technical problems. On the other hand, a noticeable increase in the drawdown values in layer 2 can be recognized at the western part of the modeled area as a result of the construction of new 100 production wells (KDP Project expansion).

The simulated drawdowns over all the stress periods have revealed a significant localized drawdown at the center of KPP and KDP well-fields and the private farms. These cones of depression became wider and wider progressively with time covering larger area. Extraction of groundwater from one layer affects the storage of the others, and this strongly confirms that these layers are hydraulically connected and behave as one system. By using Global Mapper software, V 15 and the drawdown Surfer grid files, the areas subjected to drawdown value of 1 m or more have been calculated for the three layers at every stress period as shown in Table 4 and Fig. 22.



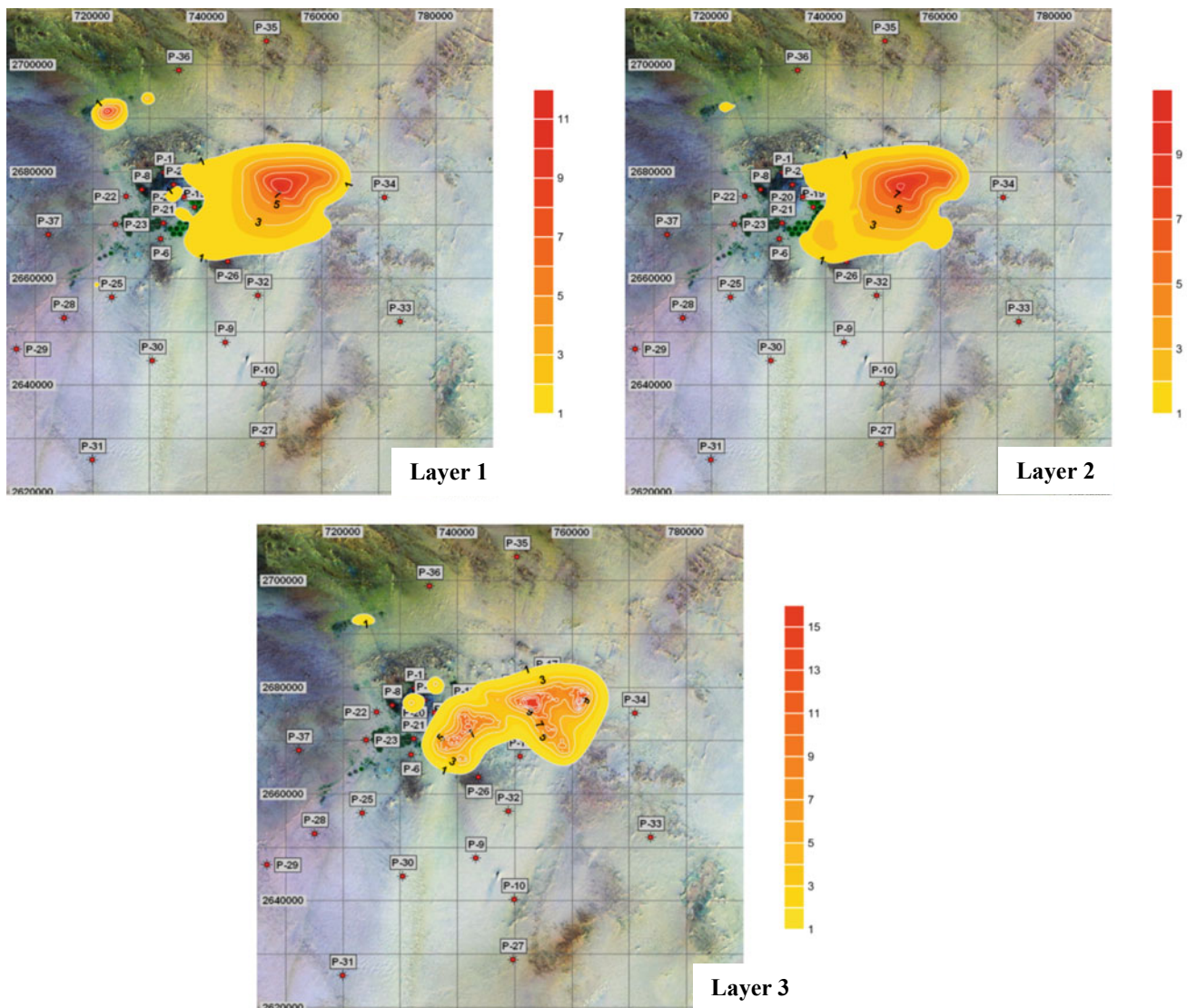


**Fig. 17** Simulated drawdown in the three model layers during stress period I (m)

## 7 Groundwater Budget of the Transient-State Model

The model is used to derive components of the groundwater budget for each of the five stress periods for the 43-year simulation. Since the whole model domain works as one system, the water budget for each stress period will be discussed for the entire model domain regardless of detailed model layers.

Negative rates indicate outflows from the groundwater system, and positive rates indicate inflows to the groundwater system. The net flow is computed by inflows minus outflows (in cubic meters per day), where drawdown reflected by negative difference and the buildup gives a positive difference. Inflow components comprise surface

recharges (irrigation water return) and head-dependent boundaries, and the outflow components consist of groundwater extraction from the pumping wells, evapotranspiration and head-dependent boundaries. The vertical exchange between the modeled layers whether it is inflow or outflow is also considered by the model as one of the water budget components. Flow into and out of storage is also considered part of the overall budget in as much as accumulation in storage effectively removes water from the flow system and storage release effectively adds water to the flow, even though neither process, in itself, involves the transfer of water into or out of the groundwater regime (Harbaugh et al., 2000). Following the convention, water entering storage is treated as an outflow (i.e., as a loss of water from the flow system), while water released from storage is treated as an inflow (i.e., a source of water to the flow system).

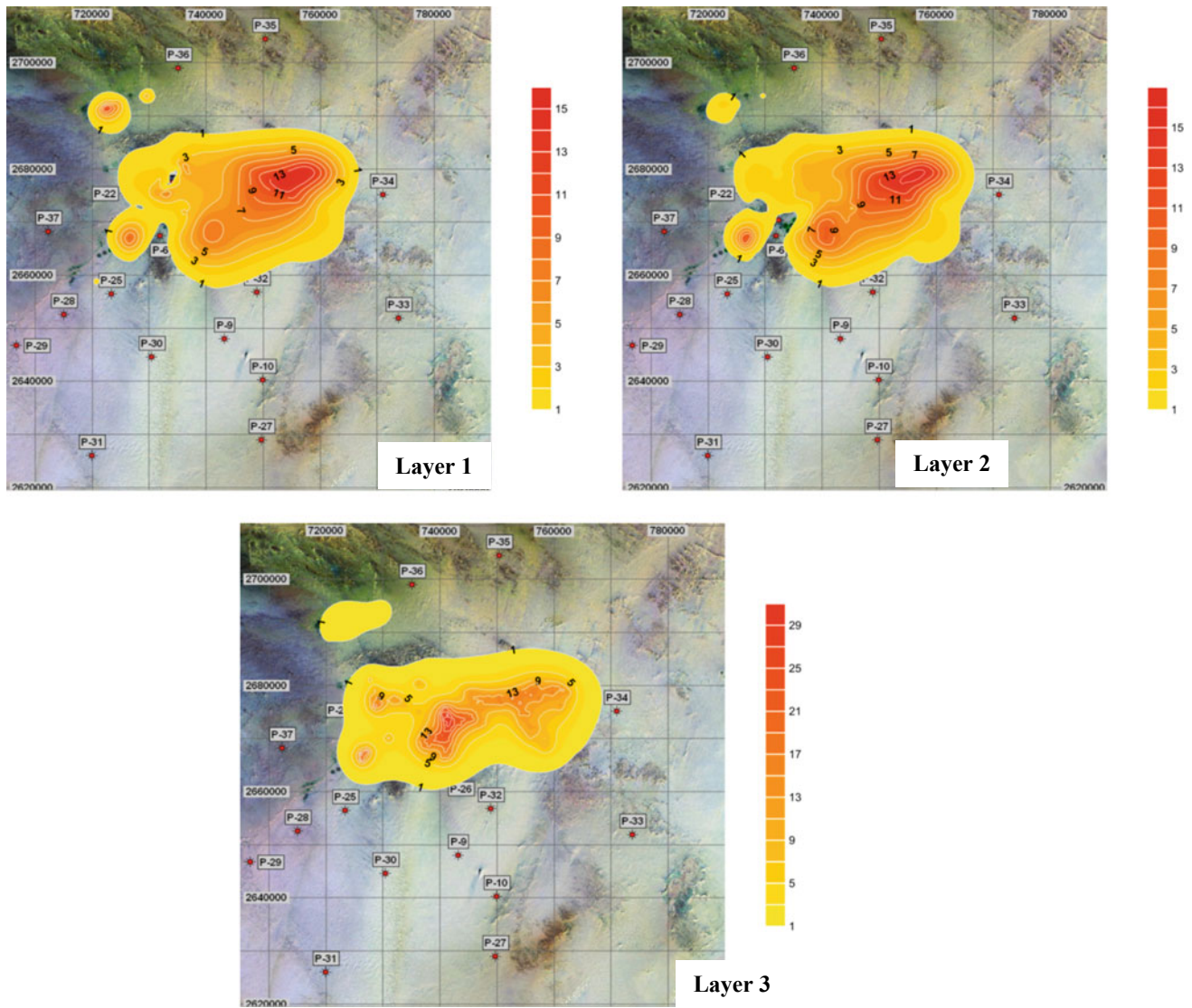


**Fig. 18** Simulated drawdown in the three model layers during stress period II (m)

Besides the drawdown calculations, the model also calculated the volumetric rate of the above-mentioned inflow and the outflow water budget components for the three layers at every stress period, but because the layers behave as one hydraulic system within the model domain, a summary of the total water budget for each stress period is presented. By examining the water budget results shown in Fig. 23, the following can be stated:

- Storage component is the dominant source of water to the aquifer system, where it contributes about 70% of the pumped water at the first period and slightly increases to 83% in period III as the water extraction increases. As the pumping from the KPP well field had been reduced during the last two periods, the storage contribution had been significantly decreased to almost 80%.
- All the budget figures show that the surface recharge from irrigation water return had insignificant part as a source in the water budget where its share had reached 12% at most.
- The inflow from the general head boundaries plays a very minor role in the water budget of the whole domain, with a maximum value less than 17% of the total inflow; this is obviously related to their remote location from the stress areas as well as to the existence of gentle gradient further away from the well field.
- The outflow component of evapotranspiration had reached up to 1.57% out of the total outflow in the first



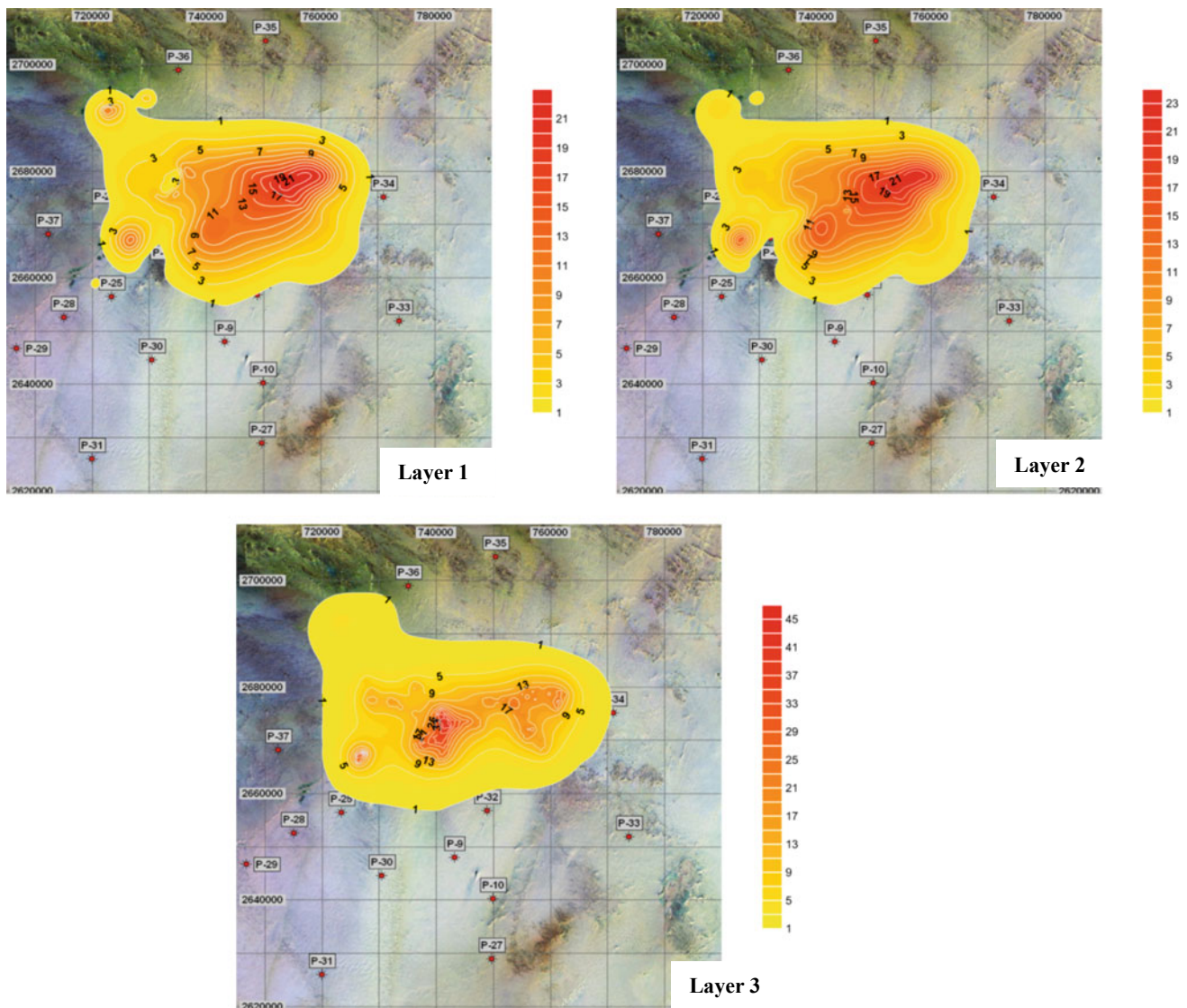


**Fig. 19** Simulated drawdown in the three model layers during stress period III (m)

period and gradually decreased to 0.67% by the end of the third period as the area affected by drawdown had widened. As the pumping had been reduced during the fourth and the fifth periods, considerable recovery of water level led to slight increase in evapotranspiration value up to 1% of the total outflow.

The groundwater budgets for both pre-development and post-development times were calculated of the whole model domain and are summarized in Table 5. Total inflow rate through the study area was about  $25.6 \times 10^3$  m<sup>3</sup>/d before development and about  $232.8 \times 10^3$  m<sup>3</sup>/d by the end of

2010. In general, groundwater pumping is supplied by a combination of two inflow sources: storage and the head-dependent boundary inflow. The head-dependent boundary inflow had been increased from  $25.6 \times 10^3$  to  $35.3 \times 10^3$  m<sup>3</sup>/d, while the head-dependent boundary outflow had been reduced from  $22.98 \times 10^3$  to  $18.060 \times 10^3$  m<sup>3</sup>/d during the simulation time. These differences in the flow rates partially provide the supply of pumping. As pumping started during the post-development time, the dominant supply of groundwater was the aquifer storage, where it reached up to  $187.1 \times 10^3$  m<sup>3</sup>/d by the end of 2010 (Table 5).

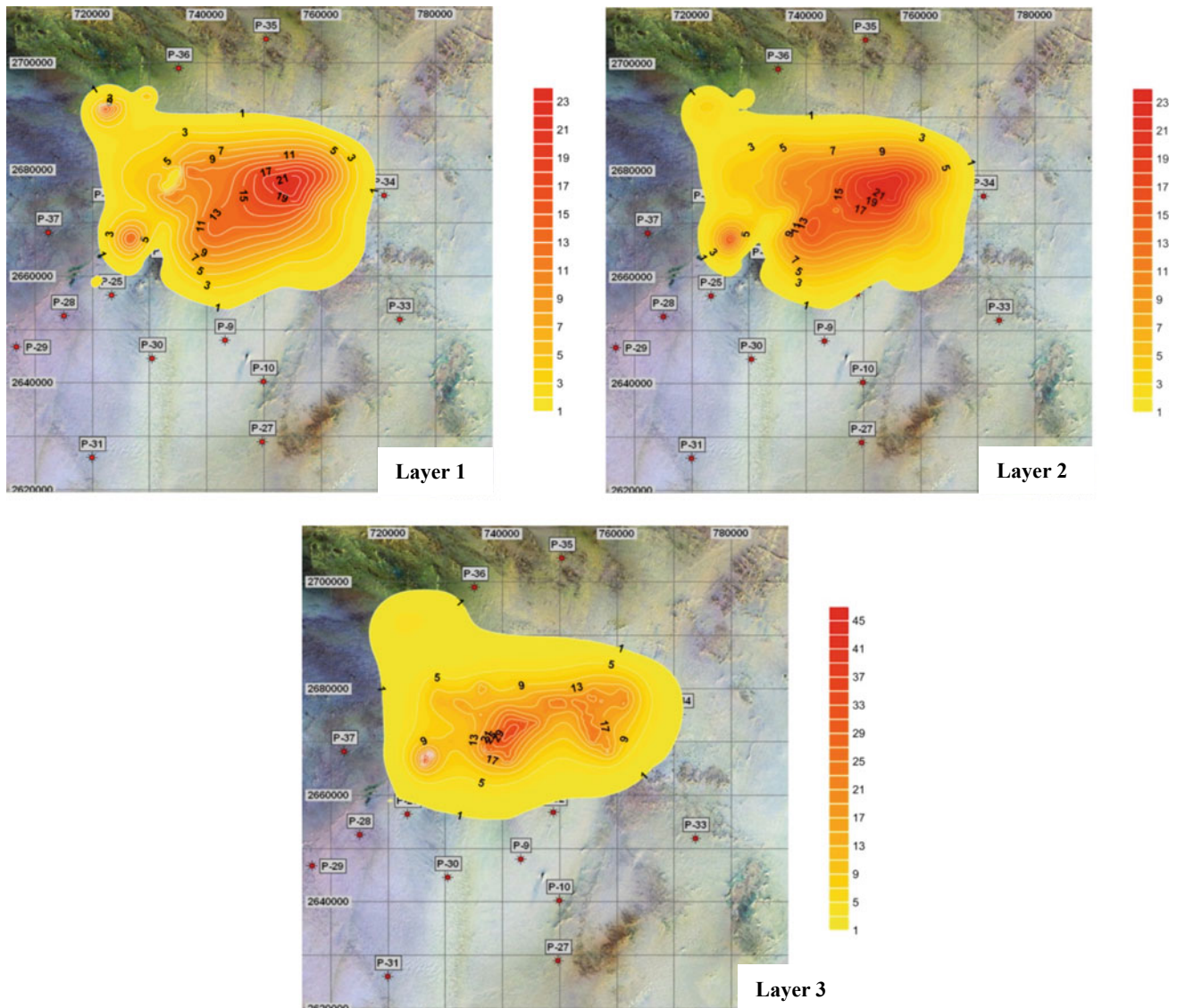


**Fig. 20** Simulated drawdown in the three model layers during stress period IV (m)

## 8 Conclusion

Based on the available data, a groundwater flow model was calibrated to generate groundwater elevations and steady-state flow in the model domain with no water budget discrepancy. A satisfactory match between simulated and observed hydraulic heads was successfully achieved. Model parameterization in the transient-state model is the same as used in the steady-state calibration, with the addition of pumpage, irrigation water return and the storage coefficient parameters that were mostly set up to follow the hydraulic conductivity zonation scheme. Unlike hydraulic conductivities, storage coefficients were varied from one model layer to the other. The transient-state model was also calibrated to

transient conditions using five stress periods (1968–2010) by traditional trial-and-error method. Final storage coefficient values are all within reasonable and expected ranges, and are consistent with about 130 aquifer test results. Other model parameters, such as boundary conditions and evapotranspiration, are the same as for the steady-state calibration. The transient model simulates fluctuations caused by groundwater extraction for irrigation and domestic purposes. Simulated historical drawdowns reflect coalescing cones of depression resulting from significant pumping from the three model layers in the study area since the mid-seventies in last century. Simulated historical variations in hydraulic heads were evaluated by comparing the model-simulated and field-measured values at 32 dual piezometers in 1976, 1986, 1998, 2004 and 2010. In general, simulations using the



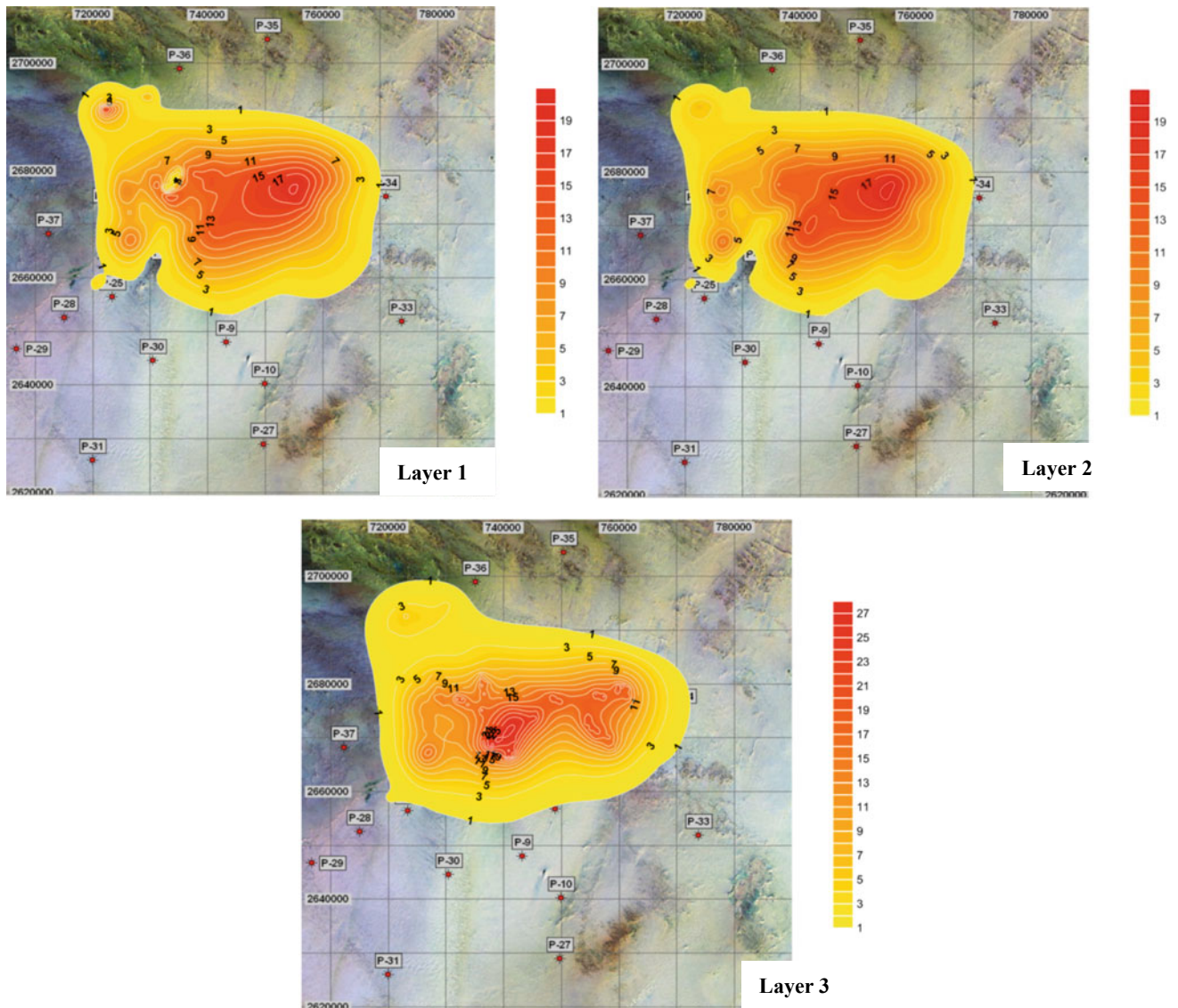


**Fig. 21** Simulated drawdown in the three model layers during stress period V (m)

**Table 4** Calculated total areas affected by drawdown in hectares

Stress period	Total area (ha)				
	I	II	III	IV	V
Layer 1	55,884	109,108	148,345	162,348	175,308
Layer 2	51,111	103,430	143,550	158,711	171,530
Layer 3	49,172	108,686	157,922	174,076	189,073



**Fig. 22** Total areas affected by one meter drawdown or more during each simulation period (in hectares)

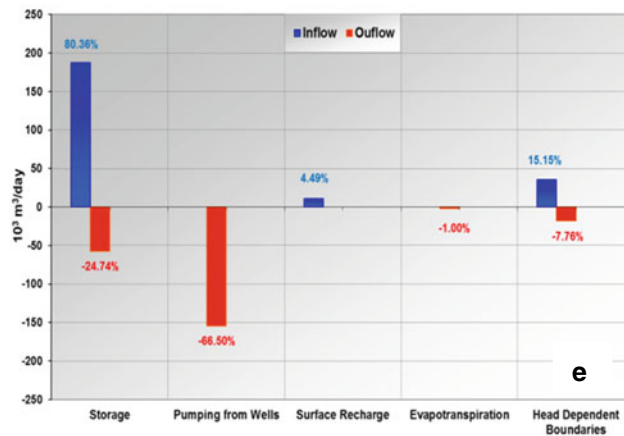
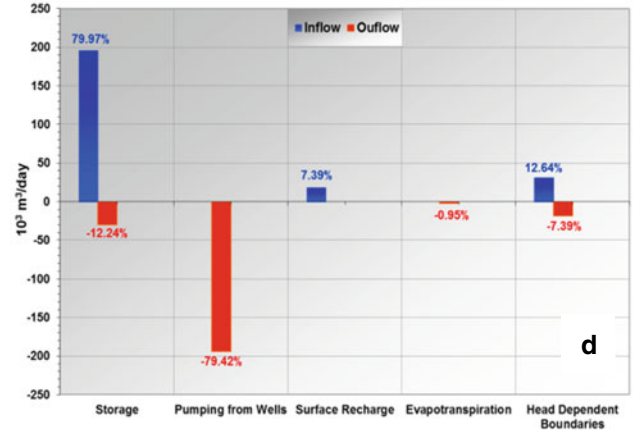
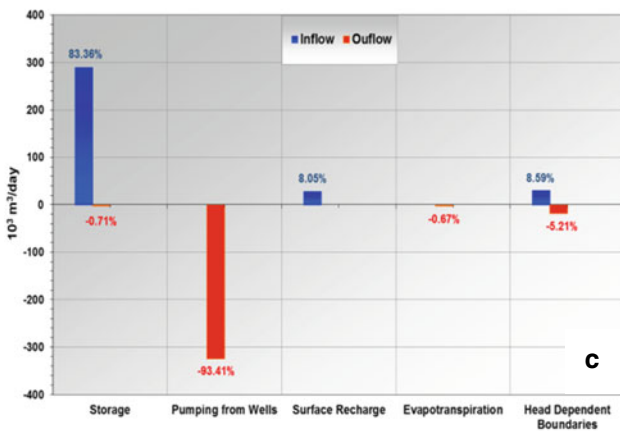
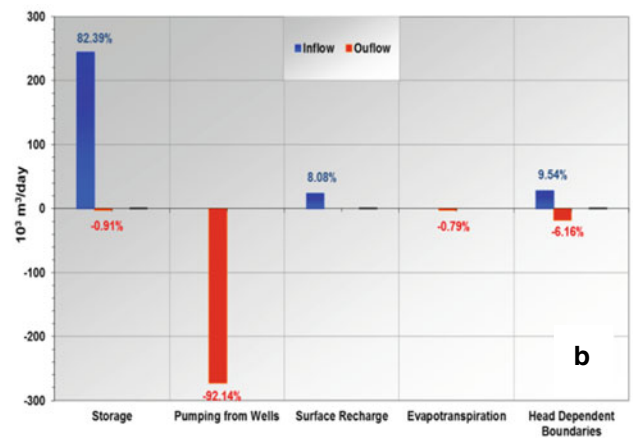
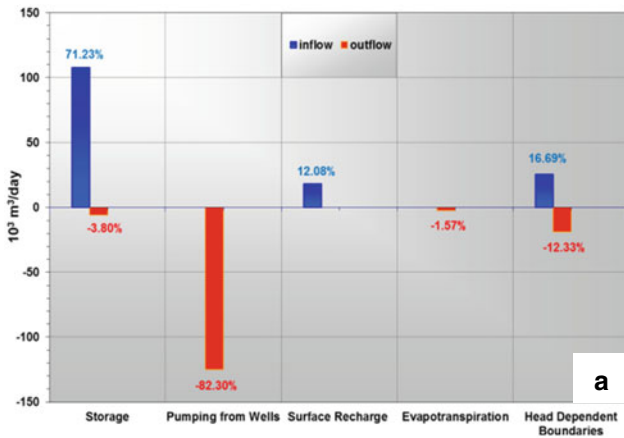
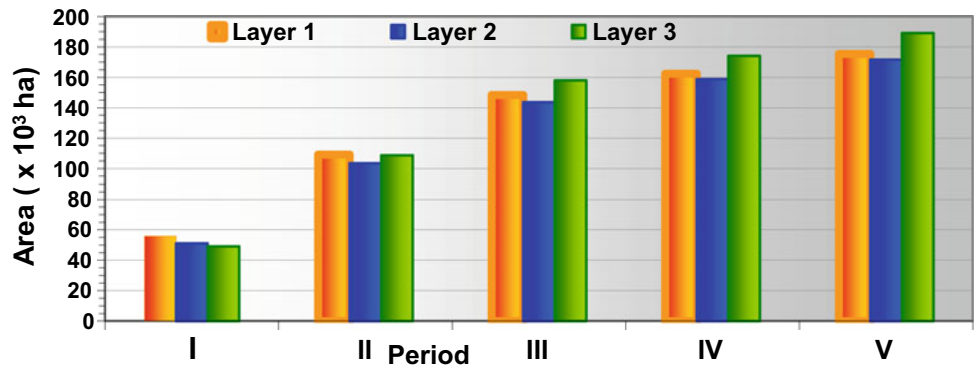


**Fig. 23** Water budget for the five stress periods; a period I, b period II, c period III, d period IV and e period V

**Table 5** Water budget outputs of the three aquifer layers for the whole transient-state model domain

Inflow	Pre-development volumetric rate (m <sup>3</sup> /d)	2010 volumetric rate (m <sup>3</sup> /d)	Component difference
Head-dependent boundaries	25,611	35,282	-9671
Storage	0	187,077	-187,077
Irrigation return (recharge)	0	10,452	-10,452
Wells	0	0	0
Evapotranspiration	0	0	0
<b>Total in</b>	<b>25,611</b>	<b>232,811</b>	<b>-207,200</b>
Outflow			
Head-dependent boundaries	22,976	18,060	4916
Storage	0	57,603	-57,603
Irrigation return (recharge)	0	0	0
Wells	0	154,833	-154,833
Evapotranspiration	2634	2324	310
<b>Total out</b>	<b>25,610</b>	<b>232,820</b>	<b>-207,210</b>

groundwater flow model developed for this study show that drawdown in the deep layer (layer 3) is much greater than in the shallow layers (layers 2 and 3), and this difference attributable to the huge quantities of water extracted by the KPP wells' tapping layer 3, i.e., significant quantities of pumped water, was derived (removed) from storage. Similarly, the total areas affected by one meter drawdown or more in layer 3 are more than those in layers 1 and 2 (it reached about  $190 \times 10^3$  ha in 2010).

## References

- CEDARE (Mohammed Bakhbaki, Regional Coordinator). (2001). *Regional strategy for the utilization of the Nubian Sand stone Aquifer System, volumes 1 to 4 and annex 1 to 2* (336 p). Cairo, Egypt: Center for Environment and Development of the Arab Region and Europe (CEDARE).
- Eddib, A. A. (1973). *A quantitative study of groundwater in Al-Kufrah Basin* (M.sc thesis) (p. 345). Athens, Ohio, USA: Ohio University.
- Fisk, E. P., & Pennigton, W. D. (1976). Groundwater geology and hydrogeology of Kufra region, Libyan Arab Republic. *Libyan Journal of Science*, 6B, 13.
- General Water Authority (GWA) (2006) General water authority, Unpublished report
- General Water Authority (GWA). (2014) (Unpublished report). General Water Authority
- German Water Group. (1977). Hydrogeological study on groundwater resources in the Kufra area. Geology (Vol. 2). Council of Agriculture Development, Kufra and Sarir Authority.
- Golden Software. Surfer v.10.7 software.
- Harbaugh, A. W., Banta, E. R., Hill, M.C., & McDonald, M. G. (2000). Modflow-2000, *The U.S. Geological Survey modular ground-water model-user guide to modularization concepts and the ground-water flow process*: U.S. Geological Survey Open-File Report 00-92, 121 p.
- Hweesh, A., & Hafi, Z. B. (2015). In K. M. Oun, Z. B. Hafi, F. M. Salloum, & S. A. Sadeg (Eds.), *Three-dimensional groundwater quantitative model (Al Kufrah Region, Southeast Libya)* (pp. 313-327). © Earth Science Society of Libya (ESSL).
- Konikow, L. F., & Reilly, T. E. (1998). Groundwater modelling. In J. W. Delleur (Ed.), *The handbook of groundwater engineering* (Vol. 20, pp. 1-20.40). Boca Raton: CRC Press.
- Pallas. P. (1980). Water resources of the socialist people's Libyan Arab Jamahiriya. M. J. Salem, M. T. Busrewil (Eds.), *The geology of Libya* (Vol. II). London: Academic Press.
- USGS. (2010). *Global Multi-resolution Terrain Elevation Data (GMTED2010)*.



# A Multivariate Analysis of Groundwater Chemistry Data

Ahmed Garba, Muhammad Mukhtar, and Aishatu Hussein Santuraki

## Abstract

Groundwater serves as the main source of water for drinking and other domestic purposes, and often it is over exploited. Nowadays, it is facing threats due to anthropogenic activities. In this study, a total of 20 groundwater samples from boreholes used for drinking, and other domestic purposes were collected from Hadejia town northeastern Jigawa State, Nigeria, and analyzed for their physicochemical characteristics and trace metal levels using standard methods aimed at assessing the groundwater quality. The well-founded techniques of principal component analysis (PCA) and cluster analysis (CA) were jointly used. PCA was used to investigate the origin of each water quality parameters and yielded five varimax factors/components with 78.69% total variance in the groundwater quality data. First two factors reveal that 47.69% of the total variance dominated by total hardness, TDS,  $\text{Cl}^-$ ,  $\text{NO}_3^-$ , Cu, EC, Fe, and Cr indicating the major variations are related to anthropogenic activities and natural processes. Cluster analysis results grouped the 15 parameters and 20 sampling sites into two and four statistically significant clusters, respectively, based on their similarities. The results showed that concentrations of Mn, Cr, and Pb are slightly higher above the maximum permissible limit of Nigerian standard for drinking water quality (NSDWQ, Nigerian Industrial Standard. NIS 554, Nigerian Standard for

Drinking Water Quality (NSDWQ). (2007). Nigerian Industrial Standard (NIS) 554:2007 ICs 13.060.20.) and hence the need for the replacement of the affected wells.

## Index Terms

Groundwater • Multivariate analysis • Physicochemical

## 1 Introduction

Groundwater constitutes the largest readily available fresh water reserve on earth. It is the most vital natural resource, which forms the core of the ecological system. It has become the major source of water supply for drinking, domestic, household, agricultural, industrial, recreational, and environmental activities, etc. The usefulness of water for particular purpose is determined by its quality. Groundwater quality is mainly controlled by the range and type of human influence as well as geochemical, physical, and biological processes occurring in the ground.

Groundwater supply schemes consist typically of a large number of hand-pumped boreholes, providing untreated, unmonitored, and often unconnected supplies (Hiscock, 2009). A poor quality of water threatens human health and plant growth (Olajire & Imeokparia, 2001), thereby adversely affecting economic development and social prosperity (Milovanovic, 2007). It is therefore crucial to establish the current status of groundwater quality in the study area and thus its appropriateness for use in drinking and other purposes.

The determination of groundwater quality for human consumption is important for the well-being of the ever-increasing population. Groundwater quality depends, to some extent, on its chemical composition (Wadie & Abduljalil, 2010) which may be affected by natural and anthropogenic factors. Variation in groundwater quality in

A. Garba (✉) · M. Mukhtar  
Department of Science Laboratory Technology, Binyaminu  
Usman Polytechnic, Hadejia, Nigeria

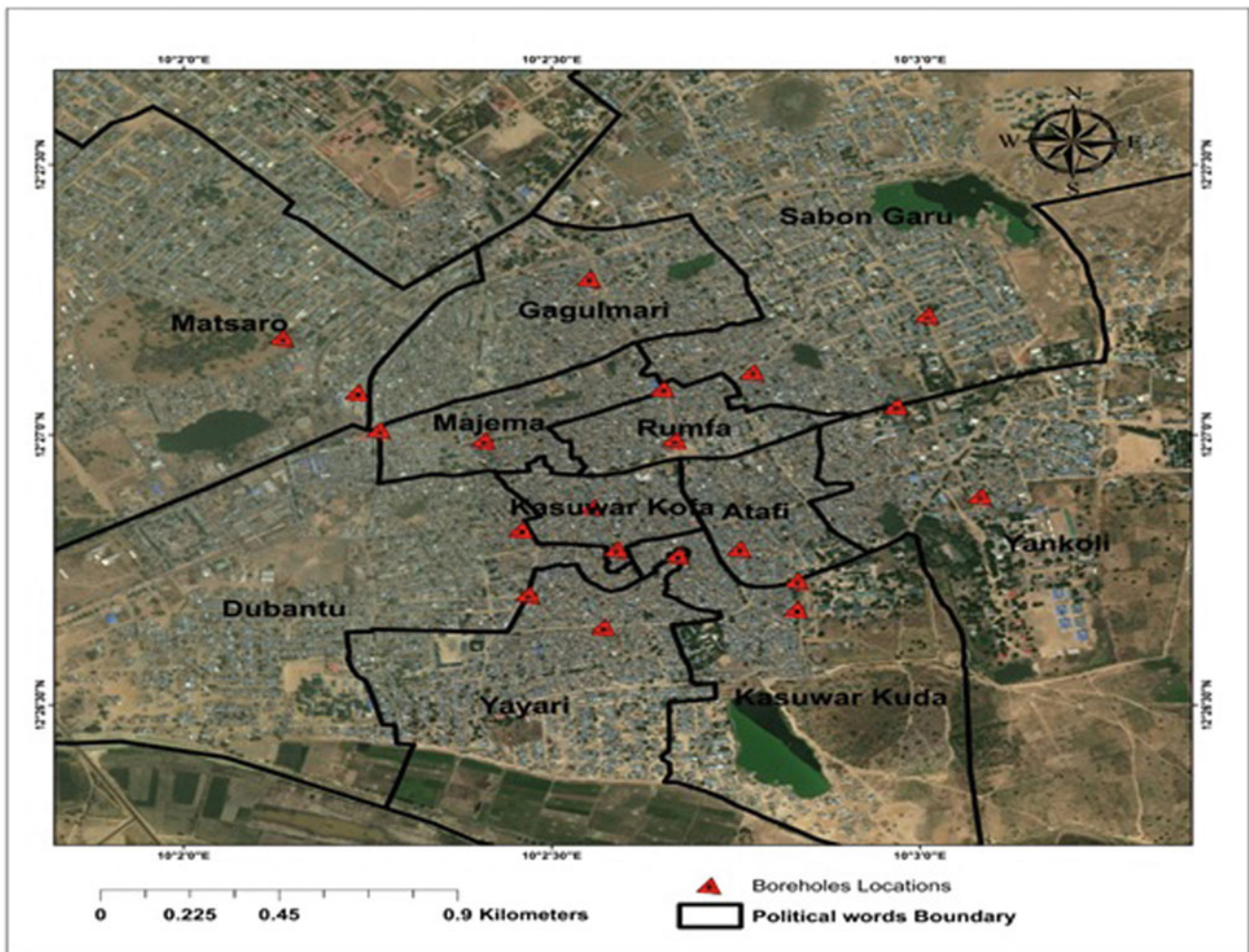
A. H. Santuraki  
Department of Chemical Sciences, Federal University Kashere,  
Gombe, Nigeria

an area is a function of physical and chemical parameters that are greatly influenced by natural processes such as geological formations and anthropogenic activities.

Multivariate techniques such as factor analysis, principal component analysis, and cluster analysis are powerful techniques to identify the underlying processes that control groundwater chemistry, grouping of samples of similar composition and origin, and to predict the variables that differentiate the sampling stations temporally and spatially. These techniques have widely been used as unbiased methods in the analysis of groundwater quality data to characterize groundwater composition influenced by natural and anthropogenic factors (Lambrakis et al., 2004; Dragon, 2006).

## 2 Study Area

This study is carried out in Hadejia Local Government Area, and it lies in the northeastern corner of Jigawa State between latitude  $12^{\circ} 13' - 13^{\circ} 60' N$  and longitude  $9^{\circ} 22' - 11^{\circ} 00'E$  (Orisakwe, 2013). The topography of the area is dominated by the river Hadejia which it lies on its Northern bank which drained into Lake Chad, which at some points is 1–2 m above the surrounding plains including the town. The climate of the area is semi-arid. It is characterized by a long dry season and a short wet season from June to September. The total annual rainfall ranges from 600 mm in the northern part to 762 mm in the southern areas (Orisakwe, 2013). The regional vegetation falls within the Sudan Savannah type.





### 3 Sample Collection and Analysis

Groundwater samples for the analysis were collected from 20 different sites monthly in February, March, and April, 2019 during the dry season. All the samples were collected and treated in accordance with the (American Society for Testing and Material, 2004; American public health association [APHA], 2005). The boreholes were allowed to flow for about 3 min before the water is collected. Temperature, pH, electrical conductivity, and total dissolved solids were measured in situ using Hanna pH 210 model microprocessor, EQ-660 digital conductivity meter, and Hatch 446,600 model TDS meter, respectively. T/H, Ca, and Mg were determined using titrimetric method (American Society for Testing and Material, 2004).  $\text{NO}_3^-$ ,  $\text{Cl}^-$ , Fe, Cu, Zn, Mn, Cr, and Pb were determined using CHEMetrics Vacu-Visual self-filling ampoules water testing kits with CHEMetrics Photometric Multi-Element Analyzer model V-2000. The samples were chemically analyzed at the Center for Energy, Research and Training, Ahmadu Bello Univeristy Zaria, Nigeria.

### 4 Results and Discussion

The values for physicochemical variables were presented in Table 1. Parameters values such as EC, pH, Temp., TDS, TH, Ca, Mg,  $\text{Cl}^-$ , and  $\text{NO}_3^-$  were found to be below or within the permissible limit set by the (NSDWQ, 2007) in majority of the boreholes. The results similarly showed that concentrations of Mn, Cr, and Pb are slightly higher above the maximum permissible limit of Nigerian

standard for drinking water quality (NSDWQ, 2007) and hence the need for the replacement of the affected wells (Table 2).

The rotated factor loading, eigenvalues, percentages of variance, and cumulative percentages of variance associated with each factor for PCA are summarized in Table 3. The results show that five (5) principal components were extracted and rotated using the varimax normalization (Liu et al., 2003) which accounts for more than 78% of the total variance, which is quite good and can be relied upon to identify the main source of variation in the hydrochemistry. The factor loading was sorted according to the criteria of (Bartram & Balance, 1996) by which strong, moderate, and weak loadings corresponds to absolute loading values of  $>0.75$ ,  $0.75-0.50$ , and  $0.50-0.30$ , respectively.

In PCA, eigenvalues are normally used to determine the number of components (PCs) that are retained for further analysis. An eigenvalue gives a measure of the significance of the factor. The factors with highest eigenvalue are the most significant. Eigenvalues of 1.0 or greater are considered significant (Shrestha & Kazama, 2007)). Number of components is equal to the number of variables in PCA.

The first component loading accounted for 30.27% of the total variance showed higher loading for TH, TDS,  $\text{NO}_3^-$ , Cu, and  $\text{Cl}^-$ , with significant contribution from Ca and Mn. It is reasonable to observe a strong positive loading of TH, TDS,  $\text{NO}_3^-$ , with  $\text{Cl}^-$ , which may be probably due to leachate from domestic waste discharge in some part of the area. The higher  $\text{Cl}^-$  and TDS is an indication that there is a possibility that the groundwater is polluted by sewage or waste from refuge dumping site (Amadi, 2010). This factor can be labeled as the hardness and anthropogenic.

**Table 1** Value of physicochemical parameter in groundwater of Hadejia

Parameter	Results range	NSDWQ (2007)	WHO (2011)
pH (Range)	5.96–7.58	6.5–8.50	6.5–8.50
Temperature (°C)	27.60–28.00	Ambient	Ambient
EC ( $\mu\text{S}/\text{cm}$ )	98.00–1306	1000	1000
TH (mg/L)	62.00–374	150	150
TDS (mg/L)	53.90–723	500	500
Fe (mg/L)	0.14–0.88	0.30	0.30
Cu (mg/L)	0.02–5.57	1.0	1.0
Zn (mg/L)	0.01–2.37	3.0	3.0
Mn (mg/L)	0.28–19.50	0.20	0.20
Cr (mg/L)	0.04–0.25	0.05	0.05
Pb (mg/L)	0.34–2.95	0.01	0.01
Ca (mg/L)	9.61–76.95	NS	75
Mg (mg/L)	6.32–56.42	50–150	50–150
$\text{Cl}^-$ (mg/L)	0.69–12.64	250	250
$\text{NO}_3^-$ (mg/L)	1.35–34.80	50	50



**Table 2** PCA rotated component matrix with Kaiser normalization

	VR1	VR2	VR3	VR4	VR5
pH	-0.103	-0.266	-0.153	-0.037	-0.58
Temp	0.066	-0.057	0.005	<b>0.877</b>	0.181
EC	-0.292	<b>-0.729</b>	0.112	0.046	-0.176
TH	<b>0.871</b>	-0.187	-0.180	-0.234	0.153
TDS	<b>0.869</b>	0.169	0.341	0.237	0.034
Ca	0.362	0.201	<b>-0.661</b>	0.069	0.395
Mg	-0.015	0.497	<b>0.665</b>	0.005	0.288
Cl <sup>-</sup>	<b>0.549</b>	-0.048	<b>0.621</b>	0.305	0.204
NO <sub>3</sub>	<b>0.891</b>	0.244	-0.003	0.063	-0.179
Fe	-0.242	<b>0.607</b>	0.109	-0.483	-0.178
Cu	<b>0.811</b>	0.285	0.317	0.203	-0.045
Zn	-0.144	-0.027	-0.08	-0.043	<b>0.906</b>
Mn	0.346	0.037	<b>0.780</b>	0.050	0.001
Cr	-0.154	<b>-0.859</b>	-0.093	0.116	-0.127
Pb	-0.03	0.168	-0.128	<b>-0.782</b>	0.289
Eigenvalues	4.54	2.615	1.974	1.624	1.051
% of variance	30.267	17.431	13.161	10.826	7.006
Cumulative %	30.267	47.698	60.858	71.684	78.690

**Table 3** Mean values of geochemistry data

Cluster	pH	Temp	EC (μS/cm)	TH (mg/L)	TDS (mg/L)	Ca (mg/L)	Mg (mg/L)	Cl <sup>-</sup> (mg/L)	NO <sub>3</sub> <sup>-</sup> (mg/L)	Fe (mg/L)	Cu (mg/L)	Zn (mg/L)	Mn (mg/L)	Cr (mg/L)	Pb (mg/L)
1 (n = 9)	6.53	27.8	235	154	207	<b>53.8</b>	30.4	1.98	7.35	0.49	0.48	0.34	0.75	0.11	1.57
2 (n = 3)	6.25	27.9	597	151	210	28	28	4.57	1.25	<b>0.53</b>	0.20	<b>0.87</b>	0.98	0.17	1.70
3 (n = 4)	6.38	27.8	286	<b>301</b>	<b>588</b>	44.8	32.5	6.79	<b>29.7</b>	0.29	3.53	0.05	<b>5.56</b>	0.08	1.39
4 (n = 4)	6.76	27.8	<b>1116</b>	145	91	19.7	20.1	0.28	2.78	0.26	0.01	0.03	0.93	<b>0.18</b>	0.99

Factor loading (VR2) accounted for 17.43% of total variance represents higher loadings for Fe and higher negative loading for Cr and Electrical conductivity, with significant contribution from Mg. These could be conceived to mainly originate from the ionic dissolution in the course of groundwater migration. This factor can be labeled as a natural process leading to heavy metal pollution. VR3 explains 13.16% of total variance and has a higher loading on Mn, Mg, Cl, and moderate negative loading on Ca with significance contribution from TDS and Cu. The major variables constituting VR3 (Ca, Mg, Cl, and Mn) are related to the hydrochemical variables originating from mineralization of groundwater.

## 5 Cluster Analysis

Cluster analysis is applied to detect the similarity among the different sampling sites. The clustering procedure generates either cluster or groups on the basis of similarity or dissimilarity of variables. Cluster analysis classifies a set of observations into two or more unknown groups based on combination of internal variables. Therefore, the cluster analysis is to discover a system of organized observations where a number of groups/variables share properties in common, and it is cognitively easier to predict mutual properties based on an overall group membership. This helps

**Fig. 1** Dendrogram of water sampling sites

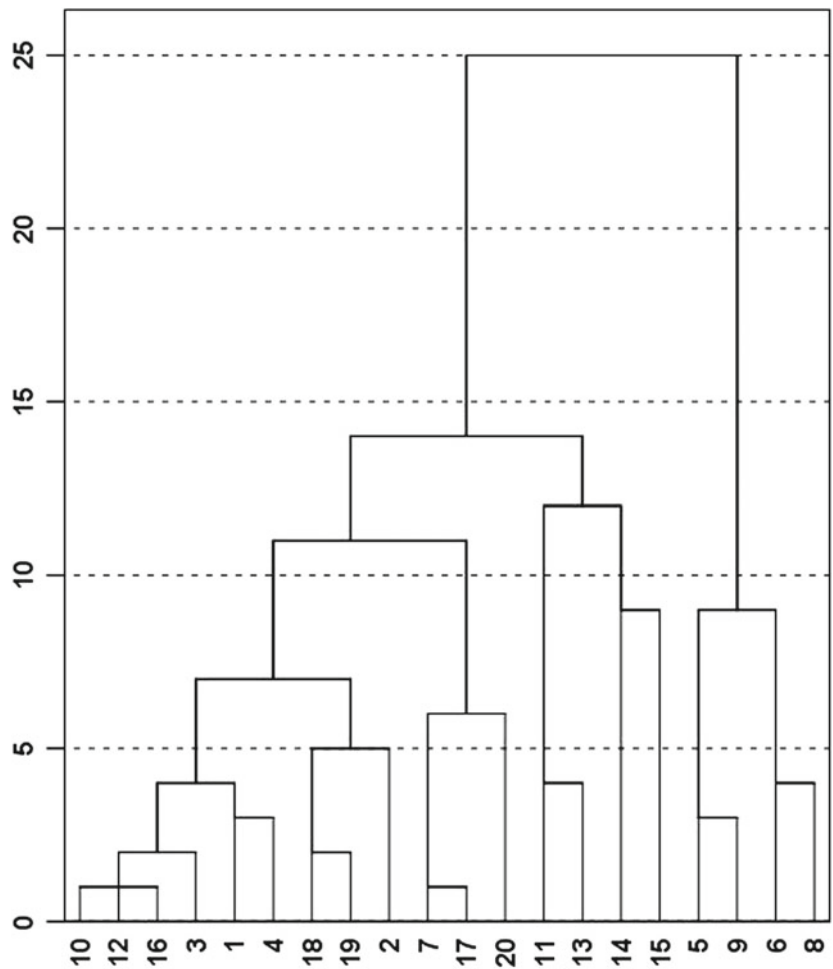
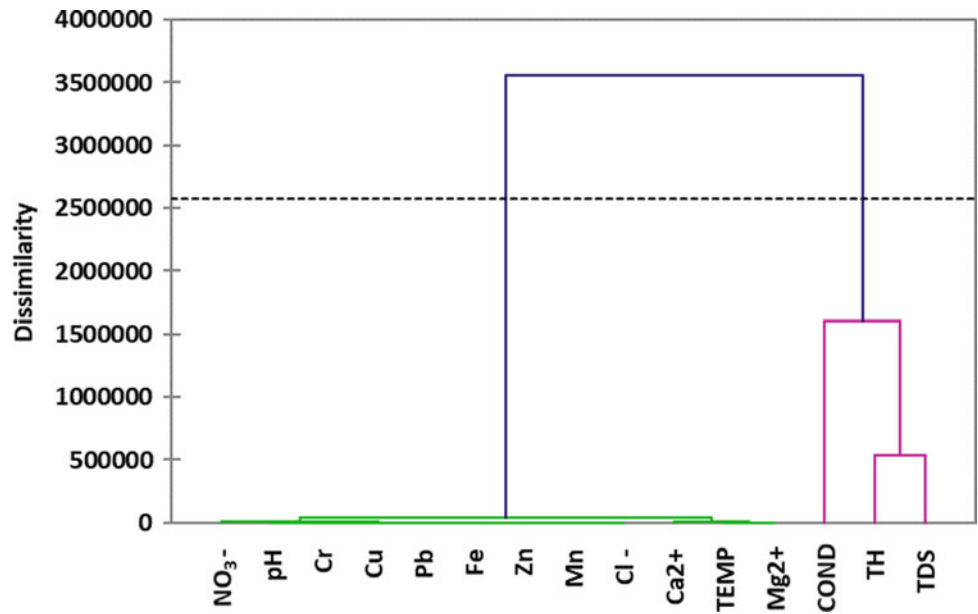


**Fig. 2** Dendrogram of hydrochemical parameters



define source profiles of variables and their interpretation in terms of possible sources. The clustering procedure generates either cluster or groups on the basis of similarity or dissimilarity of variables. From Figs. 1 and 2, the cluster analysis resulted in the grouping of 20 monitoring boreholes 15 parameters into four (4) and two (2) statistically significant clusters, respectively, based on their similarities.

Cluster 1: This includes nine (9) boreholes no. 10, 12, 16, 3, 1, 4, 18, 19, and 2(45%)

Cluster 2: It consists of three (3) boreholes which include no. 7, 17, and 20(15%)

Cluster 3: It consists of four (4) boreholes which include no. 11, 13, 14, and 15(20%)

Cluster 4: It consists of four (4) boreholes which include no. 5, 9, 6, and 8(20%).

Samples from cluster 1 are composed of nine (9) boreholes 1, 2, 3, 4, 10, 12, 16, 18, and 19, constituted 45% of the water samples, and are characterized by high concentration of Ca, and low concentration of Mn and EC in all clusters. Sample from cluster 2 is composed of three (3) boreholes 7, 17, and 20, constitutes 15% of the water samples, and is characterized by high concentration of Fe, Zn and Pb and low concentration of  $\text{NO}_3^-$  in all clusters. Samples from cluster 3 are composed of four (4) boreholes 11, 13, 14, and 15, constituted 20% of the water samples, and are characterized by high concentration of T/Hardness, TDS, Mg,  $\text{Cl}^-$ ,  $\text{NO}_3^-$ , Cu, Mn, and low concentration of Cr in all clusters. Samples from cluster 4 are composed of four (4) boreholes 5, 6, 8, and 9, constituted of 20% of the water samples, and are characterized by high concentration of EC and Cr and low concentration of T/Hardness, TDS, Ca, Mg,  $\text{Cl}^-$ , Fe, Cu, Zn, and Pb in all clusters.

## 6 Conclusion

The quality evaluation of groundwater sources in Hadejia Local Government Area of Jigawa State revealed that the results showed that concentrations of Mn, Cr, and Pb are slightly higher above the maximum permissible limit of Nigerian standard for drinking water quality (NSDWQ, 2007). The values for physicochemical variables EC, pH, Temp., TDS, TH, Ca, Mg,  $\text{Cl}^-$ , and  $\text{NO}_3^-$  were found to be below or within the permissible limit set by the (NSDWQ, 2007) in majority of the boreholes. PCA was used to investigate the origin of each water quality parameters and yielded five varimax factors/components with 78.69% total

variance, indicating that the major variations are related to anthropogenic activities and natural processes. Cluster analysis results grouped the 20 sampling points and 15 parameters into four (4) and two (2) statistically significant cluster based on their similarities.

**Acknowledgements** I want to acknowledge the Managements of the Tertiary Education Trust Fund (TETFund) Abuja, Nigeria and Binyaminu Usman Polytechnic, Hadejia, Jigawa State for sponsorship and approving to attend this conference in cash and kind, I am very much grateful.

## References

- Amadi, A. N. (2010). Effects on urbanization on groundwater quality: A case study of Port-Harcourt, southern Nigeria. *Natural and Applied Sciences Journal*, 11(2), 143–152.
- American Public Health Association (APHA). (2005). *Standard methods for the examination of water and waste water* (20th ed., pp. 65–68) Washington, D.C.
- American Society for Testing And Material. (2004). *Annual book of ASTM standards, water and environmental technology*. (Vol. 11.01, pp. pp 79–170). West Conshohocken, PA: Water (i) ASTM International.
- Bartram, J., & Balance, R. (1996). *Water quality monitoring: A practical guide to the design of fresh water quality and monitoring programmes*(pp. 34–39). London: Chapman and Hall.
- Dragon, K. (2006). Application of factor analysis to study contamination of semi-confined aquifer (Wickopolska buried valley aquifer, Poland). *Journal of Hydrology*, 331, 12–279.
- Hiscock, K. M. (2009). *Hydrology: Principles and practice* (pp. 66–75). Oxford: Blackwell Science (2009).
- Lambrakis, N., Antonakos, A., & Panagopoulous, G. (2004). The use of multi- component. statistical analysis in hydrological environmental research. *Water Resource*, 38, 1862–1872.
- Liu, C. W., Lin, K., & Kuo, Y. M. (2003). Application of factor analysis in the assignment of groundwater Quality in Blackfoot disease area in Taiwan. *The Science of the Total Environment*, 313 (1–3), 77–89.
- Milovanovic, M. (2007). Water quality assessment and determination of pollution sources along the Axios/Vardar River, southeastern Europe. *Desalination*, 213, 159–173.
- Nigerian Standard for Drinking Water Quality (NSDWQ). (2007). Nigerian Industrial Standard (NIS) 554:2007 ICs 13.060.20.
- Olajire, A. A., & Imeokparia, F. E. (2001). Water quality assessment of Osun River: Studies on inorganic nutrients. *Environmental Monitoring and Accessment*, 69(1), 17–28.
- Orisakwe, K. U. (2013). Challenge detection analysis of land uses in Hadejia township of Jigawa State of Nigeria. *International Journal of Applied Sciences and Technology*, 3(3), 60–168.
- Shrestha, S., & Kazama, F. (2007). Assessment of surface water quality using multivariate statistical techniques: A case study of the Fuji river basin, Japan. *Environmental Model, Software*, 22, 464–475.
- Wadie, A. S. T., & Abduljalil, G. A. D. S. (2010). Assessment of hydrochemical quality of groundwater under some urban areas within Sana'a Secretariat. *Ectetica Quimica*, 35(1), 77–84.

# Water Desalination and Purification Technologies



# Successfully Mutual Cooperative Collective Action: Principle of Institutional Arrangement of the Aflaj Irrigation System in Sultanate of Oman

Ahmed S. Al-Marshoudi, Suzyrman Bin Sibly,  
and Hamoon Khelghat-Doost

## Abstract

To investigate the present of the two most common analytical tools; heterogeneity and homogeneity over a mutual cooperative in an irrigation system, we considered both of these in an attempt to find an existing mutual cooperative over aflaj (singular falaj) in Oman. In an aflaj community defined-boundary shareholders group, we expect some sort of equal size distribution by which all members interested in cooperative mutual collective action with regard to system maintenance, extra water renting right, and water flow reliability. We provided the necessary demonstration of the existing institutional arrangement to further prove the theory. Although fast body of literatures discussed these rules and cooperative with the different types of the common-pool resources, this study focus over the cooperative collective action, in particular investigate the presence of cooperative collective action within the Omani ancient-aflaj system (singular falaj). In Oman, aflaj water allocation and its institutional arrangement showed relatively resilient against recent regional development. Today, in many aflaj communities, common administrative as well as allocative water delivery processes were found over almost identical structural social hierarchy. While the documented Omani measuring unit, known as ather, (based on time) indicated the first condition of the present of cooperative collective action, another associated water auctioning which used to generate income, (known as rub'ah (quarter)) has been found.

## Keywords

Aflaj system • Collective action cooperative • Measure unit • Water flow

## 1 Introduction

While many of the arid regional countries, even the temperate climatic zone countries, are facing a multitude of water problems, several analytical frameworks have been proposed in an attempt to provide social accepted solution. Substantial literatures discussion over these problems in areas like well-defined property rights structures (Alchian & Demsetz, 1973; Rosegrant & Binswanger, 1994), system maintenance (Bardhan & Dayton-Johnson, 2002), equitable distribution of water access (Baland & Platteau, 1999; Trawick, 2001). It is worth noting that these problems have been analyzed under general term 'institutional arrangements' (Meinzen-Dick, 2000; Saleth & Dinar, 2005), model of social organization (Coward, 1979) and model of the common-pool resources and property rights (Demsetz, 2002, Oakerson, 1986). Furthermore, recently economic instrument such as introducing a water market (Bjornlund, 2003; Eastert et al., 1998), establishment of cooperatives (Bardhan, 1993), and allowing more participation of the local communities (Bruns et al., 2005) have been proposed and introduced. However, since water problem is considered as a complex and poses several areas of studies like externality, wealth transfer, quality and fluctuation in water flows, several water professional and researchers attempted first to defined water problem using different perspectives. For example, Brown et al. (1982) definition of the problem reflected with two important measures (1) market bidding process determines the allocation of the scarce resources (2) the degree to which institution form preserve the natural beauty of the region. Dales (1968) placed two main conditions to solve the water ownership; a measurable unit (what

A. S. Al-Marshoudi (✉) · S. Bin Sibly · H. Khelghat-Doost  
Centre for Global Sustainability Studies, University Sains  
Malaysia (USM), Level 5, Hamzah Sendut Library,  
11800 Penang, Malaysia  
e-mail: [suzyrman@usm.my](mailto:suzyrman@usm.my)

H. Khelghat-Doost  
e-mail: [hamoon@usm.my](mailto:hamoon@usm.my)



is not owned cannot be priced) and to have a define boundary. Other scholars in the past and recently placed great deal of interest toward the most popular ancient irrigation systems in the purpose to explore their indigenous knowledge.<sup>1</sup> For instance, Trawick (2001) explored and analyzed the indigenous irrigation principle in the Northern Philippian. Wilkinson (1977) and Zekri and Al-Marshudi (2008) identified several unique features of the old and currently operated aflaj (singular falaj) system in Oman.

Since in Oman irrigated water collected and obtained from groundwater, several techniques and technologies (ranging from traditional simple ones to more complex and advanced) have been used since millennia. For example, an ancient and more primitive technique type known as al Zajrah<sup>2</sup> type well (FAO, 2008; Wilkinson, 1977) used to lift groundwater. A more complex technique uses gravity flow to transport water from the top of an aquifer through a tunnel to the field; the aflaj system. Although these systems initiated to assist the provision of water (which its availability is a crucial element for development permanent agricultural settlement areas), historically people developed a unique water collective techniques that are required for social organization setting. It is important to note the collective water techniques also found in other countries. Hamamouche et al. (2017) indicated the fact that groundwater believed to be exploited only by farmers through individual private wells and tube well. They attributed this to the fact that farmers want to be independent from state or community. Yet, they clearly indicated that many cases exist by which collective organization developed around exploitation of groundwater. While Trawick (2001) listed two main features that generally been used in reference to the indigenous system; small-scale, community based canal systems and build by local people, aflaj (singular falaj) in Oman were, and still currently operated by the local community within a boundary irrigated zone.

My own research with regard to the aflaj system in Oman (Al-Marshoudi, 2018; Al-Marshudi, 2007) suggest that we can now begin to move beyond the simple descriptive way to rather more sophisticated analysis. Furthermore, since several writers have acknowledged the system, in the past (Sutton, 1984) and more recently (Nash & Agius, 2011; Remington, 2018), it is time now to analyze the system within the context of the common property resources framework in order to make policy recommendation for resolving situation of tragedy. We believe this offers great

opportunities for research and to provide some sort of documentation researchable notes. The originality and the early development of not only the engineering techniques for these systems but also the socio-cultural factors associated with its management have formed institutional arrangements. The main purpose of these institutional arrangements was, and still currently applied, (1) to share the benefits derived from the water (2) to manage its water distribution to minimize disputes (3) auction set aside water right to the community shareholders. As Trawick (2001), pointed out many years ago, the locally-derived rules that fostered effective water management in specific cases are in urgent need of study. He meant to exploration of the irrigation system in Peruvian Andes (as he called it as the heartland of the world's great hydraulic civilization). Nowadays, these studies are urgently required to contribute toward the ever-increasing water demand problem linking some of the ancient irrigation systems over history.

## 2 Background of the Study

While Mancur Olson's publication of "the logic of collective action" in 1965 laid out the required theoretical basis for the collective action, later many scholars continued the discussion in an attempt to find solution for the common natural resources problems. In our view, the fast body of literatures with regard to the theory of collective action must be separated into two main categories. This provides the required focus over each category apart. The first ought to be placed under main heading "the operation and rules of the collective action". Schlager and Ostrom (1992) introduced five important user 'rights' to be applied with the common pool resources. These are access, withdrawal, management, exclusion, and alienation. They defined the withdrawal right as gives the holder the right to extract part of the flow of resource units (e.g., catch fish, appropriate water, etc.) and the access right, is the right to enter a resource.

The second deals with the cooperation and the dilemma game. Although in the literatures extensive theoretical analysis of water cooperative (sometimes called water association) within the game of "Prisoner's Dilemma have been conducted, few of the practical field cases studies and the use of empirical real data were found. The theoretical studies concentrated over the extent how collective action interaction among users are controlled.<sup>3</sup> For example, while, Bardham (1993) argued prison's dilemma game provides one-shot interaction of whether a defect or no cooperate, Taylor (1987) indicated that the constellation of costs and

<sup>1</sup>Trawick (2001) indicated the fact that this term has generally been used in reference to small-scale, community-based canal systems.

<sup>2</sup>FAO (2008) defined it as a system that extracts water from a dug well through the use of animals. The reporter also pointed out that this technique was the main traditional method till the introduction of pumps in the 1950s.

<sup>3</sup>Readers are directed to Bradham (1993) and Taylor (1997) for further details.

benefits of collective action on common-pool resources more favorable to the possibility of cooperation than the prisoner's dilemma game. This can be further explained as follows: Since benefits obtained from common resources require cost to acquire that benefit, individual farmer normally not capable on providing this cost. In other words, individual farmer cannot himself do the whole job, and the extra benefits from the part of the work done by him do not fairly cover his cost, as farmers tend to cooperate when others do, but defects when the other defects (Bardhan, 1993).

While prisoner's dilemma game failed in providing a solution through the use of cooperative for the water problems, several scholars used another (more practical) theoretical analytical tools. Among these two different variables used to investigate the existence of collective action. These variables can be summarised under two main types: The first type is known as 'heterogeneity. Here Bardhan and Dayton-Johnson (2002) whom argued cooperation for maintenance is a public goods because one village's action provide benefits to most or all other members of the community. Hence they suggested that inequality in holding sizes among community is considered a positive and can be of successful common resources. Irrigator's payoff from canal cleaning is large, the larger holding of wealth.

The second variable are known as 'the homogeneity variable'. Jayaraman (1981), Easter and Palanisami (1986) and Latorre et al. (2001) used the surface water irrigation to investigate the uniform of farm size. For instance Jayaraman (1981) and Easter and Palanisami (1986) studied the surface water irrigation in India and Thailand have noted the importance of a relatively what they called 'egalitarian' structure to farmers coming together to form a water user association. They stated the following: "The smaller the variation in farm size among the farmers, the more likely they are to form water user organization and have an equal benefits". Further, they argued when the farms, all of which under the boundary of the institutional are about the same size, farmers will obtain approximately equal benefits and have equal interest. Uniform distribution of benefits and this can be measured through analyzing farm size. Other scholars like Latorre et al. (2001) argued holding property rights provides a strong incentive for maintenance. Their justification of this statement based upon the fact that since individual or groups have expectations that they will get benefits from a system, they have an interest in its maintenance, but if water is insecure because supplies are irregular or water may be taken by others, then they are not interested in maintaining the system.

Although a unique and rather distinctive way is required in managing water under arid region a weak institutional arrangements will inevitably lead to major water right disputes. This is attributed to the fact that water over these regions considered highly demanded commodity. Therefore,

in Oman many aflaj community systems exit with solid institutional arrangement which was evolved over thousands of years. I say this based upon my previous and more recent studies (Al-Marshudi, 2007, 2008; Al-Marshoudi, 2018) over the topic.

The fieldwork was conducted over a period of four years in two different governing regions in the Northern part of Oman over three main cities; Nizwa, Izki, and Rustaq. Here I will limit myself to the measuring unit, locally known as ather. There are great deal of structuring water rights and its institutional arrangement which were derived through fieldwork in the form of case studies. These can be further viewed elsewhere (Al-Marshoudi, 2018) but I will not touch upon here. Note that my view with regard to the aflaj cooperative collective action in this study are based on Jayaraman (1981) and Easter and Palanisami (1986) studies. However, in case for the cooperative collective action found within aflaj system in Oman ought to be viewed carefully over existing prevailing social as well as legal context around boundary drawer rural community. Therefore, the argument for the presence of whether heterogenic or homogenous cooperative collective action must in any case rest primarily over the collected fieldwork data from the studied system. If the overall goal of the use of water brought by the system is to establish mutual cooperation, then the incentive is to maximize the output by establishing equal right. This eventually avoids conflict among shareholders. The implication of this can be significantly important not only for the theory but also can be profound for the policy makers.

---

### 3 Aflaj Community System and Literature Review

While the art of water exploitation was developed in Oman thousands of years ago to establish human settlements, many of those settlements are currently present incorporated with modern infrastructure. Each of these settlements such as the city of *Nizwa*, *Rustaq*, *Samail* and district of *Burkat Al-Muz* currently flourish with one or two aflaj systems. In addition, these aflaj have assisted greatly on the formation of what known as "settlements" or villages around legal known boundary. Currently, a law has been passed over Oman Ministerial Council to provide a protected area for the aflaj systems known as 'aflaj protected zone' on a radius of 3.5 km. This clearly provided over the past four decades a protected rule from the threat of the modern new land survey especially from the practice of digging a well which is normally owned by individual farmers.

Currently, in Oman water supply and associated crop cultivation practices are found within two main farming types, both of which use groundwater aquifer. The first and

the most modernized type is the practice of digging a well which is normally owned by individual farmers (earlier indicated). The second is through natural flows by the use of man-made tunnels and channels known as *falaj* (plural aflaj) systems. This classification is crucially important to bear in mind for the following reasons. While, the aflaj system considered as an ancient system which currently threatened by the newly developed modern system, it operates within a community property structure because a farm with its own private-owned individual well is called *mazra* literally means a farm, while farms that receive water from a public falaj are called *amwal*. This Arabic word, *amwal*, which is literally means ‘public wealth’ in its plural form, indicate community ownership.

Another factor closely related to the aflaj system is the fact this system not only transports water from the top part of the aquifer (as discussed earlier), but provides a fair water distribution among all shareholders. Since aflaj water is historically considered as community resource which is managed through social organizational setting, it is significantly important to view the concept of fairness from the angle of how the falaj systems distribute water among different shareholders within a scarce environment. This reflects the fact that disputes can be easily initiated in this type of environment because water considered to be very valuable particularly during period of drought. Although substantial literatures found with regard to this relating social organizational within arid region (Wilkinson, 1977; Costa, 1983; Speece, 1989), little studies attempted to incorporate the theory of collective action to aflaj social setting. This study as earlier indicated will investigate the presence of the cooperative collective action among aflaj irrigators within the aflaj community areas. In the past, many studies have recognized and acknowledged its performance and longevity. For example, Sutton (1984) stated that in common with many modern schemes, *falaj* systems use an imposed technology which method of construction the present user can neither understand nor copy. She went on to say that “the communities that depend upon them have kept many of these precarious water supply systems running for more than a thousand years, and it may therefore be that the organizational aspects of these long-lived cooperative water-based systems may have some features which modern schemes might consider”.

## 4 Method

The three selected *aflaj* for the study are located in separate areas. The first is *falaj daris*, located in the ancient city of *Nizwa* (the capital of the *Dakhiliya*) at coordinate of N22 59 56 E57 32:09.08). In addition, it is considered as one of the ancient *falaj* constructed by the *Yrubi* Imamate in the



**Fig. 1** The city of *Nizwa* and others which are the location all aflaj areas in the Northern part of Oman

seventeenth Century (Sultan b. *Sayf al-Yarubi* was Imam from 1650 to 1660) The second *falaj al-malki*, located in the ancient city of *Izki* at coordinate of N22 43 60 E55<sup>4</sup> and the third *ayn al-khasfah falaj* is located in other governing regions, Souter *Al Batinah*, in the city of *Rustaq* (see Fig. 1).

Historically, these *aflaj* have assisted greatly on the formation of what is known as “settlements” or villages around legal known boundary. Hence the present government has passed law of heritage protection including the aflaj cultivated zone, within a radius of 3.5 km. This consequently protected *aflaj* settlement from the threat of the modern infrastructure and the modern individual farming system (see Fig. 5). Furthermore, these settlements was developed in accordance with topography of the area by which has divided the *waliyah* (villages) into different parts. For example, *falaj daris* was constructed in a total cultivated zone of 2,382,642 m<sup>2</sup> (MRMWR, 2000), by which divided the town of *Nizwa* into two main sections; the upstream, locally referred to as the *Al allayah*, and the downstream, locally referred to as the *Asfayllah* (see Fig. 2). Similarly, *malki falaj* irrigate two different areas the *Al-Nazar* area (a total demand cultivated zone of 1,132,372 m<sup>2</sup>, which is approximately 72% of the total demand area of 1,572,739 m<sup>2</sup> (MRMWR, 2000)., sometimes referred to as the right channel, and the other to irrigate the *Al-Yemen* area, sometimes referred to as the left channel (see Fig. 3). *Ayn al-khasfah falaj* is reflect different view as follow: Unlike *daris* and *malki*, which drawing their water supply from deeper aquifers through the use of long distance tunnel reach to 3 km, *ayn al-khasfah falaj* originate their water supply from solid rocky limestone areas. It is said to be a famous hot spring and because of high temperature (reaching to 60 °

<sup>4</sup>In fact, falaj Daris and Malki was included on the UNESCO heritage list in the year 2006 (MRMWM 2008).



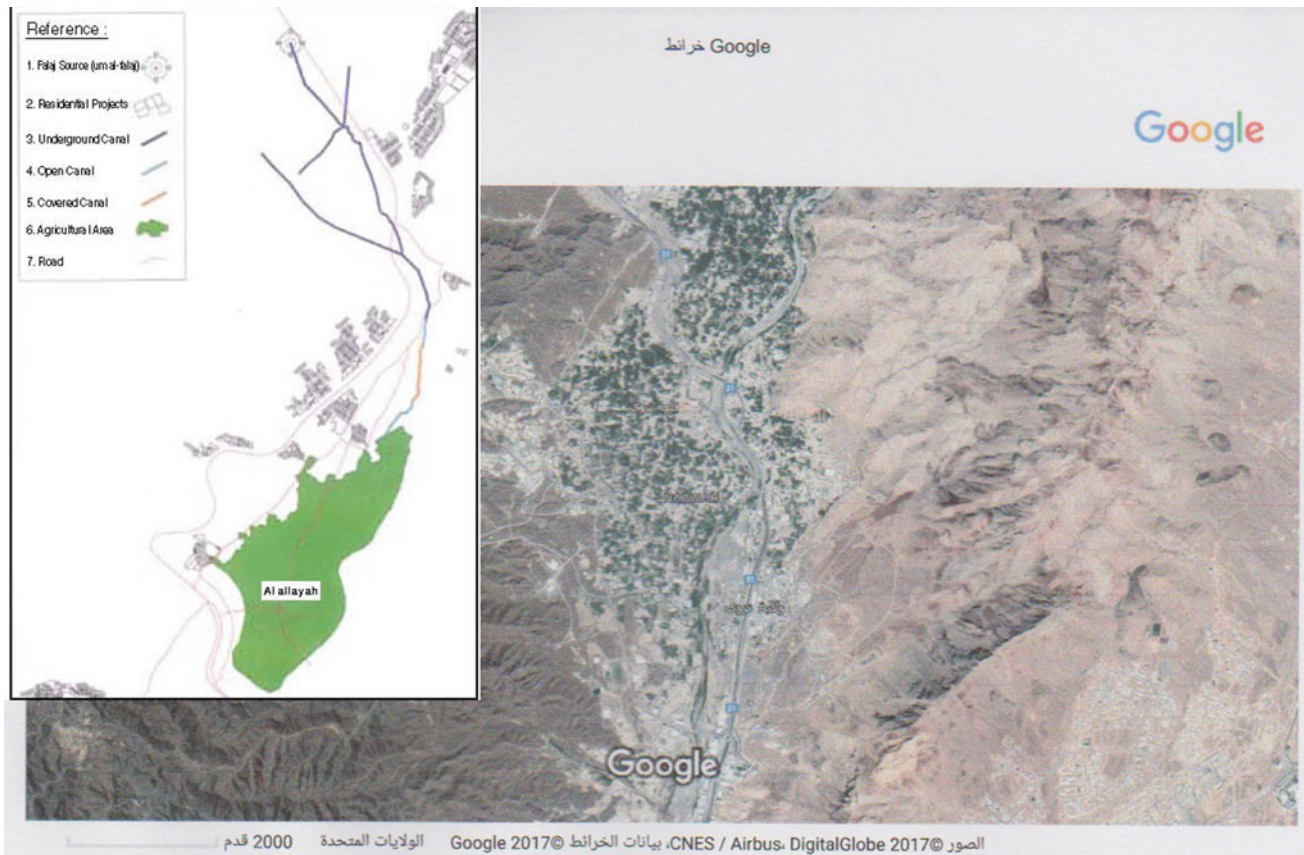


**Fig. 2** Location of *falaj daris* and the boundary of its cultivated area

C), it contains healing properties and high mineral content, especially sulphate (see Fig. 4).

Multiple visits to the study area have been conducted over the period between 2014 until 2016. The reason for the several visits has been carried out for two reasons. (1). to develop cultural understanding and norms of conduct with the Omani people whom will be interviewed for obtain information fulfilling the study objective. (2). Able to develop the research field work framework in terms sort of question needed, type of recording instrument to be used, number of important associated person to interview and any of the official governmental bodies associated to aflaj to be included.

## 5 Result

### 5.1 Local Measuring Unit

Before further elaboration of the finding, it is crucially important first to show how water flow measured within the context of the Omani institutional arrangements. While there have been found many local terms which commonly used to

ease the water process delivery, these terms over time became very known by most members of the community by custom. It was revealed that there are three main local delivery process mechanism used for water circulation among shareholders. The first and largest unit called ‘raddah (plural) raddat which simply means turn. They say today *raddat* ‘*bayt-al-mal*’ which means the flow must be diverted to farms belong to bayt-al-mal. The rest of the day the *raddat* may diverted to the privately-owned right and so on. The second is called ‘baddah’ which is a mechanism used to divide the turn (*raddah*) into two, they say ‘day time *bad-dah*’ and night *baddah* (these two equivalent to almost 12 h each). The third unit is called *ather* which is the common unit used for all shareholders, they say X farmer holds an amount of water measured in *ather* (this is equivalent to half an hour). Finally, the smallest unit is called *qiyas*, which is used to measure *ather* which they say equal to 24 *qiyas*. They say X farmer hold an amount of water flow (normally expressed over time units) 2 *ather* and 20 *qiyas* equivalent to 2.83 *ather* (we divided the 20 *qiyas* by 24).

However, in an attempt to use the simple conversion formula (discussed in the literature), difficulty in grasping a thorough understanding of the revealed information arise.

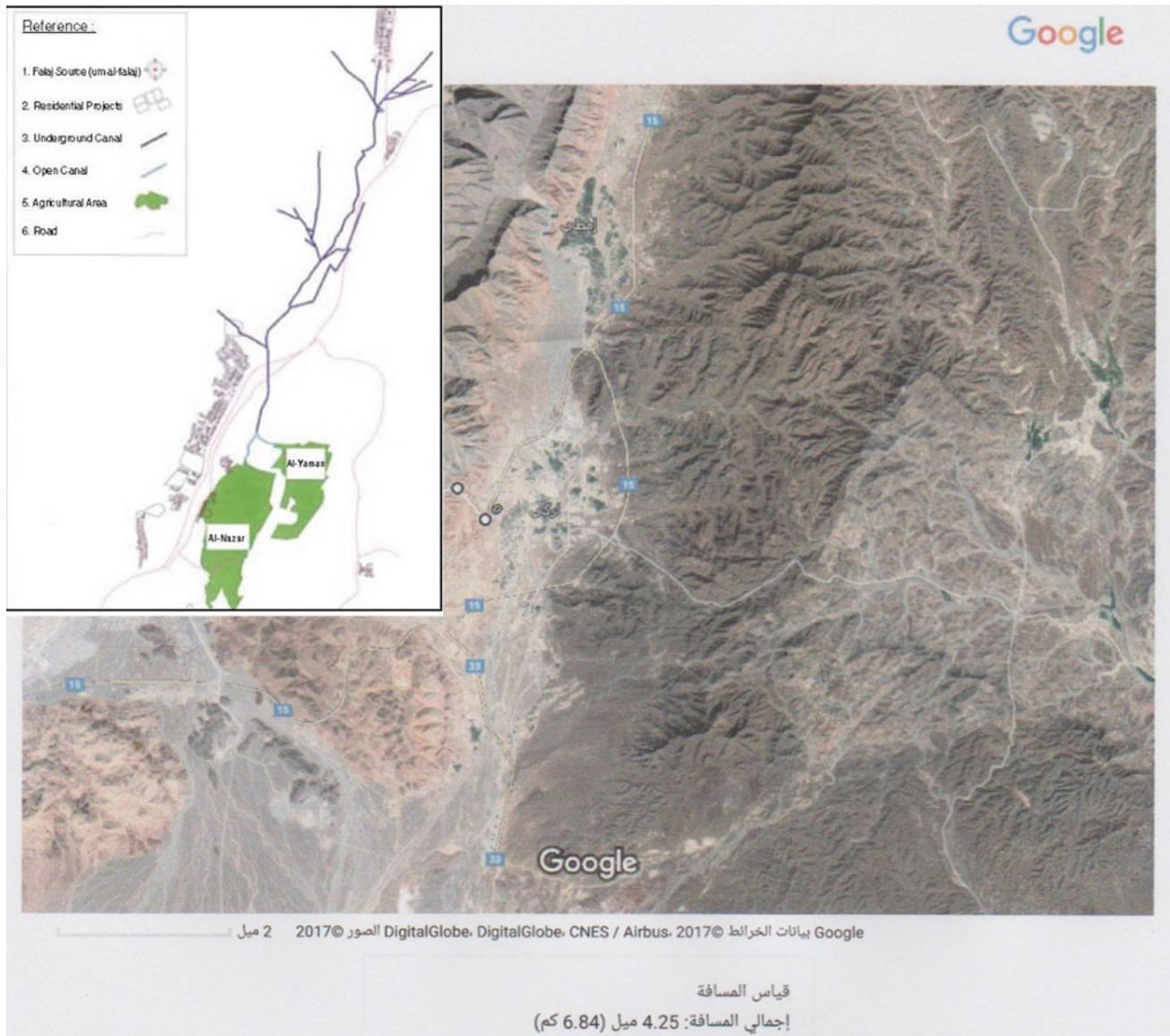


**Fig. 3** Location of *falaj al-malki* and the boundary of its cultivated area

This is attributed to the fact that original measurement units must remain and any conversion applied will reflect some sort of misleading interpretation. For example, *falaj* the service *wakeel* for *Daris falaj* orally stated *its water must be distributed among all shareholders over eight raddat which is consist of '17 baddah'*. The *wakeel* also revealed that this *falaj* holds 408 *athers* that can be delivered over the course of the eight *raddat*. Although this information appeared simple at the first sight, at a later stage difficultly experience in obtaining a thorough understanding of all given units. This can be explained as follows: It was assumed, based over the literatures conversation formula, the eight *raddat* is equivalent to eight day which must be divided into two *baddah* (12 h each). If we multiply the

eight by two (because each *raddat* hold two *baddah*) we obtain 16 *baddah*. However, it was stated by the *wakeel* this *falaj* measured over 17 *baddah*, why so the extra one *baddah*? By co-incidence an answer was obtained from another *falaj* administrative agent. The *wakeel* of *Ayn Al-Kasfah falaj* indicated that summer *ather* is 26 min and winter *ather* is 23 min. Therefore, we strongly recommend that the conversion should not be applied over these measurement units must be understood and traced to its originality. The extra *baddah* might be explained to the difference between summer and winter. In fact, Wilkinson (1974) have touch upon this issue under the discussion regarding the length of the day and night during summer and winter. He thinks that their length varies around the



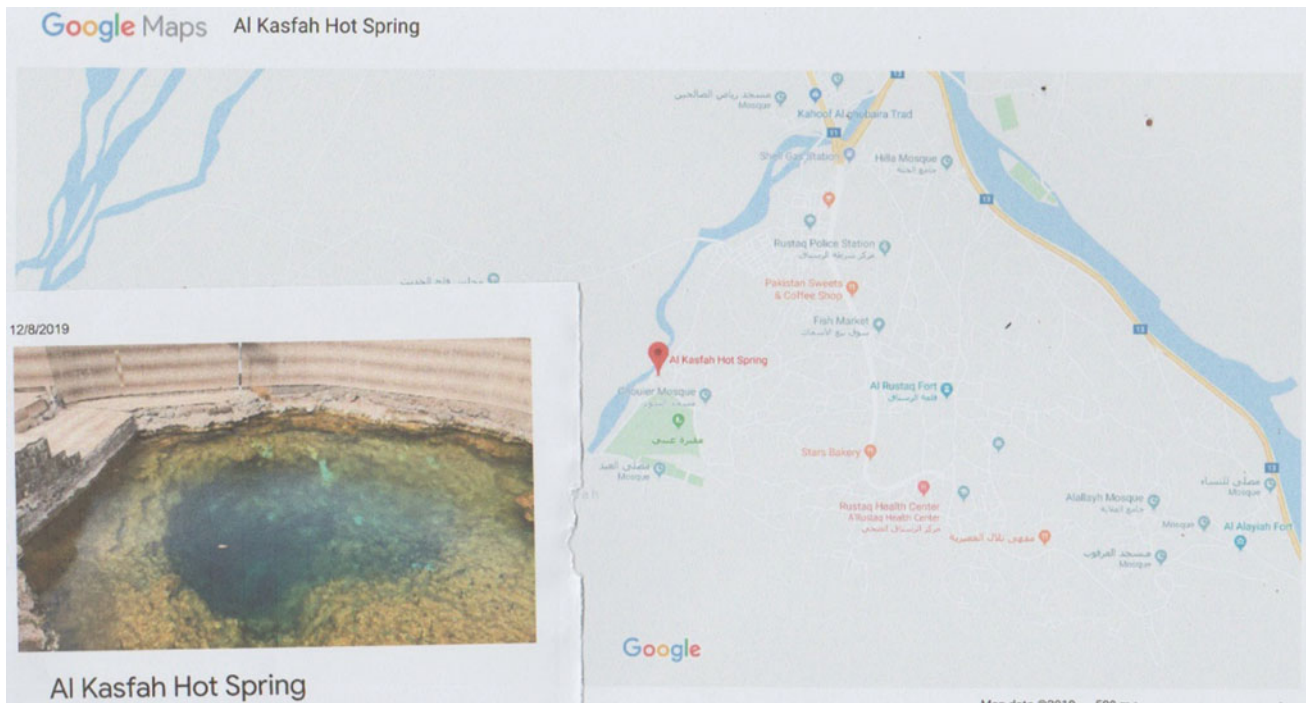


**Fig. 4** Location of the *falaj of ayn al-khasfah* and its main water source (the spring)

mean by some 9 or 10 min during the course of the year based on the latitude of Oman.

### 5.2 Privately-Owned Right Distribution

Historically water rights were initiated through the application of the *raddat* system which designated to suit the independent of water rights from landholders not on the basis who begin diversion first. Hence two types of water rights prevailed by this study; private water right and common rights. The common water rights then sub-divided into three main types; *Bayt-al-mal*, *Waqf* (endowment water rights) and *falaj* own rights.

Table 1 shows the overall prevailed water rights for the three studied *aftaj*; *daris*, *malki* and *ayn al-kasfah*. By far majority of the water rights for the *falaj malki* and *ayn al-kasfah* fall under the category of privately owned rights; 74% and 91% respectively while *falaj daris* characterized by holding more of the common water rights 75%. Readers are directed to our studies for further details of these rights (Al-Marshoudi, 2018; Al Marshoudi, 2017). However, below is a brief explanatory account with the regard to the *falaj* water rights because it is most related to the study main theme. It has been revealed that a whole day of water right set aside for the *falaj* income generation. This is rented for the potential farmers who seek extra water. During growing seasons and over drought period farmers tend to require

extra water. Hence a tradition auctioning water market initiated to fulfil this purpose. These rights are shown in column three of Table 1 and are expressed in percentage of the total *falaj* right. In general 12% and 11% for *falaj daris* and *al-malki* respectively and interestingly no right found for *falaj ayn al-khasfah*. This can be explained as follows: First, the revenues collected from the rented *falaj* water rights are considered as the primary source of income for maintenance. Second, it was revealed that while the *falaj daris* and *al-malki* are of *daudi* type,<sup>5</sup> they generally require continuous and regular maintenance; clean the accumulated rooting in the channels, repair the damaged and blocked tunnels rocks, cleaning the branches etc. In contrast *ayn Al-khasfah* which is belong to the *ayni* type which are less complex because its water supply close to the cultivated area and it was attached with an open channel and hence require no or simple maintenance.

Another finding with respect to the structural setting of the private water rights owners is the documentation and traditional registration of these rights, usually with each *falaj* administrated agent (*wakil*). A full list of these holders was

<sup>5</sup>The literature largely supports the idea that there are three types of *falaj* in Oman: *daudi*, *ghaili* and *ayni*. The *daudi falaj* extracts water from the upper part of the aquifer in the mountains, the *ghaili falaj* extracts water from the surface of an oasis, while the *ayni falaj* extracts its water from a spring which naturally comes to the surface, mainly in limestone rocks (Stanger; 1986; Wilkinson, 1977; Costra, 1983).

**Table 1** The three studied *aflaj* water rights distribution (%)

	Distribution of water rights (%)				Total
	Private	Common water rights			
		Bayt_elmal (state)	Waqf	Falaj rights	
Daris	25	24	39	12	100
Al Malki	74	None	15	11	100
Ayn Al Kasfah	91	3	6	None	100

**Table 2** Frequency distribution of the *ather* holding over the three studied *aflaj*

	Daris	Lamki	Ayn Al-Kasfah
Less than one	130	11	44
Less than two	51	59	35
Less than three	17	41	21
Less than four	2	17	16
Less than five	3	8	12
Less than six	0	6	7
More than 7	1	7	17
Total	204	149	152

obtained from the wakil. It is important to note that these are registered over the local measuring units; *ather* and *qiyas*<sup>6</sup> which are placed as conditions for the privately-owned water rights. Although both are used as measuring units for the prevailed water rights (private and the common) *ather* represent a higher unit than *qiyas*, which is considered is the smallest. Hence, they say a particular irrigator hold one *ather* and 24 *qiyas* which means he or she is entitled (or had the right to the water flow) of water flow measured over this registered unit.

Table 2 demonstrate the private water rights frequency size holding through the use of the *ather* measuring units. By far, the largest number of irrigator's for the three studied *aflaj* falls into the following categories; less than one *ather* and less than two *ather*. The concentration of the smaller size distribution varies slightly over the three *aflaj*. For example, *falaj daris* and *ayn al-kasfah* fall under the category less than one *ather* at a percentage of 64 and 29 respectively. In contrast, *falaj malki* fall under category less than two *ather* at a percentage of 40. The weighted

arithmetic mean of the holder size for the *daris* 0.461, *malki* 1.048 and *ayn al-kasfah* 0.755 *ather*. It is obvious that small size of irrigators is dominated the *aflaj* community members over the three studied *aflaj* in Oman.

## 6 Discussion and Conclusion

The present study has found two important conditions which enable *aflaj* irrigator cooperates collectively. First, when farmers have same water amount sizes then they approximately tend to share equal benefit and at the same time hold equal interest. This is usually crucial when water becomes a scarce resource and hence if the sizes are not uniform then competing toward water cannot be avoided. Second, present of a competing water market within the boundary of all irrigators assisted greatly the provision of extra water especially during the water scarcity. While the topography and the physical engineer of any irrigating system reflect the complexity and simplicity of its maintenance, development of its institutional arrangements and water rights must be online with this physical structural setting. This can be explained as follows. First, over sites of arid climatic environment, where precipitation rate is very low and evaporation (due to high temperature) is very high, availability of water considered is more valuable than land. Second, the larger the amount of water initiated to an irrigator (whether one or more of the *ather*) the larger the land can be developed. According to *Daris* wakeel, who orally explained the fact that the distributed water amount (*ather*) are strictly confined over three main factors: (1) the availability of fertile

<sup>6</sup>Originally, an *ather* unit was as follows: A three-meter high stick is anchored at the center of a flat area where there is little shade to prevent the sun from shining directly on the stick. Then the area to the west and east of the stick is divided into 24 sections; these divisions are equal to one *ather*. Now, each section is known as *qiyas* which is originally derived from the process of measuring a thing so that it is used to reflect a volume. In the past they tended to use a container made of copper with unit lines marked on the inside. *Qiyas* is considered as the smallest unit within the context of the *falaj* distributive system. Therefore, they since one *ather* is divided into 24 *qiyas*, same saying an *ather* equal to 24 *qiyas*.

soil which require continuous tillage practice (2) the topography of the land which must hold a downhill sloping to allow water naturally flow from the main source (known as mother well) to the cultivated areas (3). Canal network which recently applied cemented lining and ricked. Therefore, currently we found almost a completed land formation which are legally recognized and sometimes settlers lived on it and modern roads network were established.

While many studies discussed the view of cooperative collective action overirrigating water systems, several conditions have been initiated. First the size of the farm ought to be uniform. Second, presentan organization with a trusted and honest leadership. However, this study revealed another condition with regard to extra water which can be rented through the *aflaj* administrative agents. This water right has been initiated in the purpose to generate income for *falaj* maintenance. The *aflaj* irrigated area currently are found within a settlement village-base which are operated over a recognized boundaries. This study clearly found two different boundaries; external which was enforced by the present government through the passing of what is known as ‘*aflaj* protection zone (a radius of 3.5 km), and internal which is represented by *aflaj* institutional arrangements. While the former can be approved by strong resilience that demonstrated by the *aflaj* commanded area against the accelerated development in Oman, the later has been also approved by this study. First the unique historical locally used water measurement units, from the largest *raddat* to the most commonly explicit unit *ather*, clearly reflect the presence of cooperative collective action among irrigators. This is attributed to the fact that these *athers* units found with almost unformal distribution of *ather* sizes among all shareholders. Second condition for cooperation was found within the setting of the *aflaj* institutional arrangements. Since several regions over the northern part of the country rely heavily upon a single community-owned *falaj* for irrigating their date gardens and other annual crops, this requires a high degree of social control and cooperation to maintain the system and generate income. This was initiated by setting a whole day of the water rights, we say set aside (locally they say *raddat*) belong to the *falaj* itself for the purpose of income generation.

## References

- Al-Marshoudi, A. S. (2018). Water institutional arrangements of Falaj Al Daris in the sultanate of Oman. *International Journal of Social Sciences and Management*, 5, 12.
- Al-Marshoudi, A. S. E. A. (2017). Water institutional arrangements of Falaj Al Malki in the sultanate of Oman. *International Journal of Recent Research in Social Sciences and Humanities (IJRSSH)*, 4 (4), 94–108.
- Al-Marshudi, A. S. (2007). The falaj irrigation system and water allocation markets in Northern Oman. *Agricultural Water Management*, 91, 71–77.
- Al-Marshudi, A. S. (2008). Economic instruments for water management in the sultanate of Oman. *Water International*, 33, 361–368.
- Alchian, A. A., & Demsetz, H. (1973). The property right paradigm. *The Journal of Economic History*, 33, 16–27.
- Baland, J.-M., & Platteau, J.-P. (1999). The ambiguous impact of inequality on local resource management. *World Development*, 27, 773–788.
- Bardhan, P. (1993). Symposium on management of local commons. *The Journal of Economic Perspectives*, 7, 87–92.
- Bardhan, P. & Dayton-Johnson, J. 2002. *Unequal irrigators: Heterogeneity and commons management in large-scale multivariate research*.
- Bjornlund, H. (2003). Efficient water market mechanisms to cope with water scarcity. *International Journal of Water Resources Development*, 19, 553–567.
- Brown, L., McDonald, B., Tysseling, J., & Dumars, C. (1982). *Water and agriculture in the Western U.S.: Conservation, reallocation, and markets*. Westview Press.
- Bruns, B. R., Ringler, C., & Meinzen-Dick, R. (2005). *Water rights reform: Lessons for institutional design*. International Food Policy Research Institute.
- Costa, P. M. (1983). Notes on traditional hydraulics and agriculture in Oman. *World Archaeology*, 14, 273–295.
- Coward, E. W. (1979). Principles of social organization in an indigenous irrigation system. *Human Organization*, 38, 28–36.
- Dales, J. H. (1968). Land, water, and ownership. *The Canadian Journal of Economics/Revue Canadienne d'Economie*, 1, 791–804.
- Demsetz, H. (2002). Toward a theory of property rights II: The competition between private and collective ownership. *Journal of Legal Studies*, 31, 653–672.
- Easter, K. & Palanisami, K. (1986). *Tank irrigation in India and Thailand: An example of common property resource management*.
- Eastert, K. W., Rosegrant, M. W. & Dinar, A. (1998). *Markets for water: Potential and performance*. Kluwer Academic Publishers
- FAO, A. (2008). *Oman, country profile*. FAO.
- Hamamouche, M. F., Kuper, M., Hartani, T., & Bouarfa, S. (2017). Overlapping groundwater service markets in a Palm Grove in the Algerian Sahara. *Irrigation and Drainage*.
- Jayaraman, T. K. (1981). Farmers’ organisations in surface irrigation projects: Two empirical studies from Gujarat. *Economic and Political Weekly*, 16, A89–A98.
- Latorre, J. G., Garcia-Latorre, J., Sanchez-Picón, A. (2001). Dealing with aridity: socio-economic structures and environmental changes in an arid Mediterranean region. *Land Use Policy*, 18 53–64.
- Meinzen-Dick, R. S. (2000). Property rights and maintenance of irrigation systems. International Food Policy Research Institute.
- MRMWR, M. O. R. M. A. W. R. (2000). *Statistical and inventory of the aflaj in Sultanate of Oman*.
- MRMWR, M. O. R. M. R. W. R. (2008). *Statistical and Inventory of aflaj in Sultanate of Oman*
- Nash, H., & Agius, D. A. (2011). The use of stars in agriculture in Oman. *Journal of Semitic Studies*, 56, 167–182.
- Oakerson, R. (1986) Proceedings of the conference on common property resource management. In Panel on Common Property Resource Management, N. R. C. (Ed.), *Common property resource management, 1985* (pp. 1–229). National Academy Press.
- Remington, G. (2018). Transforming tradition: The aflaj and changing role of traditional knowledge systems for collective water management. *Journal of Arid Environments*, 151, 134–140.
- Rosegrant, M. W., & Binswanger, H. P. (1994). Markets in tradable water rights: Potential for efficiency gains in developing country water resource allocation. *World Development*, 22, 1613–1625.

- Saleth, R. M., & Dinar, A. (2005). Water institutional reforms: Theory and practice. *Water Policy*, 7, 1–19.
- Schlager, E., & Ostrom, E. (1992). Property-rights regimes and natural resources: A conceptual analysis. *Land Economics*, 68, 249–262.
- Speece, M. (1989). Aspects of economic Dualism in Oman, 1830–1930. *International Journal of Middle East Studies*, 21, 495–515.
- Stanger, G. (1986). The Hydrology of the Oman Mountains.
- Sutton, S. (1984). The falaj—A traditional co-operative system of water management. *Waterlines*, 2(5), 8–12.
- Taylor, M. (1987). *The possibility of cooperation*. Cambridge, MA: Cambridge University Press.
- Trawick, P. B. (2001). Successfully governing the commons: Principles of social organization in an Andean irrigation system. *Human Ecology*, 29, 1–25.
- Wilkinson, J. C. (1974). The organisation of the Falaj irrigation system in Oman University of Oxford, School of Geography.
- Wilkinson, J. C. (1977). *Water and tribal settlement in South-East Arabia: A study of the Aflaj of Oman*. Clarendon Press.
- Zekri, S., & Al-Marshudi, A. S. (2008). A millenarian water rights system and water markets in Oman. *Water International*, 33, 350–360.



# Monitoring and Counting *E. coli* Bacterial Growth During Low-Pressure Events in Drinking Water Distribution Networks

Ashraf Farahat

## Abstract

Maintaining clean drinking water is a key factor in maintaining sustainable development and a healthy environment. In addition to monitoring water quality at water tanks, it is important to monitor water distribution network (WDN) and pipes where water is being transported. Intrusion in WDN can be triggered by transient low-pressure events. This intrusion may result in the contamination of drinking water supplied to consumers, which may have major health impacts. This experimental study was performed to monitor and count *E. coli* bacterial intrusion into WDN. Two experiments were performed to investigate (1) the effect of low and negative pressure in WDN on bacterial intrusion; (2) the propagation and growth of bulk bacterial intrusion in WDN; (3) premeditated bacterial contamination of water sources (tanks). It was found that the rate at which bacteria reaches customers is very comparable however, higher risks are found with premeditated bacterial intrusion. It was also found that there is a small chance for *E. coli* bacteria to be intruded into the system after sudden low/negative pressure events. The experiment shows that high pressure within water networks pumps out water of the system then the mixture (water and contaminants) is sucked back into the network. It was observed that contaminants were not able to be significantly intruded into the system if water pumps were shut down for a short period of time. The minimum time required for contaminant to be intruded into the system was found to depend on the water pressure prior water pumps which were turned off.

## Keywords

*E. coli* • Drinking water • Distribution networks • Intrusion • Low pressure

## 1 Introduction

Providing clean drinking water is a key factor in maintaining sustainable development and a healthy environment. While increasing governmental investments in water supply and sanitation can increase the net economic growth and reduce the costs associated with public health care, maintaining water quality in drinking water distribution networks (WDN) requires a clear understanding of the interactions between the WDN system and the environment surrounding it.

Many attempts (Kirmeyer et al., 2001; Abo-Munassar, 2014) have been reported to predict the performance of water distribution systems against intentional and/or accidental events. Risk assessment schemes have been proposed to investigate the uncertainties associated with the performance of an existing water distribution system but they generally only take into account hydraulic criteria (Islam et al., 2015). Although intrusion is considered to be a vital mechanism for water quality contamination, not enough effort has been made to evaluate the water quality while traveling from the source to the customers. The evaluation of the quality of the water supplied to consumers usually takes part at the treatment plants, as the water at the source should match the standards. However, only minor attention is given to the water quality during the transportation stage throughout the WDN (Isovitsch & Vanbriesen, 2008).

In many countries, the safety of drinking water is expected to be facilitated and achieved in WDNs; however, there is a lack of knowledge of the microbial ecology of drinking water in WDNs as it not easy to predict the microbial nature of the soil environment surrounding pipes buried under the ground and the bacteria forming in the

A. Farahat (✉)

Department of Physics, College of General Studies,  
King Fahd University of Petroleum and Minerals,  
Dhahran, 31261, Saudi Arabia  
e-mail: farahata@kfupm.edu.sa



pipes' inner walls (LeChevallier et al., 1987; Douterelo et al., 2014). Recent developed molecular-based methods (LeChevallier et al., 1987; Pirnie et al., 2000) indicate that WDNs have a large number of bacterial and fungal colonies.

Many studies have tried to investigate microbial life within WDNs without taking into consideration the lifestyle of the microorganisms. Some of them investigate which types of microorganisms are present in the WDNs (Hellard et al., 2000; Somashekar et al., 2015), while others study the quantity of these microorganisms in a quantitative and qualitative ways (Admassu et al., 2005; Qu et al., 2013). Additionally, some studies have been carried out to examine the influence of the existence of the microorganisms in WDNs on human health (Edberg et al., 2000; Hellard et al., 2001; Murphy et al., 2016), while others have concentrated on the source and the growth of the microorganisms in the WDN (Admassu et al., 2005; Douterelo et al., 2014; Lin et al., 2016; Prest et al., 2016).

*Escherichia coli* (*E. coli*) is considered as the standard indicator for drinking water quality monitoring (Gorchev & Ozolins, 2011) and is even considered a superior indicator in determining potable water pollution (Edberg et al., 2000). The *E. coli* bacteria and/or other microorganisms could be introduced to the WDN through a replacement or repairing of the infrastructure or during an installment of a new network. Also intrusion could take place when there is depressurisation measure or other dynamic event (Besner et al., 2011). The presence of *E. coli* in water is a strong indication of recent sewage or animal waste contamination. *E. coli* contaminated drinking water can cause intestinal infection. Symptoms of intestinal infection include diarrhea, abdominal pain, and fever. Major correlation has been found between distribution system failures and waterborne disease outbreaks (Moe & Rheingans, 2006). In order to protect end users from these bacterial infections, many researchers are currently conducting studies that evaluate the effect of *E. coli* bacteria on the WDN.

This study provides a risk analysis for bacterial intrusion through water WDNs using selected hydraulic factors. The first part of the paper investigates the minimum time required for *E. coli* bacterial suspension to intrude into a WDN system under low-pressure (<1 bar) conditions. The second part evaluates the rate of bacterial propagation into the system under different operating pressures and intrusion methods. This paper also examines the theory that contaminants will be immediately intruded into the system through cracks in pipes and loose joints after power shut down is accompanied by low-pressure conditions within the WDN. It is important to mention that *E. coli* does not broadly represent a threat itself as pathogenic strains are not picked up by common methods. Only certain species and specific concentrations of *E. coli* will cause intestinal infection. It is the other pathogens from human and animal waste that are the

real concern. Not detecting *E. coli* does not indicate the absence of pathogens. In this study, *E. coli* is used as an indicator for what might happen to microorganisms in the environment under study and *E. coli* concentration measurement is simply used as an indicator of possible bacterial intrusion, growth, and transport through the WDN.

---

## 2 Material and Method

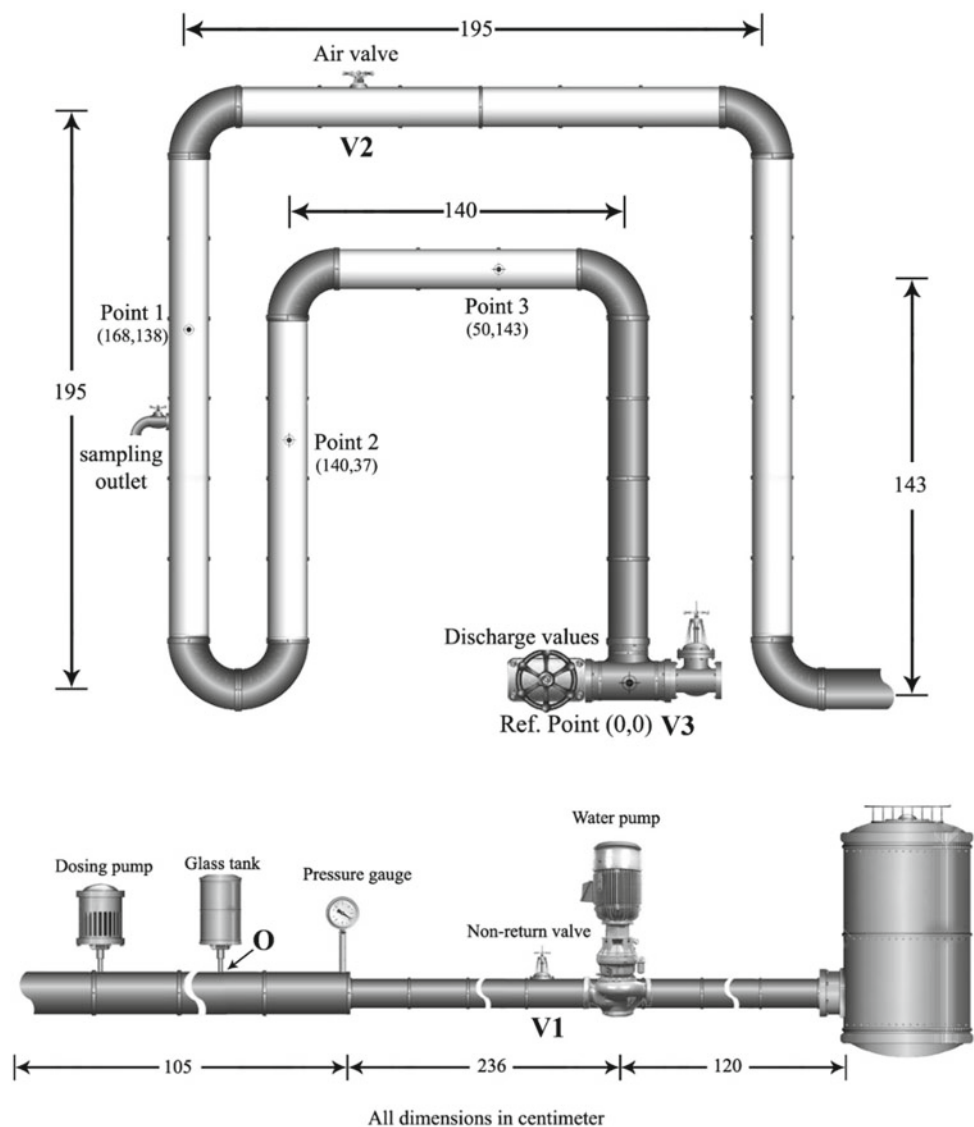
A full-scale experimental network has been constructed in order to examine the bacterial intrusion into the WDN, and the effect of various factors such as pressure magnitude and feeding location.

The experimental network is intended to imitate a real WDN, as it includes various pipe diameters, pipe materials, and pipe junctions, rises, and inclinations. The schematic diagram and photographs of the network are presented in Figs. 1 and 2, respectively, for both the side and front view. Another feature of this experimental network is its ability to be used as an open pipe system (the system tries to use the water from the source and discharge the whole of it) and as a recirculating system (water cycled back to the source).

The network system consists of two transparency loops (A, and B), constructed using several 6-ft clear acrylic pipes, with an internal diameter of 2.5 in. and an external diameter of 3 in. These loops are interconnected with certain U-shaped PVC joints and vertically installed using a steel frame. The dimensions of the internal loop (A) are 143 cm (height) × 140 cm (length), while the external loop (B) has a dimension of 195 cm for both height and length. Loop A is connected at the end with two discharge valves, one is used to flush the system and the other is used to maintain a specific pressure. They are also used to cycle the water in the system or discharge the water from the system. In contrast, loop B is connected to the source pipe on one side while the other one is connected to the beginning of loop A. Loop B contains an air release valve to sustain a full pipe flow. It also contains a sampling outlet which is well represented in Fig. 1 (front view).

The network source of water is a 1000-L tank which lies on the surface of the ground. The water is supplied to the system through a 2-in. PVC pipe with a length of 120 cm. The pressure head is maintained by using a water pump, which pumps the water into the systems through a 2-in., 236 cm PVC pipe. In addition, a non-return valve is used to ensure that the water goes in one direction and keeps the water pump safe. The last part of the network which lies on the ground is a PVC pipe with a length of 105 cm. This pipe has three interconnected parts: a pressure meter (gauge), a two-liter measured glass tank (operated by a control valve), and a dosing pump.

**Fig. 1** Schematic diagram of the water network system used in the study



The experimental setup, size, and design do not accurately represent a real-life WDN; however, it should be enough for proof of concept of the pilot study represented in this work.

### 3 Bacteria Preparation and Testing

#### 3.1 Bacterial Culture Preparation

The liquid media (nutrient broth) to be used for bacterial growth was formulated by dissolving 8 g of nutrient broth in 1L of distilled water (pH 7.5) which was then autoclaved at 121 °C at 2 bar pressure for 1800s. *Escherichia coli* K12 wild-type strain (MG 1655) was grown overnight in liquid media at 37 °C on a rotary shaker incubator (Memert INB 500, ThermoScientific) at 160 rpm. One percent aliquots of the broth medium containing *E. coli* were inoculated into a

fresh liquid medium and incubated under similar conditions. *E. coli* cells were harvested from the liquid culture by centrifugations (using a Labnet-0700 centrifuge from Hermle Germany) at  $4000 \times g$  for 600 s at 4 °C, washing twice with a sterile 0.9% NaCl solution at 4 °C and divided into two groups: test and control. In the test group *E. coli* cells were suspended in saline solution to a concentration of  $1 \times 10^8$  colonies forming units per milliliter (CFU/ml) as a start material in the tank.

#### 3.2 Preparation of Nutrient Agar Plate

The nutrient agar plates (Fig. 3) were prepared after adding 15 g of agar to 1 L of the liquid medium, then autoclaved, poured into Petri dishes and left to cool down and solidify at room temperature.

**Fig. 2** Experimental setup for the drinking water network (DWN) laboratory facility



### 3.3 Spiking *E. coli* Culture into the Testing Tank

The test tank was flushed by 1000 L of 3% of chlorine as a bacteria disinfectant in order to kill any contaminants. This step kills any existing bacteria on the tank walls or the network pipes. The bacteria disinfectant is left in the water for at least 600 s, then water is flushed by turning on the water pump until all of the water is flushed out. The tank is then

refilled up to 500 L, and the water is re-flushed. Next the tank is then refilled with another 500 L of water.

After mixing the *E. coli* bacteria in the tank, 1 ml aliquots are taken at different time intervals.

Serial dilutions were prepared with normal saline and 0.1 ml aliquots from each dilution were developed separately, spread on the nutrient agar plates and then evolved at 37 °C. Colony forming units of both groups were counted



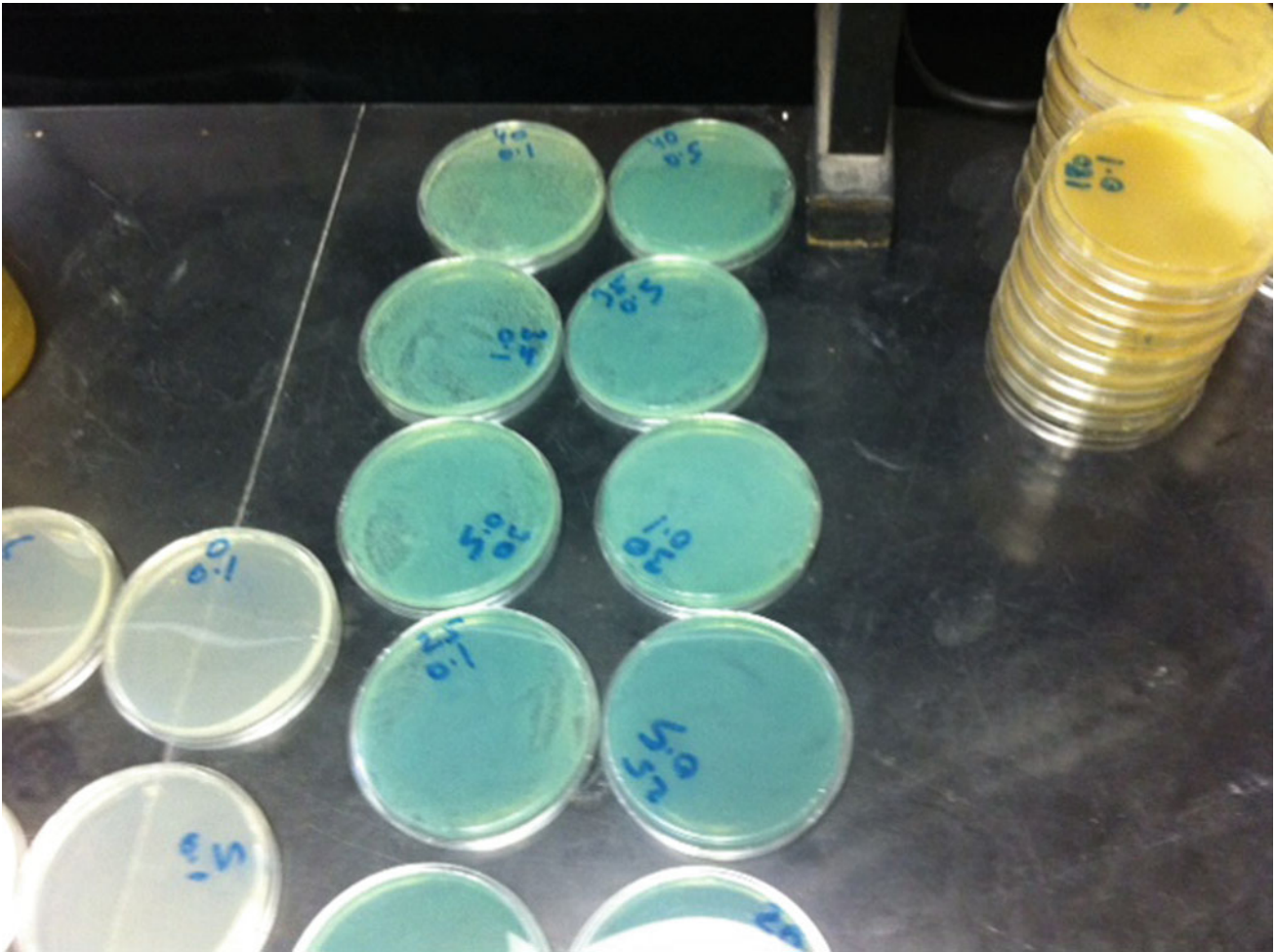


**Fig. 3** *E. coli* bacterial plates used to count the growth of the bacteria colonies

using a colony counter (Stuart Scientific, Model number 3846). After incubation at 37 °C for 24 h, plate counts were compared with each other.

## 4 Methodology

This experiment was conducted to produce the highest number of possible scenarios for *E. coli* intrusion and transport through a WDN. One of the most common reasons for bacterial intrusion is that it flows through cracks that may be found in water pipes or around connections. In the experiment, a crack was introduced to the WDN by using a valve that can control an orifice that allows *E. coli* bacteria to flow from either outside to inside the system. In this study, two main scenarios were conducted to evaluate the time required for *E. coli* bacterial intrusion into the system under negative pressure conditions (scenarios #1 and #2).

### 4.1 Scenario-1

In this stage of the experiment, low and negative pressure conditions in the WDN were simulated by increasing the water pressure within the network using a water pump and a control valve and then suddenly reducing the pressure by turning off the water pump while allowing 40 mL of *E. coli* suspension to intrude into the system through a 0.1 in. orifice (O), as shown in Fig. 1.

It was expected that, once the pressure was reduced, the *E. coli* suspension would be immediately sucked into the WDN. However, it was observed that water was pumped out of the system diluting the bacterial suspension and then the mixture was sucked slowly into the system. The time required to start sucking the mixture out was calculated from the moment the water pump was turned off.

Operating pressure is another parameter that was tested to observe its effect on the *E. coli* suspension flow rate from

outside to inside the system. The water pressure was controlled by a flow valve that was gradually increased, and on each occasion, the time required to start intruding the bacteria into the system was calculated starting from the moment at which the pump was turned off.

## 4.2 Scenario-2

It is very important to determine how long it takes for full absorption of an *E. coli* bacterial suspension into the system as this will help in estimating the bacterial volume intruded into the WDN during a sudden pressure drop.

The size of the cracks in water pipes is considered to be an important factor in determining the volume of bacteria flowing into the system during a low/negative pressure event. This is simulated by different orifice openings in our experiment.

Two cases have been checked (a) *E. coli* suspension directly added to the water source; (b) *E. coli* suspension injected into the water network; (c) *E. coli* suspension absorbed into the water network.

## 4.3 *E. coli* Suspension was Directly Added to the WDN Source (Tank)

Before the bacteria was inserted the tank was flushed by filling it to the top (1000 L) and adding a bacteria disinfectant to kill any residual bacteria that may have existed on the tank walls or inside the network. The bacteria disinfectant is left in the water for at least 10 min, then the water is flushed by turning on the water pump until all of the water is flushed out. Then the tank is refilled up to 500 L, and the water is then flushed again. The tank is then refilled with another 500 L of water. A specific volume (400 mL) of *E. coli* suspension is directly added and mixed with the water in the fiber glass tank. The pump is then turned on, and the pressure in the water network is controlled using a valve. Water is collected at the network outlet every minute to analyze the bacteria counts in the water samples.

## 4.4 *E. coli* Suspension was Injected into the Water Network

The exact same steps as described in Sect. 4.3 are followed to flush the water network and a 10 bar dosing pump (Fig. 1) is used to inject 400 mL of *E. coli* suspension into the water network. The water pressure is controlled using a manual valve attached to a pressure gauge, and water samples are collected every 30 s to analyze the bacterial concentration in the water.

## 4.5 *E. coli* Suspension was Absorbed into the Water Network

In this case, *E. coli* bacteria is allowed to be absorbed into the network due to low pressure (<1 bar) inside the network. About 400 mL of *E. coli* suspension is inserted in the glass tank in Fig. 1, the water pump is turned on and the pressure is then manually adjusted until it reaches a certain value. The pump is then turned off to allow the pressure to drop off inside the network which allows the bacteria suspension to be gradually absorbed into the system. Once the whole bacteria suspension is absorbed, the water pump is turned on again and samples are collected every 5 s.

---

## 5 Results and Discussion

### 5.1 Time Required for the System to Initially Intrude the *E. coli* Bacteria

It was found that there is a strong correlation between the operating pressure and the beginning of bacteria flowing into the system as shown in Fig. 4. It is worth mentioning that the accuracy of the results is significantly affected by the operator response time required to immediately open the orifice once the water pump is turned off. An automated system to control the orifice opening could produce better results than the manual process applied in this study. It was found that the time required to start bacterial intrusion into the system was not correlated with how long the water pump is turned on, as long as the water pump is turned on long enough to reach the desired pressure.

### 5.2 Time Required for the System to Fully Intrude the *E. coli* Bacteria

It was found that there is a direct correlation between the time required for full bacterial intrusion and the operating pressure, regardless of the orifice size, as illustrated in Table 1. This is attributed to the water pumped out of the system into the bacterial container once the water pump is turned off then sucked in again into the WDN, while the pressure gradually drops inside the system. The time for full *E. coli* absorption was found to decrease by 4 bars, contradicting the direct relationship found at pressures of 1 and 3 bars (see Fig. 5). This could be related to the high-pressure head produced in the vertical pipes in the WDN and in the water tank when the water pump operates at high pressures. This large pressure head could expedite the contaminant absorption at larger orifice sizes.

The experiment shows that, as the system is running at its capacity, *E. coli* bacterial suspension is less likely to be



**Fig. 4** Time required for the *E. coli* bacterial suspension to be intruded into the system

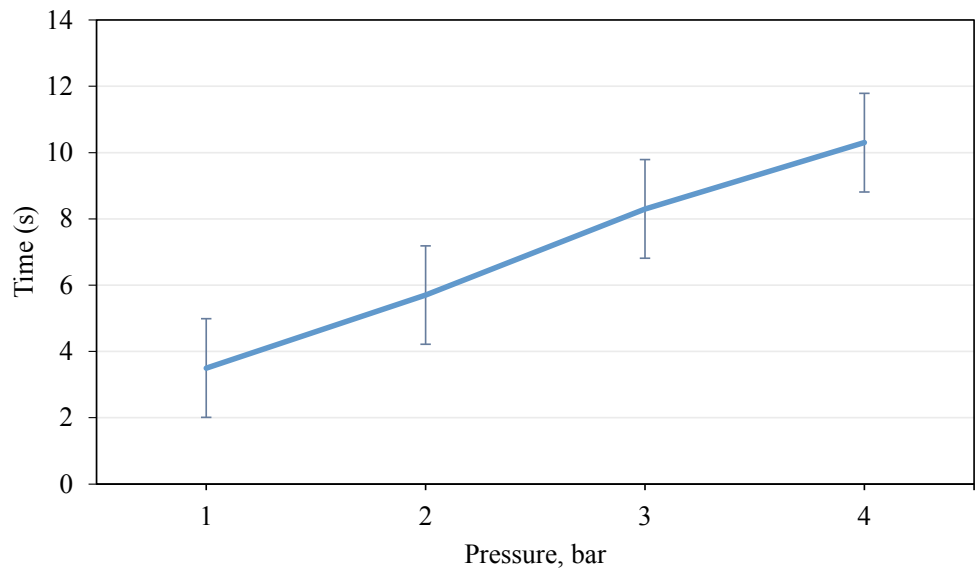
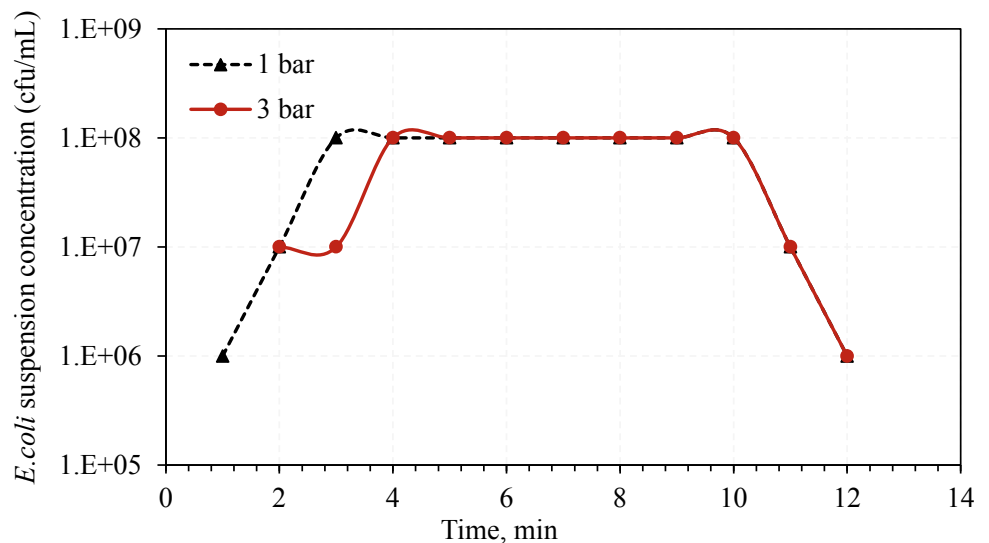


**Table 1** Time required for full *E. coli* suspension intrusion into the WDN as a function of water pressure and crack size

Crack size (in.)	0.10	0.25	0.5
Pressure (bar)	Time (s)		
1	24	26	30
2	33	30	35
3	37	41	46
4	42	34	41

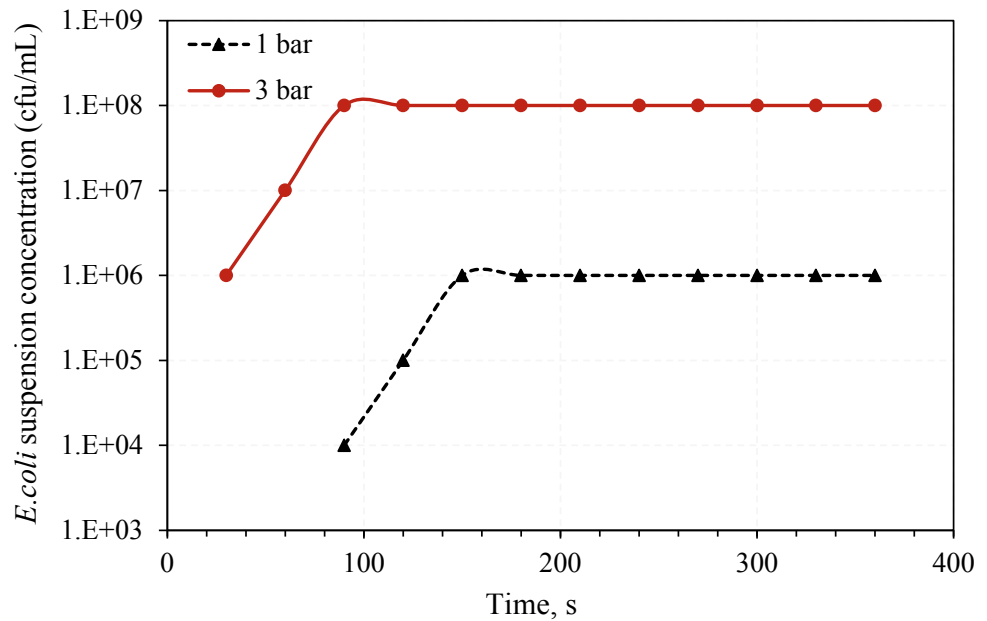
**Fig. 5** Temporal *E. coli* concentration at different pressures when bacteria is inserted in the water tank



intruded in the system. Even if the water pump is turned off, it takes a few seconds for the *E. coli* suspension to start flowing into the system based on the orifice size and the operating pressure. These results contradict the theory that contaminant and bacteria will be immediately sucked into

the WDN once a power failure takes place. This is very interesting as it is an indicator that *E. coli* bacterial growth could take place by making thin biofilms inside the pipes and that bacteria is not necessarily transported from the outside to the inside.

**Fig. 6** Temporal *E. coli* concentration at different pressures when bacteria is pumped into the water network using a dosing pump



### 5.3 Time Required to Detect *E. coli* at the WDN Outlet

#### 5.3.1 Case-1: *E. coli* Suspension was Directly Added to the WDN Source (Tank)

Figure 6 displays the *E. coli* suspension concentration at 1 and 3 bar. At 1 bar, bacteria was observed in water samples at 1 min with a concentration of  $\sim 10^6$  cfu/mL. The bacteria count directly increases with time until it becomes saturated between 3 and 10 min at  $\sim 10^8$  cfu/mL, then the bacteria count decreases with time after 10 min. At 3 bars, bacteria starts to be observed in water samples after  $\sim 2$  min with  $\sim 10^7$  cfu/mL, then it increases to  $10^8$  cfu/mL before saturation and then the bacteria count starts to decrease after 10 min. Bacteria propagates faster in water at low pressures due to higher flow rates and can be detected faster at the consumer point.

#### 5.3.2 Case-2: *E. coli* Suspension was Injected into the Water Network

Figure 6 shows the temporal variation of *E. coli* within the network. For a pressure of 1 bar, it takes 90 s for the bacteria to start to be observed at the network outlet. The bacteria count in the water sample starts to increase and then reaches saturation at  $\sim 10^6$  cfu/mL. Increasing the pressure to 3 bars shows exactly the same bacteria pattern, although bacteria is observed at 60 s and saturates at  $10^8$  cfu/mL. It is interesting to observe that direct dosing of bacteria into the system makes the propagation process faster and bacteria reaches the consumer at a higher rate than by simply placing it into the tank.

## 6 Conclusions

Many governments around the world are trying to maintain the quality of drinking water delivered to customers by applying certain standards to the water that is pumped out from water stations. However, the condition of the WDN including material, age, cracks, etc., could also impact the water quality through the intrusion of contaminants during the delivery stage. The propagation of *E. coli* bacteria in water distribution networks (WDN) was investigated using an experimental method. The theory that a sudden drop in water pressure within the WDN will result in immediate contaminant (like *E. coli* bacteria) flow into the WDN through cracks and loose joints within the pipes was examined. Our results show that, once the water pump shuts down, water is pumped out from the inside to the outside of the water network which does not allow for immediate bacterial intrusion into the network. After a certain amount of time, which depends on the WDN operating pressure before shutting down, the mixture of the pumped out water and *E. coli* bacteria is sucked into the system. It takes between 3.5 and 10.5 s for the contaminants to start flowing into the system at a network operating pressure of 1–4 bar, and it takes a minimum of 15 s (system operated at 1 bar) and 20 s (system operated at 3 bar) to observe *E. coli* at the system outlet. This contradicts the common theory that contaminant intrusion will be immediately sucked into the system after shutdown. In general, if the water pump shuts down for only a few seconds there is a slim chance for contaminants to be intruded into the system. This is an

indication that minor cracks do not represent a major risk in contaminant intrusion when the system shuts down for only a few seconds. On the other hand, it was found that directly injecting bacteria into the system represents a major risk as it takes about 30–90 s for the bacteria to reach the customer at an operating pressure of 1–3 bar. The contaminant water source represents another major risk as it was found that it takes only 5 s for the *E. coli* bacteria to reach the customer. Although the time to reach the customers is relatively comparable, direct *E. coli* bacterial dosing and contaminant water sources are more dangerous than sucking in the bacteria into the system during low-pressure events. This is because, in the two cases, municipalities will not notice the contamination before it is reported by customers although in the case of a sudden shutdown proper attention is usually given to checking the water quality before pumping it to customers.

**Acknowledgements** This project was funded by the National Plan for Science, Technology, and Innovation (MAARIFAH)—King Abdulaziz City for Science and Technology—through the Science and Technology Unit at King Fahd University of Petroleum and Minerals (KFUPM)—the Kingdom of Saudi Arabia, award number (WAT-2390-04).

## References

- Abo-Munasar, A. (2014). *Decision support system for risk and water quality management in water distribution network*. King Fahd University of Petroleum and Minerals.
- Admassu, M., Wubshet, M., & Gelaw, B. (2005). A survey of bacteriological quality of drinking water in North Gondar. *Ethiopian Journal of Health Development*, 18(2).
- Besner, M., Prévost, M., & Regli, S. (2011). Assessing the public health risk of microbial intrusion events in distribution systems: Conceptual model, available data, and challenges. *Water Research*, 45(3), 961–979.
- Douterelo, I., Boxall, J. B., Deines, P., Sekar, R., Fish, K. E., & Biggs, C. A. (2014). Methodological approaches for studying the microbial ecology of drinking water distribution systems. *Water Research*, 65, 134–156.
- Edberg, S. C., Rice, E. W., Karlin, R. J., & Allen, M. J. (2000). *Escherichia coli*: The best biological drinking water indicator for public health protection. *Journal of Applied Microbiology*, 88(S1), 106S–116S.
- Gorchev, H. G., & Ozolins, G. (2011). WHO guidelines for drinking-water quality. *WHO Chronicle*, 38(3), 104–108.
- Hellard, M. E., Sinclair, M. I., Hogg, G. G., & Fairley, C. K. (2000). Prevalence of enteric pathogens among community based asymptomatic individuals. *Journal of Gastroenterology and Hepatology*, 15(3), 290–293.
- Hellard, M. E., Sinclair, M. I., Forbes, A. B., & Fairley, C. K. (2001). A randomized, blinded, controlled trial investigating the gastrointestinal health effects of drinking water quality. *Environmental Health Perspectives*, 109(8), 773–778.
- Islam, N., Farahat, A., Al-Zahrani, M. A. M., Rodriguez, M. J., & Sadiq, R. (2015). Contaminant intrusion in water distribution networks: Review and proposal of an integrated model for decision making. *Environmental Reviews*, 23(3), 337–352.
- Isovitich, S., & Vanbriessen, J. (2008). Sensor placement and optimization criteria dependencies in a water distribution system. *Journal of Water Resources Planning and Management*, 134(2), 186–196.
- Kirmeyer G. J., Friedman, M., Martel, K. D., Noran, P. F., & Smith, D. (2001). Practical guidelines for maintaining distribution system water quality. *Journal of the American Water Works Association*, 93(7), 62–73. CR–Copyright &#169; 2001 American Water Works.
- LeChevallier, M. W., Babcock, T. M., & Lee, R. G. (1987). Examination and characterization of distribution system biofilms. *Applied and Environment Microbiology*, 53(12), 2714–2724.
- Lin, Y., Li, D., Gu, A. Z., Zeng, S., & He, M. (2016). Bacterial regrowth in water reclamation and distribution systems revealed by viable bacterial detection assays. *Chemosphere*, 144, 2165–2174.
- Moe, C. L., & Rheingans, R. D. (2006). Global challenges in water, sanitation and health. *Journal of Water and Health*, 4(1), 41–57.
- Murphy, H. M., Thomas, M. K., Schmidt, P. J., Medeiros, D. T., McFadyen, S., & Pintar, K. D. M. (2016). Estimating the burden of acute gastrointestinal illness due to Giardia, cryptosporidium, campylobacter, *E. coli* O157 and norovirus associated with private wells and small water systems in Canada. *Epidemiology and Infection*, 144(7), 1355–1370.
- Pimie, M., Szewzyk, U., Szewzyk, R., Manz, W., & Schleifer, K. H. (2000). Microbiological safety of drinking water. *Annual Review of Microbiology*, 54, 81–127.
- Prest, E. I., Hammes, F., Köttsch, S., Van Loosdrecht, M. C. M., & Vrouwenvelder, J. S. (2016). A systematic approach for the assessment of bacterial growth-controlling factors linked to biological stability of drinking water in distribution systems. *Water Science and Technology: Water Supply*, 16(4), 865–880.
- Qu, X., Alvarez, P. J. J., & Li, Q. (2013). Applications of nanotechnology in water and wastewater treatment. *Water Research*, 47(12), 3931–3946.
- Somashekar, K. M., Mahima, M. R., & Manjunath, K. C. (2015). Contamination of water sources in Mysore City by pesticide residues and plasticizer—A cause of health concern. *Aquatic Procedia*, 4(Icwrcoe), 1181–1188.



# Use of Bio-fabricated Silver Nanocomposite Capped with Mud Crab Shell (*Scylla serrata*) Chitosan for Water Purifications and Sustainable Management of Mosquito Vectors at Stagnant Water System in the Semiarid Zone of Tamil Nadu, India

Kadarkarai Murugan, Lan Wang, Jiang Shiou Hwang, Jaganathan Anitha, Devakumar Dinesh, Pandiyan Amuthavalli, Murugan Vasanthakumaran, Suresh Kumar, and Hans-Uwe Dahms

## Abstract

Mosquitoes are the major vectors of many diseases such as the malaria, filariasis, dengue, and Japanese encephalitis. Mosquitoes propagate quite successfully in a variety of aquatic habitats such as drinking water system, manmade water bodies, and sewage contaminated aquatic system. Since, water is essential for all life, without it, life won't progress and at the same time, the quality of the water also important. With the unique structural features present in chitosan bio-polymer helps to bind effectively with fine suspended particles, pollutants,

bacteria, heavy metals etc. The biocompatible and biodegradable nature of chitosan makes it a potential candidate for mosquito breeding water purification purposes. In this regard, chitosan has been extracted from freshwater crab shells *Scylla serrata* and reduced for silver nanoparticle synthesis. It has been utilized as a potent tool in control of young instars of *Aedes aegypti* and its breeding water purification. Bio-synthesized chitosan-reduced silver nanoparticles were characterized by UV-Vis spectrum, Fourier transform infrared spectroscopy (FTIR), scanning electron microscopy (SEM), energy-dispersive X-ray analysis (E-DAX), and X-ray diffraction (XRD). In laboratory condition, the chitosan silver nanocomplex was found to possess toxicity against young instars (I, II, III, and IV) of *Aedes aegypti* at the concentrations of 2, 4, 6, 8, and 10 ppm followed by chitosan treatment alone. The surface stagnant water from dengue vector breeding site checked the water purification parameters, such as water temperature (WT), pH, salinity, dissolved oxygen (DO), total dissolved solids (TDS), and electrical conductivity (EC) by using "µP Based Water & Soil Analysis Kit" (Model 1160). Further, from the results it is clearly postulated that the biomolecules present in the chitosan not only showed biopesticidal activity against mosquito larvae and pupae but also nullified the contaminants in the water and made human usage.

K. Murugan (✉) · J. Anitha · D. Dinesh · P. Amuthavalli  
Division of Entomology, Department of Zoology, School of Life Sciences, Bharathiar University, Coimbatore, Tamil Nadu 641046, India

L. Wang  
School of Life Science, Shanxi University, Taiyuan, 030006, Shanxi, China

J. S. Hwang  
Institute of Marine Biology, National Taiwan Ocean University, Keelung, 20224, Taiwan  
e-mail: [jshwang@ntou.edu.tw](mailto:jshwang@ntou.edu.tw)

J. S. Hwang  
Center of Excellence for Ocean Engineering, National Taiwan Ocean University, Keelung, 20224, Taiwan

J. S. Hwang  
Center of Excellence for the Oceans, National Taiwan Ocean University, Keelung, 20224, Taiwan

M. Vasanthakumaran  
Department of Zoology, Kongunadu Arts and Science College, Coimbatore, 641029, India

S. Kumar  
Department of Medical Microbiology and Parasitology, University Putra Malaysia, 43400 Serdang, Selangor, Malaysia

H.-U. Dahms  
Department of Biomedical Science and Environmental Biology, Kaohsiung Medical University, Kaohsiung, 80424, Taiwan

## Keywords

Mosquito vector • *Aedes aegypti* • Chitosan nanoparticle • Water purification • Water reuse

## 1 Introduction

Mosquitoes transmit pathogens that cause death and disease in humans and animals. It plays a significant role in spreading vector-borne diseases such as malaria, dengue fever, yellow fever, encephalitis and filariasis, and, very recently, Zika virus (Benelli, 2016; Ward and Benelli, 2017). *Aedes aegypti* mosquitoes mostly originated in Africa, and the mosquito has been transported globally throughout the tropical, subtropical, and parts of the temperate world. Dengue is a mosquito-borne viral disease transmitted by female mosquitoes, *Aedes aegypti* and *Aedes albopictus*. Currently, the transmission of dengue has been strappingly reached maximum in urban, semi-urban, and tropical areas worldwide, which have turned out to be an important concern in public health. Dengue infects about half a billion individuals leading to half million hospitalizations with 24,000 deaths worldwide every year (WHO, 2017).

The development of reliable, eco-friendly processes for the synthesis of nano-pesticides is an important aspect of nanotechnology. In mosquito control science, significant efforts have been carried out through investigating the efficacy of botanical products as mosquitocides (Benelli, 2015; Benelli et al., 2017a, 2017b, 2017c). Chitosan has many attractive applications in the field of biotechnology, food and pharmaceutical industry, cosmetics, environmental engineering, agriculture, and aquaculture. Though chemical procedures are widely used to extract chitin and chitosan by utilizing shrimp waste as raw material, there is not much research about how to improve the process for producing chitosan with consistent quality, especially from stored material sources (Hamidi et al., 2008).

Water is a life-sustaining drink and is essential for the survival of all living organisms. However, there are toxic contaminants present in water that cause many life-threatening health risks. So, water should be protected from contamination for public health reasons, and environmental reasons may be due to industrial development, organism breeding in stagnant water, etc. Hence, purification

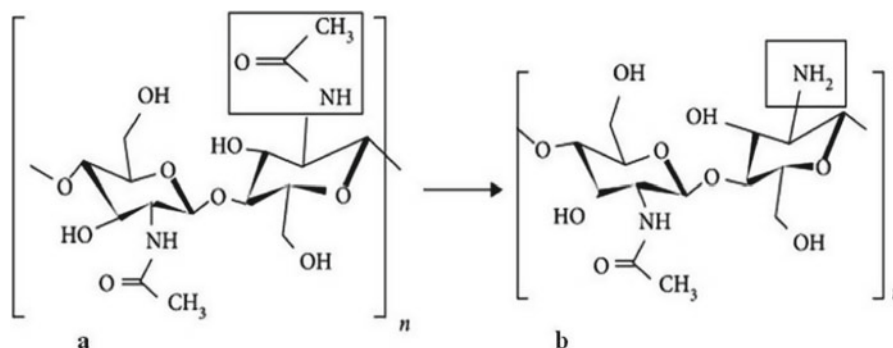
of stagnant water from mosquito breeding sites has always been a challenging task. Chitosan is a natural linear biopolymer extracted from the exoskeleton of the sea crustaceans (crabs, prawns, lobsters, shrimps, etc.). It is a sea-food waste which is produced in abundance in coastal areas. However, this humble-looking material possesses outstanding combination of properties required for water purification, food industries, cosmetics, and biomedical applications (Crini, 2005). In addition to this, chitosan is inexpensive, biodegradable, and nontoxic for mammals (Qin et al., 2006).

Chitosan is natural water coagulant/flocculent and is able to reduce turbidity, color, clay particles, etc., from water. Additionally, considerable savings in chemicals and sludge handling is achieved by using a natural coagulant like chitosan (Diaz et al., 1999). Chitosan is also effective in removal of organic pollutants, heavy metals, bacteria, etc. The US Environment Protection Agency (EPA) has given an official authorization to chitosan for drinking water purification. Hence, in the present study it was aimed to investigate the use of bio-fabricated silver nanomaterials capped with crab shell (*Scylla serrata*) chitosan for water purifications and sustainable management of mosquito vectors at stagnant water systems in Tamil Nadu, India.

## 2 Materials and Methods

### 2.1 Collection and Processing of Crab Shells

Following the method of Murugan et al. (2016), *Scylla serrata* the crab were collected from Parangipettai village, Chidambaram, Tamil Nadu, India. It is stored in ziplock bags and refrigerated overnight. Using a meat tenderizer, the exoskeletons of the crab were cut into smaller pieces. 20 g of crushed exoskeletons was measured using a Mettler balance, then labeled, and oven-dried at 65 °C for four consecutive days to obtain constant weight. The dry weight of the samples was determined, and the moisture content measured was based on the differences between the wet and the dry



Chemical structures of chitin (a) and chitosan (b)



weights. The average moisture content of the crab exoskeletons was 14.33%.

## 2.2 Extraction and Purification of Chitosan from Crab Shell

To dissolve proteins and sugars, the crushed crab exoskeletons were boiled for 1 h with sodium hydroxide (2 and 4% w/v) and thus obtained chitin was removed from the hot plate and allowed to cool for 30 min at room temperature (Lertsutthiwong et al., 2002; Lamarque, 2005). The obtained pure chitosan was demineralized using 1% HCl (v: v) and 2% NaOH according to the method of Huang (2004); 50% NaOH was added to demineralized chitosan, boiled at 100 °C for 2 h on a hot plate, and then cooled for 17–30 min at room temperature. The process was repeated to deacetylate the chitosan powder, and finally creamy-white form of chitosan was obtained (Muzzarelli & Rochetti, 1985).

## 2.3 Synthesis and Characterization of the Chitosan–Silver Nanoparticles

The AgNP was prepared by chemical reduction method, as a reducer the trisodium citrate (1% w/v) was added into AgNO<sub>3</sub> solution, and the mixture was stirred for 2 h and then treated with sonication at 1.5 kW for 30 min. The prepared silver solution was added into the chitosan solution (1% w/v in 1% acetic acid) and stirred for 4 h. The suspension was subsequently centrifuged at 12,000 g for 10 min. A brown-yellow solution indicated the formation of chitosan–Ag nanoparticles and then is used for characterization and biological assays.

The presence of chitosan–Ag nanocomplex was confirmed by sampling the reaction mixture at regular intervals, and the absorption maxima were scanned by UV–Vis, at the wavelength of 200–800 nm in a UV-3600 Shimadzu spectrophotometer at 1-nm resolution. The structure and morphological features of bio-encapsulated nanocomplex were analyzed under scanning electron microscopes (FEI QUANTA-200 SEM). In addition, XRD and EDAX were also analyzed for the presence of metals in the sample (Anitha et al., 2016).

## 2.4 *Aedes Aegypti* Rearing

*Aedes aegypti* eggs were collected from local breeding habitats at the freshwater tank in Kalveerampalayam, Coimbatore (Tamil Nadu, India) and cultured in laboratory for egg hatching in 27 °C and 75–85% RH; 14:10(L/D) photoperiod. Newly emerged larvae and pupae were used for toxicity experiments.

## 2.5 Bio-toxicity Assessment Against *Aedes Aegypti* in Laboratory Condition

In laboratory, the larvae and pupae of *Aedes aegypti* (I, II, III, or IV instars) were exposed for 24 h at the concentrations of 20, 40, 60, 80, and 100 ppm of chitosan broth and 2, 4, 6, 8, and 10 ppm of chitosan silver NPs in triplicates. Dechlorinated water without acetone served as control. Using probit analysis (Finney 1971), LC<sub>50</sub> and LC<sub>90</sub> were calculated as follows (Eq. 1):

$$\text{Percentage mortality} = \left( \frac{\text{Number of dead individuals}}{\text{Number of treated individuals}} \right) \times 100 \quad (1)$$

## 2.6 Stagnant Water Purification Property of Chitosan

The surface stagnant water from dengue vector breeding site was collected during the early morning hour (6.00 AM–8.00 AM) and pooled to check water purification parameters, such as water temperature (WT), pH, salinity, dissolved oxygen (DO), total dissolved solids (TDS), and electrical conductivity (EC) by using “µP Based Water and Soil Analysis Kit” (Model 1160).

Preparation of treatment coagulants followed methods reported by Schwarz (2000). Crab shell was powdered using an electric grinder and mixed with a small amount of clean water to form a paste. The paste was diluted to obtain the following raw water turbidity: >50, 50–150, and >150 mg/L. The final concentration was 50, 30–100, and >150 mg/L, respectively. After filtering insoluble material with a fine-mesh muslin cloth, the coagulant was added and quickly mixed for 30 s. Then, the preparation was covered for at least 1 h without disturbance.

## 2.7 Statistical Analysis

All data were subjected to analysis of variance (ANOVA). LC<sub>50</sub> and LC<sub>90</sub> values and their 95% confidence limits were estimated by getting a probit regression model to the observed relationship between percentage mortality of larvae and logarithmic 27 concentration of the substance. The goodness of the fit test was tested using Chi-Square test AP value of less than 0.05 was considered as a significant departure of the model from the observations. In case of significant departure, a heterogeneity factor was used to calculate the 90% confidence limit for LC<sub>50</sub> and LC<sub>90</sub>. All analysis was carried out using SPSS Software version 16.0.

### 3 Results and Discussion

The chitosan-mediated silver nanoparticles were characterized using UV–Vis spectrophotometer as shown in Fig. 1, where 440 nm was the maximum absorption peak. Murugan et al. (2017b) studied that the chitosan–silver nanoparticles showed UV–Vis absorption at 300–800 nm. The surface morphology of chitosan–AgNP showed spherical shape when tested under FESEM (Fig. 2). The size ranges from 40 to 90 nm in diameter, but only the particles ranging from 1 to 100 nm in diameter are considered as nanoparticles (Huang, 2004). Chitosan-fabricated AgNP-treated *E. tarda* showed a gradual increase of structural damage on surface and cell morphology with increasing concentrations of AgNP at 12.5, 25, and 50 lg/ml during a 6-h incubation period (Dananjaya et al., 2014). Alsabagh et al. (2015) studied the microscopic images of chitosan/Ag NPs/Cu NPs/CNTs multifunctional composite, and its individual components were found to be spherical.

EDX spectrum of chitosan-fabricated AgNP showed a strong Ag signal, confirming the presence of metallic silver (Fig. 3). Furthermore, EDX also showed the presence of Ca, Si, O, and Mg, suggesting that mixed precipitates were present in the chitosan (Usha & Rachel, 2014). The crystal structure and phase purity of the synthesized chitosan silver nanomaterials were identified through the XRD pattern as shown in Fig. 4. The diffractometer was operating at 40 kV and 30 mA, with a step size of  $0.02^\circ$  ( $2\theta$ ). XRD highlighted that chitosan–AgNPs, formed by the reduction of  $\text{AgNO}_3$  mediated by chitosan extract, were crystalline in resonance, consistent with previous reports (Murugan et al., 2017a).

In recent times, various routes have been anticipated for the synthesis of nanomaterials toxic against insect pests. According to the available literature, the bioactivities of the genus chitosan-synthesized nanomaterials against human pests have been scarcely studied. Hence in the present findings, Table 1 postulates the mortality of larval and pupa of *A. aegypti* (I–IV instars) when exposed to chitosan at the concentrations of 100, 200, 300, 400, and 500 ppm with  $\text{LC}_{50}$  239.165 (I), 269.825 (II), 323.823 (III), 390.86 (IV), and 447.011% (pupae). Similarly, Table 2 provides the larval and pupal toxicity of synthesized chitosan silver NPs. The toxicity was found to be higher with the doses of 10, 20, 30, 40, and 50 ppm whose  $\text{LC}_{50}$  was found to be 18.450 (I), 23.303 (II), 31.020 (III), 39.905 (IV), and 50.589% (pupae). The maximum efficacy of AgNPs was observed against the larvae of *A. aegypti*, *C. quinquefasciatus*, and *Rhipicephalus microplus* ( $\text{LC}_{50}$  = 13.90, 11.73, and 8.98 mg/L,  $r^2$  = 0.411, 0.286, and 0.479), respectively (Marimuthu et al., 2011). The comparative study of the larvicidal activity of chitosan nanoparticles and silver was also studied which shows chitosan nanoparticles started mortality at higher

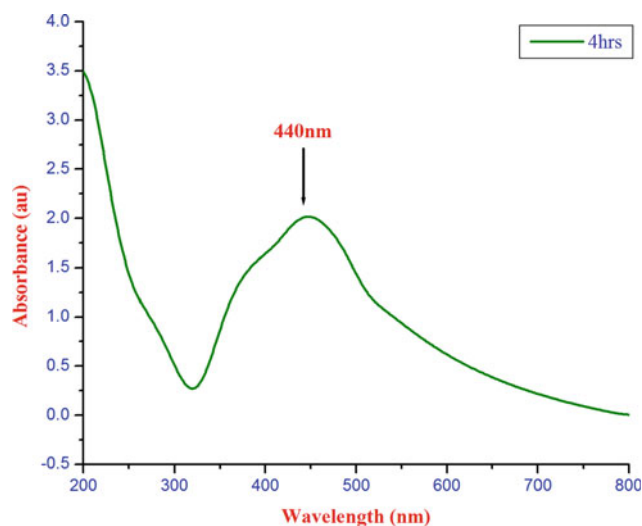


**Fig. 1** UV–vis spectra of chitosan–silver nanoparticles at four hours

concentrations, and it showed uniform rise in mortality of mosquito larvae than silver nanoparticles (Rajesh & Mahadik, 2017).

In laboratory conditions, the water purification properties were done by adding chitosan with stagnant water from mosquito breeding sites and tested its cleaning efficiency. This was achieved by analyzing the water purification properties like pH, temperature, turbidity, salinity, TDS—total dissolved solids, total hardness, alkalinity, chloride, TSS—total suspended solids, and fluoride, respectively. From Table 3, it is clear that the chitosan treatment neutralized the water purification properties at 48 h itself. It also coagulated the debris and dust present in the water as flocculation was naked before the analysis.

Recently, Pontius (2016) reported chitosan demonstrated a much narrower pH range for acceptable turbidity removal when compared to alum and ferric. Earlier, studies of Murugan et al. (2016) demonstrated that the chitosan was effective against human pathogens at lower doses. Nareshkumar et al. (2011) reported mosquitocidal and water purifying properties of different plant extracts (*Cynodon dactylon*, *Aloe vera*, *Hemidesmus indicus*, and *Coleus amboinicus*) on various mosquito vector (*A. stephensi*, *C. quinquefasciatus*, and *A. aegypti*) breeding water samples.

Removal of fine suspended particles from water is the preliminary step of the water filtration/purification process in general. The poly-cationic nature of chitosan carries positive charges along the polymer chain, which can coagulate natural particulates and colloidal materials in stagnant water, which are negatively charged. Electrostatic interaction, adsorption, charge neutralization, inter-particle bridging as well as hydrophobic flocculation work here (Zeng et al., 2008). Thus, chitosan helps in agglomeration/flocculation of the particles and helps to settle down under water for

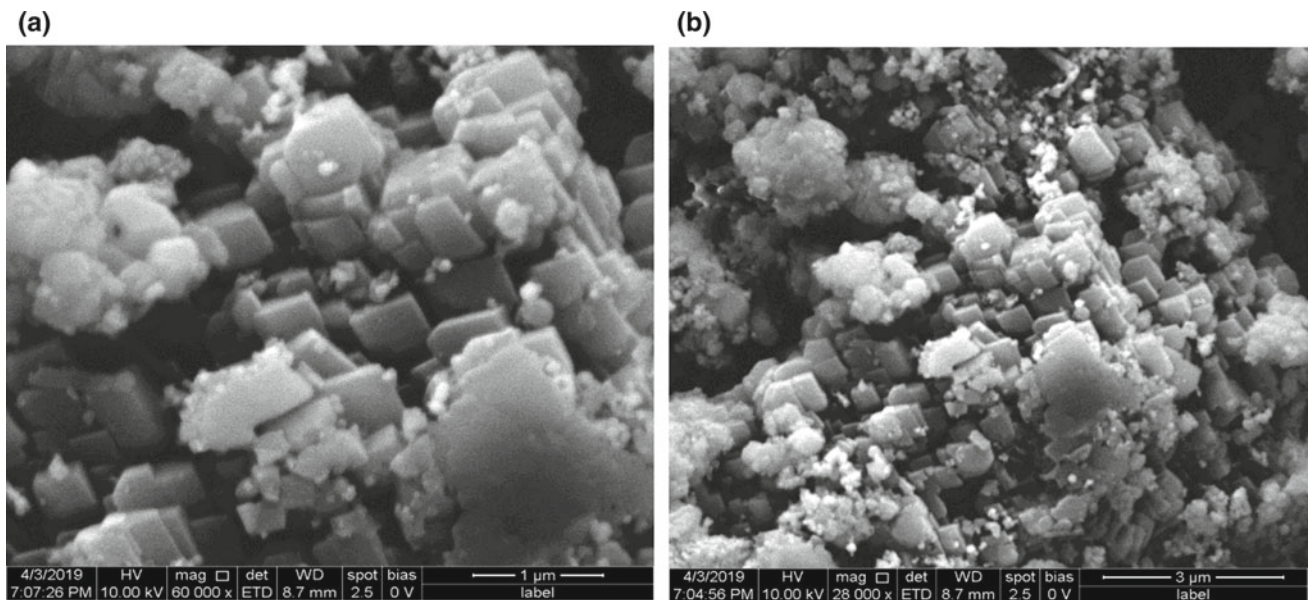
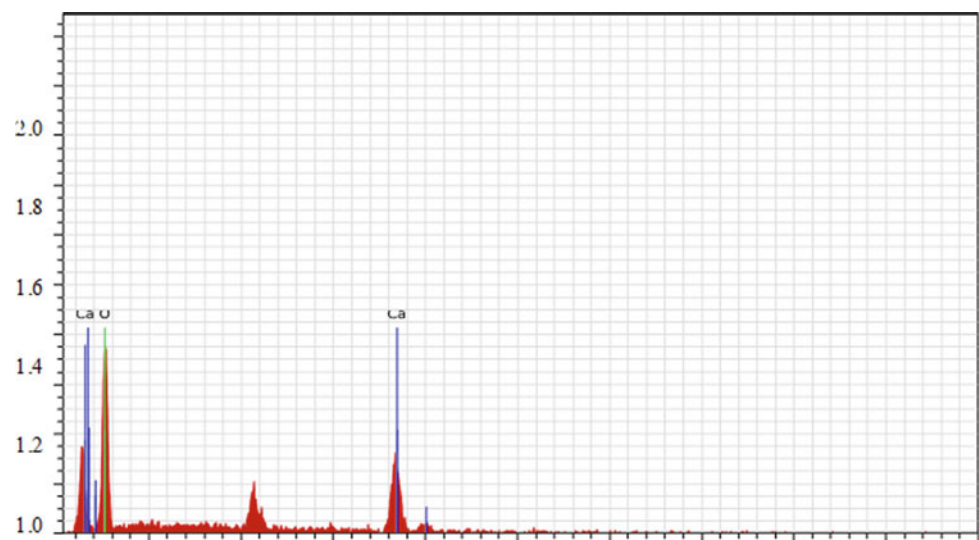


**Fig. 2** Field-emission scanning electron microscopy (FE-SEM) micrograph showing the morphological characteristics of chitosan–silver nanoparticles. **a** Higher magnification. **b** Lower magnification

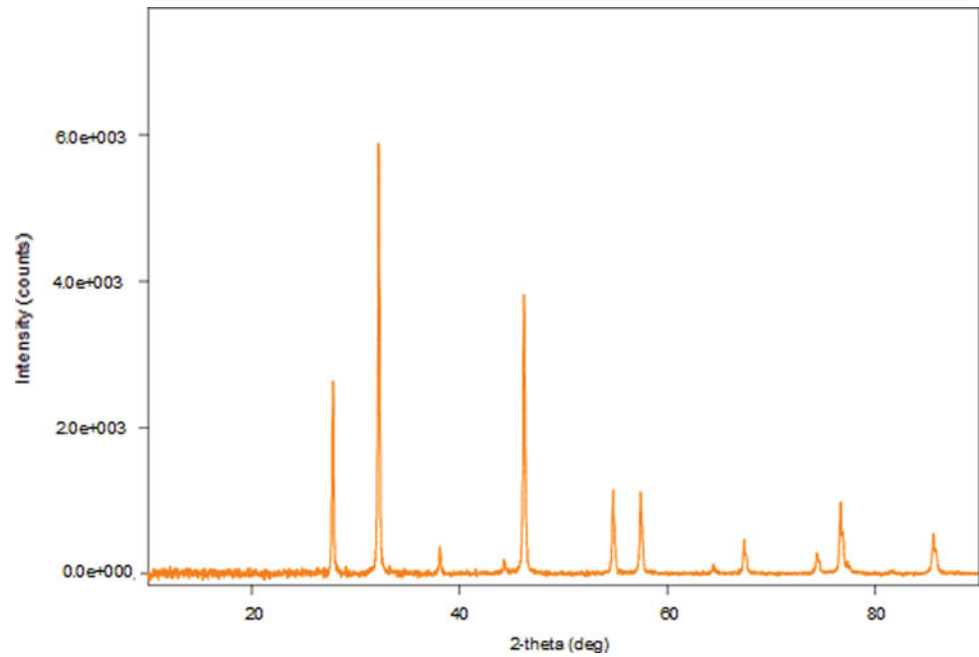
**Fig. 3** Energy-dispersive X-ray (EDX) spectrum of chitosan–silver nanoparticles



filtration. The amine groups in chitosan present along the polymer chain are strongly active with metal ions (Varma et al., 2004) which help to neutralize the chlorine content in water. However, carcinogenic chlorinated hydrocarbons such as trichloromethane, dichlorobenzene, and chlorophenol were also formed as by-products. Chitosan can effectively eliminate trichloromethane from water as the amine groups present along the chitosan chain integrate with the halides in water.

Chitosan can also effectively adsorb organic matters such as phenols, polychlorinated biphenyls, pesticides, and

surfactants. Chitosan (positively charged) can be used to design reverse osmosis/ultrafiltration membranes to filter, adsorb, and kill the microorganisms (negatively charged) in a natural way. Antimicrobial effects of chitosan are attributed to its flocculation and bactericidal activities. Qin et al. (2006) have reported a bridging mechanism for bacterial coagulation by chitosan. Chitosan molecules bind on the microbial cell surface and form an impervious layer around it. Thus, they alter the cell permeability and cause leaking of the intracellular constituents and ultimately death of the microbial cell.

**Fig. 4** XRD pattern of chitosan–silver nanoparticles**Table 1** Larval and pupal toxicity effect of chitosan nanoparticles against dengue vector, *Aedes aegypti*

Stages	LC <sub>50</sub> (LC <sub>90</sub> )	95% confidence limit LC <sub>50</sub> (LC <sub>90</sub> )		Regression equation	$\chi^2$ ( <i>d.f.</i> = 4) (ns)
		Lower	Upper		
Larva I	239.165 (474.173)	213.981 (426.967)	263.513 (545.751)	$y = -1.304 + 0.005x$	0.218
Larva II	269.825 (516.694)	245.347 (475.725)	293.132 (572.850)	$y = -1.401 + 0.005x$	5.030
Larva III	323.823 (623.955)	296.299 (564.171)	353.031 (711.621)	$y = -1.383 + 0.004x$	2.951
Larva IV	390.86 (698.480)	360.240 (626.943)	426.841 (806.158)	$y = -1.622 + 0.004x$	2.041
Pupa	447.011 (739.883)	413.992 (663.562)	490.879 (855.967)	$y = -1.956 + 0.004x$	0.815

No mortality was observed in the control

LC<sub>50</sub> = lethal concentration that kills 50% of the exposed organisms

LC<sub>90</sub> = lethal concentration that kills 90% of the exposed organisms

$\chi^2$  = chi-square value, *d.f.* = degrees of freedom, n.s. = not significant ( $\alpha = 0.05$ )

**Table 2** Larval and pupal toxicity effect of chitosan–silver nanoparticles against dengue vector, *Aedes aegypti*

Stages	LC <sub>50</sub> (LC <sub>90</sub> )	95% confidence limit LC <sub>50</sub> (LC <sub>90</sub> )		Regression equation	$\chi^2$ ( <i>d.f.</i> = 4) (ns)
		Lower	Upper		
Larva I	18.450 (41.484)	15.508 (38.188)	20.902 (45.909)	$y = -1.026 + 0.056x$	2.136
Larva II	23.303 (49.690)	14.767 (41.066)	29.388 (70.298)	$y = -1.132 + 0.049x$	6.702
Larva III	31.020 (61.847)	28.184 (55.795)	33.943 (70.783)	$y = -1.290 + 0.042x$	3.327

(continued)



**Table 2** (continued)

Stages	LC <sub>50</sub> (LC <sub>90</sub> )	95% confidence limit LC <sub>50</sub> (LC <sub>90</sub> )		Regression equation	$\chi^2$ ( <i>d.f.</i> = 4) (ns)
		Lower	Upper		
Larva IV	39.905 (76,663)	36.356 (67.298)	44.515 (91.781)	$y = -1.391 + 0.035x$	1.878
Pupa	50.589 (88.410)	45.635 (76.268)	58.253 (109.151)	$y = -1.714 + 0.034x$	4.306

No mortality was observed in the control

LC50 = lethal concentration that kills 50% of the exposed organisms

LC90 = lethal concentration that kills 90% of the exposed organisms

$\chi^2$  = chi-square value, *d.f.* = degrees of freedom, n.s. = not significant ( $\alpha = 0.05$ )

**Table 3** Water quality parameters of the mosquito-bred water (stagnant water) after the treatment of chitosan

Parameter	Control (before treatment)	Chitosan-treated water		
		24 h	48 h	72 h
pH	8.15 ± 0.79 <sup>a</sup>	7.43 ± 0.63 <sup>a,b</sup>	7.17 ± 0.53 <sup>b</sup>	6.47 ± 0.41 <sup>b,c</sup>
Turbidity (mg/L)	48.56 ± 0.65 <sup>a</sup>	32.89 ± 0.56 <sup>b</sup>	27.45 ± 0.36 <sup>c</sup>	24.43 ± 0.47 <sup>d</sup>
Dissolved oxygen (ppm)	19.2 ± 2.30 <sup>a</sup>	15.32 ± 2.15	10.26 ± 1.5	8.35 ± 1.1
Salinity (ppt)	1.857 ± 0.621 <sup>a</sup>	1.454 ± 0.427 <sup>b</sup>	1.019 ± 0.267 <sup>c</sup>	0.743 ± 0.148 <sup>d</sup>
TDS (mg/l <sup>-1</sup> )	1545. ± 11.53 <sup>a</sup>	1328 ± 12.28 <sup>b</sup>	1148 ± 10.36 <sup>c</sup>	1011 ± 10.24 <sup>c,d</sup>
Total hardness (mg/l <sup>-1</sup> )	158.43 ± 4.52 <sup>a</sup>	137.62 ± 3.86 <sup>b</sup>	125.65 ± 3.16 <sup>b,c</sup>	118.47 ± 3.29 <sup>c</sup>
Alkalinity (mg/l <sup>-1</sup> )	184.04 ± 3.52 <sup>a</sup>	147.08 ± 2.052 <sup>b</sup>	127.02 ± 2.54 <sup>c</sup>	106.18 ± 1.05 <sup>d</sup>
Chloride (mg/l <sup>-1</sup> )	215.32 ± 4.63 <sup>a</sup>	179.53 ± 5.27 <sup>b</sup>	158.12 ± 2.65 <sup>b,c</sup>	131.43 ± 2.57 <sup>c,d</sup>
TSS (mg/l <sup>-1</sup> )	38.74 ± 4.53 <sup>a</sup>	33.78. ± 3.65 <sup>b</sup>	25.39 ± 2.51 <sup>c</sup>	18.57 ± 2.39 <sup>c,d</sup>
Fluoride (mg/l <sup>-1</sup> )	5.36 ± 0.79 <sup>a</sup>	4.62 ± 0.62 <sup>b,c</sup>	3.42 ± 0.49 <sup>c</sup>	2.15 ± 0.74 <sup>c,d</sup>

WT water temperature; TDS total dissolved solids; TSS total suspended solids; mean values within the same row sharing different superscripts are significantly different ( $P < 0.05$ )

## 4 Conclusion

The present investigation was aimed to determine the toxicity against dengue vector *A. aegypti* in laboratory and in field conditions. The study of our interest shows a simple, cost-effective method for the synthesis of silver nanoparticles capped with chitosan isolated from mud crab shell *S. serrata*. The low doses of biopolymer chitosan and spherical-shaped nanoparticle exerted toxicity against young instars of *A. aegypti* in laboratory condition. It also purified the stagnant water from the mosquito breeding site with no adverse effect. Hence, it can be used as a coagulant in treatment of mosquito-bred water and as well instead using chemicals (alum) for water treatment and reducing turbidity in the water system.

**Acknowledgements** Dr. J. Anitha is grateful to the University Grant Commission (New Delhi, India), Project No. PDFSS-2014-15-SC-TAM-10125.

**Conflicts of Interest** The authors declare no conflicts of interest.

**Informed Consent** Informed consent was obtained from all individual participants included in the study.

## References

- Alsabagh, A. M., Fathy, M., & Morsi, R. E. (2015). Preparation and characterization of chitosan/silver nanoparticle/copper nanoparticle/carbon nanotube multifunctional nano-composite for water treatment: Heavy metals removal; kinetics, isotherms and competitive studies. *RSC Advances*, 69(5), 55774–55783.
- Anitha, J., Murugan, K., Panneerselvam, C., Madhiyazhagan, P., Dinesh, D., Vadivalagan, C., Aziz, A. T., Chandramohan, B., Suresh, U., Rajaganesh, R., Subramaniam, J., Nicoletti, M., Higuchi, A., Alarfaj, A. A., Murugan, M. A., Kumar, S., & Benelli, G. (2016). Earthworm-mediated synthesis of silver nanoparticles: A potent tool against hepatocellular carcinoma, *Plasmodium falciparum* parasites and malaria mosquitoes. *Parasitology International*, 65, 276–284.



- Benelli, G. (2015). Plant-borne ovicides in the fight against mosquito vectors of medical and veterinary importance: A systematic review. *Parasitology Research*, *114*, 3201–3212.
- Benelli, G. (2016). Plant-mediated biosynthesis of nanoparticles as an emerging tool against mosquitoes of medical and veterinary importance: A review. *Parasitology Research*, *115*, 23–34.
- Benelli, G., Pavela, R., Iannarelli, R., Petrelli, R., Cappellacci, L., Cianfaglione, K., Afshar, F. H., Nicoletti, M., Canale, A., & Maggi, F. (2017a). Synergized mixtures of Apiaceae essential oils and related plant-borne compounds: Larvicidal effectiveness on the filariasis vector *Culex quinquefasciatus* Say. *Industrial Crops and Products*, *96*, 186–195.
- Benelli, G., Pavela, R., Maggi, F., Petrelli, R., & Nicoletti, M. (2017b). Commentary: Making green pesticides greener? The potential of plant products for nanosynthesis and pest control. *Journal of Cluster Science*, *28*, 3–10.
- Benelli, G., Rajeswary, M., & Govindarajan, M. (2017c). Towards green oviposition deterrents? Effectiveness of *Syzygium lanceolatum* (Myrtaceae) essential oil against six mosquito vectors and impact on four aquatic biological control agents. *Environmental Science and Pollution Research International*, *25*(11), 10218–10227.
- Crini, G. (2005). recent developments in polysaccharide-based materials used as adsorbents in wastewater treatment. *Progress in Polymer Science*, *30*, 38–70.
- Dananjaya, S. H., Godahewa, G. I., Jayasooriya, R. G., Chulhong, O. H., Lee, J., & Zoysa, M. D. (2014). Chitosan silver nanocomposites (CAGNCs) as potential antibacterial agent to control *Vibrio Tapetis*, *5*(5).
- Diaz, A., Rincon, N., Escorihuela, A., Fernandez, N., Chacin, E., & Forster, C. F. (1999). A preliminary evaluation of turbidity removal by natural coagulants indigenous to Venezuela. *Process Biochemistry*, *35*, 391–395.
- Finney, D. J. (1971). Probit analysis. Cambridge University, London 68–78.
- Hamidi, M., Azadim, A., & Rafiei, P. (2008). Hydrogel nanoparticles in drug delivery. *Advanced Drug Delivery Reviews*, *60*, 638–1649.
- Huang, M. (2004). Uptake and cytotoxicity of chitosan molecules and nanoparticles: Effects of molecular weight and degree of deacetylation. *Pharmaceutical Research*, *21*(2), 344–353.
- Lamarque, G. (2005). Physicochemical behavior of homogeneous series of acetylated chitosans in aqueous solution: Role of various structural parameters. *Biomacromolecules*, *6*(1), 131–142.
- Lertsutthiwong, P., How, N. C., Chandkrachang, S., & Stevens, W. F. (2002). Effect of chemical treatment on the characteristics of Shrimp Chitosan. *Journal of Metals, Materials and Minerals*, *12*(1), 11–18.
- Marimuthu, S., Rahuman, A. A., Govindasamy, R., Thirunavukkarasu, S., Arivarasan, V. K., Chidambaram, J., Asokan, B., Zahir, A. A., Elango, G., & Chinnaperumal, K. (2011). Evaluation of green synthesized silver nanoparticles against parasites. *Parasitology Research*, *108*, 1541–2154.
- Murugan, K., Anitha, J., Dinesh, D., Suresh, U., Rajaganesh, R., Chandramohan, B., Subramaniam, J., Paulpandi, M., Vadivalagan, C., Amuthavalli, P., Wang, L., Hwang, J. S., Wei, H., Alsalhi, M. S., Devanesan, S., Kumar, S., Pugazhendy, K., Higuchi, A., Nicoletti, M., & Benelli, G. (2016). Fabrication of nano-mosquito codes using chitosan from crab shells: Impact on non-target organisms in the aquatic environment. *Ecotoxicology and Environmental Safety*, *132*, 318–328.
- Murugan, K., Dinesh, D., Paulpandi, M., Subramaniam, J., Rakesh, R., Amuthavalli, P., Panneerselvam, C., Suresh, U., Vadivalagan, C., Alsalhi, M. S., & Devanesan, S. (2017a). Mangrove helps: Sonneratia alba-synthesized silver nanoparticles magnify guppy fish predation against *Aedes aegypti* young instars and down-regulate the expression of envelope (E) gene in dengue virus (serotype DEN-2). *Journal of Cluster Science*, *28*(1), 437–461.
- Murugan, K., Jaganathan, A., Suresh, U., Rajaganesh, R., Jayasanthini, S., Higuchi, A., Kumar, S., & Benelli, G. (2017b). Towards bio-encapsulation of chitosan-silver nanocomplex? Impact on malaria mosquito vectors, human breast adenocarcinoma cells (MCF-7) and behavioral traits of non-target fishes. *Journal of Cluster Science*, *28*(1), 529–550.
- Muzzarelli, R. A. A., & Rochetti, R. (1985). Determination of the degree of deacetylation of chitosan by first derivative ultraviolet spectrophotometry. *Journal of Carbohydrate Polymers*, *5*, 461–472.
- Nareshkumar, A., Murugan, K., Madhiyazhagan, P., Kovendan, K., Prasannakumar, K., & Thangamani, S. (2011). Mosquitocidal and water purification properties of *Cynodon dactylon*, *Aloe vera*, *Hemidesmus indicus* and *Coleus amboinicus* leaf extracts against the mosquito vectors. *Parasitology Research*, *110*, 1435–1443.
- Pontius, F. W. (2016). Chitosan as a drinking water treatment coagulant. *American Journal of Civil Engineering*, *4*(5), 205–215.
- Qin, C., Li, H., Xiao, Q., Liu, Y., Zhu, J., & Du, Y. (2006). Water solubility of chitosan and its antimicrobial activity. *Carbohydrate Polymers*, *63*, 367–374.
- Rajesh, P., & Mahadik, N. (2017). Chitosan mediated nanoparticles from *Saccharomyces cerevisiae* and its Mosquito larvicidal activity. *Journal of Applied and Advanced Research*, *2*(3), 179–183.
- Usha, C., & Rachel, D. G. A. (2014). Biogenic synthesis of silver nanoparticles by *Acacia nilotica* and their antibacterial activity. *International Journal of Scientific Research*, *3*, 27–29.
- Varma, A. J., Deshpande, S. V., & Kennedy, J. F. (2004). Metal complexation by chitosan and its derivatives. *Carbohydrate Polymers*, *55*, 77–93.
- Ward, M., & Benelli, G. (2017). Avian and simian malaria: Do they have a cancer connection. *Parasitology Research*, *116*(3), 839–845.
- World Health Statistics. (2017). *Monitoring health for the SDGs*.
- Zeng, D., Wu, J., & Kennedy, J. F. (2008). Application of chitosan flocculant to water treatment. *Carbohydrate Polymers*, *71*(1), 135–139.



# Sulphate Removal from Aqueous Solution Using Modified Bentonite

Suaibu O. Badmus and Bassam Tawabini

## Abstract

Sulphate ion is a naturally occurring substance present in various mineral salts that are found in soil and various water supplies. Sulphate ions are generally considered to be non-toxic and therefore not strictly regulated, however, the consumption of drinking water containing high amounts of magnesium or sodium sulphates may result in intestinal discomfort, diarrhoea and consequently dehydration. Although there are numerous traditional adsorbents for sulphate ions removal, it is imperative to develop a cheap, easily accessible, and ecological-friendly adsorbents for the treatment of sulphates in water. This research investigated sulphate ions removal by the synthesized modified bentonite (MB) and acid-digested bentonite (ADB) as an alternative for traditional adsorbents. The modified bentonite was prepared through microwave acid digestion of raw bentonite (RB) and was subsequently coated with cationic poly-electrolytes polydiallyl dimethyl ammonium chloride (poly-DADMAC). The RB, ADB and MB were characterized using scanning electron microscopy/energy dispersive X-ray (SEM/EDX), X-ray diffraction spectroscopy (XRD) and Fourier transform infrared ray (FTIR) spectrometer. The effects of solution pH, contact time, agitation speed, the dosage of the adsorbents and initial concentration of sulphate ions on the removal from synthesized wastewater were investigated in batch adsorption studies. The characterization results showed successful impregnation of poly-DADMAC and changes in the chemical composition of the synthesized adsorbents. Results of the study showed that as high as 65% of 10 ppm sulphates were removed using 20 g/L MB dosage at pH 6, agitation speed 50 rpm within 30 min of treatment time. However, only 16% of sulphates were removed with ADB under the same conditions. The

results also showed that the sulphates removal by modified bentonite followed pseudo-first-order kinetics. It can be concluded that the Poly-DADMAC-modified bentonite has a very good removal capacity for sulphate ions in aqueous solution.

## Keywords

Sulphate • Bentonite • Poly-DADMAC • Adsorption

## 1 Introduction

The sulphate ion is one of the anionic, chemically inert, non-volatile, and non-toxic contaminants commonly found in the natural water systems in concentrations ranging from hundreds to thousands mg/L (Sadik et al., 2015; Bortolini et al., 2018). The maximum concentration level (MCL) of sulphate ions in drinking water in world health organization guidelines is 250 mg/L (Herschly, 2012). The concentration of sulphate ions is usually high in industrial wastewater, acid mine drainage and groundwater (Dong et al., 2011; Sepehr et al., 2014; Tolonen et al., 2015; Kabdaşlı et al., 2016; Pawar et al., 2016; Meng et al., 2019). Moreover, the indiscriminate release of such high sulphates containing wastewaters or effluents and its subsequent accumulation in the environment can adversely affect biodiversity and causes an imbalance in the natural environment (Zuo et al., 2018). Similarly, excessive ingestion of sulphates can endanger human health (Silva et al., 2002). Recently, the negative health and ecological implications of the presence of a high concentration of sulphates in the water attracted the attention of water regulatory agencies (Sadik et al., 2015).

Generally, sulphates can result from different sources and processes such as chemical weathering of minerals-containing sulphur, residential dwelling discharge, volcanic eruption, oxidation of sulphides and sulphur, anaerobic digestion of sulphides, groundwater infiltration, mining

S. O. Badmus (✉) · B. Tawabini  
Department of Geoscience, King Fahd University of Petroleum and Minerals, Dhahran, 31261, Saudi Arabia

drains and commercial, industrial, and agricultural discharges (Dong et al., 2011; Sepehr et al., 2014; Tolonen et al., 2015).

The treatment of sulphates in water is a complicated problem due to its strong stability and high solubility in water (Silva et al., 2010). Traditionally, large numbers of different water remediation technologies have been proposed and adopted in the treatment of sulphates in aqueous solution (Qian et al., 2015; Runtti et al., 2016; Kefeni & Mamba, 2020). Some of the conventional remediation technologies of sulphates include biological treatment (such as fluidized or packed bed reactors, anaerobic bed hybrid reactor and continuously stirred tank reactor) and physico-chemical treatment such as chemical precipitation, adsorption, ion exchange, membrane filtration and reverse osmosis. (Arahman et al., 2017; Fang et al., 2017; Hong et al., 2017; Najib et al., 2017). However, some of these methods are associated with different challenges. For instance, biological treatment encountering difficulties in the supply of carbon sources for the subsurface treatment, maintaining the quality of treated water, management of the treatment generated precipitates and lastly, the rebound of sulphates upon the suspension of the treatment (Zhang and Wang, 2016; Najib et al., 2017). Moreover, the high operational cost, high energy consumption and massive sludge generation are major challenges of physical and chemical treatment methods (Cao et al., 2011; Arahman et al., 2017; Hong et al., 2017). Although adsorption is adjudged the most reliable and attractive approach because of its rapid, efficiency, cost-effectiveness and high selectivity for sulphate ions removal and recovery (Sang et al., 2013; Sadik et al., 2015).

Bentonite is cheap, eco-friendly, non-toxic, readily available and accessible, and thus, commonly deployed in the adsorption of sulphates (Randelović et al., 2012; Moreroa and Ntuli, 2017; Meng et al., 2019). Also, bentonite had shown an impressive adsorptive capacity for cationic contaminants due to its excellent cation exchange capacity, large surface area and negative surface charges (Moreroa & Ntuli, 2017; Alexander et al., 2019). However, the hydrophilicity nature of bentonite hindered its adsorptive capacity for anionic contaminants (Koosha & Hamedi, 2019). Hence, several approaches have been proposed to aid the capacity of bentonite to remove anionic contaminants. Some of these enhancement approaches include surface modification with organic molecules, surfactants and polymers (Meng et al., 2019).

Moreover, previous studies have shown that incorporation or impregnation of organic molecules to bentonite increase its hydrophobicity (Dong et al., 2011; Sang et al., 2013; Moreroa & Ntuli, 2017). Formation of the functionalized bentonite offered better adsorption capacity due to the possession of impressive physico-chemical properties such as excellent mechanical properties, low density and toughness of the hybrid adsorbents. (Rajak et al., 2019; Wahab

et al., 2019). Also, some cationic polymers have been used to modify bentonite for the removal of anionic contaminants such as dyes, BTEX and phosphate (Dong et al., 2011; Sang et al., 2013; Moreroa & Ntuli, 2017). However, there is no clear indication that bentonite coated with polydiallyl dimethyl ammonium chloride has been used to remove sulphate ions from contaminated water.

This study, therefore, investigated the sulphates removal capacity of modified bentonite and acid-digested bentonite. Similarly, the structural, compositional and functional changes of RB with acid digestion and the subsequent functionalization of ADB with polycationic electrolyte (poly-DADMAC) were studied using different characterization techniques. The adsorption kinetics and the optimal treatment conditions of ADB and MB were equally evaluated.

---

## 2 Materials and Methods

### 2.1 Reagents

A commercially available bentonite powder produced by Loba Chemie Pvt Ltd., India was used for this study. PDADMAC chemical of MW ranges between 200,000 and 350,000 kg/mol was purchased from the local market. Deionized (DI) water was produced from the Milli-Q ultra-pure water system (millipore). Also, the sulphates solution was prepared from the sodium sulphates ( $\text{Na}_2\text{HSO}_4$ ) pellet according to the established standard. Here, 1.42 g of  $\text{Na}_2\text{HSO}_4$  was dissolved in 1000 mL DI water to prepare a stock solution of sulphates (1000 mg/L). Then, 10 mg/L of the working solution of sulphates was subsequently prepared from the stock solution. The chemicals and reagents used in this research were of analytical grade.

### 2.2 Preparation of Acid-Digested Bentonite

The acid-digested bentonite (ADB) was produced by mixing 3 g of raw bentonite (RB) in 20 mL of 65% concentrated  $\text{HNO}_3$  in each of the microwave vent vessels. The mixtures were subjected to microwave digestion at 200 °C, 400–1800 W microwave radiation for 10 min in an open glass cylinder reactor. The ADB was subsequently washed with DI water and decanted until the materials (filtrate) was neutral. Thereafter, the ADB was dried to a particle size at 103 °C in the oven for 24 h.

### 2.3 Preparation of Modified Bentonite

The modified bentonite (MB) was synthesized by mixing 5.968 g of ADB in 100 mL of polydiallyl dimethyl

ammonium chloride (poly-DADMAC) solution. The mixture of ADB and poly-DADMAC solution was sonicated for 30mins. Thereafter, the mixture was air-dried at 25–27 °C. Then, the synthesized MB was weighed, characterized and kept for the adsorption batch experiments.

## 2.4 Characterization of Adsorbent

The structural and chemical composition of raw bentonite (RB), acid-digested bentonite (ADB) and modified bentonite (MB) was investigated with field emission scanning electron microscope (FESEM) attached with energy dispersion X-ray. Also, the minerals composition of the RB, ADB and MB surfaces were examined with XRD spectroscopy. Additionally, the successful functionalization or coating of poly-DADMAC on acid-digested bentonite was determined with Fourier transform infrared (FTIR) spectroscopy.

## 2.5 Batch Adsorption Experiments

The batch adsorption studies were carried out at room temperature in graded Erlenmeyer flasks and the flasks were covered with foil to prevent interference of contaminants or extraneous matter. This study was designed to evaluate the effects of adsorbent dosage, contact time, pH and agitation rate in the adsorption of sulphates from water by ADB and MB. In each of the adsorption study, all operation parameters were fixed except the parameter under the investigation. The adsorbent dosage was varied between 2.5 to 20 g L<sup>-1</sup> while the initial concentration of sulphates was 10 mg L<sup>-1</sup>. The required pH of initial concentrations of sulphates was maintained with dropwise addition of either 0.1 M HNO<sub>3</sub> or 0.1 M NaOH solution. Analysis of initial and final concentration of sulphate ions was determined using a dual column Metrohm 850 Professional Ion Chromatograph (Metrohm, Switzerland). The % residual sulphate ions in the water and adsorption capacity  $Q$  (in mg g<sup>-1</sup>) were evaluated according to the general formulae;

$$\text{Residual Sulphates (\%)} = \left[ 1 - \left( \frac{C_i - C_e}{C_i} \right) \right] * 100\%$$

and

$$Q = \frac{C_i - C_e}{\partial}$$

where  $C_i$  and  $C_e$  are initial and final concentrations of sulphates in mg L<sup>-1</sup> while  $\partial$  and  $Q$  are adsorbent dosage and adsorptive capacity in g L<sup>-1</sup> and mg/g, respectively.

## 2.6 The Adsorption Kinetics

Kinetic models were used to estimate the sorption rate and adsorption reaction mechanisms between the adsorbate and adsorbent. For this purpose, pseudo-first-order (PFO), pseudo-second-order (PSO) and intraparticle diffusion (IPD) models were employed to investigate sorption rate and the adsorption reaction mechanisms between sulphate ions and modified bentonite (MB) or acid-digested bentonite (ADB) under the optimal treatment conditions.

The linearized equation of the PFO can be written as;

$$\ln(q_e - q_t) = \ln q_e - K_1 t$$

where  $q_t$  (mg g<sup>-1</sup>) is adsorption capacity of MB or ADB at a contact time,  $t$  (mins) and  $K_1$  is PFO rate constant (in min<sup>-1</sup>);  $q_e$  is the adsorption capacity at equilibrium (mg g<sup>-1</sup>).

The slope and intercept of the curve of  $\ln(q_e - q_t)$  against  $t$  were used to determine rate constant of PFO,  $K_1$ .

The PSO equation (Ho & McKay, 1999) is simplified as;

$$\frac{t}{q_t} = \frac{1}{K_2 q_e^2} + \frac{t}{q_e}$$

$K_2$  is the PSO rate constant (g mg<sup>-1</sup> min<sup>-1</sup>). A linearized graph of  $t/q_t$  against  $t$  produces a slope and intercept that can be used to calculate the rate constant of PSO,  $K_2$ , and theoretical  $q_e$ .

Intraparticle diffusion (IPD)-modified equation (De Castro et al., 2019) can be expressed as;

$$q_t = K_3 t^{1/2} + C$$

$K_3$  is IPD rate constant (mg g<sup>-1</sup> min<sup>-0.5</sup>). A linearized graph of  $q_t$  against  $t^{1/2}$  produces a slope and intercept that can be used to calculate the rate constant of IPD,  $K_3$ . The intercept  $C$  has a nonzero value when there are some other surface phenomena contributing to the rate-determining step, in addition to the IPD.

## 3 Results and Discussion

### 3.1 Materials Characterisation

#### 3.1.1 Surface Morphology of Synthesized Adsorbents

The surface morphological structures of RB, ADB and MB were examined with the aid of FESEM attached with EDX spectrometry. The surface structural morphologies of the RB, ADB and MB are presented in Fig. 1a–c. Also, Fig. 2 showed the EDX spectra of RB, ADB and MB. The RB particles were smooth, fine and large with limited porosity as

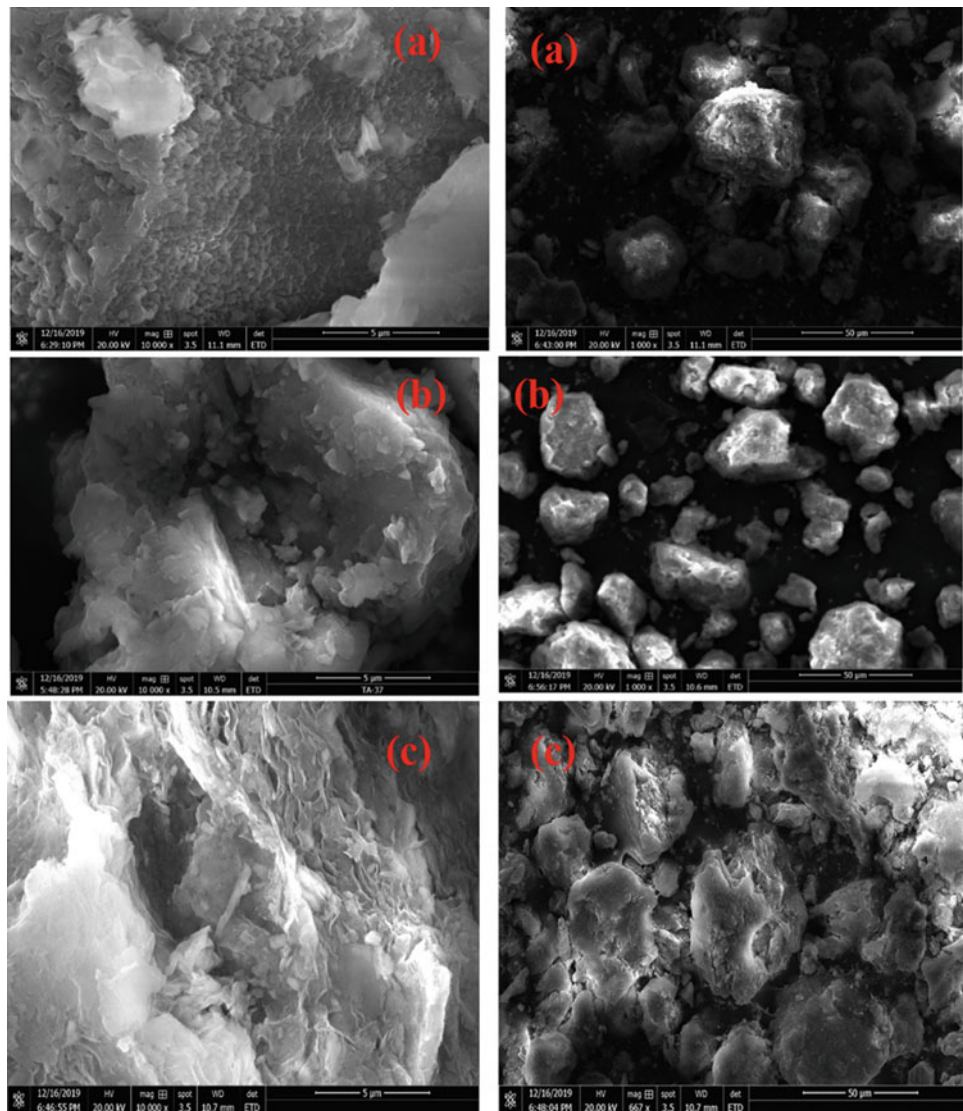
shown in Fig. 1a. However, the ADB particles were arranged singly and dispersed. The size of ADB particles was found to be sharply decreased compared with the RB. Also, the ADB particle pores were more conspicuous. This confirms the successful treatment of raw bentonite with nitric acid. The coating of ADB with poly-DADMAC agglomerate or compact the particles in MB. Hence, MB particles were larger, fined and irregular in shape. The spectrum in Fig. 2a shows that RB contained 22.6% of silicon (Si), 9.6% of aluminium (Al) and the remaining elements which are carbon, oxygen, iron, titanium, chlorine, sodium, magnesium and potassium were 6.6, 47.1, 7.7, 0.8, 0.8, 2.8, 1.3, and 0.9%, respectively. Furthermore, Fig. 2b spectrum reveals that ADB possessed 23.6% of silicon and 5.7% of aluminium as the major components. Similarly, the 2b spectrum showed the disappearance of chlorine and a significant reduction in the cationic constituents of ADB.

However, Fig. 2c spectrum shows the reappearance of chlorine and a slight increase of the cationic composition of MB. This established the successful modification of the ADB surface with poly-DADMAC.

### 3.1.2 Materials Mineral Composition.

In this section, Fig. 3 shown the results of mineral compositions of RB, ADB and MB using X-ray diffraction spectroscopy. Generally, the XRD spectra of quartz,  $\text{Al}_2\text{O}_3$  and  $\text{SiO}_2$  were found in all three materials. However, kaolinite was well pronounced in both RB and ADB while it disappears on MB. Moreover, the quartz was prominent in MB compared with ADB. In summary, the acid treatment sharply decreases the peak intensity of quartz in ADB and subsequent coating of ADB with poly-DADMAC enhanced the intensity of the quartz on MB. The major quartz, kaolinite peaks are shown on both RB and ADB correspond with

**Fig. 1** Structural morphology (a) Raw bentonite, (b) Acid-digested bentonite, (c) Modified bentonite





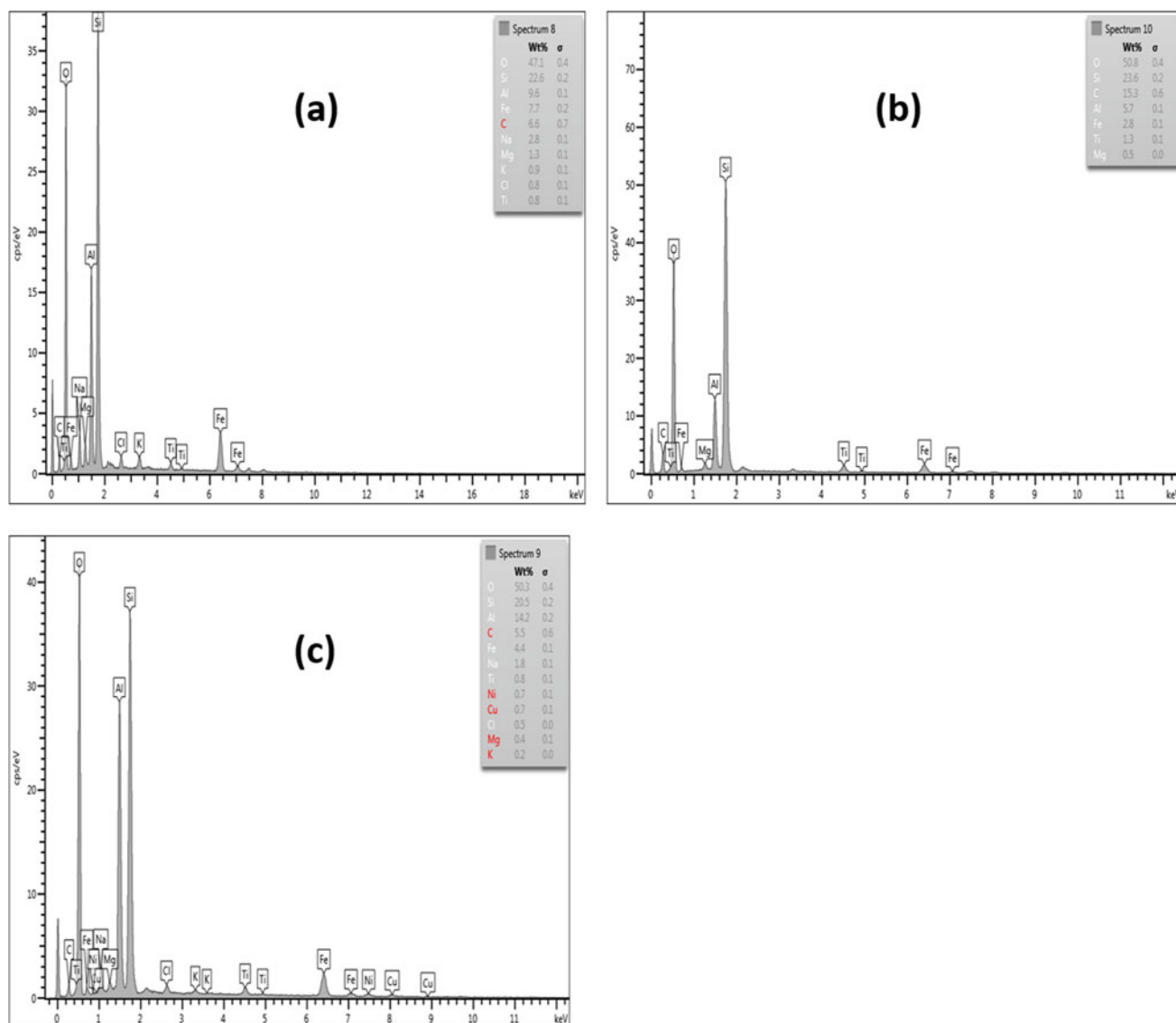


**Fig. 2** EDX spectrum of (a) raw bentonite, (b) acid-treated bentonite and (c) poly-DADMAC-modified bentonite

previous studies (Naswir et al., 2013; Al-Essa, 2018; Moraes et al., 2018).

### 3.1.3 FTIR Analysis of the Adsorbents

FTIR Spectroscopy was used to confirm the presence of the functional groups on the surface of RB, ADB and MB. FTIR spectroscopy was carried out to verify the successful coating of poly-DADMAC on ADB. The synthesized adsorbents (RB, ADB and MB) were scanned from 400 to 4000  $\text{cm}^{-1}$  and the intensity of peaks in the IR spectra was observed. Figure 4 showed the spectra of both RB and ADB and shares a similar fingerprint band and this corresponds with previous studies on bentonite (Moreroa & Ntuli, 2017; Al-Essa, 2018). This suggests that upon an acid treatment, the basic structure of RB did not deteriorate.

The spectrum of the RB exhibits OH group's absorption bands that are associated with both water molecule and octahedral  $\text{Al}^{3+}$  and these are assigned at 3440 and 1639  $\text{cm}^{-1}$ ; 3620  $\text{cm}^{-1}$ , respectively. On ADB, there was an observable decrease in the OH vibration band at 3632  $\text{cm}^{-1}$  and a small decline in the intensity of the band at 792  $\text{cm}^{-1}$ , and this process eventually creates free OH functional group sites on its surface. Also, acid digestion facilitates the disappearance of the stretching bands of  $\text{sp}^3$  C-H at 2920, 2840  $\text{cm}^{-1}$  of RB.

The coating of ADB with polyelectrolytes (poly-DADMAC) caused an increase in the intensity of the C = C absorption peak at 1637  $\text{cm}^{-1}$ . The reappearance of the stretching bands at 2920, 2840  $\text{cm}^{-1}$  and disappearance of 2340, 2370  $\text{cm}^{-1}$  showed effective coating of

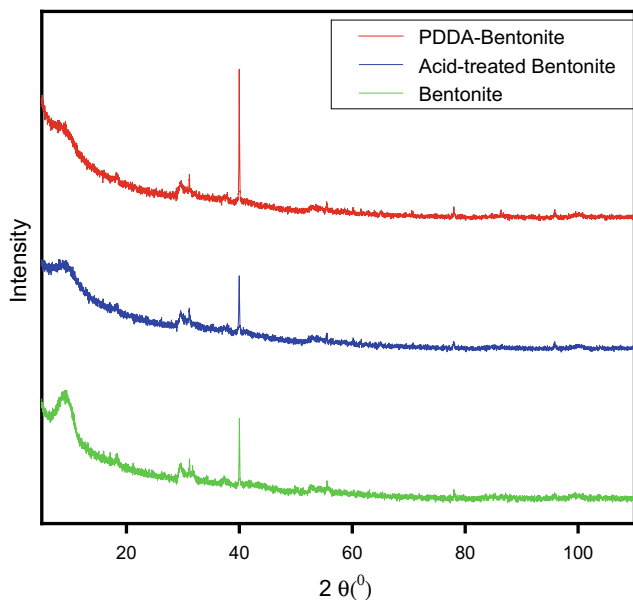


**Fig. 3** XRD spectra of MB, ADB and RB

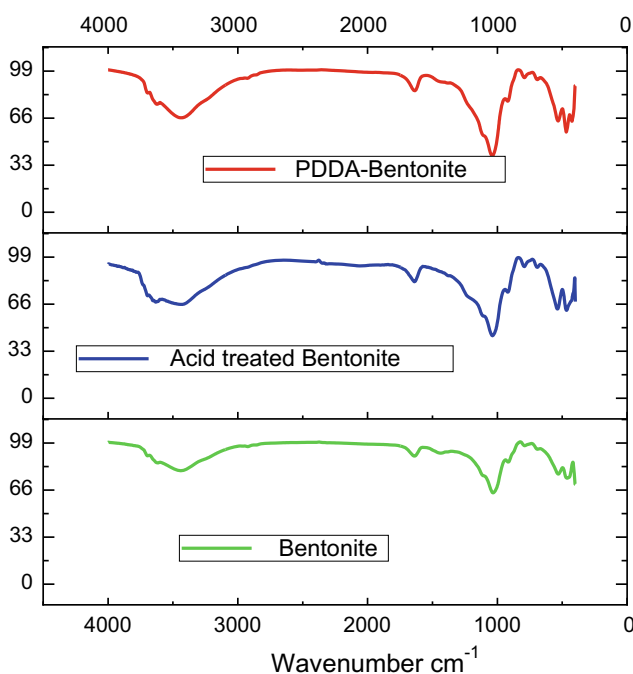


**Fig. 4** FTIR spectra of MB, ADB and RB

poly-DADMAC in MB. The peaks observed at 3439 and 3445  $\text{cm}^{-1}$  of the bentonite and ADB spectra, respectively, were also observed at 3436  $\text{cm}^{-1}$  in MB showing the availability of carboxylic acid and hydroxyl groups.

## 3.2 Removal of Sulphates by ADB and MB

### 3.2.1 Effect of Initial Concentration pH

The optimum pH of the initial concentration of sulphates was determined. Here, the pH of operating media was varied between 4 and 8, and other treatment conditions (time, dosage, agitation speed) were fixed as shown in Fig. 5a. Also, Fig. 5a revealed that sulphate ions can be effectively adsorbed by modified bentonite at pH 6. The efficiencies of sulphates removal decline as the pH increases towards alkalinity. This may be due to the competition that arise between the sulphate ions and hydroxyl ions when the pH of sulphates solution increased, thereby causing a decrease in the vacant sorption sites on the modified bentonites. The similar situation has been previously reported by Dong et al. (2011).

### 3.2.2 Effect of Agitation Speed

The optimum agitation speeds for the adsorption of sulphates by the modified bentonite and acid-digested bentonite were investigated. Here, the agitation speed was varied between 50 rpm to 200 rpm while other treatment conditions like contact time, dosage, and pH were fixed. As shown in Fig. 5b, the efficiency of sulphates removal by modified bentonite at agitation speed 50 rpm shown better performance. Hence, the optimum agitation speed for the removal of sulphates in aqueous solution was 50 rpm. The results have shown that most of the vacant adsorptive binding sites on MB were occupied at 50 rpm and any further increase in agitation speed causes undesirable desorption. The maximum adsorption was attained at 50 rpm comparable with other studies (Moreroa & Ntuli, 2017). Hence, the synthesized modified bentonite can be upscale and deploy in wastewater treatment industries. Although the ADB adsorption efficiencies were poor, however, the highest adsorption capacity of ADB was observed at 100 rpm.

### 3.2.3 Effect of Dosage

In this study, sulphates removal experiments were carried out by applying varying the dosage of ADB and MB from 2.5 to 20  $\text{g L}^{-1}$  at a pH value of 6, 10  $\text{mg L}^{-1}$  sulphate ions concentration, 50 rpm agitation rate, 30 min contact time. As shown in Fig. 5d, sulphate ions adsorption steps up with a rise in the dosage of the synthesized adsorbents, and this followed a similar report (Dong et al., 2011). The highest adsorption of sulphates with both MB and ADB was 65% and 16%, respectively. This shown that modified bentonite adsorbed better than ADB due to the polymer impregnation as shown in characterization studies.

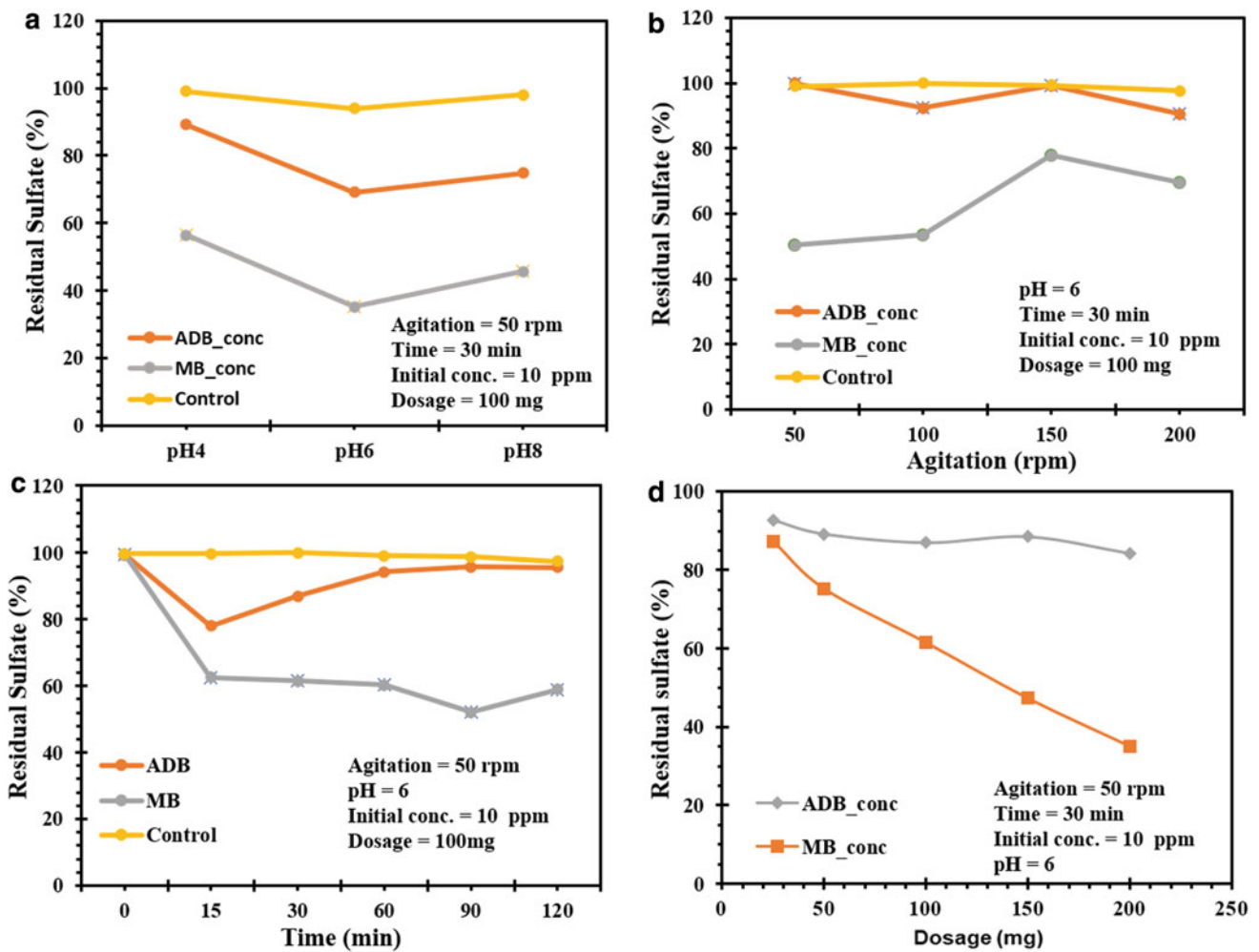


**Fig. 5** (a) Effect of the pH of initial concentration of sulphates. (b) Effects of the agitation speed. (c) Effect of contact time. (d) Effect of adsorbent dosage for the adsorption of sulphates

**Table 1** Adsorption kinetic models values for the sulphates on MB and ADB

	Pseudo-first order		Pseudo-second order			Intraparticle diffusion		
	MB	ADB		MB	ADB		MB	ADB
$R^2$	0.971	0.979	$R^2$	0.9998	0.989	$R^2$	0.990	0.848
$K_1$ (1/min)	0.004	0.0118	$K_2$ (g/mg min)	0.835	-1.160	$K_3$ (mg/g min <sup>0.5</sup> )	0.0063	-0.0298
$Q_e$ (mg/g)	0.131	0.059	$Q_e$ (mg/g)	0.516	0.054	$C$	0.4404	0.353

### 3.2.4 Effect of Contact Time

To investigate the effects of contact time for the removal of sulphate ions by modified bentonite and acid-digested bentonite, 10 mL of 10 mg L<sup>-1</sup> of sulphates was shaken with 0.1 g of ADB and MB. Other treatment conditions, pH and agitation speed, were fixed to examine the effect of contact time. As shown in Fig. 5c, after 30 min of shaking the solution, there was no significant increment in the removal efficiencies of MB. Hence, the optimum contact time for the removal of sulphates in aqueous solution was

30 min. These results have shown that most of the vacant adsorptive binding sites on MB had been occupied within 30 min. In other similar studies, the maximum adsorption of sulphates from aqueous solution usually takes between 4 and 24 h (Dong et al., 2011; Moreroa & Ntuli, 2017). The ADB adsorption efficiencies were poor owing largely to its hydrophilicity. Expectedly, the highest adsorption capacity of ADB was observed at 15 min and desorption started immediately and the binding sites were fully occupied.

### 3.2.5 Adsorption Kinetics

The experimental results obtained from the effect of contact time were fitted in PFO, PSO and IP diffusion kinetic models. The rate of constants, correlation coefficients and theoretical adsorption capacities at the equilibrium was shown in Table 1. The values of correlation coefficients and constant rate of the kinetic models for both ADB and MB showed that experimental data fitted effectively with pseudo-second order. Similarly, the values of estimated theoretical adsorptive capacity at equilibrium revealed clearly that modified bentonite significantly performed better than acid-digested bentonite for the adsorption of sulphates in aqueous solution. The results have shown that there was an exchange of ionic reaction between the chloride ions of the impregnated poly-DADMAC and sulphate ions, thus the removal of sulphates was facilitated by chemical sorption. Therefore, the impregnation of acid-digested bentonite with poly-DADMAC adequately enhanced the adsorption of sulphates in aqueous solution. The observable enhanced adsorption capacity and chemisorption of modified bentonite by effective polymer functionalization or modification have been previously reported (Dong et al., 2011; Sang et al., 2013). Also, the intraparticle models for both MB and ADB were straight lines and the intercepts were nonzero. Hence, the diffusion mechanisms occurred during the adsorption process. However, the IPD was not the rate of determining or controlling factors for adsorption of sulphate ions by MB and ADB.

## 4 Conclusion

This investigation showed the effectively removal of sulphate ions from aqueous solutions by the modified bentonite. However, the adsorption capacity of acid-digested bentonite (ADB) was not impressive and satisfactory for upscaling. The surface of the modified bentonite was rendered organophilic and hydrophobic after the coating of ADB with the polycationic electrolytes poly-DADMAC. The optimal adsorption conditions pH, dosage, agitation speed and time of modified bentonite (MB) were established. The adsorption kinetic models showed that the adsorption of sulphates on the surface of modified bentonite followed pseudo-second order. The IPD model demonstrated diffusion occurred simultaneously with the adsorption process. However, the IP diffusion model was not the rate-controlling factor of the adsorption process. In conclusion, the significant sulphate ions removal by the modified bentonite can be achieved through appropriate treatment conditions, and the process can be upscaled and deployed in wastewater treatment industries.

## References

- Al-Essa, K. (2018). Activation of Jordanian bentonite by hydrochloric acid and its potential for olive mill wastewater enhanced treatment. *Journal of Chemistry*. <https://doi.org/10.1155/2018/8385692>
- Alexander, J. A., Ahmad Zaini, M. A., Surajudeen, A., Aliyu, E. N. U., & Omeiza, A. U. (2019). Surface modification of low-cost bentonite adsorbents—A review. *Particulate Science and Technology*, 37, 534–545. <https://doi.org/10.1080/02726351.2018.1438548>.
- Arahman, N., Mulyati, S., Lubis, M. R., Takagi, R., & Matsuyama, H. (2017). Removal profile of sulfate ion from mix ion solution with different type and configuration of anion exchange membrane in electrodialysis. *Journal of Water Process Engineering*, 20, 173–179. <https://doi.org/10.1016/j.jwpe.2017.10.007>.
- Bortolini, L., Maucieri, C., & Borin, M. (2018). A tool for the evaluation of irrigation water quality in the arid and semi-arid regions. *Agronomy*, 8, 1–15. <https://doi.org/10.3390/agronomy8020023>.
- Cao, W., Dang, Z., Zhou, X. Q., Yi, X. Y., Wu, P. X., Zhu, N. W., & Lu, G. N. (2011). Removal of sulphate from aqueous solution using modified rice straw: Preparation, characterization and adsorption performance. *Carbohydrate Polymers*, 85, 571–577. <https://doi.org/10.1016/j.carbpol.2011.03.016>.
- De Castro, L. F., Brandão, V. S., Bertolino, L. C., De Souza, W. F. L., & Teixeira, V. G. (2019). Phosphate adsorption by montmorillonites modified with lanthanum/iron and a laboratory test using water from the jacarepaguá lagoon (RJ, Brazil). *Journal of the Brazilian Chemical Society*, 30, 641–657. <https://doi.org/10.21577/0103-5053.20180236>
- Dong, R., Liu, Y., Wang, X., & Huang, J. (2011). Adsorption of sulfate ions from aqueous solution by surfactant-modified palygorskite. *Journal of Chemical and Engineering Data*, 56, 3890–3896. <https://doi.org/10.1021/je200544n>.
- Fang, P., Tang, Z. X. Z. J., Chen, X. B., Huang, J. H., Tang, Z. X. Z. J., Cen, C. P., et al. (2017). Sulfate removal from wastewater using ettringite precipitation: Magnesium ion inhibition and process optimization. *Journal of Environmental Management*, 196, 518–526. <https://doi.org/10.1155/2018/1265168>.
- Herschly, R. W. (2012). Water quality for drinking: WHO guidelines. *Encyclopedia of Earth Sciences Series*, 876–883. [https://doi.org/10.1007/978-1-4020-4410-6\\_184](https://doi.org/10.1007/978-1-4020-4410-6_184)
- Ho, Y., & McKay, G. (1999). Pseudo-second order model for sorption processes. *Process Biochemistry*, 34, 451–465. [https://doi.org/10.1016/S0032-9592\(98\)00112-5](https://doi.org/10.1016/S0032-9592(98)00112-5).
- Hong, S., Cannon, F. S., Hou, P., Byrne, T., & Nieto-Delgado, C. (2017). Adsorptive removal of sulfate from acid mine drainage by polypyrrole modified activated carbons: Effects of polypyrrole deposition protocols and activated carbon source. *Chemosphere*, 184, 429–437. <https://doi.org/10.1016/j.chemosphere.2017.06.019>.
- Kabdasli, I., Bilgin, A., & Tünay, O. (2016). Sulphate control by ettringite precipitation in textile industry wastewaters. *Environmental Technology (United Kingdom)*, 37, 446–451. <https://doi.org/10.1080/09593330.2015.1026245>.
- Kefeni, K. K., & Mamba, B. B. (2020). Evaluation of charcoal ash nanoparticles pollutant removal capacity from acid mine drainage rich in iron and sulfate. *Journal of Cleaner Production*, 251, 119720. <https://doi.org/10.1016/j.jclepro.2019.119720>.
- Koosha, M., & Hamed, S. (2019). Intelligent Chitosan/PVA nanocomposite films containing black carrot anthocyanin and bentonite nanoclays with improved mechanical, thermal and antibacterial properties. *Progress in Organic Coatings*, 127, 338–347. <https://doi.org/10.1016/j.porgcoat.2018.11.028>.

- Meng, B., Guo, Q., Men, X., Ren, S., Jin, W., & Shen, B. (2019). Preparation of modified bentonite by polyhedral oligomeric silsesquioxane and sodium dodecyl sulfate in aqueous phase and its adsorption property. *Materials Letters*, 253, 71–73. <https://doi.org/10.1016/j.matlet.2019.05.144>.
- Moraes, D. S., Miranda, L. C. R., Angélica, R. S., Rocha Filho, G. N., & Zamian, J. R. (2018). Functionalization of bentonite and vermiculite after the creation of structural defects through an acid leaching process. *Journal of the Brazilian Chemical Society*, 29, 320–327. <https://doi.org/10.21577/0103-5053.20170143>
- Moreroa, M., & Ntuli, F. (2017). Removal of sulphates from acid mine drainage using TDTMA modified bentonite. *Lecture Notes in Engineering and Computer Science*, 2, 674–678.
- Najib, T., Solgi, M., Farazmand, A., Heydarian, S. M., & Nasernejad, B. (2017). Optimization of sulfate removal by sulfate reducing bacteria using response surface methodology and heavy metal removal in a sulfidogenic UASB reactor. *Journal of Environmental Chemical Engineering*, 5, 3256–3265. <https://doi.org/10.1016/j.jece.2017.06.016>.
- Naswir, M., Arita, S., & Marsi, S. (2013). Characterization of bentonite by XRD and SEM-EDS and use to increase PH and color removal, Fe and organic substances in peat water. *Journal of Clean Energy Technologies*, 1, 313–317. <https://doi.org/10.7763/jocet.2013.v1.71>.
- Pawar, R. R., Lalmunsiama, Bajaj, H. C., Lee, S. M. (2016). Activated bentonite as a low-cost adsorbent for the removal of Cu(II) and Pb (II) from aqueous solutions: Batch and column studies. *Journal of Industrial and Engineering Chemistry*, 34, 213–223. <https://doi.org/10.1016/j.jiec.2015.11.014>
- Qian, J., Lu, H., Jiang, F., Ekama, G. A., & Chen, G. H. (2015). Beneficial co-treatment of simple wet flue gas desulphurization wastes with freshwater sewage through development of mixed denitrification-SANI process. *Chemical Engineering Journal*, 262, 109–118. <https://doi.org/10.1016/j.cej.2014.09.066>.
- Rajak, D. K., Pagar, D. D., Menezes, P. L., & Linul, E. (2019). Fibre-reinforced polymer composites: Manufacturing, properties, and applications. *Polymers (Basel)*, 11(10), 1667. <https://doi.org/10.3390/polym11101667>.
- Randelović, M., Purenović, M., Zarubica, A., Purenović, J., Matović, B., & Momčilović, M. (2012). Synthesis of composite by application of mixed Fe, Mg (hydr)oxides coatings onto bentonite—A use for the removal of Pb(II) from water. *Journal of Hazardous Materials*, 199–200, 367–374. <https://doi.org/10.1016/j.jhazmat.2011.11.025>.
- Runtti, H., Luukkonen, T., Niskanen, M., Tuomikoski, S., Kangas, T., Tynjälä, P., et al. (2016). Sulphate removal over barium-modified blast-furnace-slag geopolymer. *Journal of Hazardous Materials*, 317, 373–384. <https://doi.org/10.1016/j.jhazmat.2016.06.001>.
- Sadik, R., Lakhale, R., Hssaine, N., ElHatimi, W., Diouri, M., & Sabbar, E. (2015). Sulfate removal from wastewater by mixed oxide-LDH: Equilibrium, kinetic and thermodynamic studies. *Journal of Materials and Environmental Science*, 6, 2895–2905.
- Sang, P. L., Wang, Y. Y., Zhang, L. Y., Chai, L. Y., & Wang, H. Y. (2013). Effective adsorption of sulfate ions with poly (m-phenylenediamine) in aqueous solution and its adsorption mechanism. *Transactions of Nonferrous Metals Society of China (English Edition)*, 23, 243–252. [https://doi.org/10.1016/S1003-6326\(13\)62452-8](https://doi.org/10.1016/S1003-6326(13)62452-8)
- Sephehr, M. N., Zarrabi, M., Kazemian, H., Amrane, A., Yaghmaian, K., Ghaffari, H. R., et al. (2014). Removal of hardness agents, calcium and magnesium, by natural and alkaline modified pumice stones in single and binary systems. *Applied Surface Science*, 274, 295–305. <https://doi.org/10.1016/j.apsusc.2013.03.042>.
- Silva, A. J., Varesche, M. B., Foresti, E., & Zaiat, M. (2002). Sulphate removal from industrial wastewater using a packed-bed anaerobic reactor. *Process Biochemistry*, 37, 927–935. [https://doi.org/10.1016/S0032-9592\(01\)00297-7](https://doi.org/10.1016/S0032-9592(01)00297-7).
- Silva, R., Cadorin, L., & Rubio, J. (2010). Sulphate ions removal from an aqueous solution: I. Co-precipitation with hydrolysed aluminum-bearing salts. *Minerals Engineering*, 23, 1220–1226. <https://doi.org/10.1016/j.mineng.2010.08.016>.
- Tolonen, E. T., Rämö, J., & Lassi, U. (2015). The effect of magnesium on partial sulphate removal from mine water as gypsum. *Journal of Environmental Management*, 159, 143–146. <https://doi.org/10.1016/j.jenvman.2015.05.009>.
- Wahab, N., Saeed, M., Ibrahim, M., Munir, A., Saleem, M., Zahra, M., & Waseem, A. (2019). Synthesis, characterization, and applications of silk/bentonite clay composite for heavy metal removal from aqueous solution. *Frontiers in Chemistry*, 7, 1–12. <https://doi.org/10.3389/fchem.2019.00654>.
- Zhang, M., & Wang, H. (2016). Preparation of immobilized sulfate reducing bacteria (SRB) granules for effective bioremediation of acid mine drainage and bacterial community analysis. *Minerals Engineering*, 92, 63–71. <https://doi.org/10.1016/j.mineng.2016.02.008>.
- Zuo, K., Kim, J., Jain, A., Wang, T., Verduzco, R., Long, M., & Li, Q. (2018). Novel composite electrodes for selective removal of sulfate by the capacitive deionization process. *Environmental Science and Technology*, 52, 9486–9494. <https://doi.org/10.1021/acs.est.8b01868>.



# Climate Change and Water Resources



# Rainfall Change and Spatial-Temporal Aspects of Agricultural Drought in Syria

Safwan Mohammed, Karam Alsafadi,  
Seyed Mohammad Nasir Mousavi, and Endre Harsányi

## Abstract

In the last decade, Syria has witnessed a dramatic change in rainfall patterns. These changes have badly affected vegetation cover and agricultural production. Thus, the aim of this research is to track agricultural drought changes over Syria and to highlight the most vulnerable zones to them. To achieve the study aim, monthly precipitation data observed at 36 metrological stations uniformly distributed over Syria were collected. After that, dataset was checked for homogeneity. The Standardized Precipitation Index (SPI) was then applied to detect agricultural drought. In the final steps, the results were driven to GIS and interpolated using the 'Kriging' method. The results showed that rainfall had decreased across Syria from 1990 to 2010. However, the years between 2006 and 2010 were the worst of the studied periods. Similarly, the Mann–Kendall test showed a negative trend for agricultural drought in almost all of the studied stations. All in all, this research emphasizes the negative trends of rainfall in Syria and the positive trend of agricultural drought.

## Keywords

Drought • SPI • Climate change • Syria

## 1 Introduction

Drought is one of the natural disasters that has been accelerated lately by climate change and become more intense, causing devastating damage in agricultural, environmental, and economic sectors all over the world (Rashid & Beec-ham, 2019). Generally, drought is a sudden climatic event characterized by a reduction in the amount of precipitation from the normal range over months to years. However, drought definition can vary from sector to sector due to its complexity and spatial variation from one place to another (Quiring & Papakryiakou, 2003). Within this context, drought can be categorized into four types: (1) meteorological drought; (2) hydrological drought; (3) agricultural drought; (4) socioeconomic drought; among them agricultural drought has the most serious impacts on ecosystems (Khanian et al., 2018; Alsafadi et al., 2020). Thus, many drought indices have been developed for the assessment and monitoring of drought which serve as a tool for many purposes, such as tracking the severity of drought and its distribution, as well as calculating the probability of drought as an early warning system. Even though many researchers have documented the effects and repercussions of drought on the agricultural sector, few studies can be found about the Middle East, and especially about Syria.

Syria, located in the Middle East, has suffered from drought episodes many times (Amini et al., 2016). But recently, the drought cycle has become more severe, leading to catastrophic sequences in many sectors such as agricultural and economic sectors. Nonetheless, few studies can be found about the drought in Syria with different time scales (e.g., Selby et al., 2017; Mathbout et al., 2018). Within this context, the main aim of this paper is to track agricultural drought changes over Syria and to highlight the zones most prone to drought, so that they can be addressed by the decision-makers in the rehabilitation stage after the conflict.

S. Mohammed (✉) · S. M. N. Mousavi · E. Harsányi  
Institution of Land Utilization, Technology and Regional  
Planning, University of Debrecen, Debrecen, 4032, Hungary  
e-mail: [safwan@agr.unideb.hu](mailto:safwan@agr.unideb.hu)

K. Alsafadi  
School of Geographical Sciences, Nanjing University of  
Information Science and Technology, Nanjing, 210044, China

## 2 Materials and Methods

### 2.1 Study Area and Data Collection

Syria is located in the Middle East, between latitude  $34.8021^{\circ}$  N and longitude  $38.9968^{\circ}$  E (Fig. 1). Syria's climate is classified as continental and dry, especially in the eastern parts of the country, with air temperatures reaching  $42^{\circ}\text{C}$  in summers and with very cold nights ( $<0^{\circ}\text{C}$ ) in winter. Climate is generally moderate close to the Mediterranean and in mountainous regions. The average annual rainfall ranges between 750 and 1000 mm (the coast and the western mountains) and 250 and 500 mm (inland regions). In eastern and central Syria, rainfall decreases to less than 25 mm/year. Syria has an area of 18.5 million ha, of which 6.5 million are arable land (1.4 million ha are irrigated, and 3.3 million ha are rainfed), with the irrigated area concentrated in the eastern part of the country (Deir ez-Zor, Al-Hasakah, and Raqqa). Generally, agriculture contributes 17.6–22% to GDP, and the common crops are wheat, barley, cotton, and olives (Mohammed et al., 2020).

Monthly and yearly rainfall data were collected from 36 observed metrological stations for the period 1990–2010. Data were provided by the Syrian Ministry of Agriculture (MoA). All stations are free from any impact of temporal inhomogeneity. As shown in Fig. 1, the stations are evenly distributed over space, covering the main climatic regions in Syria.

### 2.2 Trend Detection

Changes in rainfall amounts were assessed using calculated moving average by grouping the time series (1990–2010) for every station into four groups G1(1990–1995); G2 (1995–2000); G3 (2000–2005); and G4 (2005–2010). In purpose to track the changes in rainfall amount, the average rainfall was calculated per each climatic station in each group of the following G1; G2; G3; and G4, then subtracted from the general average of each station over the entire time series (1990–2010). In the final step, results were driven to GIS and interpolated using 'Kriging' method.

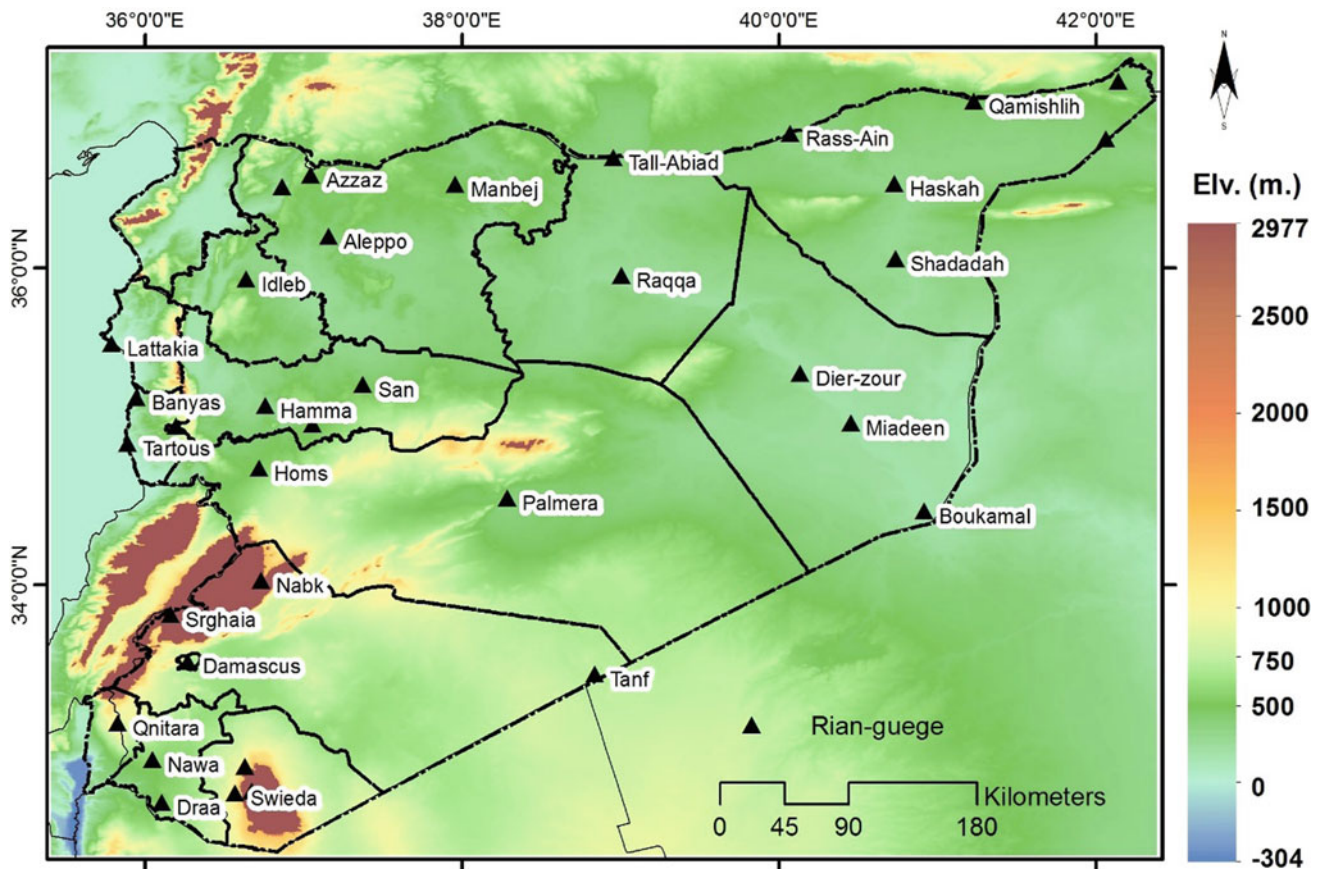


Fig. 1 Study area

**Table 1** SPI categories (McKee et al., 1993)

SPI value	Drought category
0 to -0.99	Mild drought
-1.00 to -1.49	Moderate drought
-1.5 to -1.99	Severe drought
-2.00 or less	Extreme drought

### 2.3 Standardized Precipitation Index (SPI)

Among 50 different drought indicators and indices (Enenkel et al., 2018), we chose the SPI (McKee et al., 1993) for detecting drought vulnerability in Syria, because it only needs monthly rainfall data which is available for us. On the other hand, comparing with the other indicators and indices,

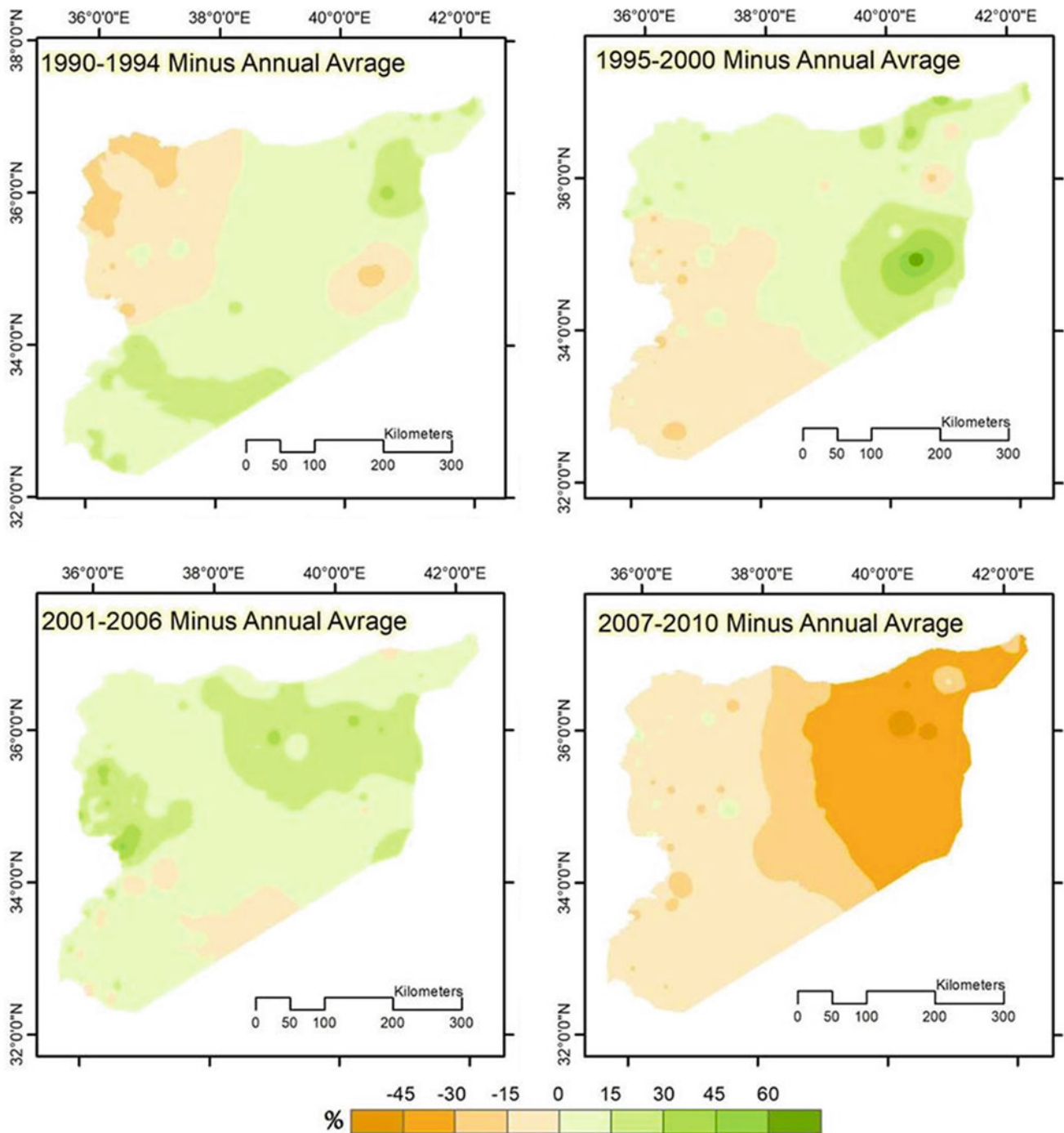


**Fig. 2** Rainfall changes over Syria from 1990 to 2010

the SPI index is less complicated and can be easily used to identify rainfall deficit for multiple time scale which give an accurate indicator of drought trend in any studied location (Lana et al., 2001; Santos et al., 2010).

Statistically, SPI converts the gamma distribution probability into a series of linear data with natural distribution, where the mean value is equal to zero and variance equal to 1 as follows:

$$g(x) = \frac{1}{B^a \Gamma(a)} x^{a-1} e^{-x/B}$$

$$\Gamma(a) = \int_0^{\infty} y^{a-1} e^{-y} dy$$

where

$\Gamma(a)$ : gamma distribution probability,  $x$  rainfall,  $a$ : shape parameter, and  $B$ : scale parameter [for details see Yang et al. (2018)]. SPI values range between (+2.00 or more) and (-2.00 or less) for wet and drought conditions, respectively, (Table 1).

In this study, the SPI was calculated for detecting agricultural drought in Syria by using the SPI- software which recommended by the World Meteorological Organization (WMO) <https://drought.unl.edu/droughtmonitoring/SPI/SPIProgram.aspx> (World Meteorological Organization (WMO) 2012). The SPI was calculated for three variable time scales: 1, 3, and 6 months, which reflecting drought events affecting agricultural system (World Meteorological Organization (WMO), 2012). In the next step, the well-known principal component analysis (PCA) was calculated for the SPI time series for defining the patterns of drought co-variability (Raziei et al., 2009). The PCA is a standard statistical method which consists in computing the covariance matrix of the SPI data with the corresponding eigenvalues and eigenvectors (World Meteorological Organization (WMO), 2012). In the next step, the varimax rotation had been applied to the “loadings” (the correlation between the SPI time series at single stations and the corresponding PCA) to identify the dominant spatial patterns of variability.

In order to determine if the SPI series has a statistically significant trend, the MK test was applied ( $H_0$ : there is no trend in the series;  $H_a$ : there is a trend in the series). The aim was to detect the trends of drought within the study area. In the final step, SPI results were keyed to GIS and interpolated using ‘Kriging’ method.

### 3 Results and Discussion

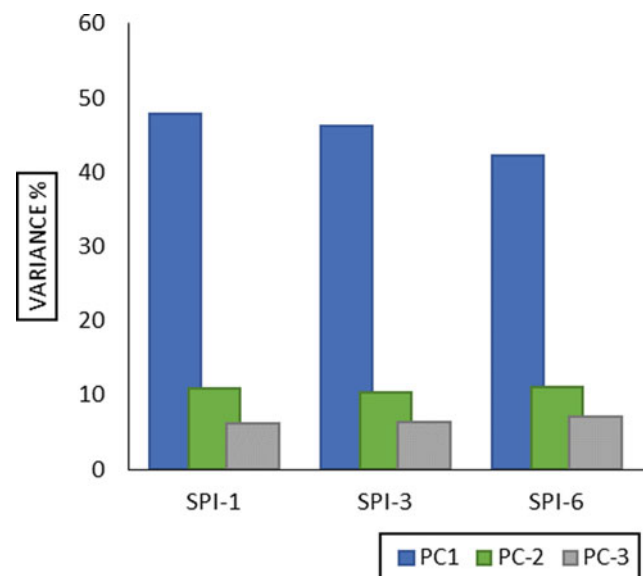
#### 3.1 Rainfall Changes (1990–2010)

Figure 2 shows that rainfall had decreased across Syria from 1990 to 2010. However, the period between 2006 and 2010 was disastrous years, where the moving average showed a reduction ranging between -10 and -45% in eastern Syria.

#### 3.2 Spatial and Temporal Patterns of Drought in Syria

The PCA for various time sets of SPI produce three components (PC1-, PC2-, and PC3) which identify three subregions of drought variability in the study area. The three main patterns—PC1, PC2, and PC3—were identified as a main component of the total variance which explained 65.064, 62.786, and 60.404% for the SPI at 1, 3, and 6 scales time series, respectively (Fig. 3).

As illustrated in Fig. 4, the drought pattern in Syria can be divided into three regions according to PC components: pattern-1 (PC1) in north-eastern Syria (i.e., Al Badia where rainfall does not exceed 200 mm); pattern-2 (PC2) in southern Syria (i.e., the Hauran plain where rainfall ranges between 200 and 400 mm); and pattern-3 (PC3) in



**Fig. 3** Variance% explained by the first three components (PC1-, PC2-, and PC3)



north-western Syria (i.e., the coastal area where rainfall exceeds 800 mm). According to the SPI values, two severe periods of drought have hit Syria, the first from 1999 to 2001, and the second from 2006 to 2009, with north-eastern Syria (PC1) being the most affected by drought throughout Syria.

The Mann–Kendall test showed a negative trend for SPI at 1-, 3-, and 6- months in almost of all the studied stations, as can be seen in Fig. 5. Negative trends were detected more clearly on longer time scales (6-months) where drought becomes more vigorous. The significant negative changes at

different confidence levels (i.e., 0.001, 0.01, and 0.05) were highlighted in 13 stations over a 6-months' time scale. For the 1- and 3-months' time scale, there were no clear significant trends (whether negative or positive), except for the two stations in northern Syria.

In recent years, Syria has been hit by successive waves of drought (Huang et al., 2015; Solh & van Ginkel, 2014), particularly in the period from 2006 to 2009, with 2008 recorded as one of the driest years in recent history (Qatna, 2010; Skaf & Mathbout, 2010; Ide, 2018; Mohammed et al., 1900), in conjunction with positive trends in temperature and

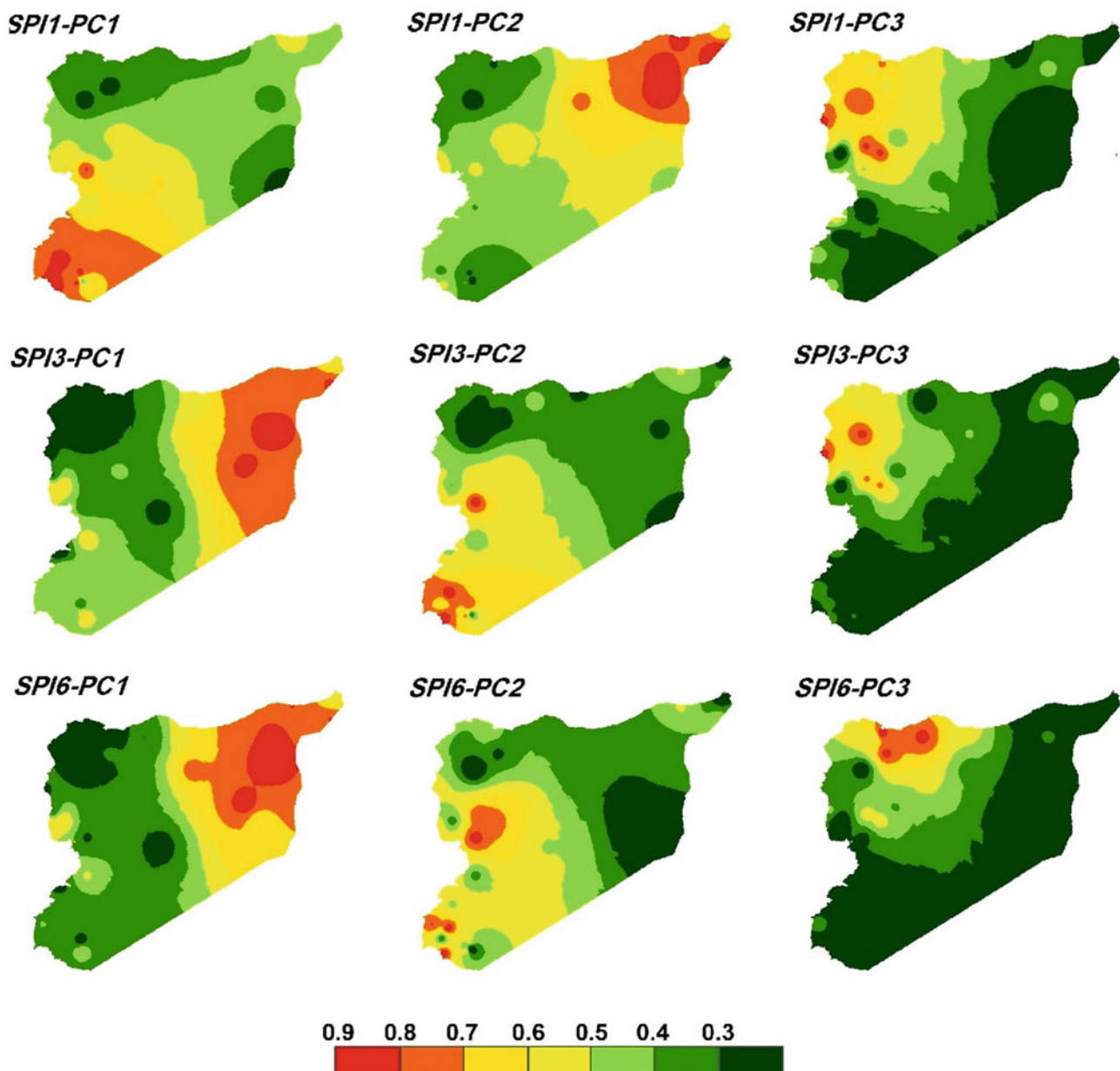


**Fig. 4** Spatial patterns of drought variability in Syria (loading patterns vs 3-PCA) for the SPI in different time scales (1-, 3-, 6- month) from 1990 to 2010

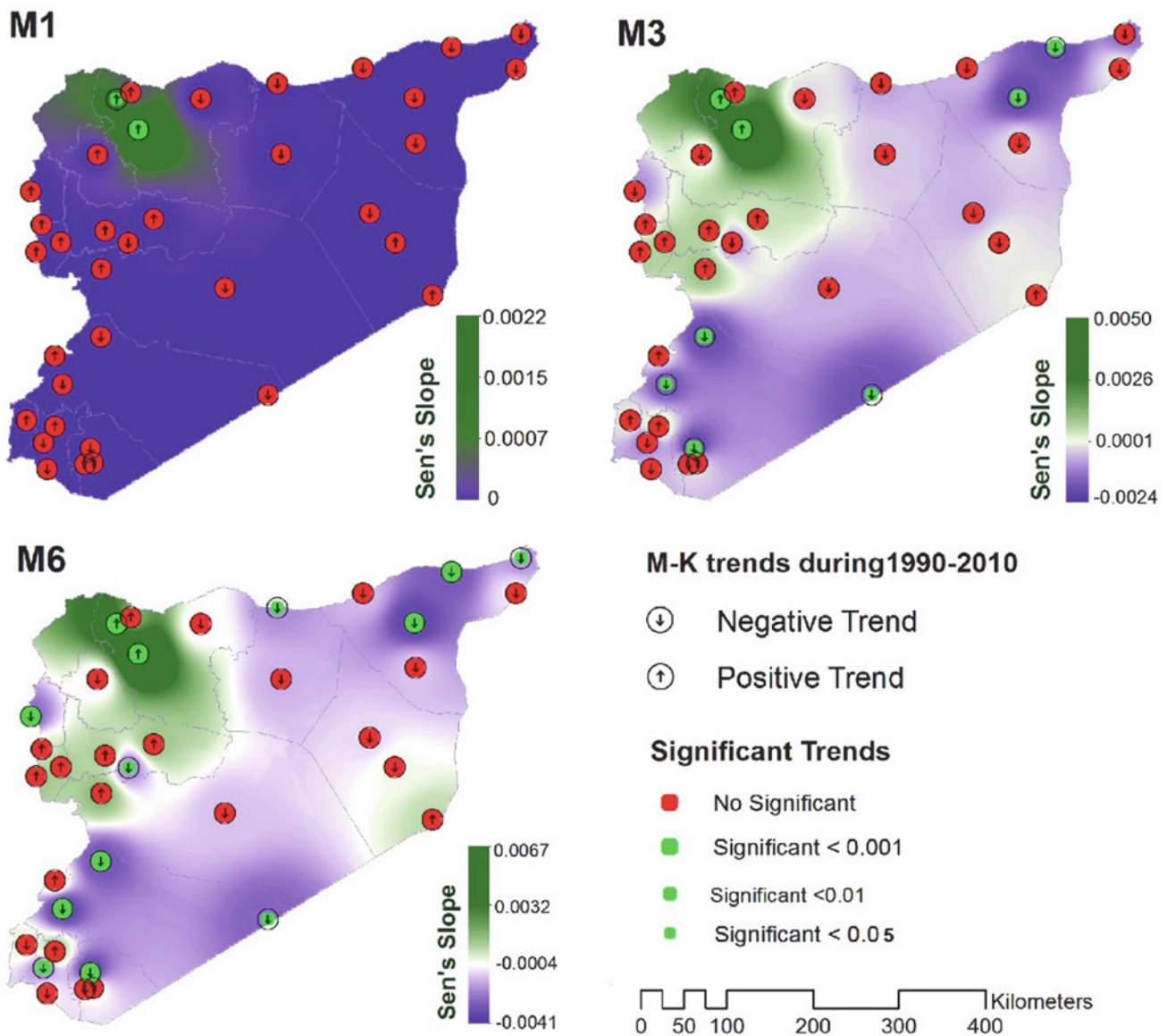


**Fig. 5** Mann–Kendall test for SPI trends at 1-, 3-, 6-months from 1990 to 2010

declines in precipitation (Tanarhte et al., 2012). However, our results indicated that SPI reached an extreme value between 2006 and 2009, and especially in 2008, resulting in catastrophic impacts in the agricultural sector, where agricultural activities are the main income source for more than 48% of the population. Syria, as well as the rest of the Mediterranean regions, was subjected to drought, especially in the Fertile Crescent which can be partly explained by changes in the rainy storm tracks generated over the Mediterranean Sea; these changes were responsible for a decrease in the amount of rainfall, which may lead to drought (Evans, 2009; Salah et al., 2018). Interestingly,

Mohammed and Fallah (2019) indicate a reduction in rainfall associated with a significant drought trend in the coastal region of Syria between 1960 and 2016, which emphasizes a drought trend on a subregional scale.

As an outcome of this research, we can highlight that the eastern part of Syria, which is mainly used for agricultural purposes, was the most vulnerable area for agricultural drought (PC1). In this area, decision-makers should track drought and rainfall deficiency as a main obstacle to future development plans. Otherwise, shifting toward an agricultural rotation will be a good solution instead of planting wheat or cotton each year.

## 4 Conclusion

In this research, the trend of both rainfall and agricultural drought were analyzed for more than 30 stations covering all Syrian land. Results showed a negative trend of rainfall especially in the eastern and central part of Syria. Similarly, statistical analysis for various time sets of SPI produce three components (PC1-, PC2-, and PC3) which identify three subregions of drought variability in the study area. Interestingly, PC1 dominated in the eastern and central part of Syria.

However, this work is a primary study for the assessment and monitoring of drought episodes in Syria, where more specific and detailed studies will be conducted in the future to measure the impact of drought on the environment, taking into consideration different ecosystem components.

## References

- Alsafadi, K., Mohammed, S. A., Ayugi, B., et al. (2020). Spatial-temporal evolution of drought characteristics over Hungary between 1961 and 2010. *Pure and Applied Geophysics*. <https://doi.org/10.1007/s00024-020-02449-5>.
- Amini, A., Zareie, S., Taheri, P., Yusof, K. B., & ul Mustafa, M. R. (2016). Drought analysis and water resources management inspection in Euphrates–Tigris Basin. In *River Basin Management*. IntechOpen. August 10, 2016.
- Enenkel, M., Farah, C., Hain, C., White, A., Anderson, M., You, L., et al. (2018). What rainfall does not tell us—Enhancing financial instruments with satellite-derived soil moisture and evaporative stress. *Remote Sensing*, *10*(11), 1819.
- Evans, J. P. (2009). 21st century climate change in the Middle East. *Climatic Change*, *92*(3–4), 417–432.
- Huang, J., Xue, Y., Sun, S., & Zhang, J. (2015). Spatial and temporal variability of drought during 1960–2012 in Inner Mongolia, north China. *Quaternary International*, *355*, 134–144.
- Ide, T. (2018). Climate war in the Middle East? Drought, the Syrian civil war and the state of climate-conflict research. *Current Climate Change Reports*, *4*(4), 347–354.
- Khanian, M., Marshall, N., Zakerhaghighi, K., Salimi, M., & Naghdi, A. (2018). Transforming agriculture to climate change in Famenin County, West Iran through a focus on environmental, economic and social factors. *Weather and Climate Extremes*, *1*(21), 52–64.
- Lana, X., Serra, C., & Burgueño, A. (2001). Patterns of monthly rainfall shortage and excess in terms of the standardized precipitation index for Catalonia (NE Spain). *International Journal of Climatology: A Journal of the Royal Meteorological Society*, *21*(13), 1669–1691.
- Mathbout, S., Lopez-Bustins, J. A., Martin-Vide, J., Bech, J., & Rodrigo, F. S. (2018). Spatial and temporal analysis of drought variability at several time scales in Syria during 1961–2012. *Atmospheric Research*, *200*, 153–168.
- McKee, T. B., Doesken, N. J., Kleist, J. (1993). The relationship of drought frequency and duration to time scales. In: *Proceedings of the 8th Conference on Applied Climatology* (Vol. 17, No. 22, pp. 179–183). Boston, MA: American Meteorological Society.
- Mohammed, S. A., Alkerdi, A., Harsányi, E., & János, N. (2020). Syrian crisis repercussions on the agricultural sector: case study of wheat, cotton and olives. *Regional Science Policy & Practice*.
- Mohammed, S., Alsafadi, K., Mohammad, S., & Mousavi, N. (2019). Drought trends in Syria from 1900 to 2015. In *Proceedings of the 4th International Congress of Developing Agriculture, Natural Resources, Environment and Tourism of Iran*. Tabriz Islamic Art University in Cooperation with Shiraz University and Yasouj University, Tabriz, Iran, August 14, 2019.
- Mohammed, S. A., & Fallah, R. Q. (2019). Climate change indicators in Alsheikh-Badr Basin (Syria). *Geography, Environment, Sustainability*, *12*(2), 87–96.
- Qatna, H. (2010). *The drought affected the north-eastern region of Syria between 2008–2009*. Damascus, Syria: Organization of Syrian Economics Science. (In Arabic).
- Quiring, S. M., & Papakryiakou, T. N. (2003). An evaluation of agricultural drought indices for the Canadian prairies. *Agricultural and Forest Meteorology*, *118*(1–2), 49–62.
- Rashid, M. M., & Beecham, S. (2019). Development of a non-stationary standardized precipitation index and its application to a South Australian climate. *Science of the Total Environment*, *657*, 882–892.
- Raziei, T., Saghafian, B., Paulo, A. A., Pereira, L. S., & Bordi, I. (2009). Spatial patterns and temporal variability of drought in western Iran. *Water Resources Management*, *23*(3), 439.
- Salah, Z., Nieto, R., Drumond, A., Gimeno, L., & Vicente-Serrano, S. M. (2018). A Lagrangian analysis of the moisture budget over the Fertile Crescent during two intense drought episodes. *Journal of Hydrology*, *560*, 382–395.
- Santos, J. F., Pulido-Calvo, I., & Portela, M. M. (2010). Spatial and temporal variability of droughts in Portugal. *Water Resources Research*, *46*(3).
- Selby, J., Dahi, O. S., Fröhlich, C., & Hulme, M. (2017). Climate change and the Syrian civil war revisited. *Political Geography*, *60*, 232–244.
- Skaf, M., & Mathbout, S. (2010). Drought changes over last five decades in Syria. In *Economics of drought and drought preparedness in a climate change context* (pp. 107–112).
- Solh, M., & van Ginkel, M. (2014). Drought preparedness and drought mitigation in the developing world's drylands. *Weather and Climate Extremes*, *3*, 62–66.
- Tanarhte, M., Hadjinicolaou, P., & Lelieveld, J. (2010). Intercomparison of temperature and precipitation data sets based on observations in the Mediterranean and the Middle East. *Journal of Geophysical Research: Atmospheres*, *117*(D12).
- World Meteorological Organization (WMO). (2012). *Standardized precipitation index user guide*. WMO-No. 1090, 24pp. [http://www.wamis.org/agm/pubs/SPI/WMO\\_1090\\_EN.pdf](http://www.wamis.org/agm/pubs/SPI/WMO_1090_EN.pdf).
- Yang, P., Xia, J., Zhan, C., Zhang, Y., & Hu, S. (2018). Discrete wavelet transform-based investigation into the variability of standardized precipitation index in Northwest China during 1960–2014. *Theoretical and Applied Climatology*, *132*(1–2), 167–180.



# Rainwater Resources of India's Desert Area in the West Rajasthan

P. R. Rakhecha

## Abstract

The western part of the Rajasthan state is the desert area of India with low and erratic rainfall and sandy soils. The real problem related to water in desert is from its inter-annual variability in rainfall. The aim of this paper, therefore, is to study the basic characteristics of rainwater resources of India's desert area in the west Rajasthan in relation to the variability of rainfall, the frequency of droughts and floods and the occurrence of maximum point and areal rain water on the basis of their latest rainfall data of 22 stations for the period from 1957 to 2012. It has been found that the annual variability in rainwater is quite large leading to a deficit in water supplies during low rainfall. When rainfall is only 186 mm or less drought conditions occur, which occurs about once in every four years, floods are rare due to low rainfall in the region but sometimes high rainfall results in flash floods as seen in the region of Barmer district in 1973. In such cases, there is a potential to utilize this flood water wisely for public consumption. The desert of West Rajasthan and other deserts of the world provide considerable hydrometeorological contrast.

## Keywords

Desert • Monsoon • Rainstorm • Flood • Drought • Season

## 1 Introduction

Rajasthan, the largest state of India, is situated in the northwestern part of the country with an area of 3, 42, 239 km<sup>2</sup> (Fig. 1). The western part of the state called 'West Rajasthan' is climatically the desert area of India with low and erratic rainfall and sandy soils. In fact the 'West Rajasthan' desert comprises the four contiguous districts of Barmer, Bikaner, Jaisalmer and Jodhpur as shown in Fig. 1 (Singh et al., 2014). This desert is a part of 'Thar Desert' or the 'Great Indian Desert' and covers an area of about a third of the total area of Rajasthan state. The name Thar is derived from 'thul' the general term for the region with great sandy ridges (Fig. 2). Although it is one of the world's largest deserts, its yearly rainwater is not as low as other deserts of the world. Essentially, this is because of the influence of the Indian southwest monsoon. This desert in West Rajasthan receives considerable quantum of rainwater of the order of 200–300 mm a year, whereas the world's other deserts such as the Sahara, Kalahari, Namib Deserts in Africa, the great sandy and Simpson Deserts in Australia and the Atacama and Peruvian Deserts in South America have their yearly rainfalls almost negligible or less than 50 mm. For example, there is evidence that the hamlet of Dakhla in the Sahara went without rain for a spell of eleven consecutive years. Also flood producing rains does occur anywhere in the desert area of West Rajasthan during the southwest monsoon season from June to September in association with monsoon depressions and cyclonic disturbances and produce millions of cubic meters of rainwater (Dhar et al. 1974). Such instances of occurring tremendous amounts of rain waters are of great importance in the development of much more surface and ground water resources to meet the water needs in very near future.

At a time, there is considerable worldwide concern about the possibility of climate change in desert regions due to global warming being caused by land use change and increasing carbon dioxide and other greenhouse gases.

P. R. Rakhecha (✉)  
D-82, Shastri Nagar, Jodhpur, 342003, India

P. R. Rakhecha  
Indian Institute of Tropical Meteorology, Pune, India



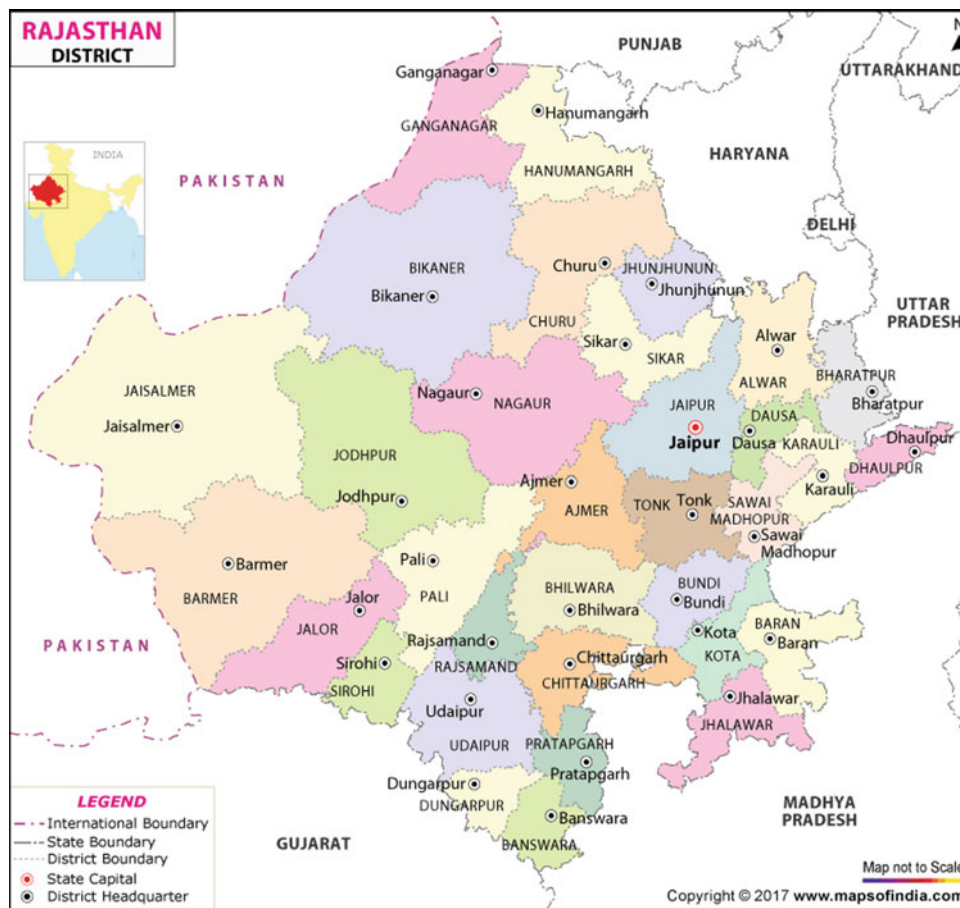


**Fig. 1** Map of Rajasthan showing the desert districts of Bikaner, Barmer, Jaisalmer and Jodhpur



**Fig. 2** Sandy ridges in West Rajasthan desert

Several numerical experiments have been carried out worldwide for climate change under double carbon dioxide scenario. Since Rajasthan rainfall mostly depends on the southwest monsoon of India, any change in its intensity under climate change would affect Rajasthan rainfall and water resources. Sikka and Pant (1992) showed that the

monsoon rainfall of northern India may increase by 5–10% and the temperature may also increase by about 1 °C. However, in the results of Lal et al. (1996) due to projected enhancement of industrialization, the rainfall showed decrease by about 5% and the temperature also showed decrease by about 1 °C. According to Sikka (1997), these scenarios are only suggestive, and the magnitude of projected change is rather quite small, much smaller in comparison with the inter-annual variability of the meteorological parameters witnessed in the instrumental period. Thus, there is hardly any cause for concern with regard to climate change due to greenhouse global warming over India or over Rajasthan desert. The real problem related to water in desert is from its inter-annual variability in rainfall. The aim of this paper, therefore, is to study the basic characteristics of rainwater resources of West Rajasthan desert in relation to the variability of rainfall, the frequency of droughts and floods and the occurrence of maximum point and areal rain water on the basis of their latest rainfall data of 22 stations for the period from 1957 to 2012 so that the results are useful for future hydrological planning wisely.



**Table 1** Area and population of the desert districts of West Rajasthan (Source MI & B, 2012)

	District	Area (km <sup>2</sup> )	% of total area	Population (2011 census)	% of total population	Density persons/km <sup>2</sup>
1	Barmer	28,387	24	2,604,453	28	92
2	Bikaner	30,248	25	2,367,745	25	87
3	Jaisalmer	38,401	32	672,008	7	17
4	Jodhpur	22,850	19	3,685,681	40	161
Total	4	119,886	100	9,329,887	100	80

## 2 Location and Population of the Desert of West Rajasthan

Climatically, the core desert area of Rajasthan consisting of the four districts (Barmer, Bikaner, Jaisalmer and Jodhpur) is located in the northwestern part between latitude 24.8° N and 28° N and longitude 69.7° E and 73° E with an area of 119,886 km<sup>2</sup>. It accounts nearly 34% of the total area of Rajasthan state and forms a natural boundary running along the border between India and Pakistan (see Fig. 1). Table 1 gives the area and population of each district. The total population of the desert area is 9,329,887 of which 80% lives in rural areas and depends on rain fed agriculture and animal husbandry. The population density varies between 17 and 161 persons/km<sup>2</sup> at the four districts. The Jaisalmer district occupying 32% of the desert area has only 7% of population which is a typical characteristic of the desert environment. However, it is worth to mention that as compared to other deserts, the population is fairly high in the desert of West Rajasthan with a density of 80 people per km<sup>2</sup>. Vegetation consists of thorny bushes, shrubs and xerophilous grass. Various species of lizards and snakes are found here.

## 3 Data and Methods

Monthly and annual averages of rainwater and rainy days for the period 1957–2012 for 22 stations in the West Rajasthan desert area are obtained from the publication rainfall structure of Thar 'The Great Indian Desert' by Singh et al. (2014) and climatic data from the climatic tables of observatories in India published by the India Meteorological Department (IMD, 1953). The commonly used statistical techniques including moving average, Poisson's probability law and the Gumbel probability distribution functions were applied.

## 4 Climate Over the Desert of West Rajasthan

The desert climate is described as BW by Koppen's classification of climate system (Pettersen, 1995). In these regions, mean annual rainfall is less than 250 mm, and surface

temperature is high. In the desert of West Rajasthan, the dry cold winter and hot summer are the two most noticeable seasons. Between these two seasons are the southwest monsoon or rainy period and the post monsoon. Thus, the desert of West Rajasthan has four distinct seasons, viz. cold winter (December to February), hot weather or summer (March to May), southwest monsoon or rainy (June to September) and cool post monsoon (October to November). The winter is a season of low-temperature averages around 10–15 °C. The winter is severe when at some places the temperature falls below 0 °C. Jaisalmer recorded the lowest temperature of –5.9 °C on January 12, 1967. The month of March marks the beginning of summer, and the temperature starts rising progressively from April through June averaging around 35–40 °C. The heat during the summer is intense, and scorching making the West Rajasthan desert the hottest region in India. Bikaner recorded the highest temperature of 49.4 °C on May 28, 1914. During summer, severe dust storms occur over most of the desert areas. The rainy season is the period between the onset dates of monsoon to its withdrawal dates. The monsoon rains begin in the West Rajasthan by about July 10–15 and end by September 7 (Sikka, 1997). Normally, the rainy season lasts for about 50–60 days. Occasionally, rain producing weather systems like 'depressions' and 'lows' during the monsoon season penetrate up to the parts of the desert and bring heavy rains and floods in the desert area.

The actual climatic data, averaged over the 60 years for Barmer (23° 45' N, 71° 23' E), is presented in Table 2. This table shows the hottest month is May, which has an average temperature of about 34.0 °C and the coldest is January with a temperature of 16.8 °C. Due to lower morning temperatures, relative humidity is higher in the morning than in the afternoon. However, the mean monthly relative humidity varies between 39% in November and 67% in August. The humidity in the monsoon months of July and August is quite high—mean monthly humidity of the order of 65–67%. The wind speed is slightly lower during the winter than during the summer monsoon. In monsoon, the average wind speed is 11.0 km/h, and in winter the average wind speed amounts to 7.3 km/h. There are three main wind regimes, typically, 11% of the days are calm, and 39% have a west/northwesterly and 31% south/southwesterly wind.

**Table 2** Climatic data for Barmer (*Source* Climatic Tables of Observatories in India, 1953)

Month	Mean daily temperature (°C)	Highest temperature (°C)	Lowest temperature (°C)	Relative humidity (%)	Rainfall (mm)	Rainy days	Wind speed (km/h)
January	16.8	32.8	-1.7	41	6.1	0.4	7.5
February	20.3	38.9	4.4	45	5.6	0.6	7.8
March	25.1	40.0	8.9	44	4.1	0.6	9.3
April	30.7	45.0	13.3	41	3.3	0.3	9.3
May	34.0	48.9	16.7	48	9.7	0.6	11.0
June	33.2	45.5	18.4	57	21.8	1.2	13.1
July	30.9	44.4	19.4	65	90.7	5.2	11.5
August	29.3	40.0	20.6	67	148.8	5.8	10.3
September	29.9	41.1	16.7	59	20.3	1.4	9.1
October	28.7	40.6	13.9	44	1.3	0.2	7.5
November	23.9	37.2	8.3	39	0.3	0.1	5.8
December	19.3	32.7	3.3	42	2.0	0.2	6.6
Mean	26.9	–	–	49	314	16.5	9.1

## 5 Rainwater in the Desert of West Rajasthan

The amount of rainwater received over various stations and regions gives the quantity of water available naturally. The mean seasonal and annual rain waters along with the coefficient of variability (CV), the number of rainy days and the highest and lowest amounts of annual rain waters worked out on the basis of data for the 56-year period (1957–2012) in the desert of West Rajasthan as a whole as also for the stations in the districts are given in Tables 3 and 4, respectively.

### 5.1 Rainwater in the Desert of West Rajasthan as a Whole

Table 3 shows that the desert area as a whole receives on an average about 250.9 mm equivalent to 30,100 million cubic

meters of rainwater every year with a CV of 38%. The average seasonal rainwater amounts are 7.8, 17.6, 218.1 and 7.4 mm for winter, summer, southwest monsoon and post monsoon contributing 3, 7, 87 and 3%, respectively, to the annual rainwater amount. The monsoon season rainwater figure of 218 mm is disappointingly lower than the country's normal of 887 mm for the June to September period. There are two reasons. First, being farthest from the seas, West Rajasthan is at the tail end of monsoon system which arrives here. Second is the existence of an inversion in the lower troposphere at about 1.5 km above sea level. This is indicative of an extremely stable density gradient in the atmosphere that tends to suppress large-scale ascent of air, and the air is never able to rise to a point of saturation despite its high humidity. That is why the mean monsoon season rainfall is way lower than country's monsoon season rainfall (Das, 1995). It is estimated that about 78% of the rainwater is lost to the atmosphere by direct evaporation and

**Table 3** Mean seasonal and annual rainwater, coefficient of variability (CV), rainy days and the highest and lowest rain waters in the Desert area (1957–2012) (*Source* Singh et al., 2014)

Seasons	Winter (December–February)	Summer (March–May)	SW monsoon (June–September)	Post monsoon (Oct–November)	Annual
Rainfall (mm)	7.8	17.6	218.1	7.4	250.9
% of annual	3	7	87	3	100
CV (%)	107	97	42	184	38
Rainy days	1.3	1.4	12.7	0.4	15.8
Highest rainfall (mm)	36 (2006)	77 (1983)	425 (1975)	69 (1998)	461 (1975)
Lowest rainfall (mm)	0 (1984)	1.1(1984)	50 (2002)	0 (1964)	73 (1968)

12% result in surface runoff and the remaining enrich the groundwater (Rakhecha, 1993).

## 5.2 Rainwater at Different Stations

It is important to know on an average in a year how much rainwater at each station in the desert area is received. The mean annual rainfall of different stations in the desert districts along with their highest and lowest annual rain waters and rainy days is given in Table 4. This table shows that the annual rainwater amounts at the 22 stations varied from 200 to 360 mm, and the average ratio of the highest recorded rainwater amount in a year to the mean annual was found to be around 2.8.

## 6 Variability in Rainwater

We have said that being located in the westernmost part of India, the desert area of West Rajasthan comes under the sway of monsoon currents after the monsoon has advanced over the rest of the country. The normal date of the advance of the monsoon over this region is between July 10 and 15, and the monsoon begins to withdraw by the end of first week of September. There are, however, significant variations from its normal behavior, and the onset of monsoon can be early or delayed by as much as two to three weeks. Late commencement of monsoon may considerably influence the amount of rainwater received during the monsoon season. To examine the variability in seasonal rain waters over the desert area, their coefficient of variability (CV) based on the data for the period 1957–2012 is given in Table 3. This table shows that among the four seasons, the lowest variability of rainwater, 42% was found in the southwest monsoon season. The frequency distribution of area average rainwater for the 56-year period (1957–2012) is given in Table 5. This table shows that there is wide variation in rainwater from year to year. In order to show the variation of rainfall over the region as a whole, average annual rain waters of West Rajasthan desert for the 56-year period have been plotted in Fig. 3. This figure shows that over the past 56 years annual rainwater amount has oscillated between 73 mm in 1968 and 461 mm in 1975. Oscillations in the annual rainwater were also subjected to a moving average filter to suppress high-frequency oscillations. The filtered series shows that the fluctuations are quite wide and the overlapping means range from 150 mm to 400 mm. The pattern of moving averages reveals a weak increasing trend in rainfall.

## 7 Abnormalities in the Monsoon Season Rainwater

The years when the monsoon season rainwater exceeded the mean monsoon rainwater by more than 50% are given in Table 6. The largest excess was 95% in 1975. Table also shows that rainwater over West Rajasthan desert was in excess of mean monsoon by more than 50% on nine occasions, giving an annual probability for this event of 16%. The interval between successive years of excess rainfall is random in nature. The probabilities of occurrence of this event in a five-year period obtained on the basis of the Poisson's probability law are given in Table 7.

## 8 Highest Point and Areal Rainfalls in the Desert of West Rajasthan

Discussion on the highest point and areal rainfalls is of great value in the design of the civil engineering water projects. Heavy point and areal rainfalls in the desert of West Rajasthan occur in association with the monsoon depressions and low pressure areas which considerably stimulate the monsoon currents. These disturbances form over the Bay of Bengal and move in the northwesterly direction across the country. After traversing Orissa and Madhya Pradesh regions, they either move across Rajasthan or merge with the seasonal trough over this region. Heavy rainfall occurs in the regions which are exposed to these disturbances. Rainfall caused by such depressions can range at a station from 400 to 800 mm in one day.

### 8.1 Highest Point Rainfalls

The daily rainfall records for stations in the desert of West Rajasthan have been examined for occurrence of the highest rainfalls of 1-day duration and the rainfalls from the severe rainstorms. The highest recorded rainfall values of 1-day duration for stations in the various districts are given in Table 8.

The highest point rainfall values represent only small areas around the recording points. The table shows that rainfall of the order of 200–350 mm in one day has occurred at individual station in the past. A glance at Table 8 conveys the impression that there have been instances when a station in this region received its mean annual rainfall in a single day. For example, Chohtan, a station in the Barmer district, recorded 356 mm on August 26, 1944, as against the annual average rainfall of 288 mm. Similarly, Balotra in Barmer

**Table 4** Rainwater at different stations in the districts

No.	Station	District	Location		Mean annual rainfall (mm)	CV (%)	Rainy days	Highest annual rainfall (mm)	Ratio of highest to mean annual rainfall	Lowest annual rainfall (mm)	Ratio of lowest to mean annual rainfall
			Lat.	Long.							
1	Barmer	Barmer	25° 45' N;	71° 23' E	264	62	14	759	2.9	37	0.14
2	Chohtan		25° 29' N;	71° 04' E	288	66	15	875	3.0	36	0.12
3	Pachpadra		25° 56' N;	72° 16' E	246	55	15	590	2.4	37	0.15
4	Sheo		26° 11' N;	71° 15' E	221	50	13	525	2.7	31	0.14
5	Siwana		25° 39' N;	72° 23' E	350	58	17	1052	3.0	34	0.1
6	Bikaner	Bikaner	28° 00' N;	73° 18' E	264	38	17	559	2.1	32	0.12
7	Lunkaransar		28° 30' N;	73° 45' E	296	53	18	783	2.6	64	0.22
8	Kolayat		–	–	268	56	16	894	3.3	60	0.22
9	Nokha		27° 35' N;	73° 29' E	315	45	20	769	2.4	71	0.23
10	Dungargarh		28° 04' N;	74° 00' E	320	52	19	904	2.5	64	0.2
11	Jaisalmer	Jaisalmer	26° 55' N;	70° 55' E	196	57	11	513	2.6	28	0.34
12	Fatehgarh		26° 30' N;	71° 11' E	176	73	9	527	3.0	16	0.09
13	Pokran		–	–	203	60	13	540	2.7	29	0.14
14	Ramgarh		–	–	134	66	8	386	2.9	2	0.02
15	Sam		–	–	181	105	9	1304	7.2	8	0.04
16	Nokh		–	–	187	7	10	522	2.8	13	0.07
17	Jodhpur		26° 18' N;	73° 01' E	360	46	20	815	2.3	91	0.25
18	Phalodi	27° 08' N;	72° 22' E	216	45	14	486	2.3	14	0.06	
19	Bilara	–	–	416	47	22	1064	2.6	128	0.3	
20	Shergarh	26° 20' N;	72° 18' E	243	3	16	677	2.8	42	0.17	
21	Osian	–	–	287	39	18	615	2.2	94	0.33	
22	Jaswantsagar	–	–	344	53	16	1088	3.2	80	0.23	

**Table 5** Frequency of area average annual rainwater in the desert area of West Rajasthan

Rainwater range (mm)	Frequency	Rainwater range (mm)	Frequency
70–90	2	271–290	2
91–110	1	291–310	3
111–130	3	311–330	2
131–150	2	331–350	3
151–170	2	351–370	4
171–190	7	371–390	4
191–210	5	391–410	2
211–230	4	411–430	0
231–250	4	431–450	1
251–270	4	451–470	1

**Fig. 3** Average annual rainwater over the desert of west Rajasthan

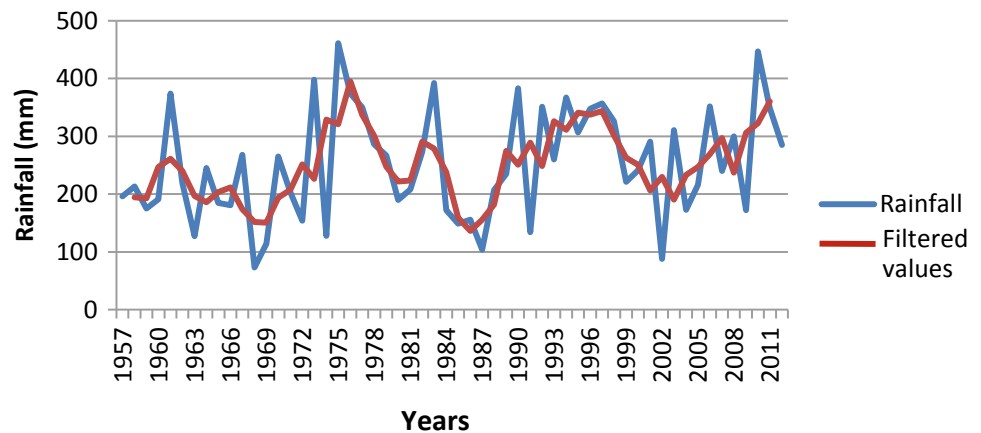


**Table 6** Years when rainwater over West Rajasthan desert was in excess of mean Monsoon rain water by more than 50% (mean monsoon rainwater = 218 mm)

Year	Deviation from mean monsoon rainwater (%)	Time interval between excessive years
1961	64	–
1973	78	12
1975	95	2
1976	58	1
1990	63	14
1992	53	2
1994	57	2
2010	89	16
2011	57	1

district and Nokh in Jaisalmer district have recorded 337 and 280 mm, respectively, in one day as against their annual average rainfalls. Heavy fall of rain exceeding 300 mm in one day is not, therefore, uncommon in the desert of West Rajasthan.

**Table 7** Probability of monsoon rainwater exceeding 50% of mean in a 5-year period

Number of exceedance in a 5-year period	Probability
0	0.45
1	0.36
2	0.14
3	0.02

### 8.2 Highest Areal Rainfalls from Severe Rainstorms

High quantum of areal rainfalls from severe rainstorms associated with the low or the cyclonic storms coming from the Bay of Bengal can result flood water in West Rajasthan. In the rainfall records of the West Rajasthan, three storms predominate. These are the storm July 30–31, 1952, over the Jodhpur district, the storm of August 17–19, 1973, over the Barmer district and July 25–27, 1995, also over the Barmer district. The storm of August 1973 brought very heavy rainwater and floods to an area around Siwana in the Barmer district, and therefore it was considered for analysis.



**Table 8** Highest recorded 1-day rainfalls (mm) in the desert of West Rajasthan

District	Station	1-day Highest Rainfall (mm)	Date	Annual rainfall (mm)	District	Station	1-day Highest Rainfall (mm)	Date	Annual rainfall (mm)
Barmer	Barmer	312	8.8.1990	264	Jodhpur	Fatehgarh	180	19.7.1993	176
	Chohtan	356	26.8.1944	288		Pokran	175	21.6.1996	203
	Pachpadra	152	26.7.1995	246		Ramgarh	180	21.9.1998	134
	Balotra	337	26.7.1995	270		Nokh	280	26.6.1996	187
	Sheo	130	23.8.2007	221		Sam	240	17.8.1972	181
	Siwana	205	18.8.1973	350		Jodhpur	157	31.7.1990	360
Bikaner	Bikaner	127	17.7.1981	264	Jodhpur	Shergarh	128	21.6.1996	243
	Lunkaransar	233	24.7.2000	296		Phalodi	168	12.7.1964	216
	Kolayat	138	6.8.1973	268		Bilara	300	31.7.1999	516
	Kokha	134	23.6.96	315		Osian	125	10.6.1998	287
	Dungargarh	262	26.7.83	320		Jaswantsagar	260	31.7.1999	344
Jaisalmer	Jaisalmer	204	16.8.1973	196	–	–			

The 1973 storm was caused by the movement of a low pressure area from the central Uttar Pradesh which stimulated the activity of the monsoon and produced heavy rainwater for a period of 7 days in the districts of Jaisalmer, Barmer and Jodhpur. Large areas of these districts were marooned for days continuously. Road and rail communications were disrupted for weeks together. The rainstorm lashed the entire West Rajasthan area during August 13–19, 1973. Some stations in the desert area received one day rainwater amounts exceeding their respective mean annual rainwater. Jaisalmer recorded 200 mm of rainwater on August 16 while its mean annual rainwater is about 180 mm. Barmer recorded 170 and 230 mm of rainwater on August 17 and 18. Figure 4 shows the isohyetal map of this rainstorm for the period August 17–19.

The depth-area-duration (DAD) values obtained during this rainstorm are given in Table 9, and the rainwater potential generated by the storm for each day of the rain spell over the desert of West Rajasthan is given in Table 10. Total volume of water generated over the desert of West Rajasthan by the August 1973 rainstorm was estimated to be about 32,293 million cubic meters during the period 13–19 August 19, 1973.

## 9 Droughts and Floods in the Desert of West Rajasthan

Cities and villages in the desert of West Rajasthan obtain their water from rainfall. Because of the inter-annual variability of rainfall, totals ranging from less than half of the average rainwater in one year to twice the average amount in another year as shown in Fig. 3, the desert of West

Rajasthan is highly susceptible to experience flooding or severe droughts. As the dominant land use is farming and animal husbandry, the occurrence of both droughts and floods is a big problem. It is, therefore, important to assess the probability of occurrence of droughts and floods in the desert of West Rajasthan. In this section, we first focused on the occurrence of the droughts in the desert area of West Rajasthan.

### 9.1 Droughts

The drought occurs over a given area when its actual rainfall received in a year significantly falls short of climatically expected rainfall of the area. For India, the India Meteorological Department (IMD, 1971) has defined a drought as a situation occurring in a region when its year's rainwater is less than 75% of the mean annual rainfall. The drought is further classified as moderate when year's rainwater is between 75 and 50% of the mean value and less than 50% as severe drought. On the basis of this criterion, the averaged rainwater of each year in the desert of West Rajasthan was classified as moderate or severe drought during the period of 1957–2012 which are listed in Table 11. This table shows that in West Rajasthan desert 15 drought years have occurred during the 56-year period (1957–2012) of which three were of severe nature. This reveals that after every 4 years of good rainfall events, one moderate or severe drought year occurs. The two contiguous severe droughts in 1968 and 1969 and one in 1987 were probably the most disastrous in their effect on the economy. It is to be mentioned here that the drought of 1987 in various parts of India was of unprecedented in intensity (Sinha Ray & Shewale, 2001).

**Fig. 4** Isohyets map of rainstorm of August 1973

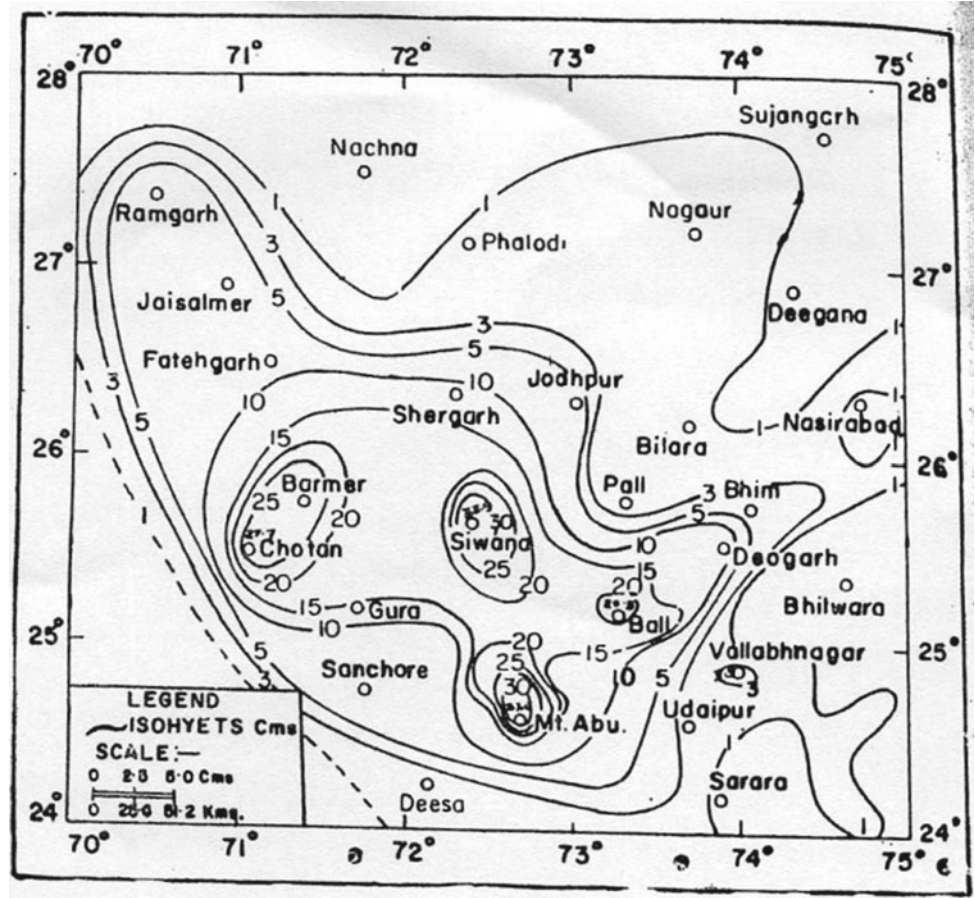


**Table 9** DAD analysis of August 1973 rainstorm over the desert of West Rajasthan

Area (sq. miles)	1-day (mm)	2-day (mm)	3-day (mm)
10	275	307	376
500	236	262	300
1000	220	241	264
5000	170	210	228
10,000	146	186	203
15,000	128	174	179
20,000	114	164	172
30,000	99	140	160
40,000	89	134	150
50,000	80	118	143

**Table 10** Volume of rainwater generated by the August 1973 rainstorm over the desert area

Date	13 August	14 August	15 August	16 August	17 August	18 August	19 August
Average rainwater depth (mm)	50	54	55	32	32	54	41
Area covered (km <sup>2</sup> )	79,901	164,651	123,102	109,749	73,072	74,721	67,081
Water generated (10 <sup>6</sup> m <sup>3</sup> )	3995	8891	6774	3512	2336	4035	2750

**Table 11** Drought and flood years

Drought year	% of annual rainfall	Drought classification	Time interval between droughts	Flood year	% of annual rainfall	Flood classification	Time interval between floods
1959	70	Moderate	–	1961	149	Moderate	–
1963	51	Moderate	4	1973	159	Severe	12
1965	74	Moderate	2	1975	183	Severe	2
1966	72	Moderate	1	1976	149	Moderate	1
1968	29	Severe	1	1983	156	Severe	7
1969	46	Severe	1	1990	153	Severe	7
1972	62	Moderate	3	1992	140	Moderate	2
1974	51	Moderate	2	1994	146	Moderate	2
1984	69	Moderate	10	1996	139	Moderate	2
1985	59	Moderate	1	1997	142	Moderate	1
1986	62	Moderate	1	1998	129	Moderate	1
1987	41	Severe	1	2003	125	–	5
1991	53	Moderate	4	2006	140	Moderate	3
2004	69	Moderate	13	2010	178	Severe	4
2009	68	Moderate	5	2012	139	Moderate	2

However, in West Rajasthan the drought years occur at irregular intervals, and the probability of occurrence of drought was found to be 27% in 56 years.

## 9.2 Floods

Floods are rare in the desert of West Rajasthan due to poor rainwater, but unusually some rainstorms can result in flooding as seen from the August 1973. In August 1973, the usually drought prone Barmer and Jaisalmer districts were hit by the flash floods and caused loss of life and damage to property. At some stations, almost the average annual amount was recorded in a single day. It is, therefore, more important in the context of desert hydrology to study the occurrence of flood rainwater. The IMD (1971) has defined flood as a situation occurring in an area in a year when the seasonal rainwater is more than 125% of mean. If the rainwater is between 125 and 150% of mean, it is called moderate flood year, and if the rainwater is more than 150% of the mean, it is called a severe flood year. On the basis of this criterion, rainfall of each year in West Rajasthan was classified as moderate or severe flood year during the period 1957–2012 and is listed in Table 11. This table shows that 15 flood rainfall years have occurred during the 56 years, and during these years the annual rainfalls were in excess of 125–183% of the mean annual rainfall. As such, on an average one flood rainfall year can be expected to occur in 4 years. It is worth to mention that one time 2 (1975, 1976) and 3 (1996, 1997, 1998) contiguous flood years with high

amounts of rainwater have occurred. Flood rains, however, occur at irregular intervals in 56 years, and the probability of occurrence of flood was about 27%.

## 10 Maximum 1-Day Rainfall for Various Return Periods

The design of minor civil engineering works such as irrigation tanks, culverts, highway bridges, urban drainage works require estimates of maximum rainfalls for various return periods. Considering the importance of the subject in this section, we provide 1-day maximum rainwater values for various return periods ranging from 2 to 100 years for stations in different districts of the West Rajasthan desert. Maximum rainfalls and floods are most commonly modeled by EV 1 distribution. The distribution is essentially a log-normal distribution with constant skewness (approximately 1.14).

Gumbel showed that the cumulative probability or the return period that any extreme value of a variable  $X$  will be equal to or greater than the given value  $x$  is given as follows:

$$1/T = 1 - \exp[-\exp\{-\alpha(x-\beta)\}] \quad (1)$$

$$X_T = \beta - 1/\alpha(\ln \ln T/T - 1) \quad (2)$$

where  $\alpha$  and  $\beta$  are scale and location parameters. The estimates of these parameters using the method of moments are the functions of the mean ( $\bar{x}$ ) and standard deviation ( $\sigma$ ) of extreme values as follows:

**Table 12** Maximum 1-day rainwater (mm) for different return periods for stations in West Rajasthan

Station	Location	2-year	5-year	10-year	25-year	50-year	100-year
Bikaner	28° 0' N, 73° 18' E	58	91	112	139	160	180
Barmer	25° 45' N, 71° 23' E	58	103	132	170	198	227
Jaisalmer	26° 55' N, 70° 55' E	50	88	113	145	169	192
Jodhpur	26° 18' N, 73° 02' E	62	89	107	130	146	163

$$1/\alpha = \sqrt{6}/\pi \cdot \sigma = 0.78\sigma$$

$$\beta = \bar{x} - 0.45\sigma$$

Substituting the parameters  $\alpha$  and  $\beta$  in Eq. (2) yields

$$X_T = \bar{x} - [0.45 + 0.78 \ln \ln (T/T - 1)]\sigma \quad (3)$$

$$X_T = \bar{x} + K \cdot \sigma \text{ and } K = -[0.45 + 0.78 \ln \ln (T/T - 1)] \quad (4)$$

In this section, the annual maximum rainfall series for the 56 years period for 1-day duration was subjected to Gumbel method, and the maximum 1-day rainfalls for different return periods from 2 to 100 years for some stations in the desert of West Rajasthan were determined using Eq. (3). The magnitude of 1-day rainwater for different return periods (2–100 years) is given in Table 12. This table shows that 1-day rainwater of the order of 50–62 mm, 90–103 mm, 107–132 mm, 130–170 mm, 146–200 mm and 163–227 mm can occur on average once every 2, 5, 10, 25, 50 and 100 years, respectively.

## 11 Conclusions

The paper provides interesting information on population and rainwater resources of India's desert area in the West Rajasthan. The availability of water in the desert of West Rajasthan is dependent on the rainwater received from the Indian southwest monsoon. The mean annual rainwater of the desert area based on records of their 56 years is 251 mm equivalent to 30,100 million cubic meters with a coefficient of variability of 38%. Thus, as compared to other desert regions of the world West Rajasthan desert receives tremendous amounts of rainwater. Also alongside, the desert area is uniquely populated with a density of 80 persons/km<sup>2</sup>. The areal average rainwater was in excess of the mean monsoon rainwater by more than 50% on nine occasions in

56 years. The largest excess was 95% in the year 1975. As also associated with the favorable meteorological situations such as monsoon depressions/lows, this desert region received heavy falls of rainwater of the order of 250–350 mm in one day. The record rainstorm of August 1973 generated a water potential of the order of about 32,293 million cubic meters in the 7-day period August 13–19. The high amount of rainwater and high density of population are the most noticeable characteristics of the West Rajasthan desert.

## References

- Das, P. K. (1995). *The Monsoons* (250pp.). India: National Book Trust.
- Dhar, O. N., Rakhecha, P. R., & Mandal, B. N. (1974). On some rainfall features of August 1973 rainstorm over Rajasthan. *International Hydrological Decade, Newsletter*, 23–36, 1–4.
- India Meteorological Department (IMD). (1953). *Climatological tables of observatories*. IMD Publication.
- India Meteorological Department (IMD). (1971). *Rainfall and droughts in India*. Report of the Drought Research Unit, IMD.
- Lal, M., Srinivasan, G., & Cubasch, U. (1996). *Current Science*, 71, 746–752.
- Ministry of Information & Broadcasting (MI & B). (2012). *India reference annual*. Government of India Publication.
- Petterssen, S. (1995). *Introduction to meteorology* (2nd ed.). McGraw-Hill Book Company, INC.
- Rakhecha, P. R. (1993). Water resources of Rajasthan. In T. S. Chouhan (Ed.), *Natural and human resources of Rajasthan*. Jodhpur: Scientific Publishers.
- Sikka, D. R. (1997). Desert climate and its dynamics. *Current Science*, 72(1), 35–46.
- Sikka, D. R., & Pant, G. B. (1992). In Y. P. Abrol et al. (Ed.), *Impact of global climatic changes on photosynthetics and plant productivity* (pp. 551–572). New Delhi: Oxford and IBH.
- Singh, S. S., Chauhan, M., & Kumawat, R. N. (2014). *Rainfall structure of Thar "The Great Indian Desert"*. IMD Publications.
- Sinha Ray, K. C., & Shewale, M. P. (2001). Probability of occurrence of drought in various sub-divisions of India. *Mausam*, 52(3), 541–546.



# Deficit Irrigation as a Strategy in Irrigating Citrus Tree Plantings Under Water Scarcity Conditions

Mohamed El-Otmani, Fatima Alahian, Charif Azrof, Chouaibi Anouar, and Redouane Choukrallah

## Abstract

Citrus is a major fruit crop produced (on 120,000 ha) and exported from Morocco, consuming 10,000 m<sup>3</sup> of irrigation water per ha annually. Currently, irrigation water is becoming very scarce, and drip irrigation is the water supply system used in plantings because of its high water use efficiency and productivity. Recent research indicates that additional water saving and higher efficiency can be obtained via adoption of deficit irrigation strategies such as sustained deficit irrigation (SDI), regulated deficit irrigation (RDI), and partial root zone drying (PRD). These irrigation strategies were applied on citrus clementine (*Citrus reticulata*) plantings for two years at different tree phenological stages. Four cultivars were included: 'Sidi Aissa' and 'Orogrande' in 2017 and 'Bruno', and 'Esbal' in 2018. Results indicate that water saving was in the range of 6 to 31% compared to control fully irrigated plantings depending on the strategy. However, deficit irrigation reduced fruit size, yield, and vegetative growth but enhanced fruit quality with PRD treatments having more significant effect than SDI or RDI. The negative effect of water deficit stress was more pronounced on total yield than on fruit size, particularly in high vapor pressure deficit (VPD) years and for PRD strategy. Under years of mild VPD, this negative effect was significant but equal for fruit size and yield. Water productivity decreased with water amounts applied. However, since clementine fruit is destined to fresh market which demands fruit of large size, it can be safe to recommend use of RDI and avoid PRD under semi-arid conditions.

## Keywords

Clementine mandarin • Deficit irrigation • Partial root zone drying • Yield • Fruit quality • Water saving • Water productivity

## 1 Introduction

In general, Morocco has a semi-arid climate, and agriculture is an important sector of the economy as it contributes 15% of GDP. Because of climate change with increasing global temperatures and decreasing annual precipitations, water is becoming scarce in many areas of the world where the resource used to be plentiful, particularly in arid and semi-arid regions of the globe (Fourouzani & Karami, 2011). With increasing urbanization and demand from industry, agriculture, and tourism, the situation may worsen by 2050 (de Wit & Stankiewicz, 2006; Godfray et al., 2010). Agriculture uses close to 80% of available freshwater resources, and this needs to be re-rationalized to satisfy the development needs of both agriculture itself and the other sectors of the economy for global and inclusive sustainable economic growth. Besides conventional water resources, non-conventional waters (such as treated wastewater, brackish water, and drainage water) can be part of the solution but not yet implemented in most countries (Allam & Allam, 2007) including Morocco. Therefore, smart water saving techniques should be developed to maintain efficient levels of crop production in all sectors. In agriculture and particularly in the fruit crop production sector, drip irrigation has been adopted for several decades as an efficient irrigation technique allowing for water saving per unit area and greater production per unit crop produced (Carr, 2012), but new and more efficient irrigation strategies have been or are being tested in several countries and on various crops from around the world to increase drought resistance and water productivity (Ferreter et al., 2003; Khanna-Chopra & Singh, 2011; Chai et al.,

M. El-Otmani (✉) · F. Alahian · C. Azrof · C. Anouar · R. Choukrallah  
Department of Horticulture, Institut Agronomique et Vétérinaire Hassan II, Complexe Horticole d'Agadir, 80150 Ait Melloul, Morocco



2016). These strategies include use of genotypes that have high water use efficiency (Condon et al., 2004; Khanna-Chopra & Singh, 2011) and irrigation management using deficit irrigation strategies (Ferrerres et al., 2003). These strategies include regulated deficit irrigation (RDI) which consists of imposing water deficit only at certain crop development stages with little or no negative effect on crop yield or quality (Chalmers et al., 1981). Ferreres et al. (2003) indicated that several researchers have tried RDI on several crops, but the results were not always encouraging, and thus, adjustments are needed in relation to crop species, variety, stage of development, soil type, and climate parameters and evaporative demand. Another version of deficit irrigation is sustained deficit irrigation (SDI) which imposes somewhat mild stress on plants throughout the crop cycle by applying 80–85% of crop water needs with no or little effect on production (Goldhamer & Viveros, 2000; Abriquesta & Ayars, 2018). Partial root zone drying (PRD) has also been developed where water deficit is applied by alternating irrigation on each side of the plant (thus, half of the root zone is irrigated alternatively) in scheduled irrigation events although with conflicting results (Sepaskhah & Ahmadi, 2010).

Citrus is major fruit crop produced (with 120,000 ha) and exported from Morocco. It consumes about 10,000 m<sup>3</sup>/ha. Under the Souss region of southwestern part of Morocco, a major citrus producing region in the country with 40,000 ha, clementine mandarins (*Citrus reticulata*) flower in the spring (March–mid-April) and fruit set in mid-April to May, whereas fruit enlargement occurs mainly during summer months (June–September) coinciding with period of high temperatures and low air humidity. Fruit maturation is mainly in August–mid-October with some variation according to the cultivar.

Under Spanish conditions, ‘Clementina de Nules’ mandarin tree response to RDI was reported to vary according to the phenological stage of application with reduced yield and fruit size and increased juice sugar and acid content when the water reduction was applied during the second half of fruit growth and early fruit maturation (Gonzaloz-Altozano & Castel, 1999, 2000). Garcia-Tejero et al. (2010) reported that, under RDI, ‘Navelina’ orange (*Citrus sinensis*) had reduced yield when the treatment was applied during flowering and fruit growth but not when it was applied during fruit maturation. Garcia-Tejero et al. (2011a) indicated that cultivars respond differently to deficit irrigation programs and that trees respond differently to the irrigation strategy applied. In particular, they reported that water saving using sustained deficit irrigation (deficit irrigation for a long period of time) caused more stress and reduced yield more than use of RDI (with much shorter period of water deficit) with supply of the same water amount. In addition, RDI allowed water saving but reduced crop yield over low frequency deficit irrigation. This was also confirmed by Nagaz et al.

(2017) on ‘Meski Maltaise’ orange trees subjected to SDI (applying 25 and 50% less water than crop needs) throughout the crop cycle (May–December); reduced yield and fruit size resulted in reduced net income to the grower. However, fruit juice sugar content increased. Gasque et al. (2016) indicated that RDI applied to ‘Navelina’ orange during initial fruit enlargement phase had no effect on yield or yield provided that stem water potential (a stress indicator) did not surpass a threshold limit of  $-2.0$  MPa.

PRD has been used with success on several fruit crops including grapes, pear, peach, olive, and apple (see Consoli et al., 2017 and the references therein). On citrus, Romero-Conde et al. (2014) indicated that water saving can be achieved with PRD if irrigation supply is properly applied. They also indicated that when PRD is used in the long term may result in severe water stress which can impair growth and physiological parameters. Consoli et al. (2017) reported that PRD supplying 50% of crop water needs to young orange trees with alternating irrigation between the two halves of the root zone at weekly interval increased water use efficiency (calculated as yield/(irrigation water + effective rainfall)). This irrigation strategy reduced vegetative growth and individual fruit weight but had no effect on yield or fruit juice content. In an experiment using PRD and SDI (applying 50% of crop needs during fruit growth) on ‘Valencia’ orange trees, Mossad et al. (2020) reported that yield was not affected by PRD but was reduced by RDI. In addition, fruit juice sugar and acid content as well as juice and sugar productivity per unit of irrigation water were increased as a result of water restriction.

The objective of this paper is to report on the results of experimental research done on four clementine mandarin plantings using SDI, RDI, and PRD applied during the crop cycle of clementine trees grown under the semi-arid climate of the Souss valley of Morocco known for its water scarcity.

## 2 Materials and Methods

The experiments were done over two years with each year in a different commercial orchard near the city of Taroudant, Morocco. To characterize the climate of the crop season, weather data was obtained from the closest weather station to each of the two experimental fields.

First year experiment was performed during 2017 in a commercial orchard where two mid-early clementine cultivars (*Citrus reticulata* Blanco) were used: ‘Sidi Aissa’ grafted on ‘Carrizo’ citrange [*Citrus sinensis* L. (Osborne) × *Poncirus trifoliata* L. (Raf.)], and ‘Orogrande’ grafted on *Citrus volkameriana*. The trees were planted in 2011 on a sandy loam soil having a field capacity of 28%, a humidity at the permanent wilting point of 14%, a pH of 7.1, and an electric conductivity (EC) of 0.22 mmhos/cm.

Trees were planted at a spacing of 6 m × 2 m (giving a planting density of 833 trees/ha) and ferti-irrigated using two lines of drippers for each tree row. Drippers were 60 cm apart (i.e., 6.6 drippers/tree) with a flow rate of 4 l/h/dripper leading a system rainfall of 2.2 mm/h. Irrigation water had a pH of 6.9 and an EC of 0.22 mmhos/cm.

Irrigation regimes were based on growers' experience coupled with frequent observations of the general status of the tree leaves and of the soil humidity level using capacitive probes. After verifying the root depth of trees and lateral extent of the root system, the net maximum water dose was calculated giving a value of 3.2 mm, i.e., irrigation duration of 1 h 30 min using the irrigation system described above. This amount corresponds to the daily tree needs in the summer period which also correspond to the supply by the grower at that season. Water supply by the grower is based on duration of irrigation. This estimation is shown to be close to crop water needs (also known as crop evapotranspiration  $ET_c$ ) which was estimated using the formula:

$$ET_c = ET_o \times K_c \quad (1)$$

where  $ET_o$  is the reference evapotranspiration and is estimated using FAO Penman–Monteith equation based on weather data from the closest meteorological station (Allen et al., 1998) and  $K_c$  is the crop cultural coefficient.  $K_c$  values varied with the season from 0.3 in the winter to 0.6 in the summer based on Doorenbos and Pruitt (1977). Water dosage was applied once a day in mid-morning between 9 and 11 am. In addition, trees received cultural practices that are optimal for the region.

Application of the irrigation strategies had begun on July 06, 2017, and lasted during the whole fruit growth and maturation stages (up to October 5, 2017) according to the specific characteristics described in Table 1.

Second year experiment used a commercial orchard planted in 2013 at tree spacing of 6 m × 3 m (leading a tree density of 555 trees/ha). 'Bruno' and 'Esbal' clementine selections (*Citrus reticulata*), respectively, grafted on *Citrus volkameriana* and *Citrus macrophylla* rootstocks were used.

Water and fertilizer application was by drip irrigation using two drip lines per row of trees, one in each side of the row to cover half of the root zone on each side of the tree. Each tree has 15 drippers delivering 1 L/h each. The drippers are 40 cm apart on the line. The soil is sandy with 90% sand and 10% clay. Maximum active root concentration is in the upper 40 cm for the 'Bruno'/*Citrus volkameriana* and 50 cm for 'Esbal'/*C. macrophylla* (data not shown). Irrigation supply was done according to grower's strategy based on irrigation duration according to leaf water visual evaluation, soil humidity level, and water availability. To avoid water loss by percolation, irrigation dose was divided in two applications per day, one in mid-morning and one in early afternoon. Soil pH in the root zone is 8.0 for 'Bruno' and 8.5 for 'Esbal' planting. Irrigation water has a pH = 8.3 and salinity of 0.5 mmhos/cm. Trees received cultural practices (fertigation, pruning, pest and disease management, etc.) that are optimal for the region. Application of irrigation regimes started on February 01, 2018, and lasted the whole crop cycle. The specifications of each irrigation program are given in Table 2. The experimental design was a complete bloc with four replications (=blocs), and five trees/experimental unit were considered in the test.

For 2017 and 2018 crop cycles, parameters observed included:

- Crop yield: at harvest (on October 2 for 2017 and October 23 for 2018), total number of fruit per tree was obtained for five trees per irrigation strategy.
- Fruit size and juice content: at maturation, composite samples of ten fruit/tree/strategy were obtained for the above five trees. These samples were weighed, and their juice extracted and weighed.
- Fruit juice quality: for the above juice samples, total soluble solids content (TSS) was obtained using a temperature-adjusted laboratory refractometer. In addition, their total acidity (TA) was obtained using a 0.1 N sodium hydroxide solution. Consequently, their maturity index (MI) was calculated as the ratio TSS/TA.

**Table 1** Irrigation regimes tested in the year 2017

Irrigation strategy	Specifications
T1 (control)	Grower's strategy: supply close to 100% $ET_c$
T2 (RD11)	regulated deficit irrigation with supply of 75% $ET_c$ from July 06 to October 05, 2017 (fruit growth to maturation)
T3 (PRD4)	Partial root zone drying (PRD) with 3–4 days alternating irrigation (supply of 50% $ET_c$ ) between the two tree root system halves from July 06 to October 05, 2017
T4 (PRD7)	Partial root zone drying (PRD) with 7 days alternating irrigation (supply of 50% $ET_c$ ) between the two tree root system halves from July 06 to October 05, 2017
T5 (RD12)	Regulated deficit irrigation with supply of 50% crop water needs during fruit maturation (Sept 11–Oct 05, 2017)

**Table 2** Irrigation regimes applied during the year 2018

Irrigation strategy	Characteristics of the strategy
T1 (control)	Supply of 100% grower's irrigation capacity (full irrigation)
T2 (SDI)	Sustained deficit irrigation with application of 73% of the full irrigation regime during the whole crop cycle (February 1–October)
T3 (RDI1)	Regulated deficit irrigation with application of 73% of the full irrigation regime during flowering and fruit set (February 1–April 30)
T4 (RDI2)	Regulated deficit irrigation with application of 73% of the full irrigation regime during fruit enlargement-to-maturation (August–October)
T5 (PRD)	Partial root zone drying applying 73% of full irrigation with one-day alternation between each root zone half during the crop cycle (February 1–October)

For 2018 crop cycle, in addition of the above, irrigation effect was also assessed on the following parameters:

- Flowering and fruit set: flower intensity and fruit set were evaluated using tagged shoots of summer 2017. Four shoots per tree and five trees per treatment were included in the study. Their number of nodes per shoot was counted (Table 3) and used as the base for estimating intensity of flowering and intensity of fruiting. Flowering was assessed by recording number of buds, number of flowers open, number of flowers at petal fall stage, and number of fruitlets set. Observations were recorded at weekly intervals starting on March 23, 2018.
- Fruit set was calculated as the ratio: [maximum number of fruits set/(maximum number of flower buds + open flowers produced)]
- Vegetative growth: Changes in vegetative growth with time were assessed using tagged 2018 spring shoots (born on the tagged 2017 summer shoots) for which shoot length was recorded at weekly intervals starting on May 09, 2018. Four tagged spring shoots per tree with five trees per treatment were used. Because of the heavy load of flowers on trees of 'Bruno,' this selection did not develop spring shoots and was thus excluded from this evaluation.
- Besides that, number of newly born summer shoots was also evaluated using the 2017 summer shoots as the base for calculating shoot development intensity. This parameter was evaluated on the 'Bruno' selection only (Table 4).

**Table 3** Characteristics of the 2017 summer shoots used in evaluating flower intensity and fruiting of trees in 2018

Irrigation strategy	Variety			
	'Bruno'		'Esbal'	
	Average shoot length (cm)	Average number of nodes/shoot	Average shoot length (cm)	Average number of nodes/shoot
T1	8.21	7.56	8.64	7.54
T2	8.68	7.67	7.55	7.60
T3 = T4	9.05	8.32	8.79	7.82

### 3 Results and Discussion

#### 3.1 Characterization of the Climate for the years 2017 and 2018

The year 2017 crop cycle was characterized by temperatures in the range of 7–30 °C in the spring, 15–45 °C in the summer, and 15–35 °C in the fall. Average air relative humidity ranged between 30 and 70%. Thus, leaf vapor pressure deficit (VPD) was in the range of 0.5–3.0 kPa with peak readings of 3.5–5.2 kPa occurring in July and August but with very short durations, coinciding with fruit enlargement. In addition, rainfall was almost nil since there were only about 6 mm total that fell between March and May. However, reference evapotranspiration was in the range of 1.8–5.6 mm/day. These data indicate that the 2017 clementine crop year was very dry and that, except for the few days of heat in the summer, weather conditions were generally acceptable for citrus tree growth and development.

For the 2018 year of study, air temperature was mostly in the range of 4–25 °C in the winter, 10–30 °C in the spring, 18–36 °C in the summer, and these values lasted through the fall (data not shown). Maximum temperature rarely exceeded 38 °C except for 5 days total between mid-July and mid-August when it reached 43 °C. Temperatures in the range of 12–36 °C are reported to be optimal for citrus tree growth and development (INRA, 1968). In addition, minimum air relative humidity was mostly in the range of 30 to

**Table 4** Effect of irrigation strategy on flowering, fruiting, and vegetative growth of ‘Bruno’ and ‘Esbal’ clementine trees (2018 year crop)

Variety	Irrigation strategy	Maximum number of flower buds + open flowers/100 nodes of summer 2017 shoots (March 21, 2018)	Maximum number of fruit set/100 nodes of summer-2017 shoots (April 18 and 25, respectively, for ‘Bruno’ and ‘Esbal’)	Fruit set (in % relative to total flowers)	Spring 2018 shoot length (cm/shoot)	Number of newly formed summer 2018 shoots/100 summer 2017 shoot nodes
‘Bruno’	T1 (control)	163.5	80.7	49.4	– <sup>z</sup>	11.0a
	T2 (SDI)	164.0	91.8	55.5	–	7.6b
	T3 (RD11)	170.0	107.6	63.0	–	12.2a
	T4 (RD12)	–	–	–	–	–
	T5 (PRD)	180.5	86.4	47.9	–	5.5b
	Significance level	NS	NS	NS	–	5%
‘Esbal’	T1 (control)	174.0	136.4	78.4	12.5	–
	T2 (SDI)	190.0	133.4	70.2	12.1	–
	T3 (RD11)	177.0	118.5	66.9	11.9	–
	T4 (RD12)	–	–	–	–	–
	T5 (PRD)	174.5	144.3	82.7	11.4	–
	Significance level	NS	NS	NS	NS	–

<sup>z</sup>Not evaluated

60%. Rainfall was 80 mm in February and 55 mm in March coinciding with flowering and 10 mm in September coinciding with end of fruit growth and initial fruit maturation. In addition, reference evapotranspiration rarely exceeded 7 mm/day (data not shown). These data gave leaf VPD values below 2.5 kPa reported to be the maximum limit for best growth and development conditions for citrus trees (Kriedmann, 1968).

Furthermore, in 2018, the main period of tree vegetative growth and that of flowering and fruit development was relatively dry with rainfall of 80, 55, and 10 mm, respectively, for the months of February, March, and September, indicating that the only stage where tree benefited from it was the flowering-early fruit set period (i.e., February–March). The period of fruit enlargement (May–August) was totally dry.

### 3.2 Flowering and Fruit Set

These parameters were evaluated in 2018 since irrigation strategies commenced in February which included flowering and fruit set, whereas in 2017, irrigation strategies begun only in July coinciding with fruit enlargement. Both ‘Bruno’ and ‘Esbal’ clementine cultivars had similar flower intensity with an average number of flower buds in the range of 163 to

180 flowers/100 nodes for ‘Bruno’ and 174–190 flowers/100 nodes for ‘Esbal’ (Table 4). Fruit set in numbers and in percent relative to number of flowers produced were generally greater for ‘Esbal’ compared to ‘Bruno.’ Furthermore, within cultivars, irrigation strategies, particularly SDI, RD11, and PRD which were applied before flowering, had no effect on these parameters with greater numbers for ‘Esbal.’

### 3.3 Vegetative Growth

This parameter was evaluated during the 2018 crop year since irrigation strategies that could affect it had begun prior to flowering and spring growth flush. Length of spring shoots was not statistically affected by irrigation strategies applied that could have any influence on this parameter (Table 4). However, influence on number of summer shoots produced was significant with lower numbers for trees receiving 73% of full irrigation whether water was supplied as SDI (T2) or as PRD regime (T5) with alternating irrigation supply between tree root zone halves at one-day interval (Table 4). Reduced vegetative growth as a result of water deficit application was reported by Consoli et al. (2017) using PRD and by Gonzalo-Altozano and Castel (1999), Perez-Perez et al. (2010) and Ballester et al. (2011) with RDI strategy on citrus trees.

### 3.4 Water Saving, Fruit Size, Crop Yield, and Water Use Efficiency

Although plantings used in 2017 were older (planted in 2011 vs. 2013) and had higher density (833 vs. 555 trees/ha) compared to those used in 2018, irrigation water needs for control trees were 6675 and 5555 m<sup>3</sup>/ha, respectively (Tables 5 and 6). The difference is mainly due to the difference in the different agro-climatic conditions in the experimental years since the climatic conditions of the year 2018 (air temperatures and leaf VPD which were milder) were more adequate for good fruit set and growth than those of the year 2017 (see above). In comparison with fully irrigated trees, restricting water supply allowed water economy between 629 and 2054 m<sup>3</sup>/ha in 2017 (Table 5) and between 338 and 1437 m<sup>3</sup>/ha in 2018 (Table 6) depending on the strategy, with the lowest amounts for RDI and the greatest for PRD, whereas SDI had intermediate amounts.

In addition, under full irrigation regime, cultivar effect on yield is high (compare 19 tons/ha for ‘Orogrande’ to 15 tons/ha for ‘Sidi Aissa’ in 2017, and 22 tons/ha for ‘Bruno’ to 30 tons/ha for ‘Esbal’ in 2018). Year weather conditions seem to have a greater effect over other agronomic factors such as tree density (yield for ‘Sidi Aissa’ and ‘Orogrande’ planted at 833 trees/ha is less than that of ‘Bruno’ and ‘Esbal’ planted at 555 trees/ha).

Effect of deficit irrigation on fruit number, fruit size, total yield, and water use efficiency was evaluated on 2017 crop of ‘Sidi Aissa’ and ‘Orogrande’ (Table 5) and on 2018 crop of ‘Bruno’ and ‘Esbal’ (Table 6) clementine trees. Fruit number per tree was greater for ‘Esbal’ compared to ‘Bruno’

(Table 5) which is mainly due to the greater number of flowers and fruit set (Table 4). Fruit number per tree was statistically not affected by irrigation strategy except for ‘Sidi Aissa’ for which fruit number was lower for trees stressed during fruit enlargement indicating that at this phenological stage, this cultivar is sensitive to water shortage which may have had a thinning effect. Ballester et al. (2011) reported that under water shortage, fruit size is significantly more affected by tree water status than tree fruit number.

Fruit size was reduced for trees subjected to reduction in irrigation water supply during fruit enlargement regardless of the variety or whether or not the irrigation restriction was applied at an earlier stage of fruit development (Tables 5 and 6). RDI during fruit maturation only had no effect on either fruit size or yield.

Furthermore, correlations between water applied and fruit size (by weight) showed positive trend. In addition, ‘Bruno’ had the lowest correlation coefficient ( $R^2 = 0.451$ , indicating that 45% only of the variability in individual fruit weight is due to total water quantity applied) followed by ‘Esbal’ (with  $R^2 = 0.758$ ), whereas ‘Orogrande’ had the greatest correlation coefficient ( $R^2 = 0.971$ ) followed by ‘Sidi Aissa’ ( $R^2 = 0.845$ ). This indicated that, overall, fruit size is more dependent on and sensitive to water supply under high VPD year (year 2017 with ‘Sidi Aissa’ and ‘Orogrande’). Garcia-Tejero et al. (2012) reported that tree water status below a certain threshold will have a significant negative effect on fruit daily growth, thus on final fruit size.

Effect of water restriction on yield was more negative with PRD than with SDI or RDI (Tables 5 and 6). In fact,

**Table 5** Effect of irrigation strategy on total water applied, fruit size, yield, and water use efficiency (WUE) for ‘Sidi Aissa’ and ‘Orogrande’ clementine mandarin (year 2017 crop)

Irrigation strategy	Quantity of water applied (m <sup>3</sup> /ha)	‘Sidi Aissa’				‘Orogrande’			
		Average fruit number/tree	Average fruit weight (g/fruit)	Estimated yield (tons/ha)	WUE (kg/m <sup>3</sup> )	Average fruit number/tree	Average fruit weight (g/fruit)	Estimated yield (tons/ha)	WUE (kg/m <sup>3</sup> )
T1 (control)	6675	334a <sup>Z</sup>	55.4a	15.5a	2.31	356a	66.4a	19.7a	2.94
T2 (RDI1)	5641 (1034; 15%) <sup>Y</sup>	318b	53.6ab (-1.8; -3%) <sup>X</sup>	14.2b (-1.3; -8%) <sup>W</sup>	2.52	335a	64.3b (-2.1; -3%) <sup>X</sup>	17.8a (-1.6; -8%) <sup>W</sup>	3.18
T3 (PRD4)	4621 (2054; 31%)	295b	51.4b (-4.0; -7%)	12.7c (-2.8; -18%)	2.74	320a	61.4c (5.0; -7%)	16.4b (3.3; -17%)	3.54
T4 (PRD7)	4621 (2054; 31%)	279b	52.6b (-2.8; -5%)	12.2c (-3.3; -21%)	2.64	325a	60.7c (5.7; -8%)	16.4b (3.3; -17%)	3.55
T5 (RDI2)	6046 (629; 10%)	348a	55.7a (-0.3; 0%)	16.2a (+7.0; +4%)	2.67	344a	65.5ab (9.0; -1%)	18.7a (1.0; -0.5%)	3.10

<sup>Z</sup>Within columns, values followed by the same letters are not significantly different (Tukey’s test at 5% level)

<sup>Y</sup>Numbers within brackets: first number indicates amount of water savings and second number indicates percent saving compared to control



**Table 6** Effect of irrigation strategy on total water applied, fruit size, yield, and water use efficiency (WUE) for ‘Esbal’ and ‘Bruno’ clementine mandarin (year 2018 crop)

Irrigation strategy	Quantity of water applied (m <sup>3</sup> /ha)	‘Bruno’				‘Esbal’			
		Average fruit number/tree	Average fruit weight (g/fruit)	Estimated yield (tons/ha)	WUE (kg/m <sup>3</sup> )	Average fruit number/tree	Average fruit weight (g/fruit)	Estimated yield (tons/ha)	WUE (kg/m <sup>3</sup> )
T1 (control)	5555	760a <sup>z</sup>	52.7a	22.2a	4.0	887a	61.3a	30.2a	5.8
T2 (SDI)	4118 (1437; 26%) <sup>y</sup>	785a	45.8b (-6.9; -13%) <sup>x</sup>	19.3bc (-2.9; -13%) <sup>w</sup>	4.7	876a	53.1c (-8.2; -13%) <sup>x</sup>	25.8b (-4.4; -15%) <sup>w</sup>	6.3
T3 (RDI 1)	4951 (604; 11%)	756a	52.5a (-0.2; -0.4%)	22.0a (0.2; 1%)	4.5	885a	61.2a (-0.1; -0.1%)	30.0a (-0.2; -0.7%)	6.1
T4 (RDI2)	5217 (338; 6%)	793a	45.0b (-7.7; -15%)	19.8b (-2.4; -11%)	3.8	904a	56.9b (-4.4; -7%)	28.6ab (-1.6; -5%)	5.5
T5 (PRD1)	4118 (1437; 26%)	756a	43.0b (-9.7; -18%)	18.0c (-4.2; -19%)	4.4	881a	50.8c (-10.5; -17%)	24.8b (-5.4; -18%)	6.0

<sup>z</sup>Within columns, values followed by the same letters are not significantly different (Tukey’s test at 5% level)

<sup>y</sup>Numbers within brackets: first number indicates amount of water savings and second number indicates percent saving compared to control

alternating irrigation between tree root zone sides had similar negative effect, with a yield reduction of 17–21% compared to full irrigation, regardless whether the alternation interval was seven days or even one day. RDI had less effect on yield (reduction between 0 and 11% with ‘the greatest reduction for ‘Bruno’), whereas SDI had an intermediate effect (13–15% reduction). Restricting water supply during fruit maturation only (RDI-2 treatment) had no effect on yield across the varieties, but water saving was very small (6–10% compared to control full irrigation).

Although the cultivars used during the two years of investigation are not the same from year-to-year, it is noteworthy that: (1) during a dry and hot year (2017), fruit yield seems to be more sensitive to water restrictions applied during fruit growth (with yield reductions between 8 and 21% for ‘Sidi Aissa’ and 8 and 17% for ‘Orogrande’) than fruit size itself (with reductions between 3 and 8% only) (Table 5); and (2) during a relatively mild year (2018), both fruit size and yield seem to be affected by irrigation water restrictions with the same degree (Table 6). This indicates that fruit yield suffers significantly more under water restrictions applied during fruit enlargement stage and high VPD. Effect of water restriction on yield and fruit size was reported to be dependent upon the phenological stage of application (Gonzalo-Altozano & Castel, 1999), rootstock genotype (Romero et al., 2006; Treeby et al., 2007), timing and severity of the degree of water deficit stress applied (Ferrerres & Soriano, 2007; Ballester et al., 2011; Nagaz et al., 2017), and the variety genotype (Garcia-Tejero et al., 2011a; b).

Water productivity values for the 2018 crop were almost double those for the 2017 crop with the lowest values recorded for ‘Sidi Aissa’ regardless of the irrigation strategy. This is certainly the result of the greater stress conditions in 2017 as well as differences in terms of variety tolerance to stress with ‘Sidi Aissa’ being the most sensitive. Furthermore, correlation coefficients between the quantity of water applied and yield were positive for all varieties tested with correlation coefficients ( $R^2$ ) values in the range 0.63 and 0.99. Increased water productivity as a result of deficit irrigation was reported by others (Nagaz et al., 2017) and Garcia-Tejero et al. (2011a, b) indicated that effect of water deficit on yield was closely related to irrigation strategy rather than to amount of irrigation water alone.

Furthermore, although no straight forward conclusion can be made for water productivity as related to irrigation strategy, it appears that it negatively correlates with water quantities applied with some differences among varieties (Table 7) which is in agreement with results of Consoli et al. (2017). In addition, at least 48% of the variability observed in water use efficiency (WUE) ( $R^2 = 0.482$ ) is explained by water amounts applied.

### 3.5 Fruit Juice Content and Quality

Effect of irrigation treatments on fruit juice content and quality was evaluated on ‘Sidi Aissa’ and ‘Orogrande’ for the 2017 crop (Table 8) and on ‘Bruno’ and ‘Esbal’ clementine for the 2018 crop (Table 9).

**Table 7** Linear and quadratic relationships between water amounts used and water use efficiency (with  $y$  in  $\text{kg}/\text{m}^3$  and  $x$  in  $\text{m}^3$ )

Variety	Quadratic equation		Linear equation	
	Equation	$R^2$	Equation	$R^2$
'Bruno'	$y = -2 \times 10^{-7}x^2 + 0.0013x + 2.3292$	0.612	$y = -0.0004x + 6.3887$	0.600
'Esbal'	$y = 3 \times 10^{-8}x^2 - 0.0006x + 8.1063$	0.482	$y = -0.0003x + 7.4975$	0.482
'Orogrande'	$y = 5 \times 10^{-8}x^2 - 0.0009x + 6.4232$	0.998	$y = -0.0003x + 4.924$	0.989
'Sidi Aissa'	$y = -10^{-7}x^2 + 0.0010x + 0.1425$	0.703	$y = -0.0001x + 3.3756$	0.598

**Table 8** Effect of irrigation strategy on fruit juice content, total soluble solids (TSS), and maturity index for 'Sidi Aissa' and 'Orogrande' clementine mandarin (year 2017 crop; date of observation: Oct 2, 2018)

Irrigation strategy	'Sidi Aissa'			'Orogrande'		
	Juice content (%)	TSS (%)	Maturity index	Juice content (%)	TSS (%)	Maturity index
T1 (control)	51.7a <sup>z</sup>	10.5c	7.7c	49.7a	11.2b	9.8c
T2 (RDI1)	48.8ab	10.8ab	8.5ab	49.4a	11.6ab	10.3ab
T3 (PRD4)	46.7b	10.9ab	8.8a	45.9b	11.7a	10.4a
T4 (PRD7)	46.3b	11.0a	8.8a	46.8b	11.7a	10.5a
T5 (RDI2)	49.3ab	10.7bc	8.3b	48.8a	11.5b	10.0bc

<sup>z</sup>Within columns, values followed by the same letters are not significantly different (Tukey's test at 5% level)

**Table 9** Effect of irrigation strategy on fruit juice content, total soluble solids (TSS), and maturity index for 'Bruno' and 'Esbal' clementine (year 2018 crop; Sept 28, 2018)

Irrigation strategy	'Bruno'			'Esbal'		
	Juice content (%)	TSS (%)	Maturity index	Juice content (%)	TSS (%)	Maturity index
T1 (control)	53.3a <sup>z</sup>	10.2b	11.9b	53.0a	9.6b	10.7b
T2 (SDI)	51.1a	11.2a	12.1a	51.3ab	11.2a	12.2a
T3 (RDI 1)	52.5a	10.5b	11.5b	53.5a	9.8b	10.7b
T4 (RDI2)	53.3a	11.1a	11.8b	49.7b	11.0a	11.8ab
T5 (PRD1)	51.9a	11.4a	12.1a	50.4b	11.4a	12.2a

<sup>z</sup>Within columns, values followed by the same letters are not significantly different (Tukey's test at 5% level)

Restricting water supply to clementine trees tended to reduce fruit juice content, but the degree of this reduction was cultivar and irrigation strategy dependent (Tables 8 and 9). In fact, PRD strategy had the greatest reduction effect compared to control full irrigation, and 'Bruno' and 'Orogrande' were less sensitive than the other two selections. Mossad et al. (2020) reported reduced fruit size and juice content for 'Valencia' orange fruit from trees under SDI (supplying 50% ETc) but not under PRD (supplying 50% ETc).

However, deficit irrigation treatments all had a significant increase effect on juice total soluble solids content which is an indicator of sugar concentration in fruit juice (Tables 8 and 9). This increase was more evident in fruit of PRD trees regardless of the irrigation alternation interval between tree root zone halves. In addition, this increase had a significant positive effect on fruit maturity index indicating an enhancement of fruit maturation as a result of water stress application. SDI and RDI treatments had an intermediate effect between control trees receiving full irrigation and PRD treatment. Increased fruit juice sugars as a result of deficit

irrigation were reported by Treeby et al. (2007) and Nagaz et al. (2017). In addition, juice and sugar productivity per unit of irrigation water was increased as a result of water restriction (Nagaz et al., 2017). Mossad et al. (2020) reported an increase in juice sugar content as well as fruit, juice, and sugar productivity per unit irrigation water for PRD and SDI.

## 4 Conclusions

Taken together, the results indicate that: (1) there is a significant cultivar and/or year effect of the response of trees to deficit stress; (2) reduced water application reduced water supply but reduced fruit size and yield with the latter being more sensitive than the former particularly during the year of high VPD year; (3) RDI had less of an effect (particularly if applied during the fruit maturation stage only), SDI had a more pronounced effect, and PRD had a severe effect; (4) deficit irrigation increased fruit sugar content, thus improving fruit quality; (5) retaining water effect on fruit

juiciness is cultivar- and irrigation strategy-dependent with the general trend that PRD reduces fruit juice content; (6) water restriction reduced vegetative growth which can be an advantage in that it should reduce pruning costs.

Enhanced quality can also be considered an advantage in that it can lead to earlier harvest time than usual which can be a comparative advantage in the market place particularly since clementine cultivars are the first citrus fruit in the market in the beginning of the citrus fruit season, and thus, earliness can bring better prices to the grower. Whether the amount of water saved, the degree of earliness in fruit maturation and potential reduction in pruning costs will offset the cost of reduced fruit size and yield, particularly for irrigation strategies with high amounts of water savings, which remains to be elucidated.

It is noteworthy that fruit of the clementine mandarin grown in the Mediterranean is mainly geared toward fresh fruit export and that fruit size matters as large fruit procures higher prices in the market place. In addition, for arid and semi-arid regions, under water scarcity conditions and very dry years, reducing water supply may be the only alternative to the citrus growers particularly under climate change and adverse climate events to ensure sustainability of the production system. It can thus be recommended to avoid using PRD strategy as it negatively affects both fruit size and yield and that RDI can be a safer strategy to adopt when water is scarce.

## References

- Abrigueta, I., & Ayars, J. E. (2018). Effect of alternative irrigation strategies on yield and quality of Fiesta raisingrapes grown in California. *Water*, 10, 583. <https://doi.org/10.3390/w10050583>
- Allam, M. N., & Allam, G. I. (2007). Water resources in Egypt: Future challenges and opportunities. *International Water Resources Association—International Water*, 32, 205–218.
- Allen, R. G., Pereira, L. S., Raes, D., Smith, M. (1998). *Crop evapotranspiration-Guidelines for computing crop water requirements-FAO Irrigation and drainage paper 56*. Rome: FAO
- Ballester, C., Castel, J., Introgliolo, D. S., & Castel, J. R. (2011). Response of Clementina de Nules citrus trees to summer deficit irrigation. Yield components and fruit composition. *Agricultural Water Management*, 98, 1027–1032.
- Carr, M. K. V. (2012). The water relations and irrigation requirements of citrus (Citrus spp.): A review. *Experimental Agriculture*, 48, 347–377.
- Chai, Q., Gan, Y., Zhao, C., Hui-Lian, Xu., Waskom, R. M., Niu, Y., & Siddique, K. H. M. (2016). Regulated deficit irrigation for crop production under drought stress: A review. *Agronomy for Sustainable Development*, 36, 3. <https://doi.org/10.1007/s13593-015-0338-6>.
- Chalmers, D. J., Mitchell, P. D., van Heek, L. (1981). Control of peach tree growth and productivity by regulated water supply, tree density and summer pruning. *Journal of the American Society for Horticultural Science*, 106, 307–312
- Condon, A. G., Richards, R. A., Rebetzke, G. J., & Farquhar, G. D. (2004). Breeding for high water-use efficiency. *Journal of Experimental Botany*, 55, 2447–2460.
- Consoli, S., Stagno, F., Vanella, D., Boaga, J., Cassiani, G., & Raccuzzo, G. (2017). Partial root-zone drying irrigation in orange orchards: Effects on water use and crop production characteristics. *European Journal of Agronomy*, 82, 190–202.
- de Wit, M., & J. and Stankiewicz. 2006. Changes in water supply across Africa with predicted climate change. *Science*, 31(311), 1917–1921. <https://doi.org/10.1126/science.1119929>
- Doorenbos, J., Pruitt, W. O. (1977). *Crop water requirements. Irrigation and Drainage*. Paper no: 24. Rome, Italy: FAO.
- Ferreres, E., & Soriano, M. A. (2007). Deficit irrigation for reducing agricultural water use. *Journal of Experimental Botany*, 58, 147–159.
- Ferreres, E., Goldhamer, D. A., & Parsons, L. R. (2003). Irrigation water management of horticultural crops. *HortScience*, 38, 1036–1042.
- Fourouzani, M., & Karami, E. (2011). Agricultural water poverty index and sustainability. *Agronomy for Sustainable Development*, 31, 415–432. <https://doi.org/10.1051/agro/2010026>.
- García-Tejero, I., Jiménez-Bocanegra, J. A., Duran-Zuazo, V. H., Romero, V. R., & Muriel-Fernandez, J. L. (2010). Positive impact of deficit irrigation on physiological response and fruit yield in citrus orchards: Implication for sustainable water savings. *Journal of Agricultural Science and Technology*, 4, 38–44.
- García-Tejero, I., Duran-Zuazo, V. H., Jiménez-Bocanegra, J. A., & Muriel-Fernandez, J. L. (2011a). Improved water use efficiency by deficit irrigation programmes: Implications for saving water in citrus orchards. *Scientia Horticulturae*, 128, 274–282.
- García-Tejero, I., Duran-Zuazo, V. H., Jiménez-Bocanegra, J. A., & Muriel-Fernandez, J. L. (2011b). Improved water-use efficiency by deficit irrigation programmes: Implications for saving water in citrus orchards. *Scientia Horticulturae*, 128, 274–282.
- García-Tejero, I. F., Duran-Zuazo, V. H., Arriaga, J., & Muriel-Fernandez, J. L. (2012). Relationships between trunk- and fruit-diameter growths under deficit irrigation programmes in orange trees. *Scientia Horticulturae*, 133, 64–71.
- Gasque, M. P., Marti, B. G., & Gonzalez-Altozano, P. (2016). Effects of long-term summer deficit irrigation on ‘Navelina’ citrus trees. *Agricultural Water Management*, 169, 140–147.
- Godfray, H. C. J., Beddington, J. R., Crute, I. R., Haddad, L., Lawrence, D., Muir, J. F., et al. (2010). Food security: The challenge of feeding 9 billion people. *Science*, 327, 812–818. <https://doi.org/10.1126/j.1439-037X.2009.00411.x>.
- Goldhamer, D. A., & Viveros, M. (2000). Effects of preharvest irrigation cutoff durations and postharvest water deprivation on almonds tree performance. *Irrigation Science*, 19, 125–131.
- González-Altozano, P., & Castel, J. R. (1999). Regulated deficit irrigation in ‘Clementina de Nules’ citrus trees. I. Yield and fruit quality effects. *The Journal of Horticultural Science and Biotechnology*, 74, 706–713
- González-Altozano, P., & Castel, J. R. (2000). Effects of regulated deficit irrigation on ‘Clementina de Nules’ citrus trees growth, yield and fruit quality. *Acta Horticulturae*, 537, 749–758.
- INRA. (1968). *Les Agrumes au Maroc. Collection Technique et Production Agricoles*. Institut National de la Recherche Agronomique, Rabat, Morocco.
- Khanna-Chopra, R., & Singh, S. (2011). Approaches to increase water use efficiency in horticultural and grain crops—An overview. *Plant Stress*, 5, 52–63.
- Kriedmann, P. E. (1968). Some photosynthetic characteristics of citrus leaves. *The Australian Journal of Biological Sciences*, 21, 895–905.
- Mossad, A., Farina, V., Lo Bianco, R. (2020). Fruit yield and quality of ‘Valencia’ orange trees under long-term partial rootzone drying. *Agronomy*, 10, 164. <https://doi.org/10.3390/agronomy10020164>
- Nagaz, K., El Mokh, F., Ben Hassen, N., Masmoudi, M. M., Ben Mechlia, N., Baba Sy, M. O., Belkheiri, O., & Ghiglieri, G. (2017). Irrigation and Drainage. <https://doi.org/10.1002/ird.2201>

- Perez-Perez, J. G. J., Garcia, J. M., & Robles and P. Botia. . (2010). Economic analysis of navel orange cv. Lane Late grown on two different drought-tolerant rootstocks under deficit irrigation in Southeastern Spain. *Agricultural Water Management*, *97*, 157–164.
- Romero-Conde, A., Kusakabe, A., & Melgar, J. C. (2014). Physiological responses of citrus to partial rootzone drying irrigation. *Scientia Horticulturae*, *169*, 234–238.
- Romero, P., Navarro, J. F., Perez-Perez, J. G., Garcia-Sanchez, F., Gomez-Gomez, A., Porras, I., et al. (2006). Deficit irrigation and rootstock: Their effects on water relations, vegetative development, yield fruit quality and mineral nutrition of Clementines mandarin. *Tree Physiology*, *26*, 1537–1548.
- Sepaskhah, A. R., & Ahmadi, S. H. (2010). A review on partial root-zone drying irrigation. *International Journal of Plant Production*, *4*, 241–258.
- Treeby, M. T., Henroid, R. E., Bevington, K. B., Milne, D. J., & Storey, R. (2007). Irrigation management and rootstock effects on navel orange [*Citrus sinensis* L. Osbeck] fruit quality. *Agricultural Water Management*, *91*, 24–32.

# **Economics and Management of Wastewater**





# Comparative Analysis on Adsorption Properties and Mechanisms of Nitrate and Phosphate Ions by a Zn Fe<sub>3</sub>O<sub>4</sub>/SiO<sub>2</sub> MCM-48 Magnetic Composite: Kinetic and Isotherm Studies

Mahmoud F. Mubarak and Rasha Hosny

## Abstract

In our research, the magnetic nanocomposite adsorbent Zn Fe<sub>3</sub>O<sub>4</sub>/SiO<sub>2</sub> MCM-48 was prepared, and the ability of this nanocomposite to remove phosphate and nitrate ions from synthetic wastewater was investigated. Various batch adsorption conditions, including different pH, temperature, contact time, initial phosphate concentration and adsorbent dosage conditions, were considered. Phosphate and nitrate adsorption kinetics were well fitted by the pseudo-second-order kinetic model for all studied adsorbents. The adsorption process was represented by Langmuir isotherms. The thermodynamic parameters  $\Delta G$ ,  $\Delta H$  and  $\Delta S$ , which were determined using the Van't Hoff equation, indicated that the phosphate adsorption reactions on the Zn Fe<sub>3</sub>O<sub>4</sub>/SiO<sub>2</sub> MCM-48 nanocomposite were spontaneous and endothermic in nature. The optimal conditions for the adsorption of phosphate and nitrate ions onto Zn Fe<sub>3</sub>O<sub>4</sub>/SiO<sub>2</sub> MCM-48 were a pH of 2.0, temperature of 340 K and contact time of 66 min. The results presented here support the potential of using the Zn Fe<sub>3</sub>O<sub>4</sub>/SiO<sub>2</sub> MCM-48 magnetic nanocomposite as a material for the treatment of phosphate and nitrate ions in wastewater.

## Keywords

Adsorption • Mechanism • Wastewater • Electrostatic attraction • Magnetite

## 1 Introduction

Water *eutrophication* is one of the main water pollution concerns worldwide. *Nitrate* (NO<sub>3</sub><sup>-</sup>) and *phosphate* (PO<sub>4</sub><sup>3-</sup>) are two main nutrients that arouse water eutrophication. They are enriched in the water body because of the human activities, resulting in the degradation of water quality and even the ecological environment. Moreover, excess NO<sub>3</sub><sup>-</sup> in water may cause infant methemoglobinemia and several types of cancers (Zikos & Hagedorn, 2017). Several physical–chemical and biological methods have been developed to manage the nitrate and phosphate in water, such as the adsorption, *chemical precipitation*, ion exchange and bacterial assimilation methods (Zhao et al., 2017). However, the application of the chemical and biological methods is restricted by potential secondary pollution, strict reaction conditions and high cost (Khedhri et al., 2017). Adsorption is a promising method of purifying polluted water in situ, with a relatively low cost and less potential of secondary pollution (Mamba & Mishra, 2016). Therefore, developing an economical and effective *adsorbent* for removing nitrate and phosphate from water is a key factor in the large-scale applications of the adsorption method.

Eutrophication is the term given to the enrichment of water bodies with nutrients, such as nitrates and phosphates. Eutrophication may occur when the concentration of phosphate is higher than 0.02 mg L<sup>-1</sup>. Adsorption is a popular method to remove nutrients, especially phosphorus, from effluent by using porous materials such as zeolites. Nitrate is an emerging pollutant in agricultural, municipal, industrial and mining wastewaters. Nitrate stimulates eutrophication, and it has been linked to the outbreak of infectious diseases. Excess nitrate in drinking water may cause methemoglobinemia, also called a blue baby disease, in newborn infants. Also nitrate can be removed in many ways such as by adsorption (Kilpimaa et al., 2014). The rapid utilization of NO<sub>3</sub><sup>-</sup> and PO<sub>4</sub><sup>3-</sup> made vibration on the environmental scientists to expand the modern techniques for removing them from

M. F. Mubarak (✉)  
Petroleum Applications Department, Core Lab. Center, Egyptian  
Petroleum Research Institute, 1—Ahmed El-Zomer,  
Box No. 11727 Nasr City, Cairo, Egypt

R. Hosny  
Production Department, Core Lab. Center, Egyptian Petroleum  
Research Institute, 1—Ahmed El-Zomer, Box No. 11727  
Nasr City, Cairo, Egypt

water. The numerous  $\text{NO}_3^{3-}$  and  $\text{PO}_4^{3-}$  removal technologies such as biological treatment, chemical precipitation, adsorption, ion exchange and membrane process were investigated in which adsorption method seems to be cost-effective and suitable at industrial level (Aswin Kumar & Viswanathan, 2019). Also there are many iron compounds like Purolite ion exchange resin and hydrous ferric oxide columns in series also removed almost all nitrate and phosphate from the wastewater with initial concentrations 5.9 mg P/L (Gupta et al., 2012),

For these reasons, the objectives of this study are to examine the feasibility of using Zn  $\text{Fe}_3\text{O}_4/\text{SiO}_2$  MCM-48 as an adsorbent for the removal of phosphate and nitrate ions from aqueous solutions by studying the effects of the pH, temperature, contact time, initial phosphate and nitrate concentration, and adsorbent dosage; assessing the potential adsorption capacity and investigating the adsorption mechanism associated with these conditions.

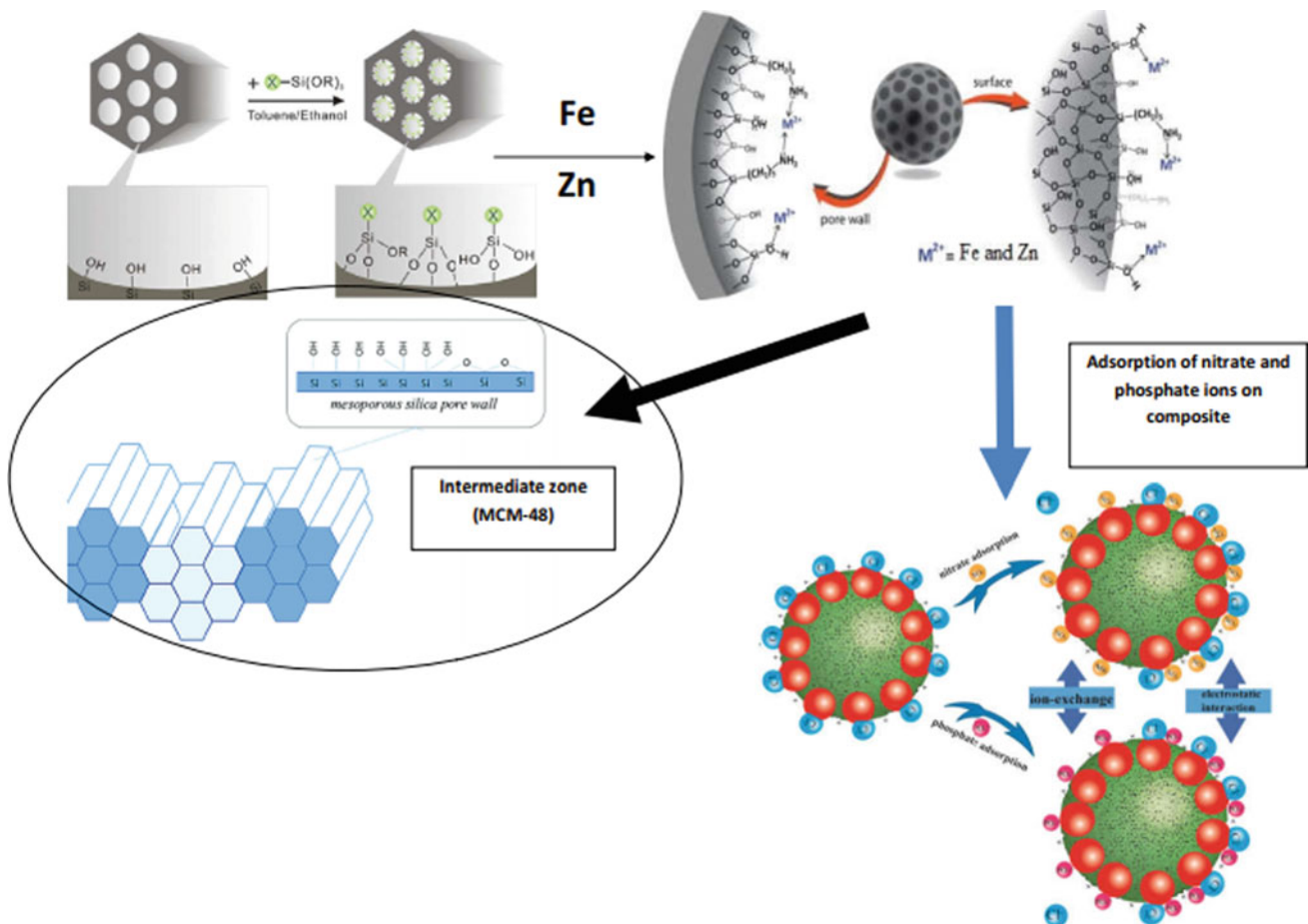
## 2 Materials and Methods

All the reagents and starting materials used were of analytical grade, and distilled water was used to prepare all solutions. The following chemical reagents were used in the

study: potassium dihydrophosphate, potassium nitrate III, potassium nitrate V, 35–38% hydrochloric acid, sodium hydroxide and 99.5–99.9% acetic acid. All the reagents were analytically pure and were purchased from POCH S.A. (Poland). HCl (35–38%),  $\text{NH}_4\text{VO}_3$  (98.0%) and  $(\text{NH}_4)_6\text{Mo}_7\text{O}_{24}$  ( $\geq 99.0\%$ ) were acquired from Merck, India. The typical  $\text{PO}_4^{3-}$  and  $\text{NO}_3^{3-}$  stock solutions were prepared by dissolving of 1.4329 g of anhydrous  $\text{KH}_2\text{PO}_4$  ( $\geq 98.0\%$ ) and 1.6305 g of anhydrous  $\text{KNO}_3$  ( $\geq 98.0\%$ ) in 1000 mL of double distilled (DD) water separately. AR grade of all other reagents was utilized.

### 2.1 Synthesis of Mesoporous MCM-48

MCM-48 mesoporous was synthesized according to the procedure described in the literature (Fathy et al., 2019; Korzeniowska et al., 2019) using TEOS as a silicon source, sodium aluminate, 50% NaOH, hexamethylenimine and aniline (AN, >99%, Sigma Aldrich) in the following molar ratios:  $\text{Si}/\text{Al} = 11.5$ ,  $\text{OH}/\text{Si} = 0.18$ ,  $\text{HMI}/\text{Si} = 0.1$ ,  $\text{H}_2\text{O}/\text{Si} = 45$  and  $\text{AN}/\text{Si} = 0.2$ . The crystallization was carried out for 6 and 2 h in a 200 ml Teflon-lined autoclave at 143 °C. The products were activated as above.



**Schema 1** Shows the nanocomposite for adsorption of phosphate and nitrate anions

## 2.2 Preparation of Zn Fe<sub>3</sub>O<sub>4</sub>/SiO<sub>2</sub> MCM-48 Nanocomposites

A 10 wt% of FeCl<sub>2</sub>, FeCl<sub>3</sub> (1:2) and 1 wt% Zn(NO<sub>3</sub>)<sub>2</sub> impregnated on MCM-48 catalysts were prepared by a wet impregnation method. In a typical procedure, the calculated quantity of FeCl<sub>3</sub> and Zn(NO<sub>3</sub>)<sub>2</sub> was dissolved in 40 mL of methanol, which was stirred for 5 min, followed by the slow addition of MCM-48 to the solution and kept for 6 h at room temperature under stirring. Then, solvent was evaporated on a rotavapour, and finally the catalysts were calcined at 373 K for 1 h (Fathy et al., 2019; Sakate et al., 2018).

## 2.3 Adsorption Experiments

Standard nitrate and phosphate stock solution was prepared by dissolving an appropriate amount of sodium nitrate (NaNO<sub>3</sub>) and potassium dihydrogen phosphate (KH<sub>2</sub>PO<sub>4</sub>) into water. The nitrate and phosphate solution was obtained by stepwise dilution of the stock solutions with purified water. The batch adsorption procedures were conducted to reveal the adsorption isotherms by adding 0.1 g of Zn Fe<sub>3</sub>O<sub>4</sub>/SiO<sub>2</sub> mesoporous MCM-48 into a series of flasks with the nitrate and phosphate solution (0.5–100 mg/L) for 6 h at initial pH values (6.80) and different temperature (288, 298 and 308 K). The adsorption kinetics were investigated by mixing 0.1 g of Zn Fe<sub>3</sub>O<sub>4</sub>/SiO<sub>2</sub> mesoporous MCM-48 with 50 mL of nitrate solution (250 mg/L) and 50 mL of phosphate solution (500 mg/L) in each flask at initial pH values (6.80) and temperature of 288, 298 and 308 K in an orbital shaker at 120 rpm. The investigation was conducted in triplicate. At certain time intervals, Zn Fe<sub>3</sub>O<sub>4</sub>/SiO<sub>2</sub> mesoporous MCM-48 was filtered off, and the concentrations of nitrate (210 nm) and phosphate (700 nm) were measured using a UV–visible spectrophotometer (UV2600, Unico, USA) (Fathy et al., 2016).

## 3 Results and Discussion

### 3.1 Characterization of the Adsorbent Nanocomposites

#### 3.1.1 TEM Image

Figure 1 shows a TEM image of Zn Fe<sub>3</sub>O<sub>4</sub>/SiO<sub>2</sub>MCM-48. The core–shell structure of Zn Fe/Si MCM-48 is not as clearly observable as that of previously reported silica/magnetic nanoparticles. Zn Fe<sub>3</sub>O<sub>4</sub>/SiO<sub>2</sub>MCM-48 sample displayed a skeleton structure with different sizes of nanorods, which is further confirmed by TEM observation

(Fig. 1) (Heba et al., 2017). The HR-TEM image (Fig. 1) reveals that the lattice fringes with crystal plane distances of 0.334 and 0.318 nm, which corresponded to the spacing of the (040) plane of Fe<sub>2</sub>O<sub>3</sub> and the (101) plane of Zn(OH)<sub>2</sub>.

### 3.2 XRD Analysis

The XRD pattern of the A-MCM-48 is shown in (Fig. 2). It demonstrated that the A-MCM-48 has the typical long-range ordered hexagonal mesoporous structure. The structure can be verified by the observation of four distinct diffraction peaks indexed as (1 0 0), (1 1 0), (2 0 0) and (2 1 0) in the low  $2\theta$  region (Zhang et al., 2016d). In addition, the interplanar distance of the sample is 5.29 nm. The hexagonal unit cell parameter  $a_0 = 2d_{100}/1.732$  of the sample is 6.11 nm (Liu et al., 2013). In addition, the XRD plot of the hexagonal ZnO structure contains nine prominent peaks, which indicates that the single phase is within the detection limit. The diffraction peaks of the Zn Fe<sub>3</sub>O<sub>4</sub>/SiO<sub>2</sub>MCM-48 nanocomposite are sharp, and their  $2\theta$  positions can be observed at 32° and 38°, indicating the presence of magnetite Fe<sub>3</sub>O<sub>4</sub> or maghemite  $\gamma$ -Fe<sub>2</sub>O<sub>3</sub> that were well indexed to Fe<sub>2</sub>O<sub>3</sub> (JCPDS 02-0282). Due to the high diffractogram resolution, only the mean crystallite size of the Zn Fe/Si MCM-48 sample could be inferred from the X-ray plot, with a value of 60 nm.

### 3.3 FT-IR Analysis

The functional groups of Zn Fe<sub>3</sub>O<sub>4</sub>/SiO<sub>2</sub>MCM-48 nanocomposite are shown in the FT-IR spectra (Fig. 3). The spectra presented characteristics and adsorption peaks indicated the complex nature of the sample compositions. The strong and *broad band* around 3039–3710 cm<sup>-1</sup> of Zn Fe<sub>3</sub>O<sub>4</sub>/SiO<sub>2</sub>MCM-48 nanocomposite could be assigned to the O–H groups, carboxylic groups stretching, corresponding to the vibration of functional groups in Zn Fe<sub>3</sub>O<sub>4</sub>/SiO<sub>2</sub>MCM-48 nanocomposite (Hosny et al., 2016). The peak located at 1447.06 cm<sup>-1</sup> was attributed to the stretching vibration of stretching vibrations of Si–O–Si and to the stretching of silanol groups ( $\equiv$ Si–OH). The decreased adsorption peak in Zn Fe<sub>3</sub>O<sub>4</sub>/SiO<sub>2</sub>MCM-48 nanocomposite at 734.7 and 1167 cm<sup>-1</sup> was caused by the stretching vibration of SiO in (Mahmoud Fathy et al., 2015). The band around 1634 cm<sup>-1</sup> is attributed to the characteristics of water molecules inside the framework, and the bands around 3445 cm<sup>-1</sup> correspond to OH<sup>-</sup> group from water molecules. This illustrated that the sample is hydrophilic, and it adsorbs some water when it is exposed to the air (Liu et al., 2013).

**Fig. 1** TEM image of Zn Fe<sub>3</sub>O<sub>4</sub>/SiO<sub>2</sub>MCM-48

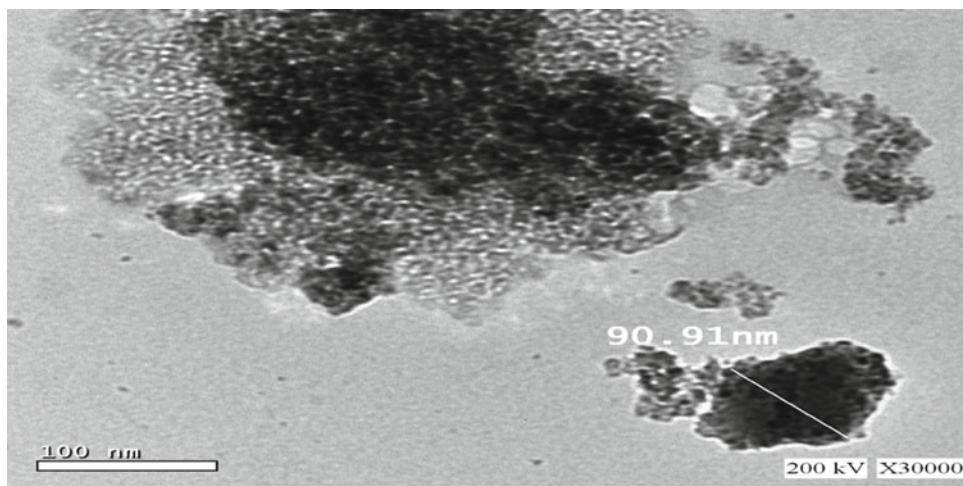


**Fig. 2** X-ray diffraction (XRD) spectra of the Zn Fe<sub>3</sub>O<sub>4</sub>/SiO<sub>2</sub>MCM-48 nanocomposite

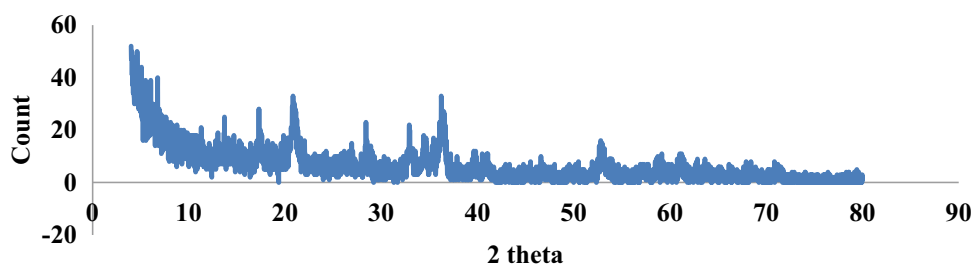
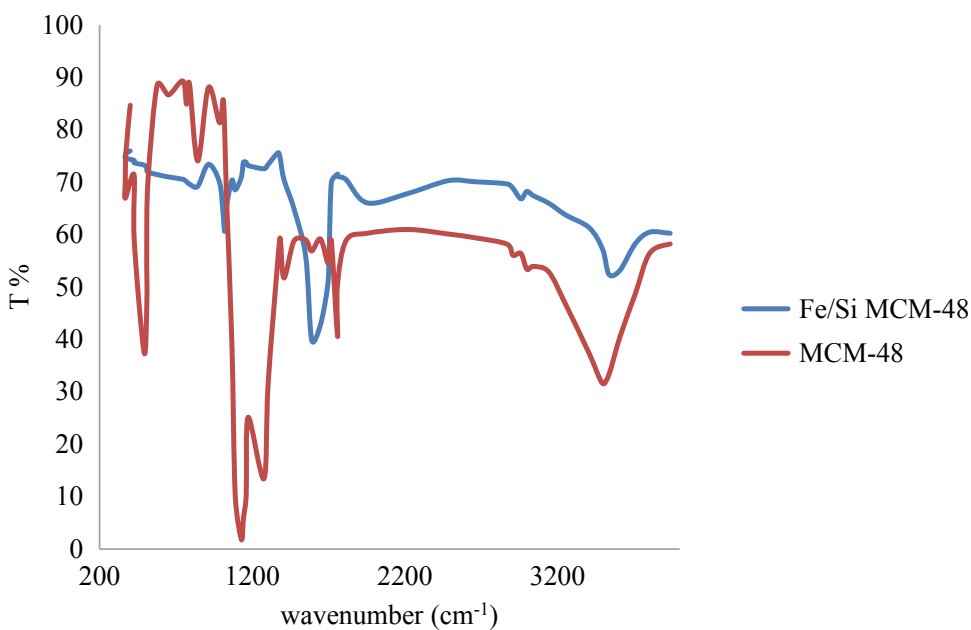


**Fig. 3** FT-IR spectrum of the Zn Fe<sub>3</sub>O<sub>4</sub>/SiO<sub>2</sub>MCM-48 nanocomposite sintered at various temperatures



The FT-IR spectra indicated that the modification reaction resulted in the intensity variation and peak shift, and the functional groups (amine groups) were successfully loaded onto Zn Fe<sub>3</sub>O<sub>4</sub>/SiO<sub>2</sub>MCM-48 nanocomposite samples. Also this result suggests that Si atoms are replaced by Zn ions on the surface to form Si–O–Zn bonds.

### 3.4 Adsorption Studies

#### 3.4.1 Effect of Dose

The effect of adsorbent dosage (Zn Fe<sub>3</sub>O<sub>4</sub>/SiO<sub>2</sub>MCM-48) on simultaneous nitrate and phosphate removal is illustrated in (Fig. 4). With increasing adsorbent dosage from 0.2 to



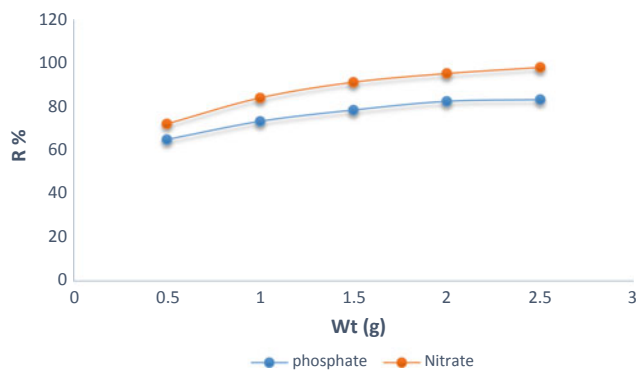


**Fig. 4** Effect of magnetic sorbent amounts of nitrate and phosphate ions on the solid phase of (Zn Fe/Si MCM-48) pre-concentration phosphate ions

1.0 g/L, the removal rates of nitrate and phosphate increased from 84 to 96.5%, 62 to 82%, respectively. However, the removal rates of nitrate and phosphate decreased to 98.3 and 87.1% when adsorbent dosage was increased to 1.5 g/L. As the adsorbent dosage was further increased to 2.0 g/L, the removal rates of nitrate and phosphate continued to decrease. This may be attributed to the decrease of available activated sites due to the aggregation of adsorbent (Keränen et al., 2015). That behaviour of increasing the amine cross-linked tea wastes dosage from 1 to 8 g/L increased the nitrate removal from 57.4 to 89.2%. Less amine cross-linked tea wastes were needed to remove phosphate, as increasing the amine cross-linked tea wastes dose from 0.4 to 2 g/L increased the phosphate removal from 45.3 to 92.3%. There was no critical increase in the removal rates for nitrate and phosphate when the ACTW dosage was >8 and 2 g/L, respectively (Qiao et al., 2019).

### 3.4.2 Effects of pH on Anions Adsorption

For anion pollutant adsorption, the pH value is a significant factor. The adsorption of nitrate and phosphate ions on adsorbents at different pH conditions is shown in Fig. 5. Figure 5 shows that the removal rates of nitrate and phosphate on Zn Fe<sub>3</sub>O<sub>4</sub>/SiO<sub>2</sub>MCM-48 adsorbent increased with increasing pH from 3.8 to 6.2, and it can be clearly found that the nitrate removal rate at pH = 3.8 was higher than that at pH of 4–6. It may be due to the high adsorption rate (Kazemi et al., 2015). The nitrate removal rate began to decrease when the pH value was higher than 6.2, which may be ascribed to that the increasing hydroxide ions would compete with nitrate for the adsorption sites of the Zn Fe<sub>3</sub>O<sub>4</sub>/SiO<sub>2</sub>MCM-48 adsorbent. Therefore, the nitrate adsorption was retarded. Usually, the form of phosphate compound, such as H<sub>3</sub>PO<sub>4</sub>, H<sub>2</sub>PO<sub>4</sub><sup>−</sup>, HPO<sub>4</sub><sup>2−</sup> and PO<sub>4</sub><sup>3−</sup>, depends on the solution pH value (Zhang et al., 2016b). Figure 5 shows that

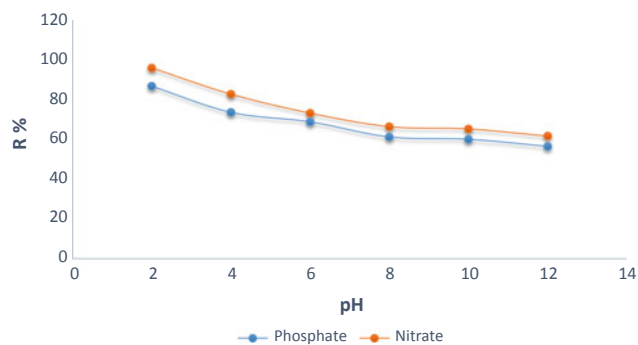


**Fig. 5** The nitrate and phosphate adsorption by Zn Fe/Si MCM-48 at different pH values

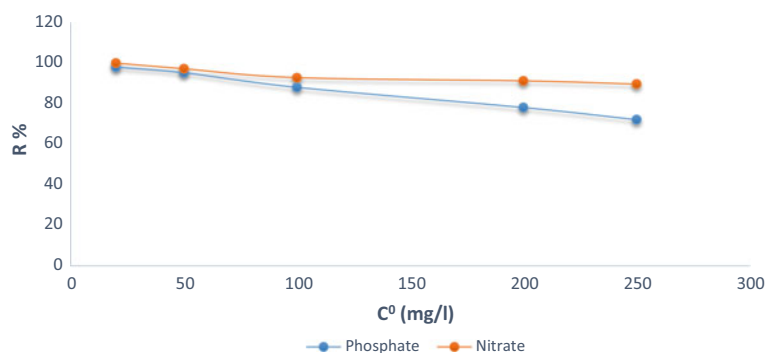
the average removal rate of phosphate reached 90.6% when the pH was 3.2. Meanwhile, the mainly chemical form of phosphorus is H<sub>2</sub>PO<sub>4</sub><sup>−</sup>—under acid condition and the surface protonation of Zn Fe<sub>3</sub>O<sub>4</sub>/SiO<sub>2</sub>MCM-48 adsorbent enhanced the adsorption of phosphate by electrostatic attraction (Zhang et al., 2016a). The removal rate of phosphate was greatly reduced as the pH value was increased to more than 7, which is ascribable to that the electrostatic attraction was shifted to electrostatic repulsion because of the deprotonation of Zn Fe<sub>3</sub>O<sub>4</sub>/SiO<sub>2</sub>MCM-48 adsorbent. Furthermore, the competition between hydroxide ions and phosphate ions was also responsible for the low adsorption efficiency (Zhang et al., 2016f). We observe that results of high phosphate removal efficiency were observed between pH 5 and 9, whereas high nitrate removal was achieved at pH 7. 2. And high nitrate removal was achieved at pH 7, whereas high phosphate removal was observed in the range of pH 5–9. The decrease in nitrate removal above pH 7 could be due to stronger competition with hydroxide ions, while low removal below pH 7 can be attributed to instability of oxides of SWR at lower pH (Berkessa et al., 2019).

### 3.4.3 Different Initial Solution Concentrations

Initial contaminating *ion concentration* was also an important parameter for nitrate and phosphate adsorption by Zn Fe<sub>3</sub>O<sub>4</sub>/SiO<sub>2</sub>MCM-48 (Fig. 6). As the initial concentration of either ion increased, the adsorption capacities of the Zn Fe<sub>3</sub>O<sub>4</sub>/SiO<sub>2</sub>MCM-48 for those ions gradually reached equilibrium and then their respective maximum adsorption capacities, 232.26 and 222 mg/g. At low initial concentrations, the low adsorption capacities might reflect the fact that active sites on the surface of the adsorbent had not reached fullness (Zhang et al., 2016e). The adsorption capacities increased drastically with increased initial nitrate and phosphate concentration, possibly since higher initial nitrate or phosphate ion concentration would increase the driving force



**Fig. 6** Removal efficacy of phosphate ions by Zn Fe<sub>3</sub>O<sub>4</sub>/SiO<sub>2</sub>MCM-48 at different concentrations



to overcome the mass transfer resistance of nitrate or phosphate between the solid and aqueous phases and because of a more intense interaction between nitrate/phosphate and the adsorbent. The plateau occurs when the active sites on the surface of the Zn Fe<sub>3</sub>O<sub>4</sub>/SiO<sub>2</sub>MCM-48 reach saturation. It is worth noting that the adsorption capacity of the Zn Fe<sub>3</sub>O<sub>4</sub>/SiO<sub>2</sub>MCM-48 for an applied nitrate solution of 250 mg/L nitrate aqueous was 232.2 mg/g (Fig. 6), which is significantly higher than the adsorption capacities of other reported cross-linked agricultural by-products (Zhang et al., 2016d). At low adsorption doses (10 mg), Zn Fe<sub>3</sub>O<sub>4</sub>/SiO<sub>2</sub>MCM-48 also showed high adsorption capacity (249 mg/g) for removal of phosphates (Fig. 6), which is significantly higher than the adsorption capacities of other reported cross-linked agricultural by-products (Zhang et al., 2016g). Same results and same behaviour were observed in Berkessa et al. (2019) where the effect of adsorbate concentration on the adsorption was investigated by varying the initial concentration of phosphate between 0.2 and 260 mg/L and that of nitrate–nitrogen between 3 and 19 mg/L. The decrease in nitrate adsorption could suggest lack of available area required for the high initial concentration of nitrate. This result is similar with the observation made by Katal et al. where there is a decrease in the percentage removal of nitrate from 94.5 to 46.3% with the increase in initial concentration from 50 to 300 mg/L.

#### 3.4.4 Effect of Temperature

The adsorption equilibria of nitrate and phosphate on Zn Fe<sub>3</sub>O<sub>4</sub>/SiO<sub>2</sub>MCM-48 at different temperatures are shown in Fig. 7. As seen in the figure, the adsorption % increased correspondingly with increasing temperature and that because the mass transfer driving force increased as the initial concentration increased, thereby increasing adsorption capacity (Zhang et al., 2016c). The adsorption capacity of nitrate and phosphate on Zn Fe<sub>3</sub>O<sub>4</sub>/SiO<sub>2</sub>MCM-48 was 12.42 and 20.13 mg/g at 100 mg/L and 288 K, respectively. The decreased values of  $q_e$  at the increased temperature revealed that the adsorption process may be exothermic to a certain extent (Zhang et al., 2016c).

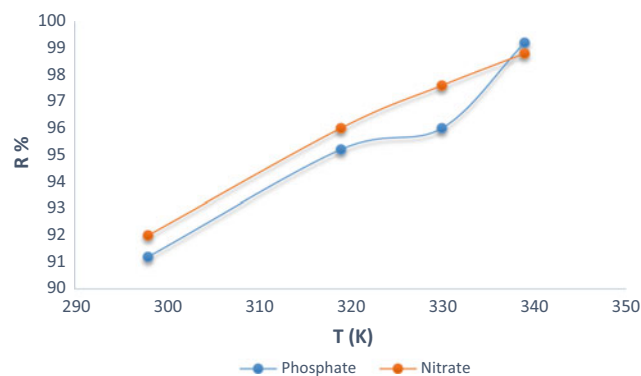


**Fig. 7** Effect of temperature on the adsorption of phosphate ions by Zn Fe/Si MCM-48 nanocomposites

#### 3.4.5 Adsorption Isotherms

The dependences of phosphate adsorbed onto Zn Fe<sub>3</sub>O<sub>4</sub>/SiO<sub>2</sub>MCM-48 at equilibrium concentrations and at a pH of 7.0 for both the Langmuir and Freundlich equations are described in Figs. 8 (Zhang et al., 2016d).

Langmuir isotherm is used to describe single layer adsorption. The linearized form of Langmuir isotherm model is given as (Aljbour et al., 2016)

$$1/q_e = 1/q_m + 1/bq_m C_e \quad (1)$$

where  $q_e$  is the amount adsorbed per unit weight of adsorbate (mg/g),  $C_e$  is the equilibrium concentration of adsorbate in the solution after sorption (mg/L), and  $q_m$  and  $b$  are the Langmuir constants.  $q_m$  indicates the saturated monolayer sorption capacity (mg/g), and  $b$  represents the sorption equilibrium constant (L/mg). The Langmuir isotherm parameters can be obtained by plotting  $1/q_e$  versus  $C_e$  as shown in Fig. 8.

#### Freundlich Isotherm

The Freundlich isotherm is used for heterogenous surface systems. The linearized form of Freundlich isotherm equation is given as (Aljbour et al., 2016)

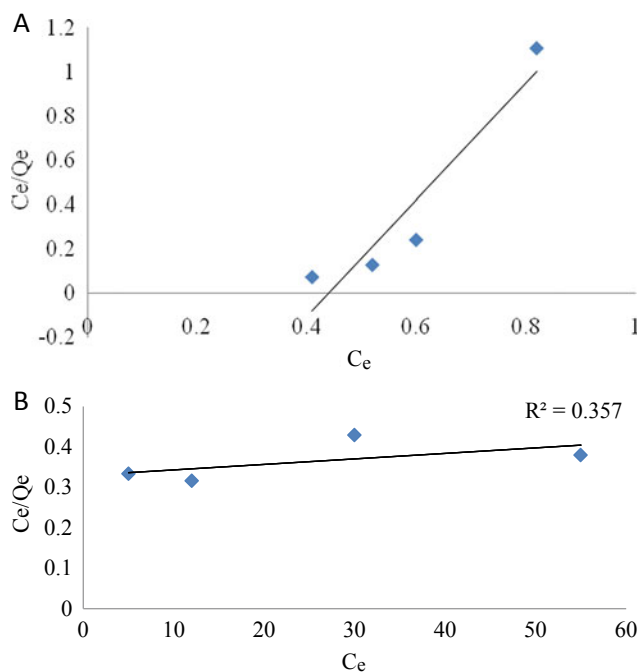


**Fig. 8** Langmuir adsorption isotherm between  $1/C_e$  and  $1/Q_e$  for **a** phosphate and **b** nitrate ions on the prepared Zn Fe<sub>3</sub>O<sub>4</sub>/SiO<sub>2</sub>MCM-48 composite

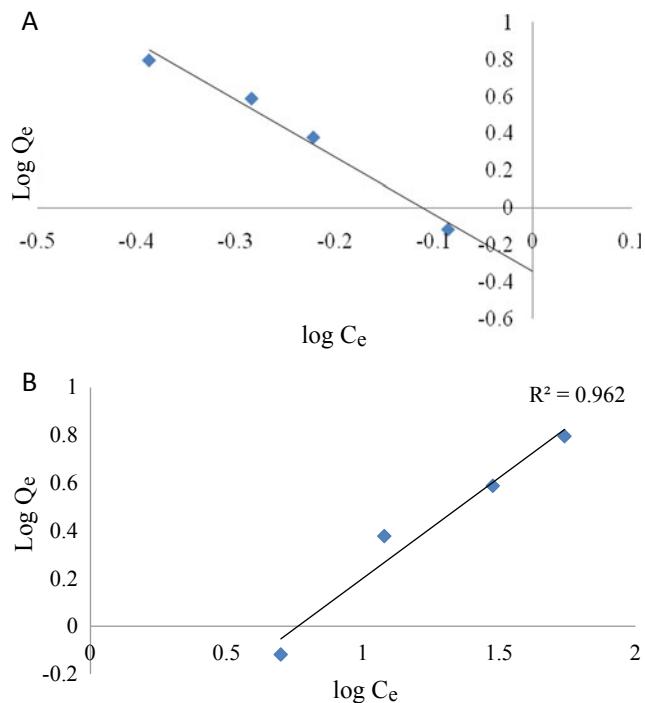


**Fig. 9** Freundlich adsorption isotherm between  $\log C_e$  and  $\log Q_e$  for **a** phosphate and **b** nitrate ions on the prepared Zn Fe<sub>3</sub>O<sub>4</sub>/SiO<sub>2</sub>MCM-48 composite

$$\log qe = \log K + 1/n \log Ce \quad (2)$$

where  $q_e$  is the amount adsorbed per unit weight of adsorbate (mg/g),  $C_e$  is the equilibrium concentration of adsorbate in the solution after sorption (mg/L), and  $K$  and  $n$  are the Freundlich constants.  $K$  indicates the sorption capacity, and  $n$  represents the reaction energy. The Langmuir isotherm parameters can be obtained by plotting  $\log qe$  versus  $\log C_e$  as shown in Fig. 9.

The isotherm equations and their linear plot details are shown in Tables 1 and 2. The single layer type of adsorption was governed by Langmuir which was plotted by  $C_e$  versus  $C_e/q_e$ . The multilayer type adsorption was governed by Freundlich which was plotted by  $\log q_e$  versus  $\log C_e$ , and the best fit in these parameters is listed in Tables 1 and 2. The  $1/n$  and  $n$  values should be around 0 to 1 and 1 to 10 for the adsorption to be feasible. In Freundlich isotherm, it was detected that  $1/n$  values were dropping between 0 and 1, whereas  $n$  values falling between 1 and 10 denote the favourable nature of NO<sub>3</sub><sup>-</sup> and PO<sub>4</sub><sup>3-</sup> adsorption onto Zn Fe<sub>3</sub>O<sub>4</sub>/SiO<sub>2</sub>MCM-48 composite beads (Hydro).

### 3.4.6 Thermodynamic Study

The thermodynamic experiments were used to examine the thermodynamic probability of the adsorption system and calculating their parameters like standard entropy change ( $\Delta S^\circ$ ), standard enthalpy change ( $\Delta H^\circ$ ), standard free energy change ( $\Delta G^\circ$ ) and activation energy ( $E_a$ ) (Alagha et al., 2020). These thermodynamic parameters can be calculated from following Eq. (3–5)

$$\Delta G = -RT \ln Kd \quad (3)$$

$$\ln K = \Delta S - \Delta H/RT \quad (4)$$

where  $T$  is the experimental temperature (Kelvin) and  $R$  is the gas constant (8.314 J/(mol/K)). Moreover, the activation energy ( $E_a$ ) delivers the nature of sorption system which is generally physisorption or chemisorption, and it was examined using the following equation.

$$E_a = \Delta H_{ads} + RT \quad (5)$$

The Gibbs free energy reflects the spontaneity degree of the adsorption process, where more negative values suggest an energetically favourable adsorption process. Commonly, for physisorption, the change in free energy is between -20 and 0 kJ/mol, but the change in free energy in the case of chemisorption ranges between -80 and 400 kJ/mol.

The free energy of the process at all temperatures was negative and changed with the rise in temperature (Tables 3 and 4; Fig. 10). This indicates that the adsorption process

**Table 1** Phosphate ions adsorption by Zn Fe<sub>3</sub>O<sub>4</sub>/SiO<sub>2</sub>MCM-48

Isotherm equation	Zn Fe <sub>3</sub> O <sub>4</sub> /SiO <sub>2</sub> MCM-48				X2
	298	319	330	339	
<i>Langmuir</i>					12
$q^0$ (mg g <sup>-1</sup> )	22	18.327	17.2803	18.256	
$K$ (L mg <sup>-1</sup> )	0.001354	0.001383	0.001756	0.002078	
$R^2$	0.597509	0.512908	1	0.727058	
$RL$	0.806452	0.373134	0.37037	0.42735	
<i>Freundlich</i>					11
$k_f$	0.841883	0.890105	0.880918	0.886283	
$n$	0.640624	0.58855	0.59743	0.62917	
$R^2$	0.98084	0.99482	0.99664	0.99944	

**Table 2** Nitrate ions adsorption by Zn Fe<sub>3</sub>O<sub>4</sub>/SiO<sub>2</sub>MCM-48

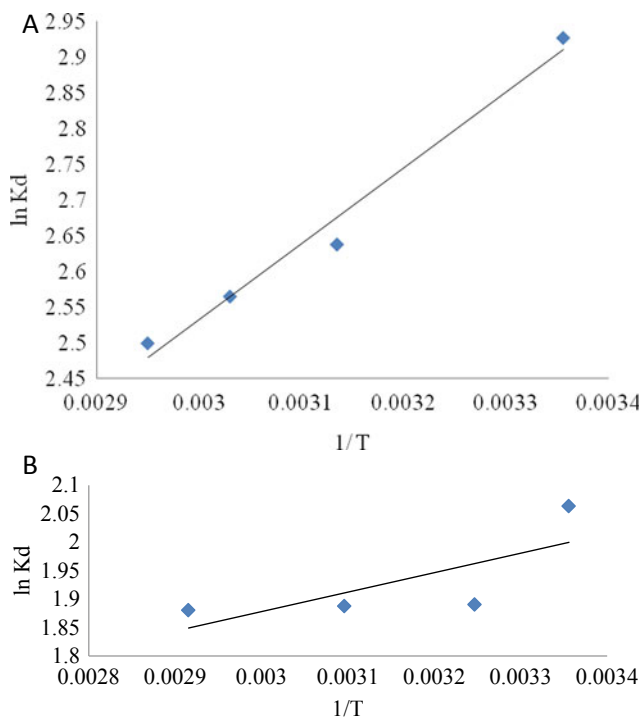
Isotherm equation	Zn Fe <sub>3</sub> O <sub>4</sub> /SiO <sub>2</sub> MCM-48				14
	298	319	330	339	
<i>Langmuir</i>					14
$q^0$ (mg g <sup>-1</sup> )	20	17.17573	16.1636	16.073	
$K$ (L mg <sup>-1</sup> )	0.004114	0.00068	0.00194	0.004817	
$R^2$	0.56896	0.11107	1	0.631983	
$RL$	0.806452	0.373134	0.37037	0.42735	
<i>Freundlich</i>					17
$k_f$	0.629954	0.635777	0.579245	0.599785	
$n$	0.131389	1.22648	1.34087	1.33288	
$R^2$	0.9854	0.9478	0.9554	0.9221	

**Table 3** linear kinetic data for the adsorption of phosphate onto Zn Fe/Si MCM-48

Order	$C^0$	$K_1$	$Q_e$	$R^2$
1 <sup>st</sup> order model	20 mg/l	-0.0104	0.1723	0.9664
	50 mg/l	-0.0072	0.2543	0.9492
	100 mg/l	-0.0035	0.3075	0.9931
	250 mg/l	-0.0012	0.3796	0.9853
2 <sup>nd</sup> order model	$C_0$	$K_2$	$Q_e$	$R^2$
	20 mg/l	58.707	0.017	0.8445
	50 mg/l	101.689	0.0098	0.6940
	100 mg/l	50	0.02	1
	250 mg/l	220	0.004	1
Intraparticle diffusionmodel	$C_0$	$a$	$k_d$	$R^2$
	20 mg/l	0.09491	32.747	0.8819
	50 mg/l	0.09491	28.327	0.8819
	100 mg/l	0.0813	29.714	0.8964
	250 mg/l	0.0669	32.747	0.8039

**Table 4** Linear kinetic data for the adsorption of nitrate onto Zn Fe/Si MCM-48

Order	$C^0$	$K_1$	$Q_e$	$R^2$
1 <sup>st</sup> order model	20 mg/l	-0.0017	0.17445	0.96207
	50 mg/l	-0.00724	0.25432	0.949202
	100 mg/l	-0.00734	0.28834	0.982115
	250 mg/l	-0.0017	0.3746	0.928332
2 <sup>nd</sup> order model	$C_0$	$K_2$	$Q_e$	$R^2$
	20 mg/l	58.7	0.0170	0.9844
	50 mg/l	91.26	0.0109	0.9407
	100 mg/l	50	0.02	1
	250 mg/l	240	0.004	1
Intraparticle diffusion model	$C_0$	$a$	$k_d$	$R^2$
	20 mg/l	0.0883	21.242	0.8761
	50 mg/l	0.0883	25.476	0.8761
	100 mg/l	0.0419	13.239	0.7062
	250 mg/l	0.0478	21.242	0.6806

**Fig. 10** Van't Hoff plot of the adsorption of 100 mg/L (initial concentration) of phosphate and nitrate by Zn Fe<sub>3</sub>O<sub>4</sub>/SiO<sub>2</sub>MCM-48

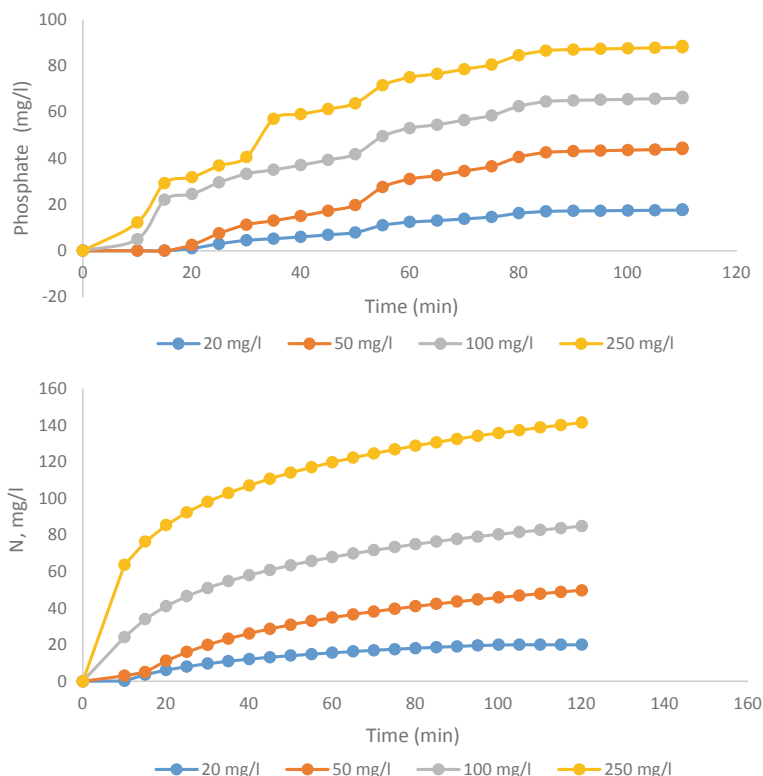
was spontaneous and thermodynamically favourable. The more negative values of  $\Delta G$  imply a greater driving force for the adsorption process. As the temperature increased, the  $\Delta G$  value increased, indicating a higher driving force resulting in a greater adsorption affinity at higher

temperatures (El-Naggar et al., 2019). The value of  $\Delta H$  was positive, indicating that the adsorption process was endothermic in nature (Fathy et al., 2014). The positive value of  $\Delta S$  suggested increased randomness at the solid/solution interface with some structural changes in the adsorbate and the adsorbent and an affinity of the adsorbent towards phosphate. Though the adsorption of dyes is currently described as an exothermic phenomenon (Afroze & Sen, 2018), endothermic adsorption was also reported in the literature: acid orange 7 dye in aqueous solutions using spent brewery grains, methylene blue adsorption using wheat shells and malachite green and basic red using activated carbon and activated slag (Dong et al., 2019). However in case of nitrate, the entropy increased like in the present work and the same phenomenon was reported by Gupta et al. (2003). These differences may be attributed to the physical and chemical characteristics of the anions and adsorbents, which play an important role in adsorption (Boopathy et al., 2013). Many adsorbents show that the thermodynamics parameters show the effect of temperature on adsorption capacity, thus imply the spontaneity of the process. Standard Gibbs free energy was all negative and decreased as temperature increased, suggesting that the adsorption is spontaneous and favours high temperature. The positive standard enthalpy indicates that the process is endothermic; therefore, high temperature can promote adsorption (Gupta et al., 2020).

### 3.4.7 Contact Time Effect

For successful application of Zn Fe<sub>3</sub>O<sub>4</sub>/SiO<sub>2</sub>MCM-48 for nitrate removal, it is important to achieve high adsorption

**Fig. 11** Effect of the contact time on the adsorption of nitrate and phosphate by the Zn Fe<sub>3</sub>O<sub>4</sub>/SiO<sub>2</sub>MCM-48 nanocomposite



capacity for nitrate in a short time. According to Fig. 11, the rate of anion removal by the Zn Fe<sub>3</sub>O<sub>4</sub>/SiO<sub>2</sub>MCM-48 was sharp at initial times followed by a long slow decline, as reported by (Bavaresco et al., 2017). About 72, 54 and 58% of adsorption occurred at the first 5 min for nitrate and phosphate, respectively. The adsorption equilibrium was fully established after 90 min for nitrate. For phosphate, adsorption continued over 100 min (Fig. 11). The results showed that adsorption of nitrate was higher and faster than that of phosphate. Keränen et al. (2015) showed that about 40% of nitrate adsorption on Mg–Al–LDH (3:1) occurred within the first 5 min. Keränen et al. (2015) reported that about 93% of adsorption of phosphate by Mg–Al–LDH (2:1) was obtained within 5 min. The percentage removal depends on the type and initial concentration of anion as well as Zn Fe<sub>3</sub>O<sub>4</sub>/SiO<sub>2</sub>MCM-48 characteristics such as Zn Fe<sub>3</sub>O<sub>4</sub>/SiO<sub>2</sub>MCM-48 type, calcination, crystallization of Zn Fe<sub>3</sub>O<sub>4</sub>/SiO<sub>2</sub>MCM-48, molar ratio of M<sup>2+</sup>/M<sup>3+</sup> and method of synthesis (Khalid et al., 2015). The percentage of removal decreased with increasing initial phosphate concentration. In these studies, besides the difference in the initial concentrations, higher absorption rate of nitrate and phosphate within the first 5 min could be due to the active site percentage with respect to the concentrations of ions. Removal of nitrate higher than phosphate ions may be due to the higher nitrate

adsorption capacity and selectivity of Zn Fe<sub>3</sub>O<sub>4</sub>/SiO<sub>2</sub>MCM-48, obtained from preliminary experiments.

### 3.4.8 Kinetic Mechanism of Adsorption

The adsorption kinetics study describes the absorption uptake capacity of the solute and the time required to reach dense absorption at the solid solution interface, including the effect of diffusion. The effect of the contact time on batch adsorption at 20, 50, 100, 250 mg L<sup>-1</sup> initial phosphate ion concentrations, 303 K and pH 7.0 was investigated, and the results are shown in Figs. 12 and 13.

The pseudo-first-order kinetic model, pseudo-second-order kinetic model and intraparticle diffusion model (Zhang et al., 2016f) were used to investigate the mechanism of adsorption. The dynamic experimental data were obtained at particle sizes of 200 nm. The adsorption mechanism depends on the physical and chemical characteristics of the adsorbent and the mass transfer process. Such kinetic models can be expressed by the following Eqs. (6–8):

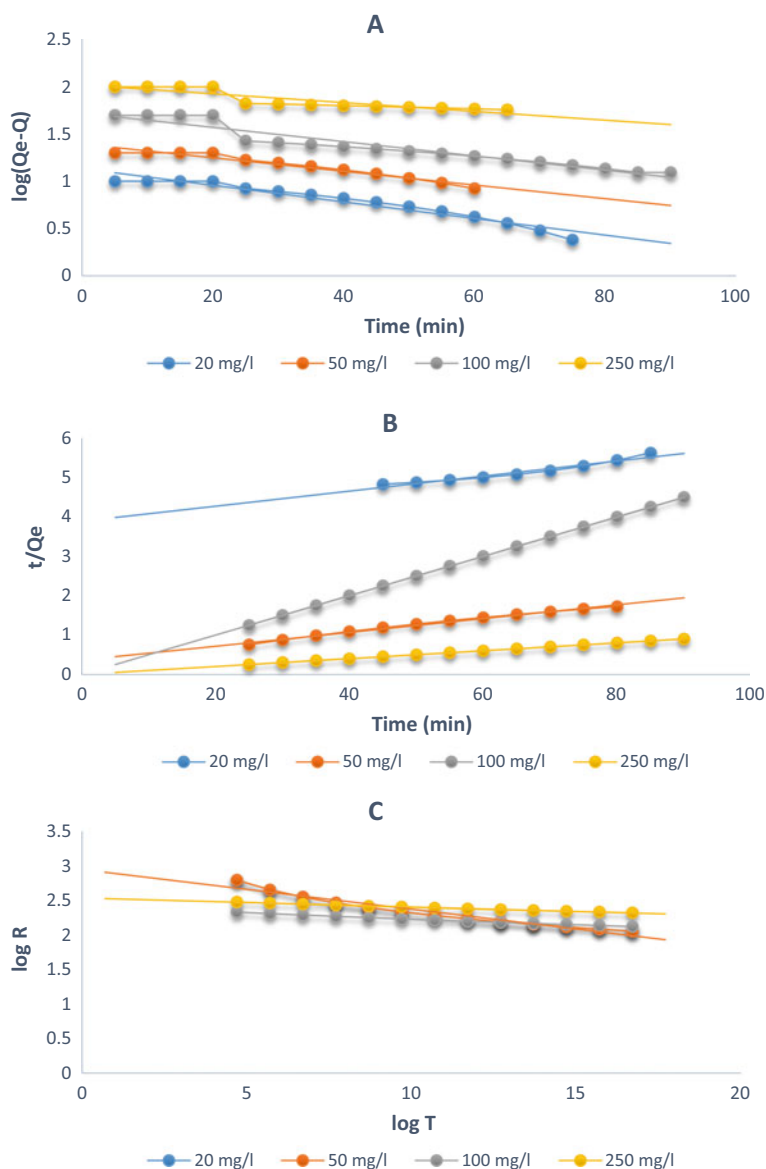
$$qt = qe(1 - e^{-k_1t}) \quad (6)$$

$$qt = k_2q_2et_1 + k_2qet \quad (7)$$

$$qt = kpt^{1/2} \quad (8)$$



**Fig. 12** Linear kinetic model A) 1st pseudo order, B) 2nd pseudo order and C) intraparticle diffusion models of phosphate adsorption by Zn Fe<sub>3</sub>O<sub>4</sub>/SiO<sub>2</sub>MCM-48

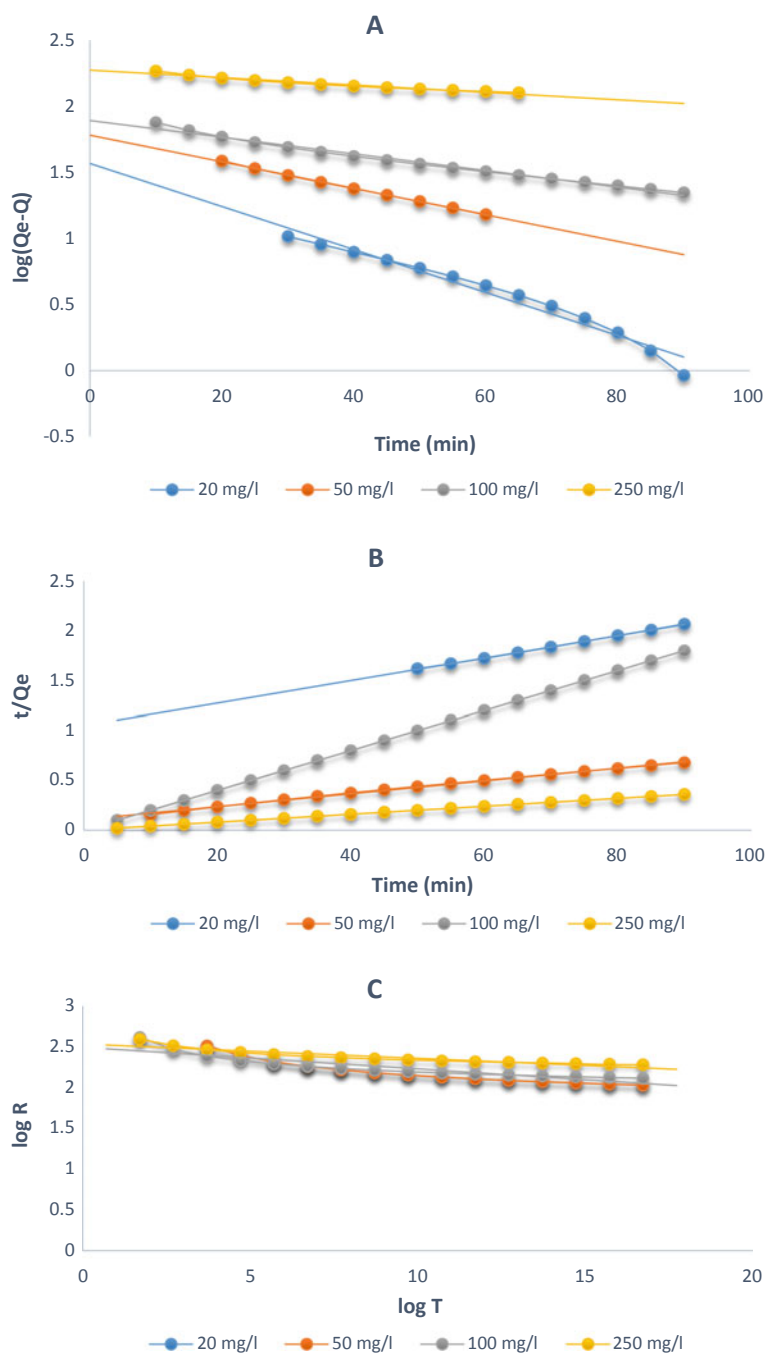


where  $q_e$  (mg/g) and  $q_t$  (mg/g) are the quantities of phosphate ions adsorbed at equilibrium and at time  $t$ , respectively; the rate constants of the pseudo-first-order and second-order reactions are  $k_1$  ( $s^{-1}$ ) and  $k_2$  (g/mg/min), respectively; and the constant of intraparticle diffusion is  $k_p$  (mg/g/half minute). In addition, all the correlation coefficients and other parameters were calculated from the models given in Tables 5 and 6.

As evidenced by the higher  $R^2$  (3, 4), the experimental data of nitrate and phosphate adsorption on the Zn Fe<sub>3</sub>O<sub>4</sub>/SiO<sub>2</sub>MCM-48 were better fitted to the pseudo-second-order

model. In addition, for all three anions the calculated ion adsorbed at equilibrium time ( $q_e$ ) from the pseudo-second-order model was more close to the experimental data. The experimental  $q_e$  values for nitrate and phosphate were obtained, 250 and 240 mg/l, respectively. Among the kinetics models, pseudo-first order and pseudo-second order have been widely used for oxyanion adsorption by Zn Fe<sub>3</sub>O<sub>4</sub>/SiO<sub>2</sub>MCM-48 (Hoque et al., 2016). These common models are used in order to determine the rate constants of adsorption and to find out information about the adsorption mechanisms.

**Fig. 13** Linear kinetic model A) 1st pseudo order, B) 2nd pseudo order and C) intraparticle diffusion models of the adsorption of nitrate by Zn Fe<sub>3</sub>O<sub>4</sub>/SiO<sub>2</sub>MCM-48



## 4 Conclusions

The novel Zn Fe<sub>3</sub>O<sub>4</sub>/SiO<sub>2</sub>MCM-48 adsorbent was prepared and characterized, and the adsorption behaviours of nitrate and phosphate on Zn Fe<sub>3</sub>O<sub>4</sub>/SiO<sub>2</sub>MCM-48 in binary systems were investigated. The surface of Zn Fe<sub>3</sub>O<sub>4</sub>/SiO<sub>2</sub>MCM-48 was rougher, and the intensity variation of related functional

groups appeared in the FT-IR spectra. The adsorption process could be described by the Langmuir isotherm and pseudo-second-order equation, and the maximum adsorption capacity, as calculated from the Langmuir equation at 298 K of nitrate and phosphate on Zn Fe<sub>3</sub>O<sub>4</sub>/SiO<sub>2</sub>MCM-48, was 220 and 190 mg/g, respectively. The adsorption of nitrate and phosphate on Zn Fe<sub>3</sub>O<sub>4</sub>/SiO<sub>2</sub>MCM-48 was spontaneous and exothermic. Therefore, Zn Fe<sub>3</sub>O<sub>4</sub>/SiO<sub>2</sub>MCM-48 is

**Table 5** Linear kinetic data for the adsorption of phosphate onto Zn Fe<sub>3</sub>O<sub>4</sub>/SiO<sub>2</sub>MCM-48

Order	C <sub>0</sub>	K <sub>1</sub>	Q <sub>e</sub>	R <sup>2</sup>
1 <sup>st</sup> -order model	20 mg/l	-0.01046	0.17239	0.966431
	50 mg/l	-0.00724	0.25432	0.949202
	100 mg/l	-0.00353	0.30756	0.99311
	250 mg/l	-0.00129	0.37963	0.985357
2 <sup>nd</sup> -order model	C <sub>0</sub>	q <sub>e</sub>	k <sub>2</sub>	R <sup>2</sup>
	20 mg/l	-58.7075	0.017034	-0.84456
	50 mg/l	101.6891	0.009834	0.694044
	100 mg/l	50	0.02	1
	250 mg/l	220	0.004	1
Intraparticles model	C <sub>0</sub>	a	k <sub>d</sub>	R <sup>2</sup>
	20 mg/l	0.09491	32.74783	0.881992
	50 mg/l	0.09491	28.32762	0.881992
	100 mg/l	0.08132	29.71492	0.896456
	250 mg/l	0.06695	32.74783	0.803917

**Table 6** Linear kinetic data for the adsorption of nitrate onto Zn Fe<sub>3</sub>O<sub>4</sub>/SiO<sub>2</sub>MCM-48

Order	C <sub>0</sub>	K <sub>1</sub>	Q <sub>e</sub>	R <sup>2</sup>
1 <sup>st</sup>	20 mg/l	-0.0017	0.17445	0.96207
	50 mg/l	-0.00724	0.25432	0.949202
	100 mg/l	-0.00734	0.28834	0.982115
	250 mg/l	-0.0017	0.3746	0.928332
2 <sup>nd</sup>	C <sub>0</sub>	q <sub>e</sub>	k <sub>2</sub>	R <sup>2</sup>
	20 mg/l	88.62014	0.011284	0.999823
	50 mg/l	154.4531	0.006474	0.999084
	100 mg/l	50	0.02	1
	250 mg/l	250	0.004	1
Intraparticles model	C <sub>0</sub>	a	k <sub>d</sub>	R <sup>2</sup>
	20 mg/l	0.08837	21.24239	0.876113
	50 mg/l	0.08837	25.47686	0.876113
	100 mg/l	0.04192	13.23901	0.706256
	250 mg/l	0.04789	21.24239	0.680608

appropriate for nitrate and phosphate removal from aqueous solutions in binary systems.

## References

- Alagha O., Manzar M. S., Zubair M., Anil I., Mu'azu N. D., & Qureshi A. (2020). Comparative adsorptive removal of phosphate and nitrate from wastewater using biochar-MgAl LDH nanocomposites: Coexisting anions effect and mechanistic studies. *Nanomaterials (Basel)*, 10(2): 336. <https://doi.org/10.3390/nano10020336>
- Afroze, S., & Sen, T. K. (2018). A review on heavy metal ions and dye adsorption from water by agricultural solid waste adsorbents. *Water, Air, & Soil Pollution*, 229(7), 225. <https://doi.org/10.1007/s11270-018-3869-z>.
- Aljbour, S. H., Al-Harshesh, A. M., Alieedeh, M. A., Al-Zboon, K., & Al-Harshesh, S. (2016). Phosphate removal from aqueous solutions by using natural Jordanian zeolitic tuff. *Adsorption Science & Technology*, 35(3-4), 284-299. <https://doi.org/10.1177/0263617416675176>.
- Aswin Kumar, I., & Viswanathan, N. (2019). Fabrication of zirconium (IV) cross-linked alginate/kaolin hybrid beads for nitrate and phosphate retention. *Arabian Journal of Chemistry*. <https://doi.org/10.1016/j.arabjc.2019.06.006>.
- Bavaresco, J., Fink, J. R., Rodrigues, M. L. K., Gianello, C., BarrÓN, V., & Torrent, J. (2017). Chromium adsorption in different mineralogical fractions from subtropical soils. *Pedosphere*, 27(1), 106-111. [https://doi.org/10.1016/S1002-0160\(17\)60300-X](https://doi.org/10.1016/S1002-0160(17)60300-X).
- Berkessa, Y. W., Mereta, S. T., & Feyisa, F. F. (2019). Simultaneous removal of nitrate and phosphate from wastewater using solid waste from factory. *Applied Water Science*, 9(2), 28. <https://doi.org/10.1007/s13201-019-0906-z>.

- Boopathy, R., Karthikeyan, S., Mandal, A. B., & Sekaran, G. (2013). Adsorption of ammonium ion by coconut shell-activated carbon from aqueous solution: Kinetic, isotherm, and thermodynamic studies. *Environmental Science and Pollution Research*, 20(1), 533–542. <https://doi.org/10.1007/s11356-012-0911-3>.
- Dong, J., Du, Y., Duyu, R., Shang, Y., Zhang, S., & Han, R. (2019). Adsorption of copper ion from solution by polyethylenimine modified wheat straw. *Bioresource Technology Reports*, 6, 96–102. <https://doi.org/10.1016/j.biteb.2019.02.011>.
- El-Naggar, I., Ahmed, S. A., Shehata, N., Sheneshen, E., Fathy, M., & Shehata, A. (2019). A novel approach for the removal of lead (II) ion from wastewater using Kaolinite/Smectite natural composite adsorbent. *Applied Water Science*, 9(1), 7.
- Fathy, M., Abdel Moghny, T., Mousa, M. A., El-Bellihi, A.-H.A.-A., Awadallah, A. E. (2016). Absorption of calcium ions on oxidized graphene sheets and study its dynamic behavior by kinetic and isothermal models. *Applied Nanoscience* 1–13. <https://doi.org/10.1007/s13204-016-0537-8>
- Fathy, M., Moghny, T. A., Mousa, M. A., Abdelraheem, O., Emam, A. A. (2019). Synthesis and study bromophenol blue dye adsorption efficiency of reduced graphene oxide produced by catalytic acid spray (CAS) method. *Journal of the Australian Ceramic Society*, 1–11
- Fathy, M., Moghny, T. A., Mousa, M. A., El-Bellihi, A.-H. A., Awadallah, A. E. (2014). *Sulfonated ion exchange polystyrene composite resin for calcium hardness removal*.
- Fathy, M., Zayed, M. A., & Moustafa, Y. (2019). Synthesis and applications of CaCO<sub>3</sub>/HPC core–shell composite subject to heavy metals adsorption processes. *Heliyon*, 5(8), e02215.
- Gupta, M. D., Loganathan, P., & Vigneswaran, S. (2012). Adsorptive Removal of Nitrate and Phosphate from Water by a Purolite Ion Exchange Resin and Hydrous Ferric Oxide Columns in Series. *Separation Science and Technology*, 47(12), 1785–1792. <https://doi.org/10.1080/01496395.2012.658487>.
- Gupta, N. K., Saifuddin, M., Kim, S., & Kim, K. S. (2020). Microscopic, spectroscopic, and experimental approach towards understanding the phosphate adsorption onto Zn–Fe layered double hydroxide. *Journal of Molecular Liquids*, 297, 111935. <https://doi.org/10.1016/j.molliq.2019.111935>.
- Heba, H., El-Maghrabi, R. H., Ramzi, M., & Fathy, M. (2017). Novel mesoporous silica (MCM-41) and its characterization for oil adsorption from produced water injected in water injection projects using fixed bed column processes. *Desalination and Water Treatment*, 60, 70–77.
- Hoque, M. A., Hassan, F. M., Seo, M.-H., Choi, J.-Y., Pritzker, M., Knights, S., et al. (2016). Optimization of sulfur-doped graphene as an emerging platinum nanowires support for oxygen reduction reaction. *Nano Energy*, 19, 27–38. <https://doi.org/10.1016/j.nanoen.2015.11.004>.
- Hosny, R., Fathy, M., Ramzi, M., Moghny, T. A., Desouky, S., & Shama, S. (2016). Treatment of the oily produced water (OPW) using coagulant mixtures. *Egyptian Journal of Petroleum*, 25(3), 391–396.
- Kazemi, E., Dadfarnia, S., & Haji Shabani, A. M. (2015). Dispersive solid phase microextraction with magnetic graphene oxide as the sorbent for separation and preconcentration of ultra-trace amounts of gold ions. *Talanta*, 141, 273–278. <https://doi.org/10.1016/j.talanta.2015.04.024>.
- Keränen, A., Leiviskä, T., Hormi, O., & Tanskanen, J. (2015). Removal of nitrate by modified pine sawdust: Effects of temperature and co-existing anions. *Journal of Environmental Management*, 147, 46–54. <https://doi.org/10.1016/j.jenvman.2014.09.006>.
- Khalid, A., Al-Juhani, A. A., Al-Hamouz, O. C., Laoui, T., Khan, Z., & Atieh, M. A. (2015). Preparation and properties of nanocomposite polysulfone/multi-walled carbon nanotubes membranes for desalination. *Desalination*, 367, 134–144. <https://doi.org/10.1016/j.desal.2015.04.001>.
- Khedhri, I., Afli, A., & Aleya, L. (2017). Structuring factors of the spatio-temporal variability of macrozoobenthos assemblages in a southern Mediterranean lagoon: How useful for bioindication is a multi-biotic indices approach? *Marine Pollution Bulletin*, 114(1), 515–527. <https://doi.org/10.1016/j.marpolbul.2016.10.023>.
- Kilpimaa, S., Runtti, H., Kangas, T., Lassi, U., & Kuokkanen, T. (2014). Removal of phosphate and nitrate over a modified carbon residue from biomass gasification. *Chemical Engineering Research and Design*, 92(10), 1923–1933. <https://doi.org/10.1016/j.cherd.2014.03.019>.
- Korzeniowska, A., Grzybek, J., Kalańska, K., Kubu, M., Roth, W. J., & Gil, B. (2019). The structure-catalytic activity relationship for the transition layered zeolite MCM-56 with MWW topology. *Catalysis Today*. <https://doi.org/10.1016/j.cattod.2019.09.044>.
- Liu, M., Hou, L.-a, Yu, S., Xi, B., Zhao, Y., & Xia, X. (2013). MCM-41 impregnated with A zeolite precursor: Synthesis, characterization and tetracycline antibiotics removal from aqueous solution. *Chemical Engineering Journal*, 223, 678–687. <https://doi.org/10.1016/j.cej.2013.02.088>.
- Mahmoud Fathy, T. A. M., Mousa, M. A., ElBellhi, A.-H.-A., & Awadallah, A. E. (2015). Sulfonated ion exchange polystyrene composite resin for calcium hardness removal. *International Journal of Emerging Technology and Advanced Engineering*, 5 (10), 20–29.
- Mamba, G., & Mishra, A. K. (2016). Graphitic carbon nitride (g-C<sub>3</sub>N<sub>4</sub>) nanocomposites: A new and exciting generation of visible light driven photocatalysts for environmental pollution remediation. *Applied Catalysis B: Environmental*, 198, 347–377. <https://doi.org/10.1016/j.apcatb.2016.05.052>.
- Qiao, H., Mei, L., Chen, G., Liu, H., Peng, C., Ke, F., et al. (2019). Adsorption of nitrate and phosphate from aqueous solution using amine cross-linked tea wastes. *Applied Surface Science*, 483, 114–122. <https://doi.org/10.1016/j.apsusc.2019.03.147>.
- Sakate, S. S., Shinde, S. H., Kasar, G. B., Chikate, R. C., & Rode, C. V. (2018). Cascade synthesis of dihydrobenzofuran via Claisen rearrangement of allyl aryl ethers using FeCl<sub>3</sub>/MCM-41 catalyst. *Journal of Saudi Chemical Society*, 22(4), 396–404. <https://doi.org/10.1016/j.jscs.2017.08.006>.
- Gupta, S. S., Ton, V.-K., Beaudry, V., Rulli, S., Cunningham, K., & Rao, R. (2003). Antifungal activity of amiodarone is mediated by disruption of calcium homeostasis. *Journal of Biological Chemistry*, 278(31), 28831–28839
- Zhang, Q., He, M., Chen, B., & Hu, B. (2016a). Preparation, characterization and application of *Saussurea tridactyla* Sch-Bip as green adsorbents for preconcentration of rare earth elements in environmental water samples. *Spectrochimica Acta Part B: Atomic Spectroscopy*, 121, 1–10. <https://doi.org/10.1016/j.sab.2016.04.005>.
- Zhang, Y., Huang, Y., Wang, X., Guo, Y., Jia, D., Tang, X. (2016b). Improved electrochemical performance of lithium iron phosphate in situ coated with hierarchical porous nitrogen-doped graphene-like membrane. *Journal of Power Sources*, 305, 122–127. <https://doi.org/10.1016/j.jpowsour.2015.11.092>
- Zhang, Y., Si, L., Zhou, B., Zhao, B., Zhu, Y., Zhu, L., & Jiang, X. (2016c). Synthesis of novel graphene oxide/pristine graphene/polyaniline ternary composites and application to super-capacitor. *Chemical Engineering Journal*, 288, 689–700. <https://doi.org/10.1016/j.cej.2015.12.058>.
- Zhang, X.-Z., Zhou, Y., Zhang, W., Zhang, Y., & Gu, N. (2016d). Polystyrene@Au@prussian blue nanocomposites with enzyme-like activity and their application in glucose detection. *Colloids and Surfaces A: Physicochemical and Engineering Aspects*, 490, 291–299. <https://doi.org/10.1016/j.colsurfa.2015.11.035>.

- Zhang, Y., Zhang, Y., Huang, L., Zhou, Z., Wang, J., Liu, H., & Wu, H. (2016e). Hierarchical carambola-like  $\text{Li}_4\text{Ti}_5\text{O}_{12}$ - $\text{TiO}_2$  composites as advanced anode materials for lithium-ion batteries. *Electrochimica Acta*, 195, 124–133. <https://doi.org/10.1016/j.electacta.2016.02.092>.
- Zhang, Z., Zhai, S., Wang, M., Ji, H., He, L., Ye, C., et al. (2016f). Photocatalytic degradation of rhodamine B by using a nanocomposite of cuprous oxide, three-dimensional reduced graphene oxide, and nanochitosan prepared via one-pot synthesis. *Journal of Alloys and Compounds*, 659, 101–111. <https://doi.org/10.1016/j.jallcom.2015.11.027>.
- Zhang, Z., Zhang, H., Zhu, L., Zhang, Q., & Zhu, W. (2016g). Hierarchical porous  $\text{Ca}(\text{BO}_2)_2$  microspheres: Hydrothermal–thermal conversion synthesis and their applications in heavy metal ions adsorption and solvent-free oxidation of benzyl alcohol. *Chemical Engineering Journal*, 283, 1273–1284. <https://doi.org/10.1016/j.cej.2015.08.073>.
- Zhao, Y., Zhang, Z., Dai, L., Mao, H., & Zhang, S. (2017). Enhanced both water flux and salt rejection of reverse osmosis membrane through combining isophthaloyl dichloride with biphenyl tetraacyl chloride as organic phase monomer for seawater desalination. *Journal of Membrane Science*, 522, 175–182. <https://doi.org/10.1016/j.memsci.2016.09.022>.
- Zikos, D., Hagedorn, K. (2017) Competition for water resources from the European perspective A2—Ziolkowska, Jadwiga, R. In: J. M. Peterson (ed.) *Competition for Water Resources* (pp 19–35). Elsevier. <https://doi.org/10.1016/B978-0-12-803237-4.00002-1>.





# Effect of Treated Wastewater on the Growth and Yield of Two Sweet Corn Varieties: Impact of Doses and Systems of Irrigation

Afaf Belabhir, Imane Mansir, Lhoussaine Bouchaou,  
Mohamed El Otmani, Bouchra Yaacoubi, and Redouane Choukr-Allah

## Abstract

The limited availability of freshwater and succession of drought years and climate change have put the pressor to look for alternative water resources including treated wastewater, in order to meet the demands of agriculture in the Souss-Massa, Morocco. This study focuses on the use of treated wastewater for growing sweet corn under different systems and doses of irrigation. An open field experiment was carried out in the Agadir region using two sweet corn varieties: Prime-plus and SF681 and two irrigation systems subsurface drippers (SSD) and surface drippers (SD) also two irrigation doses regime 100 and 120% of the ETM determined using Lysimeters. The growth and yield components of sweet corn were improved by irrigation under surface dripper, using high dose of irrigation. However, the high accumulation of salts in the root zone under subsurface drip irrigation reduced the growth and yield of corn. Adding a leaching fraction of 20% of ETM, improve growth and yield of both sweet corn varieties. The highest yield was achieved by SF681 variety with 20 T/ha, under (SD) irrigated with

120% of ETM. Reducing water application by 20% decreases yield production up to 24.4% under (SD) and gave the same yield for both 100 and 120% of ETM under (SSD). Despite that (SSD) saves water, it increased soil salinity, even in sandy soil, due to the accumulation of salts in the root zone. Under treated wastewater irrigation, the sweet corn water consumption was 186 mm, allowing a saving of conventional water. Furthermore, it generated an economic gain in terms of fertilizers: 240 kg/ha of N and 60 kg/ha of CaO in addition to 10.38 kg/ha of P<sub>2</sub>O<sub>5</sub> and 65.12 kg/ha of K<sub>2</sub>O in the case of 100% ETM and 12.45 kg/ha of P<sub>2</sub>O<sub>5</sub> and 78.14 kg/ha of K<sub>2</sub>O in the case of 120% ETM.

## Keywords

Treated wastewater • Sweet corn • Irrigation • Yield • Water saving • Salts accumulation

A. Belabhir (✉) · M. E. Otmani · R. Choukr-Allah  
Laboratory of Salinity and Plant Nutrition, Hassan II Institute of  
Agronomy and Veterinary Medicine, BP 6202 Ait Melloul,  
Morocco  
e-mail: [afaf.belabhir.iav@gmail.com](mailto:afaf.belabhir.iav@gmail.com)

I. Mansir  
Laboratory of Mechanic, Process Energy and Environment,  
National School of Applied Sciences, BP 1136 Agadir, Morocco

L. Bouchaou  
Laboratory of Geology and Geo-Environment,  
Ibn Zohr University, Agadir, Morocco

L. Bouchaou  
International Water Research Institute, Mohammed VI  
Polytechnic University, Benguerir, Morocco

B. Yaacoubi  
Laboratory of Aquatic Systems: Marine and Continental  
Environment, Ibn Zohr University, BP 32/S CP 80000 Agadir,  
Morocco

## 1 Introduction

Morocco, as part of the Mediterranean countries located in the North-West Africa, is suffering from water scarcity for several decades (Fig. 1). Morocco's water shortage has important implications for the water management. This explains the current Moroccan policy of seeking new alternative water resources (wastewater reuse and desalination of brackish or marine). Moroccan water resources are unevenly distributed over its regions and heavily dependent on climatic variations. Souss-Massa region which is located in the south-west of Morocco (Fig. 1) is among the regions that suffers the most from water stress due to the arid climate. In addition, the economy of the region is mainly based on agriculture (ABHSM, 2006). So, the availability of water is a major factor for the economic development of the region. Increased demand for drinking water for tourism, industry and above all agriculture has led to the over-exploitation of

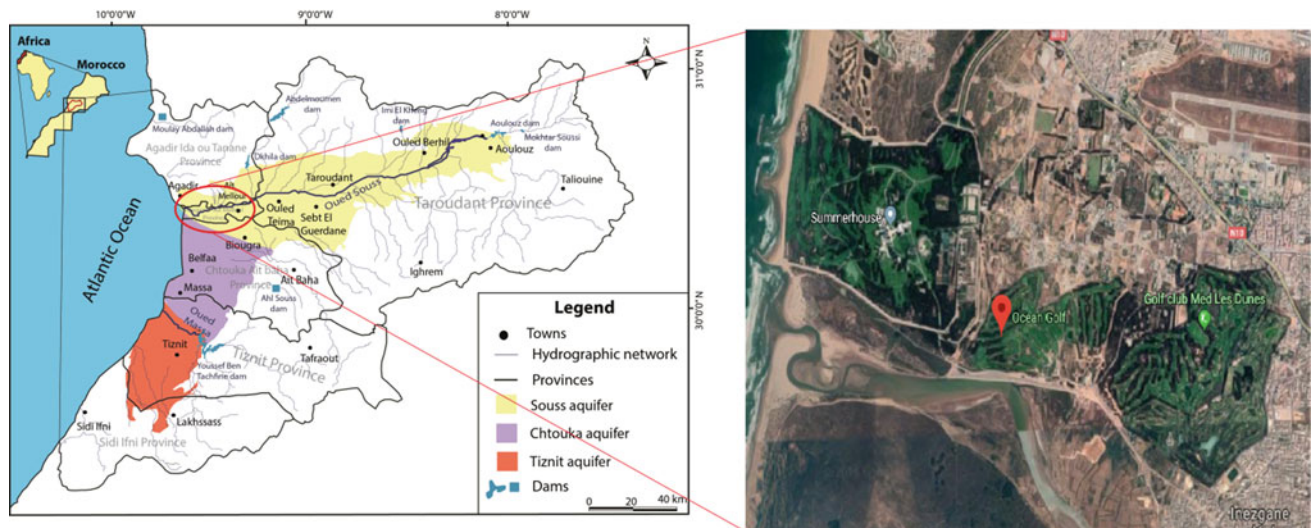


**Fig. 1** Souss-Massa region map (Mansir et al., 2018) and Ocean Golf course situation

the groundwater resources, with major implications for the country's socioeconomic development.

The water master plan developed by the Souss-Massa Hydraulic Basin Agency (ABHSM) responds to the framework directive of the integrated water resource management in Morocco. The driving forces are strong population growth and urbanization; tourism and industrialization; globalization; and climate variability and change leading to decreasing precipitation and increasing the frequency of droughts. This situation has increased the interest in recycling treated wastewater in agriculture and the integration of non-conventional water in planning and mobilization strategy and water resources management within the river basin.

Reuse of treated wastewater is one of the key solutions to solve durably the problems of water stress. The interest in the reuse of treated wastewater in agriculture or for landscaping is growing, as additional water resources, and a source of plant nutrients. It can generate a significant economic gain up 1500 and 3500 MAD/ha for field crops (Choukr-Allah, 1995). In addition to these benefits, treatment and reuse of wastewater contribute to the protection of the receiving environment.

Maize is the third worldwide cultivated crop after rice and wheat (Eagles & Lothrop, 1994). It is one of the most important cereals both for human and animal consumption and is grown as fresh vegetable and forage crop. A significant increase of 50% in global maize demand will occur from 1995 to 2020 (Ekboir, 2002). By 2020, demand for maize in developing countries will surpass the demand for both wheat and rice. Usually, those crops require a high amount of irrigation water, and they are relatively susceptible to excessive concentration of salts. Increasing soil salinity may induce various primary and secondary salt stress effects in cultivated plants. Salt stress is one of the

most widespread abiotic constraints in food production. One of the innovative alternatives to save water is the use of the new irrigation technologies such as a subsurface drip irrigation system (SSD) which is considered more water efficient compared to surface drip irrigation system (SD).

In addition, using treated wastewater for irrigation will lead to increase soil salinity as it contains high level of soluble salts. Therefore, there is a need to add a leaching fraction reducing salt accumulation in the root zone. The application of 120% ETM irrigation regime instead of 100% ETM is one of the best strategies to reduce soil salt accumulation. Consequently, installation of drainage system is mandatory in order to control the salinity and the elements percolation through the groundwater.

For this reason, it is important to implement a demonstration unit in Agadir city which is the capital of the Souss-Massa region with the aims to establish an integrated reuse of treated wastewater project for landscaping, orchards and other crops. This will provide the municipality of Agadir and farmers in the region with a good practice guide and help them to improve the management of treated wastewater. Agronomic and Veterinary Institute Hassan II (IAV) in collaboration with different local institutions are providing to this project all their research, facilities and their experience and expertise, accumulated over recent years at regional, national and international level.

## 2 Materials and Methods

This work was carried out to study the effect of irrigation using treated wastewater on growth and yield of sweet corn (*Zea mays saccharata*) and on physicochemical parameters of the soil.

The treated wastewater used comes from the L'Mzar station which is located approximately 8.5 km south of the city of Agadir on the coastal dunes L'Mzar. The western boundary of the site is about 1500 m from the sea. Wastewater at the L'Mzar station is treated up to the tertiary level by U.V rays. Table 1 shows treated wastewater characteristics.

This treated wastewater is characterized by high electrical conductivity (EC) and is very rich in terms of nitrogen. The high conductivity is mainly due to salt discharges from the various fish canning factories. This source of salts, if not controlled, may pose serious problems that can limit the use of treated water for irrigation of salt-sensitive species. That is why the Moroccan company in charge for MWW treatment (RAMSA) has forced fish canneries to separate the internal sanitation network. The separation of liquid discharges to salt water and unsalted waters is necessary in order to not disturb the progress of the urban water treatment process and to avoid clogging. In addition, we will compare two irrigation systems (surface drip irrigation and subsurface irrigation) and two irrigation doses (100% of ETM and 120% of ETM) on the behavior of two varieties of sweet corn. This experiment was implemented in the experimental open field of Ocean Golf in Agadir (Fig. 1). Some physical and chemical properties of the experimental site soil are given in Table 2.

The experimental plot has an area of 322 m<sup>2</sup>. In order to investigate the performance of irrigation technologies and irrigation doses using treated wastewater on the yield production of two sweet corn varieties, a study was conducted on a complete randomized blocks design and four replications. Table 3 and Fig. 2 show combinations and trial layout.

Each experimental unit contains one cultivated row bed with two dripper lines. Two irrigation systems were installed, SD and SSD, which were buried at depth of 15 cm from soil surface at the root zone. Sowing two local sweet corn varieties Prime-plus and SF681 at a density of 50,000 plant/ha took place in May 18, 2017; under two irrigation regimes 100% of ETM and 120% of ETM. For the calculation of daily irrigation requirements, the lysimetric method is used which is based on the drained water. In order to follow up the drainage, four lysimeters were installed in the field. Before the first irrigation, the quantity of water drained from the previous day is measured to be taken into consideration to calculate the irrigation requirement of the next day. The daily irrigation requirement  $I(j)$  is determined from the difference between the irrigation requirement of the previous day  $I(j - 1)$  and the drained water of the previous day  $D(j - 1)$ :

$$I(j) = I(j - 1) - D(j - 1) \quad (1)$$

**Table 1** Quality of treated wastewater used for irrigation and the recommended limits

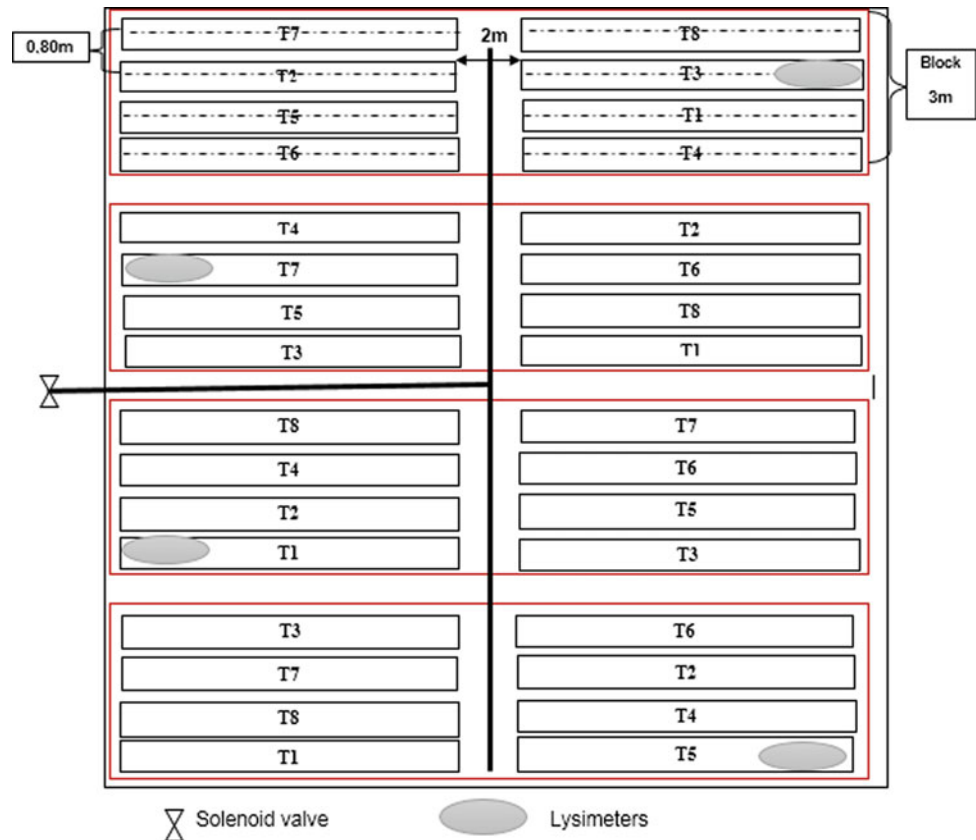
Parameters	Measured values	Recommended limits (FAO, 2011)
pH	7.02	6.5–8.4
Conductivity (25 °C) (μS/cm)	4.11	12
Chloride (mg/l)	795.2	350
Bicarbonate (mg/l)	549.00	518
Nitrate (mg/l)	430.99	30
Phosphorus (mg/l)	1.45	–
Calcium (mg/l)	203.95	–
Sodium (mg/l)	115.71	69
Magnesium (mg/l)	61.49	–
Potassium (mg/l)	31.86	–
Copper (mg/l)	0.008	2
Iron (mg/l)	0.06	5
Manganese (mg/l)	0.02	0.2

**Table 2** Physical–chemical characteristics of the soil before sowing

Particle size distribution (%)			Soil texture	pH	EC	Elements (mg/kg)		
Sand	Silt	Clay			(μS/cm)	N	Na	Cl
94.35	2.15	1.60	Sandy soil	8.42	206.0	12.8	260.36	532.5

**Table 3** Different combinations of the experimental trial

Symbol	Irrigation system	Dose as % of ETM	Variety
T1	SD	120	Prime-plus
T2	SD	100	Prime-plus
T3	SD	120	SF681
T4	SD	100	SF681
T5	SSD	120	Prime-plus
T6	SSD	100	Prime-plus
T7	SSD	120	SF681
T8	SSD	100	SF681

**Fig. 2** Experimental layout adopted in the trial

The water volumes of different irrigation treatments were applied at the same irrigation time, by changing the discharge of drippers. Therefore, we installed dripper lines with different discharges of emitters (5 l/h or 6 l/h) depending on the applied treatment (120% or 100% of ETM) in each plot. In the case of 100% ETM, we installed two drippers with different discharges, one of 2 l/h and the other of 3 l/h. To obtain 120% of ETM at the same time of irrigation, we installed two drippers with the same discharge 3 l/h. In regard to fertilization, it consists on a mineral supplement of potassium and phosphorus for plant growth due to their low

content in treated wastewater. As the trial progresses, and in order to show possible differences between the different treatments, agronomic and physiological measurements are carried out to follow up on the growth and development of the plants. Similarly, physicochemical analyzes were carried out at a depth of 20 cm of the soil to determine the impact of wastewater irrigation on physicochemical properties of the soil.

Statistical analysis was carried out using the “Minitab version 16” software. All statistical differences were significant at test used to reveal homogeneous groups.

### 3 Results and Discussion

#### 3.1 Climatic Conditions

It was important to record climatic data during the crop cycle of sweet corn because of the high temperatures that hinder the growth of plants (Birch et al., 2003).

According to Fig. 3, there are high-temperature peaks exceeding 45 °C at the end of June and during the first week of July. In addition to the absence of rain, this period is marked by Chergui (hot and dry wind blowing from the southeast). Fortunately, this climate has not lasted long and has not affected the production of biomass.

#### 3.2 Dry Shoot, Root Weight and Dry Root/Shoot Ratio

Roots, stems and leaves are functionally interdependent, and these three systems maintain a dynamic balance in biomass which reflects relative abundance of above-ground resources (light and CO<sub>2</sub>) compared with root zone resources (water and nutrients) (Poorter et al., 2012).

According to the results shown in the two graphs in Fig. 4, there is no significant difference between the two varieties in terms of dry shoot production. For the Prime-plus variety, at the end of vegetative stage, the statistical analysis showed that there is a high significant

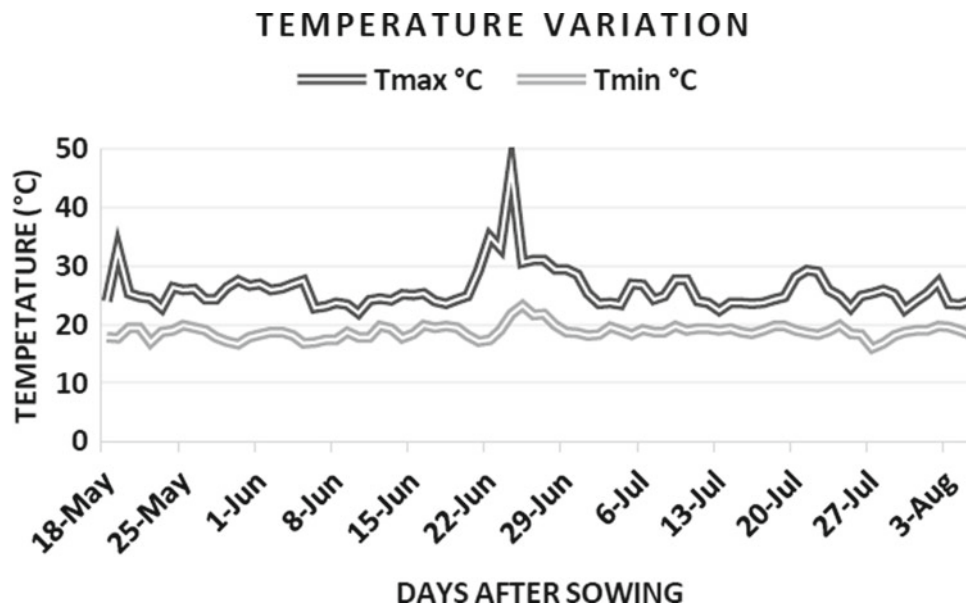


Fig. 3 Temperature variation recorded during the crop cycle of sweet corn

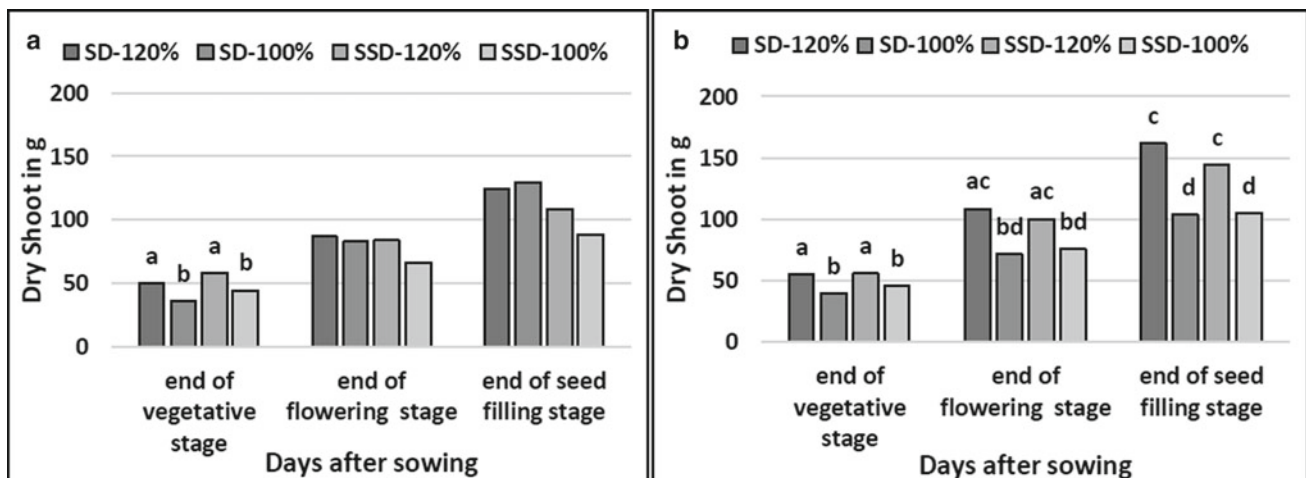
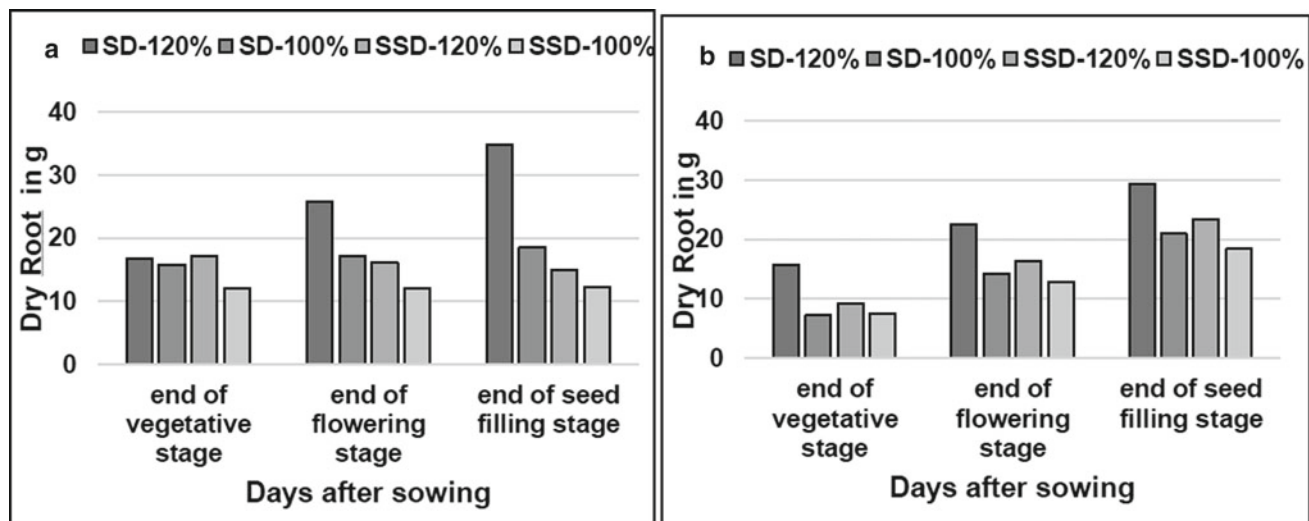


Fig. 4 Impact of the different irrigation combinations on the total dry shoot of the sweet corn varieties Prime-plus (a) and SF681 (b) during the life cycle. Means having different letters are significantly different at 5% level





**Fig. 5** Impact of the different irrigation doses and systems on the dry root weight for the two varieties Prime-plus (a) and SF681 (b) during the life cycle

difference ( $p = 0.006$ ) between the irrigation systems (SSD and SD), where the plants under SSD developed more shoot than that under SD system. Also, it revealed a high significant difference ( $p = 0.003$ ) between the irrigation doses (100 and 120% of ETM). However, no significant difference was found at the end of flowering stage also at the end of seed filling stage. The water stress leads to 11.5% of biomass reduction at the end of vegetative stage (under 120% ETM regime, the biomass was 54.88 g against 41.58 g for 100% ETM regime).

For the SF681 variety, at the end of vegetative stage there is significant difference ( $p = 0.05$ ) between the irrigation doses in terms of the shoot dry weight. The maximum value is recorded for the plants that received 20% supplement need water which is 55.67 g against 42.83 g for plants irrigated under 100% of ETM. Statistical analysis did not reveal any significant difference between the irrigation systems.

At the end of flowering stage, the maximum value of dry shoot weight is recorded by the plants irrigated under 120% of ETM with a value of 104.38 g against 73.63 g under 100% of ETM. The statistical analysis revealed high significant difference ( $p = 0.021$ ) between the irrigation doses and no significant difference between the irrigation systems in terms of shoot dry weight. Same scenario is at the end of seeds filling, and the plants under 120% of ETM have a shoot dry value of 153.1 g against 104.4 g for 100% of ETM.

For dry root production and for both varieties, we register significant difference ( $p = 0.036$ ) between the irrigation systems. The plants under the SD have developed more roots than that under SSD and can lead to 27.7% of reduction in term root development throughout the life cycle.

At the other hand, the statistical analysis revealed a significant difference ( $p = 0.019$ ) between the two irrigation

doses 120 and 100% of ETM. As it is clearly shown in Fig. 5 for both varieties, the plants under the 100% of ETM have reduced their root development of 30.22% compared to that under 120% of ETM during the life cycle.

The statistical analysis did not reveal significant difference between the responses of the two varieties in terms of dry root/shoot ratio.

Our data (Fig. 6) show that there is no impact of the irrigation doses on the root/shoot ratio for the both varieties. The statistical analysis revealed a significant difference ( $p = 0.012$ ) between the irrigation systems SSD and SD in terms of dry ratio. The plants cultivated under the subsurface drip irrigation system presented 24.4% reduction of the root/shoot ratio with, indicating that they produce more shoots than roots.

### 3.3 Yield Components and Fresh Yield Production

The main goal of this experiment is to improve sweet corn production under the irrigation using the treated wastewater with different irrigation systems (SSD and SD) and different doses (120 and 100% of ETM).

The presented data shown in Fig. 7 indicate that under the SD irrigation system the ears number is higher for the 120% of ETM irrigation dose than 100% of ETM. However, under the SSD irrigation system, the two irrigation doses have approximately the same ears number.

The statistical analysis revealed significant difference ( $p = 0.042$ ) between the irrigation doses, indicating that more water is added, the higher ears number is obtained. For the varieties under (SD) irrigation with 100% of ETM, it has

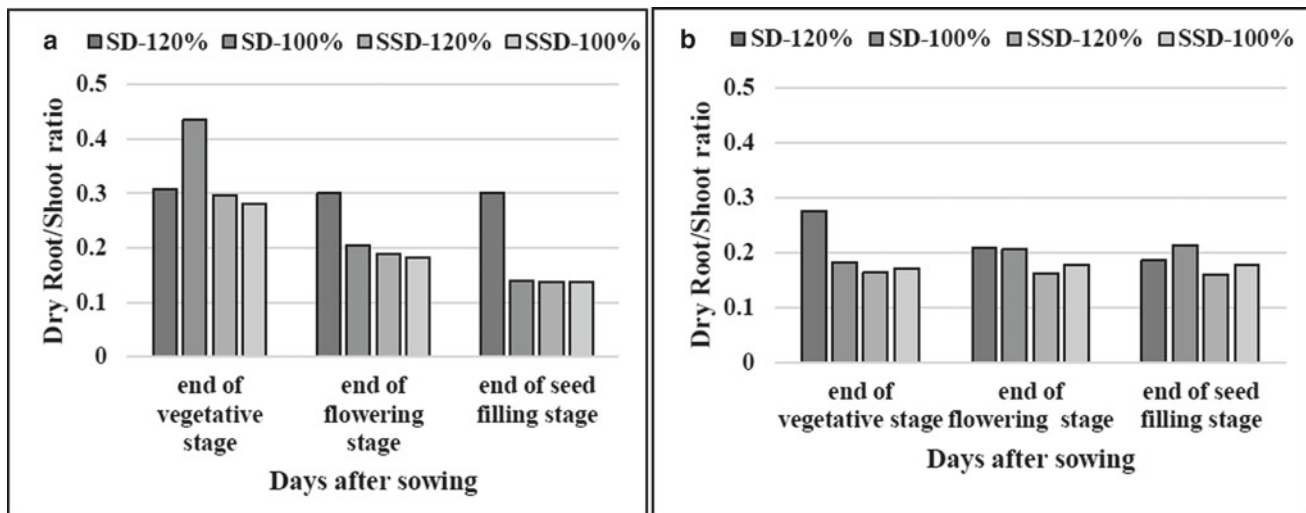


**Fig. 6** Impact of the different irrigation systems and irrigation doses on the dry root/shoot ratio evolution of the varieties Prime-plus (a) and SF681 (b) during the life cycle

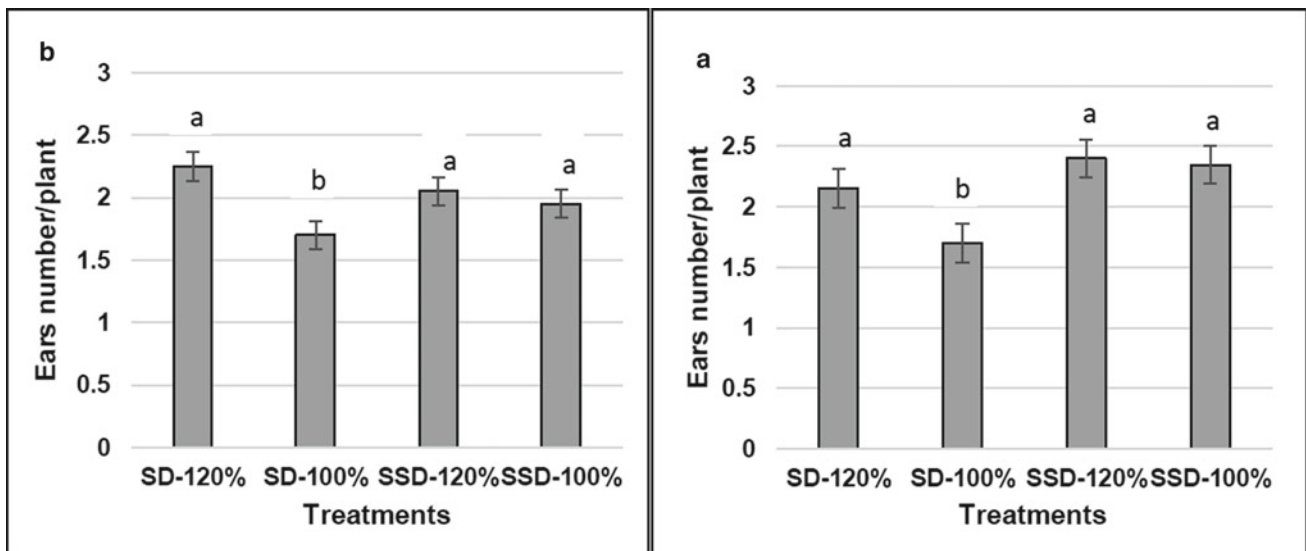


**Fig. 7** Impact of the investigated irrigation systems and doses on the ears number of both varieties of sweet corn Prime-plus (a) and SF681 (b). Means having different letters are significantly different at 5% level

reduced the ears number by 21 and 24.4% [respectively for Prime-plus (a) and SF681 (b)] compared to that irrigated with 120% of the same variety. In case of the SSD irrigation system, the reduction in terms of ears number is negligible at 100% of ETM 2.1% (a) and 4.9% (b) compared to 120% of ETM.

Deep analysis of the data indicates that the irrigation doses have a great influence on the fresh yield production. There is a positive relationship between the water supply and the fresh ears production. In the case of SD irrigation, the higher is the irrigation dose, the higher is the yield production (T/ha).

Figures 8 and 9 show that when the plants received during the crop cycle a supplement of 20% of the plant water

needs corresponding 120% of ETM, they give the highest yield production of an average of 18.09 T/ha with an increase nearly of 21% more than that produced under the 100% of ETM. This is explained by the intake of excessive water in the 120% of ETM regime, in fact Ayache (1995) reported that the water intake with a slight excess favors the growth consequently the production.

Regarding the SSD irrigation system, the variation in terms of fresh yield production between the two doses was not notable compared to SD irrigation. The statistical analysis of the data revealed a significant difference ( $p = 0.026$ ) between the irrigation doses (100 and 120% of ETM) and no significant difference between the two irrigation systems (SD

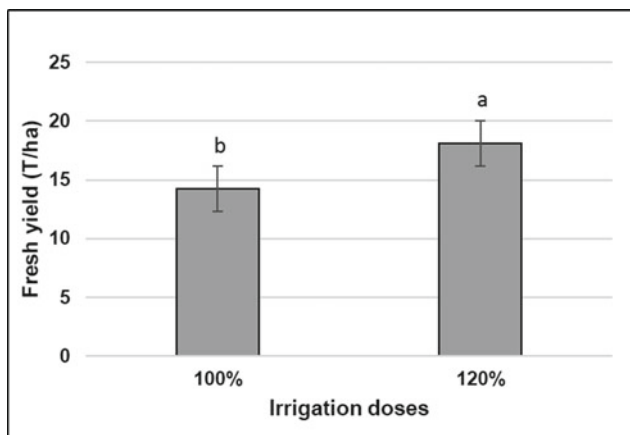


**Fig. 8** Impact of the irrigation doses on the fresh yield of the sweet corn irrigated using treated wastewater (Means having different letters are significantly different at 5% level)

and SSD). Therefore, under SSD irrigation, we do not need to add 20% more water since we obtain the same yield. Similarly, Douh and Boujelben (2012) recorded, in addition to a water saving, there is an improvement in the yield of irrigated maize in favor of SSD compared to SD.

### 3.4 Physiological Parameters

#### 3.4.1 Proline Accumulation in the Sweet Corn Leaves

The leaves proline concentration at the end of different sweet corn stages under the two irrigation regime using the two varieties treated wastewater is given in Figs. 10 and 11.

Our data show that the proline accumulated in leaves of the two varieties is variable from one crop stage to another (Fig. 10). Therefore, the behavior of the varieties versus to investigated treatment is different during the crop cycle.

At the end of vegetative stage, SF681 variety was more stressed than Prime-plus variety as it accumulates  $3.64 \mu\text{mol g}^{-1}$  of leaves fresh weight against  $2.44 \mu\text{mol g}^{-1}$  of leaves fresh weight, statistically no significant difference was found between the two varieties. Also at the end of flowering stage, there is no significant difference between Prime-plus and SF681, and they have nearly the same proline concentration. But, at the end of seed filling, statistical analysis revealed a significant difference ( $p = 0.044$ ) between the varieties. Prime-plus variety accumulated the highest proline concentration value of  $2.50 \mu\text{mol g}^{-1}$  of fresh weight compared to 1.33 for SF681.

Statistical analysis revealed a significant difference ( $p = 0.007$ ) between irrigation doses 120 and 100% of ETM. According to Fig. 11, the 120% of ETM which gave 20% of ETM as water supplement to the plants indicate the lower proline accumulation under all investigated irrigation system treatments. This holds true for both investigated varieties.

Under the studied SSD irrigation system, proline concentrations recorded are very high than the one recorded under the SD irrigation, which means that the SSD promote stressed conditions for the plants more that the SD irrigation system. Statistically, there is no significance between irrigation systems SSD and SD. The increase in proline content occurs late and slowly in the excised foliage stem (Thellier et al., 2000).

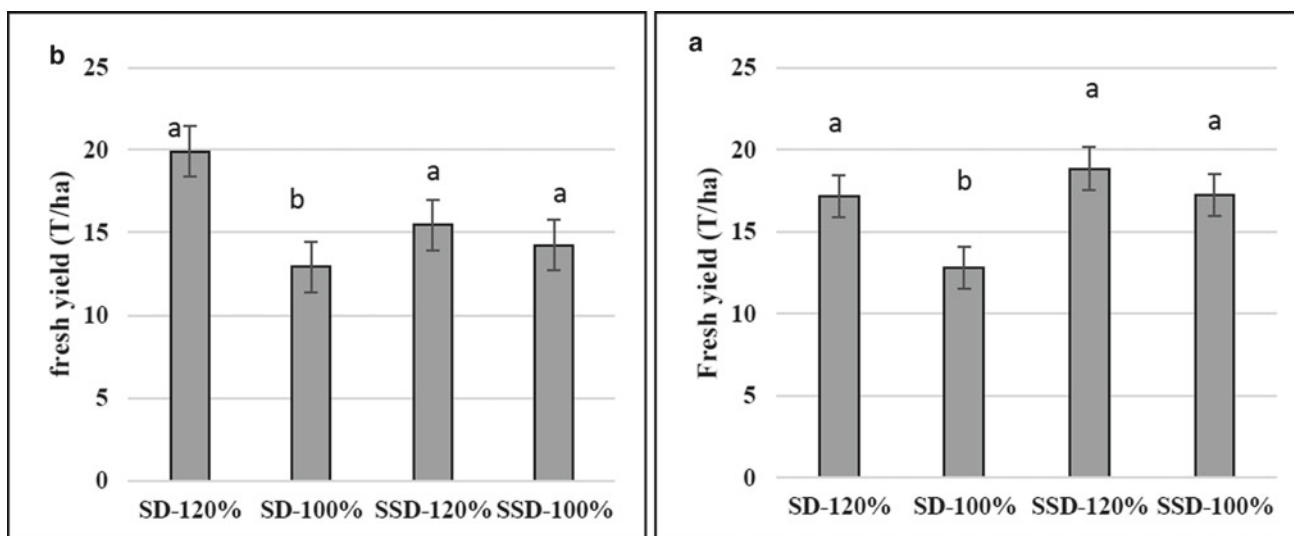
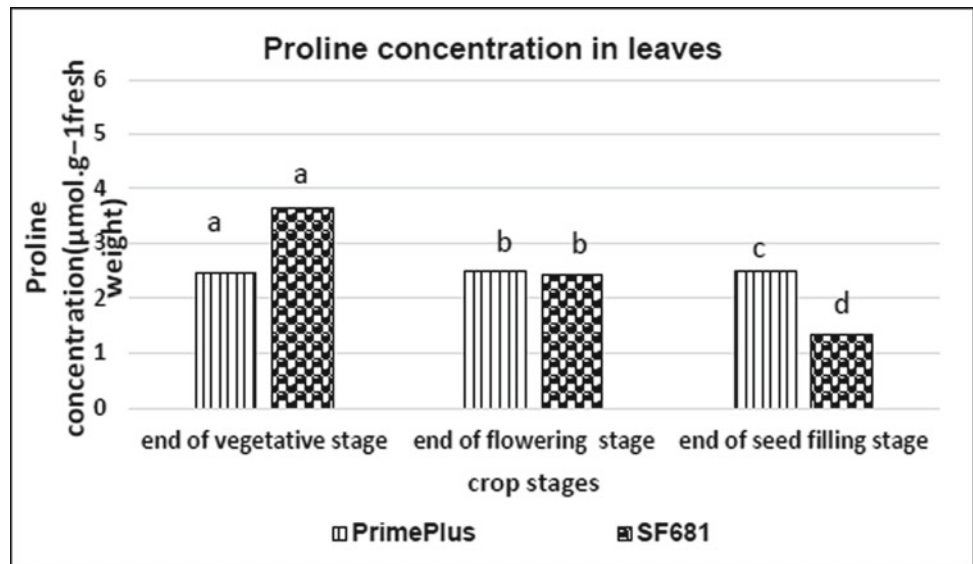


**Fig. 9** Impact of the irrigation systems and doses on the fresh yield of the both varieties Prime-plus (a) and SF681 (b)

**Fig. 10** Impact of the irrigation using treated wastewater on the proline accumulation in leaves of sweet corn varieties under the investigated treatments (Means having different letters are significantly different at 5% level)



### 3.4.2 Leaf Chlorophyll Content

The leaf chlorophyll (Chla and Chlb) content at the end of the three crop stages under the different investigated treatment is presented in Fig. 12.

The presented data indicate that for both investigated varieties, there is a gradual reduction in chlorophyll components (especially Chla) with a gradual life cycle progress. The reduction was not equal for both studied chlorophyll components; however, Chla was more affected presenting the lowest values, whereas Chlb showed the highest value, and this is clearly demonstrated in Fig. 12.

Statistical analysis did not reveal a significant difference between the two varieties (Prime-plus and SF681) neither between the two irrigation doses and also between the two irrigation systems.

This reduction may be explained by the salts accumulation in the soil due to the use of treated wastewater with high electrical conductivity. This conclusion is confirmed by Levitt, (1980); Megdiche et al., (2008) and Akram et al., (2011) showing that the interactive effect of maize and salinity levels indicates that chlorophyll components decreased significantly with the increase in irrigation salinity level.

The variation in photosynthetic pigments is not only a function of waters EC values, but also to the applied nitrogen rate by the irrigation with treated wastewater that contains enough nitrogen mostly in the form of nitrate (Table 1). The increase in N application up to 240 kg/ha led to a highly significant increase in Chlb and Chla under saline water of 8dS/m being 1.6 and 1.7 times, respectively, higher than the value recorded under N application 120Kg/ha. According to Akram et al. (2011), nitrogen is, therefore, very effective in the formation of the chlorophyll components under saline irrigation practices.

### 3.5 Water Consumption During the Crop Cycle and Nutrient Requirements

Our data (Fig. 13) show the variation of water application for both irrigation regimes (100 and 120% of ETM) and the variation of water cumul consumption throughout the sweet corn cycle.

At the beginning of the crop cycle, the water application was low in the order of 0.1 L/plant/day. As biomass and leaf area increased as well as increasing the photosynthesis mechanism, these water intakes have increased to 1.40 L/plant /day. This increase is due to the increment in the temperature during this period, when there was a significant water deficit in the air, causing an increase in the evaporation power of the climate. The decrease in water application after this period corresponds to the end of the sweet corn cycle. The total applied water amounted to 186 mm.

The data in Table 4 summarize the quantity of water applied during the sweet corn life cycle, in addition the quantity of major nutrient elements provided by the application of the treated wastewater for irrigation.

As it is clearly shown in Table 3, the treated wastewater used for irrigation during the sweet corn development supplied twice the crop nitrogen requirements, and the same goes for the quantity of calcium that is very high and exceeds the plant needs in terms of calcium.

For the phosphorus and potassium, the quantity required is completed by fertilizers supplement. The economic gain generated in terms of fertilizer allowed to save: 240 kg/ha of N and 60 kg/ha of CaO in addition to 10.4 kg/ha of P<sub>2</sub>O<sub>5</sub> and 65.1 kg/ha of K<sub>2</sub>O in the case of 100% ETM and 12.5 kg/ha of P<sub>2</sub>O<sub>5</sub> and 78.1 kg/ha of K<sub>2</sub>O in the case of 120% ETM.

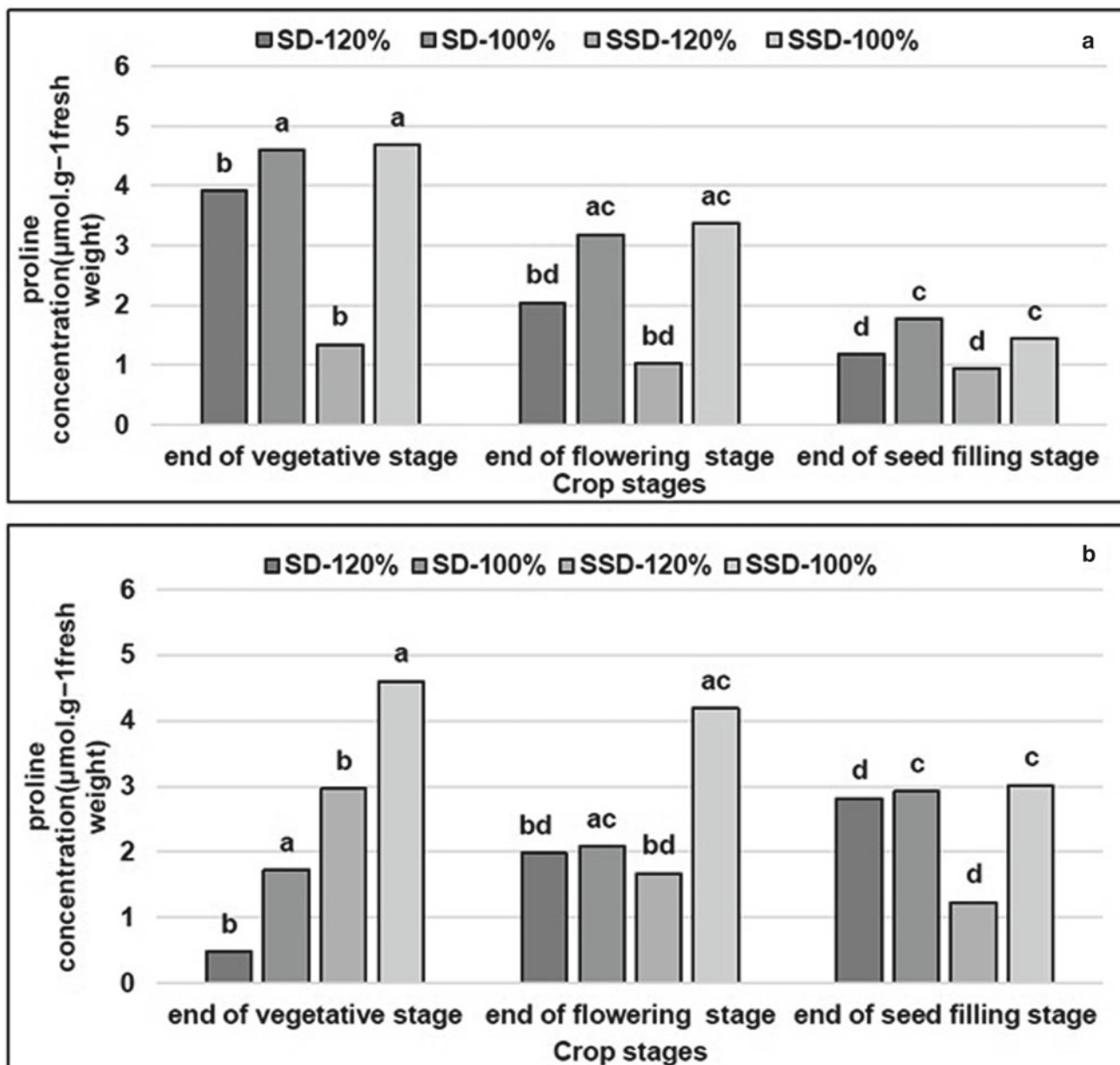


**Fig. 11** Impact of the investigated irrigation systems and doses on the proline accumulation in sweet corn leaves for the two varieties Prime-plus (a) and SF681 (b)

Because of the excessive amount of elements leached under treated wastewater irrigation, a drainage system to control salts and prevent groundwater contamination is needed.

### 3.6 Effect of the Water Regime and Irrigation System on the Soil EC with Irrigation Using Treated Wastewater

Presenting data in Fig. 14 indicates clearly an increase in the soil EC of the both systems and both doses of irrigation, particularly under SSD irrigation system.

Statistical analysis revealed no significant difference between irrigation doses (120 and 100% of ETM) unlike irrigation systems (SD and SSD) where we found a very high significant difference ( $p = 0.0003$ ). The SSD irrigation system caused an increment of soil EC up to 35% increment compared to SD irrigation system. This increase can be explained by the salts accumulations in the soil (at the root zone) under the SSD system comparing, as in the SD system the salts were leached to the drained water.



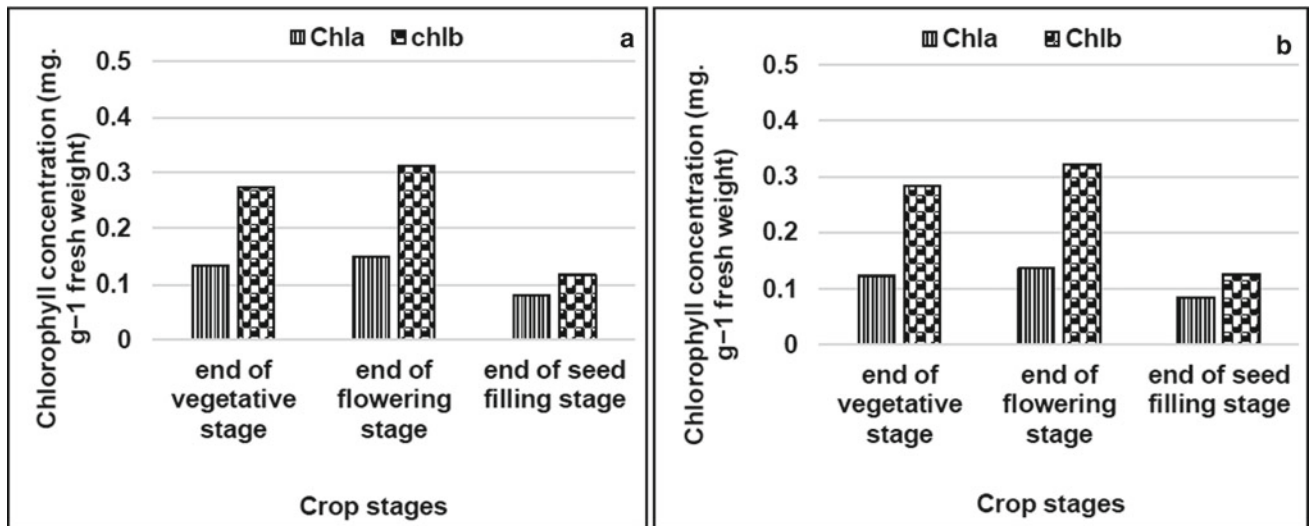


**Fig. 12** Effect of the different systems and doses of irrigation under the irrigation using wastewater on the photosynthetic pigments content in leaves during the life cycle of two varieties Prime-plus (a) and SF681 (b) of sweet corn

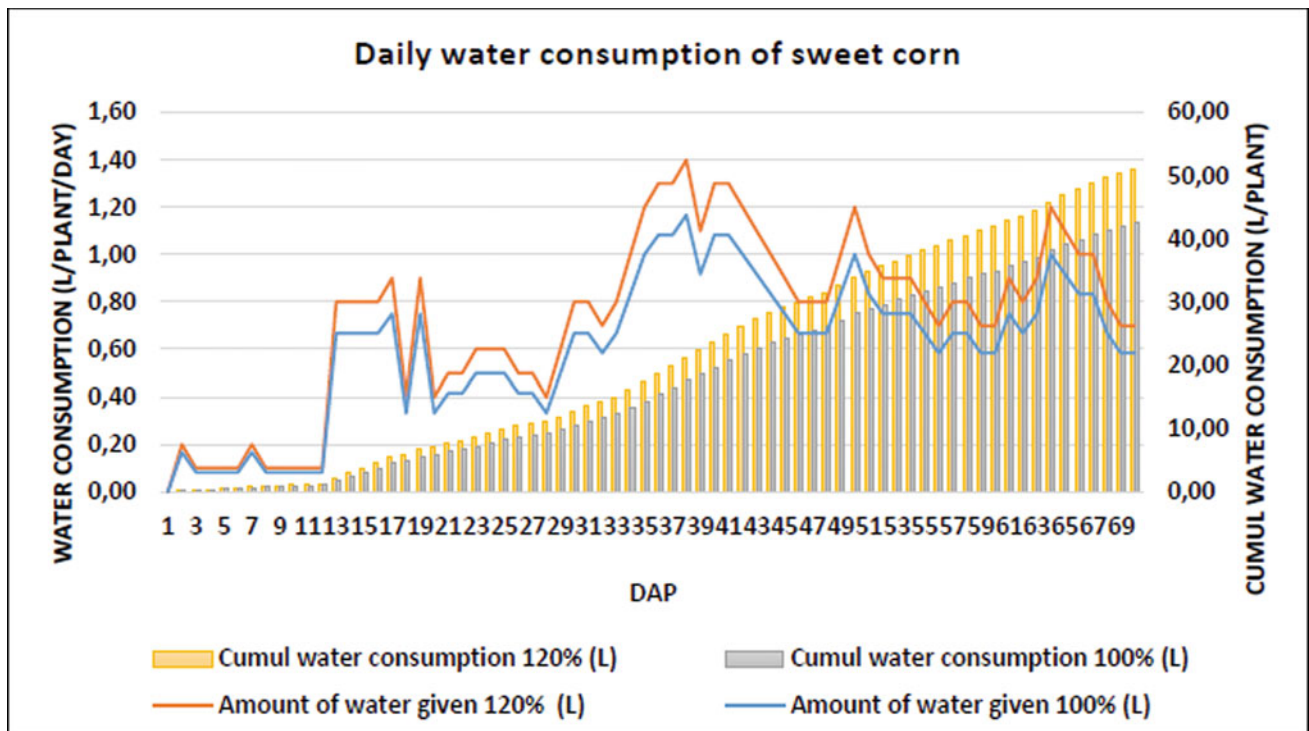


**Fig. 13** Variation of the daily water consumption during the sweet corn life cycle

#### 4 Conclusions

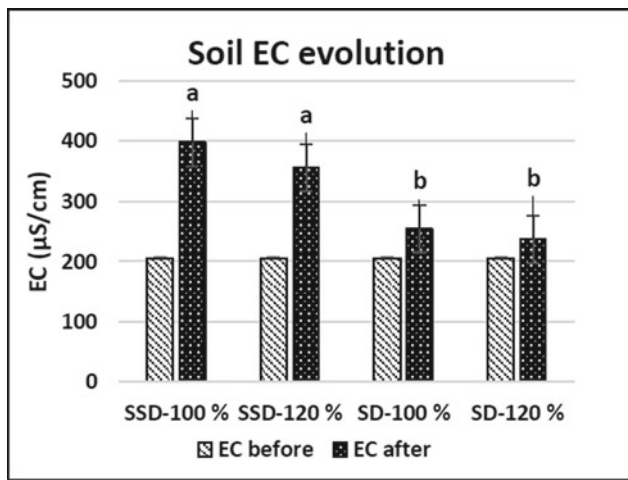
Under water scarcity, the use of treated wastewater in irrigation is a necessity for a better water resources management and economy to cope with the shortage of water in agriculture and urban landscaping. As the salinity of Agadir

treated wastewater is high, it will be important to modify the current irrigation system as well as the applied water and crop management practices to cope with the inevitable damage due to an increase in soil salinity.

Our findings indicate that sweet corn irrigated with treated wastewater showed a high yield production. According to Choukr-Allah and Hamdy (2004), irrigation using treated

**Table 4** Nutrient elements given by the treated wastewater during the crop cycle

Water consumption during the crop cycle			100% of ETM	120% of ETM
In m <sup>3</sup>			27.2	32.64
In m <sup>3</sup> /ha			1689.4	2027.3
Nutrient elements	Unit	Nutrient requirements of sweet corn (CPIF, 2014)	100% of ETM	120% of ETM
N	Kg/ha	240	456.10	547.32
P <sub>2</sub> O <sub>5</sub>	Kg/ha	90	10.38	12.45
K <sub>2</sub> O	Kg/ha	270	65.12	78.14
CaO	Kg/ha	60	413.56	496.28

**Fig. 14** Soil electrical conductivity evolution under different irrigation doses and irrigation systems (before and after irrigation with treated wastewater)

wastewater has given similar results and sometimes better than freshwater irrigation in terms of yield, that equals or exceeds to the one irrigated with freshwater and yielded 20 T/ha compared to 17–20 T/ha, of fresh yield. The supply of 186 mm to satisfy the crop consumption needs allows us to save on conventional water by using treated wastewater. Furthermore, an important economic gain is generated in term of the fertilizers use. We can save 240 kg/ha of N and 60 kg/ha of CaO in addition to 10.38 kg/ha of P<sub>2</sub>O<sub>5</sub> and 65.12 kg/ha of K<sub>2</sub>O in the case of 100% ETM and 12.45 kg/ha of P<sub>2</sub>O<sub>5</sub> and 78.14 kg/ha of K<sub>2</sub>O in the case of 120% ETM.

The addition of a leaching fraction (20%) to the irrigation requirements under saline conditions significantly improved the growth and the yield production (up to 24.4% of yield increment) of sweet corn varieties irrigated with treated wastewater.

Under the SD irrigation system, we found that reducing the applied water from 120 to 100% of ETM affects significantly the yield production up to 24.4%, but under SSD irrigation system we found nearly the same yield of both

100% of ETM and 120% of ETM. Therefore, we can save the 20% of water under SSD system. Despite that SSD allows to save water, we found significant increase in soil salinity, even in sandy soil, due to the accumulation of salts in the root zone.

Persistent management practices, such as applications of soil amendments that provide calcium to replace sodium; periodic leaching to reduce salt accumulation; frequent aerifications to maintain infiltration, percolation and drainage; regular soil and plant monitoring, and selection and use salt-tolerant crops will be helpful in mitigating the negative impact and ensuring continued success in using recycled wastewater for irrigation (Qian & Mecham, 2005).

**Acknowledgements** We are thankful to WASA and REUSE project for the financial support.

## References

- ABHSM. (2006). *Agence du Bassin Hydraulique du Souss-Massa. Etude de révision du plan directeur d'aménagement intégré des ressources en eau (PDAIRE) des bassins du Souss-Massa*, Vol. 10. Demande en eau agricole.
- Akram, M., Ashraf, M. Y., Jamil, M., Iqbal, R. M., Nafees, M., & Khan, M. A. (2011). Nitrogen application improves gas exchange characteristics and chlorophyll fluorescence in maize hybrids under salinity conditions. *Russian Journal of Plant Physiology*, 58(3), 394–401.
- Ayache, A. (1995). *Besoins en eau du haricot vert conduit sous serre dans la région du Souss*.
- Birch, C. J., Robertson, M. J., Humphreys, E., & Hutchins, N. (2003). Agronomy of maize in Australia in review and prospect. In *Versatile Maize-Golden Opportunities: 5th Australian Maize Conference* (pp. 45–57).
- Choukr-Allah, R. (1995). Utilisation des eaux usées en irrigation, approche globale du traitement des effluents, comparaison de différents systèmes d'irrigation sur diverses cultures et leurs aspects institutionnels et organisationnels. *Gembloux, Belgique, faculté universitaire des sciences agronomiques de Gembloux*: 4.
- Choukr-Allah, R., & Hamdy, A. (2004). Best management practice for sustainable reuse of treated wastewater. WASAMED Workshop, Cairo, Egypt.
- CIPF. (2014). *Centre indépendant de promotion fourragère*. Available on <https://cipf.be/fr/mais/varietes-semis/resultats-varietaux-annees-precedentes/resultats-2014>. Accessed on 03/05/2017.

- Douh, B., & Boujelben, A. (2012). Diagnostic des pratiques d'irrigation localisée souterraine en Tunisie effet sur la variation du stock en eau du sol, le rendement d'une culture de maïs et l'efficacité de l'utilisation de l'eau. *LARHYSS Journal*. ISSN 1112-3680.
- Eagles, H. A., & Lothrop, J. E. (1994). Highland maize from Central Mexico—Its origin, characteristics, and use in breeding programs. *Crop Science*, 34(1), 11–19.
- Ekboir, J. (2002). *Developing no-till packages for small-scale farmers* (pp. 1–38). International Maize and Wheat Improvement Center
- FAO. (2011). Food and Agriculture Organization of the United Nations. Ministry of Agriculture and Maritime Fishing, Secretariat of State in the Ministry of Energy, Mines, Water and the Environment in charge of Water and Environment. *Capacity Building project on the Safe Use of Wastewater in Agriculture*. National report of Morocco Mixt Program FAO/UNW-DPC/UNU-INWEH.
- Levitt, J. (1980). *Responses of plants to environmental stress*, Volume 1: *Chilling, freezing, and high temperature stresses*. Academic Press.
- Mansir, I., Bouchaou, L., Choukr-allah, R., Chebli, B., & El Otmani, M. (2018). Groundwater resources scarcity in Souss-Massa region and alternative solutions for sustainable agricultural development. In *Groundwater and global change in the Western Mediterranean Area* (pp. 189–197). Springer, Cham.
- Megdiche, W., Hessini, K., Gharbi, F., Jaleel, C. A., Ksouri, R., & Abdelly, C. (2008). Photosynthesis and photosystem 2 efficiency of two salt-adapted halophytic seashore *Cakilemaritima* ecotypes. *Photosynthetica*, 46(3), 410–419.
- Poorter, H., Niklas, K. J., Reich, P. B., Oleksyn, J., Poot, P., & Mommer, L. (2012). Biomass allocation to leaves, stems and roots: Meta-analyses of interspecific variation and environmental control. *New Phytologist*, 193, 30–50.
- Qian, Y. L., & Mecham, B. (2005). Long-term effects of recycled wastewater irrigation on soil chemical properties on golf course fairways. *Agronomy Journal*, 97, 717.
- Thellier, M., Le Sceller, L., Norris, V., Verdus, M. C., & Ripoll, C. (2000). Long-distance transport, storage and recall of morphogenetic information in plants. The existence of a sort of primitive plant 'memory'. *Comptes Rendus de l'Académie des Sciences-Series III-Sciences de la Vie*, 323(1), 551–557.



# Ecotoxicological Assessment of Three Types of Wastewater Effluents: Catalase as a Biomarker of Oxidative Stress in Marine Bivalves

Abdellah Meknachi, Mustapha Djellali, and Abdelmalek Badis

## Abstract

Catalase (CAT) is an important enzyme in the antioxidant defense system in marine bivalves. This present work consists first of all in studying the effect, of an acute exposure (bioassays) of the mussels *Mytilus galloprovincialis* to three types of real effluents [industrial wastewater (IW), desalination station effluent (DSE) and harbor effluents (HE)], on the enzymatic activities CAT. In situ, the transplantation of mussels into natural environments was carried out in the same context. The medium size class of the *Mytilus* mussel has proven to be the most resistant to contamination by the IW. Notwithstanding, this same size class showed hypersensitivity to contamination by the SDE, thus translating the high toxicity of the latter which led to very high CAT inductions whatever the concentration tested. Furthermore, under controlled laboratory conditions, the HE demonstrated a certain toxicity by inducing the CAT enzyme. On the other hand, the *Mytilus* mussels transplanted to the khemesti port site are found all dead after ten days of immersion. The deoxygenation of the medium probably had an additional and aggressive effect on our specimens of mussels. This study makes it possible to qualify catalase as a relevant, sensitive, rapid and effective defense biomarker in the evaluation of the health state of the surrounding environment. However, more studies must be made on metabolic activities and energy reserves while adopting the multi-biomarker approach.

## Keywords

Catalase • Oxidative stress • Effluents • *Mytilus galloprovincialis* • Transplantation

## 1 Introduction

Surface and coastal waters are often contaminated by many chemicals released by industry, agriculture and urban communities. The estuarine and coastal zones, under strong continental influence, are the most affected by this type of contamination. The problems posed by the dispersion of pollutants into the environment have attracted the interest of the scientific community for many decades now. Awareness of the need to preserve aquatic ecosystems has led to the emergence of certain issues, including the fate of these pollutants in the environment and their effects on animal and plant communities (Bouzahouane et al., 2018; Cappello et al., 2013; Flammarion et al., 2001; Jing et al., 2019; Sillero-Rios et al., 2018; Vlahogianni et al., 2007).

In order to know and monitor the evolution of chemical contamination of aquatic ecosystems, research and monitoring programs based on the measurement of contaminants concentration in water and sediments have been implemented. However, the chemical analysis of the pollutants present in the various compartments of the aquatic ecosystems is not always possible because of the multiplicity of the molecules present, and this often at concentrations lower than the limits of analytical detection, which makes sampling and measurement techniques quite complex. The risks of contamination at the time of sampling and analysis are numerous, making measurements difficult. These problems have been overcome by the use of “ultra-clean” techniques in sampling. However, the direct measurement of contaminants in water uses sophisticated analytical techniques that are difficult to apply in a perennial network for the routine measurement of the quality and health of aquatic

A. Meknachi (✉) · M. Djellali · A. Badis  
National Center for Research and Development of Fisheries and Aquaculture, CNRDPA-BouIsmaïl, 11 Bd Colonel Amirouche BouIsmaïl, Tipasa, Algeria  
e-mail: [meknachi@gmail.com](mailto:meknachi@gmail.com)

A. Meknachi · A. Badis  
Laboratory of Chemistry of Natural Substances and Biomolecules LCSN-BioM, USDB1 University of Blida-1, B.P. 270, Route de Soumaa, Blida, Algeria

ecosystems. Moreover, the temporal variability of the littoral and limnic environment confers little representativity to a point measurement in the water column. Finally, such an approach does not provide information on the risks faced by animal or plant populations exposed to pollutants, and cannot, on its own, predict the biological effects of contaminant mixtures (synergies, etc.) or simply quantify the bioavailability of contaminants for living organisms. As a result, the manager lacks information on the urgency of taking action to improve the health status of these ecosystems, or to protect biodiversity and the integrity of these ecosystems (Aouini et al., 2018; Barillet et al., 2011; Boukadida et al., 2017; Brooks et al., 2015; Casas and Bacher, 2006; Mejdoub et al., 2017).

With this in mind, Goldberg (1975) proposed monitoring the concentrations of contaminants in living organisms to monitor the surrounding environment. This is the principle of “quantitative bioindicators” based on the fact that aquatic organisms concentrate contaminants at concentrations higher than those present in the environment (Aouini et al., 2018; Arienzo et al., 2019; Benali et al., 2017; Casas and Bacher, 2006).

Current surveillance strategies are diverse, and the use of fixed molluscs and relatively sedentary fish are most commonly developed in environmental monitoring programs. *Mytilus galloprovincialis* mussels and other marine bivalves have characteristics that make them good bioindicators of coastal water contamination (Akaishi et al., 2007; Arienzo et al., 2019; Aslan et al., 2018; Cappello et al., 2013; Casas and Bacher, 2006; Forbes et al., 2006; Sparks et al., 2019).

Other tools, the biomarkers (reflecting an interaction between a biological system and a potential hazard) can be used to study the bioavailability of contaminants. They are then studied more for their contribution to the mechanistic understanding of the action of pollutants (Al-Fanharawi et al., 2018; Aslan et al., 2018; Beiras, 2018; Peric et al., 2017; Sparks et al., 2019).

In this context, the National Center for Research and Development of Fisheries and Aquaculture CNRDPA-BouIsmaïl is currently developing a program of management of aquatic ecosystems and environmental monitoring contributing to the research of pollution indicators. Within this framework, we carried out our research on the Mediterranean mussel “*Mytilus galloprovincialis*” as a biological model in order to better define the ecotoxicology research topics of real effluents, in laboratory and in situ, whose main objective is the contribution looking for biomarkers like an early response that can provide integrated information on the state of the aquatic ecosystem as well as on bioaccumulation phenomena.

## 2 Materials and Methods

### 2.1 Experimental Procedure

The different experiments were conducted and carried out at the CNRDPA-BouIsmaïl pilot shellfish breeding center (Fig. 1).

On the map below are indicated the sampling points of the different liquid discharges used in this study, as well as the collection points of the *Mytilus* mussels and the transplant sites of artificial cages (mussels caging).

#### 2.1.1 First Series of Ecotoxicity Tests

*Mytilus galloprovincialis* mussels, which are used as a biological model, are collected from the sea buoyage signals of the Fouka marine seawater desalination plant (Fig. 1). Sampling targeted the three size classes (22 mm; 28 mm), (43 mm; 52 mm) and (71 mm; 86 mm). After the collection of the mussels, the latter are sorted, cleaned, cleared of their epibionts and measured using a Vernier caliper before their adaptation. The set of mussels is maintained under identical environmental conditions, and the use of air pumps ensures the aeration of the water tanks. A daily renewal of the rearing water is carried out during the adaptation period and throughout the entire experimental cycle.

In order to minimize other factors that may constitute a source of disturbance or interference of ours results, a measurement of the physicochemical parameters (temperature, salinity, pH and dissolved oxygen) is carried out each day during the whole experimental cycle before and after the change of water using a YSI 556 multiparameter.

The strategy of the ecotoxicity tests is to contaminate the *Mytilus* mussels, of different size classes (large, medium and small), by the waters of an industrial wastewater (IW), discharging directly at sea in BouIsmaïl Bay (Fig. 1), and this at different concentrations by dilution in tanks of 70 L.

Thus, the mussels are exposed for four days at four increasing concentrations ( $C1 = 0.01\%$ ;  $C2 = 0.15\%$ ;  $C3 = 0.3\%$  and  $C4 = 0.5\%$  (v/v)) of the IW. The manipulation is automatically compared to a control aquarium (0 mg/L pollutant).

The four selected concentrations were tested to establish dose–response relationships between the chemical pressure represented by the pollutants of the release and the biological responses observed in the mussels.

#### 2.1.2 Second Series of Experience

In the second series of experiments, we chose to work on the medium-sized class (juvenile mussels) judged to be the most resistant. The experimental conditions are the same as the



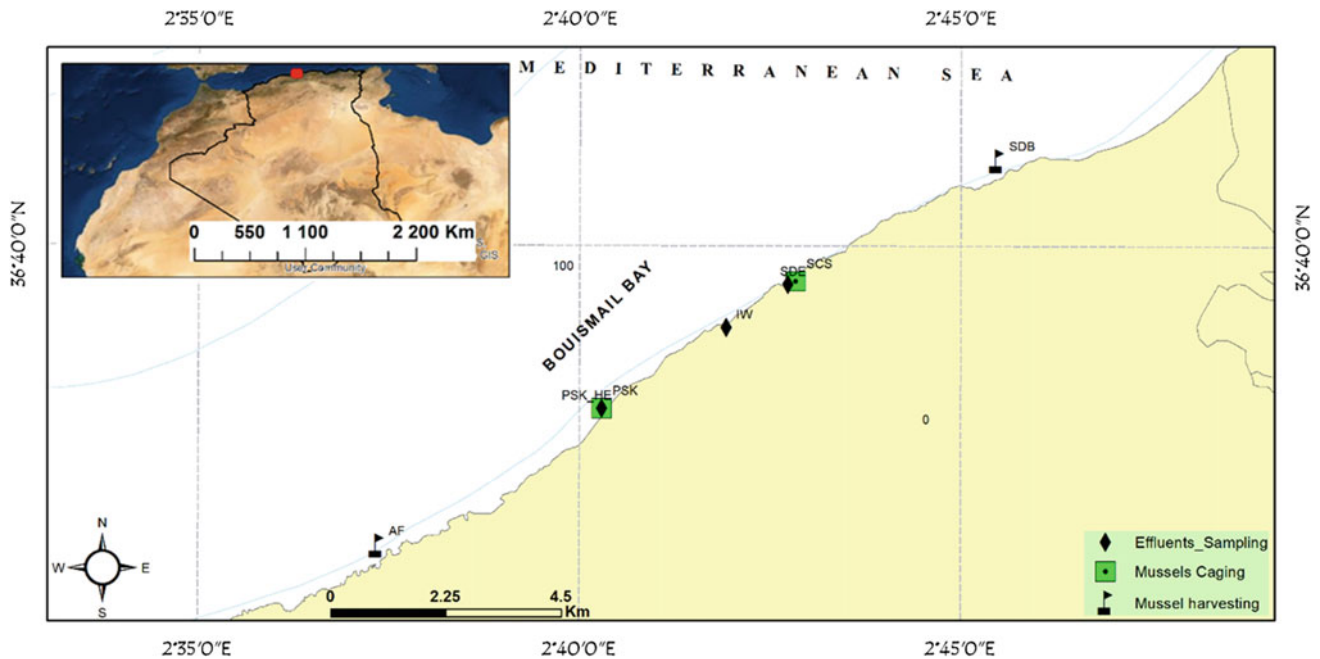


**Fig. 1** Map of BouIsmaïl Bay with points of discharge locations, mussels harvesting and mussels caging

first series of tests. But this time, the mussel specimens are exposed to two types of effluents, namely the water discharge from the BouIsmaïl seawater desalination plant (DSE) and the water from the site port of Khemisti (HE) (Fig. 1). The concentrations chosen are the following: C2 = 0.15%; C3 = 0.3% and C4 = 0.5% (v/v), and the exposure time is always 96 h.

### 2.1.3 In Situ Study: Artificial Cage Transplantation Technique

The mussels this time from an aquaculture farm (AF) located at Ain-Tagourait (Fig. 1) (Tipasa, Algeria) are put in plastic nets (40 cm × 30 cm and mesh 20 mm) and divided into four lots of 15 individuals in wool pockets. The nets are stiffened by a 30 mm diameter PVC tube split in their width and threaded on the upper part.

The artificial stations (mussels caging) were transplanted at two sites: Khemisti port site (PSK Fig. 1) (contaminated environment) and in an open environment (low contamination site) near the shellfish center (SCS) (see map). The immersion time of the stations was planned for one month with a periodic sampling of mussels every ten days. However, we were limited to ten days following the total mortality of transplanted individuals in the port site.

## 2.2 Analytical Methods and Biochemical Assays

Total proteins are assayed by Lowry method using bovine serum albumin (BSA) as standard. Catalase activity is determined according to the method of Lartillot et al. 1988 described by Atli et al. (2006).

In ice-cold, tissues are homogenized (1/10 w/v) in Tris (tris (hydroxymethyl) aminomethane) buffer (20 mM, pH 7.8) for three minutes using a mixer. Centrifugation of the homogenate is done at 10,000 g for 30 min at 4 °C. The supernatant thus obtained (Fraction S9) is used to assay the proteins and catalase.

In our practice, 2.5 ml of substrate solution (25 mM H<sub>2</sub>O<sub>2</sub> in 75 mM phosphate buffer at pH7) are placed in a cuvette of the spectrophotometer already set in the kinetic mode. 50 µl of the S9 fraction (enzyme source) are added to the mixture; thus, the kinetic mode of the spectrophotometer is triggered and the decomposition of hydrogen peroxide is monitored in a time interval of 60 s.

## 2.3 Statistical Analyzes

Data are tested for normality and homoscedasticity using Shapiro–Wilk and Levene tests, respectively. A statistical

analysis is then performed using a bilateral analysis of variance (ANOVA 2), followed by a post hoc analysis of Tukey. The significance was set at  $p < 0.05$ . The results of the in situ study are tested using ANOVA one way (STATISTICA 6.0).

### 3 Results

#### 3.1 First Series of Experiments

The results relating to the determination of catalase (CAT) in mussels (*Mytilus galloprovincialis*) contaminated by industrial rejection are shown in Fig. 2.

Concerning the medium-sized *Mytilus* mussel, the statistical analyzes did not show any significant effect of the contamination, by industrial effluent, on the responses of the defense enzyme catalase, and this compared to the controls and to the gradient concentration examined. The four concentrations of pollutants tested did not seem to have a remarkable effect on the induction of the antioxidant defense mechanism where no significant effect was measured between concentrations.

A significant effect of contamination by industrial discharge is noted in *Mytilus* mussels of the large size class exposed to concentrations C2 and C3. Also, compared to the control individuals (CAT:  $307.89 \pm 23.86$  U/mg Proteins/min), a proportional increase in catalase activity is measured in mussels exposed to the effluent xenobiotics for concentrations C1, C2 and C3. The activities achieved, respectively, are  $545.89 \pm 106.65$ ,  $623.71 \pm 81.48$  and  $688.09 \pm 35.33$  U/mg proteins/min. The C4 concentration (CAT:  $551.08 \pm 90.46$  U/mg Proteins/min) had an insignificant and identical effect as that of the C1 concentration on the induction of the antioxidant enzyme CAT.

In mussels of the small size class, individuals of the latter have shown a hyperactivity in the induction of the antioxidant

mechanism translated by the CAT. Thus, compared to the controls, the highest induction of catalase (253.25%) is measured under the effect of the C4 concentration. Also, the trend was almost proportional with the four concentrations tested. This time, no significant effect was noted between the concentration C1 (CAT:  $737.59 \pm 4.33$  U/mg Protein/min) and C3 (CAT:  $760.33 \pm 64.27$  U/mg Proteins/min), while a very significant effect of the concentration is marked compared to controls ( $416.13 \pm 65.25$  U/mg Protein/min).

The study of the independent effect of each concentration on the CAT response in the three size classes reveals significant and non-significant effects depending on the case considered. Thus, the measured values of the catalase activity in the control individuals (no contaminant) did not show any significant difference between the three classes studied. Under the effect of the C2 concentration, the statistical difference is significant whatever the size class studied. Also, compared to the small size class, the difference is always significant between the compared size classes. However, the statistical analysis reveals an insignificant effect between the medium and large size class and this under the effect of concentrations C1, C3 and C4.

In light of the results obtained, the statistical analysis of the effects of the contaminant concentration and the interaction with the size class revealed that the *Mytilus* mussels of the medium size class (juveniles) are the most resistant to contamination. *Mytilus* individuals of the large size class showed medium sensitivity, while small *Mytilus* appeared the most sensitive to concentration.

#### 3.2 Second Series of Experiments

##### • Comparative study between the different types of effluents (*Mytilus* mussel, medium size)

The results relating to the determination of catalase (CAT) in the mussel (*Mytilus galloprovincialis* of medium size) contaminated by the different types of liquid discharges are represented by Fig. 3.

Whatever the concentration tested for industrial liquid discharge (IW), ANOVA-2 ( $P < 0.05$ ) did not highlight any significant difference between the CAT activities measured (Fig. 3). Also, for the harbor effluent (HE), compared to the effect of the concentration C2, the statistical analysis did not show any significant difference in the CAT activities. However, the difference in the activity of the antioxidant enzyme being significant ( $P < 0.01$ ) between the effect of concentration C3 and that of concentration C4.

In addition, the discharge from the seawater desalination station (DSE) led to very large CAT inductions proportional to the concentrations tested. The highest induction (573.22%) of the antioxidant enzyme is noted under the

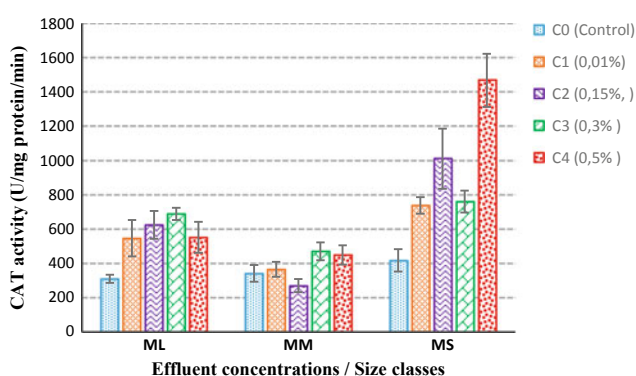


**Fig. 2** Variation in catalase activity in *Mytilus galloprovincialis* contaminated by IW

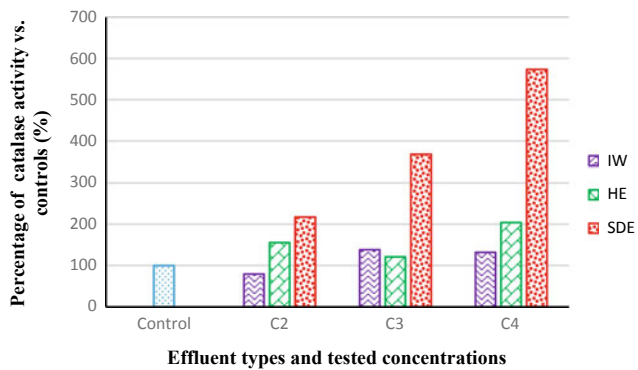


**Fig. 3** Variation in catalase activity in young *Mytilus* mussels under the effect of different effluents

effect of the C4 concentration. The differences in CAT activities were very significant ( $P < 0.0001$ ) regardless of the concentration used for the rejection (DSE).

The study of the independent effect of the concentration C2 (ANOVA-2;  $P < 0.05$ ) on the CAT responses did not show any significant difference ( $P < 0.05$ ) between the port discharge and that of the desalination plant. Notwithstanding, the difference being significant between IW and HE but still very significant between IW and DSE.

For the concentration C3, there was no significant difference of the effect of the nature of effluents between IW and HE. However, the differences are clearly significant between IW-DSE and HE-DSE.

Whatever the type of liquid effluent tested, the differences in CAT activity measured under the effect of the concentration C4 are significant ( $P < 0.05$ ) between IW-HE and very significant ( $P < 0.0001$ ) between IW-DSE and HE-DSE.

### 3.3 Mussels Caging

The results relating to the determination of catalase (CAT) activity in the mussel (*Mytilus galloprovincialis*) transplanted in the port of Khemisti (PSK) and in an open environment (SCS) near the shellfish farming center of CNRDPA-Boulsmail are represented in Fig. 4.

According to the graph in Fig. 4, it emerges that the catalase activity in mussels transplanted in an open medium (SCS) like that of origin of provenance (AF) is identical examining ANOVA one way ( $P < 0.05$ ).

The conditions of the open transplant medium (for ten days) were within the tolerance range for *Mytilus* individuals, which did not lead to a variation in the activity of the antioxidant enzyme CAT. It is also likely that the two media are not really affected by a source of contamination by the different types of xenobiotic.

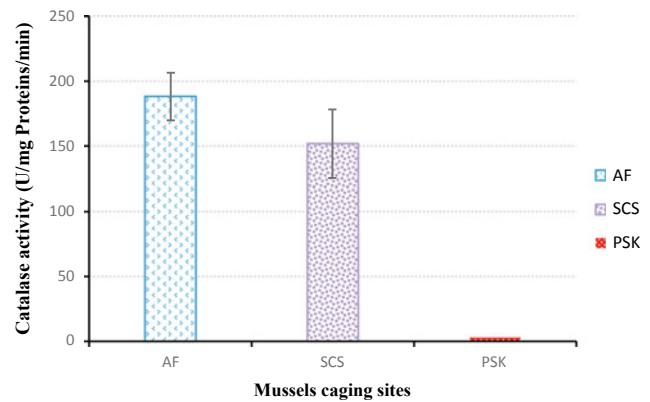


**Fig. 4** Variation in catalase activity in transplanted mussels. *Note* The mussels transplanted into the port of khemisti (PSK) were found all dead on the tenth day of exposure

Furthermore, the mussels transplanted to the Khmesti port site (PSK) were unable to survive, when they showed a total mortality on the tenth day. It is likely that the environmental conditions were not favorable for the mussel specimens to be able to exercise their physiological activity of basic metabolism (respiration, nutrition, etc.) in an optimal manner without any external aggression due to environmental conditions.

## 4 Discussion

### 4.1 First and Second Series of Experiment

Since the development of the “Mussel Watch” program by Goldberg in 1975, the use of bivalve molluscs has been widespread in order to monitor the improvement or degradation of the environment and to study its biological and physiological impacts (Arienzo et al., 2019; Benali et al., 2017; Dong et al., 2019; Pellerin and Amiard, 2009; Zorita et al., 2008). By their filtration capacity of sea water, in order to feed on suspended matter, bivalves can ingest a large quantity of contaminants and therefore concentrate the trace elements (chemical or biological) at concentrations higher than those encountered in its environment (Aouini et al., 2018; Arienzo et al., 2019; Box et al., 2007; Gorbi et al., 2013; Maanan, 2008; Pellerin and Amiard, 2009; Perosevic et al., 2018; Silva Dos Santos et al., 2018). In bivalves, the accumulation of contaminants is mainly by passive diffusion via gill respiration and by active transport resulting from the filtration of water and the ingestion of the particles present (Aasen et al., 2006; Casas and Bacher, 2006). Tissues directly exposed to xenobiotics accumulate these according to their bioavailability (e Silva et al., 2006). The accumulation of chemicals in organisms is the cause of oxidative stress (Aouini et al., 2018; Vlahogianni et al., 2007).

Indeed, by their redox properties, many xenobiotics such as hydrocarbons, metals, quinones or even certain pesticides are known to exert their deleterious effects through the formation of reactivated oxygen species (ROS) (Akcha et al., 2000; Boukadida et al., 2017; Mejdoub et al., 2017; Peric et al., 2017; Verlecar et al., 2008; Vlahogianni et al., 2007). The reactivity of ROS can be the cause of harmful biological effects (oxidation of components such as DNA, proteins, lipids and general disturbance of the redox state) in invertebrates (Barillet et al., 2011; Bouzahouane et al., 2018; Sparks et al., 2019; Vernon and Jha, 2019; Yavasoglu et al., 2016).

In fact, to cope with the production of ROS, aquatic organisms have developed antioxidant defense systems made up of enzymes (superoxide dismutase, **catalase CAT**, glutathione peroxidase) and molecules which trap radical species at the level of membranes (vitamin E,  $\beta$ -carotene) or the aqueous phase (ascorbic acid, uric acid and glutathione). The antioxidant defense enzyme CAT is known to be induced to deal with oxidative stress (Al-Fanharawi et al., 2018; Bao et al., 2018; Barillet et al., 2011; Boukadida et al., 2017; Cappello et al., 2013; Damiens et al., 2004). Measured in the *Mytilus galloprovincialis* mussel, the catalase activity can tell us about the levels of pollution (Box et al., 2007; Vlahogianni et al., 2007) and the degree of cell damage (Akcha et al., 2000; da Silva Barreto et al., 2018; Di Giulio et al., 1993; Teixeira et al., 2017).

In fact, the CAT activities noted in this study, under the effect of the various liquid discharges, can clearly tell us about the degree of toxicity of each effluent. Effluent from the desalination plant is the most toxic regardless of the concentration tested.

In situations of severe stress, defense enzymes are induced very quickly and amply to cope with the endured effects. Sometimes, the end result of such a situation is the inhibition of the activity of the various defense mechanisms (Aouini et al., 2018; Benali et al., 2017). In our study, we noted remarkable mortalities at the end of the exposure of the mussels to the different concentrations of rejection from the desalination station, thus reflecting the total impairment of the different physiological mechanisms of the *Mytilus* mussels as a bioindicator of the level of contamination. Under the effect of industrial discharge and that of port effluent, no mortality was noted. Thus, it is easy to conclude on the high toxicity of the discharge from the desalination plant.

The bioaccumulation of xenobiotics varies according to their chemical properties giving a good indication of their bioavailability in the environment. Acquiring knowledge on the type and rate of contamination will make it possible to analyze the risks they represent at different physiological levels (e Silva et al., 2006; Lemaire et al., 2006; Pellerin and Amiard, 2009).

The introduction of different concentrations of industrial (IW) and port effluents (HE) did not lead to any variation in the physicochemical parameters of the water in aquariums compared to the control groups. So, the deleterious effect on our specimens can be attributed to the xenobiotics present in the two effluents. On the other hand, the liquid discharge of the desalination station (SDE) led to an increase in the salinity and the conductivity of the water in the aquariums. The effect of the xenobiotics present in the effluent therefore combines and probably increases with the increase in salinity leading to a multiplication of the stress signal (CAT).

As was the case in our study, industrial effluents are generally discharged directly into receiving environments (in our case coastal waters) without any pretreatment and are often very loaded with suspended matter, dissolved salts, trace chemical elements organic and/or inorganic. Reaching the receiving environment, liquid effluents can have very harmful effects on the biological component of the environment as they can modify the physicochemical properties of the water column and even sedimentary funds following the accumulation and precipitation of xenobiotics transported by the continuous flow of liquid discharges.

Certain contaminants have the particularity of not being eliminated by living organisms, thus generating a bioaccumulation throughout the food chain with remarkable harmful effects in particular: neurotoxicity, immunotoxicity, stress and oxidative damage, behavior modification, growth inhibition and impaired reproduction (Coppola et al., 2017; Oliveira et al., 2018). The effects are very worrying if we consider the direct short and long-term impact on the receiving environment.

Also, the continuous flow rates of industrial liquid discharges will certainly bring a significant load in xenobiotics on the one hand, but also on the other hand, it can lead to a slight reduction in the salinity of the coastal waters which receive them. The sensitivity of aquatic organisms to the decrease in salinity has been reported by several scientists.

(Hamer et al., 2008) showed an increased mortality of mussels *Mytilus galloprovincialis* under lowest salinities during two acclimation experiments at high/low seawater temperature (27/13 °C), especially during the summer period. Their results revealed that the oxygen consumption rate of mussels increase inversely with the salinity. Furthermore, the DNA integrity from mussels sampled in the winter period showed a significantly lower DNA integrity status than those sampled during the summer season.

Under stressful environmental conditions, homeostasis of organisms is compromised. The hypothesis is that this will in turn increase the susceptibility of mussels to other stresses. The hypothesis is that this will in turn increase the susceptibility of mussels to other stresses.

According to Bussell et al. (2008), the reducing seawater salinity to half that of normal caused a significant reduction



in several measures of immune function, including the concentration of hemocytes, percentage of eosinophilic hemocytes and phagocytosis. Wang et al (2011) found that clearance rate, absorption efficiency, respiration rate and scope for growth of the mussel *Perna viridis* decreased with decreasing salinity and dissolved oxygen concentration. (Bakhmet et al., 2005) report that, when exposed to moderate hyposalinity (15 g/L), the mussel *Mytilus edulis* showed a significant decrease in the heart rate with respect to the control salinity (25 g/L). The heart beat quickly accelerated in all organisms when they were returned to the control salinity medium. In the mussel *Mytilus galloprovincialis*, Freitas et al. (2017) notice that, at low salinity, despite an increase of antioxidant enzymes activity, lipids peroxidation (LPO) increased, probably as a result of ROS overproduction from higher electron transport system activity.

On the other hand, discharges from desalination plants can increase the salinity of the areas close to the outfalls. The dispersion of brine can vary considerably depending on site-specific characteristics, the volume of effluent, the method of discharge and the existing hydrographic conditions. However, salinity and temperature are higher than the reference standards for discharge sites (Fernández-Torquemada et al., 2009).

The southern shore of the Mediterranean is considered to be one of the world's poorest regions of water. As a result, desalination efforts around the Mediterranean are concentrated mainly on its southern and eastern shores, as well as in Spain. In 2013, more than 1532 seawater desalination plants were set up around the Mediterranean Sea with a total cumulative capacity of around 12 Mm<sup>3</sup>/day. Spain was the main producer (31% of total capacity), while in third place comes Algeria followed by Libya with 20 and 11%, respectively (POL, 2015). Given the desalination effort thus mentioned, the biodiversity of our coastal waters is therefore compromised.

Salinity and temperature have long been perceived as environmental factors that inhibit the survival and growth of marine biota (Murray and Wingard, 2006; Wiltshire et al., 2010).

Laboratory and mesocosm experiments have shown the sensitivity of certain seagrass beds to hypersalinity with tolerances which vary from one species to another. Generally, physiology, leaf growth and survival rate are affected (Fernández-Torquemada and Sánchez-Lizaso, 2011; Fernández-Torquemada et al., 2005; Koch et al., 2007; Marín-Guirao et al., 2013; Ruíz et al., 2009; Sandoval-Gil et al., 2012).

In the field, it has been shown that a shallow *Posidonia oceanica* meadow was affected after six years of exposure to brine (Sanchez-Lizaso et al., 2008), while the benthic community was changed (de-la-Ossa-Carretero et al., 2016;

Del-Pilar-Ruso et al., 2008; Ruso et al., 2007) with disappearance of certain echinoderm.

In the distant vicinity of the outlets of the liquid discharges of the present study, we observed a disappearance of the herbarium *Posidonia oceanica*, of the sea urchin *Paracentrotus lividus*, while the spat of *Mytilus* mussels installed on hard substrates did not find the opportunity to grow.

Several authors agree on the importance of salinity, and their results show its influence as much as an abiotic factor on metabolic activity and above all on enzyme responses (Hamer et al., 2008).

Results found by Carregosa et al. (2014) showed that clams under salinity associated stress can alter their biochemical mechanisms, such as increasing their antioxidant defenses, to cope with the higher oxidative stress resulting from hypo and hypersaline conditions. Among the physiological and biochemical parameters that they analyzed: glycogen and protein content, lipid peroxidation levels, antioxidant enzymes (Catalase and especially superoxide dismutase), the latter proved to be sensitive biomarkers to assess the impact of salinity in clams. Among the physiological and biochemical parameters that they analyzed: glycogen and protein content, lipid peroxidation levels, antioxidant enzymes (Catalase and especially superoxide dismutase), the latter proved to be sensitive biomarkers to assess the impact of salinity in clams.

## 4.2 Mussels Caging Discussion

Several authors describe the transplantation of mussels from a reference site that is not/or little polluted to more polluted sites, as a very promising and very relevant technique and strategy in order to assess the degree of contamination of marine ecosystems (Box et al., 2007; Cappello et al., 2017, 2013; Gherras Touahri et al., 2016; Risso-de Faverney et al., 2010; Schintu et al., 2008; Verlecar et al., 2008).

According to Box et al. (2007) and Sillero-Rios et al. (2018), measuring the same biomarker simultaneously in different localities provides information on the degree of pollution of the latter and provides a better understanding of the mechanisms of the mode of action of pollutants in the environment on transplanted organisms. In fact, Box et al. (2007) found that the degree of induction of CAT activity was greater in mussels (*Mytilus galloprovincialis*) transplanted in estuaries most affected by urban discharges than in specimens transplanted in estuaries little affected by anthropogenic activity for which they measured a lesser induction of the antioxidant enzyme CAT.

In agreement with Cappello et al. (2013), significantly greater CAT activity was recorded in mussels caged at the site influenced by anthropogenic activities compared to the reference site. By applying passive biomonitoring of



pollution in coastal areas from the Saronikos Gulf of Greece, Vlahogianni et al. (2007) found that CAT activity was increased 2–3 times at the polluted sites, with high activity in the winter and spring time, compared to the control site. Data for increases in CAT activity demonstrate a disturbance from pollutants in the Elefsis Bay with seasonal variations reflecting the intensity of pollution in the area.

In fact, it is easy to attribute the induction levels of the antioxidant enzyme CAT, from the present study, to the overall quality of the different mussels caging sites. In addition to chemical analyzes of bioaccumulation, the measurement of biomarkers provides information on the nature and level of chemical contamination but also on the health of living organisms and populations of aquatic ecosystems (Aouini et al., 2018; Benali et al., 2017; Gorbi et al., 2008; Kopecka et al., 2006; Verlecar et al., 2008; Vlahogianni et al., 2007).

It is recognized that the biological responses of organisms (growth, bioaccumulation and detoxification of chemical pollutants, enzymatic responses of biomarkers, etc.) can be affected not only by chemical pollutants but also by a certain number of natural stressors such as temperature, salinity, dissolved oxygen, food availability and the reproductive state (Balbi et al., 2017; Blanco-Rayon et al., 2019; Cappello et al., 2017; Chatel et al., 2010; Gonzalez-Fernandez et al., 2017; Nardi et al., 2018; Richir and Gobert, 2014). Thus, to exclude the effect of fluctuating temperatures and the reproductive cycle on the signals of the CAT biomarker, the immersion of artificial stations was carried out during the period of sexual rest in the months of June and July.

In terms of volume, the port of Khemisti is small. The discharges reaching the latter are of domestic, industrial origin (two activities are located nearby) and those linked to fishing activities, which leads to a significant concentration of pollution in situ.

The dissolved oxygen contents, which are the result of physical, chemical and biological factors (photosynthesis, respiration, redox reaction, etc.) and which govern the majority of chemical and biological processes, oscillate between a minimum of 3.93 mg/L and a maximum of 4.41 mg/L in the port of Khemisti (PSK), while in SCS and AF sites, the values often exceed 7 mg/L. In assessing the degree of a given pollution, direct measurement of the dissolved oxygen level can tell us about the eutrophication of aquatic ecosystems. Eutrophication can lead to water suffocation (Mucci, 1997). Dissolved oxygen is therefore a sensitive and practical indicator in a first assessment of an environmental diagnosis. In fact, the lower content of dissolved oxygen in the port of Khemisti is the likely result of the latter's eutrophication. Adding to this, the presence of xenobiotics of different forms, the defense system of mussels transplanted in the port site did not have the possibility of coping with the stresses endured, ultimately leading to total

mortality of the transplanted individuals. Dellali et al. (2001) reported that a decrease in the oxygen content is at the origin of an increase in the activity of catalase in the mussels of the lagoon of Bizerte (Tunisia).

Toxic molecules interact with biological molecules. Consequently, the exposed organisms develop various defense mechanisms: avoidance and/or isolation, active elimination, neutralization by complexation with proteins, etc. (Jean-Claude and Claude, 2008). Studies of metabolism and biomass production in organisms exposed to toxins (Ducrot, 2005) have shown that these defense mechanisms are costly for the organism in terms of energy. These defense costs are added to maintenance costs: there is therefore a quantitative correlation between the organism's defense capacity (survival) and its biomass production capacity (growth and reproduction). In addition, energy allocation for the defense, repair and regeneration of cells is favored over growth and reproduction. In extreme situations, the survival of the living is uncertain. According to Jean-Claude and Claude (2008), defense biomarkers allow organisms to fight and survive in the presence of pollutants at reasonable levels, but this has an energy cost for the individual.

In mussels, since the avoidance or isolation strategy is not possible, the use of antioxidant enzymes seems to be the best strategy for dealing with xenobiotics. The excretion and sequestration of xenobiotics in the tissues can also intervene. However, it has been shown that the first responses to the presence of contaminants are those linked to the antioxidant system (Aouini et al., 2018; Box et al., 2007; Damiens et al., 2004; Verlecar et al., 2008; Vlahogianni et al., 2007).

In addition, valve closure is a known behavior in bivalves in response to environmental stress (Freitas et al., 2017; Geffard et al., 2001). As a result, the decrease in the volume of water filtered by the mussels will lead to a decrease in food capture which will have a direct effect on energy intake. Consequence: bad physiological activities. On the other hand, damage to the digestive enzyme by port pollutants either by trophic route or via water will probably have an effect on the efficiency of food energy conversion. The digestive gland is the main organ involved in food processing, digestion and nutrient delivery, and these processes could interfere with the processes of accumulation, detoxification and elimination of pollutants (Arrighetti et al., 2019; Blanco-Rayon et al., 2019; Faggio et al., 2018).

The results obtained in this study have shown that the *Mytilus* mussel has a number of characteristics which make it an excellent bioindicator of the quality of the marine environment, the importance of which has already been emphasized in numerous research studies (Arienzo et al., 2019; Benali et al., 2017; Boukadida et al., 2017; Chatel et al., 2010). Also, the CAT as a stress biomarker demonstrates its sensitivity, its precocity and its effectiveness in predicting the deleterious effects of the real effluents of the

present study. Also, the major interest of catalase as a biomarker resides in the non-specific character of its response, which constitutes an advantage in the context of multiple contamination of aquatic ecosystems. According to several authors, the biomarkers of defense like CAT help maintain the organism's homeostasis. The latter depends on the dose, duration/effect relationship (Al-Fanharawi et al., 2018; Aouini et al., 2018; Bao et al., 2018; Benali et al., 2017).

Catalase can be influenced by intrinsic or extrinsic factors beyond the control of the researcher. Thus, to compensate for the variations in biomarker responses due to these factors, the multimarker approach seems to be a promising key for a better interpretation of the results and thus a more precise evaluation of the health state of the aquatic environment.

## 5 Conclusion

In conclusion, the practice of biomarkers, in our present study, has proven to be very interesting from the point of view of precocity of rest of the measured signals and their correlations with the levels of pollution. They can indeed constitute an obvious complement to chemical monitoring programs by translating a risk for organisms in aquatic ecosystems. As a result, biomarkers can be used and are still of great ecological relevance, particularly in the case of a long-term monitoring program for the coastal and estuarine environments.

Furthermore, the integration of these biological variables into a long-term monitoring and measurement network will provide managers of aquatic environments with better information on the evolutionary trend of the monitored environments (sign of good management or degradation) and will allow scientists to better understand the functioning of the systems studied.

**Acknowledgements** This work could not have happened without the support of some people. I particularly want to thank Mr Djamel Eddine ABASSI for his contribution to the English translation. Also, I am very grateful to Mr Amar DILMI who counted enormously in the outcome of this work. I am also very grateful to the intern Mr Nabil KRITLI.

## References

- Aasen, J. A., Hardstaff, W., Aune, T., & Quilliam, M. A. (2006). Discovery of fatty acid ester metabolites of spirolide toxins in mussels from Norway using liquid chromatography/tandem mass spectrometry. *Rapid Communications in Mass Spectrometry: An International Journal Devoted to the Rapid Dissemination of Up-To-The-Minute Research in Mass Spectrometry*, 20, 1531–1537.
- Akaishi, F. M., St-Jean, S. D., Bishay, F., Clarke, J., da, S. R. I., & de Oliveira Ribeiro, C. A. (2007). Immunological responses, histopathological finding and disease resistance of blue mussel (*Mytilus edulis*) exposed to treated and untreated municipal wastewater. *Aquatic Toxicology*, 82, 1–14.
- Akcha, F., Izuel, C., Venier, P., Budzinski, H., Burgeot, T., & Narbonne, J. (2000). Enzymatic biomarker measurement and study of DNA adduct formation in benzo [a] pyrene-contaminated mussels, *Mytilus galloprovincialis*. *Aquatic Toxicology*, 49, 269–287.
- Al-Fanharawi, A. A., Rabee, A. M., & Al-Mamoori, A. M. J. (2018). Biochemical and molecular alterations in freshwater mollusks as biomarkers for petroleum product, domestic heating oil. *Ecotoxicology and Environmental Safety*, 158, 69–77.
- Aouini, F., Trombini, C., Volland, M., Elcafsi, M., & Blasco, J. (2018). Assessing lead toxicity in the clam *Ruditapes philippinarum*: Bioaccumulation and biochemical responses. *Ecotoxicology and Environmental Safety*, 158, 193–203.
- Arienzo, M., Toscanesi, M., Trifuoggi, M., Ferrara, L., Stanislao, C., Donadio, C., et al. (2019). Contaminants bioaccumulation and pathological assessment in *Mytilus galloprovincialis* in coastal waters facing the brownfield site of Bagnoli, Italy. *Marine Pollution Bulletin*, 140, 341–352.
- Arrighetti, F., Landro, S. M., Lambre, M. E., Penchaszadeh, P. E., & Teso, V. (2019). Multiple-biomarker approach in the assessment of the health status of a novel sentinel mussel *Brachidontes rodriguezii* in a harbor area. *Marine Pollution Bulletin*, 140, 451–461.
- Aslan, E., Ugru Gorgun, A., Katalay, S., Filizok, I., Becerik, S., & Aydemir, T. (2018). An investigation on the seasonal variations of the biomarkers of oxidative stress response and their correlations to Polonium-210 in mussel (*Mytilus galloprovincialis*) and common sole (*Solea solea*) from Izmir Bay, Turkey. *Journal of Environmental Radioactivity*, 189, 103–108.
- Atli, G., Alptekin, Ö., Tükel, S., & Canli, M. (2006). Response of catalase activity to Ag<sup>+</sup>, Cd<sup>2+</sup>, Cr<sup>6+</sup>, Cu<sup>2+</sup> and Zn<sup>2+</sup> in five tissues of freshwater fish *Oreochromis niloticus*. *Comparative Biochemistry and Physiology Part C: Toxicology & Pharmacology*, 143, 218–224.
- Bakhmet, I., Berger, V. J., & Khalaman, V. (2005). The effect of salinity change on the heart rate of *Mytilus edulis* specimens from different ecological zones. *Journal of Experimental Marine Biology and Ecology*, 318, 121–126.
- Balbi, T., Fabbri, R., Montagna, M., Camisassi, G., & Canesi, L. (2017). Seasonal variability of different biomarkers in mussels (*Mytilus galloprovincialis*) farmed at different sites of the Gulf of La Spezia, Ligurian sea, Italy. *Marine Pollution Bulletin*, 116, 348–356.
- Bao, M., Huo, L., Wu, J., Ge, D., Lv, Z., Chi, C., et al. (2018). A novel biomarker for marine environmental pollution of CAT from *Mytilus coruscus*. *Marine Pollution Bulletin*, 127, 717–725.
- Barillet, S., Adam-Guillermin, C., Palluel, O., Porcher, J. M., & Devaux, A. (2011). Uranium bioaccumulation and biological disorders induced in zebrafish (*Danio rerio*) after a depleted uranium waterborne exposure. *Environmental Pollution*, 159, 495–502.
- Beiras, R. (2018). *Biological Tools for Monitoring* (pp. 265–291)
- Benali, I., Boutiba, Z., Grandjean, D., de Alencastro, L. F., Rouane-Hacene, O., & Chevre, N. (2017). Spatial distribution and biological effects of trace metals (Cu, Zn, Pb, Cd) and organic micropollutants (PCBs, PAHs) in mussels *Mytilus galloprovincialis* along the Algerian west coast. *Marine Pollut. Bull.*, 115, 539–550.
- Blanco-Rayon, E., Guilhermino, L., Irazola, M., Ivanina, A. V., Sokolova, I. M., Izagirre, U., & Mari Gomez, I. (2019). The influence of short-term experimental fasting on biomarker responsiveness in oil WAF exposed mussels. *Aquatic Toxicol.*, 206, 164–175.
- Boukaidida, K., Cachot, J., Clerandeaux, C., Gourves, P. Y., & Banni, M. (2017). Early and efficient induction of antioxidant defense

- system in *Mytilus galloprovincialis* embryos exposed to metals and heat stress. *Ecotoxicology and Environmental Safety*, 138, 105–112.
- Bouzahouane, H., Barour, C., Sleimi, N., & Ouali, K. (2018). Multi-biomarkers approach to the assessment of the southeastern Mediterranean Sea health status: Preliminary study on *Stramonita haemastoma* used as a bioindicator for metal contamination. *Chemosphere*, 207, 725–741.
- Box, A., Sureda, A., Galgani, F., Pons, A., & Deudero, S. (2007). Assessment of environmental pollution at Balearic Islands applying oxidative stress biomarkers in the mussel *Mytilus galloprovincialis*. *Comparative Biochemistry and Physiology Part C: Toxicology & Pharmacology*, 146, 531–539.
- Brooks, S. J., Farnen, E., Heier, L. S., Blanco-Rayon, E., & Izagirre, U. (2015). Differences in copper bioaccumulation and biological responses in three *Mytilus* species. *Aquatic Toxicology*, 160, 1–12.
- Bussell, J. A., Gidman, E. A., Causton, D. R., Gwynn-Jones, D., Malham, S. K., Jones, M. L. M., et al. (2008). Changes in the immune response and metabolic fingerprint of the mussel, *Mytilus edulis* (Linnaeus) in response to lowered salinity and physical stress. *Journal of Experimental Marine Biology and Ecology*, 358, 78–85.
- Cappello, T., Maisano, M., Mauceri, A., & Fasulo, S. (2017). (1)H NMR-based metabolomics investigation on the effects of petrochemical contamination in posterior adductor muscles of caged mussel *Mytilus galloprovincialis*. *Ecotoxicology and Environmental Safety*, 142, 417–422.
- Cappello, T., Mauceri, A., Corsaro, C., Maisano, M., Parrino, V., Lo Paro, G., et al. (2013). Impact of environmental pollution on caged mussels *Mytilus galloprovincialis* using NMR-based metabolomics. *Marine Pollution Bulletin*, 77, 132–139.
- Carregosa, V., Velez, C., Soares, A. M., Figueira, E., & Freitas, R. (2014). Physiological and biochemical responses of three Veneridae clams exposed to salinity changes. *Comparative Biochemistry and Physiology Part B: Biochemistry and Molecular Biology*, 177, 1–9.
- Casas, S., & Bacher, C. (2006). Modelling trace metal (Hg and Pb) bioaccumulation in the Mediterranean mussel, *Mytilus galloprovincialis*, applied to environmental monitoring. *Journal of Sea Research*, 56, 168–181.
- Chatel, A., Hamer, B., Talarmin, H., Dorange, G., Schroder, H. C., & Muller, W. E. (2010). Activation of MAP kinase signaling pathway in the mussel *Mytilus galloprovincialis* as biomarker of environmental pollution. *Aquatic Toxicology*, 96, 247–255.
- Coppola, F., Almeida, A., Henriques, B., Soares, A., Figueira, E., Pereira, E., & Freitas, R. (2017). Biochemical impacts of Hg in *Mytilus galloprovincialis* under present and predicted warming scenarios. *Science of the Total Environment*, 601–602, 1129–1138.
- da Silva Barreto, J., de Melo Tarouco, F., de Godoi, F. G. A., Geihs, M. A., Abreu, F. E. L., Fillmann, G., et al. (2018). Induction of oxidative stress by chlorothalonil in the estuarine polychaete *Laeonereis acuta*. *Aquatic Toxicology*, 196, 1–8.
- Damiens, G., His, E., Gnassia-Barelli, M., Quiniou, F., & Roméo, M. (2004). Evaluation of biomarkers in oyster larvae in natural and polluted conditions. *Comparative Biochemistry and Physiology Part C: Toxicology & Pharmacology*, 138, 121–128.
- de-la-Ossa-Carretero, J. A., Del-Pilar-Ruso, Y., Loya-Fernández, A., Ferrero-Vicente, L. M., Marco-Méndez, C., Martínez-García, E., and Sánchez-Lizaso, J. L. (2016). Response of amphipod assemblages to desalination brine discharge: Impact and recovery. *Estuarine, Coastal and Shelf Science* 172, 13–23.
- Del-Pilar-Ruso, Y., De-la-Ossa-Carretero, J. A., Giménez-Casalduero, F., & Sánchez-Lizaso, J. L. (2008). Effects of a brine discharge over soft bottom Polychaeta assemblage. *Environmental Pollution*, 156, 240–250.
- Dellali, M., Romeo, M., & Aissa, P. (2001). Suiivi annuel de l'activité catalase chez des moules et des palourdes originaires de la lagune de Bizerte. *Oceanologica Acta*, 24, 263–271.
- Di Giulio, R. T., Habig, C., & Gallagher, E. P. (1993). Effects of Black Rock Harbor sediments on indices of biotransformation, oxidative stress, and DNA integrity in channel catfish. *Aquatic Toxicology*, 26, 1–22.
- Dong, S., Yang, Y., Cheng, B., Ren, C., Zhang, H., Xu, H., et al. (2019). Responses of antioxidant defenses in the clam *Macra veneriformis* to 2,2',4,4'-tetrabromodiphenyl ether exposure. *Comparative Biochemistry and Physiology Part C: Toxicology & Pharmacology*, 217, 98–105.
- Ducrot, V. (2005). *Compréhension et modélisation des relations entre les caractéristiques biologiques et écologiques et la sensibilité aux contaminants des communautés d'invertébrés benthiques: perspectives pour l'évaluation des effets des substances chimiques*. Université Paul Verlaine-Metz.
- e Silva, C. A. R., Smith, B. D., & Rainbow, P. S. (2006). Comparative biomonitors of coastal trace metal contamination in tropical South America (N. Brazil). *Marine Environmental Research*, 61, 439–455.
- Faggio, C., Tsarpali, V., & Dailianis, S. (2018). Mussel digestive gland as a model tissue for assessing xenobiotics: An overview. *Science of the Total Environment*, 636, 220–229.
- Fernández-Torquemada, Y., González-Correa, J. M., Loya, A., Ferrero, L. M., Díaz-Valdés, M., & Sánchez-Lizaso, J. L. (2009). Dispersion of brine discharge from seawater reverse osmosis desalination plants. *Desalination and Water Treatment*, 5, 137–145.
- Fernández-Torquemada, Y., & Sánchez-Lizaso, J. L. (2011). Responses of two Mediterranean seagrasses to experimental changes in salinity. *Hydrobiologia*, 669, 21.
- Fernández-Torquemada, Y., Sánchez-Lizaso, J. L., & González-Correa, J. M. (2005). Preliminary results of the monitoring of the brine discharge produced by the SWRO desalination plant of Alicante (SE Spain). *Desalination*, 182, 395–402.
- Flammarion, P., Devaux, A., & Garric, J. (2001). Marqueurs biochimiques de pollution dans les écosystèmes aquatiques continentaux. Exemples d'utilisation et perspectives pour le gestionnaire. *Bulletin Français de la Pêche et de la Pisciculture*, 209–226.
- Forbes, V. E., Palmqvist, A., & Bach, L. (2006). The use and misuse of biomarkers in ecotoxicology. *Environmental Toxicology and Chemistry*, 25, 272–280.
- Freitas, R., De Marchi, L., Bastos, M., Moreira, A., Velez, C., Chiesa, S., et al. (2017). Effects of seawater acidification and salinity alterations on metabolic, osmoregulation and oxidative stress markers in *Mytilus galloprovincialis*. *Ecological Indicators*, 79, 54–62.
- Geffard, A., Amiard-Triquet, C., Amiard, J. C., & Mouneyrac, C. (2001). Temporal variations of metallothionein and metal concentrations in the digestive gland of oysters (*Crassostrea gigas*) from a clean and a metal-rich site. *Biomarkers*, 6, 91–107.
- Gherras Touahri, H., Boutiba, Z., Benguedda, W., & Shaposhnikov, S. (2016). Active biomonitoring of mussels *Mytilus galloprovincialis* with integrated use of micronucleus assay and physiological indices to assess harbor pollution. *Marine Pollution Bulletin*, 110, 52–64.
- Gonzalez-Fernandez, C., Albertosa, M., & Sokolova, I. (2017). Interactive effects of nutrition, reproductive state and pollution on molecular stress responses of mussels, *Mytilus galloprovincialis* Lamarck, 1819. *Marine Environment Research*, 131, 103–115.
- Corbi, S., Avio, G. C., Benedetti, M., Totti, C., Accoroni, S., Pichierri, S., et al. (2013). Effects of harmful dinoflagellate *Ostreopsis cf. ovata* exposure on immunological, histological and oxidative responses of mussels *Mytilus galloprovincialis*. *Fish & Shellfish Immunology*, 35, 941–950.
- Corbi, S., Lamberti, C. V., Notti, A., Benedetti, M., Fattorini, D., Moltedo, G., & Regoli, F. (2008). An ecotoxicological protocol with caged mussels, *Mytilus galloprovincialis*, for monitoring the impact of an offshore platform in the Adriatic sea. *Marine Environment Research*, 65, 34–49.

- Hamer, B., Jakšić, Ž., Pavičić-Hamer, D., Perić, L., Medaković, D., Ivanković, D., et al. (2008). Effect of hypoosmotic stress by low salinity acclimation of Mediterranean mussels *Mytilus galloprovincialis* on biological parameters used for pollution assessment. *Aquatic Toxicology*, 89, 137–151.
- Jean-Claude, A., & Claude, A.-T. (2008). *Les biomarqueurs dans l'évaluation de l'état écologique des milieux aquatiques*. Lavoisier.
- Jing, W., Lang, L., Lin, Z., Liu, N., & Wang, L. (2019). Cadmium bioaccumulation and elimination in tissues of the freshwater mussel *Anodonta woodiana*. *Chemosphere*, 219, 321–327.
- Koch, M., Schopmeyer, S., Kyhn-Hansen, C., Madden, C., & Peters, J. (2007). Tropical seagrass species tolerance to hypersalinity stress. *Aquatic Botany*, 86, 14–24.
- Kopecka, J., Lehtonen, K. K., Barsiene, J., Broeg, K., Vuorinen, P. J., Gercken, J., & Pempkowiak, J. (2006). Measurements of biomarker levels in flounder (*Platichthys flesus*) and blue mussel (*Mytilus trossulus*) from the Gulf of Gdansk (southern Baltic). *Marine Pollution Bulletin*, 53, 406–421.
- Lemaire, N., Pellerin, J., Fournier, M., Girault, L., Tamigneaux, E., Cartier, S., & Pelletier, E. (2006). Seasonal variations of physiological parameters in the blue mussel *Mytilus* spp. from farm sites of eastern Quebec. *Aquaculture*, 261, 729–751.
- Maanan, M. (2008). Heavy metal concentrations in marine molluscs from the Moroccan coastal region. *Environmental Pollution*, 153, 176–183.
- Marín-Guirao, L., Sandoval-Gil, J. M., Bernardeau-Esteller, J., Ruiz, J. M., & Sánchez-Lizaso, J. L. (2013). Responses of the Mediterranean seagrass *Posidonia oceanica* to hypersaline stress duration and recovery. *Marine Environment Research*, 84, 60–75.
- Mejdoub, Z., Fahde, A., Loufi, M., & Kabine, M. (2017). Oxidative stress responses of the mussel *Mytilus galloprovincialis* exposed to emissary's pollution in coastal areas of Casablanca. *Ocean & Coastal Management*, 136, 95–103.
- Mucci, A. (1997). Chimie des Milieux Aquatiques. Chimie des Eaux Naturelles et des Interfaces dans l'Environnement. *Geochimica Et Cosmochimica Acta*, 61, 2158–2159.
- Murray, J. B., & Wingard, G. L. (2006). *Salinity and temperature tolerance experiments on selected Florida Bay mollusks*. Rep. No. 2331–1258.
- Nardi, A., Benedetti, M., d'Errico, G., Fattorini, D., & Regoli, F. (2018). Effects of ocean warming and acidification on accumulation and cellular responsiveness to cadmium in mussels *Mytilus galloprovincialis*: Importance of the seasonal status. *Aquatic Toxicology*, 204, 171–179.
- Oliveira, P., Lirio, A. V., Canhoto, C., & Guilhermino, L. (2018). Toxicity of mercury and post-exposure recovery in *Corbicula fluminea*: Neurotoxicity, oxidative stress and oxygen consumption. *Ecological Indicators*, 91, 503–510.
- Pellerin, J., & Amiard, J.-C. (2009). Comparison of bioaccumulation of metals and induction of metallothioneins in two marine bivalves (*Mytilus edulis* and *Mya arenaria*). *Comparative Biochemistry and Physiology Part C: Toxicology & Pharmacology*, 150, 186–195.
- Peric, L., Nerlovic, V., Zurga, P., Zilic, L., & Ramsak, A. (2017). Variations of biomarkers response in mussels *Mytilus galloprovincialis* to low, moderate and high concentrations of organic chemicals and metals. *Chemosphere*, 174, 554–562.
- Perošević, A., Joksimović, D., Durović, D., Milasević, I., Radomirović, M., & Stanković, S. (2018). Human exposure to trace elements via consumption of mussels *Mytilus galloprovincialis* from Boka Kotorska Bay, Montenegro. *Journal of Trace Elements in Medicine and Biology*, 50, 554–559.
- Pol, J. S. M. (2015). *Environment programme mediterranean action plan*.
- Richir, J., & Gobert, S. (2014). The effect of size, weight, body compartment, sex and reproductive status on the bioaccumulation of 19 trace elements in rope-grown *Mytilus galloprovincialis*. *Ecological Indicators*, 36, 33–47.
- Risso-de Faverney, C., Guibolini-Sabatier, M. E., & Francour, P. (2010). An ecotoxicological approach with transplanted mussels (*Mytilus galloprovincialis*) for assessing the impact of tyre reefs immersed along the NW Mediterranean Sea. *Marine Environment Research*, 70, 87–94.
- Ruiz, J. M., Marín-Guirao, L., & Sandoval-Gil, J. M. (2009). Responses of the Mediterranean seagrass *Posidonia oceanica* to in situ simulated salinity increase. *Botanica Marina*, 52, 459–470.
- Ruso, Y. D. P., De la Ossa Carretero, J. A., Casalduero, F. G., & Lizaso, J. S. (2007). Spatial and temporal changes in infaunal communities inhabiting soft-bottoms affected by brine discharge. *Marine Environment Research*, 64, 492–503.
- Sanchez-Lizaso, J. L., Romero, J., Ruiz, J., Gacia, E., Buceta, J. L., Invers, O., et al. (2008). Salinity tolerance of the Mediterranean seagrass *Posidonia oceanica*: Recommendations to minimize the impact of brine discharges from desalination plants. *Desalination*, 221, 602–607.
- Sandoval-Gil, J. M., Marín-Guirao, L., & Ruiz, J. M. (2012). Tolerance of Mediterranean seagrasses (*Posidonia oceanica* and *Cymodocea nodosa*) to hypersaline stress: Water relations and osmolyte concentrations. *Marine Biology*, 159, 1129–1141.
- Schintu, M., Durante, L., Maccioni, A., Meloni, P., Degetto, S., & Contu, A. (2008). Measurement of environmental trace-metal levels in Mediterranean coastal areas with transplanted mussels and DGT techniques. *Marine Pollution Bulletin*, 57, 832–837.
- Sillero-Rios, J., Sureda, A., Capo, X., Oliver-Codorniu, M., & Arechavala-Lopez, P. (2018). Biomarkers of physiological responses of *Octopus vulgaris* to different coastal environments in the western Mediterranean Sea. *Marine Pollution Bulletin*, 128, 240–247.
- Silva Dos Santos, F., Neves, R. A. F., Carvalho, W. F., Krepsky, N., & Crapez, M. A. C. (2018). Evaluation of the immune responses of the brown mussel *Perna perna* as indicators of fecal pollution. *Fish & Shellfish Immunology*, 80, 115–123.
- Sparks, C., Marnewick, J., Toefy, R., Snyman, R., & Odendaal, J. (2019). Baseline levels of antioxidant activities in *Mytilus galloprovincialis* along the coast of Cape Town, South Africa. *Marine Pollution Bulletin*, 140, 287–293.
- Teixeira, M., Almeida, A., Calisto, V., Esteves, V. I., Schneider, R. J., Wrona, F. J., et al. (2017). Toxic effects of the antihistamine cetirizine in mussel *Mytilus galloprovincialis*. *Water Research*, 114, 316–326.
- Verlecar, X., Jena, K., & Chainy, G. (2008). Seasonal variation of oxidative biomarkers in gills and digestive gland of green-lipped mussel *Perna viridis* from Arabian Sea. *Estuarine, Coastal and Shelf Science*, 76, 745–752.
- Vernon, E. L., & Jha, A. N. (2019). Assessing relative sensitivity of marine and freshwater bivalves following exposure to copper: Application of classical and novel genotoxicological biomarkers. *Mutation Research*, 842, 60–71.
- Vlahogianni, T., Dassenakis, M., Scoullou, M. J., & Valavanidis, A. (2007). Integrated use of biomarkers (superoxide dismutase, catalase and lipid peroxidation) in mussels *Mytilus galloprovincialis* for assessing heavy metals' pollution in coastal areas from the Saronikos Gulf of Greece. *Marine Pollution Bulletin*, 54, 1361–1371.
- Wang, Y., Hu, M., Wong, W. H., Shin, P. K., & Cheung, S. G. (2011). The combined effects of oxygen availability and salinity on physiological responses and scope for growth in the green-lipped mussel *Perna viridis*. *Marine Pollution Bulletin*, 63, 255–261.
- Wiltshire, K. H., Kraberg, A., Bartsch, I., Boersma, M., Franke, H.-D., Freund, J., et al. (2010). Helgoland roads, North Sea: 45 years of change. *Estuaries and Coasts*, 33, 295–310.

- Yavasoglu, A., Ozkan, D., Guner, A., Katalay, S., Oltulu, F., & Yavasoglu, N. U. K. (2016). Histopathological and apoptotic changes on marine mussels *Mytilus galloprovincialis* (Lamark, 1819) following exposure to environmental pollutants. *Marine Pollution Bulletin*, *109*, 184–191.
- Zorita, I., Ortiz-Zarragoitia, M., Apraiz, I., Cancio, I., Orbea, A., Soto, M., et al. (2008). Assessment of biological effects of environmental pollution along the NW Mediterranean Sea using red mullets as sentinel organisms. *Environmental Pollution*, *153*, 157–168.





# Preparation and Characterization of Activated Carbon Derived from Sewage Sludge for Pollutant Removal from Wastewater

Abdulbari A. Ahmad and Marwan Alraggad

## Abstract

The preparation of activated carbon derived from aerobic biological treatment of the activated sludge (SSAC) is a promising way to dispose of sewage sludge as well as to produce a low-cost adsorbent for pollutant removal methylene blue (MB). In this work, the activated carbon was developed from aerobic biological treatment of the activated sludge using KOH as a chemical activation reagent. The SSAC was characterized by scanning electron microscope (SEM) and Fourier transforms infrared spectroscopy (FTIR) analysis. The SEM study showed that the activated carbon was not large and uniform porous. The main functional groups present in the prepared activated carbon were quinone and aromatic rings. The highest removal of methylene blue dye obtained at prepared SSAC optimum conditions (Temp. 500 °C, time 180 min, KOH 30 g) was 99.92%. It is concluded that the activated carbon from sewage sludge is promising for pollutant removal from wastewater using adsorption process.

## Keywords

Sewage sludge • Activated carbon • Production • Characterization • Methylene blue • Adsorption

## 1 Introduction

In Yemen, the total number of wastewater treatment stations in Yemen is nine stations in function; the total actual flow of the treated wastewater is around 92,000 cubic meter per day and around 33.5 million cubic meter per year (Abdul-Malik,

A. A. Ahmad (✉) · M. Alraggad  
Inter-Islamic Network On Water Resources Development and Management, 70 Ahmed Tarawneh st. Jubeiha, Amman, 11941, Jordan  
e-mail: [abdulbari@Inwrdam.org.jo](mailto:abdulbari@Inwrdam.org.jo)

2002). Primary sewage sludge is containing in large quantities soil contaminants, such as organic compounds, heavy metals, pesticides and human pathogens. Most of the conventional means of sewage sludge disposal like open dumping, sanitary landfilling, aerobic and anaerobic digestion and incineration have created more serious problems like soil and plant toxicity, surface and ground water contamination and air pollution. Furthermore, the ever-increasing cost and unavailability of land near urban areas, more stringent waste disposal regulations and public awareness have made open dumping and landfilling increasingly expensive and impractical.

Wastewater treatment plants produce a large quantity of sludge which has to be disposed. Secondary sewage treatment plants (Fig. 1) typically generate a primary sludge in the primary sedimentation stage of treatment biological treatment. Approximately, 70% of the main raw sewage components is composed of proteins and urea (nitrogenous compounds); sugars, cellulose and starches (carbon hydrates); cooking oil, greases and soaps (fats). About 30% of the solids consist of inorganic components such as metallic salts, road grit and chloride where sewerage and storm water are combined (Spellman, 1996). Typically, the chemicals are used either to facilitate the precipitation of hard to remove substances or to improve suspended solid removal (Turovskiy and Mathai, 2006).

Wastewater contains large quantity undesirable components, including organic, inorganic and toxic substances, as well as pathogenic or disease-causing micro-organisms. In the biological treatment phase, the coagulation and removal of the non-settleable colloidal solids and the stabilization of the organic matter are accomplished biologically using a variety of micro-organisms, principally bacteria (Chobanoglous, 1987). In the third treatment stage, the elimination of phosphorous and nitrogen takes place. Nitrogen elimination may be achieved by a two-stage process: nitrification and denitrification. Ammonia in the wastewater is first oxidized to nitrate (nitrification), and thereafter, the nitrate is

**Fig. 1** Activated sludge wastewater treatment plant



converted to free nitrogen (denitrification) before it is discharged (Werther & Ogada, 1999). Phosphorous compounds can be eliminated through chemical precipitation using additives followed by the sedimentation of the sludge formed, or through biological treatment, where phosphorous compounds are incorporated in the cell tissues which are thereafter removed through sedimentation (Werther & Ogada, 1999).

A promising way for sewage sludge disposal that has been widely studied is the thermal application such as pyrolysis process (Thipkhunthod et al., 2006). Sewage sludge is carbonaceous in nature and rich in organic materials. Hence, it has the potential to be converted into activated carbon if pyrolyzed under controlled conditions or with some chemical treatment (Smith et al., 2009). Many researchers have recognized sewage sludge as a resource with much potential for beneficial reuse other than direct disposal (Kim & Parker, 2008; Massanet-Nicolau et al., 2008).

The fixed carbon contents are considered satisfactorily high, indicating that precursors are suitable to be converted into activated carbon. The fixed activated carbon content increases steadily while volatile declines over temperatures. At higher temperatures, organic substances become unstable as the heat provides energy to the molecules to break their bonding and linking, and once it is broken, the substances will be discharged both as gas and liquid products. The volatile matter content of the precursors decreases significantly after undergoing the carbonization process, whereas the fixed carbon content increases in the activated carbons (Ahmad, 2010). It is seen that sewage sludge contains large amounts of ash. Ash in activated carbon is undesirable and is regarded as impurity.

Activated carbon production from sewage sludge can be considered as an attractive method in reducing of the large quantity sludge volume. There are two processes for the production of activated carbon: chemical activation and physical activation. Chemical activation method is known as a single step of preparation of activated carbon using chemical agents. Physical activation involves carbonization

of carbonaceous materials followed by the activation of the resulting char in the presence of activating agents such as carbon dioxide (CO<sub>2</sub>) or steam (Klijanienko et al., 2008). The chemical activation temperature is lower than physical activation. In addition, the chemical activation can improve the pore development in the carbon structure because the effect of chemical agents (Diao et al., 2002). The carbon yields of chemical activation are higher than the physical one (Sudaryanto et al., 2006). Therefore, in this work, activated carbon was prepared from aerobic sewage sludge by potassium hydroxide activation at different conditions.

The purpose of this study is to present the preparation and characterization of activated carbon derived from aerobic biological treatment of the activated sludge by chemical activation method using KOH for wastewater treatment. The effect of parameters on textural characterization of the SSAC, such as surface morphology, surface chemistry and adsorption uptake, was investigated.

## 2 Materials and Methods

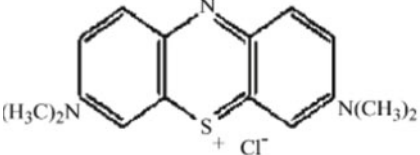
### 2.1 Sample Preparation

The sewage sludge used in this study was collected from the Sana'a Wastewater Treatment Plant (SWTP) located in Bani Al-Hareth, in the north of Sana'a city. The sample's collecting method was in accordance with the standard method (ASTM D346-90, 1999). The sample of sewage sludge was first dried at 105 °C for 24 h, crushed and sieved into a uniform size of 0.5–0.1 mm.s

### 2.2 Methylene Blue Dye

Methylene blue supplied by Sigma–Aldrich (M) Sdn Bhd was used as an adsorbate. The characteristics of the dye are listed in Table 1. The dye stock solution was prepared by dissolving accurately weighed dye in distilled water to a concentration of 1000 mg/L. The experimental solution was

**Table 1** Properties and characteristics of methylene blue dye

Generic name	Methylene blue
Chemical name (IUPAC)	3,7-bis (Dimethylamino)-phenazathionium chloride tetramethylthionine chloride
Chemical formula	C <sub>16</sub> H <sub>18</sub> ClN <sub>3</sub> S·3H <sub>2</sub> O
Molecular weight (g/mol)	373.90
Molecular volume (cm <sup>3</sup> /mol)	241.9
Molecular diameter (nm)	0.80
$\lambda_{\max}$ (nm)	668
Color index number	52,015
Chemical structure	

obtained by diluting the dye stock solution in accurate proportions to different initial concentrations.

### 2.3 Preparation of Activated Carbon

The sludge sample was first dried at 105 °C at constant weight and subsequently crushed and sieved into a uniform size of less than 1 and 2 mm. The resulted granular particles were then impregnated with a 40% (vol) potassium hydroxide (KOH) solution at 25 °C at a ratio of 1:1, 1:2, 1:3, 1:4 (weight). The impregnation ratio (IR) is given by:

$$IR = (\text{weight of KOH in solution}) : (\text{weight of precursor}) \quad (1)$$

After impregnation, the sample solution was filtered to remove the residual KOH, and the sample was subjected to dry at 105 °C.

### 2.4 Chemical Activation of Impregnate Samples

The activation of KOH impregnate raw material was carried out by carbonizing under a purified nitrogen (99.995%) flow (150 cm<sup>3</sup>/g) at a constant heating rate of 10 °C/min a horizontal furnace with a temperature programming heating rate. Experiments were conducted at different carbonization temperatures (400–600 °C) and carbonization times (1–3 h). After activation, the samples were cooled down under a nitrogen flow and were washed sequentially several times with hot distilled water (70 °C). The pH of the washing solution was reached 6–7. Finally, samples were dried in an oven at 110 °C for 24 h and then stored in plastic containers before use.

### 2.5 Activated Carbon Yield

The activated carbon yield was calculated based on Eq. (2).

$$\text{Yield}(\%) = \frac{w_c}{w_o} \times 100 \quad (2)$$

where  $w_c$  (g) is the dry weight of final activated carbon, and  $w_o$  (g) is the dry weight of precursor.

### 2.6 Characterization of Activated Carbon

Scanning electron microscopy analysis was carried out on the precursor, precursor impregnated with KOH and SSAC. The sample was placed on the aluminum tub and coated with gold for electron reflection. The sample was then vacuumed for 5–10 min prior to analysis.

FTIR analyzer was used to investigate the presence of active carbon surface functional group. A disk containing fine carbon with 0.1 wt% potassium bromide (12.7 mm internal diameter and 1 mm thickness) was prepared prior to analysis. The disk was then placed inside the analysis chamber and exposed to infrared light wavelength ranging from 400 to 4000 cm<sup>-1</sup>.

### 2.7 Adsorption Studies

The experiments were conducted by adding a fixed amount of adsorbent to a series of 250 mL glass stopper flasks filled with 200 mL diluted MB solutions with an initial concentration of 100 mg/L placed in each flask. The pH of the solution was not adjusted. 0.30 g of each of the prepared activated carbon, with particle size of 200–500 μm, was

added to each flask. Aqueous samples were taken from the solutions, and the concentrations were analyzed. The concentrations of MB in the supernatant solutions before and after adsorption were determined using double beam UV–VIS spectrophotometer (UV-1601 Shimadzu, Japan) at its maximum wavelength of 668 nm. The dye percentage removal can be calculated as follows:

$$\text{Percentage removal} = 100 \times (C_o - C_e)/C_o \quad (3)$$

where  $C_o$  and  $C_e$  (mg/l) are the liquid-phase concentrations of dye at initial and equilibrium, respectively.

### 3 Results and Discussion

The characterization of raw materials using the desorption process is presented in Table 2, showing that the basic quality parameters of the sewage sludge samples of heavy metals such as Fe, Zn and Pb were analyzed according to the methods prescribed in APHA (Clesceri & Eaton, 1992).

#### 3.1 Characteristics of ACS

##### 3.1.1 Surface Morphology

The SEM of the sewage sludge and the prepared activated carbon are illustrated in Fig. 2. As show in Fig. 2a, the structure of raw sludge is dense, and there are almost no pores. After the carbonization and activation process, the structure became different. The surface of the carbonized product was loose, and pores of different size and shapes appeared (Fig. 2b) due to the decomposition of organic matter (KOH) during carbonization process. And the pores on the surface of SSAC were different from that of carbonized product, contributing to the drilling and expansion of steam to pores during the activation process. These textural structures may consist of well-developed graphite layers, and the spaces between the carbon layer planes and the gaps between the stacks will form an interconnected network of slit-shaped pores, ultimately accommodate the adsorbate molecules during the adsorption process.

##### 3.1.2 Surface Chemistry

The surface chemistry of activated carbons is basically determined by the acidity and basicity of their surface. The existence of functional groups such as carboxyls, phenols,

aldehydes, ketones, quinones, hydroquinones and anhydrides on activated carbon surfaces has been postulated (Ahmad & Idris, 2014). These functional groups determine the acid-base character of carbon materials. The acidic and basic properties are caused by the oxygen-containing groups (Ahmad & Idris, 2014). In Fig. 3, the FTIR spectrum obtained for the prepared activated carbon displayed the following bands; 3841 and 3736  $\text{cm}^{-1}$  were attributed to (O–H) vibrations in hydroxyl groups. The location of hydrogen-bonded OH groups, usually in the range of 3394–3841  $\text{cm}^{-1}$  for alcohols and phenols, involved in hydrogen bonding may be due to adsorbed water (Jindarom et al., 2007); 2375  $\text{cm}^{-1}$  denotes C=O stretching from ketones, aldehydes or carboxylic groups, while 1622  $\text{cm}^{-1}$  is C=C stretching vibration of the aromatic rings. The major absorption band of the SSAC is 1053  $\text{cm}^{-1}$  assigned to either Si–O–Si or Si–O–C structures, which is associated with the silicon content in sewage sludge and SSAC whilst the band at 617  $\text{cm}^{-1}$  is C–O–H twist broad. However, if one closely looks at the spectra, one might find an increasingly upward drift in the baseline of the spectrum from low to high wave numbers at the high pyrolysis temperature, probably due to the increase in aromatics content of char during pyrolysis process (Boehm, 2002).

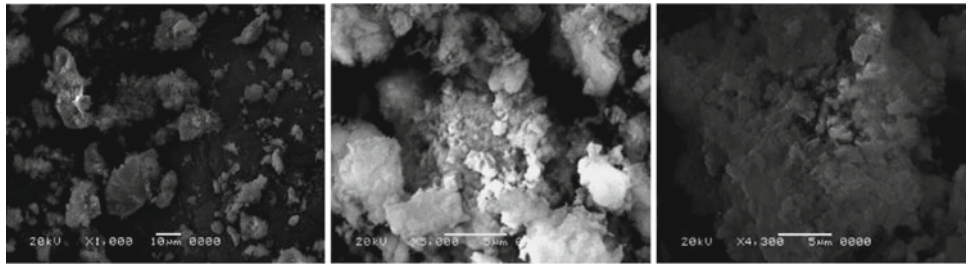
#### 3.2 Adsorption Study

Table 3 shows the removal on percentage of methylene blue. It is found that the rate of removal was rapid during the initial 60 min, and thereafter, no significant change in the rate of removal was observed. MB removal was obtained at optimum conditions (Temp. 500 °C, time 180 min, KOH 30 g) and (Temp. 600 °C, time 60 min, KOH 20 g) where 99.92% and 98.4%, respectively.

Table 3 lists the comparison of the maximum percentage of MB removed by various conditions. Possibly, at the beginning, the solute molecules were adsorbed by the exterior surface of adsorbent particles, so the adsorption rate was fast. When the adsorption of the exterior surface reached saturation, the molecules will need to diffuse through the pores of the adsorbent into the interior surface of the particle. This phenomenon takes relatively long contact time. The monolayer adsorption and surface mass transfer, whereas the linear part at the later period of contact, show the effect of intra-particle diffusion.

**Table 2** Characterization of the raw materials using desorption process

Time (hour)	Fe (mg/kg)	Zn (mg/kg)	Pb (mg/kg)
1	177	20.1	–
2	159	26.1	–
3	117	18	–
4	36	30	0.297



**Fig. 2** SEM images of **a** raw sludge, **b** carbonized product and **c** SSAC

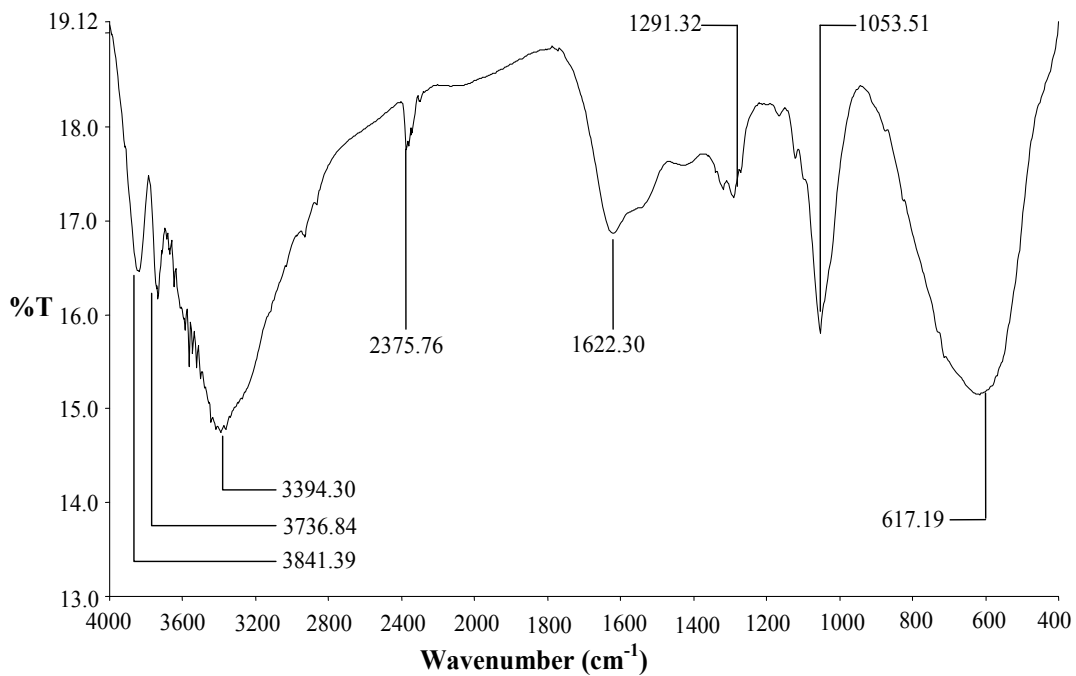
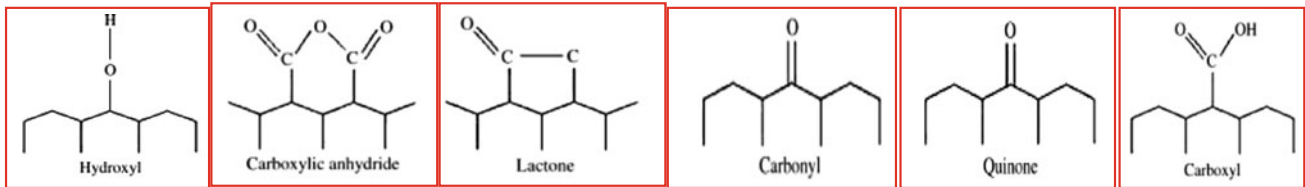


**Fig. 3** FTIR spectrum of SSAC

**Table 3** Comparison of the maximum percentage of MB removal by various conditions

Temp. (°C)	Time (min)	KOH (g)	AC yield (%)	MB removal (%)
500	180	20	24.9	99.99
500	180	30	29.0	99.92
600	60	20	30.6	98.4
600	60	30	30.5	98.8



The activated carbon prepared in this work showed relatively large percentage of MB removed, as compared to some previous works reported in the literature.

#### 4 Conclusion

- The selected waste by-products were promising precursors for the preparation of sewage sludge activated carbon using the chemical activation method.
- Characterization of prepared activated carbon sewage sludge activated carbon:
  - The SEM study showed that the activated carbon was not large and of uniform porosity.
  - The main surface functional groups present in the derived activated carbon were basic and acidic; these functional groups are favorable for removal of pollutants from wastewater.
- Methylene blue was found to adsorb good onto the surface of the sewage sludge-based activated carbon as determined through a batch adsorption test. The highest removal was obtained at optimum conditions (Temp. 500 °C, time 180 min, KOH 30 g).
- The activated carbon production from sewage sludge could be an interesting alternative route for the inexpensive and environmentally acceptable synthesis of carbon-based adsorbents.

**Acknowledgements** The corresponding author gratefully acknowledges the fellowship from Institute of International Education- Scholar Rescue Fund (IIE-SRF). Thanks, are especially due to the Inter-Islamic Network on Water Recourses Development and Management (INWRDAM) staff who helped throughout the different stages of this project.

#### References

Abdul-Malik, Q. Y. (2002). *Yemen water resources and treated wastewater, central water monitoring unit*. Ministry of Agriculture & Irrigation, Yeman.

- Ahmad, A. (2010). *Preparation and characterization of activated carbons from rattan and bamboo waste for color and COD removal* (Ph. D thesis, University Science Malaysia).
- Ahmad, A., & Idris, A. (2014). Preparation and characterization of activated carbons derived from bio-solid: A review. *Desalination Water Treat*, 52(25–27), 4848–4862.
- Boehm, H. P. (2002). Surface oxides on carbon and their analysis: A critical assessment. *Carbon*, 40(2), 145–149.
- Chobanoglous, G. (1987). *Wastewater engineering, treatment, disposal and reuse*. Tata McGraw-Hill.
- Clesceri, L., & Eaton, A. (1992). *Standard methods for the examination of water and wastewater*. Washington, DC: American Public Health Association.
- Diao, Y., Walawender, W., & Fan, L. (2002). Activated carbons prepared from phosphoric acid activation of grain sorghum. *Bioresource Technology*, 81(1), 45–52.
- Jindarom, C., Meeyoo, V., Kitiyanan, B., Rirksomboon, T., & Rangsunvigit, P. (2007). Surface characterization and dye adsorptive capacities of char obtained from pyrolysis/gasification of sewage sludge. *Chemical Engineering Journal*, 133(1–3), 239–246.
- Kim, Y., & Parker, W. (2008). A technical and economic evaluation of the pyrolysis of sewage sludge for the production of bio-oil. *Bioresource Technology*, 99(5), 1409–1416.
- Klijanienko, A., Lorenc-Grabowska, E., & Gryglewicz, G. (2008). Development of mesoporosity during phosphoric acid activation of wood in steam atmosphere. *Bioresource Technology*, 99(15), 7208–7214.
- Massanet-Nicolau, J., Dinsdale, R., & Guwy, A. (2008). Hydrogen production from sewage sludge using mixed microflora inoculum: Effect of pH and enzymatic pretreatment. *Bioresource Technology*, 99(14), 6325–6331.
- Smith, K., Fowler, G., Pullket, S., & Graham, N. J. D. (2009). Sewage sludge-based adsorbents: A review of their production, properties and use in water treatment applications. *Water Research*, 43(10), 2569–2594.
- Spellman, F. R. (1996). *Wastewater biosolids to compost*. CRC Press.
- Sudaryanto, Y., Hartono, S., Irawaty, W., Hindarso, H., & Ismadji, S. (2006). High surface area activated carbon prepared from cassava peel by chemical activation. *Bioresource Technology*, 97(5), 734–739.
- Thipkhunthod, P., Meeyoo, V., Rangsunvigit, P., Kitiyanan, B., Siemanond, K., & Rirksomboon, T. (2006). Pyrolytic characteristics of sewage sludge. *Chemosphere*, 64(6), 955–962.
- Turovskiy, I. S., & Mathai, P. (2006). *Wastewater sludge processing*. Wiley.
- Werther, J., & Ogada, T. (1999). Sewage sludge combustion. *Progress in Energy and Combustion Science*, 25(1), 55–116.

## Urban Water



# Water Quality Investigation of Recent Wells Which Were Randomly Dug at the Left Side of Mosul City

Mohammed F. O. Khattab, Eman Sami Al-Sarraj, Hazim J. Mahmood, and Oliver Wiche

## Abstract

Groundwater is the second biggest source of freshwater of our planet, and it is the only resource that can be access to face the problem of stopping water supply during war and disaster periods. However, there are several challenges facing water quality, particularly in arid and semi-arid regions where climate conditions, type of reservoir rock, geological setting and anthropogenic activities have a significant impact on the groundwater quality. In this work, 13 groundwater samples were taken to evaluate the water quality and investigate its suitability for various uses, such as drinking water, irrigation and household water supply at the left side of Mosul City. These samples were collected from the wells that were dug during the time of liberation the city from ISIS fighters. Attention was given on the examination of EC, TDS, pH,  $\text{Ca}^{+2}$ ,  $\text{Mg}^{+2}$ ,  $\text{Na}^+$ ,  $\text{K}^+$ ,  $\text{SO}_4^{-2}$ ,  $\text{Cl}^-$ ,  $\text{NO}_3^-$  and other water quality parameters, such as sodium adsorption ratio, sodium percentage and magnesium adsorption ratio, as well as heterotrophic bacteria and coliform bacteria. The results of factor analysis proved that the geochemical composition of groundwater is mainly controlled by chemical weathering of carbonate–sulfate minerals and the contamination by municipal activities in the city. The results of the assessment of groundwater proprieties for drinking

and irrigation purposes will give for both decision makers and people good insights for managing the groundwater during crises at this part of Mosul City.

## Keywords

Water quality • Recent wells • Mosul • Groundwater

## 1 Introduction

Water is the basis of survival for human beings and all other living things. Thus, clean potable water is the essential human right demand no one can be prevent it to anyone (Dev & Bali, 2018), where groundwater is a second biggest source of freshwater of our planet and playing important role to providing people with water for different uses in the arid and semi-arid region (Srinivas et al., 2015). It is also the only source can easily be developed to meet the demand of water for during wars or damage to the water systems (Faour & Fayad, 2014; Robins & Fergusson, 2014). Assessment of chemical physical and biological characteristics for groundwater quality is essential to development and successful management of this source (Ndoye et al., 2018). Especially in arid and semi-arid regions, where each of the climate conditions, type of reservoir rock, geological setting and anthropogenic activities have a significant impact on groundwater quality (Zaki et al., 2019). Accordingly, 13 groundwater samples have been taken to analyze and discover the physical, chemical and biological characteristics for the left side of Mosul City. Mosul is the second largest city located in northwestern Iraq and constitutes the main trading center of the northwestern portion of the country (Augustyn et al., 2019). City of Mosul separated by the Tigris River into two halves: the left bank and the right bank with an estimated population about 1.5 million and more than half of them settling at the left side of the city

M. F. O. Khattab (✉)  
Center of Remote Sensing, University of Mosul, Mosul, Iraq

E. S. Al-Sarraj  
Department of Biology Collage of Science, University of Mosul,  
Mosul, Iraq

H. J. Mahmood  
Dams and Water Resources Research Center, University of Mosul,  
Mosul, Iraq

O. Wiche  
Department of Biology, TU Freiberg University, Freiberg,  
Germany

(Al-Sabawi, 2008; UNAMI, 2017). During control ISIS fighters on the city and the military operations which took 10 months to liberation the city, people suffered from water scarcity. To handle this situation, city inhabitants digged wells at each district to draw underground water for different uses without any studying.

The current study included collection 13 groundwater samples from these wells which are located at the left side of Mosul City and to analyze the groundwater quality, where chemical and physical parameters such as EC, TDS, pH,  $\text{Ca}^{+2}$ ,  $\text{Mg}^{+2}$ ,  $\text{Na}^+$ ,  $\text{K}^+$ ,  $\text{SO}_4^{-2}$ ,  $\text{Cl}^-$  and  $\text{NO}_3^-$  investigated as well as heterotrophic bacteria and coliform bacteria. Also, evaluated suitability the groundwater at this part of the city for different uses according to WHO standards and Iraqi references. This work aims to give for both decision makers and people good insights for managing the groundwater during crises at left bank of Mosul City.

## 2 Materials and Methods

### 2.1 Location of Study Area

Mosul city (Capital of Ninawa Governorate) is located northwestern Iraq, about 465 km northwest of Baghdad (Fig. 1). Geographically, It has location coordinates 36.34 latitude and 43.12 longitude with 228 m above sea level (AtlasWorld, 2019). Mosul is split into two separate sides by the Tigris River, with the left bank being Mosul's north-eastern side and the right being the city's southwest. The total area of the left side about 140 km<sup>2</sup> is divided into 51 residential districts with inhabitants reach to more than 750,000 (UN-Habitat, 2016).

### 2.2 Geological and Hydrogeological Setting

The study area is a semi-arid region, where Mosul's climate is classified as warm and temperate where the summers are sweltering, arid and sunny and the winters are cold and partly cloudy (Climate-Data.Org, 2019; WeatherSpark, 2019). Average annual rainfall is about 370.4 mm, and the highest temperatures are in July (32.9 °C), while the coldest month is January (7.2 °C). Tigris River separates the city to the two sides with mean annual discharge range 270–1371 m<sup>3</sup>/s (Khattab & Merkel, 2012; Saleh, 2010).

Geologically, the study area is covered by the sedimentary formations which range in age from late miocene to recent (Fig. 2). These formations can order of the oldest as follow, Fatha formation is the oldest sediments comprises at

the area of interest sandstone and claystone with lenses or strata of anhydrite, gypsum, limestone and marl which are mostly covered by recent sediments (Mahder-Bashi & Khattab, 2009; Al-Naqib et al., 2018). Injana formation comprises of sandstone, siltstone and claystone which exposed at north of the study area. Quaternary deposits are represented by terrace deposits which composed of conglomerate, gravel with lenses of sand and silt, residual soil that covered most of the left bank of Mosul City included sandy and loamy soil (Sissakian et al., 1995).

Finally, flood plain deposits that covered the areas which are close from the Al-Khoser River (cross the study area from the east to west) and Tigris River. Generally, the trend of the groundwater movement is mainly from north and northeast toward south and southwest to the east of Tigris River, with local exceptions (Al-Jiburi & Al-Basrawi, 2015).

### 2.3 Sample Collection and Analysis

The current study included collected 13 groundwater samples were preselected to cover whole area of the left bank of Mosul City (Fig. 1). These samples were taken during November 2018, and the geographical location of each well was fixed by handheld GPS device. The wells examined have different depths ranging from 12 to 60 m. All samples were captured after pumping until the electrical conductivity (EC), pH and temperature reach to steady. The samples for ICP-MS analysis were collected using polyethylene 50 ml bottles after rapidly filtered on site by a 0.2 µm membrane filter and acidified with HNO<sub>3</sub> before storage.

Samples for analysis NO<sub>3</sub> and Cl were 50 ml polyethylene bottles after filtered and stored without acidified, while 50 ml glass bottles were used for measuring bicarbonate. For analysis heterotrophic and fecal coliform bacteria, a 100 ml sterile glass bottle was used and stored inside a cool box and shift directly to the laboratory. Temperature, EC, pH and total dissolved soil (TDS) were measured at the field by portable multi-probe Hanna devices. Heterotrophic and *F. coli* bacteria have been analysed according to the standard methods (APHA, 2005). Each of concentrations the HCO<sub>3</sub> and Cl was measured by titration. NO<sub>3</sub> was measured by UV spectrophotometer method. The concentrations of Ca, Mg, Na, K and S were determined with an ICP-MS (inductively coupled plasma mass spectrometry, Thermo Scientific Element XSERIES 2 ICP-MS). An internal standard with three elements was added to each sample before analysis to verify the accuracy of the analyses. Depending on the element, the measurement was done either in direct, reaction or collision mode.

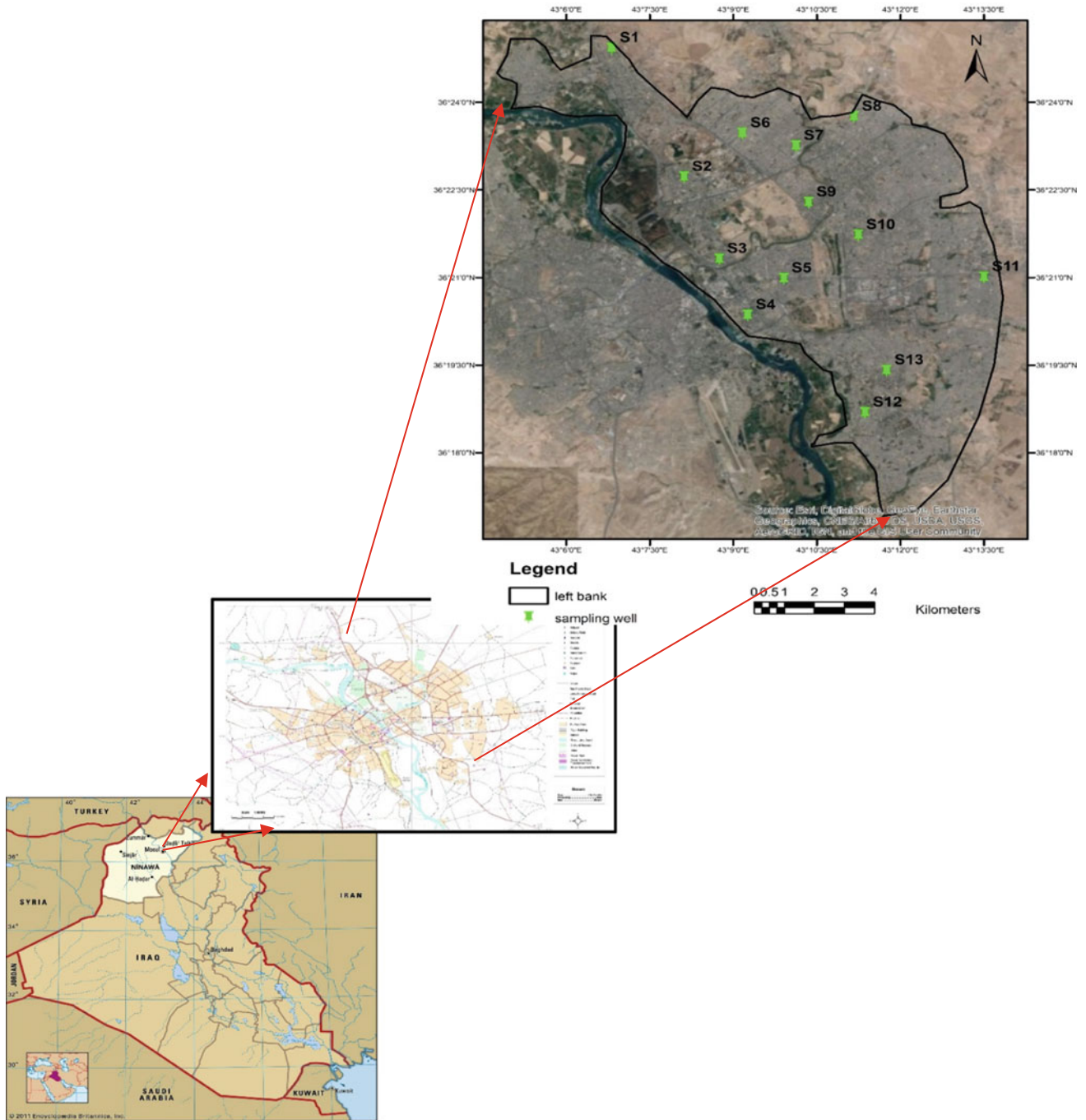


**Fig. 1** Location map of study area showing samplings locations wells

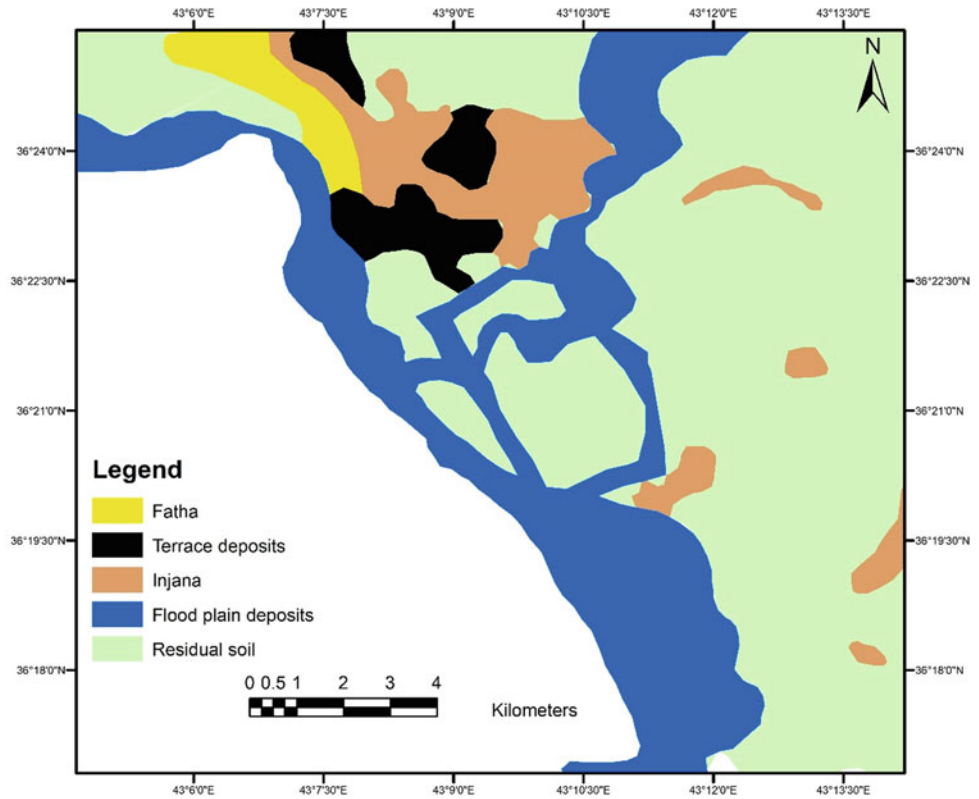
### 2.4 Water Quality Assessment

The current research includes assessment the propriety of groundwater for using as potable water by correlate the results of analysis with International standard of World Health Organization for drinking water and Iraqi sandard specification for drinking water (ICS, 2001; WHO, 2017). The present study selected 15 water quality

parameters which are overall the main key for most water quality evaluation (He et al., 2018; Khattab & Merkel, 2015). These parameters are TPC, F. coliform, pH, TDS, Ca<sup>++</sup>, Mg<sup>++</sup>, Na<sup>+</sup>, Cl<sup>-</sup>, SO<sub>4</sub><sup>2-</sup>, HCO<sub>3</sub><sup>-</sup> and NO<sub>3</sub><sup>-</sup>. Also, the validity of water for irrigation was examined by computing the indicators of irrigation water, where each of sodium adsorption ratio (SAR), sodium percentage (Na %) and magnesium adsorption ratio



**Fig. 2** Geological map of study area ( modified from Sissakian et al., 1995)



(MAR) were calculated as follows (He et al., 2018; Jassas & Merkel, 2015)

$$\text{SAR} = \frac{\text{Na}^+}{\sqrt{(\text{Ca}^{++} + \text{Mg}^{++})/2}}$$

$$\text{Na}\% = \frac{\text{Na}^+ + \text{K}^+}{\text{Ca}^{++} + \text{Mg}^{++} + \text{Na}^+ + \text{K}^+} \times 100$$

$$\text{MAR} = \frac{\text{Mg}^{++}}{\text{Ca}^{++} + \text{Mg}^{++}} \times 100$$

## 2.5 Factor Analysis

Factor analysis is one of the statistical techniques widely used in dealing with large sets of data to determine the relationship between a number of variables at the same time (Kumru, 2001), a statistical method that summarizes many variables for a less known number of factors so that each set of variables is strongly associated with one factor so that reduce the dimensionality of the data matrix (Jolliffe, 2002; Menció & Mas-Pla, 2008). In this study, factor analysis using principal component analysis method with statistical package SPSS 19 for windows was carried out in order to determine the main factors affecting on the hydrochemistry of the studied area.

## 3 Results and Discussion

### 3.1 Hydrogeochemical Characteristics

General information of the groundwater samples is presented in Table 1. pH values do not show a significant change among the samples; this behavior is in line with that of carbonate and bicarbonate ions (Nasrabadi & Abbasimaedeh, 2013). Total dissolved solid and electrical conductivity values ranged between 834-3214  $\mu\text{s}$  and 1008-3829 ppm, respectively. It is known that variance in EC values depends mainly on the variation in TDS values. As for the variation in TDS values, it seems that the difference in their values in the studied wells depends mainly on the dissolution processes of sulfate minerals (mainly Gypsum) (Fig. 3a), as well as the contribution of Tigris water in reduction of TDS values in the near-river wells (Al-Nuaimy, 2010). Calcium is the dominant cation in the studied samples (Table 1), and its concentration ranges from 110.4 to 597.6 ppm, while of  $\text{Mg}^{+2}$  is from 51.7 to 197.6 ppm. The chemical weathering of carbonate and evaporate rocks is the main source of these two ions in natural water (Bouwer, 1978).

Such rocks and rock fragments which belong to the Al-fatha formation are widely spread in the study area. The strong correlation and positive relationship between  $\text{Ca}^{2+}$  and  $\text{SO}_4^{2-}$  (Table 2 and Fig. 3b) indicate that the main source of calcium in the studied area is sulfate minerals, and

**Table 1** General information of samples

Sample	pH	EC	TDS	Cations (ppm)					Anions (ppm)			Bacteria	
		$\mu\text{s}/\text{cm}$	ppm	$\text{Ca}^{2+}$	$\text{Mg}^{2+}$	$\text{Na}^+$	$\text{K}^+$	$\text{HCO}_3^-$	$\text{SO}_4^{2-}$	$\text{Cl}^-$	$\text{NO}_3^-$	TPC	F.coli
1 M	6.98	2922	2480	597.6	99.3	87.8	4.0	375.2	1648.7	70.0	20.5	$6 * 10^3$	0
2 M	7.14	2116	1756	226.3	133.7	108.1	11.5	402.5	976.1	46.0	4.8	$4 * 10^3$	1
3 M	7.37	1310	1097	136.5	66.2	80.4	23.0	345.3	429.2	56.0	9.4	$4 * 10^3$	0
4 M	7.19	1814	1505	226.2	107.2	78.7	9.0	362.1	814.2	66.0	7.7	$4 * 10^3$	3
5 M	7.04	2721	2312	468.5	165.0	46.1	25.2	512.4	1412.5	76.0	0.7	$4 * 10^3$	0
6 M	7.22	1612	1328	162.5	105.8	83.0	1.8	375.8	522.0	100.4	46.0	$7 * 10^3$	2
7 M	7.19	1814	1505	198.4	141.8	56.0	1.4	429.3	702.8	76.0	22.5	$6 * 10^3$	0
8 M	7.15	2015	1673	172.5	143.3	164.4	1.6	479.8	728.8	136.0	42.7	$6 * 10^3$	2
9 M	7.34	3829	3214	547.2	197.6	290.1	5.3	457.4	2154.7	185.9	10.2	$9 * 10^3$	1
10 M	7.19	1612	1330	191.0	100.5	88.9	1.4	387.2	556.9	66.0	35.2	$7 * 10^3$	0
11 M	7.1	1008	834	110.4	51.7	78.7	1.7	323.2	187.2	78.0	51.8	$7 * 10^3$	2
12 M	7.47	1310	1123	232.5	78.0	31.8	1.2	354.5	598.2	26.0	14.2	$4 * 10^3$	0
13 M	7.2	1914	1589	287.8	81.3	84.7	2.1	400.2	676.4	94.0	52.8	$3 * 10^3$	0
Min.	7.0	1008.0	834.0	110.4	51.7	31.8	1.2	323.2	187.2	26.0	0.7	$3 * 10^3$	0.0
Max.	7.5	3829.0	3214.0	597.6	197.6	290.1	25.2	512.4	2154.7	185.9	52.8	$9 * 10^3$	3.0

that between  $\text{Mg}^{2+}$  and  $\text{HCO}_3^-$  (Table 2 and Fig. 3c) refers to the dolomite as the main source of  $\text{Mg}^{2+}$  in the study area, while the positive correlation between  $\text{Mg}^{2+}$  and  $\text{SO}_4^{2-}$  (Table 2) may indicate to the Al-fatha formation as the main source of carbonate and sulfate minerals in the studied area. Sodium is characterized by its high mobility in the aquatic environment and can be derived from multiple sources, and the most important in the studied area is dissolution processes of evaporite rocks (Dhannoun & Mahmood, 2014). This is what the positive correlation (Table 2) between  $\text{Na}^+$ , and each of  $\text{Cl}^-$ , TDS and  $\text{SO}_4^{2-}$  indicates. Potassium concentration ranged from 1.2 to 25.2 ppm  $\text{K}^+$  is derived from dissolution of potassium bearing minerals and cation exchange (Li et al., 2013). The main source of  $\text{HCO}_3^-$  and  $\text{SO}_4^{2-}$  in the studied area is the Al-fatha formation rocks, and this is why a positive correlation between sulfates and bicarbonates is shown in Table 2.  $\text{Cl}^-$  and  $\text{NO}_3^-$  have high solubility and rarely participate in precipitation processes (Mason, 1966). These ions are naturally present at low concentrations in continental water (Hem, 1985), and the increase in their concentration may indicate a case of contamination with sewage or agricultural land water (Heath, 1987; Yuan et al., 2007). In this study,  $\text{Cl}^-$  and  $\text{NO}_3^-$  concentrations ranged from 26 to 185.9 and 0.7 to 52.8 ppm, respectively, and the positive correlation between  $\text{Cl}^-$  and  $\text{Na}^+$  refers to the halite mineral, as indicated previously.

### 3.2 Factor Analysis

Factor analysis revealed two main factors representing more than 74% of the total variance. The first factor explains 52.28% of the variance, while the second factor explains 21.97% (Table 3). The first principal component constitutes a large proportion of the total variance, a unipolar factor which has positive loading of the following variables ( $\text{Ca}^{2+}$ ,  $\text{Mg}^{2+}$ ,  $\text{Na}^+$ ,  $\text{HCO}_3^-$ ,  $\text{SO}_4^{2-}$ ,  $\text{Cl}^-$  and TDS) (Fig. 4). This factor represents the dissolution processes of the mineral composition in the studied area, represented by the carbonate and evaporate (Gypsum and Anhydrite) rocks of Al-fatha formation which is located under the recent sediments and is exposed in the highlands surrounding the study area (Al-Naqib & Aghwan, 1993). The second principal component constitutes (21.97%) of the total variance is less effective than the first factor. It has positive loadings of  $\text{NO}_3^-$ , TCP and *F. coli* and is associated with the first factor influencing chloride ion concentration (Fig. 4). It is clear from the variables loaded on this factor that it represents the contamination factor in the area, due to the leakage from the septic tanks and sewage from the residential neighborhoods, especially as the level of groundwater in the study area ranges from 7 to 18 m.

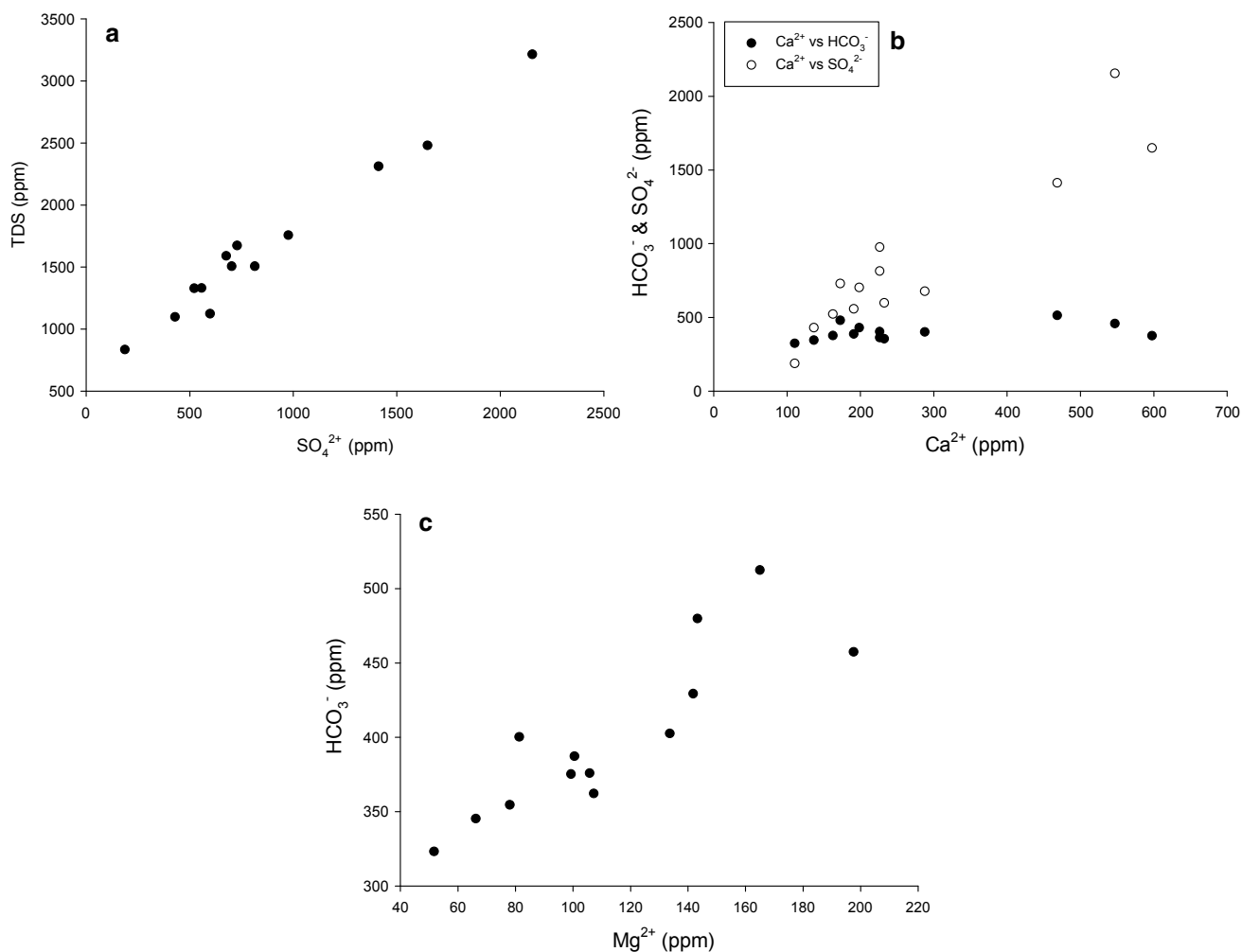


**Fig. 3** Relation between **a** TDS and  $\text{SO}_4^{2-}$ ; **b**  $\text{Ca}^{2+}$  and each of  $\text{HCO}_3^-$  and  $\text{SO}_4^{2-}$ ; **c**  $\text{Mg}^{2+}$  and  $\text{HCO}_3^-$

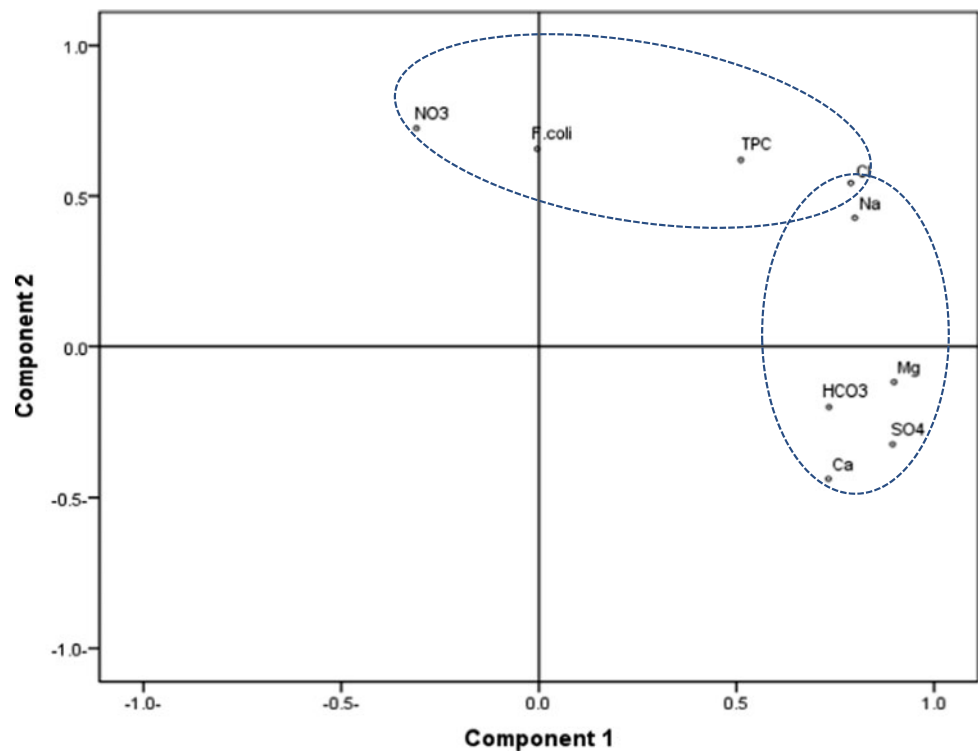
**Table 2** Correlation coefficient matrix of major parameters

Variables	$\text{Ca}^{+2}$	$\text{Mg}^{+2}$	$\text{Na}^+$	$\text{K}^+$	$\text{HCO}_3^-$	$\text{SO}_4^{-2}$	$\text{Cl}^-$	$\text{NO}_3^-$	TDS
$\text{Ca}^{+2}$	1.000	0.532	0.370	0.167	0.440	<b>0.934</b>	0.343	-0.407	<b>0.898</b>
$\text{Mg}^{+2}$		1.000	0.604	0.154	<b>0.861</b>	<b>0.749</b>	0.618	-0.427	<b>0.801</b>
$\text{Na}^+$			1.000	-0.146	0.370	0.601	<b>0.872</b>	-0.029	<b>0.686</b>
$\text{K}^+$				1.000	0.244	0.184	-0.205	-0.662	0.133
$\text{HCO}_3^-$					1.000	0.556	0.525	-0.229	<b>0.643</b>
$\text{SO}_4^{-2}$						1.000	0.510	-0.512	<b>0.984</b>
$\text{Cl}^-$							1.000	0.228	<b>0.638</b>
$\text{NO}_3^-$								1.000	-0.400
TDS									1.000

Bold indicates correlation is significant at the 0.01 level (2-tailed)

**Table 3** Factor loadings, variance, eigen values and communalities of the main PC

Variables	Component 1	Component 2	Communalities
Ca <sup>+2</sup>	0.783	-0.398	0.771
Mg <sup>+2</sup>	0.887	-0.049	0.789
Na <sup>+</sup>	0.772	0.478	0.824
HCO <sub>3</sub> <sup>-</sup>	0.723	-0.139	0.542
SO <sub>4</sub> <sup>-2</sup>	0.928	-0.268	0.933
Cl <sup>-</sup>	0.751	0.595	0.917
NO <sub>3</sub> <sup>-</sup>	-0.347	0.699	0.609
TDS	0.972	-0.148	0.966
F. coli	-0.046	0.655	0.431
TPC	0.469	0.651	0.644
Eigenvalues	5.23	2.20	
Variance (%)	52.28	21.97	
Cumulative (%)	52.28	74.25	

**Fig. 4** Graphical representation of the first and second components

## 4 Groundwater Quality Assessment

### 4.1 A: Drinking Water

Although Tigris River in Mosul City is the only freshwater source for municipal purposes under the normal circumstances, groundwater was replaced this resource during time of control ISIS fighters on the city and liberation processes. Therefore, finding out the range of groundwater validity for

domestic purposes will evaluate the previous period and gave a good understanding to manage the city during crisis. This study included assess the suitability of groundwater at the left bank of Mosul City for drinking according to standard guidelines of World Health Organization for drinking water and Iraqi standard specification for drinking water (Table 4).

When comparing the results of groundwater models analysis with the WHO scale and the Iraqi drinking water standard, it is clear that the groundwater is not suitable for

**Table 4** Standard guidelines for drinking water of WHO (2017) and ICS (2001)

Parameter	WHO (2017)	ICS (2001)
pH	6.5–9.2	6.5–8.5
TDS	1000	500 ppm
Na <sup>+</sup>	200	ni
Ca <sup>++</sup>	200	75 ppm
Mg <sup>++</sup>	150	50 ppm
K <sup>+</sup>	12	ni
Cl <sup>-</sup>	250	200 ppm
S	ni	200 ppm
HCO <sub>3</sub> <sup>-</sup>	ni	ni
NO <sub>3</sub> <sup>-</sup>	50	15 ppm
TPC	<100	<100
F. coli	<50	0

drinking because it exceeds the limits allowed for most parameters.

## 4.2 B: Agricultural Purposes

There are several indicators used to discover the propriety of water for irrigation. In this research, the assessing water quality for irrigation is evaluated by the total concentration of dissolved salts expressed by (EC), sodium percentage (Na %), sodium adsorption ratio (SAR) and magnesium adsorption ratio (MAR). According to EC, more than 60% of the samples were categorized in permissible class, and 26% were categorized in doubtful class while less than 14% categorized in doubtful class unsuitable class (Table 5). The (Na%) is a familiar parameters to evaluate the possible effect of sodium by irrigation water (He et al., 2018), where the higher concentration of Na % reducing the permeability of soil (Todd & Mays, 2005). As shown in (Table 5), all

samples are classified as excellent or good for irrigation purposes. MAR index is representing the ratio between Ca<sup>++</sup> and Mg<sup>++</sup> in groundwater. The higher value of magnesium hazard lead to increasing the soil alkalinity and thus reducing in crop production (Xu et al., 2019). 80% of groundwater samples showed that the groundwater is suitable for irrigation based on the MAR parameters (Table 5).

Also, SAR can be considered indicator for permeability of soil, and higher value of it lead to reduce the water absorption by crops (Xu et al., 2019). The values of SAR for the samples are ranged between 0.4 and 2.6 which indicates that the water can be classified as excellent based on SAR indicator (Table 6).

This research included plotting the groundwater samples on Wilcox diagram (Fig. 5) shows that most of the samples that fell into C3-S1 class, which indicated a threat of alkalization of soils irrigated with such water (Belic et al., 2013). According to FAO, this type of water characterized by each of salinity and infiltration are slight to moderate.

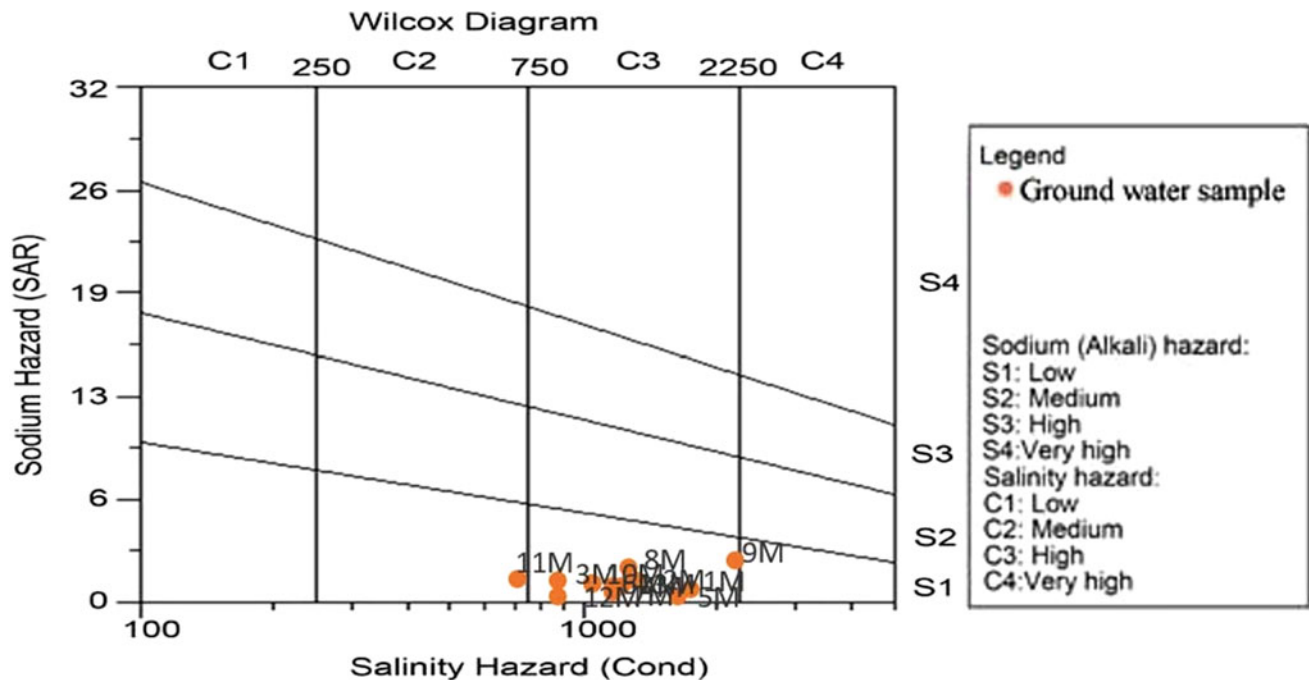
**Table 5** Classification of groundwater quality for irrigation purposes based on (EC), (Na %) and (MAR)

Parameter	Range	Water class	Numbers	Numbers%
EC (μs/cm)	250<	Excellent	–	
	250–750	Good	–	
	750–2000	Permissible	9	60
	2000–3000	Doubtful	4	26.6
	>3000	Unsuitable	2	13.3
Na %	20<	Excellent	10	66.6
	20–40	Good	5	33.3
	40–60	Permissible	–	
	60–80	Doubtful	–	
	>80	Unsuitable		
MAR	50<	Suitable	12	80
	>50	Unsuitable	3	20



**Table 6** Suitability of water for irrigation with different value of SAR

SAR	Suitability for irrigation
1–10	Suitable for all types of crops and soil except for those crops sensitive to sodium
10–18	Suitable for coarse texture or organic soil with permeability
18–26	Harmful for almost all soil
>26	Unsuitable for irrigation

**Fig. 5** Wilcox diagram with groundwater samples of Mosul left bank

## 5 Conclusions

The present study reached to set of conclusions of which that the groundwater of left side of Mosul City unsuitable for drinking water according to WHO and Iraqi standard specification for drinking water, whereas these water for irrigation purposes are good enough to use. Also chemical weathering of carbonate and sulfate minerals is the most important factor controlling the groundwater in the study area. Finally, the municipal activities in the city are contaminating shallow groundwater with nitrates, chlorides and bacteria in the study area. This is reinforced by the result of factor analysis.

**Acknowledgements** The authors are very grateful to the University of Mosul/Dams and Water Resources Research Center for their provided facilities, which helped to improve the quality of this work.

## References

- Al-Jiburi, H. K., & Al-Basrawi, N. H. (2015). Hydrogeological map of Iraq, Scale 1: 1000 000 2nd edition, 2013. *Iraqi Bulletin of Geology and Mining*, 11(1), 17–26.
- Al-Naqib, S., Al-Youzbakey, K. T., & Suleman, A. M. (2018). Hydrochemistry and groundwater level fluctuations (2009-2011) in selected wells at the Eastern part of Mosul City, Northern Iraq. In *The 9th Periodical Scientific Conference* (pp. 19–34). Mosul-University.
- Al-Naqib, S. Q., & Aghwan, T. A. (1993). Sedimentological study of clastic units of the lower Faris formation. *Iraqi Geological Journal*, 26(3), 108–121.
- Al-Nuaimy, H. J. (2010). Hydrochemistry and water quality of some wells distributed at Wana area Northern Iraq. *Iraqi Journal of Earth Science*, 10(2), 45–62.
- Al-Sabawi, L. H. A. (2008). Distribution of health centers in the city of Mosul A comparative study between actual and ideal distribution using information systems Geographically. *Journal of Education and Science*, 15(3), 332–359.

- APHA. (2005). *Standard methods for the examination of water and waste water* (21st ed.). Washington, D.C: American Public Health Association.
- AtlasWorld. (2019). *Where Is Mosul, Iraq?* Retrieved from <https://www.worldatlas.com/as/iq/ni/where-is-mosul.html>
- Augustyn, A., Bauer, P., Duignan, B., Eldridge, A., Gregersen, E., McKenna, A., ... Zelazko, A. (2019). Mosul. In *britannica*. Retrieved from <https://www.britannica.com/place/Mosul>
- Belic, S., Belic, A., & Vranesevic, M. (2013). Water quality as a limiting factor for irrigated agriculture. In *Understanding Freshwater Quality Problems in a Changing World* (pp. 243–249). Gothenburg, Sweden: IAHS Publ.
- Bowser, H. (1978). *Groundwater hydrology*. New York: McGraw-Hill Book.
- Climate-Data.Org. (2019). *Climate Mosul*. Retrieved from <https://en.climate-data.org/asia/iraq/nineveh/mosul-1248/>
- Dev, R., & Bali, M. (2018). Evaluation of groundwater quality and its suitability for drinking and agricultural use in district Kangra of Himachal Pradesh, India. *Journal of the Saudi Society of Agricultural Sciences*. <https://doi.org/10.1016/j.jssas.2018.03.002>
- Dhannoun, H. Y., & Mahmood, H. J. (2014). Hydrochemistry of Tigris River water from its Iraqi's territory entry to Baghdad city. *Iraqi Journal of Earth Science*, 14(1), 67–89.
- Faour, G., & Fayad, A. (2014). Water environment in the coastal basins of Syria—Assessing the impacts of the war. *Environmental Processes*, 1(4), 533–552. <https://doi.org/10.1007/s40710-014-0043-5>.
- He, X., Wu, J., & He, S. (2018). Hydrochemical characteristics and quality evaluation of groundwater in terms of health risks in Luohe aquifer in Wuqi County of the Chinese Loess Plateau, northwest China. *Human and Ecological Risk Assessment: An International Journal*, 1–20. <https://doi.org/10.1080/10807039.2018.1531693>
- Heath, R. C. (1987). *Basic Ground-Water Hydrology*. Washington, DC: ICS, I. C., & S. for drinking water. (2001). *Iraqi Criteria and Standards for drinking water*. No. 417. Baghdad.
- Jassas, H., & Merkel, B. (2015). Assessment of hydrochemical evolution of groundwater and its suitability for drinking and irrigation purposes in Al-Khazir Gomal Basin, Northern Iraq. *Environmental Earth Sciences*, 74. <https://doi.org/10.1007/s12665-015-4664-4>
- Jolliffe, I. T. (2002). *Principal component analysis* (2nd ed). New York: Springer. <https://doi.org/10.1007/B98835>
- Khattab, M. F. O., & Merkel, B. (2015). Secchi disc visibility and its relationship with water quality parameters in the photosynthesis zone of Mosul Dam Lake, Northern Iraq. *Freiberg Online Geology*, 39, 87–101.
- Khattab, M. F. O., & Merkel, B. J. (2012). Distribution of hetrotrophic bacteria and water quality parameters of Mosul Dam Lake, Northern Iraq. In C. A. Brebbia (Ed.), *Water Pollution XI* (pp. 195–207). Southampton: WIT Press.
- Kumru, M. N. (2001). Factor analysis in the geochemical studies along the Gediz river, Turkey. *Journal of Radioanalytical and Nuclear Chemistry*, 249(3), 617–624. <https://doi.org/10.1023/A:1013258601527>.
- Li, P., Qian, H., Wu, J., Zhang, Y., Zhang, H. (2013). Major ion chemistry of shallow groundwater in the Dongsheng Coalfield, Ordos Basin, China. *Mine Water and the Environment*, 32, 195–206
- Mahder-Bashi, T. D., & Khattab, M. F. O. (2009). The use of hydrograph analysis to evaluate the groundwater contribution to Tigris River flow at Mosul city. *Iraqi Journal of Earth Sciences*, 9 (1), 73–84.
- Mason, B. (1966). *Principals of Geochemistry* (3rd Ed). Wiley International Publication.
- Menció, A., & Mas-Pla, J. (2008). Assessment by multivariate analysis of groundwater–surface water interactions in urbanized Mediterranean streams. *Journal of Hydrology*, 352, 355–366. <https://doi.org/10.1016/j.jhydrol.2008.01.014>.
- Nasrabadi, T., & Abbasimaedeh, P. (2013). Groundwater quality degradation of urban areas (case study: Tehran city, Iran). *Environmental Science and Technology*, 11. <https://doi.org/10.1007/s13762-013-0340-y>
- Ndoye, S., Fontaine, C., Gaye, B., & Razack, M. (2018). Groundwater Quality and Suitability for Different Uses in the Saloum Area of Senegal. *Water*, 10(12), 1837. <https://doi.org/10.3390/w10121837>
- Robins, N. S., & Fergusson, J. (2014). Groundwater scarcity and conflict—Managing hotspots. *Earth Perspectives*, 1(1), 6. <https://doi.org/10.1186/2194-6434-1-6>.
- Saleh, S. (2010). *Stream gage descriptions and streamflow statistics for sites in the Tigris River and Euphrates River basins, Iraq*. Reston, Virginia
- Sissakian, V. K., Hagopian, D. H., & Hasan, E. A. (1995). *The geology of Al-Mosul quadrangle sheet NJ-38-3 (GM 4) scale 1:250 000*. Baghdad.
- Srinivas, R., Bhakar, P., & Singh, A. (2015). Groundwater Quality Assessment in Some Selected Area of Rajasthan, India Using Fuzzy Multi-criteria Decision Making Tool. *Aquatic Procedia*, 4, 1023–1030. <https://doi.org/10.1016/j.aqpro.2015.02.129>
- Todd, D., & Mays, L. (2005). *Groundwater hydrology* (Vol. 3). Hoboken: Wiley.
- UN-Habitat. (2016). *City profile of Mosul, Iraq. Multi-sector assessment of a city under siege*. Retrieved from [http://unhabitatiraq.net/mosulportal/wp-content/uploads/2017/05/UN-Habitat\\_MosulCityProfile\\_MEdRes\\_170409\\_V6.pdf](http://unhabitatiraq.net/mosulportal/wp-content/uploads/2017/05/UN-Habitat_MosulCityProfile_MEdRes_170409_V6.pdf)
- UNAMI. (2017). *Report on the Protection of Civilians in the context of the Ninewa Operations and the retaking of Mosul City, 17 October 2016–10 July 2017*. Retrieved from [http://www.uniraq.org/images/factsheets\\_reports/Mosul\\_report17Oct2016-10Jul201731October\\_2017.pdf](http://www.uniraq.org/images/factsheets_reports/Mosul_report17Oct2016-10Jul201731October_2017.pdf)
- WeatherSpark. (2019). *Average weather in Mosul*. Retrieved from <https://weatherspark.com/y/102754/Average-Weather-in-Mosul-Iraq-Year-Round>
- WHO. (2017). *Guidelines for drinking water quality: Fourth edition incorporating the first addendum*. Geneva.
- Xu, P., Feng, W., Qian, H., & Zhang, Q. (2019). Hydrogeochemical characterization and irrigation quality assessment of shallow groundwater in the Central-Western Guanzhong Basin, China. *International Journal of Environmental Research and Public Health*, 16(9), 1492. <https://doi.org/10.3390/ijerph16091492>.
- Yuan, F., Miyamoto, S., & Anand, S. (2007). Changes in major element hydrochemistry of the Pecos River in the American Southwest since 1935. *Applied Geochemistry*, 22, 1798–1813. <https://doi.org/10.1016/j.apgeochem.2007.03.036>.
- Zaki, S. R., Redwan, M., Masoud, A. M., & Abdel Moneim, A. A. (2019). Chemical characteristics and assessment of groundwater quality in Halayieb area, southeastern part of the Eastern Desert. *Egypt. Geosciences Journal*, 23(1), 149–164. <https://doi.org/10.1007/s12303-018-0020-5>.



# Social Network Analysis of Collaborative Management: Assessment of Human Network Stability in Water Resources Management of Iran

Iman Islami

## Abstract

Human management and social communication networks play an important role in water resources management, especially in arid and semi-arid regions. Active actors and a coherent network of individuals are very useful in establishing an appropriate collaborative governance to face the current constraints of water management, conservation, control, and optimal management. In this study, special attention pay to the human role of local actors in the context of a water management social network in central part of Iran with severe water restrictions and under the effects of repeated droughts. Due to the challenges in water distribution as well as local conflicts, it is evaluated based on social network analysis method. The relationships of actors were tested based on indices of density, reciprocity, and focus on local active networks throughout Yazd province during the year 2018–2019. The results show that lack of individuals as mediators between two or more close groups makes it difficult to transfer different information (social, environmental, and economic) between different groups. The lack of inter-group collaboration relationships has created structural holes (empty space) throughout the network that is reduced the direct contact between the actors. The absence of these people with appropriate distribution, who are able to get different ideas from different sources and share innovative ideas with others, has reduced creativity and innovation necessary in dealing with environmental problems especially drought. This study has provided to achieve ideal governance plan by introducing vital actors and presenting weaknesses at the macro level of the human relations network.

## Keywords

Governance • Social cohesion • Social network analysis (SNA) • Network stability • Arid region

## 1 Introduction

Over the past decade, widespread use of the term social capital in various social, economic, political, environmental sciences and especially water resources management indicates the key and important role of this type of capital in achieving the development and sustainable use of natural resources and its protection.

Social capital has come under the scrutiny of sociologists because of its importance to the unique role of human beings and human relationships. Social capital in many sociological studies is a network of social interactions between individuals who manage a community and can lead to social cohesion, a desire to participate in social activities (e.g., Putnam, 1995; Veenstra, 2000). In this view, social capital is a network of collaborative governance or participatory management in a society that facilitates the solution of problems requiring collective action (Brahm & Rahn, 1997; Emerson & Gerlak, 2014; Fliervoet et al., 2016; Sen et al., 2019).

Social capital in the area of environmental resources and natural resources (such as water management) includes resources or benefits from stakeholder relationships that place them in formal or informal local networks. Stakeholder engagement not only develops communication resources but also provides collective benefits for stakeholders who are active in the field. These benefits, which can be considered as social capital, are the primary benefits such as the development of collective cooperation in the face of natural disasters (e.g., drought, floods), productivity growth, and the

I. Islami (✉)

Tarbiat Modares University, Noor, Iran  
e-mail: [i.eslami@modares.ac.ir](mailto:i.eslami@modares.ac.ir)

production of human and material capital in projects that they have mutual and environmental benefits. The activities, as well as the benefits that are ultimately created, resulting from the strong relationships between the groups participating in and out of a local community (e.g., social capital within the group, between the group and the interface) and to social stability and sustainability helps the environment. The debate over participatory management and the term governance and participatory governance have been added to the literature for many years. Various studies have so far criticized the purely governmental role in natural resource management without regard to the role of different stakeholders, and, given the various failures and low yields, the new participatory management system based on the role of different stakeholders has gradually replaced it (Lienert et al., 2013; Fliervoet et al., 2016). It has also received widespread popularity around the world. Local government has relied on local forces for years, although in recent years because of different reasons, it has not been as favorable as in the past.

Network governance in the social network of local water users in Yazd province, including stakeholders in livestock, agriculture, and horticulture sectors, indicates their participation in these areas under difficult ecosystem conditions.

Despite all the problems and severe natural constraints, such as limited rainfall and drying up of water resources, cooperation and collaboration between local residents without government intervention have preserved the habitat and nature. In recent years, the weakening of the human relations network has a major impact on social order and the environmental order. Increasing social conflicts in the development and use of water resources, rather than the social participation of stakeholders, has many natural disasters. Unlawful digging of illegal wells, competition in the exploitation of water resources, depletion of underground water resources, failure to pay attention to the environmental potential of rural areas, and encroachment on industries and mines against water resources are examples of these natural damages. In the meantime, the development of trust and interactions among stakeholders is a key factor in participatory management of water resources (Carlsson & Sandström, 2008). Sociologists' consensus on the index of trust in measuring social capital may be due to the necessity and importance of this component in the development of continuous social relationships. In many studies, including collaborative management of natural resources management, social network analysis based on modeling relationships among actors has been the turning point (Van Eeten et al., 2002). Network analysis helps sociologists gain access to hidden dimensions and reveals the truth of human relations interactions. Social network analysis is a well-used method for evaluating relationships and understanding human

communication chats that understanding them is a great achievement for managers to solve structural problems (Sen et al., 2019; Wang et al., 2019).

The results show that network management is not the same with different structures of relationship density, degree of continuity, subgroup interconnections, and degree of centrality (Bodin & Crona, 2009). Studies of water management show that given the different water consumption by different stakeholders that are often at odds, and network analysis can reflect a deep insight into the power relations and limitations facing institutional management and social relations (Hiwasaki & Arico, 2007).

Researchers have attempted to apply this approach and to analyse the relationships of local communities in order to provide suggestions and solutions to the problems of the area. For example, Mandarano (2009) cites the impact of social networking on achieving successful participatory planning and shows that organizations, by overcoming differences, are able to build new relationships and thus new capital.

The present study emphasizes the importance of network analysis and its combination with other aspects of governance network analysis in further studies. How stakeholders are linked to social relations is an important factor in the sustainable forecasting, control, and management of rural water resources in Yazd province. This method has also been used in various studies. For example, a study of density indices, degree of concentration, and centrality by Prell et al. (2009) in the UK shows that actors with a high centrality are crucial for developing mediator communication and also using network analysis. Power decided to choose the people (Prell et al. 2009). In general, actors with a high degree of centrality and communication have greater social power in society. Naturally, low-center actors are less influential, so accurate understanding of actors is an important factor in successful collaborative management.

Investigating the trust and participatory network and understanding the structure of relationships in this study can be effective in solving the problem ahead. To this end, the present study investigated the quantity and quality of participatory management of local beneficiaries of Yazd province. In this research, the challenges of structuring social relationships of these stakeholders have been analyzed using network analysis by examining the components of trust, participation, and social cohesion in the local governance network.

The goal of this research is network analysis of local water consumers' relationships in Yazd province in central part of Iran as a highlighted arid region of Iran to identify and show the vital roles of mediators in human cohesions and stability of this network. All this is for one ultimate



purpose and the effect that this human network sustainability can have on the social and ecological sustainability of local settlements.

## 2 Methodology

This part of study deals with introducing the study area, the method of network analysis, and the examined indices.

### 2.1 The Study Area

The area under study is Yazd province located in 29° and 35 min to 35° and 7 min of north latitude and 52° and 50 min to 58° and 16 min of east longitude. In this ecological border, local beneficiaries of water living in 50 villages of Yazd province in an area of 3.6 million hectares having a grazing license ( $n = 44$ ) were studied. The method used in this research is complete network analysis. In this method, census is conducted for population relations of actors instead of sampling method. All the involved beneficiaries were studied in order to correct politicizing which was required by managers and planners. The individuals under study were consumers of water resources, from the department of natural resources organization. Figure 1 indicates the study area of this study (Yazd Province) in central part of Iran. This figure shows the distribution of

local stakeholders of water consumption in the geographical area of Yazd province.

### 2.2 Questionnaire of Network Analysis

Social network analysis studies the relations between certain elements (individuals, groups, and organizations, etc.). Its important feature is that it considers communicational and network data in the analysis. Communicational data is the special relationship between a pair of elements, and it is possible that network generates from this pair of elements and their relations. Using a questionnaire of network analysis, the present study deals with studying the relations of trust and participation in local beneficiaries' network of water in Yazd. To identify beneficiaries and receive communicational, a list of all beneficiaries of Yazd was made, and respondents were asked to choose those names in whom they trust and in another list choose those names with whom they have participated in managing water resources at rural, original, or province level. This method can be performed more quickly but requires skill and knowledge of researcher (Scott, 1987). Necessary data was collected based on information obtained from active rural development offices in rural areas that had the most interactions with other stakeholders. In the final step, after forming and entering data matrix, data was analyzed, and graphs were drawn using UCINET (version 6.611) and NetDraw (version 2.159) softwares.

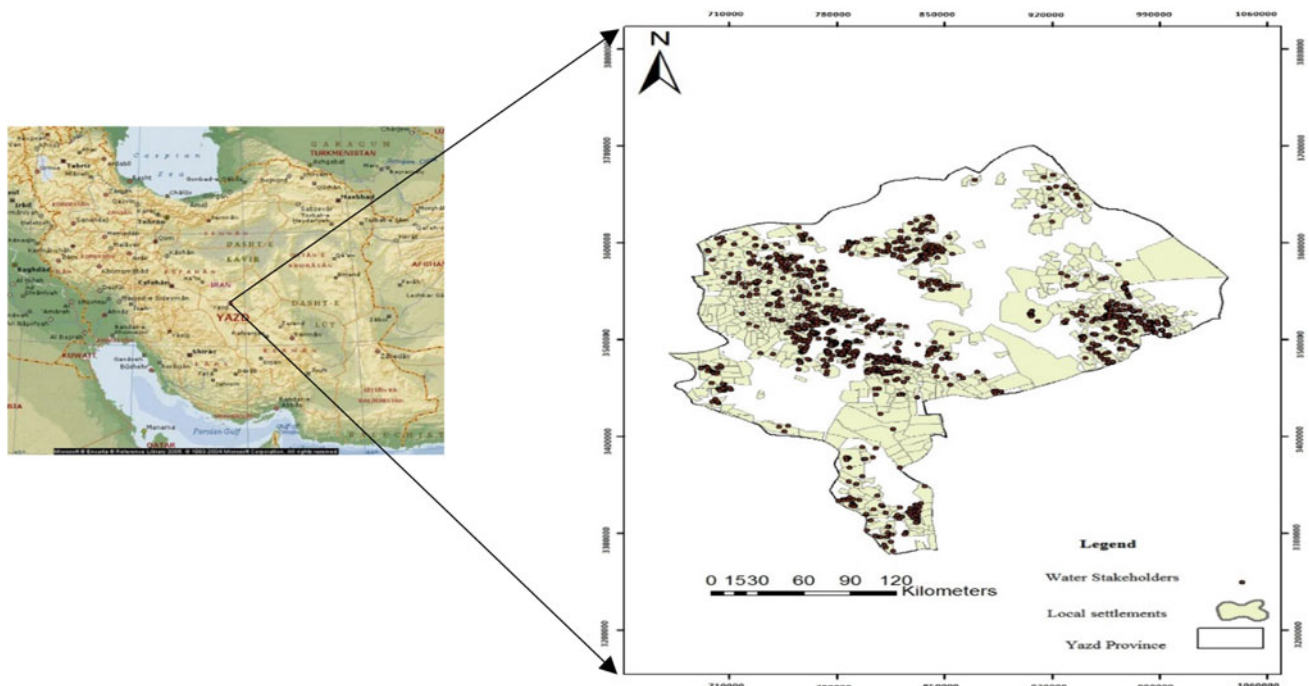


**Fig. 1** Geographical location of study area in Iran and distribution of local water consumers



### 2.3 The Indices of Network Analysis

In the present study, concepts of cut points and structural hole were used to study the structure of the network, and indices like density, size of the network, link reciprocity, and network centralization were used to analyze the statuses of trust and participation. Here, indices, concepts, and the relationships between them are briefly introduced.

**Density:** It shows the ratio of all existing links to all possible links. The number of possible links can be detected based on the number of actors, and the number of existing links is the very size of the network that represents the links formed in the studied networks (Olsson et al., 2004). The relationship between density and structural cohesion is built on the same basis because structural cohesion index includes links that lead to the most and basic communications and eliminating them can cut the communication (Mody & Douglas, 2003). The index shows the minimum number of actors that if removed would disconnect the communications in the network (Mody & Douglas, 2003).

In the case of disconnection of communications of several links, fixed holes are developed that can be filled by connecting a few links. The concept of the structural hole that is negation of the concept of density, links with the idea of social capital, since actors who are mediators between different groups have a direct role in creating dense connections between actors and groups of a network. The more these links are dominant, the components of trust and participation become stronger, and thus, different levels of social capital rise, and participatory management is developed (Leahy & Anderson, 2008). There are actors whose roles are more critical than others so that eliminating them can divide the network into two or more disconnected parts. To determine these vulnerable points, elimination of which causes division of the network, blocks, and cut points indices is used. Networks without such points have high densities in their relationships.

Social researchers measure the role of an actor using degrees. Degrees show the number of communication. However, besides the quantity of communication, quality of communication is also important in network analysis. For this purpose, there are several indices studying this quality. For example, in studies networks, the more the index of link reciprocity is, the more trust and participation will be and thus the more stable the network will be (Leahy & Anderson, 2008).

Another index, which is important at the whole network, is centralization, representing key actors in a network. Centralized networks have high-percentage links on the basis of one or more actors. Decentralized networks are those having low diversity in the number of actors' links.

## 3 Results

### 3.1 Density Index, Reciprocity Index, Network Size, Cohesion Status Analysis, and Social Capital in the Network

The results of the density index analysis in the whole network of Yazd consumers in trust link and participation link are 38.2 and 34.4%, respectively, which indicates poor confidence and participation of local beneficiaries in Yazd Province. Low trust between beneficiaries has led to low participation and thus poor social cohesion in the process of participatory management of water resources. The results show that the process of participatory management has low cohesion and social capital. Low participation and trust are two important factors indicating that. So basic and radical measures, including identifying and solving barriers to participation, strengthening social cohesion, and appropriate promoting measures in order to increase the density index are clearly required.

An important point understood from density index is that because of its lowness, the resilience of beneficiaries against environmental stresses (factors such as drought) has also come down, and it can be expected that comprehensive measures, which increase the density index, also increase the resilience of the local community against environmental changes. The reciprocity index, which also was analyzed in this study, was 36% in participation link and 42% in trust link that indicates the stability of networks is, respectively, week and average. One reason for the success of project management is the collective and mutual cooperation between individuals, known as social trade-offs. Examples are included in shared rangelands and collective participation in the supply and development of water resources, which need to be strengthened. Increasing indices like the density index, it is expected that social capital is strengthened, and social resilience to problems of water restrictions that have affected beneficiaries is also increased. So through pathology of the issue and working to remove barriers to mutual cooperation, reciprocity index percentage can get close to its optimal level (Table 1).

### 3.2 The Results of Network Centralization Index in the Network of Local Beneficiaries in Yazd Province

The centralization index, which has been shown in percentage in this study, as mentioned before, is the percentage of the network, which is enclosed by a limited number of central actors. The results obtained from this index, which is

**Table 1** Indices of density, reciprocity, network size in the network of trust and participation

Socio-ecological border	Kind of link	Number of individuals (persons)	Density (percent)	Reciprocity (percent)
Yazd rural areas	Participation	44	34.4	36
	Trust	44	38.2	42

presented in Table 2, indicate higher percentage of centralization of external links than internal links.

This result makes clear a few points. First, an overall comparing of internal and external centralization indicates that receiving trust and participation (network centralization in internal links) has a better status than spreading trust and participation (network centralization in external links). And also in both networks of participation and trust, given the high levels of centralization in external link in proportion to internal link, central actors have important roles at the network level. Secondly, a high degree of centralization in the network has decreased beneficiaries' participation since in the whole network high-percentage link has centralized only on one or a few actors. However, participatory management requires cooperation links to be spread in the whole network until it is not limited only to a few actors.

### 3.3 Visual Analysis of Network Structure of Participation and Trust of Beneficiaries in Yazd Province

As mentioned in the previous section, outlining the networks of participation and trust allows visual analysis. NetDraw was used in this study organize the network and to make the network presentation and visual analysis possible. Figure 2 presents the network of local communities of water consumer of Yazd province. In Fig. 2, people have been distinguished with blue points. These individuals have been identified basis for social policy makers' planning in the development of participatory management of local communities in the areas of natural resources of Yazd province. The role of these people is of great importance especially in accessing information and developing participatory management policies between beneficiaries community. These people in the role of mediators between different individuals often form weak links. This is in line with the study of Granovetter (1973) in which he argued that information could be received and flow provided that the communicational bridges were weaker than strong links. Given the more cohesion in the network (having integrity and

less discontinuity), it is hoped that participatory management projects and governance network will be implemented successfully.

In the field of access to information, despite the communication intervals, Burt (1999) raised the term of "structural holes" between groups. These structural holes can be seen due to the formation of separate clusters in the network of beneficiaries in Yazd. Blue points represent the existing structural holes and cut points. Eliminating these cut points, shown in blue, many individuals are divided into two or more small clusters. Figure 3 indicates the four clusters created by the removal of cut points in the primary network. In fact, the cohesion of the network has been eroded by the elimination of these important actors that had the role of connecting small networks. Due to the presence of small number of these important mediators in the network of beneficiaries, maintaining and developing communication between various groups have been problematic and complicated. On the other hand, lack of individuals as mediators between two or more close groups makes it difficult to transfer different information (social, environmental, and economic) between different groups. An important advantage of these people as Burt (1999) referred to is their emphasis on discovering and developing great opportunities. So individuals who can mediate between groups are so valuable. For example, in the community under study here, many conflicts overusing water take place due to the misunderstanding and misinterpretation made by fellows in other groups, and the presence of these key mediators, with mentioned specifications, significantly prevent the occurrence of these events.

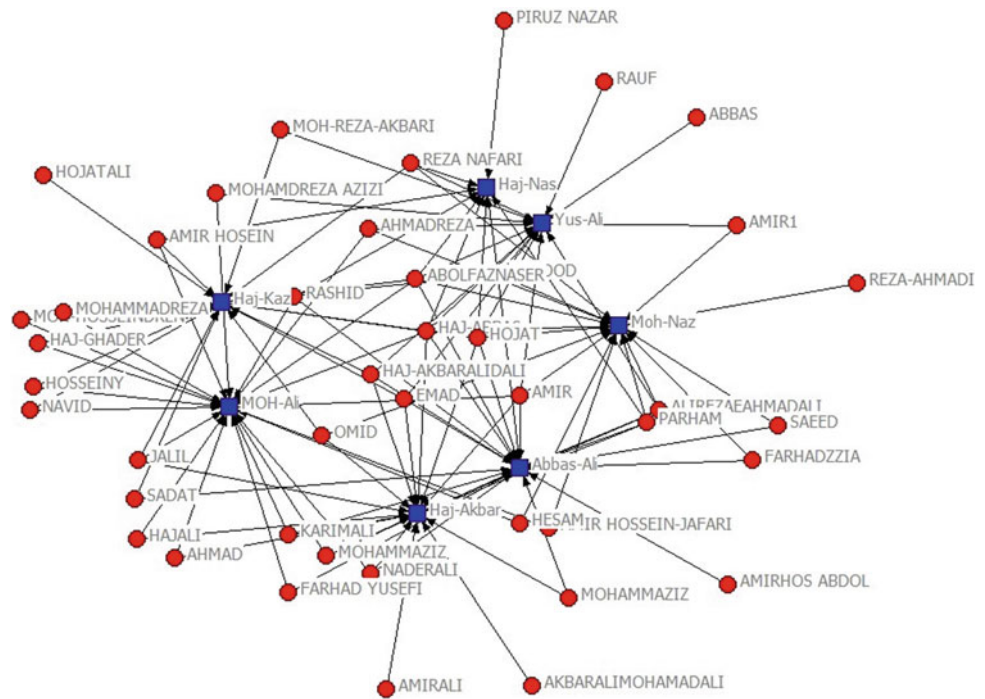
## 4 Discussion and Conclusion

The present research has studied and analyzed the status of network governance of beneficiaries based on the SNA. Therefore, it has analyzed participation and trust, which are important components of social capital. Our first issue was to evaluate the sustainability of the network structure of human

**Table 2** Network centralization based on external and internal links

Socio-ecological border	Kind of link	Network centralization based on external links (percent)	Network centralization based on internal links (percent)
Yazd rural areas	Participation	47	36
	Trust	44	32

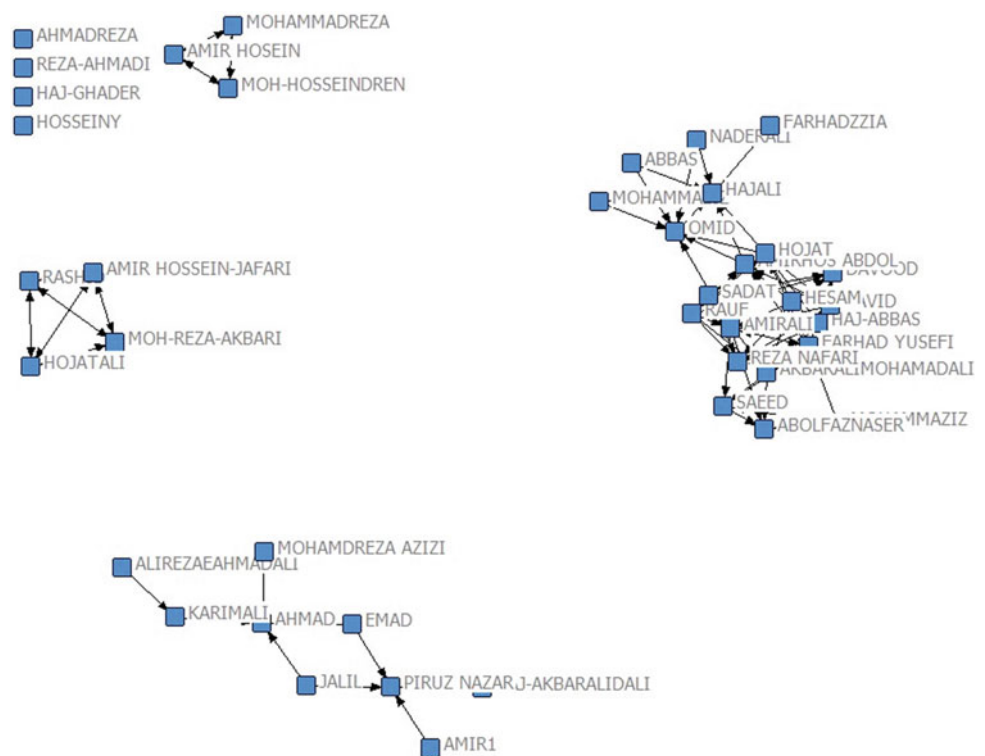
**Fig. 2** Network of local collaborative management of water consumers in Yazd province (Iran)



consumers based on the relationship between density index and social cohesion (Olsson et al., 2004). Analyzing relations based on indices of density, reciprocity, and network size and visual analyzing based on the concepts of cut points

and structural holes helped to assess social structure of local beneficiaries in Yazd province using mathematical elements and to assess their social organization in participatory management.

**Fig. 3** Removing cut points and fragmentation of the primary network (discrete clusters)



The results obtained in this study indicate that unfortunately none of the indices has optimal status. Evaluation shows that the density index in both network of participation and trust was weak, indicating poor social cohesion and reduced resilience of beneficiaries when facing with environmental stresses. Lack of communication links between beneficiary individuals and groups makes the size index be much lower than expected. Reciprocity index, representing mutual cooperation, is also weak in the participation network which demonstrates low stability of this network in the beneficiaries' community in Yazd. These conditions are slightly better, in the trust network, but not at an optimal level. Analysis of motioned indices shows that the relations structure of this community suffers from a social disorder. As Lawson and Garrod (2001) state, poor trust and participation as supporter mechanisms creating a sense of security in emergencies (such as situation that beneficiaries in Yazd are now facing with) have failed to facilitate social actions and solve the problem requiring collective actions. Coleman (1990) and Brehm and Rahn (1997) referred to these items as tasks of trust and participation. Weakness in these two important components of social capital reduces social cohesion of the community and the desire to participate in collective cooperation. It can be understood from the network of Yazd beneficiaries that social participation of individuals and accessing information is more homogenous inside local groups than in between-group relationships. There is lack of those individuals who are mediators between groups. The prominent characteristic of these people is their ability to access information and have necessary experience for transferring it (Newig et al., 2010; Bodin & Prell, 2011; Lienert et al., 2013; Koutsou et al., 2014), the case that is the need of the participatory management of the area under study.

The absence of these mediators or the presence of weak links between groups has made various structural holes in the networks of trust and participation. According to the results obtained from the analysis, trust network, having more links and density ratio higher than participation network, has a relatively better social cohesion; however, this structural weakness is obvious in both networks especially in participation network. The present study is compatible with the study of Burt (1999, 2000, 2002) in which he referred to these individuals, with mentioned specifications, as social capitals of network since the absence of these people prevents creating an integrated and cohesion network. In the beneficiaries' network in Yazd, lack of these individuals, with mentioned specifications, has declined communicational social capital with such efficiency. Lack of these mediators has reduced density at the whole network, resulting in, as stated by various researchers including Oh et al. (2004), Bodin and Norberg (2005), Bodin and Crona (2009), Sandstro and Rova (2010), reduced strength of trust

and participation and decelerate developing participatory management.

It can be clearly understood that beneficiaries in Yazd focus on the activities inside their own groups that are often based on family ties, lack of possible links has made holes in the flow of information and between-group cooperation at the macro-level of network of Yazd beneficiaries, and in simpler terms, structural holes have been made. The reason of lacking mediators and communicational bridges can be traced in high centralization of network. Studying centralization index indicates that spreading participation and trust, between beneficiaries, are weaker than receiving participation and trust, and this is the result of high centralization in external links than in internal links. Lack of centralization in external links in certain clusters has caused non-appropriate distribution of cooperation links at the whole network, and in general, it can be a barrier to establish ideal participatory management. High centralization of central actors in internal links rather than in external links is a factor preventing the formation of intermediate relationships at the macrolevel of Yazd consumers' network. The results of the present study are in line with those of the study by Prell et al. (2009) and Scholz (2011) in which they confirmed the role of central actors and their influence in communicational mediating and establishing successful participatory management. This study is compatible with the study of Watts (1999) in which he approved that through small number of mediators but with special features, communicational bridges can be built in the social world. These small numbers of links, despite large geographical distances, can produce bigger clusters. The absence of these people with appropriate distribution, who are able to get different ideas from different sources and share innovative ideas with others, has reduced creativity and innovation necessary in dealing with environmental problems especially drought. As time passes and water shortage shows its effects in social lives of beneficiaries including livelihood, social cohesion and resilience necessary in dealing with environmental stresses are reduced. It can be concluded that the network of beneficiaries in Yazd was weak. According to sociologists such as Coleman (1990) and Putnam (1993) who define social capital with regard to its function, it can be stated that due to the weakness in the formation of an appropriate social capital, there will be no facilitation for collective actions and solving problems that require participation. Social network analysis based on indices and concepts helped in analysis the networks of trust and participation at the macrolevel resulting in solid understanding of the social structure of beneficiaries' community in Yazd province.

What can be referred to at the end of this discussion is the necessity of creating and strengthening ideal social spaces based on social trade-offs, the case, which is needed in the community of beneficiaries in Yazd province. It is hoped



that realizing collective actions at an appropriate level help the realization of successful participatory management based on local communities.

**Acknowledgements** This research was supported supported by Tarbiat Modarres University (TMU). We thank our colleagues who provided insight and expertise. We would also like to show our gratitude to the WRAA2020 conference team for sharing their pearls of wisdom with us during this research, and we thank “anonymous” reviewers for their so-called insights.

## References

- Bodin, O., & Crona, B. I. (2009). The role of social networks in natural resource governance: What relational patterns make a difference? *Global Environmental Change*, 19(3), 366–374. <https://doi.org/10.1016/j.gloenvcha.2009.05.002>.
- Bodin, O., & Norberg, J. (2005). Information network topologies for enhanced local adaptive management. *Environmental Management*, 35(2), 175–193. <https://doi.org/10.1007/s00267-004-0036-7>.
- Bodin, O., & Prell, C. (2011). Social network in natural resources management. Cambridge University Press. <https://doi.org/10.1017/CBO9780511894985>
- Brehm, J., & Rahn, W. (1997). Individual-level evidence for the causes and consequences of social capital. *American Journal of Political Science*, 41(3), 999–1023. <https://doi.org/10.2307/2111684>.
- Burt, R. S. (1999). The social capital of opinion leaders. *Annals*, 566, 37–54. <https://doi.org/10.1177/000271629956600104>.
- Burt, R. S. (2000). The network structure of social capital. In: R. I. Sutton & B. M. Staw (Eds.), *Research in organizational behavior* (pp. 345–423). Greenwich Conn.: JAI Press. [https://doi.org/10.1016/S0191-3085\(00\)22009-1](https://doi.org/10.1016/S0191-3085(00)22009-1)
- Burt, R. S. (2002). The social capital of structural holes. In M. F. Guillén, R. Collins, P. England, & M. Meyer (Eds.), *The new economic sociology* (pp. 148–192). New York: Russell Sage Foundation. <https://faculty.chicagobooth.edu/ronald.burt/research/files/SCSH.pdf>
- Carlsson, L., & Sandström, A. (2008). Network governance of the commons. *International Journal of the Commons*, 2(1), 33–54. <https://www.readcube.com/articles/10.18352%2Fijc.20>
- Coleman, J. (1990). *Foundation of social theory*. Cambridge, MA: Harvard University Press. <https://doi.org/10.1525/awr.1991.12.3.19>
- Emerson, K., & Gerlak, A. (2014). Adaptation in collaborative governance regimes. *Environmental Management*, 54(4), 768–781. <https://doi.org/10.1007/s00267-014-0334-7>.
- Fliervoet, J. M., Geerling, G. W., Mostert, E., & Smits, A. J. M. (2016). Analyzing collaborative governance through social network analysis: a case study of river Management along the Waal River in The Netherlands. *Environmental Management*, 57(2), 355–367. <https://doi.org/10.1007/s00267-015-0606-x>.
- Granovetter, M. S. (1973). The strength of weak ties. *American Journal of Sociology*, 78, 1360–1380. <https://doi.org/10.1016/B978-0-12-442450-0.50025-0>.
- Hiwasaki, L., & Arico, S. (2007). Integrating the social sciences into ecohydrology: Facilitating an interdisciplinary approach to solve issues surrounding water. *Environment and People, Ecohydrology & Hydrobiology*, 17(1), 3–9. [https://doi.org/10.1016/S1642-3593\(07\)70184-2](https://doi.org/10.1016/S1642-3593(07)70184-2).
- Koutsou, S., Partalidou, M., & Ragkos, A. (2014). Young farmers’ social capital in Greece: Trust levels and collective actions. *Journal of Rural Studies*, 34, 204–211. <https://doi.org/10.1016/j.jrurstud.2014.02.002>.
- Lawson, T., & Garrod, J. (2001). *Dictionary of sociology* (273 p.). London; Chicago: Fitzroy Dearborn Publishers, English. ISBN: 1579582915. <https://trove.nla.gov.au/work/17619814?q&versionId=42701659>
- Leahy, E., & Anderson, H. (2008). Trust factors in community–water resource management agency relationships. *Journal of Landscape and Urban Planning*, 87, 100–107 (London). <https://doi.org/10.1016/j.landurbplan.2008.05.004>
- Lienert, J., Schnetzer, F., & Ingold, K. (2013). Stakeholder analysis combined with social network analysis provides fine-grained insights into water infrastructure planning processes. *Journal of Environmental Management*, 125, 134–148. <https://doi.org/10.1016/j.jenvman.2013.03.052>.
- Mandarano, L. A. (2009). Social network analysis of social capital in collaborative planning. *Society and Natural Resources*, 22(3), 245–260. <https://doi.org/10.1080/08941920801922182>.
- Mody, J., & Douglas, R. W. (2003). Structural cohesion and embeddedness: A hierarchical concept of social groups. *American Sociological Review*, 68(1), 103–127. <https://doi.org/10.2307/3088904>.
- Newig, J., Günther, D., & Pahl-Wostl, C. (2010). Synapses in the network: Learning in governance networks in the context of environmental management. *Ecology and Society*, 15(4), 24. <http://www.ecologyandsociety.org/vol15/iss4/art24/>
- Oh, H., Chung, M. H., & Labianca, G. (2004). Group social capital and group effectiveness: The role of informal socializing ties. *Academy of Management Journal*, 47(6):860–875. <https://www.jstor.org/stable/20159627>
- Olsson, P., Folke, C., & Berkes, F. (2004). Adaptive comanagement for building resilience in social-ecological systems. *Environmental Management*, 34(1), 75–90. <https://doi.org/10.1007/s00267-003-0101-7>.
- Prell, C., Hubacek, K., & Reed, M. (2009). Stakeholder analysis and social network resources. *Society and Natural Resources*, 22(6), 501–518. <https://doi.org/10.1080/08941920802199202>.
- Putnam, R.D. (1993). *Making democracy work: Civic traditions in modern Italy* (280 p.). Princeton University Press. [https://doi.org/10.1016/S0030-4387\(96\)90074-5](https://doi.org/10.1016/S0030-4387(96)90074-5)
- Putnam, R. D. (1995). Tuning in, tuning out: The strange disappearance of social capital in America. *PS: Political Science & Politics*, 28(4), 664–683. <https://doi.org/10.2307/420517>
- Sandstrom, A., & Rova, C. (2010). Adaptive co-management networks: A comparative analysis of two fishery conservation areas in Sweden. *Ecology and Society*, 15(3), 14. <https://www.ecologyandsociety.org/vol15/iss3/art14/>
- Scholz, R. W. (2011). *Environmental literacy in science and society: From knowledge to decisions* (631 pp). Cambridge: Cambridge University Press; New York, USA; Hardback. ISBN 978-0-521-19271-2; Paperback, ISBN 978-0-521-18333-8. <https://doi.org/10.1111/jieec.12091>
- Scott, J. (1987). Social network analysis: A handbook (Vol. 17(1), pp. 3–9). Sage Publication. <https://dx.doi.org/10.4135/9781446294413>
- Sen, S. M., Singh, A., Varma, N., Sharma, D., & Kansal, A. (2019). Analyzing social networks to examine the changing governance structure of Springsheds: A case study of Sikkim in the Indian Himalayas. *Environmental Management*, 63(2), 233–248. <https://doi.org/10.1007/s00267-018-1128-0>.
- Van Eeten, M. J. G., Loucks, D. P., & Roe, E. (2002). Bringing actors together around large-scale water systems: Participatory modeling and other innovations. *Journal of Knowledge, Technology, and Policy*, 14(4), 94–108. <https://doi.org/10.1007/s12130-002-1017-x>.



- Veenstra, G. (2000). Social capital, SES and health: An individual-level analysis. *Social and Medicine*, 50(5), 619–629. [https://doi.org/10.1016/S0277-9536\(99\)00307-X](https://doi.org/10.1016/S0277-9536(99)00307-X).
- Wang, S., Shen, W., Tang, W., Wang, Y., Duffield, C. F., & Hui, F. K. P. (2019). Understanding the social network of stakeholders in hydropower project development: An owners' view. *Renewable Energy*, 132, 326–334. <https://doi.org/10.1016/j.renene.2018.07.137>.
- Watts, D. J. (1999). Networks, dynamics, and the small-world phenomenon. *American Journal of Sociology*, 105(2), 493–527. <https://doi.org/10.12691/ajie-1-3-1>.

# Techno-economic Analysis of Membrane Distillation to Provide Potable Water to the Hormuz Island

Ramin Haghighi Khoshkhoo, Ameneh Moumivand, and Mohammad Namazizadeh

## Abstract

This paper is aimed to study the technical and economical supply of minimum potable water in the southern regions of Iran (isolated areas with lack of access to national water and electricity networks), especially on Hormuz Island. In this regard, the techno-economic analysis of solar membrane distillation and membrane distillation is carried out as a package (mobile desalination). The cost of thermal energy in each of these systems is zero. At present, the minimum required potable water on Hormuz Island is 30 m<sup>3</sup>/d. The cost of water generated from the solar membrane distillation is 6 \$/m<sup>3</sup>, and the cost of water produced in the mobile desalination is 1 \$/m<sup>3</sup>. Furthermore, the problems of the potable water transfer in a mobile desalination are also met.

## Keywords

Techno-economic • Solar membrane and mobile distillation • Potable water • Isolated areas of utilities

## Nomenclature

AGMD	Air gap membrane distillation
CC	Initial investment cost
$C_{\text{brine}}$	The cost of disposing of salt water
$C_{\text{fixed}}$	Fixed investment cost
$C_{\text{I\&C}}$	Cost of instrumentation and control
$C_{\text{installation}}$	Installation cost
$C_{\text{labor}}$	Labor cost
$C_{\text{O\&M}}$	Maintenance cost
$C_p$	Seawater specific heat capacity

$C_{\text{total}}$	Total production cost
DCMD	Direct contact membrane distillation
$d_{\text{fib}}$	The diameter of each string of membranes
MD	Membrane distillation
$E_{\text{max}}$	Maximum sun exposure on sunny days
$E(t)$	Radiation of the sun reached the collector surface (W/m <sup>2</sup> )
$f$	The amount of access to the unit
IRR	Internal rate of return
$K_m$	Membrane permeability coefficient
$K_{\text{mo}}$	Knudsen's permeability
$L$	Total collector length
$M$	Unit capacity
$m_{\text{dist}}$	Flow rate distilled water
$m_o$	Flow rate in solar collector
MED	Multi-effect distillation
MSF	Multi-stage flash
$N$	System life
NPV	Net present value
$n_{\text{fib}}$	Number of strings
$P_s$	Saturation vapor pressure
$P_{\text{vacuum}}$	Vacuum pressure
VMD	Vacuum membrane distillation
RO	Reverse osmosis
$T_i$	Internal membrane temperature (K)
$T_{\text{ref}}$	The initial temperature
$T_z$	Temperature variations along the membrane (K)
$t_{\text{sunset}}$	Sunset time (hour)
$t_{\text{sunrise}}$	Sunrise time (hour)
$\rho$	The density of liquids used (kg/m <sup>3</sup> )
$\sum \text{CAPEX}$	Total investment cost
$\sum \text{CPEC}$	The current value of all purchased equipment

R. Haghighi Khoshkhoo (✉) · A. Moumivand · M. Namazizadeh  
 Faculty of Mechanical and Energy Engineering,  
 Shahid Beheshti University, Tehran, Iran  
 e-mail: [r\\_haghighi@sbu.ac.ir](mailto:r_haghighi@sbu.ac.ir)

## 1 Introduction

Demand for potable and fresh water has increased gradually in the last two decades (Mohammad Namazizadeh & Joda, 2020). Utilizing desalination in islands and coastal areas is an important method for overcoming water shortage (Guo et al., 2016; Qi et al., 2017). Reverse osmosis (RO) in membrane distillation (MD) and multi-effect distillation (MED) in thermal desalination are mainly referred to (Karagiannis & Soldatos, 2008; Sadri et al., 2017).

Using desalination, many attractive features, such as low operating temperature and cost-effective process, have been considered. MD is a technology that lies at the interface between membrane and thermal desalination (Bamuffleh et al., 2017).

There are many ways that heat integrated within the process and with the MD desalination and optimal design of equipment should be provided due to the geographical condition of the case study and the lack of access to fuel, water, and power (Guo et al., 2016; Li et al., 2017).

This type of desalination can be built on small scales, and it uses excess heat, such as thermal energy from sunlight (because it requires less temperature) and is much more energy efficient than other methods. Membrane and distillation will be affordable. In this type of technology, membranes with less price can also be used that can be effective in the overall economy of the process. Since the size of the cavities of MD is larger than RO, the membrane obstruction will be less. Excretion of 100% (theoretically) ions, colloids, macromolecules, and other non-volatile substances, operating temperature lower than distillation, less operating pressure compared to pressure separation processes such as reverse osmosis, reduction of required mechanical properties for membrane stability, reduced spaces needed for steam, in comparison with the distillation process are the advantage of membrane distillation in comparison with other natural separation operations (Camacho et al., 2013).

MD is less susceptible to membrane fouling than RO, given the absence of a high hydraulic pressure and the discontinuity of the liquid phase. So, MD can be operated without feed water pre-treatment, making it an ideal process for standalone seawater desalination applications. Furthermore, MD systems can be made from inexpensive materials to reduce process investment and operational costs. Finally, MD can be operated at low feed temperature (Duong et al., 2016; Ravisankar et al., 2016). Thus, low-grade heat sources such as solar thermal energy can be utilized to meet MD energy demands.

To supply water to certain areas, such as the countryside, inland waters, in addition to electricity and water, and the islands renewable energy sources such as the wind and solar can be used as the source of power and energy. MD is one of

the desalination technologies that are commonly utilized in these conditions. It is arguably the most suitable platform for small-scale and off-the-grid seawater desalination applications (Mericq et al., 2011; Plattner et al., 2017). On Hormuz Island, in addition to solar energy, the thermal energy from the combustion products of the diesel engine for offshore floating can also be exploited (the original idea of the researcher). The use of sea vessels, while not requiring a grid system and distribution of fuel, will eliminate the problems of water transmission and environmental pollution. Researchers have provided many studies on MD. Some researchers have investigated the impact of membrane properties and transport phenomena on the energetic performance of MD desalination (Deshmukh & Elimelech, 2017). A. Khalifa et al. (2017) conducted experimental and theoretical investigations on water desalination using direct contact MD. Hung C. Duong assessed the performance of solar thermal-driven MD for seawater desalination using computer simulation (Duong et al., 2017).

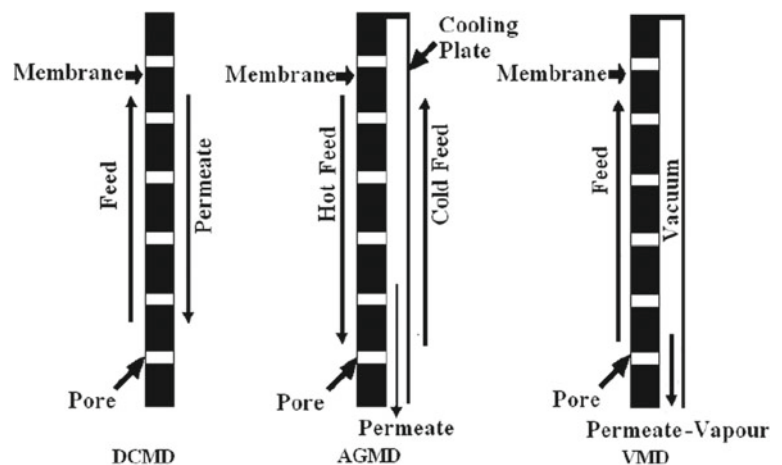
Chafidz et al. (2014) designed and manufactured a prototype of an MD system for an arid location in Saudi Arabia. Escher et al. (2012) designed and modeled a prototype porous solar MD system in remote areas and, then, investigated and evaluated it. Alkudhiri et al. (2012) reviewed the process of MD. Al-Obaidani et al. (2008) studied the potential of the direct contact MD process in energy sewage sweetening. Chang et al. (2010) modeled and optimized the air gap MD system and supplied the thermal energy and electricity of this system through the solar system. Cipollina et al. (2012) examined the development of solar MD (photovoltaic panel and solar collector). Numerical methods are reliable and cost effective in modeling and optimizing the engineering systems (Namazizadeh et al., 2020). Therefore, in most of studies, modeling and optimization in the field of one configuration of MD have been addressed. In this paper, MD is a main technology for desalting highly saline waters on Hormoz Island, and from among the MD configurations, vacuum membrane distillation (VMD) is selected. Using direct contact membrane distillation (DCMD) is economical, and using air gap membrane distillation (AGMD) is energy efficient. However, VMD is both economical and energy efficient. VMD has once been used in the solar system and once in the sea vessel body. The economic analysis of these two systems is carried out and, ultimately, compared. The innovation of this article lies in the package designed in the sea vessel body and the use on a ship to transfer drinking water to various parts of the island. It is possible to use any kind of refrigeration in one area. However, the islands and remote areas will be different. The sub-objectives of this research are multi-fold and include: selecting desalination suitable in terms of power and heat consumption for Hormoz Island, solar MD desalination study and modeling study of

the layout of a desalination package on the ship and economic opportunity of selective technologies.

## 2 Membrane Configuration of MD

In desalination, different MD configurations that have been used to separate the aqueous feed solution using a micro-porous hydrophobic membrane will be examined. In DCMD configuration, the hot solution is in direct contact with the hot membrane side surface. Therefore, evaporation takes place at the feed-membrane surface. The vapor is moved by the pressure difference across the membrane to the permeate side and condenses inside the MD module. Because of the hydrophobic characteristics, the feed cannot penetrate into the membrane (only the gas phase exists inside the membrane pores). DCMD is the simplest MD shape and is widely employed in desalination processes and acid manufacturing. The main drawback to this design is the heat lost by conduction. In AGMD, the feed is in direct contact with the hot side on the membrane surface only. Stagnant air is introduced between the membrane and the condensation surface. The vapor crosses the air gap to condense over the cold surface inside the membrane. The benefit from this design is the reduced heat lost by conduction. However, additional resistance for mass transfer is created, which is considered a disadvantage. This shape is appropriate for desalinating and removing volatile compounds from aqueous solutions. In VMD, a pump is used to prepare a vacuum in the permeate membrane side. The heat lost by conduction is negligible, which is considered a great advantage. This type of MD is used to separate aqueous volatile solutions (Deshmukh & Elimlech, 2017; Plattner et al., 2017). In Fig. 1, MD configurations are observed.

Fig. 1 MD configurations



## 3 Solar MD Desalination

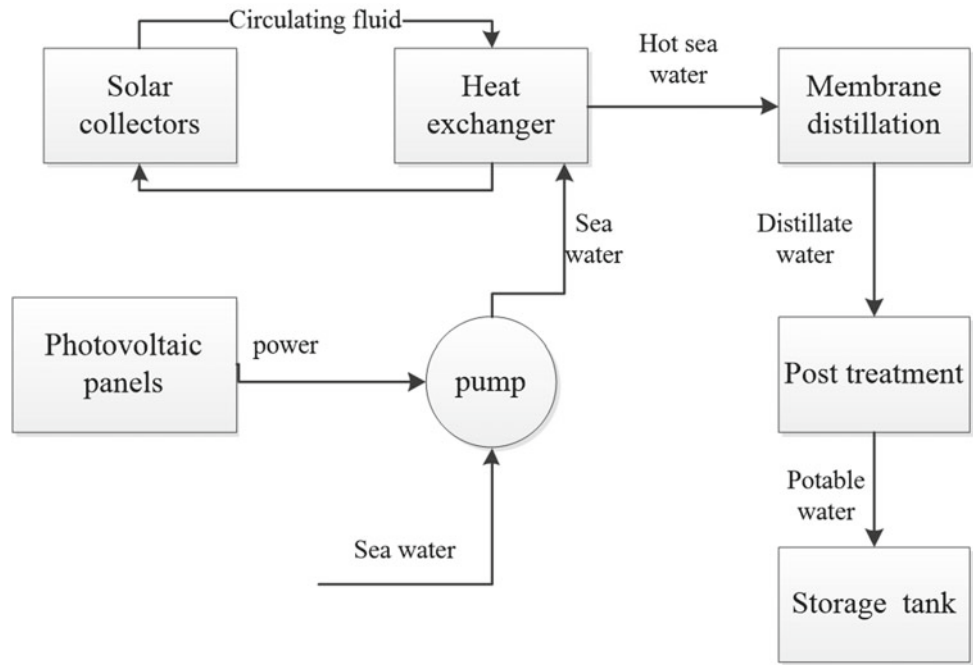
The solar collector, photovoltaic panel, membrane distillation module, and pump are the main components of this system. Heat exchangers and heat storage devices are added to the process loop, depending upon the project. In Fig. 2, a schematic diagram of the solar MD system, which is analyzed for this paper, is technically feasible.

Solar energy can be used to convert saline water into potable water with simple, low cost, and economical technology; thus, it is suitable for small communities, rural areas, and areas where the income level is very low. Recent developments have described that solar-powered desalination processes are better than the alternative MD technologies, like RO. Two types of solar MD are classified as direct and indirect systems. The direct systems are those, in which the heat gaining and desalination processes take place naturally in the same device (solar still). In the indirect method, the plant is separated into two subsystems, a solar collector and a desalination unit. The solar collector can be a flat plate, evacuated tube, solar PV cell, or solar concentrator; it can be integrated with any of the distillation unit types, which use the evaporation and condensation principle, such as MSF, MED, and MD of possible combinations of thermal desalination with solar energy. Systems that use PV panels tend to produce power to operate MD in solar MD. The most important advantage is that the operating temperature of the MD process is in the range of 40–100 °C.

## 4 Innovation of Mobile Desalination

The mobile desalination system, introduced in this paper, includes filtering, pre-treatment tank, heat exchanger, membrane distillation, pump, and post-treatment. Seawater

**Fig. 2** Schematic diagram of the solar MD system



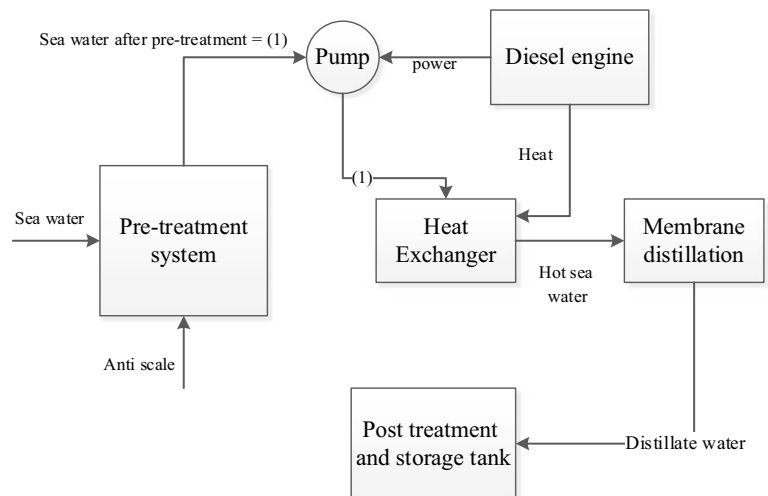
is pumped to the heat exchanger. The pre-treatment system and pump are installed on the sea vessel body. Seawater in the heat exchanger increases its temperature by receiving heat from the flue gas from the engine. Then, the seawater enters the membrane module. Distilled water is produced, and then, the final purge (post-treatment) in the tank is collected.

Water is collected in the reservoir after passing through the purification system and is converted into drinking water. The overall schematic of this system, which is in the form of a package in the corresponding float, is shown in Fig. 3.

### 5 Profile of Hormuz Island

Hormuz Island has population of 6000 people. According to Hormozgan Meteorological Organization’s research on Hormuz Island, there are 362 days of the 365 days in Hormozgan, which shows there is a real potential for solar energy. Hormuz Island has longitude of 28.56 and latitude of 27.4° north and is isolated from the electrical power (is away from the electricity grid) and potable water. Per capita, water consumption per person, is considered between 80 and

**Fig. 3** Form of a package in the corresponding sea vessel





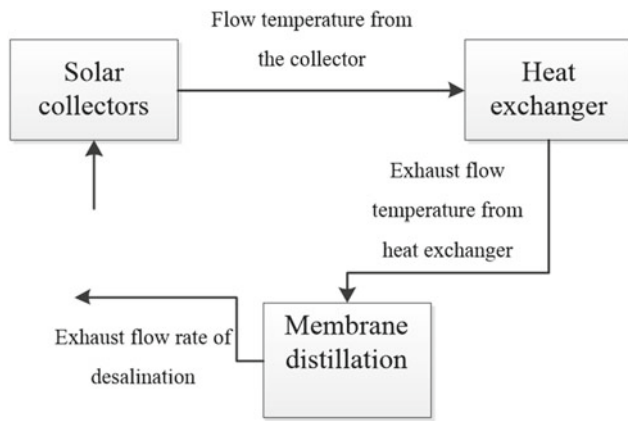


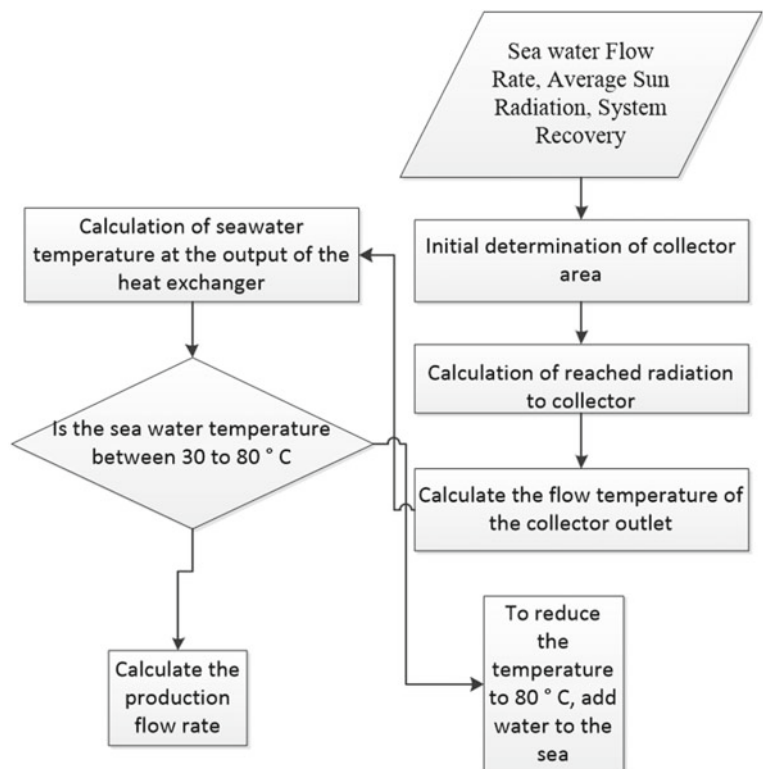
**Fig. 4** Step-by-step modeling of the solar MD process

120 L per day. This amount includes drinking, agricultural, and industrial consumption. More than 95% of this amount is for agricultural and industrial use. This article is about drinking water and cooking. Therefore, at least 5 L per day per person (30 m<sup>3</sup>/d) is considered (Moradi & Kabiri, 2012).

## 6 Modeling Solar MD

To model the entire system, each of the equipment must be modeled. The inputs and outputs of every equipment are determined. Step-by-step modeling of the MD process is shown in Fig. 4.

**Fig. 5** Modeling solar MD flowchart



The modeling of solar MD flowchart is illustrated in Fig. 5. In the MD module, the membrane is sensitive to temperatures above 80 °C. A temperature less than 30 °C does not result in a two-phase mode.

## 7 Designing Mobile Desalination

To design the smallest land craft as a sea vessel, the electricity power from the diesel engine is taken into consideration. Various types of floating vessels with capacities, ranging from 200 kW to more than 10 MW, are designed and built in Iran. Considering the dimensions of the package of the system in question and the amount of drinking water required by Hormuz Island, the types of sea vessel made, landing craft and towels that have suitable space, are selected. The design steps are such that depending on the amount of water produced, the MD module is selected. The next stage is to design a heat exchanger, a pump selection, and a storage tank.

## 8 Results of Modeling

The results from the modeling of solar MD showed that the highest amount of solar radiation was in the summer, and its lowest was in the winter. Note that the solar radiation reaching the surface was the input of modeling in the

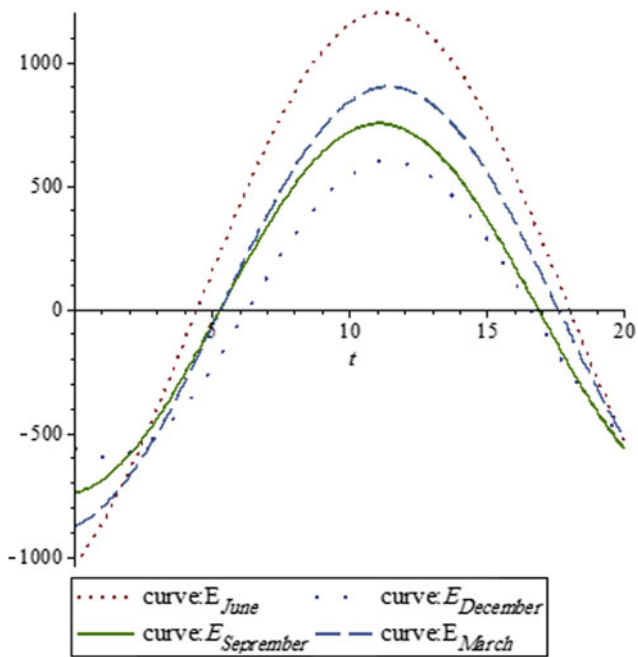
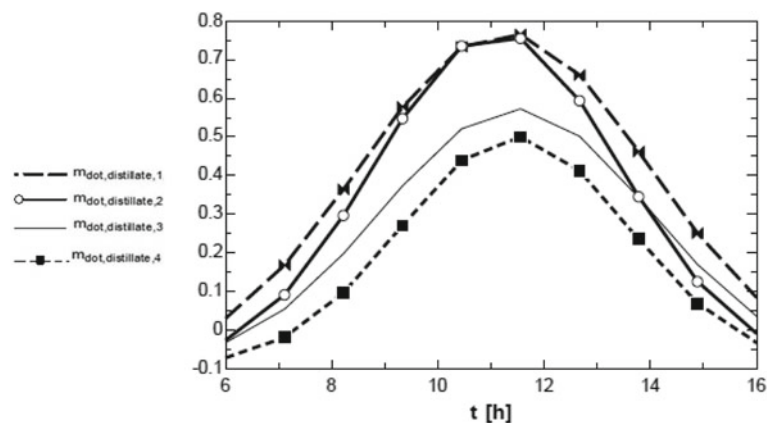


**Fig. 6** Amount of solar radiation reaching the collector in Hormuz Island for four days from different seasons of the year

collector sector. The final output of distilled water from the production and the exhaust of the membrane was affected by solar radiation, with the highest production during the summer and the lowest in winter (Fig. 6). The results were related to the four days of the year and had the lowest and highest radiation for two days and the two days between them. Using NASA's meteorological information and having geographical latitude and longitude of Hormuz Island, four days were considered in June, December, September, and March, respectively. The radiation of the sun varied throughout the day and on different days of the year, and the sinusoidal equation was considered for simplicity in modeling. The output of the first stage was the hot fluid temperature, the second stage was the output of the seawater

**Fig. 7** Flow rate of distilled water in an MD system in four days from four seasons



temperature at the output of the heat exchanger, and the final output of the distilled water was obtained from the MD module, as seen in Fig. 7.

The initial area considered in this calculation was  $10,000 \text{ m}^2$ . The area of the collector was  $7 \text{ m}^3$  per day during the winter and  $25 \text{ m}^3$  on average during summer to produce the stems. Therefore, the area of collectors should be increased (Fig. 7).

Therefore, it was decided to initially use the same area for economical production of Hormuz Island drinking water by using an MD system. If an economic justification is achieved, the collector area will be increased to produce more drinking water. The modeling results of mobile desalination are generated in each package designed to be  $8 \text{ m}^3$  per day, which is required for the needs of the district's four packets.

An MD module that generates  $1 \text{ m}^3$  of water per day was used, with eight of these modules packed in each package. The design of the heat exchanger was based upon the flow rate of combustion products.

## 9 Economic Evaluation

In general, to estimate the cost of water produced from desalination, the three parameters of the initial investment cost, fixed annual cost, and annual cost variables were used. The initial investment cost included the purchase cost of the equipment, the installation cost, and the cost of control and measurement. The fixed and variable annual costs varied depending on the selected system. The cost model is shown in Fig. 8.

The initial investment cost included the cost of purchasing equipment, the cost of installation, and the cost of control and instrumentation. The annual costs incurred after the exploitation involve fixed and variable costs. The cost of the MD module depended on the area used. For example, each MD module cost four hundred times of its area. Economic

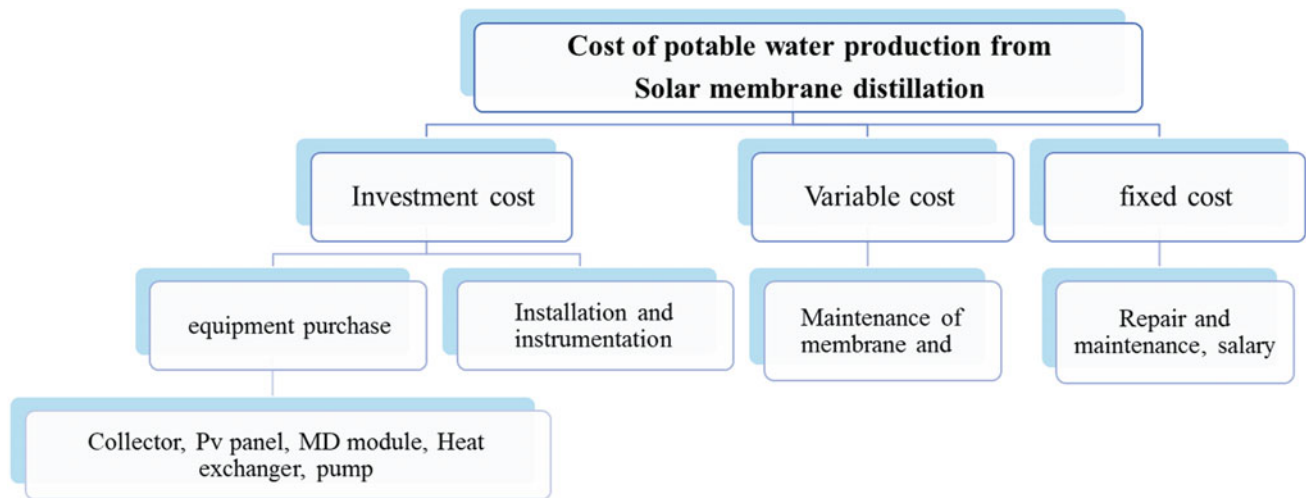


Fig. 8 Cost model desalination

evaluation was calculated both formally and using COMFAR software.

The price of each equipment was extracted from the equipment available on the world market. Cost of equipment purchase, installation cost, and cost of instrumentation was the initial investment cost. Maintenance cost was variable cost. Given the longevity of the equipment and the discount rate in COMFAR software, these economic calculations were performed in the paper.

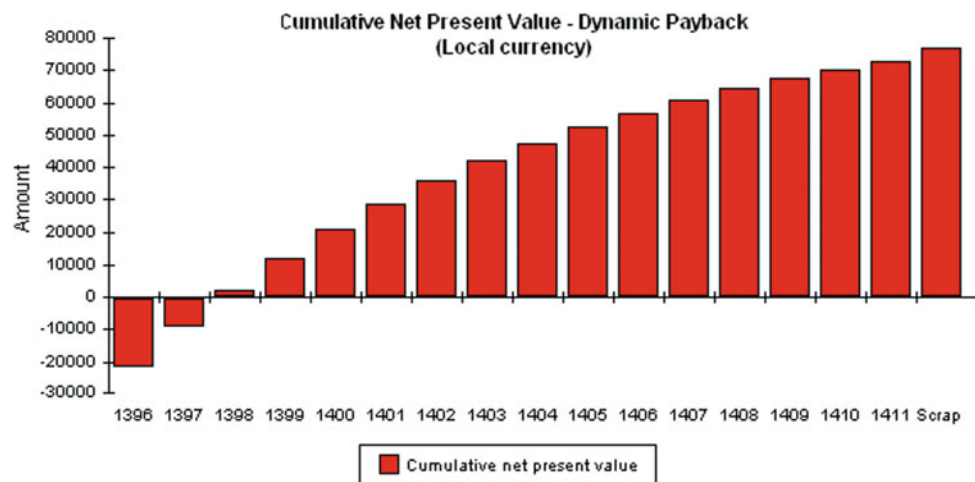
The cost of producing water from the solar MD was 6 \$/m<sup>3</sup> and was 1 \$/m<sup>3</sup> while produced from mobile desalination. In addition, the economic feasibility of the mobile desalination was carried out (Fig. 9).

And the results from this feasibility study can be seen in figure. The NPV was positive, and the IRR has gone up from the discount rate. And payback period for this project was two years.

## 10 Discussion

The issue of minimum potable water in areas that do not have access to potable water and electricity is a very important. In this paper, the goal is to provide an optimal supply scheme for potable water from Hormuz Island. For this purpose, different types of desalination were studied. Solar MD and PV-RO systems were selected. Then, MATLAB, ROSA, EES, and COMFAR (cost analysis) software were employed. The economic evaluation of these two systems was carried out using the existing relationships in the engineering economics. The results showed that the two systems were technical and energy-efficient. But economically, due to the high cost of solar equipment, they were not cost effective. Finally, the idea of using the existing harbors in the area of Hormuz Island under the name of a

Fig. 9 Dynamic payback period



mobile water tank was studied. From the heat of combustion products and output of the diesel engine, these sea vessels were used to supply the heat and power required by the MD system. The results of the mathematical modeling of the designed system indicated that using this method not only solves the problem of water transfer to different parts of the island but also is a technically and economically suitable method. The cost of producing potable water by moving desalination is 1 \$/m<sup>3</sup>, and time for invest return, using this method and considering the discounting rate of 12%, is 2 years.

In this research, an innovation is proposed:

- Using electrical and thermal power of landing craft motors to supply potable water required by MD method.
- Reducing economic problems and drinking water transmission by landing craft to different islands and coasts.
- On Hormuz Island, in addition to solar energy, thermal energy from the combustion products of the diesel engine for the offshore floating can also be exploited (the original idea of the researcher).
- The use of sea vessels, while not requiring a grid system and distribution of fuel, will eliminate the problems of water transmission and environmental pollution. This innovation is mobile desalination.
- The mobile desalination system, introduced in this research, includes filtering, pre-treatment tank, heat exchanger, MD, pump, and post-treatment.
- Seawater is pumped to the heat exchanger.
- The pre-treatment system and pump are installed on the sea vessel body.
- Seawater in the heat exchanger increases its temperature by receiving heat from the flue gas from the engine.
- Then, the seawater enters the membrane module.
- Distilled water is produced, and then, the final purge (post-treatment) in the tank is collected.

Comparison of the selected desalination on Hormoz Island:

- Solar MD system.  
Modeling by EES software.  
Selecting two days a year with the lowest and highest levels of solar radiation.  
Initial guessing for solar collector area.  
7 m<sup>3</sup> per day in winter (minimum solar radiation) and 25 m<sup>3</sup> per day in summer (highest solar radiation).  
Preliminary economic evaluation before increasing collector area (to increase the amount of water produced).  
Production of 6\$/m<sup>3</sup> of water and economical choice of this system.
- Photovoltaic—reverse osmosis system (PV–RO).

Photovoltaic panel modeling using MATLAB software and RO in ROSA software.

Modeling based on a day in the winter with the least radiation.

Economic evaluation and production of \$ 9.2 per m<sup>3</sup> of water and economical selection of this system.

- Introducing innovative portable water production system on Hormuz Island using heat and electricity of diesel engines in the Persian Gulf.

Selecting and designing the components of the package according to the size, space, and number of the floating diesel engine.

Using MD desiccant due to the use of low-temperature heat and low power consumption.

Heat exchanger design using thermophysical properties of diesel engine combustion products and the Persian Gulf water features.

Pump selection, pre- and post-filtration system, etc.

Economic value and \$ 1 per m<sup>3</sup> of water production.

## 11 Conclusion

MD is a separation process, in which only vapor molecules transfer through a membrane. This process has various applications, such as desalination, wastewater treatment, and in the food industry. Hormuz Island is isolated from water and electricity; MD desalination was selected to produce potable water on this island, because this process requires less electricity and heat. Solar MD and mobile desalination into the sea vessel design to produce potable water on the island of Hormuz. Both desalination types are energy efficient; however, mobile desalination is economical. Although the use of solar systems in terms of energy consumption is an appropriate option, it is not economically feasible due to the high price of its equipment. If the cost of investment decreases, the use of solar equipment will enter the economic competition. It should be noted that due to lack of electricity in this area, RO has been neglected.

## References

- Al-Obaidani, S., Curcio, E., Macedonio, F., Di Profio, G., Al-Hinai, H., & Drioli, E. (2008). Potential of membrane distillation in seawater desalination: Thermal efficiency, sensitivity study and cost estimation. *Journal of Membrane Science*, 323(1), 85–98.
- Alkhudhiri, A., Darwish, N., & Hilal, N. (2012). Membrane distillation: A comprehensive review. *Desalination*, 287, 2–18.
- Bamufleh, H., Abdelhady, F., Baaqeel, H. M., & El-Halwagi, M. M. (2017). Optimization of multi-effect distillation with brine treatment via membrane distillation and process heat integration. *Desalination*, 408, 110–118.

- Camacho, L. M., Dumée, L., Zhang, J., Li, J.-D., Duke, M., Gomez, J., et al. (2013). Advances in membrane distillation for water desalination and purification applications. *Water*, 5(1), 94–196.
- Chafidz, A., Al-Zahrani, S., Al-Otaibi, M. N., Hoong, C. F., Lai, T. F., & Prabu, M. (2014). Portable and integrated solar-driven desalination system using membrane distillation for arid remote areas in Saudi Arabia. *Desalination*, 345, 36–49.
- Chang, H., Wang, G.-B., Chen, Y.-H., Li, C.-C., & Chang, C.-L. (2010). Modeling and optimization of a solar driven membrane distillation desalination system. *Renewable Energy*, 35(12), 2714–2722.
- Cipollina, A., Di Sparti, M., Tamburini, A., & Micale, G. (2012). Development of a membrane distillation module for solar energy seawater desalination. *Chemical Engineering Research and Design*, 90(12), 2101–2121.
- Deshmukh, A., & Elimelech, M. (2017). Understanding the impact of membrane properties and transport phenomena on the energetic performance of membrane distillation desalination. *Journal of Membrane Science*, 539, 458–474.
- Duong, H., Cooper, P., Nelemans, B., Cath, T., & Nghiem, L. (2016). Evaluating energy consumption of membrane distillation for seawater desalination using a pilot air gap system. *Separation and Purification Technology*, 166, 55–62.
- Duong, H. C., Xia, L., Ma, Z., Cooper, P., Ela, W., & Nghiem, L. D. (2017). Assessing the performance of solar thermal driven membrane distillation for seawater desalination by computer simulation. *Journal of Membrane Science*, 542, 133–142.
- Guo, H., Ali, H. M., & Hassanzadeh, A. (2016). Simulation study of flat-sheet air gap membrane distillation modules coupled with an evaporative crystallizer for zero liquid discharge water desalination. *Applied Thermal Engineering*, 108, 486–501.
- Karagiannis, I. C., & Soldatos, P. G. (2008). Water desalination cost literature: Review and assessment. *Desalination*, 223(1–3), 448–456.
- Khalifa, A., Ahmad, H., Antar, M., Laoui, T., & Khayet, M. (2017). Experimental and theoretical investigations on water desalination using direct contact membrane distillation. *Desalination*, 404, 22–34.
- Li, W., Song, B., Li, X., & Liu, Y. (2017). Modelling of vacuum distillation in a rotating packed bed by Aspen. *Applied Thermal Engineering*, 117, 322–329.
- Mericq, J.-P., Laborie, S., & Cabassud, C. (2011). Evaluation of systems coupling vacuum membrane distillation and solar energy for seawater desalination. *Chemical Engineering Journal*, 166(2), 596–606.
- Moradi, M., & Kabiri, K. (2012). Red tide detection in the Strait of Hormuz (east of the Persian Gulf) using MODIS fluorescence data. *International Journal of Remote Sensing*, 33(4), 1015–1028.
- Namazizadeh, M., Gevari, M. T., Mojaddam, M., & Vajdi, M. (2020). Optimization of the splitter blade configuration and geometry of a centrifugal pump impeller using design of experiment. *Journal of Applied Fluid Mechanics*, 13(1).
- Namazizadeh, M., & Joda, F. (2020). Effect of air gap on thermohydraulic performance of finned tube bundles. *Thermal Science and Engineering Progress*, 100687.
- Ong, C. L., Escher, W., Paredes, S., Khalil, A., & Michel, B. (2012). A novel concept of energy reuse from high concentration photovoltaic thermal (HCPVT) system for desalination. *Desalination*, 295, 70–81.
- Plattner, J., Naidu, G., Wintgens, T., Vigneswaran, S., & Kazner, C. (2017). Fluoride removal from groundwater using direct contact membrane distillation (DCMD) and vacuum enhanced DCMD (VEDCMD). *Separation and Purification Technology*, 180, 125–132.
- Qi, C., Wang, X., Feng, H., & Lv, Q. (2017). Performance analysis of low-temperature multi-effect distillation system under different feeding modes. *Applied Thermal Engineering*, 112, 1452–1459.
- Ravisankar, V. A., Seaman, R., Mirchandani, S., Arnold, R. G., & Ela, W. P. (2016). Solar-driven membrane distillation demonstration in Leupp, Arizona. *Reviews on environmental health*, 31(1), 79–83.
- Sadri, S., Ameri, M., & Khoshkhoo, R. H. (2017). Multi-objective optimization of MED-TVC-RO hybrid desalination system based on the irreversibility concept. *Desalination*, 402, 97–108.



## Subsurface Hydrology



# Groundwater Pollution in an Arid Region, Southwest of Iran

Hassan Daneshian, Nasrollah Kalantari, and Farshad Alijani

## Abstract

The sources of groundwater pollution in Behbahan plain, southwest of Iran, as an urban aquifer in arid climate, were determined using hydrogeochemistry. Groundwater samples were collected from 40 water wells in both wet and dry periods, June 2017 and April 2018. The water samples were analyzed for determination of major ions, nitrate, fluoride, and bromide. The quality of groundwater pollution in the Behbahan plain was affected by natural groundwater recharge (R) and discharge (D) areas, Marun (M) and Bonehbasht (B) irrigation and drainage networks, contact with gypsum bedrock (G) of the Gachsaran formation, and wastewater of Behbahan City (T). The spatial variation of electrical conductivity, chloride, ionic ratios, and nitrate concentrations was investigated to determine anomalous groundwater zones associated with urban sources of groundwater pollution. Cluster analysis (CA) was also employed to evaluate the recharge sources, where it was observed that both natural and anthropogenic factors were affecting the groundwater quality. Two major water types Ca-SO<sub>4</sub> and Ca(Na)-SO<sub>4</sub>(Cl) were present in the Behbahan groundwater plain. The high concentrations of sulfate, calcium, and magnesium were reflected in moderate-to-high TDS (about 3000 mg/l). The dominant hydrogeochemical processes in the aquifer were dissolution of gypsum and somewhat halite, dedolomitization, scant normal and reverse cation exchange, and mixing. The main sources of the nitrate pollution of groundwater were leaching of organic manure applied on cultivated areas as well as wastewater of Behbahan City. The minimum and maximum

concentrations of nitrate in groundwater of the Behbahan plain were 5–105 mg/L and 5–150 mg/L in dry and wet periods, respectively. About one third of groundwater samples in the Behbahan plain had nitrate concentrations above drinking water standard (45 mg/L).

## Keywords

Hydrochemistry • Pollution sources • Nitrate • Groundwater • Iran

## 1 Introduction

Groundwater is the source of drinking water for many people around the world, especially in arid regions. This has become the most concerning issue for most countries in the Middle East. In addition to being vital for drinking, agriculture, and industries, it can contribute to socio-environmental problems. The population of Iran has rapidly doubled in the past 40 years, and as a result, the use of water for different purposes has increased enormously in this country. Agriculture uses the major portion of available freshwater where about 60% of this water is wasted due to inefficient agriculture methods and leaky irrigation systems. In addition to this, pesticides and fertilizers are also leached into the aquifers.

Groundwater can become contaminated naturally or because of numerous types of anthropogenic activities. Urban, industrial, and agricultural activities can degrade groundwater quality in different ways. Immethodical use of fertilizers, irrigation activities, and infiltration of urban wastewater can lead to elevated nitrate levels in the subsoils which can leach into the aquifer, causing degradation of groundwater quality, especially in the urban aquifers. The sustainability of safe groundwater resources is the most important challenge in the urban areas, as exacerbated by the increasing water shortage in arid climates. The exploitation

H. Daneshian · N. Kalantari  
Faculty of Earth Sciences, Shahid Chamran University of Ahvaz,  
Ahvaz, Iran

F. Alijani (✉)  
Department of Minerals and Groundwater Resources, Faculty of  
Earth Sciences, Shahid Beheshti University, Tehran, Iran  
e-mail: [f\\_alijani@sbu.ac.ir](mailto:f_alijani@sbu.ac.ir)

of groundwater is related to understanding groundwater sources, groundwater quality, and anthropogenic activities.

The effect of human activities on groundwater chemistry is probably greatest in vulnerable hydrogeologic settings, such as karstic aquifers or shallow parts of sand and gravel aquifers. The occurrence of high nitrate concentrations in groundwater in response to the interaction of agricultural activities, wastewater, and septic effluent infiltration in urban areas has been reported in many previous studies (Burow et al., 2010; Zhang et al., 2018).

Over the past few decades, many investigations have dealt with application of hydrochemical methods (Monjerezi et al., 2011; Nandimandalam 2012; Xiao et al., 2015; Yidanaet al., 2017), multivariate statistical techniques (Kshetrimayum 2015; Kshetrimayum and Laxmi 2017; Bodrud-Doza et al., 2018; Khanoranga 2018), and so forth to identify the origins and pollution sources of groundwater. When it comes to urban aquifers, a great deal of ambiguity arises in the interpretation of hydrogeochemistry caused by the simultaneous effects of geogenic and anthropogenic factors or mixing (Fukada et al., 2004; Choi et al., 2005; Bottrell et al., 2008; Hosono et al., 2010; Salcedo Sánchez et al., 2017). The anomalous hydrochemistry is complex, especially with respect to groundwater flow. The hydrochemical studies in an urban aquifer should be done with regards to the amounts and duration of infiltration and rising of groundwater level. However, evaluating the impact of recharge on groundwater resources in an urban environment is different from assessing the effect on natural systems for three reasons (Tam and Nga 2018): (1) recharge sources being radically different; (2) lack of detailed information on the sewerage system and water distribution system as well as the position, duration, and volume of water leaked from these systems; and (3) reduction of recharge and decline of groundwater level due to urbanization. They are inter-related as mentioned above, which cannot be independently quantified by a single simulation. Multivariate statistics are useful tools to conclude other findings and obtain significant information from complex hydrochemical datasets in aquifers.

This study aims to identify the pollution sources of the Behbahan aquifer, as a typical aquifer in the arid region of Iran, as well as main hydrogeochemical processes controlling groundwater quality in order to capture the effects of water–rock interactions, recharge, and mixing. Despite the reported pollution of the Behbahan alluvial aquifer, detailed studies of the hydrogeochemistry and groundwater contamination have not been conducted yet. In the Behbahan plain, the southern part of the plain functions as an urban aquifer, where nitrate contaminations of groundwater (more than 45 mg/L  $\text{NO}_3$ ) have also been reported over the last decades. Irrigation water is mainly supplied from the Marun and

Bonehbasht irrigation as well as drainage networks across 80 km<sup>2</sup> of the plain. The main objective of this paper is to describe pollution plume of the groundwater in Behbahan alluvial aquifer using graphical and multivariate statistical methods in order to identify various sources of contamination, with emphasis on nitrate pollution of the aquifer.

## 2 Materials and Methods

### 2.1 Study Area, Geology, and Hydrogeology

The study area is a 430 km<sup>2</sup> alluvium at 330 m A.S.L., located in the southwest of Iran, approximately 200 km northeast of Ahvaz and 1100 km southwest of Tehran (Fig. 1). The study area is located between the 30°30' and 30°40' and the 50°08' and 50°23' geographic latitude and longitude, respectively.

The main river running through the Behbahan plain is the Marun River. The study area includes the Behbahan City plus the Marun and Bonehbasht irrigation and drainage networks. In the surrounding environs, the primary land use is agriculture in the networks with crops such as corn and rice grown by farmers. In the study area, Behbahan City is the main population center, with over 130,000 inhabitants.

The average annual rainfall is 310 mm, with the major part of the precipitation resulting from late autumn and early spring thunderstorms. The main annual temperature is 30 °C, with a July high of 50 °C and a February low of 5 °C. The average annual transpiration from free surface of water is 2900 mm. The climate across the Behbahan requires farmers to supplement precipitation with irrigation to sustain their crops. Overall, 70% of all irrigations originate from surface water of the Marun and Bonehbasht rivers, about 150 MCM in the year on the southern part of the plain. The remaining cultivation areas are supplied by groundwater as 30 MCM per year.

The commonly used N and P fertilizers include urea, ammonium sulfate, and super phosphate. The N fertilizers are applied to the vast grain fields on the early February, with an application rate of 100 kg/ha. The Marun River flows in the middle of the plain with an average discharge of 80 m<sup>3</sup>/s which is considered as the northern boundary of the study area. The drinking water for Behbahan City, 10 MCM per year, is supplied from Kheirabad River, 10 km east of the plain.

Concerning regional geology, Behbahan region is located in the folded Zagros. Geological formations from Oligo-Miocene to recent age have outcrops in Behbahan area (Fig. 1). Thick limestones of the Asmari formation are overlaid by gypsum and marl beds of Gachsaran formation, sandstone and marl of the Mishan and Aghajari formations, conglomerate of the Bakhtiari formation, and alluvial

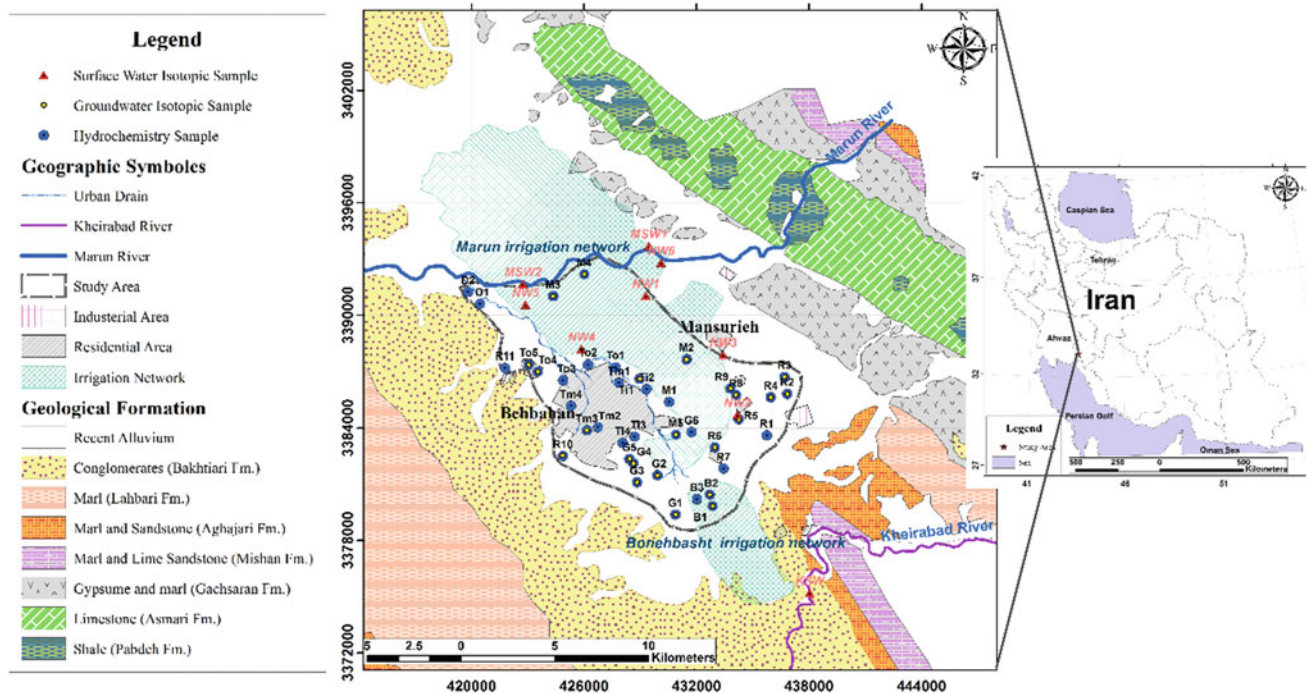


**Fig. 1** Location map of the Behbahan plain in the southwest of Iran

sediments, respectively. Although Gachsaran formation have some outcrops in the margin of the plain (Fig. 2), there are residuals of this formation, including gypsum, halite, and marl in the alluvium considerably deteriorating the groundwater quality. Quaternary sediments include pebble, gravel, sand, and some silt composed of alluvial fans in the border of Behbahan plain. Fine sediments such as silt, clay, and fine sand are deposited beneath the plain locally. The thickness of unconfined Behbahan aquifer ranges from 40 m in the marginal areas to over 150 m in the middle parts.

The Behbahan unconfined aquifer is composed of gravel and silty sand deposits with hydraulic conductivity ranging from 1 to 7 m/day. This lithological unit overlies fine sediments (silt and clay) with very low hydraulic conductivity in the east of the plain. The main surface recharges to the Behbahan alluvial aquifer include infiltration of rainfall, irrigation water, as well as the Marun and Bonehbasht irrigation and drainage networks. The Khaviz karst aquifer, in the north east of the Behbahan plain, is the main source for subsurface recharge of the aquifer, though the underground recharge from the Bakhtiari and Gachsaran formations also occurs, with high and low quality of groundwater, respectively.

Depth to the water table ranges from 3 m in the Behbahan City to higher than 32 m in the northwest of the plain. The iso-potential map (Fig. 2) provides a good description of the alluvial aquifer. According to the iso-potential map of the aquifer, it can be seen that the groundwater elevations range

from 335 m in the recharge areas in the southeast of the plain to lower than 290 m in the discharge area in the west. The highest groundwater elevations exist in the north of the plain. The groundwater head distribution for the Behbahan aquifer shows recharge zones, on the eastern and northern sides of the plain through the Bakhtiari and Asmari formations, respectively. The groundwater flow lines are oriented toward the discharge area in the west of the plain. Although the main recharge sources of the aquifer are infiltration from the irrigation networks and wastewater of Behbahan City, the directions of flow lines are not affected significantly.

Groundwater has been exploited from the Behbahan aquifer to supply agricultural activities. Surface water infiltration of the Behbahan aquifer from the irrigation water (150 MCM annually) and the presence of fine layers in the uppermost part of the aquifer cause rising groundwater levels in the west of plain, despite the occurrence of drought since 2008, causing serious problems for the Behbahan City.

### 3 Data Collection

The groundwater sampling (number of water samples, periods of sampling, types of water sources, depth of sampling, and selection of representative samples) is dependent on the aim and type of the study, spatial changes in groundwater quality, extent and type of the aquifer, and economical considerations. Groundwater samples were



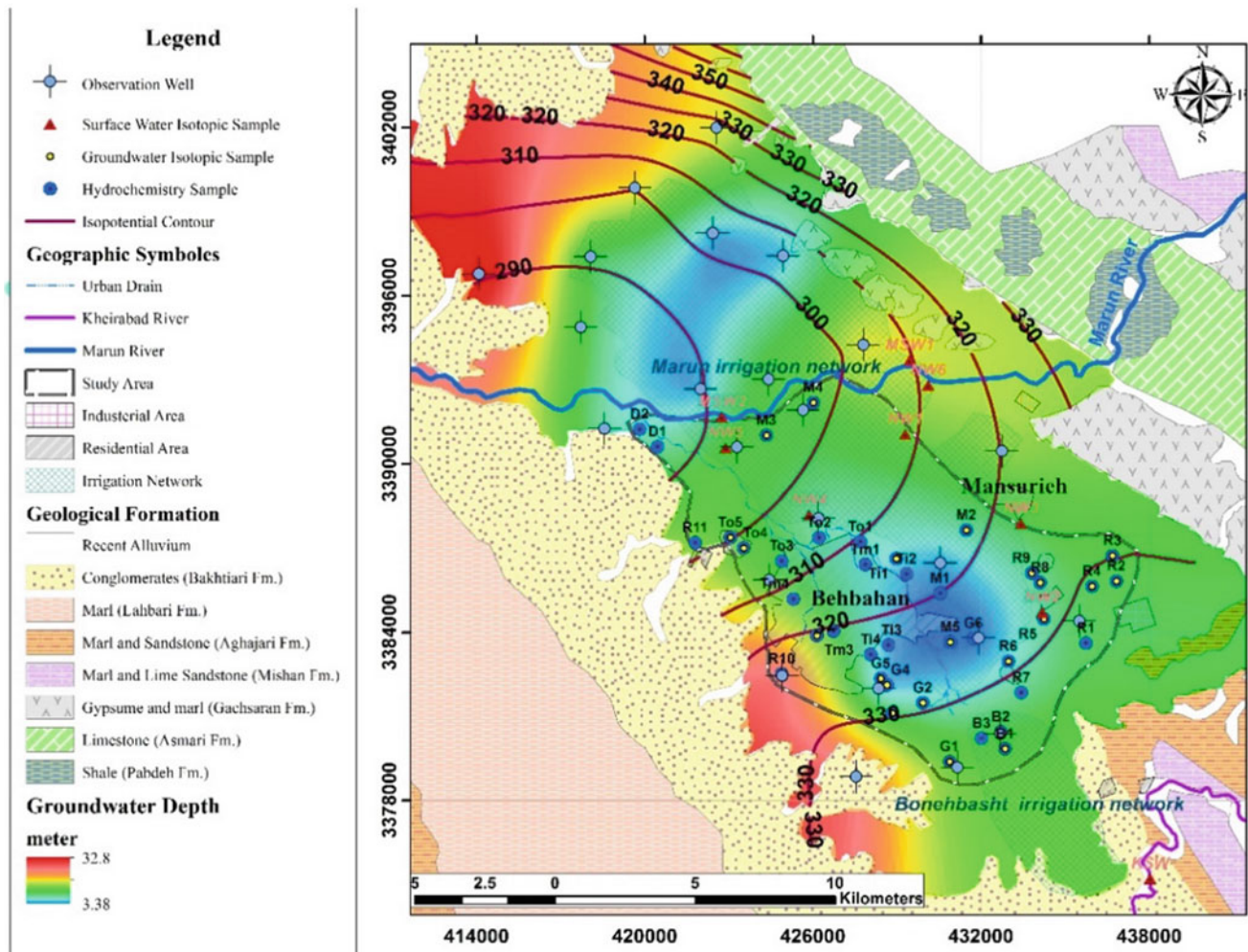


**Fig. 2** Location of groundwater samples on hydrogeological map of the Behbahan plain

collected from 40 water wells in the Behbahan plain in both wet and dry periods, June 2017 and April 2018. They are named with respect to their probable origins as (1) natural groundwater recharge (R) and (2) discharge (D) areas, (3) the Marun (M) and (4) Bonehbasht (B) irrigation and drainage networks, (5) in contact with gypsum bedrock (G) of the Gachsaran formation, and (6) wastewater of Behbahan City (T). The sampled wells were distributed throughout the southern part of the Behbahan plain (Fig. 2). Sampling procedures consisted of well purging, sample collection, and sample preservation (when required). The water samples were analyzed for determining major ions, nitrate, fluoride, and bromide for both periods.

The pH, temperature, and EC were measured in the field using a portable instrument model HACH. One sample was placed in 250 ml polyethylene bottle (for analyses of major ions,  $\text{NO}_3$ , Br, and F). Samples were acidified to  $\text{pH} < 4$  with concentrated  $\text{HNO}_3$  for cation analysis. Water samples were filtered with 45  $\mu\text{m}$  filter in the field and kept at

approximately 5 °C during transport and storage. Hydrochemical analyses were performed at Khuzestan Water and Power Authority (KWPA) Laboratory, in Ahvaz, Iran.

Concentrations of Ca, Mg,  $\text{HCO}_3$ , and Cl were analyzed by volumetric titrations, while the concentration of sulfate was measured by turbidimetric method. Also, those of Na and K were determined using a flame photometer. The analytical errors were determined to be lower than 5% based on cation–anion concentrations balance for all samples. The results of hydrochemical of groundwater samples in the Behbahan plain have been obtained in both period of the study which are given in Tables 1 and 2.

## 4 Methodology

After describing the hydrochemical data and determining the types of water using Piper diagrams, the spatial variations of electrical conductivity, chloride, sulfate, fluoride, bromide,



**Table 1** Results of hydrochemical analysis of groundwater samples in the Behbahan plain in June 2017 as dry season (EC as  $\mu\text{S}/\text{cm}$ , major ion concentrations as  $\text{meq}/\text{l}$ ,  $\text{NO}_3$ , F, and Br as  $\text{mg}/\text{l}$ )

ID	T	EC	pH	Ca	Mg	Na	K	$\text{HCO}_3$	Cl	$\text{SO}_4$	$\text{NO}_3$	F	Br
Ti1	26.5	4410	7	29.43	19.94	11.68	0.22	3.5	8.9	48.5	57.7	1.24	0.45
Ti2	26	4730	6.9	30.24	10.35	19.64	0.22	5.4	17.6	37.1	11.1	1.48	0.4
Ti3	26.5	3800	7.1	23.66	20.79	7.77	0.24	4.05	7.9	40.2	72.9	1.6	0.48
Ti4	26.2	4710	6.7	33.83	7.09	14	0.46	4.78	13.7	36.6	102.9	0.58	0.86
Tm1	27.2	5710	7.2	31.4	17.97	20.16	0.56	4.76	18.9	46.1	83.8	2.18	0.59
Tm2	29.2	3470	6.7	25.6	3.54	8.42	0.24	4.79	9.8	22.8	31.4	0.8	0.23
Tm3	26.5	2880	7	22.49	10.16	5.57	0.17	4.32	4.8	28.9	77.2	1.3	0.21
Tm4	28.7	2730	7.3	22	7.75	5.04	0.22	2.6	3.3	28.8	31.1	1.27	0.29
To1	27.5	3470	7.1	15.4	6.84	14.6	0.14	4.71	13.7	18.2	19.5	1.6	0.34
To2	27	5700	6.6	30.3	16.83	22.8	0.24	5.63	20.0	44.2	41.5	0.9	0.9
To3	28	3610	6.7	24.66	12.86	7.93	0.23	5.48	7.8	32.1	69.2	1.24	0.22
To4	27	3120	7	23.82	13.36	10.6	0.19	4	4.5	39.1	44.4	1.27	0.6
To5	29.5	3930	7.1	25.45	18.45	9.82	0.5	4.35	5.7	43.8	58.9	1.6	0.61
D1	24	6610	8	22.94	17.47	27.85	0.95	4.44	20.5	44.1	64.4	1.5	0.89
D2	23	5610	8	20.62	14.27	22.8	0.14	4.86	17.3	35.5	50.9	1.3	0.62
G1	26	4630	7	27.72	21.3	14	0.29	4.42	12.5	46.0	80.5	1.58	1.05
G2	25.7	4380	6.7	36.41	3.13	13.4	0.1	4.84	14.9	33.0	18.7	1.84	0.48
G3	25	4820	6.7	32.83	11.36	13.6	0.34	4.28	16.5	37.0	29.7	1.33	1.07
G4	28	4650	6.7	28.04	16.6	14.92	0.5	4.38	13.4	42.0	65.0	2.11	0.88
G5	26.9	4185	6.8	24.9	17.2	12.2	0.3	6.5	13.6	33.6	82.0	0.58	0.39
G6	27.4	4250	6.7	27.57	3.28	13.16	0.22	4.67	18.3	20.9	23.7	0.99	0.37
M1	27	4900	7	29.97	24.19	14.6	0.29	5	12.2	51.5	20.2	1.97	0.33
M2	27	3360	7.2	21.43	6.13	13.1	0.1	5.22	12.7	22.5	6.2	1.39	0.33
M3	22.5	2880	7.1	11.3	4.57	16.18	0.11	5.4	12.3	14.1	41.7	0.46	0.32
M4	24.5	3050	7.1	15.31	5.54	13.4	0.12	4.94	14.2	14.9	22.4	0.33	0.37
M5	26.5	1537	7.6	8.81	1.11	7.15	0.06	3.06	7.4	6.4	25.0	1.73	0.46
R1	27	1682	7.2	16.1	6.1	3.45	0.12	5	4.5	17.1	44.0	0.86	0.53
R9	24.5	2670	7	17.93	4.93	9.27	0.21	4	10.0	18.0	13.4	0.98	0.556
R2	29	1872	7	16.96	5.49	1.6	0.12	3.1	1.6	19.2	39.9	1.46	0.27
R3	27.8	2960	7.1	26.61	8.22	4.42	0.2	2.38	4.6	32.1	32.8	1.06	0.27
R4	26.5	1991	7	17.48	6.52	1.91	0.13	3.86	1.6	20.2	40.3	1.14	0.26
R5	26	2830	7	19.17	5.27	8.84	0.13	3.77	10.5	18.8	37.6	1.07	0.41
R6	25.5	2550	7.8	15.02	5.93	8.6	0.12	3.96	10.7	14.7	59.0	0.77	0.48
R7	25.4	2870	7.5	24.2	10.3	4.2	0.12	3.6	6.2	28.8	16.0	0.76	0.35
R8	27	2570	7.1	16.08	5.01	8.59	0.13	3.29	9.4	16.8	19.9	0.86	0.1
R10	28	2610	7.4	13.52	8.59	8.09	0.18	3.7	5.9	20.5	41.0	0.95	0.26
R11	26.5	3096	7	21.9	7.8	4.9	0.13	3.85	3.5	27.2	28.6	1.18	0.3
B1	26.8	2929	7.3	21.1	10.8	5.5	0.22	4.1	7.4	26.3	8.8	0.85	0.45
B2	27.1	3660	7	27.4	8.8	5.9	0.2	5.6	7.9	28.8	16.5	0.94	0.65
B3	27.5	3904	6.9	32.2	7.3	9.41	0.22	5.1	10.3	35.2	18.9	0.92	0.52

Natural groundwater recharge (R) and discharge (D) areas, Marun (M) and Bonehbasht (B) irrigation and drainage networks, contact with gypsum bedrock (G) of Gachsaran formation, and wastewater of Behbahan City (T)

**Table 2** Results of hydrochemical analysis of groundwater samples in the Behbahan plain in April 2018 as the wet season (EC as  $\mu\text{S}/\text{cm}$ , major ion concentrations as  $\text{mg}/\text{l}$ ,  $\text{NO}_3$ , F, and Br as  $\text{mg}/\text{l}$ )

ID	T	EC	pH	Ca	Mg	Na	K	$\text{HCO}_3$	Cl	$\text{SO}_4$	$\text{NO}_3$	F	Br
Ti1	26	3660	6.9	27.23	8.18	13.70	0.15	3.1	13.3	32.5	53.4	1.13	0.42
Ti2	26.7	4350	7	28.80	9.91	14.92	0.11	4.9	14.7	33.8	16.8	1.37	0.45
Ti3	24.2	5180	7.1	33.13	12.99	18.16	0.37	4.2	19.9	40.2	66.1	1.68	0.48
Ti4	25.5	6190	6.9	36.46	13.30	26.80	0.56	4.5	24.8	47.5	98.2	0.72	0.95
Tm1	25.3	5840	7.3	30.59	21.14	23.36	0.56	5.6	19.2	50.4	80.6	1.85	0.55
Tm2	25.8	3390	7	23.61	8.20	8.14	0.21	4.3	9.7	25.9	32.2	0.95	0.28
Tm3	25.2	2592	7	22.10	8.10	4.30	0.15	3.9	4.3	26.0	76.0	0.34	0.22
Tm4	25.5	2800	7.4	20.50	9.38	6.12	0.24	2.5	3.3	30.1	31.4	1.40	0.32
To1	24.2	3620	7.2	16.75	7.59	17.20	0.16	4.9	14.0	22.4	17.0	1.69	0.27
To2	26.5	5125	6.9	30.21	15.80	19.80	0.19	5.6	18.1	42.1	41.5	2.11	1.12
To3	26.6	3540	6.8	28.30	14.74	8.26	0.21	4.2	7.2	39.8	61.3	1.32	0.29
To4	26	3040	6.6	24.70	14.22	5.98	0.24	4.5	4.4	35.9	46.4	1.45	0.67
To5	23	3760	7	28.61	16.52	9.58	0.50	3.8	5.2	45.8	56.0	1.53	0.58
D1	24.5	5260	6.6	25.88	16.36	25.64	0.88	4.7	20.1	43.5	65.1	1.33	0.92
D2	24	4550	6.8	23.54	10.51	21.72	0.56	5.5	17.2	33.3	50.9	1.45	0.86
G1	27	4300	6.9	27.42	18.74	14.30	0.28	3.8	11.5	45.1	76.4	1.69	1.12
G2	26	4470	6.8	30.85	20.69	14.00	0.37	4.5	11.6	49.5	17.1	1.34	0.35
G3	25	5830	6.9	37.68	25.94	21.72	0.27	3.4	16.9	64.9	28.7	1.56	0.95
G4	23.5	4670	7	31.01	27.41	12.82	0.22	6.1	8.5	56.6	154.0	1.98	0.83
G5	24	4550	6.8	29.07	11.79	19.64	0.30	4.5	17.7	38.2	72.2	0.74	0.37
G6	25.8	4450	7	26.68	9.81	15.36	0.24	4.3	19.5	28.0	25.9	0.81	0.39
M1	26	3870	6.9	34.33	10.18	9.97	0.18	3.6	9.7	41.1	16.3	1.57	0.34
M2	23.5	3380	7	21.43	5.96	12.82	0.10	4.9	12.0	23.1	4.7	1.34	0.35
M3	26.5	2800	6.6	11.96	5.42	17.50	0.14	4.8	12.1	17.8	41.0	0.65	0.39
M4	23.9	3420	6.6	19.68	5.94	16.28	0.10	4.7	16.1	20.9	23.2	0.43	0.34
M5	24.5	4510	6.9	29.07	10.83	15.80	0.30	4.3	16.9	34.4	27.4	1.38	0.48
R1	28	1682	7	14.80	6.13	2.33	0.10	4.3	3.4	15.3	37.4	0.95	0.55
R9	24.9	1705	7.7	13.66	5.40	1.45	0.11	2.6	1.5	16.1	15.2	0.89	0.52
R2	23.6	2760	7.3	23.83	7.96	3.48	0.18	2.4	4.2	28.9	34.9	1.55	0.32
R3	24.1	2120	7.1	17.41	7.56	2.07	0.14	3.6	1.5	21.8	30.4	1.21	0.24
R4	26	2180	7.4	16.44	8.33	4.30	0.13	3.0	4.9	20.9	36.9	1.26	0.25
R5	26	2420	6.8	16.40	4.54	8.60	0.12	3.3	10.4	15.7	40.6	1.13	0.37
R6	26.5	2870	6.9	25.27	10.35	3.95	0.15	3.5	5.2	30.7	56.6	0.79	0.45
R7	25.1	2490	7.4	13.37	4.24	9.58	0.13	3.1	11.1	12.8	13.6	0.67	0.33
R8	25.2	3560	7	26.31	6.57	10.08	0.23	4.1	11.7	27.0	27.3	1.02	0.15
R10	23.9	2090	7.4	14.98	5.83	7.00	0.15	3.3	3.8	20.5	38.4	1.03	0.24
R11	26.5	2580	7	19.08	7.42	8.59	0.15	3.8	4.0	27.2	23.9	0.96	0.32
B1	21.9	2462	7.3	17.80	9.10	4.80	0.18	3.4	6.2	22.1	11.2	0.57	0.37
B2	22.4	3050	7.1	22.80	8.50	5.76	0.20	4.0	7.2	26.1	18.1	0.74	0.42
B3	23.6	3200	7	24.90	7.70	6.70	0.21	4.2	7.6	27.5	12.8	1.02	0.49

Natural groundwater recharge (R) and discharge (D) areas, Marun (M) and Bonehbasht (B) irrigation and drainage networks, contact with gypsum bedrock (G) of Gachsaran formation, and wastewater of Behbahan City (T)

and nitrate concentrations, ionic ratios ( $\text{Na}/\text{Cl}$ ,  $\text{SO}_4/\text{Cl}$ ,  $\text{Ca}/\text{Mg}$ , and  $\text{Br}/\text{Cl}$ ), were investigated to determine anomalous groundwater zones with regards to the urban sources of groundwater pollution. Hydrochemical maps are usually compiled to display the regional distribution of water composition and quality with respect to recharge sources as well as the water/rock interaction. Hydrochemical mapping has been used by many researchers for the representation of spatial variability of ion concentrations in the aquifer (Ghesquière et al., 2015; Maurya et al., 2018; Romero-Sierra et al., 2018; Zereg et al., 2018).

To evaluate the analytical data, multivariate statistical techniques, i.e., item analysis and cluster analysis (CA), were used in this study using MINITAB (version 18.0) software. Cluster analysis was applied to identify groups or clusters of similar water wells based on similarities and differences in hydrochemical specifications. Hierarchical clustering is the most popular approach, which provides intuitive similarity relationships between any sample and the entire dataset, and can be illustrated by a dendrogram (McKenna, 2003). The input hydrochemical data including major ion,  $\text{NO}_3$ , F, and Br concentrations, and EC values were chosen for cluster analysis. After standardization, the hydrochemical data were clustered using the Ward's linkage method with squared Euclidean distances as the similarity measurement between two samples.

## 5 Results and Discussion

### 5.1 General Hydrochemistry

The results of chemical analyses of water samples in dry and wet periods were used for hydrogeochemical investigations of the Behbahan alluvial aquifer. The solute chemistry of major ions in the two periods is demonstrated in Piper diagrams (Fig. 3). The groundwater samples in Piper diagrams show cluster and line patterns in cationic and anionic triangles, respectively. There are two major water types  $\text{Ca-SO}_4$  and  $\text{Ca(Na)-SO}_4(\text{Cl})$ . The high concentrations of sulfate, calcium, and magnesium are reflected in moderate-to-high TDS (about 3000 mg/l). In the dry period, the samples are more outspread than in wet periods because of no mixing due to recharge from precipitation or irrigation.

According to the hydrochemical data in the Behbahan aquifer, the groundwater has a Ca concentration ranging from 11.2 to 37.7 meq/L and from 8.80 to 36.4 meq/L in wet and dry periods, respectively, with the mean concentrations of 23.3 and 24.2 meq/L. The mean concentrations of  $\text{SO}_4$  ranged from 12.84 to 64.91 meq/L and from 6.37 to 51.53 meq/L in wet and dry periods, respectively, with the mean concentrations 32.0 and 29.8 meq/L, where dissolution of gypsum is the most probable source of  $\text{SO}_4$ . On the

other hand, differences in Ca and  $\text{SO}_4$  concentrations are to some extent involved in dedolomitization possibly causing elevated Mg concentrations with the mean concentrations of 10.9 and 10.3 meq/L.

In addition, the mean concentrations of Cl have been 10.8 and 10.4 meq/L while those of Na have 11.8 and 11 meq/L. The strong correlation between Cl and Na in the Behbahan aquifer suggests that there is no evidence of cation exchange.

In the study area, the mean concentrations of  $\text{HCO}_3$  have been 4.1 and 4.4 meq/L, respectively, indicating that the carbonate dissolution is a minor hydrochemical process in the aquifer. Nevertheless, this could be a result of saturation with respect to calcite and dolomite in the formation groundwater in the entrance of the alluvial aquifer as recharge areas.

The occurrence of high-fluoride groundwater has been reported in a few regions in Iran (Battaleb-Looie et al., 2013; Akhavan et al., 2016; BaghalAsghari et al., 2017; Dehbandi et al., 2018; Dehghani et al., 2018; Enalou et al., 2018; Karimi et al., 2018;) as well as in other countries (Li et al., 2017; Raj and Shaji 2017; Colombani et al., 2018; Emenike et al., 2018; Gupta and Misra 2018; Wu et al., 2018) because of its considerable effects on human health. Long-term exposure to high-fluorine water can seriously affect the health of the body, leading to chronic fluorosis (Wang & Cheng, 2001). As an essential trace element in the human body, the concentration of F in drinking water should not exceed 0.7–2.1 mg/L in cold and hot months, respectively, Biglari et al. (2016) depending on the concentration and daily ingested dose.

According to the standard of drinking water, the optimum concentration of fluoride in drinking water is 0.7 mg/L during warm months, while it is 2.1 mg/L in the cold months. The average fluoride concentration of groundwater samples in the Behbahan aquifer ranged from 0.33 to 2.18 mg/L with a mean concentration of 1.19 mg/L in the dry period (Table 1).

Bromide is commonly found in nature along with sodium chloride, owing to the dissimilar physical and chemical properties, though in smaller quantities. The natural source of bromide is usually geothermal, seawater, and dissolution of rocks (Bero et al., 2016; Nair et al., 2016; Hildenbrand et al., 2017). In residential areas, due to treatment of water for drinking by disinfection processes, bromide gets converted into bromate which is a potential carcinogen. In addition, agricultural fertilizers contribute to a significant amount of bromide in groundwater as well. The concentrations of bromide in groundwater samples in the study area ranged from 0.1 to 1.07 mg/L (Table 1).

Nitrate is the major contaminant of groundwater resources in urban areas in Iran. In recent decades, the average levels of nitrate have increased in groundwater resources due to the urban, industrial, and agricultural sewage. The data

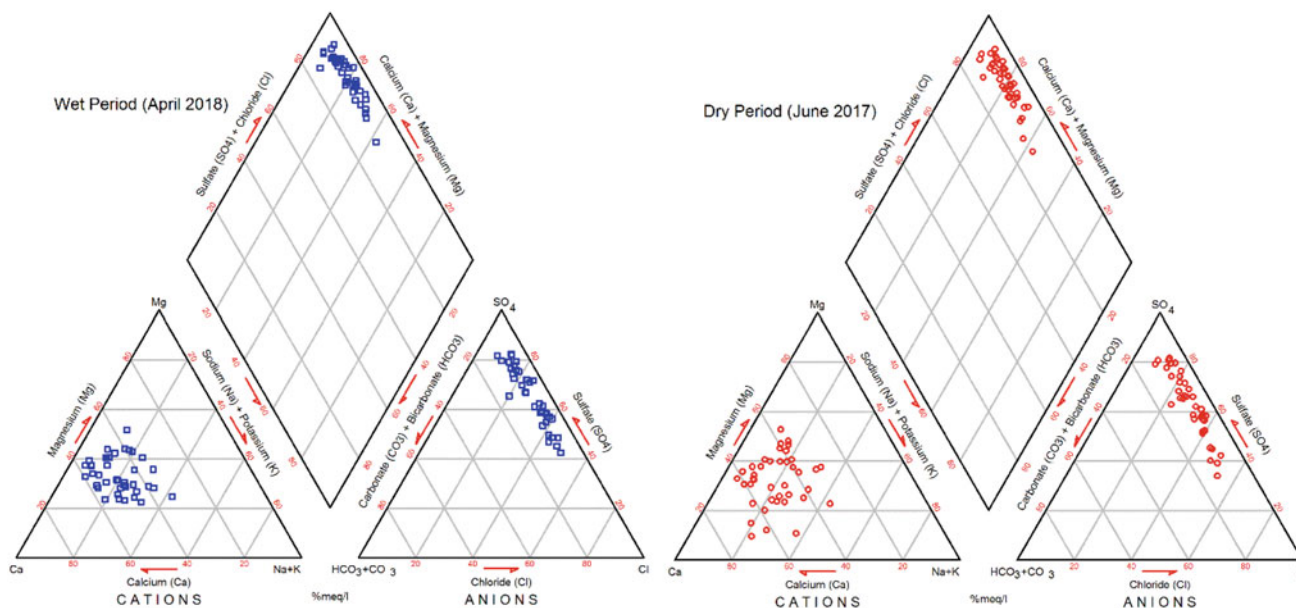


**Fig. 3** Piper diagram of groundwater samples in Behbahan plain (June 2017 and April 2018)

reveal that the groundwater has a concentration of  $\text{NO}_3^-$  ranging from 4 to 154 mg/L and from 6 to 103 mg/L in wet and dry periods, respectively, with the mean concentrations of 41.2 and 41.9 mg/L. Among 40 samples of groundwater in the Behbahan plain, 15 and 13 samples in wet and dry period, respectively, had the concentration above World Health Organization's (WHO) permissible limit for nitrate in drinking water which has been set at 45 mg/L. In the study area, 27 samples were polluted samples whose nitrate concentration was above 25 mg/L; in comparison, only one sample could be regarded as unpolluted with a nitrate concentration less than 10 mg/L.

## 5.2 Spatial Variations of Hydrochemistry

The chemical composition of groundwater is a result of many hydrogeochemical factors including the composition of initial water that infiltrates to the aquifer, its reactions with minerals in the rock matrix, hydraulic properties of the aquifer (residence time), evapotranspiration, mixing with infiltration of wastewater resulting from residential, industrial, and agricultural sources, and so forth. The major ion analyses of groundwater seek to produce basic, yet valuable, information concerning the water composition and quality. The hydrochemical maps of both sampling periods in the Behbahan plain were prepared and investigated preliminarily with respect to each sampling period to capture the hydrochemical processes. According to these maps, it is observed that the data of the wet period are slightly indeterminate possibly due to mixing with infiltration of precipitation.

Then, the hydrochemical maps of the Behbahan plain in the dry season (June 2017) have been presented as electrical conductivity (EC), chloride, sulfate, fluoride, bromide, and nitrate concentrations (Fig. 4), and ionic ratios ( $\text{Na}/\text{Cl}$ ,  $\text{SO}_4/\text{Cl}$ ,  $\text{Ca}/\text{Mg}$ , and  $\text{Br}/\text{Cl}$ ) (Fig. 5) to determine anomalous groundwater zones concerning demodulation of recharge sources of groundwater in the urban aquifer.

The total dissolved solids concentrations, which could be expressed by EC, are one of the most important factors originating from the progress of hydrochemical processes and infiltration of irrigation and sewage of urban areas, especially in arid and semi-arid regions. In the Behbahan plain, the EC map (Fig. 4a) shows elevated EC from the upstream to the mid parts of the plain, homogeneously, while in the central area near the Behbahan City, the EC tends to decrease. The infiltration of wastewater of Behbahan city could be potentially characterized by low salinity. On the other hand, the increase in EC is remarkable in the downstream area, which is probably related to the evapotranspiration in the fine sediments of shallow groundwater depths in the northwestern part of the plain. Further, the imperceptible rise of the EC in the Marun irrigation network area is likely due to significant groundwater recharges with lower dissolved solid concentrations than in the background aquifer.

The  $\text{Cl}^-$  concentrations range between 1.44 meq/L in recharge areas and 20.41 meq/L in the discharge area (Fig. 4b). The observed pattern of  $\text{Cl}^-$  values in the Behbahan aquifer may arise from an array of factors including dissolution of evaporate minerals and the recharge from miscellaneous sources. The  $\text{Cl}^-$  concentrations of the Behbahan alluvial aquifer are strongly affected by the residuals of the



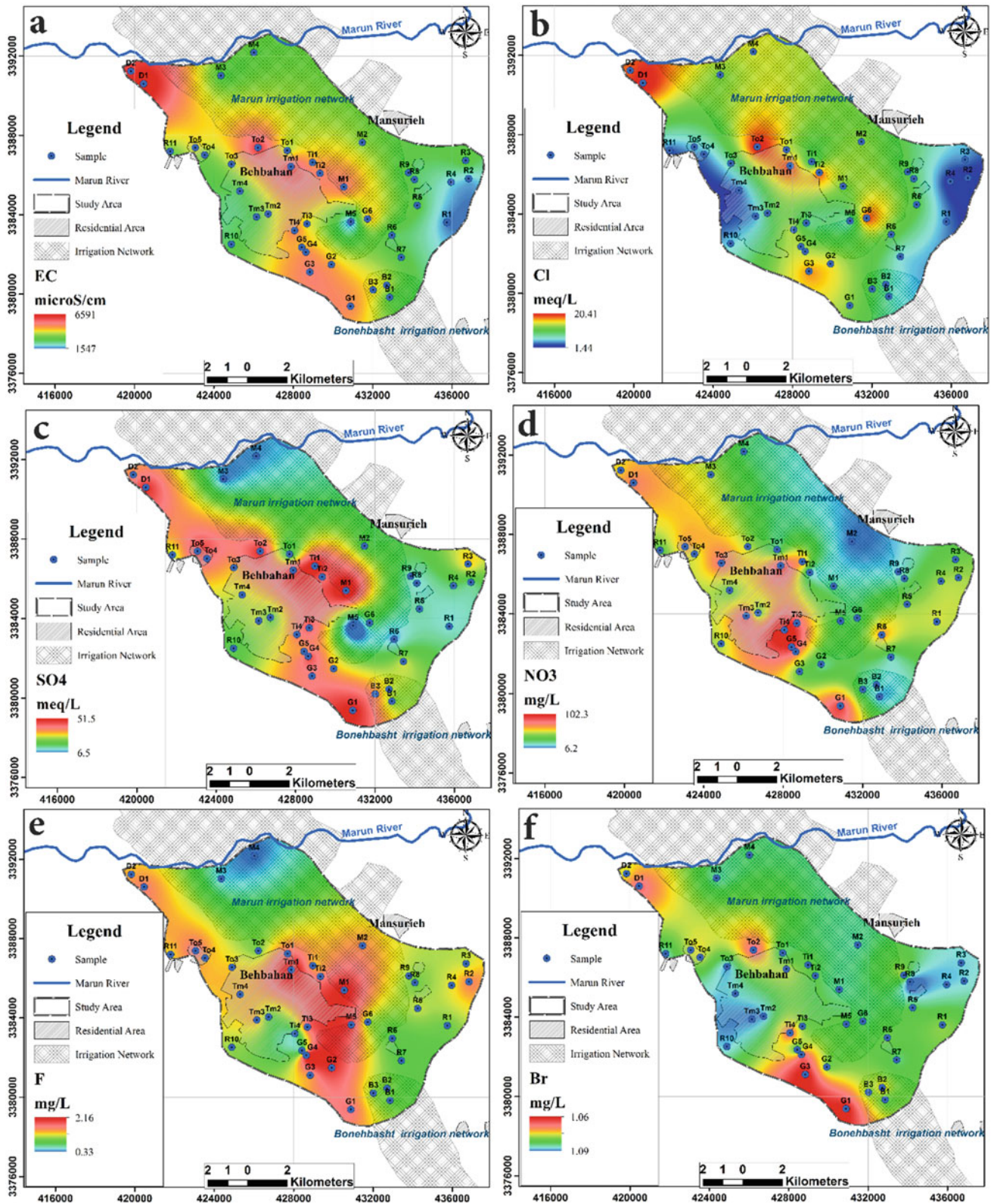


Fig. 4 Hydrochemical maps of Behbahan aquifer in the dry season (June, 2017)



Gachsaran formation in the plain. The maximum chloride concentration was observed in separated points in the middle and the northwest of the Behbahan plain. In these areas, groundwater samples are probably in contact with halite beds of the Gachsaran formation.

Sulfate appears to be the most dominant anion in the aquifer (Fig. 4c) with the data suggesting that in much of the area,  $\text{SO}_4$  and Cl concentrations are higher than the Iranian recommended maximum permissible concentration for drinking purposes. The high concentrations of  $\text{SO}_4$  in groundwater of the plain are essentially due to the dissolution of weathered minerals such as gypsum and anhydrite in the alluvium and recharge from gypsum karst aquifer of the Gachsaran formation in the north and east of the plain as well as the bedrock. Initially, through the dissolution process in the aquifer, the concentrations of Ca and  $\text{SO}_4$  have been elevated in the aquifer; however, eventually the concentration of Ca would be compensated by Mg, given the dedolomitization in the study area. The Gachsaran formation (the upstream eastern and northern boundaries of the plain) constitutes a potential sulfate source, making it the predominant ion in the aquifer. The  $\text{SO}_4$  map shows a spatial decline in the central parts of the plain in response to the infiltration of municipal wastewater with low sulfate concentrations. In the Marun and Bonehbasht irrigation network areas, the concentration of  $\text{SO}_4$  is lower than expected. This implies that a groundwater recharge (due to irrigation) causes  $\text{SO}_4$  depletion. Nevertheless, the gypsum dissolution proceeds continuously in the aquifer.

Among the two sampling periods, the maximum concentrations of nitrate in the groundwater occurred in April 2018. Oxidation of ammonium resulting from rapid leaching of organic fertilizers applied on the irrigation networks and wastewater of Behbahan City caused elevated  $\text{NO}_3$  in the groundwater. According to the iso-nitrate map of the alluvial aquifer in June 2017 (Fig. 4d), it is observed that the nitrate concentration in the middle parts in neighborhood areas of Behbahan City is greater than the maximum permissible concentration for drinking water, 45 mg/L. In Behbahan City, many aspects of the relationship between the details of groundwater flow and geochemical processes that influence the nitrogen discharge from shallow aquifers have not been resolved yet. In particular, it has been suggested that geochemical reactions, such as denitrification, may have the capacity to substantially reduce nitrogen loads in the alluvial aquifer. Denitrification is a process by which bacteria obtain energy through the chemical reduction of nitrate and the oxidation of organic matter or other reduced compounds in the absence of oxygen. If proceeded completely, denitrification transforms dissolved nitrate to nitrogen gas. Denitrification and fall of  $\text{NO}_3$  concentrations of groundwater in the urban areas resulted from the occurrence of reducing conditions in the aquifer.

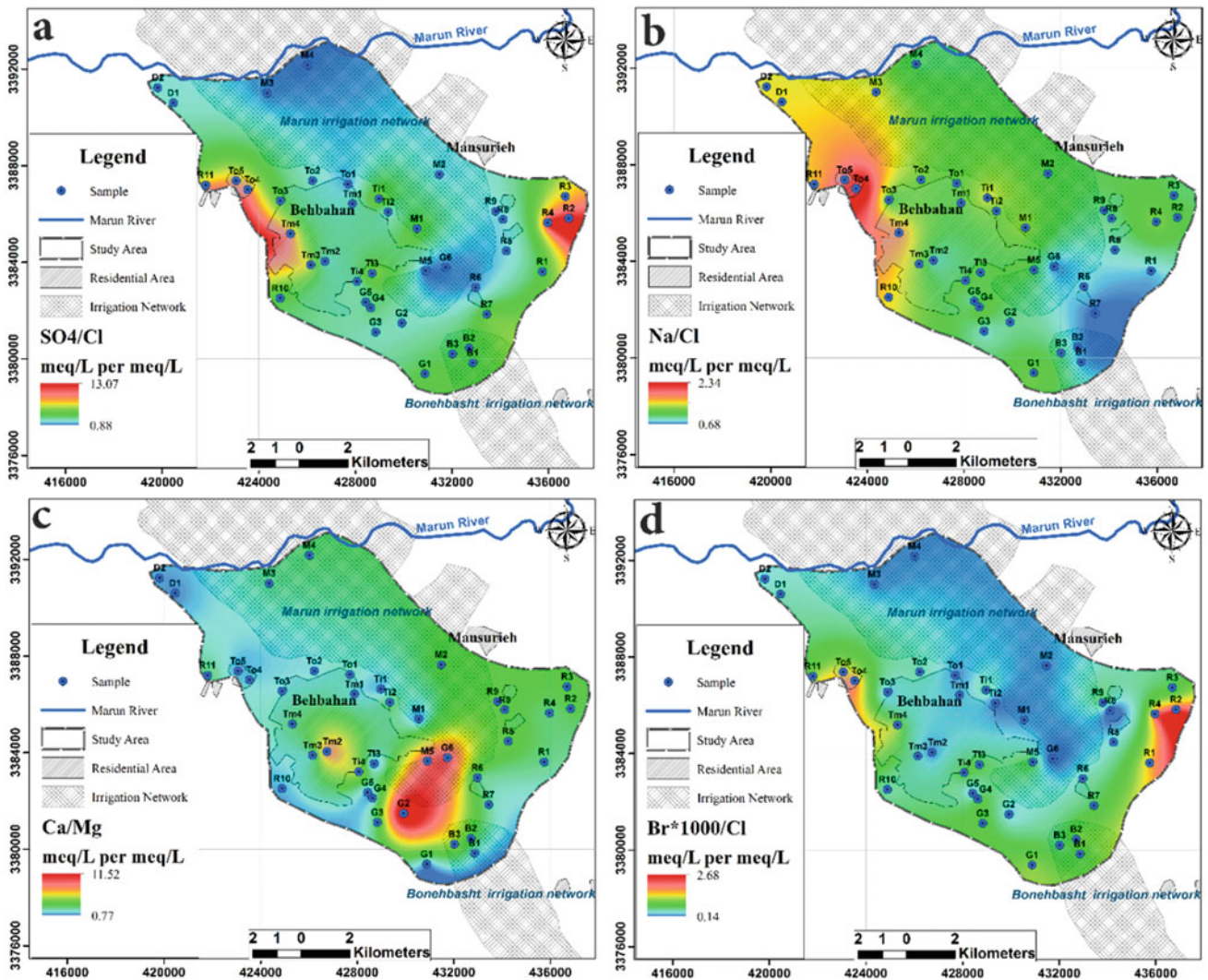
The distribution suggests a high degree of variability of Br concentrations in the groundwater (Fig. 4f). This may indicate a wide range of geogenic and anthropogenic sources which vary in the study area. The F concentration map (Fig. 4e) represents a relatively similar trend of spatial variability with Br, though it is comparable with EC map. The possible sources of variation in the concentrations of the F are in accordance with  $\text{SO}_4$  in the terrain.

The representative ionic ratios for the study are shown in Fig. 6. The values of  $\text{SO}_4/\text{Cl}$  (Fig. 5a) have been mainly greater than 1, given the dominant dissolution of gypsum in the area. The highest ratios in two parts of the aquifer, in the recharge areas, exclusively indicate the gypsum dissolution with slight or no dissolution of halite. The inequality of Na and Cl concentrations, Na/Cl ratio higher than 1.5 (Fig. 5b), could be related to ion exchange processes in northwestern parts of the aquifer. The higher sorption sites for the ions in fine sediments in the aquifer contribute to a relatively higher charge density in the alluvium. The Ca/Mg ratio higher than 5 (Fig. 5c) as coincidence with gypsum dissolution, especially in the southeast of the Behbahan City, could be associated with the dedolomitization process, leading to the relative high abundance of the Mg in relation to Ca in groundwater. The ratio of Br/Cl (Fig. 5d) diminishes from the border of the aquifer to the middle parts as a result of mixing with infiltration of irrigation and municipal wastewater originating from Marun River.

### 5.3 Composition Diagrams and Cluster Analysis

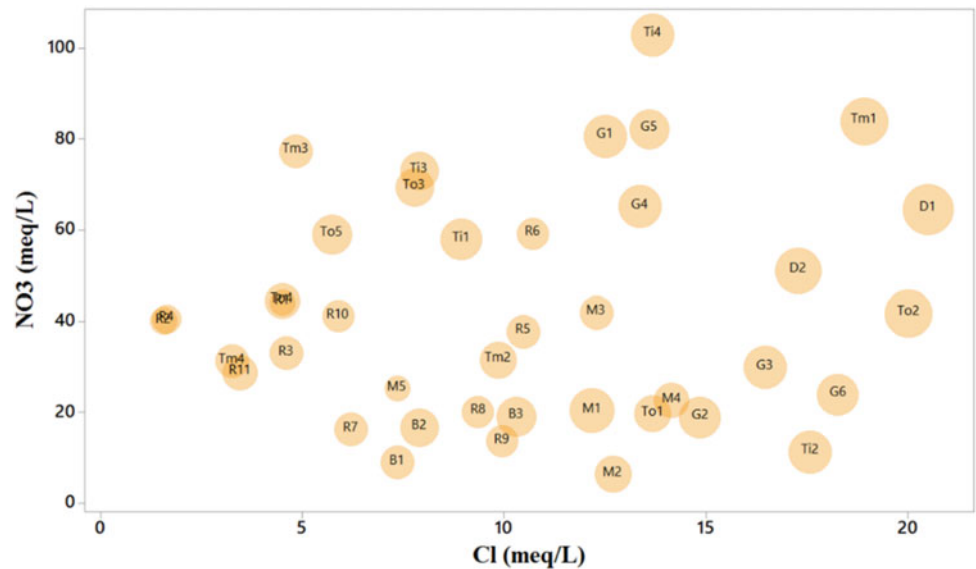
The composition bivariate diagram of  $\text{NO}_3$  versus Cl, as two indicator conservative ions, bubbled with EC in the dry season (Fig. 6) is used to display the anthropogenic and natural hydrochemical effects on the groundwater quality of Behbahan plain. The groundwater in recharge areas (mostly R samples) has low Cl and moderate-to-high  $\text{NO}_3$  concentrations plus moderate EC values, lower than 2000 micromhos/cm. Although the urban samples (denoted by T) show Cl concentrations and EC values slightly higher than those of recharge samples, the nitrate concentrations have been doubled. The highest EC values are related to groundwater in contact with gypsum bedrock (G samples) in accordance with high values of nitrate concentrations, mainly above 60 mg/L. Some of G samples have high EC and Cl values with minimum values of nitrate concentrations. Groundwaters affected by irrigation water in Marun (M samples) and Bonehbasht (B samples) networks have low  $\text{NO}_3$  values and moderate EC and Cl values. However, some deviation from the expected hydrochemical behavior is inevitable possibly due to the mixing process.

A combination of graphs has been used to illustrate all of the hydrochemical parameters together in one figure (Fig. 7),



**Fig. 5** Ionic ratio maps of the Behbahan aquifer in the dry season (June, 2017)

**Fig. 6** Composition bivariate diagram of  $\text{NO}_3$  versus Cl bubbled with EC of Behbahan aquifer in the dry season (June, 2017)



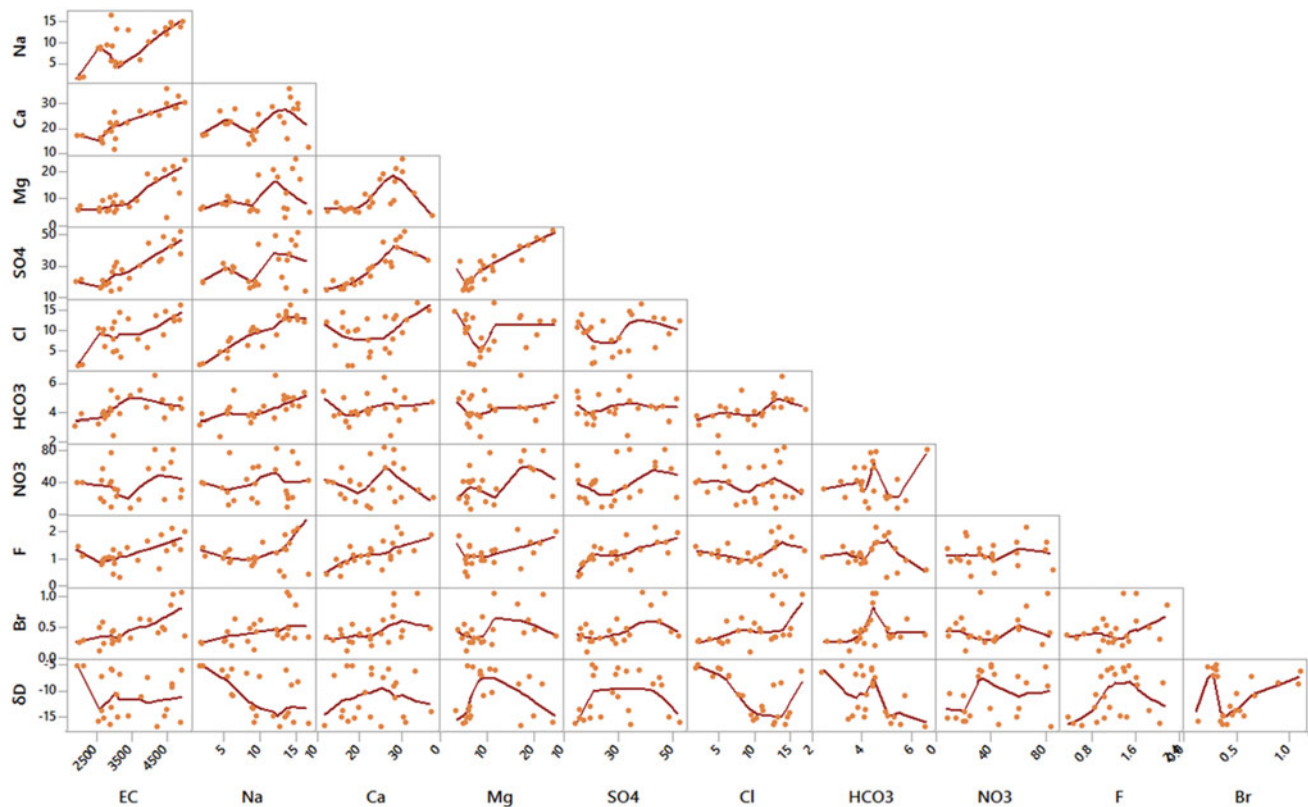


**Fig. 7** Conjugate diagram of hydrochemical parameters of Behbahan aquifer in the dry season (June, 2017)

so that their interactions with each other can be displayed. It could be observed that the concentrations of major ions, except for  $\text{HCO}_3$ , F, and Br have been elevated with EC, while  $\text{NO}_3$  values have had no obvious relationship with dissolved solids. Among all diagrams in item analysis, the correlations of Na with Cl; F, Mg, and  $\text{SO}_4$  with Ca;  $\text{SO}_4$  with Mg; Br with Cl; and F with Br are noticeable.

Cluster analysis was performed using hydrochemical parameters illustrated by two dendrograms grouping all 40 groundwater samples of the Behbahan plain into five statistical clusters, according to the main recharge sources (Fig. 8). Concerning the dendrogram in the dry season, by considering improbability of mixing with precipitation recharge, five clusters with similar hydrogeochemical compositions were distinguished with a high congruence with the initial grouping of samples based on location and most probable sources of water. The largest cluster is related to the underground recharge samples (R) with two samples of B1 and Tm4 revealing similarities with them. The samples of M2 to M4 as well as To1 composed a cluster which could be attributed to Marun irrigation network. A strange cluster in the middle of the dendrogram including a blend of waters B, Tm, Ti, and G may be related to gypsum bedrock. The discharge samples (D) have a greater similarity with Tm1 and To2. Although the municipal clusters are mainly

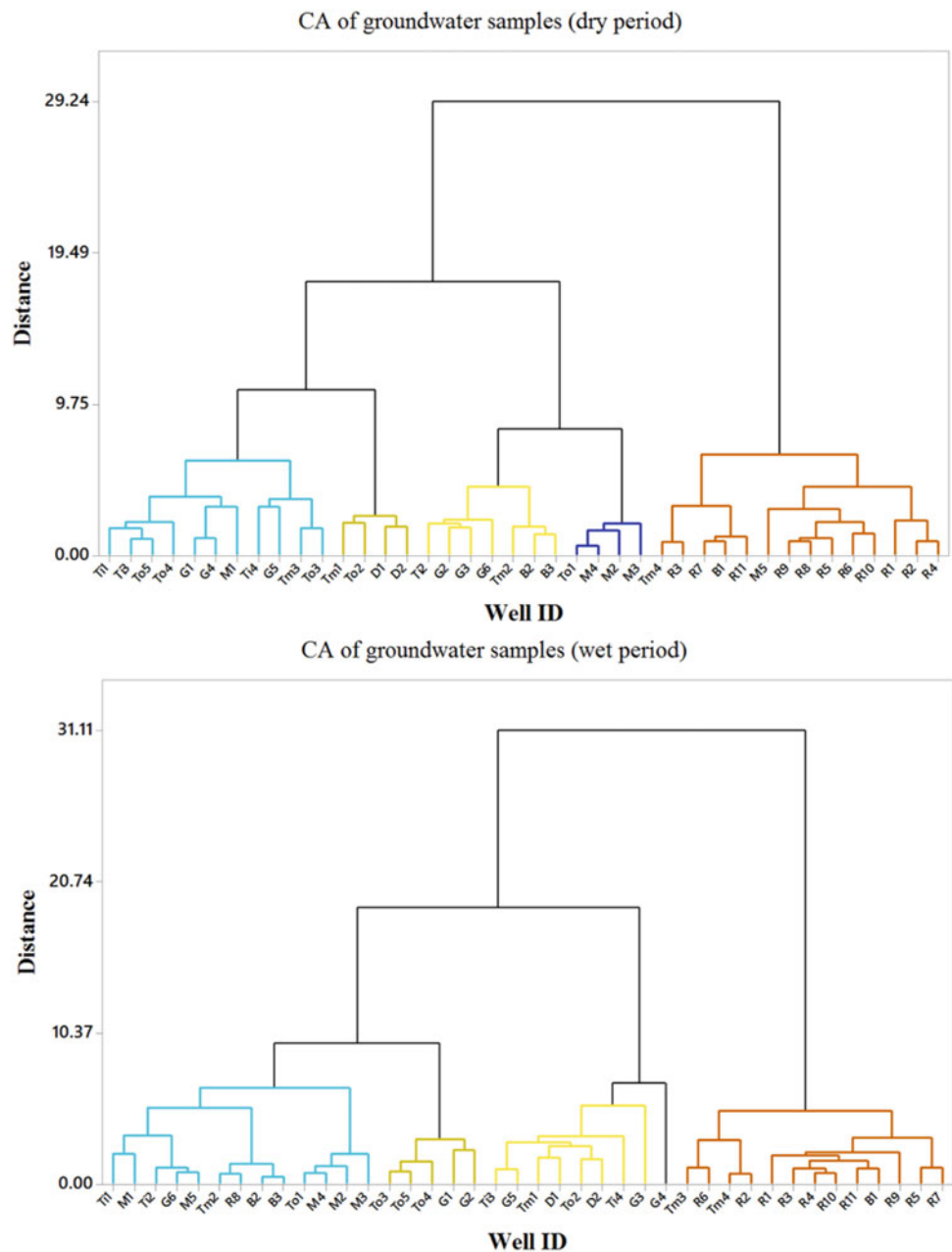
characterized by T samples, samples G1, G4, G5, and M1 are similar to these waters.

## 6 Conclusion

Although it is believed urbanization often results in the deterioration of groundwater quality, in the Behbahan aquifer, groundwater freshening could occur with reduction of EC,  $\text{SO}_4$ , Cl, and especially  $\text{NO}_3$  content. In the Behbahan aquifer urbanization, the quality of underlying unconfined aquifer is improved by making the recharge from urban wastewater and irrigation return flow. However, the recharge from urban wastewater leads to elevated levels of nitrate and probably pathogens in the residential areas. The hydrochemical evolution revealed that diminished EC and other dominant anion concentrations, as observed on their maps, are strongly influenced by recharge events resulting from urbanization.

The hydrochemical mappings illustrate their evolutions on the spatial scale, basically controlled by gypsum, and to some extent by halite dissolution, abnormal hydrochemical behavior is apparent in the middle parts of the plain due to the Marun irrigation network and urban areas of Behbahan City.

**Fig. 8** Dendrogram based on cluster analysis of hydrochemical parameters of Behbahan aquifer in the dry season (June, 2017)



The nitrate remains the major pollutant in the groundwater of the Behbahan plain, and high concentrations of this ion are due to the use of wastewater to irrigation networks and municipal wastewater. In the spatial scale, the main type of the nitrate pollution of groundwater is non-point or diffuse source, and it covers most parts of the plain, which is probably due to recharge from irrigation networks and the sewage from Behbahan City. The significant decreases of nitrate seem to be due to the denitrification in the extremely reduced environment beneath the Behbahan City.

Generally, the maximum concentrations of nitrate in the groundwater of the Behbahan plain are presented in urban areas and are higher than 45 mg/L. The fine-textured aquifer

materials, thin unsaturated zones, and direct infiltration of highly polluted urban wastewater lead to lower nitrate concentrations due to denitrification occurrence. The dissolution of gypsum was presented as the primary process of  $\text{SO}_4$  and Ca enrichment with EC values higher than 3000 micromohs/cm as this evaporate mineral is easily dissolved.

Cluster analysis based on both hydrochemical data identified the sources responsible for water samples and confirmed that in addition to geochemical process, the anthropogenic effect is another major source responsible for groundwater quality deterioration in Behbahan aquifer causing reduced  $\text{SO}_4$  and elevated  $\text{NO}_3$  concentrations.



## References

- Akhavan, G., Dobaradaran, S., & Borazjani, J. M. (2016). Data on fluoride concentration level in villages of Asara (Alborz, Iran) and daily fluoride intake based on drinking water consumption. *Data in Brief*, 9, 625–628.
- BaghalAsghari, F., Mohammadi, A. A., Aboosaedi, Z., Yaseri, M., & Yousefi, M. (2017). Data on fluoride concentration levels in cold and warm season in rural area of Shout (West Azerbaijan, Iran). *Data in Brief*, 15, 528–531.
- Battaleb-Looie, S., Moore, F., Malde, M. K., & Jacks, G. (2013). Fluoride in groundwater, dates and wheat: Estimated exposure dose in the population of Bushehr, Iran. *Journal of Food Composition and Analysis*, 29(2), 94–99.
- Bero, N. J., Ruark, M. D., & Lowery, B. (2016). Bromide and chloride tracer application to determine sufficiency of plot size and well depth placement to capture preferential flow and solute leaching. *Geoderma*, 262, 4–100.
- Biglari, H., Chavoshani, A., Javan, N., & Mahvi, A. H. (2016). Geochemical study of groundwater conditions with special emphasis on fluoride concentration, Iran. *Desalination and Water Treatment*, 57, 22392–22399.
- Bodrud-Doza, M., Bhuiyan, M. A. H., Didar-UI, S. M., Rahman, M. S., Haque, M. M., Fatema, K. J., et al. (2018). Hydrogeochemical investigation of groundwater in Dhaka City of Bangladesh using GIS and multivariate statistical techniques. *Groundwater for Sustainable Development*, 8, 226–244.
- Bottrell, S., Tellam, J., Bartlett, R., & Hughes, A. (2008). Isotopic composition of sulfate as a tracer of natural and anthropogenic influences on groundwater geochemistry in an urban sandstone aquifer, Birmingham, UK. *Applied Geochemistry*, 23(8), 2382–2394.
- Burow, K. R., Nolan, B. T., Rupert, M. G., & Dubrovsky, N. M. (2010). Nitrate in groundwater of the United States. *Environmental Science and Technology*, 44(13), 4988–4997.
- Choi, B. Y., Yun, S. T., Yu, S. Y., Lee, P. K., Park, S. S., Chae, G. T., & Mayer, B. (2005). Hydrochemistry of urban groundwater in Seoul South Korea: Effects of land-use and pollutant recharge. *Environmental Geology*, 48(8), 979–990.
- Colombani, N., Di Giuseppe, D., Kebede, S., & Mastrocicco, M. (2018). Assessment of the anthropogenic fluoride export in Addis Ababa urban environment (Ethiopia). *Journal of Geochemical Exploration*, 190, 390–399.
- Dehbandi, R., Moore, F., & Keshavarzi, B. (2018). Geochemical sources, hydrogeochemical behavior, and health risk assessment of fluoride in an endemic fluorosis area, central Iran. *Chemosphere*, 193, 763–776.
- Dehghani, M. H., Haghghat, G. A., & Yousefi, M. (2018). Data on fluoride concentration in drinking water resources in Iran: A case study of Fars province; Larestan region. *Data in Brief*, 19, 842–846.
- Emenike, C. P., Tenebe, I. T., & Jarvis, P. (2018). Fluoride contamination in groundwater sources in Southwestern Nigeria: Assessment using multivariate statistical approach and human health risk. *Ecotoxicology and Environmental Safety*, 156, 391–402.
- Enalou, H. B., Moore, F., Keshavarzi, B., & Zarei, M. (2018). Source apportionment and health risk assessment of fluoride in water resources, south of Fars province, Iran: Stable isotopes ( $\delta^{18}\text{O}$  and  $\delta\text{D}$ ) and geochemical modeling approaches. *Applied Geochemistry*, 98, 197–205.
- Fukada, T., Hiscock, K. M., & Dennis, P. F. (2004). A dual-isotope approach to the nitrogen hydrochemistry of an urban aquifer. *Applied Geochemistry*, 19(5), 709–719.
- Ghesquière, O., Walter, J., Chesnaux, R., & Rouleau, A. (2015). Scenarios of groundwater chemical evolution in a region of the Canadian Shield based on multivariate statistical analysis. *Journal of Hydrology: Regional Studies*, 4, 246–266.
- Gupta, R., & Misra, A. K. (2018). Groundwater quality analysis of quaternary aquifers in Jhajjar District, Haryana, India: Focus on groundwater fluoride and health implications. *Alexandria Engineering Journal*, 57(1), 375–381.
- Hildenbrand, Z. L., Carlton, D. D., Meik, J. M., Taylor, J. T., Fontenot, B. E., Walton, J. L., et al. (2017). A reconnaissance analysis of groundwater quality in the Eagle Ford shale region reveals two distinct bromide/chloride populations. *Science of the Total Environment*, 575, 672–680.
- Hosono, T., Siringan, F., Yamanaka, T., Umezawa, Y., Onodera, S., Nakano, T., & Taniguchi, M. (2010). Application of multi-isotope ratios to study the source and quality of urban groundwater in Metro Manila, Philippine. *Applied Geochemistry*, 25(6), 900–909.
- Karimi, A., Radfard, M., Abbasi, M., Naghizadeh, A., Biglari, H., Alvani, V., & Mahdavi, M. (2018). Fluoride concentration data in groundwater resources of Gonabad, Iran. *Data in Brief*, 21, 105–110.
- Khanoranga, S. K. (2018). An assessment of groundwater quality for irrigation and drinking purposes around brick kilns in three districts of Balochistan province, Pakistan, through water quality index and multivariate statistical approaches. *Journal of Geochemical Exploration*, 197, 14–26.
- Kshetrimayum, K. S., & Laxmi, T. (2017). A hydrogeochemical approach to evaluate the occurrence and source of salinization in the shallow aquifers of the southeastern Imphal valley in the Indo-Myanmar range of Northeast India. *Environment and Earth Science*, 76, 714.
- Kshetrimayum, K. S. (2015). Hydrochemical evaluation of shallow groundwater aquifers: A case study from a semiarid Himalayan foothill river basin, northwest India. *Environmental Earth Sciences*, 74, 7187–7200.
- Li, J., Zhou, H., Qian, K., Xie, X., Xue, X., Yang, Y., & Wang, Y. (2017). Fluoride and iodine enrichment in groundwater of North China Plain: Evidences from speciation analysis and geochemical modeling. *Science of the Total Environment*, 598, 239–248.
- Maurya, P., Kumari, R., & Mukherjee, S. (2018). Hydrochemistry in integration with stable isotopes ( $\delta^{18}\text{O}$  and  $\delta\text{D}$ ) to assess seawater intrusion in coastal aquifers of Kachchh district Gujarat, India. *Journal of Geochemical Exploration*, 196, 42–56.
- McKenna, J. J. E. (2003). An enhanced cluster analysis program with bootstrap significance testing for ecological community analysis. *Environmental Modelling and Software*, 18(3), 205–220.
- Monjerezi, M., Vogt, R. D., Aagaard, P., & Saka, J. D. K. (2011). Hydro-geochemical processes in an area with saline groundwater in lower Shire River valley, Malawi: An integrated application of hierarchical cluster and principal component analyses. *Applied Geochemistry*, 26, 1399–1413.
- Nair, I. S., Brindha, K., & Elango, L. (2016). Identification of salinization by bromide and fluoride concentration in coastal aquifers near Chennai, southern India. *Water Science*, 30(1), 41–50.
- Nandimandalam, J. R. (2012). Evaluation of hydrogeochemical processes in the Pleistocene aquifers of Middle Ganga Plain, Uttar Pradesh, India. *Environmental Earth Sciences*, 65, 1291–1308.
- Raj, D., & Shaji, E. (2017). Fluoride contamination in groundwater resources of Alleppey, Southern India. *Geoscience Frontiers*, 8(1), 117–124.
- Romero-Sierra, P., Rivas, D., Almazán-Becerril, A., & Hernández-, L. (2018). Hydrochemistry and hydrodynamics of a Mexican Caribbean Lagoon: Nichupté Lagoon System. *Estuarine, Coastal and Shelf Science*, 215(31), 185–198.
- Salcedo Sánchez, E. R., GarridoHoyos, S. E., Esteller, M. V., Martínez, M., & Ocampo, A. A. (2017). Hydrogeochemistry and water-rock



- interactions in the urban area of Puebla Valley aquifer (Mexico). *Journal of Geochemical Exploration*, 181, 219–235.
- Tam, V. T., & Nga, T. T. V. (2018). Assessment of urbanization impact on groundwater resources in Hanoi, Vietnam. *Journal of Environmental Management*, 227, 107–116.
- Wang, G. X., & Cheng, G. D. (2001). Fluoride distribution in water and the governing factors of environment in arid north-west China. *Journal of Arid Environments*, 49, 601–614.
- Wu, C., Wu, X., Qian, C., & Zhu, G. (2018). Hydrogeochemistry and groundwater quality assessment of high fluoride levels in the Yanchi Endorheic region, northwest China. *Applied Geochemistry*, 98, 404–417.
- Xiao, J., Jin, Z. D., Wang, J., & Zhang, F. (2015). Hydrochemical characteristics, controlling factors and solute sources of groundwater within the Tarim River Basin in the extreme arid region, NW Tibetan Plateau. *Quaternary International*, 1–10.
- Yidana, S. M., Bawoyobie, P., Sakyi, P., & Fynn, O. F. (2017). Evolutionary analysis of groundwater flow: Application of multivariate statistical analysis to hydrochemical data in the Densu Basin, Ghana. *Journal of African Earth Sciences*, 138, 167–176.
- Zereg, S., Boudoukha, A., & Benaabidate, L. (2018). Impacts of natural conditions and anthropogenic activities on groundwater quality in Tebessa plain, Algeria. *Sustainable Environment Research*, 28, 340–349.
- Zhang, Q., Wang, H., & Wang, L. (2018). Tracing nitrate pollution sources and transformations in the over-exploited groundwater region of north China using stable isotopes. *Journal of Contaminant Hydrology*, 218, 1–9.



# Aquifer Characteristics and Evidence of Saltwater Intrusion in Coastal Groundwater of Niger Delta (Nigeria) Based on Historical and Recent Data

Aniekan Edet 

## Abstract

The economic expansion of Niger Delta region depends on groundwater resource for various uses. Therefore, there is need for an understanding of the hydrogeological and hydrochemical characteristics as an integral for management of the resource. Hence, this study was aimed at delineating areas of saltwater intrusion in the area. Geological and hydrogeological data were used to delineate two aquifers: alluvial aquifer (upper designated as A and lower designated as B) and a coastal plain aquifer (designated as C). Groundwater in the area was classified as fresh ( $<1500 \mu\text{S}/\text{cm}$ ), brackish ( $1500\text{--}3000 \mu\text{S}/\text{cm}$ ), and saline ( $>3000 \mu\text{S}/\text{cm}$ ). Among the groundwater samples ( $n = 105$ ), 95% from A, B, and C were classified as fresh, while 2 and 3% of the samples from A were classified as brackish and saline, respectively. The main groundwater facies were Na–Cl, Mg–Cl, and Na–HCO<sub>3</sub> respectively, for A, B, and C aquifers. The enrichment of Na<sup>+</sup> and Cl<sup>-</sup>, freshwater–seawater mixing ratio, cross plots, and classifications by means of different schemes indicated that seawater intrusion was occurring in the A aquifer. In terms of drinking and irrigation use, the A aquifer water is of poor quality relative to the groundwater from B and C aquifers. The study highlights the potential danger of contaminated groundwater in the coastal areas occupied by low income dwellers. Hence, seawater intrusion should be continuously monitored for sustainable development and management of groundwater in coastal areas.

## Keywords

Coastal aquifer • Contamination • Saltwater • Niger Delta • Nigeria

## 1 Introduction

Niger Delta Region is one of the major petroleum-bearing basins of the world. In this area, groundwater is the major source of water for most drinking, domestic, agricultural, and industrial uses. However, the quantity and quality of groundwater have been affected by natural and human-induced activities associated with rapid development in terms of urbanization and industrialization. In coastal regions like the Niger Delta, salinization is one of the major problems due to over exploitation (Khaska et al., 2013; Anders et al., 2014; Yolcubal et al., 2019). Besides over pumping, other sources and processes which may contribute to salinization of groundwater in coastal regions have been documented in previous studies. Some of these include leakage of saline water trapped in silty and clayey layers (Walter et al., 2017), domestic and industrial effluents, polluted surface water (Fakir et al., 2002; Sanchez-Martos et al., 2002; Carwright et al., 2004; Ghabayen et al., 2006), and discharge from oil and oil-related companies in the Niger Delta Region (Edet, 2005, 2006, 2008, 2009). The Niger Delta Region, which is one of the topmost wetlands in the world, is located in the south most end of Nigeria, sharing a boundary with the Atlantic Ocean in the south. Urban and rural settlements and factories are widespread in the area which host different oil and oil-related industrial facilities mainly flow stations, oil terminals, gas plants, petrochemicals, refineries, liquefied natural gas, fertilizers, etc. These facilities require groundwater for their daily activities, and this is achieved through pumping groundwater.

## Electronic supplementary material

The online version of this chapter ([https://doi.org/10.1007/978-3-030-67028-3\\_29](https://doi.org/10.1007/978-3-030-67028-3_29)) contains supplementary material, which is available to authorized users.

A. Edet (✉)

Department of Geology, University of Calabar, Calabar, Nigeria  
e-mail: [aniekanedet@yahoo.com](mailto:aniekanedet@yahoo.com)

Several methods have been used to elucidate seawater intrusion into coastal aquifers, for example, parameters such as electrical conductivity (EC), total dissolved solids (TDS), sodium, chloride, and bromide are used as markers of seawater influence (Sukhija et al., 1996; Capaccioni et al., 2005; de Montety et al., 1996). Also ionic ratios ( $\text{Na}/\text{Cl}$ ,  $\text{Cl}/\text{HCO}_3$ ,  $\text{Ca}/\text{Na}$ ,  $\text{Br}/\text{Cl}$ ,  $\text{Ca}/\text{Cl}$ ,  $\text{Mg}/\text{Cl}$ ,  $\text{SO}_4/\text{Cl}$ ,  $\text{Ca}/\text{HCO}_3 + \text{SO}_4$ ), seawater mixing ratios, trace elements, and isotopes have been applied to evaluate the degree of saltwater intrusion into freshwater aquifer (Edet & Okereke, 2001; Barbecot et al., 2000; Vengosh et al., 2002; Cartwright et al., 2004; Faye et al., 2005; Walraevens et al., 2005; El Moujabber et al., 2006; Ghabayen et al., 2006; de Montety et al., 2008; Park et al., 2012; Wang & Jiao, 2012; Khaska et al., 2013; Giambastiani et al., 2013; Anders et al., 2014; Abdalla, 2016; Yolcubal et al., 2019). The existence of other processes such as rock weathering, cation exchange, and human activities tends to mask distinguishing salinization process and requires other methods of assessment. Hence, this study applies several tools to determine the degree of groundwater pollution in coastal aquifers due mainly to natural sea water intrusion process and anthropogenic activities.

Most of the available literature on the geology and hydrogeology of the area are localized in scope. Such studies include identification and characterization of the aquifers (Etu-Efeotor and Akpokoje, 1990; Etu-Efeotor, 2000), documentation of aquifer parameters from drilling records (Offodile, 2014), water supply problem (Etu-Efeotor and

Odigi, 1983), quality status of groundwater (Etu-Efeotor, 1981; Edet, 1993; Ofoma et al., 2005; Udom & Amah, 2006; Udom et al., 1998, 1999; Esu & Amah, 1999; Onwuka & Omonona, 2017), and seawater intrusion (Amadi et al., 1989; Amadi & Amadi, 1990; Edet & Okereke, 2001, Edet, 2008, 2017, 2018; Edet & Worden, 2009; Edet et al., 2003, 2012). This study is therefore a conglomeration of historical and recent data to unravel and further contribute to the current situation of groundwater for sustainable development of the Niger Delta Basin. The objectives of the present study are (i) to further delineate and characterize the different aquifers in area, (ii) to determine the major ion chemistry of groundwater and delineate areas of saltwater intrusion using different approaches, and (iii) to assess the groundwater suitability for drinking and agricultural use.

## 2 Study Area Description

The study area is located in southern parts of Nigeria and is roughly bounded by latitudes  $4^\circ 20' - 5^\circ 20'$  North and longitudes  $5^\circ 30' - 8^\circ 00'$  East (Fig. 1). The area experiences tropical climate with distinct wet and dry seasons. The basin is characterized by high temperatures and rainfall. The temperature range is  $21 - 43^\circ$ , and the average annual rainfall is about 2500 mm. The average annual rainfall exceeds 3500 mm along the coast and decreases to about 2000 mm inland (Akpokoje, 1987).

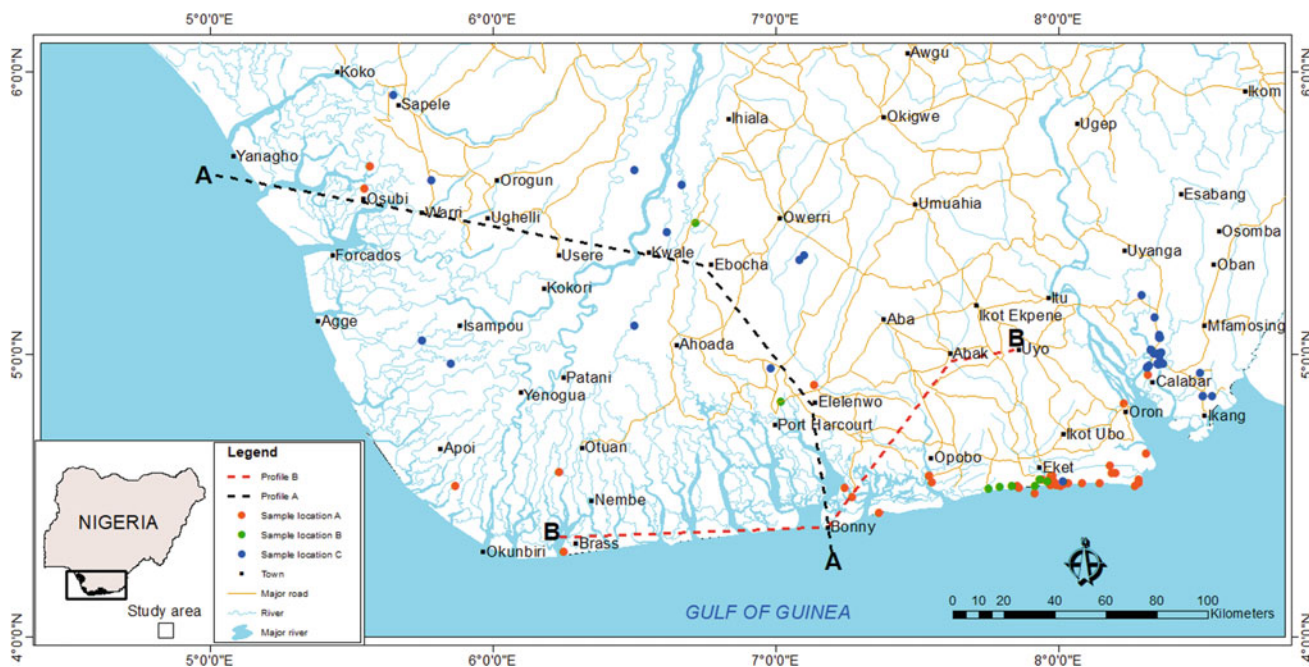


**Fig. 1** Regional map of Niger Delta including sample locations (dashed lines A-A and B-B, show lines of hydrogeological profiles for Figs. 2a and 2b)

The geomorphology and geology of the Niger Delta have been described in details by various authors (Allen, 1965a, b; Akpokoje, 1987; Reyment, 1965; Short & Stauble, 1967; Weber, 1971; Murat, 1972; Kogbe, 1976; Petters, 1982; Whiteman, 1982; Wright, 1989). The formation of the present Niger Delta started during Early Paleocene, and it resulted from the buildup of fine grained sediments eroded and transported by river Niger and its tributaries. The subsurface geology consists of three lithostratigraphic units: Akata, Agbada, and Benin Formations. These formations are overlain by Quaternary deposits. The Benin Formation which underlies the study area is composed of sand of various varieties with intercalations of clay and silts (Allen, 1965a; b). The Quaternary deposits generally consist of alternating sequences of gravel, sand, silt, and clay (Etu-Efeotor & Akpokoje, 1990). Hydrogeology of the Niger Delta Basin has been studied by several workers. Etu-Efeotor and Akpokoje (1990) gave a detailed stratigraphic analysis of the various geomorphological and geologic units in order to delineate local and regional aquifers in the basin, while Etu-Efeotor (2000) studied the hydraulic properties of the subsurface materials in different wells and identified four aquiferous horizons. Recent work in the area is mainly localized on dynamics of static water level (Nghah & Nwankwoala, 2013), estimation of porosity and hydraulic conductivity (Okiongbo & Soronnadi-Ononiwu, 2015; George et al., 2017), groundwater potential and aquifer protective capacity (Rasaq, 2017), and groundwater quality assessment (Ejoro et al., 2015; Nwankwoala & Nghah, 2014).

### 3 Materials, Methods, and Data Handling

#### 3.1 Geological and Hydrogeological Data Acquisition

Geological data were collected from existing records and those acquired during the duration of this study. The data were geological and hydrogeological information such as lithology, depth of wells and boreholes, water levels, and aquifer characteristics. Field surveys were conducted at various times to study the surficial geology, measure groundwater levels, and collect groundwater samples for chemical analyses. Groundwater level monitoring was undertaken at some locations within the study area across different seasons and tidal changes using existing hand-dug wells.

Lithological logs were used to draw hydrogeological cross sections and estimate the storage capacity of the aquifers as area  $\times$  depth  $\times$  porosity. The porosity of the aquifers was assumed to be 23% (George et al., 2017).

Recharge (R) to the aquifers was estimated from rainfall data by means of chloride mass balance (CMB) method (Wood & Sandford, 1995) as:

$$R = \text{rainfall amount} \times \text{Cl}_p / \text{Cl}_{\text{gw}} \quad (1)$$

where  $\text{Cl}_p$  and  $\text{Cl}_{\text{gw}}$  are chloride concentrations in precipitation and groundwater, respectively.

#### 3.2 Groundwater Sampling and Analysis

A total of 105 groundwater samples were collected between 1990 and 2018 from monitoring wells, hand-dug wells, and boreholes for physicochemical parameters' determinations and assessment. The locations of the sampling points are presented as Table 1. Temperature, pH, electrical conductivity (EC), total dissolved solids (TDS), and dissolved oxygen (DO) were measured in the field using standard equipment. Groundwater samples were collected in polyethylene bottles, which were soaked in  $\text{HNO}_3$  for 24 hr and rinsed several times prior to use. At the sampling sites, the bottles were rinsed with the water to be sampled prior to filling the bottles with the samples. The samples were filtered through 0.45  $\mu\text{m}$  membrane filters into sterilized polyethylene bottles. Samples collected for major ions analysis were preserved by acidifying with  $\text{HNO}_3$  to achieve a pH of  $\leq 2$ . The samples were kept at 4  $^\circ\text{C}$  in laboratory prior to analyses.

The samples were analyzed at various times for major cations (Na, K, Ca, Mg) and anions ( $\text{Cl}$ ,  $\text{SO}_4$ ,  $\text{NO}_3$ ) using ion chromatograph (Dionex Dx-120) at the Institute of Geosciences, University of Tuebingen (Germany) and Thermo Scientific X Series 2 high-resolution ICP-MS, Ion Chromatography Metrohm 872 Extension Module, and Ion Chromatography Metrohm 881 Extension Module at the Department of Hydrogeology, TU Bergakademie, Freiberg (Germany). Bicarbonate was estimated by titration with  $\text{H}_2\text{SO}_4$  standard solution using methyl orange as indicator at the Institute of Oceanography, University of Calabar (Nigeria).

#### 3.3 Seawater Contamination Assessment

The Niger Delta Basin is in direct contact with the Atlantic Ocean; hence, it was necessary to access the level of sea water intrusion into the freshwater system. The sea water fraction in groundwater was estimated using chloride concentration since chloride has been considered as a conservative tracer, not affected by ion exchange (Custodio, 1987) and calculated as follows (Appelo & Postma, 1999):

$$f_{\text{sea}} = \text{C}_{\text{clsample}} - \text{C}_{\text{clfresh}} / \text{Cl}_{\text{clsea}} - \text{Cl}_{\text{clfresh}} \quad (2)$$

where  $\text{C}_{\text{clsample}}$  is  $\text{Cl}^-$  concentration in sample,  $\text{C}_{\text{clfresh}}$  is  $\text{Cl}^-$  concentration in freshwater, and  $\text{Cl}_{\text{clsea}}$   $\text{Cl}^-$  concentration in seawater.

**Table 1** Historical and recent groundwater sample locations in Niger delta

No	Code	North	East	Data type	Source <sup>a</sup>	No	Code	North	East	Data type	Source <sup>a</sup>
1	1A	4° 50.00	5° 40.00	HD	1	54	54B	4° 32.10	7° 50.02	HD	1
2	2A	4° 18.00	6° 15.00	HD	1	55	55B	4° 31.85	7° 47.47	HD	1
3	3A	4° 32.00	5° 52.00	HD	1	56	56B	4° 31.38	7° 45.25	HD	1
4	4A	5° 40.00	5° 34.01	HD	1	57	57B	4° 50.00	7° 01.01	HD	1
5	5A	5° 34.01	5° 33.00	HD	1	58	58B	5° 28.01	6° 43.00	HD	1
6	6A	5° 22.01	5° 13.00	HD	1	59	59C	5° 26.01	6° 37.00	HD	1
7	7A	4° 35.00	6° 14.00	HD	1	60	60C	5° 06.00	6° 30.00	HD	1
8	8A	4° 26.37	7° 22.00	HD	1	61	61C	4° 58.01	5° 51.00	HD	1
9	9A	4° 32.60	8° 02.00	HD	1	62	62C	5° 39.07	6° 30.00	HD	1
10	10A	4° 30.50	7° 55.00	HD	1	63	63C	5° 20.01	7° 05.09	HD	1
11	11A	4° 33.05	7° 59.00	HD	1	64	64C	5° 36.07	6° 40.00	HD	1
12	12A	4° 31.70	7° 51.69	HD	1	65	65C	5° 37.00	5° 47.00	HD	1
13	13A	4° 32.15	7° 51.19	HD	1	66	66C	5° 03.00	5° 45.00	HD	1
14	14A	4° 34.07	7° 58.31	HD	1	67	67C	5° 55.01	5° 38.89	HD	1
15	15A	4° 33.44	7° 56.49	HD	1	68	68C	5° 21.01	7° 06.00	HD	1
16	16A	4° 32.87	7° 59.09	HD	1	69	69C	4° 57.00	6° 59.00	HD	1
17	17A	4° 32.40	7° 59.10	HD	1	70	70C	4° 33.08	8° 00.86	HD	1
18	18A	4° 34.81	8° 11.32	HD	1	71	71C	5° 07.86	8° 20.32	HD	3
19	19A	4° 34.84	8° 12.20	HD	1	72	72C	4° 57.20	8° 18.77	HD	4
20	20A	4° 36.44	8° 11.02	HD	1	73	73C	4° 57.23	8° 18.73	HD	4
21	21A	4° 33.41	8° 16.96	HD	1	74	74C	4° 57.26	8° 18.79	HD	4
22	22A	4° 32.55	8° 17.12	HD	1	75	75C	4° 57.19	8° 18.75	HD	4
23	23A	4° 32.76	8° 17.02	HD	1	76	76C	4° 58.09	8° 22.09	HD	4
24	24A	4° 31.68	7° 14.65	HD	1	77	77C	4° 58.07	8° 22.04	HD	4
25	25A	4° 29.62	7° 16.22	HD	1	78	78C	4° 58.06	8° 22.06	HD	4
26	26A	4° 19.57	7° 17.21	HD	1	79	79C	4° 58.04	8° 22.01	HD	4
27	27A	4° 53.56	7° 08.27	HD	1	80	80C	5° 00.39	8° 21.66	HD	4
28	28A	4° 32.11	8° 16.16	HD	2	81	81C	5° 00.45	8° 21.65	HD	4
29	29A	4° 32.17	7° 58.35	HD	2	82	82C	5° 00.35	8° 21.61	HD	4
30	30A	4° 32.49	7° 59.53	HD	2	83	83C	5° 00.31	8° 21.60	HD	4
31	31A	4° 34.21	7° 32.52	HD	2	84	84C	5° 01.01	8° 19.54	HD	4
32	32A	4° 34.04	7° 58.40	HD	2	85	85C	5° 01.05	8° 19.51	HD	4
33	33A	4° 32.25	7° 59.55	HD	2	86	86C	5° 01.07	8° 19.53	HD	4
34	34A	4° 32.17	7° 58.35	HD	2	87	87C	5° 01.09	8° 19.58	HD	4
35	35A	4° 34.21	7° 32.52	HD	2	88	88C	4° 57 36	8° 19 15	RD	6
36	36A	4° 32.50	8° 01.01	HD	2	89	89C	5° 04 03	8° 21 18	RD	6
37	37A	4° 32.07	8° 00.48	HD	2	90	90C	5° 00 11	8° 20 04	RD	6
38	38A	4° 32.80	8° 01.07	HD	2	91	91C	4° 57 52	8° 21 14	RD	6
39	39A	4° 32.65	8° 08.69	HD	2	92	92C	4° 58 38	8° 21 34	RD	6
40	40A	4° 32.69	8° 04.94	HD	2	93	93C	5° 03 53	8° 21 51	RD	6
41	41A	4° 38.94	8° 18.65	HD	2	94	94C	5° 03 78	8° 21 45	RD	6
42	42A	4° 49.61	8° 13.89	HD	2	95	95C	5° 03 51	8° 21 33	RD	6
43	43A	4° 33.10	7° 58.30	HD	2	96	96C	5° 00.13	8° 20.94	RD	6
44	44A	4° 32.76	7° 59.04	HD	2	97	97C	4° 59.95	8° 20.92	RD	6

(continued)



**Table 1** (continued)

No	Code	North	East	Data type	Source <sup>a</sup>	No	Code	North	East	Data type	Source <sup>a</sup>
45	45A	4° 32.91	7° 33.11	HD	2	98	98C	5° 00.05	8° 21.23	RD	6
46	46A	4° 33.43	7° 56.43	HD	2	99	99C	5° 00.02	8° 21.59	RD	6
47	47A	4° 34.16	7° 58.65	HD	2	100	100C	4° 51.18	8° 30.69	RD	6
48	48A	4° 34.03	7° 58.26	HD	2	101	101C	4° 51.22	8° 30.65	RD	6
49	49A	4° 55.64	8° 18.99	HD	3	102	102C	4° 56.11	8° 30.02	RD	6
50	50A	4° 32.50	7° 58.60	HD	1	103	103C	4° 51.14	8° 32.50	RD	6
51	51B	4° 33.50	7° 56.00	HD	1	104	104C	4° 58.04	8° 21.05	HD	5
52	52B	4° 33.10	7° 57.49	HD	1	105	105C	5° 12.52	8° 17.67	RD	6
53	53B	4° 32.09	7° 55.03	HD	1						

Upper alluvial aquifer (code A, SCW), Lower alluvial aquifer (code B, DCW) and coastal plain aquifer (code C, DIW)

<sup>a</sup>1 Edet (2008), 2 Edet (2017), 3 Edet (2018), 4 Edet and Worden (2009), 5 Edet et al (2003), 6 Recent data Recent data (RD) and HD (Historical data)

The  $f_{sea}$  is used to calculate the theoretical concentration of each cation resulting from conservative mixing of seawater and freshwater using the following formula:

$$C_{imix} = f_{sea} \times C_{isea} + (1 - f_{sea}) \times C_{ifresh} \quad (3)$$

where  $C_{i\ mix}$  is conservative mixing,  $C_{i\ sea}$  is concentration of cation in seawater, and  $C_{i\ fresh}$  is concentration of cations in freshwater. For each cation, the difference between the concentration of conservative mixing ( $C_{i\ mix}$ ) and measured concentration of the cation simply represents the change in concentration (delta,  $\Delta$ ), resulting from any chemical reaction occurring with mixing (Fidelibus, 2003; Zghibi et al., 2013):

$$\Delta C_i = C_{isample} - C_{imix} \quad (4)$$

When  $\Delta C_i$  is positive, groundwater is enriched for that particular ion  $i$ , whereas a negative value indicates depletion compared to theoretical mixing (Appelo & Postma, 1999; Anderson et al., 2005; Slama, 2010).

### 3.4 Geochemical Classification of Groundwater

#### 3.4.1 Chloride and Bicarbonate

Revelle (1941) and Krishnakumar et al. (2014) used the ratio of  $Cl^-/HCO_3^-$  to classify the effect of seawater on fresh groundwater system. The classification is as follows: <0.5 (not affected by sea water); 0.5–6.6 (slightly/moderately affected by sea water), and >6.6 (strongly affected by sea water).

#### 3.4.2 Chloride-Nitrate Classification

The groundwater samples were classified into four groups using concentrations of chloride and nitrate which, respectively, reflect the influences of sea water and human activities (Cardona et al., 2004). This was done by obtaining threshold values of  $Cl^-$  and  $NO_3^-$  from the inflection points of cumulative frequency distribution plots (Sinclair, 1974, 1976).

#### 3.4.3 Stuyfzand Classification

Groundwater classification by Stuyfzand (1986, 1993) method involves four levels: primary, type, subtype, and class (Table 2). The primary type is based on chloride content; type is determined on the basis of hardness, while classification into subtypes is based on dominant cations and anions (facies). Lastly, the class is determined on the basis of  $Na^+ + K^+ + Mg^{2+}$  (meq/l) corrected for sea water contribution according to the formula:

$$Na^+ + K^+ + Mg_{corrected}^{2+} = Na^+ + K^+ + Mg_{measured}^{2+} - 1.061 Cl^- \text{ (meq/l)} \quad (5)$$

The parameter is tested against  $\sqrt{0.5}Cl^-$  as a margin of error in order to arrive at a meaningful positive (marine cation surplus, positive cation code), negative (marine cation deficit; negative cation exchange code), or equilibrium value (cation exchange code  $\emptyset$ ). Mtoni et al. (2013), further added that, the classification allows for the recognition of cation exchange.

## 4 Results and Discussion

### 4.1 Aquifer Framework, Characteristics and Recharge

Groundwater occurs in the Niger Delta Basin in two main aquifers, an upper unconfined shallow aquifer, designated as

**Table 2** Stuyfzand Classification parameters

Classification	Parameter	Description	Code
Main type	Cl <sup>-</sup> (mg/l)	< 150	Fresh (F)
		150–300	Fresh-Brackish (Fb)
		300–1,000	Brackish (B)
		1,000–10,000	Brackish salt (Bs)
		> 10,000	Salt (S)
Type	Total hardness (mmol/l)	0–0.5	Very soft (*)
		0.5–1	Soft (0)
		1–2	Moderately hard (1)
		2–4	Hard (2)
		4–8	Very hard (3)
		8–16	Extremely hard (4)
		16–32	Extremely hard (5)
		32–64	Extremely hard (6)
		64–128	Extremely hard (7)
Class	[Na <sup>+</sup> + K <sup>+</sup> + Mg <sup>2+</sup> ] (meq/l)	(Na <sup>+</sup> + K <sup>+</sup> + Mg <sup>2+</sup> ) <sub>corrected</sub> > $\sqrt{I}/2Cl^{-}$	+
	corrected for seawater contribution	$(-\sqrt{I}/2Cl^{-}) \leq (Na^{+} + K^{+} + Mg^{2+})_{corrected} \leq \sqrt{I}/2Cl^{-}$	∅
		(Na <sup>+</sup> + K <sup>+</sup> + Mg <sup>2+</sup> ) <sub>corrected</sub> < $-\sqrt{I}/2Cl^{-}$	-

alluvial aquifer, and a lower unconfined to semi-confined deep aquifer, designated as coastal plain aquifer. The alluvial aquifer dominates the coastal area, while the coastal plain characterizes the inland area. Upper parts of the alluvial aquifer are harnessed through hand-dug wells, (designated as A) and the lower parts through shallow boreholes (designated as B), while the coastal aquifer is harnessed through deep boreholes (designated as C).

The alluvial aquifer is at a depth of generally <30 m. It is composed of clayey sand to sand with varying proportions of silt and gravel. The aquifer is found within the alluvial deposits, especially within the coastal areas and ranges in thickness from < 0 to 30 m (Fig. 2a). Water levels vary between 0.75 and 15.0 m with an average value of 4.28 m. The aquifer is limited in lateral extent due to clay/shale intercalations. The hydraulic conductivities of shallow aquifer estimated from grain size distribution curve using Hazen's method (Fetters, 2001; Al-Shaibani, 2008) and pumping test data, ranged between 0.001 and 68 m/day with an average value of 11.02 m/day. The average transmissivity value was 259.7 m<sup>2</sup>/day with range of 204.5–315 m<sup>2</sup>/day. Specific yield values varied from 108 to 432 m<sup>3</sup>/hr/m (average 214.8 m<sup>3</sup>/hr/m). The estimated volume of storage for the alluvial aquifer is about 29 M m<sup>3</sup> based on data on

Table 3. Abstraction of water from this aquifer is through hand-dug wells and shallow boreholes.

The coastal plain aquifer is the main aquifer within the Niger Delta Basin. The aquifer serves as the main source of water for the entire area, and abstraction is through shallow and deep boreholes. The aquifer occurs at depth >30 m with thickness reaching >150 m (Fig. 2b). The aquifer is characterized by sand, gravelly sand, and gravel with intercalations of clay/shale and silt. Static water level varies between 2.9 and 21.0 m with a mean 8.4 m below the ground surface. For this aquifer, the specific yield is in the range 10.5–1404 m<sup>3</sup>/hr/m with average value of 216.8 m<sup>3</sup>/hr/m (Offodile, 2014). Transmissivities of the aquifer varied between 154.5 and 6500 m<sup>2</sup>/day with average of 1227.0 m<sup>2</sup>/day, and well discharge ranged between 1392 and 7200 m<sup>3</sup>/day with an average of 3345 m<sup>3</sup>/day. Hydraulic conductivities of the coastal plain aquifer ranged between 1.4 and 75.0 m/day averaging 16.2 m/day. The estimated volume of storage for the coastal aquifer is about 1304 M m<sup>3</sup> using data in Table 3.

The groundwater level contour map shown on Fig. 3 summarizes the distribution of piezometric head in the aquifer system within the Niger Delta Basin. The general groundwater flow is north–south with variations in north–east–southwest and northwest–southeast directions under

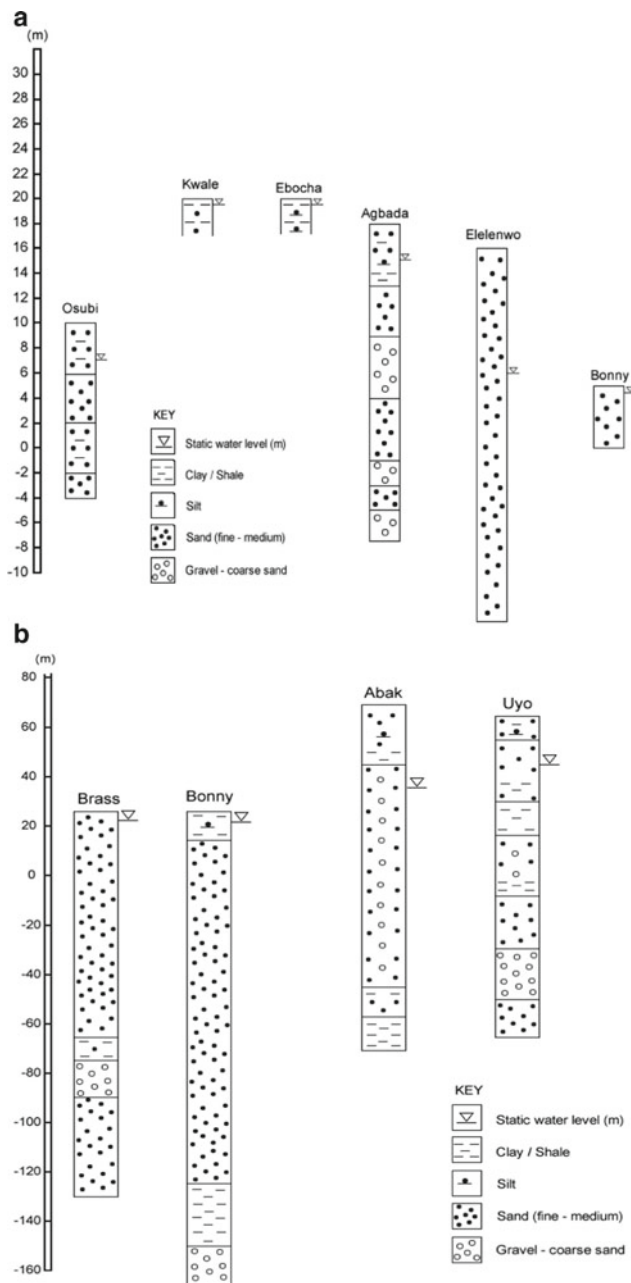


**Fig. 2** a Hydrogeological profile across alluvial aquifer, b Hydrogeological profile across coastal plain aquifer

hydraulic gradient of 0.00007–0.00104. Detailed groundwater level measurements within the shallow aquifer at six locations (8A, 31A, 42A, 49A, 63C, and 69C, Table 1) indicate fall in static water level with respect to the ground level (SWLwrtgl) by about 4.50 m on the average in dry season and corresponding increase in wet season by an average of 3.50 m. Change ( $\Delta$ SWL) in water level between wet (May–October) and dry (November–April) seasons varied between 0.40 and 2.70 m (average 1.00). Also, local monitoring at three locations (4A, 6A, and 7A, Table 1)

indicated SWLwrtgl at low tide varied from 0.25 to 2.00 m with an average of 0.91 m, while at high tide, SWLwrtgl varied from 0.14 to 1.75 m with an average of 0.74 m. The change in water levels between low and high tides ranged between 0.11 and 0.25 m with an average of 0.18 m. This is due to shallow water level (<1.0 m) and porous alluvial materials. These variations in water levels during different seasons and tidal changes are the main form of recharge mechanism in the basin.

Chloride mass balance (Eq. 1) was used to estimate the recharge in the area. The input data for this estimation are given in Table 3. In the area, chloride concentration in groundwater increases toward the coast with average values varying from 272.9 mg/l in A (coastal area) through 66.9 mg/l in B (between the coastal and inland area) to 21.9 for C (inland area). From CMB, the recharge estimate for the area varied from 6 mm through 15–25 mm representing 0.2, 0.6, and 1.25% of precipitation, respectively, for areas A, B, and C.

## 4.2 Groundwater Chemistry and Quality

Detailed and average values of the various physicochemical constituents for all and the different aquifers are presented in Table 4 and Online Resource 1.

### 4.2.1 General Physicochemical Composition of Niger Delta Basin

The electrical conductivity (EC) of the groundwater ranged from 16.28 to 21,583  $\mu$ S/cm. Ten percent of all the groundwater samples exceeds the WHO (2004, 2006) maximum limit for drinking water for in respect of EC, suggesting influence of sea water. According to electrical conductivity (EC) levels (Rai, 2004; Mondal et al., 2010), groundwater was classified as fresh (<1500  $\mu$ S/cm), brackish (1500–3000  $\mu$ S/cm), and saline (>3000  $\mu$ S/cm). Among the groundwater samples ( $n = 105$ ), 95% from A, B, and C were classified as fresh, while 2 and 3% of the samples from A were classified as brackish and saline, respectively. The water is acidic to alkaline in nature, with pH values ranging from 3.72 to 8.5. Sixty-five percent of all the groundwater samples were not within the WHO (1993,2004) range of 6.5–8.5 for drinking water. Dissolved oxygen (DO) concentration varied from 1.19 to 10.7 mg/l. Low DO value (<5.0 mg/l) for 54% of the groundwater samples is attributed to high organic matter.  $\text{Na}^+$  is the dominant cation. It ranged from 0.06 mg/l in the coastal plain aquifer (sample 67C) to 1280.80 mg/l in the upper alluvial aquifer (sample 17A). This represents an average of 52% of all the cations. Six out of 105 samples representing about 6% of all the samples are higher than the WHO (1993) maximum permissible of 200 mg/l for  $\text{Na}^+$  in drinking water.  $\text{Ca}^{2+}$  ranged between

**Table 3** Details of Parameters used for computation of aquifer storage capacity and estimation of recharge through Chloride Mass Balance Method

Area	Aquifer	Total area km <sup>2</sup>	Area considered for capacity km <sup>2</sup>	Average thickness km	Average porosity %	Source of groundwater	Designation	P mm	Cl <sub>p</sub> mg/l	Cl <sub>gw</sub> <sup>a</sup> mg/l
Coastal	Upper alluvial	7,000	4,200	0.03	23	Handug well	A	3500	0.5	272.9
	Lower alluvial					Shallow borehole	B	2750	0.4	66.9
Inland	Coastal sand	63,000	37,800	0.15	23	Deep borehole	C	2000	0.3	21.9

<sup>a</sup>See Table 4

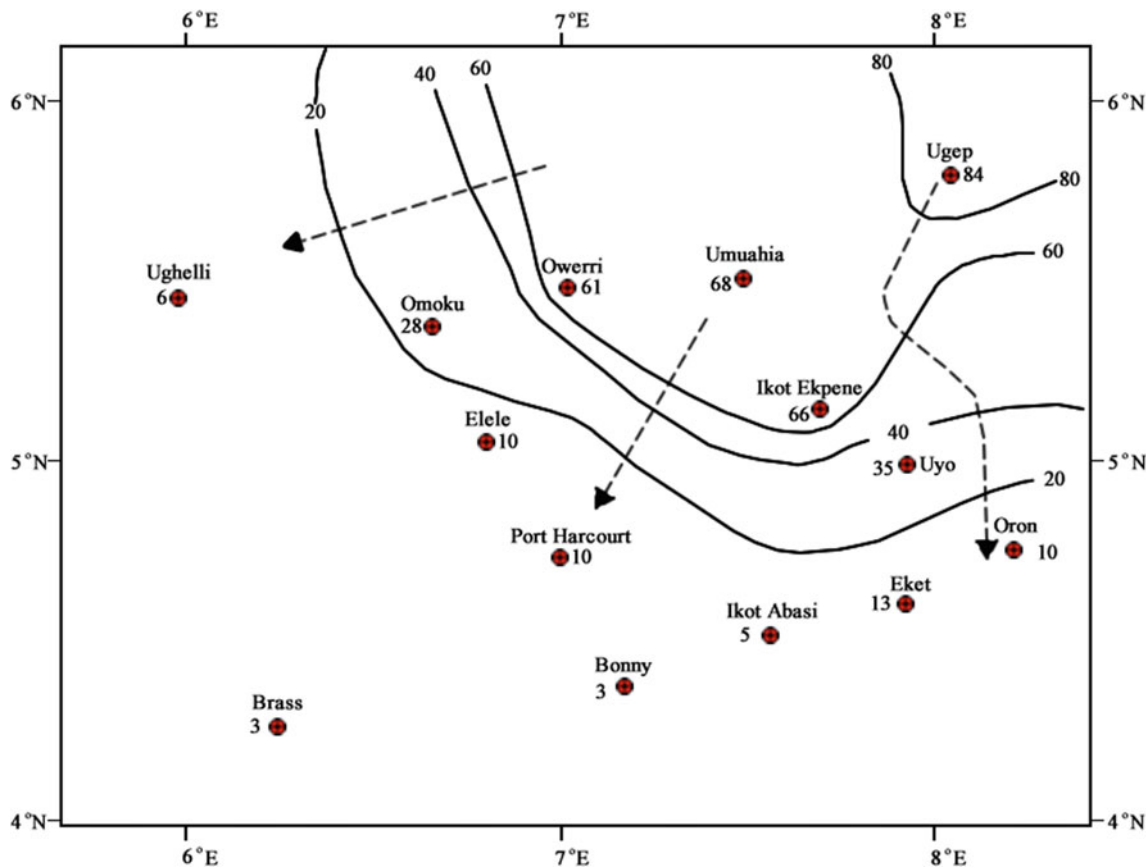


**Fig. 3** Regional groundwater flow map of the Niger Delta (Updated and modified from Edet, 2008)

0.01 (82C & 83C) and 520.3 mg/l (25A), while Mg<sup>2+</sup> varied from 0.01 (86C) to 230.7 (17A) mg/l. These average values represents 21.8 and 20.5% of the total cations for Ca<sup>2+</sup> and Mg<sup>2+</sup>, respectively, in the groundwater samples. However, 4 and 5% of Ca<sup>2+</sup> and Mg<sup>2+</sup> exceed the WHO (1993) maximum limit for drinking water. K<sup>+</sup> concentrations represent on the average 5.7% of the total cations in groundwater samples. The concentration of K<sup>+</sup> ranged from 0.01 (55B) to 159.6 (25A) mg/l. Concentration of Cl<sup>-</sup> varied from 0.32 (sample 80C) to 2670 (sample 17A) mg/l with 11% of the groundwater samples exceeding the WHO maximum limit of

250 mg/l. Bicarbonate concentrations ranged from 0.2 (67C) to 787.2 (25A) mg/l. 2% of the groundwater samples exceeds the WHO limit (2004) of 600 mg/l. SO<sub>4</sub><sup>2-</sup> concentrations ranged from 0 (79C, 80C, 81C, 82C, 83C, 84C, 85C, 86C, 87C, 88C, 89C, 91C, 92C, 96C, 97C, 98C, and 99C) to 968.9 (24A) mg/l. Two samples of groundwater analyzed had SO<sub>4</sub><sup>2-</sup> higher than WHO (2004) maximum drinking water limit of 250 mg/l. The concentration of NO<sub>3</sub><sup>-</sup> varied between 0 (80C) and 59.60 (73C) mg/l. The mean concentrations of Na and Cl (Table 4) increased by ~80 and 1000 times relative to those of freshwater (rainwater), while

**Table 4** Average values for physicochemical parameters from different aquifers. Units in mg/l, except EC ( $\mu\text{S/cm}$ ) and pH (no unit) and error are presented as  $\pm\text{SD}$  (standard deviation)

Aquifer	All	Alluvial						Coastal Plain												
		Mean $\pm\text{SD}$ (n = 105)	> WHO (2006)	no	%	Upper (A)	> WHO	no	%	Lower (B)	> WHO	no	%	Mean $\pm\text{SD}$ (n=44)	> WHO	no	%	WHO <sup>a</sup>	Rain water	Seawater
EC		707.07 $\pm$ 2825.74	5	5	1372.73 $\pm$ 4054.27	5	10	51.90 $\pm$ 22.89	0	0	136.75 $\pm$ 120.17	0	0	1500	(Near 41A) <sup>b</sup>	0	0	1500	25.00	(Near 28A, 29A) <sup>b</sup>
pH		6.16 $\pm$ 0.99	62	59	6.58 $\pm$ 0.97	26	52	5.27 $\pm$ 0.76	0	0	5.87 $\pm$ 0.86	36	77	6.5–8.5		0	0	62	7.42	
DO		5.01 $\pm$ 1.82	57	54	4.91 $\pm$ 1.63	24	48	5.175 $\pm$ 1.36	4	50	5.08 $\pm$ 2.09	29	62	5 min		0	0	5	3.0	
Na <sup>+</sup>		64.31 $\pm$ 183.06	5	5	121.10 $\pm$ 257.30	5	10	8.88 $\pm$ 6.75	0	0	15.60 $\pm$ 15.11	0	0	200		0	0	200	1.51	8520.2
K <sup>+</sup>		10.31 $\pm$ 25.39	17	16	18.53 $\pm$ 34.52	15	30	1.88 $\pm$ 2.36	2	25	2.86 $\pm$ 5.79	0	0	12		0	0	12	0.26	459.7
Ca <sup>2+</sup>		22.84 $\pm$ 68.76	2	2	40.68 $\pm$ 97.09	2	4	9.18 $\pm$ 15.17	0	0	6.91 $\pm$ 13.34	0	0	200		0	0	200	1.83	325.1
Mg <sup>2+</sup>		15.51 $\pm$ 36.39	2	2	27.61 $\pm$ 49.51	2	4	14.98 $\pm$ 23.14	0	0	3.26 $\pm$ 6.44	0	0	150		0	0	150	0.16	1009.0
Cl <sup>-</sup>		142.50 $\pm$ 393.06	12	11	272.90 $\pm$ 547.37	11	22	66.90 $\pm$ 98.76	1	13	21.9 $\pm$ 29.42	0	0	250		0	0	250	0.27	14611.7
HCO <sub>3</sub> <sup>-</sup>		56.11 $\pm$ 107.23	2	2	84.68 $\pm$ 149.29	2	4	7.713 $\pm$ 6.16	0	0	35.02 $\pm$ 31.16	0	0	600		0	0	600	0.76	658.8
SO <sub>4</sub> <sup>2-</sup>		22.55 $\pm$ 95.15	2	2	40.67 $\pm$ 137.29	2	4	3.78 $\pm$ 3.15	0	0	7.18 $\pm$ 11.82	0	0	250		0	0	250	0.74	1973.2
NO <sub>3</sub> <sup>-</sup>		6.87 $\pm$ 13.11	2	2	3.23 $\pm$ 8.33	1	2	0.40 $\pm$ 0.32	0	0	11.67 $\pm$ 16.29	1	2	50		1	2	50	1.04	

<sup>a</sup>WHO (1993, 2004, 2006, 2008) <sup>b</sup>See Table 1 for locations



**Table 5** Pearson correlation coefficients between physicochemical parameters for the different aquifers

Aquifer	Parameter	EC	Na <sup>+</sup>	K <sup>+</sup>	Ca <sup>2+</sup>	Mg <sup>2+</sup>	Cl <sup>-</sup>	HCO <sub>3</sub> <sup>-</sup>	SO <sub>4</sub> <sup>2-</sup>	NO <sub>3</sub> <sup>-</sup>
Upper alluvial	EC	1.000	<b>0.790</b>	<b>0.794</b>	<b>0.969</b>	<b>0.513</b>	<b>0.747</b>	<b>0.915</b>	<b>0.711</b>	-0.098
	Na <sup>+</sup>		1.000	<b>0.615</b>	<b>0.682</b>	<b>0.807</b>	<b>0.977</b>	<b>0.603</b>	<b>0.496</b>	-0.128
	K <sup>+</sup>			1.000	<b>0.803</b>	<b>0.509</b>	<b>0.631</b>	<b>0.767</b>	<b>0.574</b>	-0.055
	Ca <sup>2+</sup>				1.000	<b>0.448</b>	<b>0.658</b>	<b>0.929</b>	<b>0.711</b>	-0.114
	Mg <sup>2+</sup>					1.000	<b>0.880</b>	<b>0.399</b>	<b>0.326</b>	-0.144
	Cl <sup>-</sup>						1.000	<b>0.565</b>	<b>0.384</b>	-0.143
	HCO <sub>3</sub> <sup>-</sup>							1.000	<b>0.677</b>	-0.097
	SO <sub>4</sub> <sup>2-</sup>								1.000	-0.077
	NO <sub>3</sub> <sup>-</sup>									1.000
Lower alluvial	EC	1.000	0.615	0.485	0.266	0.015	0.141	0.359	0.060	<b>0.726</b>
	Na <sup>+</sup>		1.000	<b>0.753</b>	<b>0.843</b>	0.576	<b>0.730</b>	0.028	0.334	0.270
	K <sup>+</sup>			1.000	<b>0.792</b>	0.668	<b>0.771</b>	-0.225	0.417	0.010
	Ca <sup>2+</sup>				1.000	<b>0.905</b>	<b>0.974</b>	0.027	0.648	0.024
	Mg <sup>2+</sup>					1.000	<b>0.974</b>	0.133	<b>0.853</b>	-0.225
	Cl <sup>-</sup>						1.000	0.038	<b>0.752</b>	-0.136
	HCO <sub>3</sub> <sup>-</sup>							1.000	0.539	0.474
	SO <sub>4</sub> <sup>2-</sup>								1.000	-0.161
	NO <sub>3</sub> <sup>-</sup>									1.000
Coastal Plain	EC	1.000	<b>0.324</b>	-0.017	-0.199	-0.081	-0.062	0.274	0.131	<b>0.716</b>
	Na <sup>+</sup>		1.000	<b>0.679</b>	0.125	<b>0.352</b>	<b>0.715</b>	<b>0.825</b>	0.106	0.156
	K <sup>+</sup>			1.000	0.280	0.241	<b>0.557</b>	<b>0.575</b>	0.094	-0.036
	Ca <sup>2+</sup>				1.000	0.224	<b>0.640</b>	<b>0.401</b>	0.255	-0.167
	Mg <sup>2+</sup>					1.000	<b>0.432</b>	<b>0.476</b>	0.215	-0.183
	Cl <sup>-</sup>						1.000	<b>0.655</b>	0.129	-0.279
	HCO <sub>3</sub> <sup>-</sup>							1.000	0.019	0.148
	SO <sub>4</sub> <sup>2-</sup>								1.000	0.218
	NO <sub>3</sub> <sup>-</sup>									1.000

Marked correlations in bold are significant at  $p < .05000$

those of K, Ca, Mg, and SO<sub>4</sub> increased by ~70, 20, 175, and 55 times, respectively, suggesting influence of seawater. However, the values of all the physicochemical parameters are below that of typical sea water (Table 4).

#### 4.2.2 Physicochemical Composition of Different Aquifer Systems

##### Upper Alluvial Aquifer Harnessed Through Hand-Dug Wells (A)

EC of the upper alluvial aquifer ranged from 100 to 21,538  $\mu\text{S}/\text{cm}$ . Groundwater on the average is acidic with 48% of all the samples not within the WHO limit for drinking and domestic purposes. Dissolved oxygen (DO) concentration varied from 1.30 to 8.79 mg/l. Low DO values (<5.0 mg/l)

was recorded for 48% of the samples. Na<sup>+</sup> is the dominant cation, ranging from 0.56 to 1280.8 mg/l. This represents an average of 48% of all the cations. Ca<sup>2+</sup> ranged between 0.02 and 520.30 mg/l, while Mg<sup>2+</sup> varied from 0.47 to 230.7 mg/l. These values represent, respectively, 24.6 and 20.3% of Ca<sup>2+</sup> and Mg<sup>2+</sup> relative to the total cations. K<sup>+</sup> represents on the average 5.7% of total cations in groundwater samples of the basin. Concentration of K<sup>+</sup> varied from 0.40 to 159.60 mg/l. Concentration of Cl<sup>-</sup> varied from 3.54 to 2670 mg/l. Bicarbonate concentration ranged from 1.0 to 787.20. SO<sub>4</sub><sup>2-</sup> concentration varied between 0.22 and 968.90 mg/l. Concentration of NO<sub>3</sub><sup>-</sup> varied from 0.08 to 51.62 mg/l. All the parameters showed varying exceedances above WHO standard limits for drinking. Statistical evaluation by means of Pearson's correlation (Table 5) of the groundwater analyses show that EC had significant positive

correlation at  $p < 0.05$  with  $\text{Na}^+$ ,  $\text{K}^+$ ,  $\text{Ca}^{2+}$ ,  $\text{Mg}^{2+}$ ,  $\text{Cl}^-$ ,  $\text{HCO}_3^-$ , and  $\text{SO}_4^{2-}$ . All the parameters ( $\text{Na}^+$ ,  $\text{K}^+$ ,  $\text{Ca}^{2+}$ ,  $\text{Mg}^{2+}$ ,  $\text{Cl}^-$ ,  $\text{HCO}_3^-$ , and  $\text{SO}_4^{2-}$ ) showed significant positive correlation with each other, except with  $\text{NO}_3^-$ . Besides, evaluation of the concentration of the major ions indicate Na-Ca-Cl- $\text{HCO}_3^-$  water type suggesting seawater intrusion as the major process controlling water chemistry, while ion exchange and silicate weathering as the minor processes.

#### Lower Alluvial Aquifer Harnessed Through Shallow Boreholes (B)

Groundwater samples from lower alluvial aquifer showed that the pH varied from 4.08 to 6.40 indicating acid groundwater. EC varied from 21 to 80  $\mu\text{S}/\text{cm}$ . These values of EC are within acceptable limit for drinking and domestic purposes. DO concentration varied from 4.00 to 8.40 mg/l. Among the cations,  $\text{Na}^+$  varied from 2.20 to 21.80 mg/l;  $\text{K}^+$  from 0.01 to 6.70 mg/l;  $\text{Ca}^{2+}$  from 1.10 to 46.10 mg/l and  $\text{Mg}^{2+}$  from 0.10 to 60.20 mg/l. Among the anions,  $\text{Cl}^-$  varied between 10.20 and 307.40 mg/l;  $\text{HCO}_3^-$  varied from 0.50 to 18.90 mg/l;  $\text{SO}_4^{2-}$  from 1.24 to 10.70 mg/l, and  $\text{NO}_3^-$  from 0.09 to 0.82 mg/l. These values are within the limits of WHO for drinking and domestic purposes, except for DO and  $\text{K}^+$  in some samples. In lower alluvial aquifer as presented in Table 5, EC is positively correlated with  $\text{NO}_3^-$ , while Na + is positively correlated with  $\text{K}^+$ ,  $\text{Ca}^{2+}$ , and  $\text{Cl}^-$ . Also  $\text{K}^+$  positively correlated with  $\text{Ca}^{2+}$  and  $\text{Cl}^-$ .  $\text{Cl}^-$  correlates positively with  $\text{Ca}^{2+}$  and  $\text{Mg}^{2+}$ , while  $\text{SO}_4^{2-}$  positively correlates with  $\text{Mg}^{2+}$  and  $\text{Cl}^-$ . This pattern of relationship is attributable to cation exchange due mainly to significant positive correlation between  $\text{Na}^+$  and  $\text{Ca}^{2+}$  and  $\text{Ca}^{2+}$  and  $\text{Cl}^-$ . The main groundwater chemical facies are Mg-Na-Cl. Significant positive correlation between EC with  $\text{NO}_3^-$  is attributable to anthropogenic pollution.

#### Coastal Plain Aquifer Harnessed Through Deep Boreholes (C)

Groundwater pH values from coastal plain aquifer ranged from 3.72 to 7.16. EC values ranged from 16.28 to 457.80  $\mu\text{S}/\text{cm}$ . Based on EC values, all the samples analyzed are classified as fresh ( $\text{EC} < 1500 \mu\text{S}/\text{cm}$ ) according to Rai (2004) and Mondal et al. (2010). DO concentration varied from 1.19 to 10.7 mg/l. Concentration of  $\text{Na}^+$  varied from 0.06 to 64.60 mg/l, while  $\text{K}^+$  varied from 0.02 to 30.30 mg/l.  $\text{Ca}^{2+}$  and  $\text{Mg}^{2+}$  in the analyzed groundwater samples from coastal plain aquifer ranged from 0.01 to 67.80 mg/l and 0.01 to 28.30 mg/l, respectively.  $\text{Cl}^-$  concentration ranged from 0.32 to 116 mg/l. The concentration of  $\text{NO}_3^-$  in groundwater ranged from 0.00 to 59.60 mg/l. The values of  $\text{SO}_4^{2-}$  in the groundwater samples ranged from 0.00 to 47.47 mg/l, while  $\text{HCO}_3^-$  concentration ranged

from 0.20 to 117.50 mg/l. These values within the various limits are specified by WHO for drinking and domestic purposes, except for pH, DO, and  $\text{NO}_3^-$  in some samples. (Table 4). In the coastal plain aquifer, EC correlated positively with  $\text{Na}^+$  and  $\text{NO}_3^-$ , while  $\text{Na}^+$  correlated positively with  $\text{K}^+$ ,  $\text{Mg}^{2+}$ ,  $\text{Cl}^-$ , and  $\text{HCO}_3^-$ . In addition,  $\text{Cl}^-$  correlated positively with  $\text{K}^+$ ,  $\text{Ca}^{2+}$ , and  $\text{Mg}^{2+}$ , while  $\text{HCO}_3^-$  is also positively correlated with  $\text{K}^+$ ,  $\text{Ca}^{2+}$ ,  $\text{Mg}^{2+}$ , and  $\text{Cl}^-$ . It is observed that  $\text{Na}^+$ ,  $\text{K}^+$ ,  $\text{Ca}^{2+}$ ,  $\text{Mg}^{2+}$ ,  $\text{Cl}^-$ , and  $\text{HCO}_3^-$  were poorly correlated with  $\text{SO}_4^{2-}$  and  $\text{NO}_3^-$  due to contribution from anthropogenic pollution. However, significant correlation between  $\text{Na}^+$  and  $\text{HCO}_3^-$  suggests contribution from silicate weathering. Na-Ca- $\text{HCO}_3^-$  constitutes the dominant hydrochemical facies.

Average concentrations of all the parameters were higher concentration in groundwater from A relative to groundwater from B and C aquifers. However, the average values of DO,  $\text{Ca}^{2+}$ ,  $\text{Mg}^{2+}$ , and  $\text{Cl}^-$  were higher in B relative to C. Considering analytical results for the entire study area, the standard deviation (SD) is high for EC, TDS  $\text{Na}^+$ ,  $\text{K}^+$ ,  $\text{Ca}^{2+}$ ,  $\text{Mg}^{2+}$ ,  $\text{Cl}^-$ ,  $\text{NO}_3^-$ ,  $\text{SO}_4^{2-}$ , and  $\text{HCO}_3^-$  suggesting dispersion of ionic concentration from average value (Table 4). SD was low for pH and DO suggesting their limited variability (Vasu et al., 2017).

#### 4.2.3 Seawater Contamination

The ratio of  $\text{Na}^+/\text{Cl}^-$  for analyzed groundwater samples ranged from 0.01 to 15.64 for the entire groundwater with an average of  $1.73 \pm 2.28$ . The average values for A, B, and C were  $0.95 \pm 0.68$ ,  $0.44 \pm 0.38$ , and  $2.73 \pm 3.01$ , respectively. The deviation of these values relative to that of seawater (0.86) is shown in Fig. 4a, b. Figure 4a, b includes freshwater and seawater dilution line, which shows simple mixing of both freshwater and seawater end members (Mtoni et al., 2013). A deviation from the dilution line is related to ion exchange, suggesting an excess or depletion of  $\text{Na}^+$  relative to  $\text{Cl}^-$  (Walraevens & Van Camp, 2005). Excess  $\text{Na}^+$  in groundwater plotting above mixing line (1:1 line) in Fig. 4b indicates silicate weathering or freshening. On the other hand, depletion of  $\text{Na}^+$  in groundwater indicated by plotting below the mixing line (Fig. 4b) suggests seawater intrusion. In addition, concentrations of EC and  $\text{Cl}^-$  are good indicators of sea water contamination (El Moujabber et al., 2006). Contamination of seawater is represented by elevated concentration of  $\text{EC} > 1500 \mu\text{S}/\text{cm}$  and  $\text{Cl}^- (>250 \text{ mg/l})$ . The concentrations of EC and  $\text{Cl}^-$  in the basin varied from 16 to 21, 538  $\mu\text{S}/\text{cm}$  and from 0.32 to 2670 mg/l, respectively. Values of EC (1992.5–21,538  $\mu\text{S}/\text{cm}$ ) at 1A, 5A, 17A, 24A, and 25A (upper alluvial aquifer) and  $\text{Cl}^-$  (307.4–2324.0 mg/l) at 1A, 2A, 3A, 5A, 17A, 24A, 25A, 27A, 35A, 38A (upper alluvial aquifer), and 53B (lower alluvial aquifer) (Appendix 1) further support intrusion of seawater.

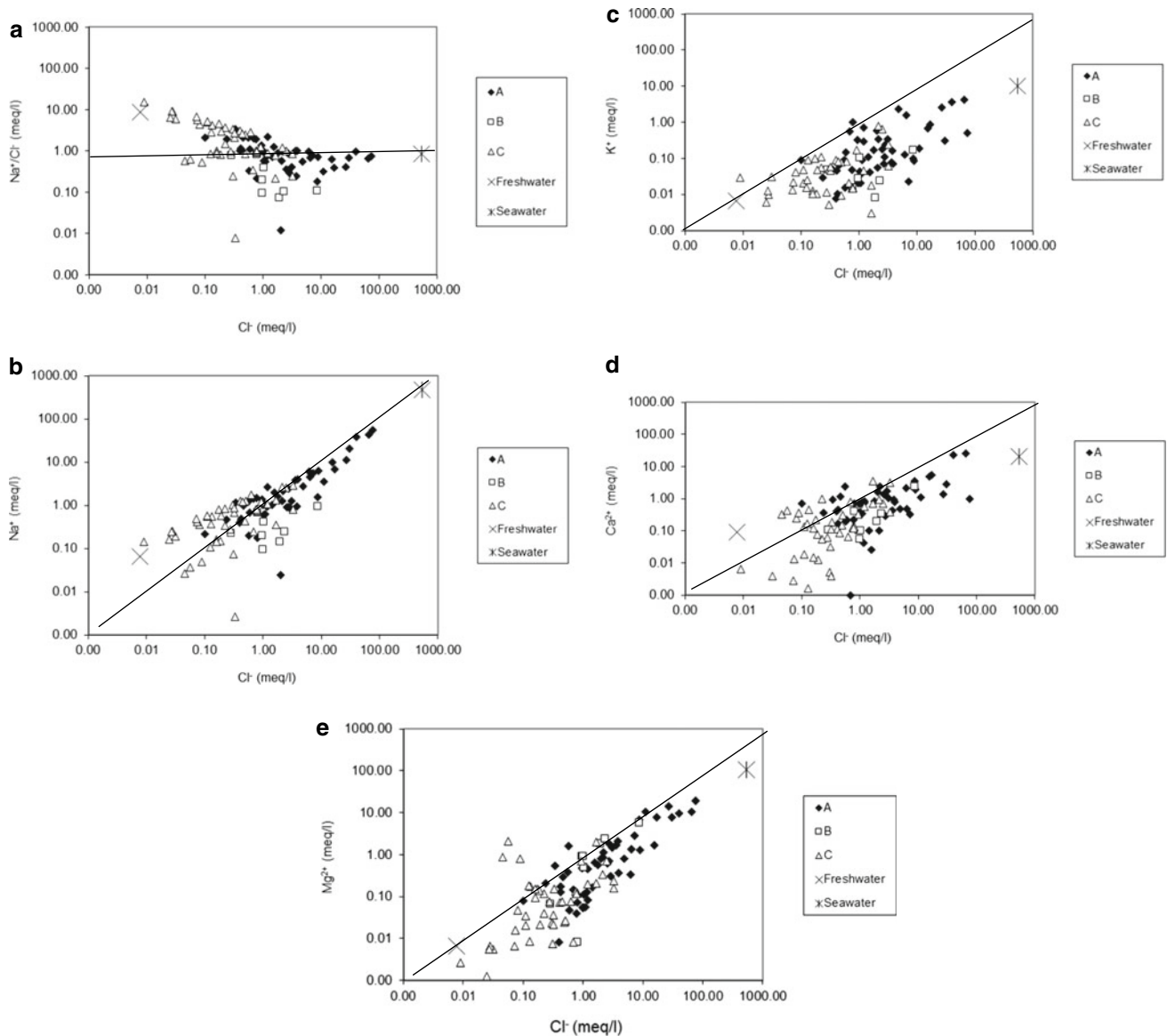


**Fig. 4** **a** Plot of  $\text{Na}^+/\text{Cl}^-$  versus  $\text{Cl}^-$  for upper alluvial (A), lower alluvial (B) and coastal plain (C) aquifers, **b** Plot of  $\text{Na}^+$  versus  $\text{Cl}^-$  for upper alluvial (A), lower alluvial (B) and coastal plain (C) aquifers, **c** Plot of  $\text{K}^+$  versus  $\text{Cl}^-$  for upper alluvial (A), lower alluvial (B) and

coastal plain (C) aquifers, **d** Plot of  $\text{Ca}^{2+}$  versus  $\text{Cl}^-$  for upper alluvial (A), lower alluvial (B) and coastal plain (C) aquifers, **e** Plot of  $\text{Mg}^{2+}$  versus  $\text{Cl}^-$  for upper alluvial (A), lower alluvial (B) and coastal plain (C) aquifers

To quantify the mixing ratios of seawater and freshwater in the basin, the chloride mass balance (Eqs. 2–4) was applied. The computed values of fraction of seawater in freshwater (% F) are presented in Table 6. The delta values varied from 0.0002 to 13.8% for the entire basin. The average values for the different aquifers were  $1.41 \pm 2.83$ ,  $0.34 \pm 0.51$ , and  $0.11 \pm 0.15$  for A, B, and C, respectively. The F values > 1% (range 1.13–13.8%) at 1A, 2A, 3A, 5A, 7A, 8A, 17A, 24A, 25A, 26A, 27A, 35A, and 38A in upper alluvial aquifer and 53B in lower alluvial aquifer also support evidence of seawater contamination. Figure 4b–e demonstrate that there is an enrichment of  $\text{Cl}^-$

with respect to cations ( $\text{Na}^+$ ,  $\text{K}^+$ ,  $\text{Ca}^{2+}$ , and  $\text{Mg}^{2+}$ ) with distinctive patterns that are lower than the theoretical mixing line. This is confirmed by the computed ionic delta and presented as Table 6 and Fig. 5. Most of the groundwater samples display enrichment of  $\text{Na}^+$  compared to pure mixing model, ranging between -3.35 and 3.13 with an average value  $1.83 \pm 1.36$ , except in 1A, 2A, 3A, 5A, 8A, 17A, 24A, and 25A (A aquifer) which have negative values. The depletion of  $\text{Na}^+$  is accompanied by enrichment of  $\text{K}^+$ ,  $\text{Ca}^{2+}$ , and  $\text{Mg}^{2+}$ . Enrichment of  $\text{Ca}^{2+}$  and  $\text{Mg}^{2+}$  suggest ion exchange process (Pulido-Leboeuf, 2004; Trabelsi et al., 2012).

**Table 6** Summary of fraction of seawater in fresh water and computed ionic deltas and mixing expected according to a theoretical freshwater/seawater mixing model

Aquifer	Statistics	%F	$\Delta\text{Na}$	$\Delta\text{K}$	$\Delta\text{Ca}$	$\Delta\text{Mg}$	$\text{Na}_{\text{mix}}$	$\text{K}_{\text{mix}}$	$\text{Ca}_{\text{mix}}$	$\text{Mg}_{\text{mix}}$
All	Mean	0.73	1.83	0.59	1.06	0.71	0.67	0.29	0.37	0.30
	Min	0.0002	-3.35	-0.03	-0.09	-0.28	0.07	0.01	0.08	0.01
	Max	13.80	3.13	6.93	22.54	10.02	6.20	1.73	1.81	2.09
	SD	2.03	1.36	1.06	2.95	1.56	0.95	0.47	0.47	0.50
Upper alluvial (A)	Mean	1.41	0.82	0.69	1.61	1.22	0.49	0.01	0.10	0.01
	Min	0.02	-3.35	-0.03	-0.09	-0.01	0.07	0.01	0.08	0.01
	Max	13.80	2.31	6.93	22.54	10.02	4.29	0.04	0.27	0.06
	SD	2.83	1.20	1.50	4.21	2.15	0.86	0.01	0.04	0.01
Lower alluvial (B)	Mean	0.34	2.38	0.29	1.14	0.42	0.18	0.01	0.09	0.01
	Min	0.05	1.95	0.01	0.09	0.15	0.08	0.01	0.08	0.01
	Max	1.59	2.60	0.98	1.96	0.85	0.55	0.01	0.10	0.01
	SD	0.51	0.20	0.33	0.67	0.25	0.15	0.00	0.01	0.00
Coastal plain (C)	Mean	0.11	2.81	0.53	0.46	0.21	0.95	0.64	0.71	0.65
	Min	0.0002	-1.43	0.03	-0.08	-0.28	0.08	0.01	0.08	0.01
	Max	0.60	3.13	1.73	0.62	1.48	6.20	1.73	1.81	2.09
	SD	0.15	0.69	0.26	0.16	0.21	1.05	0.54	0.54	0.57

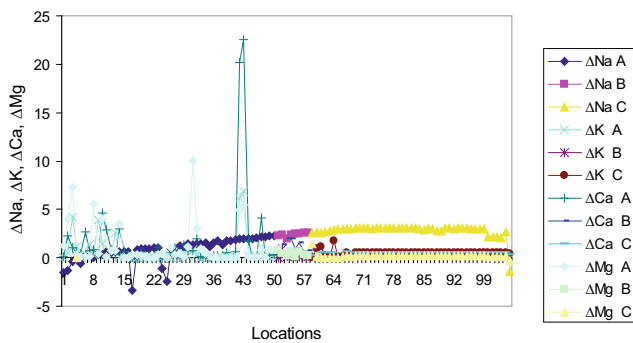


**Fig. 5** Plot of ionic delta for the different groundwater in the study area

The clayey sand layers in the aquifer could be the required ion exchanger. This phenomenon may be responsible for low  $\text{Na}^+/\text{Cl}^-$  ratios observed in some locations. The plot of  $\text{Cl}^-/\text{HCO}_3^-$  vs  $\text{Cl}^-$  (Fig. 6) indicates  $\text{Cl}^-/\text{HCO}_3^-$  ratios ranging between 0.05 and 695.13 with an average value of  $16.88 \pm 70.48$  for all the groundwater samples. The different aquifers displayed ratios in the following range: 0.12 to 695.13 (average  $26.27 \pm 99.25$ ) for upper alluvial aquifer; 1.29 to 120.63 (average  $40.42 \pm 48.15$ ) for lower alluvial aquifer, and 0.05 to 101.28 (average  $3.36 \pm 101.38$ ) for coastal plain aquifer.

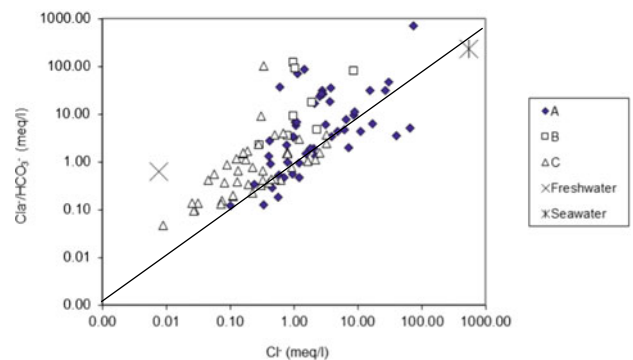


**Fig. 6** Plot of  $\text{Ca}^{2+}/\text{HCO}_3^-$  versus  $\text{Cl}^-$  for upper alluvial (A), lower alluvial (B) and coastal plain (C) aquifers

#### 4.2.4 Classification of Groundwater Chloride and Bicarbonate

On the basis of  $\text{Cl}^-/\text{HCO}_3^-$  classification scheme, 47.6% of the groundwater samples were not affected by sea water intrusion, 6.7% are slightly/moderately affected by sea water intrusion, while 45.7% are strongly affected by sea water intrusion. The unaffected samples were obtained from coastal plain aquifer. Twenty-five and 75% of the samples from A aquifer were not affected and strongly affected by sea water intrusion, respectively, while 54, 6, and 40% of groundwater samples from B aquifer were not affected,

**Table 7** Classification of groundwater based on different criteria and schemes (including chloroalkaline indices for cation exchange and reverse cation exchange process)

Classification	Criteria	Remarks	Aquifer					
			A	B	C	A	B	C
			No			%		
Revelle ratio	< 0.5	not affected by seawater	9	27	14	25	54	74
	0.5–6.6	slightly/moderately affected by sea water		3	4	0	6	21
	> 6.6	strongly affected by seawater	27	20	1	75	40	5
Chloride-nitrate classification	$\text{Cl}^- < 35 \text{ mg/l}$ , $\text{NO}_3^- < 2 \text{ mg/l}$	Low chloride and low nitrate	10	3	13	20	37.5	29.5
	$\text{Cl}^- < 35 \text{ mg/l}$ , $\text{NO}_3^- > 2 \text{ mg/l}$	Low chloride and high nitrate	6		25	12		56.8
	$\text{Cl}^- > 35 \text{ mg/l}$ , $\text{NO}_3^- < 2 \text{ mg/l}$	High chloride and low nitrate	30	5	6	60	62.5	13.6
	$\text{Cl}^- > 35 \text{ mg/l}$ , $\text{NO}_3^- > 2 \text{ mg/l}$	High chloride and high nitrate	4			8		

A upper alluvial aquifer, B lower alluvial aquifer and C coastal plain aquifer

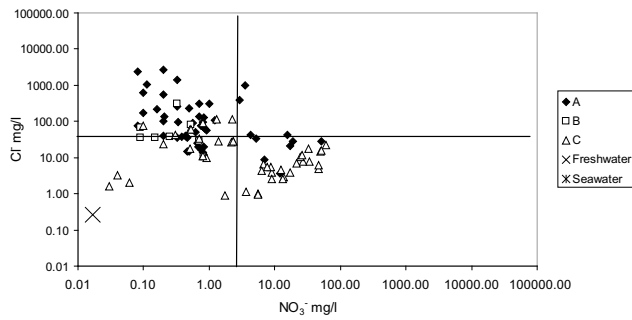


**Fig. 7** Groundwater classification based on  $\text{Cl}^-$  and  $\text{NO}_3^-$  (Group 1-row 1, column 1; Group 2 row 1, column 2; Group 3 row 2, column 1 and Group row 2, column 2) for upper alluvial (A), lower alluvial (B) and coastal plain (C) aquifers

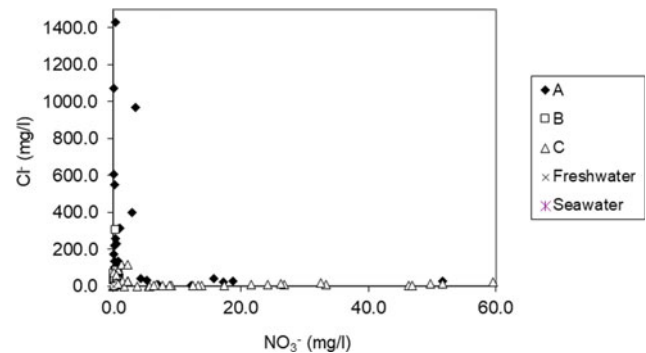


**Fig. 8** Plot of  $\text{Cl}^-$  versus  $\text{NO}_3^-$  for upper alluvial (A), lower alluvial (B) and coastal plain (C) aquifers

slightly/moderately affected, and strongly affected by sea water intrusion. For the groundwater samples from C aquifer, 73.7% were not affected; 21.1% were slightly/moderately affected, while 5.3% are strongly affected by sea water intrusion (Table 7). Above show that samples from the A aquifer were strongly affected by sea water relative to the B and C aquifers.

#### Chloride and Nitrate Classification

Analytical results indicated that about 20 and 14% of the groundwater samples from A and B aquifers exceeded the WHO (1993) limit for chloride and 2% of same set of groundwater samples show nitrate concentrations greater than WHO (1993). The threshold values following method of Sinclair (1974, 1976) were 35 and 2 mg/l for  $\text{Cl}^-$  and  $\text{NO}_3^-$ , respectively. The classification of groundwater of the

study area is presented in Fig. 7. Group 1 account for 20, 37.5, and 29.55%, respectively, for A, B, and C aquifers and are relatively low in chloride and nitrate ( $\text{Cl}^- < 35 \text{ mg/l}$  and  $\text{NO}_3^- < 2 \text{ mg/l}$ ). Sixty percent, 62.5, and 13.64% of the groundwater, respectively, for A, B, and C aquifers were classified as group 3, which is enriched in chloride and poor in nitrate ( $\text{Cl}^- > 35 \text{ mg/l}$  and  $\text{NO}_3^- < 2 \text{ mg/l}$ ). Group 2 with low chloride and high nitrate ( $\text{Cl}^- < 35 \text{ mg/l}$  and  $\text{NO}_3^- > 2 \text{ mg/l}$ ) contained 12% from A aquifer and 56.82% from C aquifer, while Group 4 with high chloride and high nitrate content ( $\text{Cl}^- > 35 \text{ mg/l}$  and  $\text{NO}_3^- > 2 \text{ mg/l}$ ) has 8% of samples from A aquifer. Majority of the groundwater samples in Groups 3 are from A and B aquifers suggesting influence of seawater contamination, while the majority of samples in Group 2 are from C aquifer suggesting input from human activities (Table 7). The arithmetic plot for  $\text{Cl}^-$  and  $\text{NO}_3^-$  shows two pathways (Fig. 8). One pathway shows an



**Table 8** Stuyfzand Classification<sup>a</sup> of groundwater of Niger Delta basin

Class	A	B	C	Class	A	B	C
B3-NaCl-	1A,			F4-NaCaHCO <sub>3</sub> +	47A		
B7-MgNaCl-	2A, 5A,			F3-NaClHCO <sub>3</sub> +	49A		
B7-MgCl-	3A, 8A			F4-NaCaCl-	50A		
Fb5-NaKCl-	4A,			F4-MgCl-		52B	
F6-MgNaCl-	6A,			F7-MgCl-		53B	
Fb-5NaCl-	7A			F5-MgCl-		54B	
F4-NaCl-	13A, 19A	51B	60C	F4-MgCl-		55B	
F5-NaCl-	10A		59C	F3-MgNaCl-		56B	
F4-NaCaCl-	11A			F6-MgCl-		58B	
F6-CaNaCl-	12A			F4-CaCl-			64C
F6-CaNaCl-	14A			F0-NaCl-			65C
F6-CaCl-	15A, 31A		61C	F4NaMgCl+	66C		
F6-MgCl-	16A			F3-CaCl-	67C		
Bs7-NaCl-	17A, 25A			F6-MgClHCO <sub>3</sub> +	68C		
F3-NaCl-	18A, 20A, 22A, 41A, 45A			F2-NaCl-	69C, 70C		
F4-CaNaCl-	21A			F5-NaHCO <sub>3</sub> ClØ	71C		
F5-CaNaCl-	23A			F0-NaHCO <sub>3</sub> +	72C, 87C		
F4-NaCl+	9A			F2-NaHCO <sub>3</sub> Cl+	73C		
Bs7-NaCl+	24A			F2-NaHCO <sub>3</sub> Cl+	74C		
Fb6-NaCl-	26A			F1-NaHCO <sub>3</sub> +	75C		
B7-NaCl-	27A			F4-NaCaSO <sub>4</sub> +	76C		
F5-NaCl+	28A, 29A			F3-NaSO <sub>4</sub> Cl+	77C		
F5-MgHCO <sub>3</sub> +	30A			F3-NaSO <sub>4</sub> +	78C		
F6-CaCl+	32A			F*-NaHCO <sub>3</sub> +			79C, 80C, 81C, 82C, 83C, 84C, 86C, 91C
F6-CaClHCO <sub>3</sub> +	33A		63C	F*-NaHCO <sub>3</sub> ClØ			85C
F5-CaNaCl+	34A			F3-NaHCO <sub>3</sub> +			88C
B6-NaCl-	35A			F2-NaHCO <sub>3</sub> Cl+			89C
F5-NaCl+	36A		62C	F2-NaHCO <sub>3</sub> +			90C
F5-NaCaHCO <sub>3</sub> +	37A, 48A			F*-NaHCO <sub>3</sub> ClØ			92C
Fb6-NaCl-	38A			F5-MgHCO <sub>3</sub> Cl+			93C
F1-NaHCO <sub>3</sub> +	39A			F5-MgSO <sub>4</sub> <sup>2</sup> HCO <sub>3</sub> +			94C
F4-NaCaHCO <sub>3</sub> -	40A			F6-MgSO <sub>4</sub> HCO <sub>3</sub> +			95C
F4-CaCl+	42A			F1-NaHCO <sub>3</sub> Cl-			96C
F4-KHCO <sub>3</sub> Cl-	43A			F2-NaMgClHCO <sub>3</sub> -			97C
F2-NaCl-	44A	57B	100C, 103C	F3-MgNaClHCO <sub>3</sub> -			98C, 99C
F3-NaCl-	22A		101C, 102C	F2-NaHCO <sub>3</sub> +			104C
F5-NaHCO <sub>3</sub> +	46A			F4-NaCl-			105C

A upper alluvial aquifer, B lower alluvial aquifer and C coastal plain aquifer

increasing trend for chloride values along the  $y$ -axis. This pathway reflects seawater contamination. The second pathway is an increase in nitrate values along the  $x$ -axis and suggests human activities. This is in line with the work of Kim et al. (2004), Min et al. (2003), and Stumm and Morgen (1996). From above, samples from upper and lower alluvial aquifers are affected by high concentration of chloride, suggesting influence of sea water, while samples from coastal plain aquifer are affected by high nitrate due to human activities.

#### Stuyfzand Classification

Majority of the groundwater samples are grouped as Fresh, F (Table 8) accounting for 72, 88.5, and 100% for A, B, and C aquifers, respectively. The second most important group is Brackish (B) accounting for 14 and 12.5%, respectively, for A and B aquifers. The third group is fresh-brackish (Fb) and accounts for 8% of groundwater in A aquifer. Brackish-salt (Bs) is the least account for 6% of samples from the A aquifer.

Total hardness varies from very soft (\*) with value of 0.02 mmol/l for sample 86C from C aquifer to extremely hard (7) with value of 646.7 mmol/l for groundwater sample 25A from A aquifer. Most of the groundwater samples are hard (11.4%) to very hard (15.2%) in C aquifer and extremely hard (4, 5, 6) constituting 17.1, 17.1, and 15.2%, respectively, in coastal plain aquifer. On the basis of dominant ions, most of the groundwater is classified as Na-Cl representing 44, 25, and 23% in A, B, and C aquifers. Mg-Cl is the major groundwater type in B aquifer, while Na-HCO<sub>3</sub> constitutes the main groundwater type in C aquifer. Most of the groundwater samples analyzed from the area have positive cation exchange code (+) for C aquifer suggesting freshening or recharge water, while negative cation exchange code (-) dominates groundwater from A aquifer, suggesting salt water contamination. Again this supports the fact that the upper alluvial aquifer is affected by sea water relative to the lower alluvial and coastal plain aquifers.

#### 4.2.5 Impact of Human Activities

Human activities such as irrigation including application of fertilizers and disposal of waste have been linked to variations of electrical conductivity, total dissolved solids, cations, and nitrate in groundwater (Jalali, 2009; Marghade et al., 2012). This is supported by the significant correlation ( $r = > 0.50$ ,  $p < 0.05$ ) between TDS with Na<sup>+</sup> ( $r = 0.80$ ), Cl<sup>-</sup> ( $r = 0.76$ ), and SO<sub>4</sub><sup>2-</sup> ( $r = 0.72$ ). However, correlation between NO<sub>3</sub><sup>-</sup> with Cl<sup>-</sup> ( $r = 0.17$ ); TDS with (NO<sub>3</sub><sup>-</sup> + Cl<sup>-</sup>)/Na<sup>+</sup> ( $r = 0.0022$ ) and TDS with (NO<sub>3</sub><sup>-</sup> + Cl<sup>-</sup>)/HCO<sub>3</sub><sup>-</sup> ( $r = 0.21$ ) does not suggest human activities, rather more of

halite dissolution, sea water intrusion on one hand and mineral dissolution on the other (Choi et al., 2005).

#### 4.2.6 Analysis of Historical and Recent Data

An analysis of the historical and recent data was for the coastal aquifer since data were only available for this aquifer. Comparative assessment shows that the impact of seawater contamination cannot be deciphered between the two hydrochemical data sets as given in Table 9. From Table 9, the average seawater indicators (EC, TDS, Na<sup>+</sup>, and Cl<sup>-</sup>) for historical period of study were 143.18 μS/cm, 130.59 mg/l, 16.77 mg/l, and 22.21 mg/l, respectively. For the recent study period, the values for the same indicators were 129.86 μS/cm, 75.45 mg/l, 14.11 mg/l, and 17.70 mg/l, respectively. This is attributable to limited number of data for the recent time ( $n = 17$ ) relative to historical time (30).

#### 4.2.7 Assessment of Groundwater Quality for Drinking and Irrigation Use

Groundwater in the study area is assessed for drinking and irrigation purposes. Drinking water used for drinking is compared with WHO (2006) standard, while for irrigation use, assessment is based on electrical conductivity (EC), sodium adsorption ratio (SAR), and percent sodium (%Na).

##### Drinking Purpose

Groundwater samples from upper alluvial aquifer show elevated concentrations above WHO limits for drinking in all parameters ranging between 2% for nitrate and 59% for pH (Table 4). Groundwater samples show concentrations higher than WHO limits in dissolved oxygen (DO), potassium, and chloride representing 50, 25, and 13% of all the samples from lower alluvial samples (B), while 77, 62, and 2% of groundwater samples from coastal plain aquifer exceeded WHO limits in pH, DO, and nitrate (Table 4). The groundwater samples with elevated concentrations are not suitable for drinking purpose. Seawater contamination represented by high EC, TDS, Na<sup>+</sup>, and Cl<sup>-</sup> and improper waste disposal represented by low DO and high NO<sub>3</sub><sup>-</sup> maybe responsible for groundwater contamination.

In order to provide an overall water quality assessment, the water quality index (WQI) approach was applied to the analyzed data. Water quality approached has been used by several workers to assess the quality of water. Such studies include but not limited to Banoeng-Yakubo et al. (2009), Bhutiani et al. (2016), Cude (2001), Edet et al. (2013), Ewaid and Abed (2017), Kumar et al. (2015), Li et al. (2010); Oni (2016), and Saeedi et al. (2009). The procedures of using WQI to assess water quality are well documented in the above studies and will not be introduced in this write

**Table 9** Comparison of historical (n = 30) and recent data (n = 17) for coastal aquifer (C). Units in mg/l, except EC (μS/cm) and pH (no unit) and error are presented as ±SD (standard deviation)

Data type Statistics	Historical				Recent			
	Mean	Min	Max	SD	Mean	Min	Max	SD
EC	143.18	16.28	457.80	125.51	129.86	23.00	367.00	115.69
TDS	130.59	12.37	314.40	97.46	75.45	10.50	183.00	62.40
pH	6.14	5.20	7.16	0.49	5.34	3.72	7.03	1.12
DO	5.22	3.00	10.70	1.83	4.97	1.19	10.50	2.52
Na <sup>+</sup>	16.77	0.06	60.10	15.00	14.11	0.60	64.60	15.87
K <sup>+</sup>	3.71	0.02	30.30	6.94	1.16	0.40	3.22	1.02
Ca <sup>2+</sup>	8.88	0.01	67.80	16.52	3.45	0.03	8.70	2.78
Mg <sup>2+</sup>	2.21	0.01	24.30	4.70	3.64	0.08	25.30	6.34
Cl <sup>-</sup>	22.21	0.32	115.30	29.19	17.70	1.60	116.00	27.37
HCO <sub>3</sub> <sup>-</sup>	39.21	0.20	117.50	34.57	27.91	6.24	83.30	24.44
SO <sub>4</sub> <sup>2-</sup>	8.43	0.00	47.47	13.90	4.76	0.00	21.96	7.12
NO <sub>3</sub> <sup>-</sup>	13.20	0.00	59.60	17.87	9.61	0.03	51.69	13.56

up. The classification of water for overall assessment is as follows: WQI < 25 (Excellent quality), 25 < WQI < 50 (Good quality), 50 < WQI < 100 (Medium quality) 100 < WQI < 150 (Poor quality), and WQI > 150 (Very poor quality), and assessment is given in Table 9.

As given in Table 9, of all the samples, 58, 88, and 98% from upper alluvial, lower alluvial, and coastal plain aquifers, respectively, are of excellent quality, while 22, 13, and 2% are of good quality. In the samples from upper alluvial aquifer, 8, 4, and 8%, respectively, are of medium, poor, and very poor quality.

**Irrigation Purpose**

The United States Department of Agriculture (USDA, 1954) was used to classify the groundwater for irrigation use with respect to electrical conductivity (EC), sodium adsorption ratio (SAR), and percent sodium (%Na). SAR and %Na are computed as Eqs. 6 and 7 with units in meq/l:

$$SAR = Na + (\sqrt{Ca^{2+} + Mg^{2+}}) / 2 \tag{6}$$

$$\%Na = (Na + /Na^{+} + K^{+} + Ca^{2+} + Mg^{2+}) * 100 \tag{7}$$

The calculated SAR ranges from 0.02 to 17.51, 0.14 to 1.47, and 0.01 to 8.48 for upper alluvial, lower alluvial, and coastal plain aquifers, respectively. Almost all the samples are in the excellent (SAR < 10) and good (SAR 10–18) irrigation water classes (Table 10). The USDA (1954) also classified irrigation water on the basis of EC as presented in Table 10. Most of the groundwater samples in lower alluvial and coastal plain aquifers are in the low salinity class (EC < 250 μS/cm), while most samples in upper alluvial aquifer (46%) and 26% of samples in coastal plain aquifer

are in the medium salinity class (EC 250–750 μS/cm). Thirty-six percent, 10%, and 8% of the samples from upper alluvial aquifer are in low, high, and very high salinity classes, respectively. Percent sodium (%Na) was also used to evaluate sodium hazard and computed as given in Table 9. According to Khodpanah et al. (2009), water with %Na > 60% may result in sodium accumulations that will result in breakdown of physical properties of soil. The values of %Na range from 0.80 to 82.92%, 6.41 to 60.97%, and 0.77 to 95.53%, respectively, for upper alluvial, lower alluvial, and coastal plain aquifers. It is observed that 34% (upper alluvial aquifer), 13% (lower alluvial aquifer), and 60% (coastal plain aquifer) have very high %Na, suggesting very poor quality for irrigation.

In addition, the USSL (1954) scheme was applied in this study to further evaluate the quality of groundwater for irrigation use. The scheme classifies water on the basis of EC and SAR. EC is classified into four salinity zones (C<sub>1</sub> [<250 μS/cm], C<sub>2</sub> [250–750 μS/cm], C<sub>3</sub> [750–2250 μS/cm], and C<sub>4</sub> [>2550 μS/cm]) and SAR into four hazard zones (S<sub>1</sub> [<10], S<sub>2</sub> [10–18], S<sub>3</sub> [18–26], and S<sub>4</sub> [>26]). Classification of groundwater is presented in Table 9. The data show that 36, 100, and 77% of groundwater from upper alluvial, lower alluvial, and coastal plain aquifers, respectively, are characterized as C<sub>1</sub>-S<sub>1</sub> (low salinity-low sodium hazard), which is very suitable for irrigation use, while 46 and 23% of samples from upper alluvial and coastal plain aquifers are in the class C<sub>2</sub>-S<sub>1</sub> (medium salinity-low sodium hazard), classed as suitable. 10, 6, and 2%, respectively, of groundwater samples from A are classed as C<sub>3</sub>-S<sub>1</sub> (medium salinity-low sodium hazard), C<sub>4</sub>-S<sub>1</sub> (very high salinity-low sodium hazard), and C<sub>4</sub>-S<sub>2</sub> (very high salinity-low sodium hazard).

**Table 10** Classification of groundwater for human and irrigation use

Classification	Criteria	Remarks	Source of water					
			A	B	C	A	B	C
			No			%		
Water quality index (WQI)	< 25	Excellent	29	7	46	58	88	98
	25–50	Good	11	1	1	22	13	2
	50–100	Medium	4			8		
	100–150	Poor	2			4		
	>150	Very poor	4			8		
Percent sodium (% Na)	< 20	Excellent	5	5	6	10	62.5	13
	20–40	Good	13	1	6	26	12.5	13
	40–60	Permissible	15	1	7	30	12.5	15
	60–80	Doubtful	16	1	10	32	12.5	21
	> 80	Unsuitable	1		18	2	0	38
Electrical conductivity (EC) ( $\mu\text{S}/\text{cm}$ )	100–250	Low salinity ( $C_1$ )	18	8	35	36	100	74
	250–750	Medium salinity ( $C_2$ )	23		12	46		26
	750–2250	High salinity ( $C_3$ )	5			10		
	> 2250	Very high salinity ( $C_4$ )	4			8		
Sodium adsorption ratio (SAR)	< 10	Excellent (low- $S_1$ )	49	8	47	99	98	100
	10–18	Good (medium- $S_2$ )	1			1	2	
	18–26	Doubtful (high- $S_3$ )						
	> 26	Unsuitable (very high- $S_4$ )						
$C_1$ - $S_1$		Low salinity-low sodium hazard	18	8	36	36	100	77
$C_2$ - $S_1$		Medium salinity-low sodium hazard	23		11	46		23
$C_3$ - $S_1$		High salinity-low sodium hazard	5			10		
$C_4$ - $S_1$		Very high salinity-low sodium hazard	3			6		
$C_4$ - $S_2$		Very high salinity-medium sodium hazard	1			2		

A upper alluvial aquifer, B lower alluvial aquifer and C coastal plain aquifer

## 5 Conclusions

Historical and recent geological, hydrogeological, and hydrochemical data were used to study the aquifers of the Niger Delta Region of Nigeria. Lithologic logs and aquifer characteristics including water levels, well and boreholes depths, hydraulic conductivity, and transmissivity were used to delineate two aquifers: alluvial aquifer (upper and lower) and coastal plain aquifers in the Niger Delta Region (Nigeria). Many methods have been used to attempt to examine the processes controlling groundwater chemistry. The methods applied include enrichment of  $\text{Na}^+$ ,  $\text{K}^+$ ,  $\text{Ca}^{2+}$ ,  $\text{Mg}^{2+}$ ,  $\text{Cl}^-$ ,  $\text{HCO}_3^-$ , and  $\text{SO}_4^{2-}$ , and seawater mixing ratio, cross plots, and different classification schemes were used to confirm seawater intrusion, anthropogenic pollution, and processes controlling groundwater chemistry. The groundwater is

acidic, while most of the groundwater samples (95%) from A, B, and C are fresh, while 2 and 3% of the samples from A are brackish and saline, respectively. The main groundwater facies are Na-Cl, Mg-Cl, and Na- $\text{HCO}_3$ , respectively, from A, B, and C.

$\text{Cl}^-$  showed significant correlation with  $\text{Na}^+$ ,  $\text{K}^+$ ,  $\text{Ca}^{2+}$ ,  $\text{Mg}^{2+}$ ,  $\text{Cl}^-$ ,  $\text{HCO}_3^-$ , and  $\text{SO}_4^{2-}$  in upper and lower alluvial aquifer and  $\text{Cl}^-$  with  $\text{Na}^+$ ,  $\text{K}^+$ ,  $\text{Ca}^{2+}$ ,  $\text{Mg}^{2+}$ ,  $\text{Cl}^-$ , and  $\text{HCO}_3^-$  in coastal plain aquifer which demonstrated the mixing of seawater and freshwater. However, correlation of EC and  $\text{NO}_3^-$  in lower alluvial and coastal plain aquifer indicate anthropogenic pollution. The cross plots of  $\text{Na}^+/\text{Cl}^-$ ,  $\text{K}^+/\text{Cl}^-$ ,  $\text{Ca}^{2+}/\text{Cl}^-$ , and  $\text{Mg}^{2+}/\text{Cl}^-$  with  $\text{Cl}^-/\text{HCO}_3^-$  and  $\text{Cl}^-/\text{NO}_3^-$  and classification indicated seawater intrusion was occurring in the upper alluvial aquifer and decreased inland through lower alluvial aquifer to the coastal plain aquifer. In terms of drinking and irrigation use, the upper alluvial aquifer water

is of poor quality relative to the groundwater from lower alluvial and coastal plain aquifers. The study has shown that the upper alluvial aquifer had relatively higher salinity and is due to sea water intrusion. This study highlights the potential danger of contaminated groundwater in the coastal areas the home of low income dwellers. Hence, seawater intrusion should be continuously monitored for sustainable management of coastal groundwater affected by seawater.

**Acknowledgements** Literature for this work was possible as a result of Fellowship from Alexander von Humboldt Foundation, Germany. Also to my hosts Prof Dr BJ Merkel and Prof Dr Peter Grathwhöl in Germany at various times for facilitating the sample analyses and for their hospitality. **Compliance with Ethical Standards** Part of this study was funded through a fellowship by Alexander von Humboldt, Germany (3.4-NRI/101071296 STP) at TU Bergakademie, Freiberg, and Institute of Geosciences, University of Tübingen, Germany.

**Conflict of Interest** The author declares that he has no conflict of interest.

## References

- Abdalla, F. (2016). Ionic ratios as tracers to assess seawater intrusion and to identify salinity sources in Jazan coastal aquifer, Saudi Arabia. *Arabian Journal of Geosciences*, 9, 40. <https://doi.org/10.1007/s12517-015-2065-3>.
- Akpokoje, E. G. (1987). The Engineering geological characteristics and classification of major superficial soils of Niger Delta. *Engineering Geology*, 23, 193–211.
- Al-Shaibani, A. M. (2008). Hydrogeology and hydrochemistry of a shallow alluvial aquifer, western Saudi Arabia. *Hydrogeology Journal*, 16, 155–165.
- Allen, J. R. L. (1965). Late Quaternary Niger Delta and adjacent areas: Sedimentary environment and lithofacies. *American Association of Petroleum Geologists*, 49, 549–600.
- Allen, J. R. L. (1965b). *Aspects of the geology of Nigeria* (133p.). Nigeria: University of Ibadan Press.
- Amadi, P. A., Ofoegbu, C. O., & Morrison, T. (1989). Hydrochemical assessment of groundwater quality in parts of the Niger Delta, Nigeria. *Environmental Geology and Water Sciences*, 14(3), 195–202.
- Amadi, U. M. P., & Amadi, P. A. (1990). Saltwater migration in coastal aquifers of southern Nigeria. *Journal of Mining and Geology*, 26(1), 35–44.
- Anders, R., Mendez, G. O., Futa, K., & Danskin, W. R. (2014). A geochemical approach to determine sources and movement of saline groundwater in a coastal aquifer. *Groundwater*, 52(5), 756–768.
- Andersen, M. S., Nyvang, V., Jakobsen, R., & Postma, D. (2005). Geochemical processes and solute transport/freshwater interface of a sandy aquifer. *Geochimica Et Cosmochimica Acta*, 69, 3979–3994.
- Appelo, C. A. J., & Postma, D. (1999). *Geochemistry, groundwater and pollution* (p. 536). Rotterdam: AA Balkema.
- Banoeng-Yakubo, B., Yidana, S. M., Emmanuel, N., Akabzaa, T., & Asiedu, D. (2009). Analysis of groundwater quality using water quality index and conventional graphical methods: The Volta region. *Ghana Environmental Earth Sciences*, 59, 867–879.
- Barbecot, F., Marlin, C., Gilbert, E., & Dever, L. (2000). Hydrochemical and isotopic characterization of the Bathonian and Bajocian coastal aquifer of the Caen area (northern France). *Applied Geochemistry*, 15, 791–805.
- Bhutiani, R., Khanna, D. R., & Kulkarni, D. B. (2016). Assessment of Ganga river ecosystem at haridwar, Uttarakhand, India with reference to water quality indices. *Applied Water Science*, 6, 107–113.
- Capaccioni, B., Didero, M., Paletta, C., & Didero, L. (2005). Saline intrusion and refreshing in a multilayer coastal aquifer in the Catanian Plain (Sicily, Southern Italy): Dynamics of degradation processes according to hydrochemical characteristics of groundwaters. *Journal of Hydrology*, 307, 1–16.
- Cardona, A., Rivera, J. J. C., Alvarez, R. H., & Castro, G. E. (2004). Salinization in coastal aquifers of arid zone: An example from Santo Domingo, Baja California Sur, Mexico. *Environmental Geology*, 45, 350–366.
- Carwright, I., Weaver, T. R., Fulton, S., Nichol, C., Reid, M., & Cheng, X. (2004). Hydrogeochemical and isotopic constrains on the origins of dryland salinity, Murray basin, Victoria, Australia. *Applied Geochemistry*, 19, 1233–1254.
- Chadha, D. K. (1999). A proposed new diagram for geochemical classification of natural waters and interpretation of chemical data. *Hydrogeology Journal*, 7, 431–439.
- Choi, B. Y., Yun, S. T., Yu, S. Y., Lee, P. K., Park, S. S., & Chae, G. T. (2005). Hydrochemistry of urban groundwater in Seoul, South Korea: Effect of landuse and pollution recharge. *Environmental Geology*, 48, 979–990.
- Cude, C. (2001). Oregon water quality index: A tool for evaluating water quality management effectiveness. *Journal of the American Water Resources Association*, 37, 125–137.
- Custodio, E. (1987). Hydrogeochemistry and tracers. In Custodio, E. (Ed.), *Groundwater problems in coastal areas studies and reports in hydrology* (Vol 45, pp. 213–269). UNESCO, Paris
- de Montety, V., Radakovitch, O., Vallet-Coulomb, C., Blavoux, B., Hermitte, D., & Valles, V. (2008). Origin of groundwater salinity and hydrogeochemical processes in a confined coastal aquifer. Case of the Rhône delta (southern France). *Applied Geochemistry*, 23, 2337–2349.
- El Moujabber, M., BouSamra, B., Darwish, T., & Atallah, T. (2006). Comparison of different indicators for groundwater contamination by seawater intrusion on the Lebanese Coast. *Water Resources Management*, 20, 161–180.
- Edet, A. E. (1993). Groundwater quality assessment in parts of eastern Niger delta, Nigeria. *Environmental Geology*, 22, 41–46.
- Edet, A. E., & Okereke, C. S. (2001). A regional study of saltwater intrusion in southeastern Nigeria based on analysis of geoelectrical and hydrochemical data. *Environmental Geology*, 40(10), 1278–1289.
- Edet, A. (2005–2006). Groundwater vulnerability assessment using soil and hydrogeological data in the petroliferous Niger Delta, southern Nigeria. *Journal of Environmental Systems*, 32(2), 109–123
- Edet, A. (2008). Hydrogeochemical characteristics of groundwater in the in parts of the Niger Delta. In *Proceedings 1st Postgraduate Researchers Conference on Meeting Environmental Challenges in the Coastal Regions of Nigeria*. 29–30 September 2008. University of Abertay Dundee, United Kingdom.
- Edet, A. E. (2009). Characterization of groundwater contamination using factor analysis in the Niger Delta (Nigeria). *Journal of Hydrologic Engineering*, 14(11), 1255–1261.
- Edet, A (2017) Hydrogeology and groundwater evaluation of a shallow coastal aquifer, southern Aiwá Ibom State (Nigeria). *Applied Water*



- Science*, 7(5), 2397–2412. <https://doi.org/10.1007/s13201-016-0432-1>.
- Aniekan, E. (2018). Seasonal and spatio-temporal patterns, evolution and quality of groundwater in Cross River State, Nigeria: Implications for groundwater management. *Sustainable Water Resources Management*. <https://doi.org/10.1007/s40899-018-0236-6>.
- Edet, A., & Worden, R. (2009). Monitoring of Physical parameters and evaluation of the chemical composition of river and groundwater in Calabar (Southeastern Nigeria). *Environmental Monitoring Assessment*, 157, 243–258.
- Edet, A. E., Worden, R. H., Mohammed, E. A., & Preston, M. R. (2012). Hydrogeochemical processes in a populated shallow Coastal Plain Sand Aquifer southeastern Nigeria. *Environmental Earth Sciences*, 65, 1933–1953.
- Edet, A. E., Merkel, B. J., & Offiong, O. E. (2003). Trace element hydrochemical assessment of the Calabar Coastal Plain Sands, southeastern Nigeria using statistical methods. *Environmental Geology*, 44, 137–149.
- Edet, A., Ukpong, A., & Nganje, T. (2013). Hydrochemical studies of Cross River Basin (southeastern Nigeria) river systems using cross plots, statistics and water quality index. *Environmental Earth Sciences*, 70, 3043–3056.
- Ejiro, A. K., Anthony, A. I., & Oghenero, O.-A. (2015). Characterization of groundwater quality from surface geoelectrics: The case of the Sombreiro – Warri Deltaic Plain Aquifer, Western Niger Delta, Nigeria. *Journal of Environment and Earth Science*, 5(8), 5–12.
- El Moujabber, M., Bou Samra, B., Darwish, T., & Atallah, T. (2006). Comparison of different indicators for groundwater contamination by seawater intrusion on the Lebanese coast. *Water Resources Management*, 20, 161–180.
- Esu, E. O., & Amah, E. A. (1999). Physico-chemical and bacteriological quality of natural waters in parts of Akwa Ibom and Cross river States, Nigeria. *Global Journal of Pure and Applied Sciences*, 5(4), 525–552.
- Etu-Effetor, J. O. (1981). Preliminary hydrogeochemical investigations of subsurface waters in parts of the Niger Delta. *Journal of Geology and Mining*, 18(1), 103–107.
- Etu-Effetor, J. O., & Odigi, M. I. (1983). Water Supply problems in the eastern Niger Delta. *Journal Mining and Geology*, 20(1 & 2), 183–193.
- Etu-Effetor, J. O., & Akpokoje, E. G. (1990). Aquifer systems of the Niger Delta. *Journal of Mining and Geology*, 26(2), 279–284.
- Etu-Effetor, J. O. (2000). Hydraulic characteristics of the aquifers within the Oligocene-Recent Coastal Plains Sands part of southern Nigeria. *Global Journal of Pure and Applied Sciences*, 6(1), 107–115.
- Ewaid, S. H., & Abed, S. A. (2017). Water quality index for Al-Gharraf River, southern Iraq. *Egypt Journal of Aquatic Research*, 43(2), 117–122.
- Fakir, Y., Mernissi, M. E., Kreuser, T., & Berjami, B. (2002). Natural tracer approach to characterize groundwater in coastal Sahel of Qualidia (Morocco). *Environmental Geology*, 43, 197–202.
- Faye, S. P., Maloszewski, W., Stichler, P., Trimbom, S. C., & Gaye, C. B. (2005). Groundwater salinization in the Saloum (Senegal) delta aquifer: Minor elements and isotropic indicators. *Science of the Total Environment*, 343, 243–259.
- Fetters, C. W. (2001). *Applied hydrogeology* (4th ed., p. 598). Eaglewood Cliffs, NJ, USA: Prentice Hall.
- Fidelibus, M. D. (2003). Environmental tracing in coastal aquifers: Old problems and new solutions. In *Coastal Aquifer Intrusion Technology: Mediterranean Countries* (Vol II, pp. 79–111). Publ. IGME, Madrid.
- George, N. J., Akpan, A. E., & Akpan, F. S. (2017). Assessment of spatial distribution of porosity and aquifer geohydraulic parameters in parts of the Tertiary – Quaternary hydrogeoresource of south-eastern Nigeria. *NRIAG Journal of Astronomy and Geophysics*, 6(2), 422–433. <https://doi.org/10.1016/j.nrjag.2017.09.001>.
- Ghabayen, S. M. S., McKee, M., & Kemplowski, M. (2006). Ionic and isotopic ratios for identification of salinity sources and missing data in the Gaza aquifer. *Journal of Hydrology*, 318(1–4), 360–373.
- Giambastiani, B. M. S., Colombani, N., & Mastrocicco, M. (2013). Characterization of the lowland coastal aquifer of Comacchio (Ferrara, Italy): Hydrology, hydrochemistry and evolution of the system. *Journal of Hydrology*, 50, 53–44.
- Jalali, M. (2009). Geochemistry characterization of groundwater in an agricultural area of Razan, Hamadan, Iran. *Environmental Geology*, 56, 1479–1488.
- Khaska, M., La Salle, C.L., Lancelot, J., Aster Team, Mohammad, A., Verdoux, P., Noret, A., & Simler, R. (2013). Origin of groundwater salinity (current seawater vs saline deep water) in coastal karst aquifer based on Sr and Cl isotopes. Case study of the La Clape massif (southern France). *Applied Geochemistry*, 37, 212–227.
- Khodpanah, L., Sulaiman, W. N. A., & Khodpanah, N. (2009). Groundwater quality assessment for different purposes in Eshtehard District, Tehran, Iran. *European Journal of Scientific Research*, 36(4), 543–553.
- Kim, K., Rajmohan, N., Kim, H. J., Hwang, G. S., Cho, M. J. (2004). Assessment of groundwater chemistry in coastal region (Kunsan, Korea) having a complex contaminant sources: A stoichiometric approach. *Environmental Geology*, 46, 763–774. <https://doi.org/10.1007/s00254-004-1109-x>
- Kogbe, C. A. (1976). *Geology of Nigeria*. Lagos: Elizabeth Publishing Co.
- Krishnakumar, P., Lakshumanan, C., Kishore, V. P., Sundararajan, M., Santhiya, G., & Chidambaram, S. (2014). Assessment of groundwater quality in and around Vedaranyam, South India. *Environmental Earth Sciences*, 71, 2211–2225.
- Kumar, S. K., Logeshkumaran, A., Magesh, N. S., Godson, P. S., & Chandrasekar, N. (2015). Hydro-geochemistry and application of water quality index (WQI) for groundwater quality assessment, Anna Nagar, Part of Chennai City, Tamil Nadu, India. *Applied Water Science*, 5, 335–343.
- Li, P., Qian, H., & Wu, J. (2010). Groundwater quality assessment based on improved water quality index in Pengyang County, Ningxia, Northwest China. *European Journal of Advanced Chemistry Research*, 7(S1), S209–S216. <https://doi.org/10.1155/2010/451304>.
- Marghade, D., Malpe, D. B., & Zade, A. B. (2012). Major ion chemistry of shallow groundwater of a fast growing city of Central India. *Environmental Monitoring and Assessment*, 184, 2405–2418. <https://doi.org/10.1007/s10661-011-2126-3>.
- Min, J. H., Yun, S. T., Kim, K., Kim, H. S., & Kim, D. J. (2003). Geologic controls on the chemical behavior of nitrate in Riverside alluvial aquifers, Korea. *Hydrological Processes*, 17, 1197–1211.
- Mondal, N. C., Singh, V. P., Singh, V. S., & Saxena, V. K. (2010). Determining the interaction between groundwater and saline water through groundwater major ion chemistry. *Journal of Hydrology*, 388, 100–111.
- Mtoni, Y., Mjemah, I. C., Bakundukize, C., Camp, M. V., Martens, K., & Walraevens, K. (2013). Saltwater intrusion and nitrate pollution in the coastal aquifer of Dar es Salaam, Tanzania. *Environment and Earth Science*, 70, 1091–1111.
- Murat, R. C. (1972). Stratigraphy and paleogeography of the Cretaceous and Lower Tertiary in southern Nigeria. In T. F. G. Dessauvage & A. J. Whiteman (Eds.), *African Geology* (pp. 251–266). Geology Department: University of Ibadan.
- Ngh, S. A., & Nwankwoala, H. O. (2013). Assessment of Static Water Level Dynamics in parts of the Eastern Niger Delta. *The International Journal of Engineering and Science*, 2(11), 136–141.

- Nwankwoala, H. O., & Ngah, S. A. (2014). Groundwater resources of Niger Delta: Quality implications and management considerations. *International Journal of Water Resources and Environmental Engineering*, 6(5), 155–163.
- Offodile, M. E. (2014). *Hydrogeology: Groundwater supply and development in Nigeria* (3rd ed., 636pp).
- Ofoma, A. E., Omologbe, D. A., & Aigberua, P. (2005). Physico-chemical quality of groundwater in parts of Port-Harcourt city eastern Niger Delta, Nigeria. *Water Resources*, 16, 18–24.
- Okiongbo, K. S., & Soronadi-Ononiwu, G. C. (2015). Estimation of porosity and hydraulic conductivity of shallow quaternary alluvial aquifer in Yenogoa, southern Nigeria using electrical measurements. *IFE Journal of Science*, 17(2), 493–504.
- Omi, O., & Fasakin, O. (2016). The use of water quality index method to determine the potability of surface water and groundwater in the vicinity of a municipal solid waste dumpsite in Nigeria. *American Journal of Engineering Research*, 5(10), 96–101.
- Onwuka, O.S., & Omonona, O.V. (2017). Hydrogeochemical characteristics of coastal aquifers from Port Harcourt, southern Nigeria. *Environmental Earth Sciences*, 76(17), 609. <https://doi.org/10.1007/s12665-017-6933-x>.
- Park, Y., Lee, J.-Y., Kim, J.-H., & Song, S.-H. (2012). National scale evaluation of groundwater chemistry in Korea coastal aquifers: Evidences of seawater intrusion. *Environment and Earth Science*, 66, 707–718.
- Petters, S. W. (1982). Central West African Cretaceous-Tertiary Benthic Foraminifera and Stratigraphy. *Palaeontographica, A*, 179, 1–104.
- Pulido-Leboeuf, P. (2004). Seawater intrusion and associated processes in a small coastal complex aquifer (Castell de Ferro, Spain). *Applied Geochemistry*, 19, 1517–1527.
- Rai, N. S. (2004). *Role of mathematical modelling in groundwater resources management*. Hyderabad: Sri Vinayaka Enterprises.
- Rasaq, B. (2017). Investigation of Groundwater Potential and Aquifer Protective Capacity of Part of Effurun, Delta State, Nigeria. *International Journal Geology and Mining*, 3(3), 141–150.
- Reyment, R. A. (1965). *Aspects of the geology of Nigeria* (p. 145p). Nigeria: University of Ibadan Press.
- Revelle, R. (1941). Criteria for recognition of sea water in groundwater. *Transactions. American Geophysical Union*, 22(593), 597.
- Saeedi, M., Abessi, O., Sharifi, F., & Meraji. (2009). Development of groundwater index. *Environmental Monitoring and Assessment*. <https://doi.org/10.1007/s10661-009-0837-5>
- Sanchez-Martos, F., Pulido-Bosch, A., Molina-Sanchez, L., & Vallejos-Izquierdo, A. (2002). Identification of the origin of salinization in groundwater using minor ions (Lower Andarax, Southeast Spain). *Science of the Total Environment*, 297, 43–58.
- Short, K. C., & Stauble, A. J. (1976). Outline of the geology of the Niger Delta. *Bulletin—American Association of Petroleum Geologists*, 54, 761–779.
- Sinclair, A. J. (1974). Selection of thresholds in geochemical data using probability graphs. *Journal of Geochemical Exploration*, 3, 129–149.
- Sinclair, A. J. (1976). *Application of probability graphs in mineral exploration* (p. 95). Association of Exploration Geochemists, Rexdale.
- Slama, F. (2010). Field experimentation and modelling of salt transfer in Korba coastal plain: Impact of the seawater intrusion and irrigation practices. Ph.D. Thesis. University of Neuchatel, Centre of Hydrogeology, p. 112.
- Stumm, W., & Morgan, J. J. (1996). *Aquatic chemistry*. New York: Wiley.
- Stuyfzand, P. J. (1986). A new hydrogeological classification of water types: principles and application to the coastal dunes aquifer system of the Netherlands. In: *Proceedings 9th Salt Water Intrusion Meeting (SWIM): Delft, The Netherlands*, pp 641–656.
- Stuyfzand, P. J. (1993). *Hydrochemistry and hydrology of the coastal dune area of the Western Netherlands*. PhD dissertation. Free University (VU), Amsterdam. 90-74741-01-0:366
- Sukhija, B. S., Varma, V. N., Nagabhushanam, P., & Reddy, D. V. (1996) *Differentiation of paleomarine and modern seawater intruded salinities in coastal groundwaters (of Karaikal and Tanjavur, India)*.
- Trabelsi, R., Abid, K., Zouari, K., & Yahyaoui, H. (2012). Groundwater salinization processes in shallow coastal aquifer of Djefara plain of Medenine, Southern Tunisia. *Environmental Earth Sciences*, 66(2), 641–653.
- Udom, G. J., Esu, E. O., & Ekwere, S. J. (1998). Quality status of groundwater in Calabar Municipality, southeastern Nigeria. *Global Journal of Pure and Applied Sciences*, 4(2), 163–169.
- Udom, G. J., Etu-Efeotor, J. O., & Esu, E. O. (1999). Hydrochemical evaluation of groundwater in parts of Port Harcourt and Tai-Eleme Local Government Areas, Rivers State. *Global Journal of Pure and Applied Sciences*, 5(5), 545–552.
- Udom, G. J., & Amah, E. A. (2006). Quality status of groundwater in Yenogoa and its environs, Bayelsa State, Nigeria. *Journal of Scientific and Industrial Studies*, 4(1), 45–51.
- USDA. (1954). *Agriculture handbook No 60*. Washington DC, USA: United States Department of Agriculture, US Government Print Office.
- United States Salinity Laboratory (USSL). (1954). Diagnosis and improvement of saline and alkali soils. In *Agriculture handbook No 60* (pp. 69–81). US Department of Agriculture (USDA), Washington.
- Vasu, D., Singh, S. K., Tiwary, P., Sahu, N., Ray, S. K., Butte, P., & Duraisami, V. P. (2017). Influence of geochemical processes on hydrochemistry and irrigation suitability of groundwater in parts of semi-arid Deccan Plateau, India. *Applied Water Science*. <https://doi.org/10.1007/s13201-017-0528-2>.
- Vengosh, A., Gill, J., Davission, M. L., & Hudson, G. B. (2002). A multi-isotope (B, Sr, O, H and C) and age dating (3H, 3He and 14C) study of groundwater from Salinas Valley, California: Hydrochemistry, dynamics and contamination processes. *Water Resources Research*, 38(1), 1008. <https://doi.org/10.1029/2001WR000517>.
- Walraevens, K., Van Camp, M. (2005). *Advances in understanding natural groundwater quality controls in coastal aquifers* (pp 451–460). 18 Saltwater Intrusion Meeting (SWIM). Cartagena 2004, Spain.
- Walter, J., Chesnaux, R., Cloutier, V., & Gaboury, D. (2017). The influence of water/rock-water/clay interactions and mixing in salinization processes in groundwater. *Journal of Hydrology*, 13, 168–188.
- Wang, Y., & Jiao, J. J. (2012). Origin of groundwater salinity and hydrogeochemical processes in the confined quaternary aquifer of Pearl River Delta, China. *Journal of Hydrology*, 325(1–4), 35–55.
- Weber, K. J. (1971). Sedimentological aspects of oil fields in Niger delta. *Geologie En Mijnbouw*, 50, 559–576.
- Whiteman, A. J. (1982). *Nigeria: Its petroleum geology resources and potential* (Vols. 1 and 2, 394p). London: Graham and Trotman.
- Winograd, I. J., & Farlekas, G. M. (1974). Problem in 14C dating of waters from aquifers of deltaic origin. *Isotope hydrology* (pp. 69–93). Vienna: IAEA.
- Wood, W. W., & Sandford, W. E. (1995). Chemical and isotopic methods for quantifying groundwater recharge in a regional, semi-arid environment. *Groundwater*, 33, 458–468.
- World Health Organization (WHO). (1993). Guidelines for drinking water quality. In *Revision of the 181 Guidelines Final Task Group Meeting*, 21–25 Sept 1992, WHO Geneva, Switzerland.
- World Health Organization (WHO). (2004). *Guidelines for drinking water quality vole 1 recommendations* (3rd ed.). Switzerland: WHO Geneva.

- World Health Organization (WHO). 2006. *Guidelines for drinking water quality vol 1 recommendations* (3rd ed.) Geneva, Switzerland: WHO.
- WHO (2008) *The guideline for drinking-water quality 3rd edition incorporating the first and second addenda Vol 1 recommendations*. Geneva: World Health Organization.
- Wright, J. B. (1989). Review of the origin and evolution of the Benue Trough in Nigeria. In: C. A. Kogbe (Ed.), *Geology of Nigeria* (pp. 359–376). Rock View (Nigeria) Limited.
- Yolcubal, I., Gündüz, Ö. C. A., & Kurtuluş, N. (2019). Origin of salinization and pollution sources and geochemical processes in urban coastal aquifer (Kocaeli NW Turkey). *Environmental Earth Sciences*, 78, 181. <https://doi.org/10.1007/s12665-019-8181-8>.
- Zghibi, A., Tarhouni, J., & Zouhri, L. (2013). Assessment of seawater intrusion and nitrate contamination on the groundwater quality in the Korba coastal plain of Cap\_Bon (North-east of Tunisia). *Journal of African Earth Sciences*, 87, 1–12.



# Hydrogeophysical Investigation of Fractured Shale Aquifers in Ikwo and Environs, South-Eastern Nigeria

Amobi C. Ekwe, Georgebest Azuoko, Olufemi V. Omonona, Obialo S. Onwuka, and Julius Onwuka

## Abstract

Results obtained from the interpretation of vertical electrical sounding (VES) were combined with geological data to determine the groundwater potential of the study area. The dominant lithology in the area is the shales of the Asu River group of Albian age. The tectonic activities that took place in Santonian times resulted in folding, uplift, and intense fracturing of the shales of the study area. The challenge lies on how to map the fracture zones in the shales in order to optimally exploit the groundwater resources in the area. Ten (10) vertical electrical soundings (VESs) with maximum current electrode (AB) spread of 300 m were acquired using the Schlumberger configuration. Four (4) of the soundings were carried out near existing boreholes for comparative purposes between the geological and geoelectric sections. Layer parameters (aquifer thickness, depth to water, transverse resistance, etc.) were obtained after data processing with the IP12 Win™ software. The derived layer parameters were combined with borehole logs and pumping test data from existing boreholes to estimate aquifer hydraulic parameters in other locations without boreholes. Results show that the depth to the fractured shale aquifer ranges from 22.1 to 54.9 m at Ekpelu (VES 9) and Ndufu Alike II (VES 2), respectively, while aquifer thicknesses vary from 19 m at Ndufu Alike I and II (VES 1 and VES 2) to 56.4 m at Amainyima (VES 10). Hydraulic conductivity varies between 0.0047 m/day at Ndufu Alike I (VES 1) and 0.300 m/day at Onyikwa playground (VES 5), while

transmissivity varies between 0.0893 m<sup>2</sup>/day at Ndufu Alike I (VES 1) and 9.780 m<sup>2</sup>/day at Onyikwa Playground (VES 5).

## Keywords

Aquifer parameters • Vertical electrical sounding • Fractures • Groundwater

## 1 Introduction

Shales are defined as non-aquifers on hydrogeology maps and often overlooked as a source of sustainable source of groundwater supply in poor communities not underlain by conventional aquifer materials like sandstones (Struckmier and Margarat 1995). MacDonald and Davies (2000) have shown that approximately 70 million people in Sub-Saharan Africa live in rural communities underlain by shales and mudstones. Many of such communities are located within Ikwo and environs, and the areas have continued to witness a surge in population following the establishment of a Federal University in the area. The entire area is underlain by consolidated shales of the Asu River group. It is a well-known fact that shales are classified as low permeability formations because of little or no interconnectivity between individual pores within the rock matrix. The permeability of the shales can be greatly enhanced when fractured. Fractured shale aquifers can yield significant volumes of water because of their enhanced porosity and permeability. Several workers have used the electrical resistivity method to characterize aquifer types and geometry (Onuoha & Mbazi, 1988; Ekwe et al., 2006; Ekwe & Opara, 2012; Opara et al., 2012). Some more recent works have been done by employing the electrical resistivity to prospect for water in low permeability formations (e.g., shales) and hard rock terrains (Ekwe et al., 2010; Omeje et al., 2015; Loke et al., 2013; Okonkwo & Ezeh, 2013; Okonkwo et al., 2017). MacDonald et al. (2001)

A. C. Ekwe (✉) · G. Azuoko · O. V. Omonona  
Department of Geology and Geophysics, Alex Ekwueme Federal University Ndufu Alike, Ebonyi, Nigeria  
e-mail: [amobiekwe@yahoo.com](mailto:amobiekwe@yahoo.com)

O. S. Onwuka  
Department of Geology, University of Nigeria, Nsukka, Nigeria

J. Onwuka  
Department of Geophysics, Federal University Oye Ekiti, Ekiti, Nigeria

applied geophysical techniques to locate groundwater in low permeability sedimentary rocks in southeast Nigeria. The present study would involve the integration of geophysics, geology, and geographic information system (GIS) to map and characterize the fractured shale aquifers of Ikwo and environs to guide water resource planners and developers in the area.

## 2 Location of the Study Area

The study area (Fig. 1) falls within Ikwo local government area of Ebonyi state and has an elevation profile of about 100 m above the mean sea level. Some important towns within the study area include Amegu, Nwakpu, Enyigba, and Ndufu Alike. The area is situated within the tropical rain

forest of Nigeria. Two seasons are prominent in the area—dry and rainy seasons. It has a humid tropical climate with high temperature, with a mean daily maximum and minimum annual temperatures of 32.2 and 23 °C, respectively. The annual rainfall rate is about 1820 mm, while mean daily temperature ranges from 30 °C during the rainy season to about 34 °C in the dry season. The annual mean of the relative humidity in the area is 71%, while the rate of evaporation is about 3.4 mm/yr. Soil temperature measurements at depths of 5, 10, 20, 30, 50, and 100 cm gave values of 32, 31, 30, 30.5, 27, and 30 °C, respectively, while the average monthly sunshine hours for the months of February–June 2014 are about 6.6 h (Federal University Ndufu Alike Ikwo Weather Station data, 2014). The study area is drained by the Ebonyi River and its numerous tributaries. The pattern is dendritic.

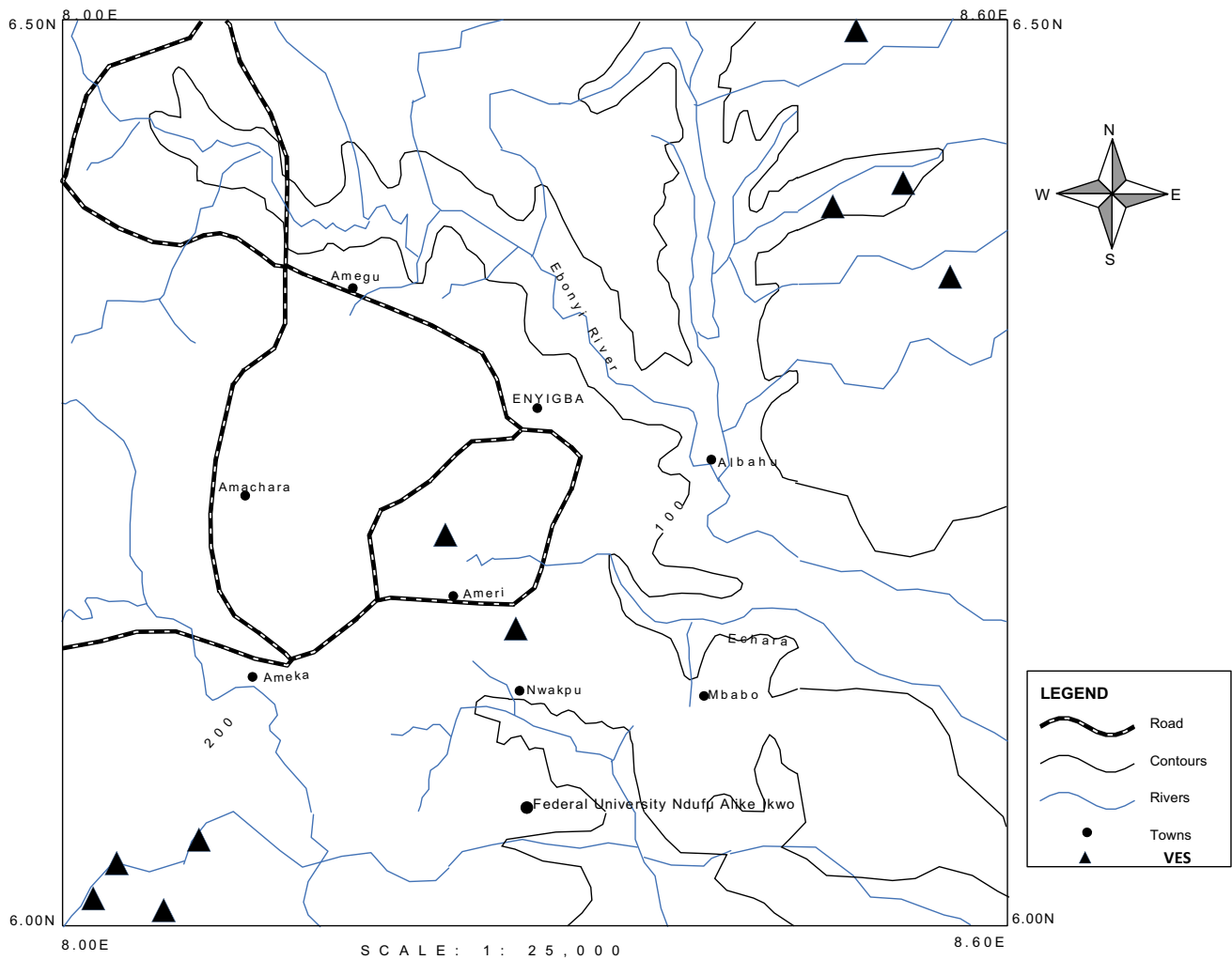


**Fig. 1** Topographic map of the study area showing VES points, important towns, and drainage pattern



### 3 Geology of the Study Area

The study area lies within the Lower Benue Trough. The Benue Trough is a SW-NE trending elongate structure with a sedimentary fill ranging from over 2000 m in the northern limit to 7000 m in the southern region. The lithologic unit underling the study area is mainly the shales of the Asu River group (Fig. 2) and the Abakaliki shale formation (Reyment, 1965). The shales are fissile, thinly laminated, highly fractured, and weathered. The shales have been classified based on their lithologic characteristics, structures, and stratigraphic positions by Obarezi and Nwosu (2013) into two units with colors ranging from dark to black to grayish brown, reddish, and pinkish.

### 4 Methodology

A detailed literature review was carried out before actual field work and subsequent acquisition of ten (10) vertical soundings (VESs) with the Schlumberger configuration. The method involves the injection of direct current (5 mA) from a 12 V battery source into the ground through a pair of current electrodes and measuring the resulting potentials through another pair of potential electrodes. The geoelectrical data was acquired using ABEM SAS 1000, with a maximum current electrode spacing (AB) of 300 m. Few of the soundings were carried out near existing boreholes for comparative purposes. The data obtained was plotted as a graph of apparent resistivity against half current electrode

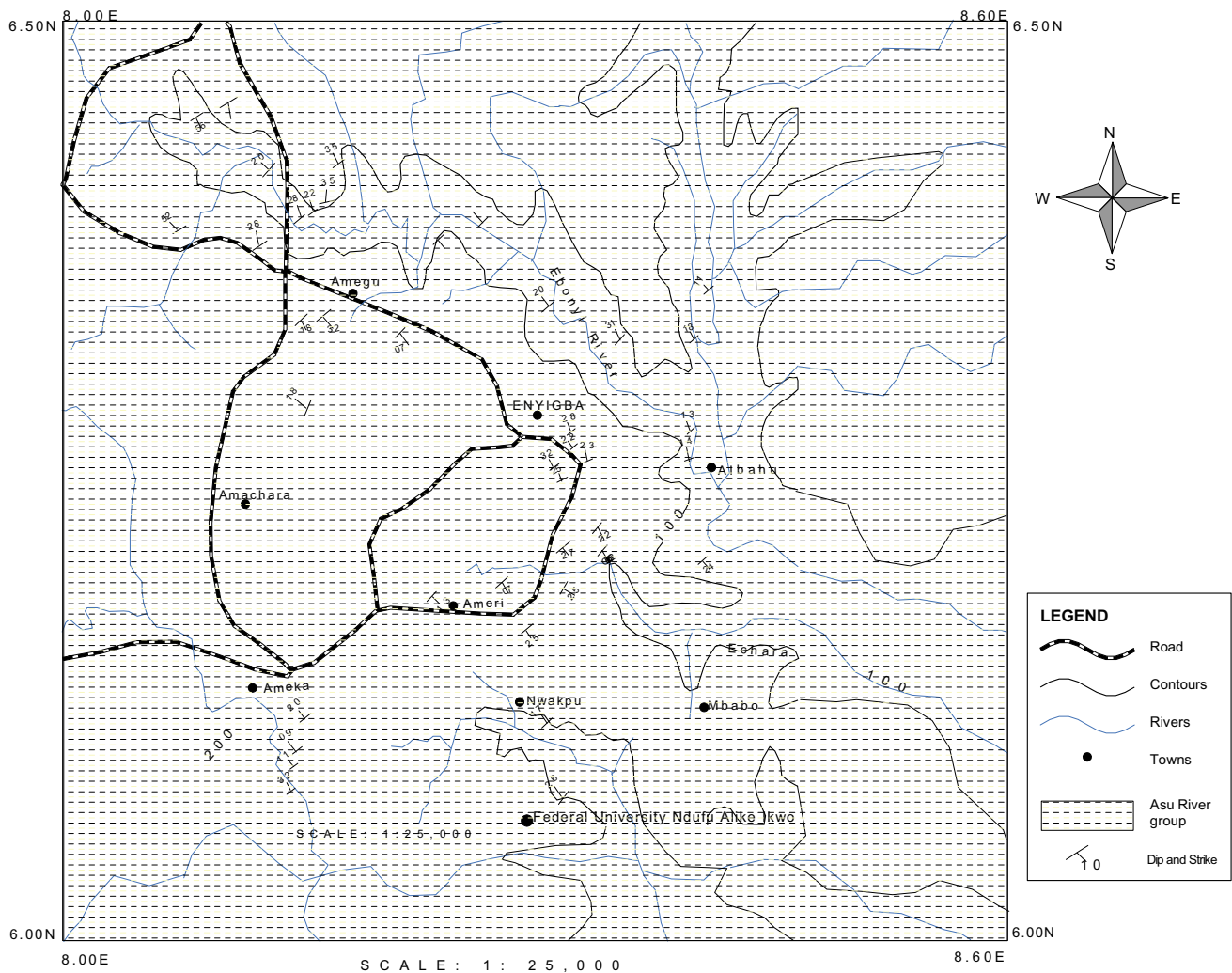


Fig. 2 Geologic map of the study area

spacing and the electrode spacing at which inflection occurs on the graph provides an idea of the depth to the interface. The apparent resistivity ( $\rho_a$ ) for the Schlumberger array is given by Eq. 1.

$$\rho_a = \pi R \left( \frac{a^2}{b} - \frac{b}{4} \right) \quad (\text{Keller \& Frischknecht, 1979; Ekwe et al., 2006}) \quad (1)$$

where  $a$  = half current electrode spacing,  $b$  = potential electrode spacing,  $R$  = resistance, while  $\pi \left( \frac{a^2}{b} - \frac{b}{4} \right)$  is the geometric factor. The geometric factor depends on the electrode configuration in use. The apparent resistivity ( $\rho_a$ ) is usually obtained by multiplying the measured resistance with the geometric factor.

## 5 Determination of Aquifer Hydraulic Parameters from Geoelectrical Data

Previous researchers have shown that in areas of similar geology and water quality, the product of hydraulic conductivity ( $K$ ) and electrical conductivity ( $\sigma$ ) remains fairly constant (Niwas & Singhal, 1981; Onuoha & Mbazi, 1988; Ekwe et al. 2006; Okonkwo & Ezech, 2013). An empirical relation exists between aquifer transmissivity and transverse resistance on the one hand, and aquifer transmissivity and longitudinal conductance on the other hand (Niwas & Singhal, 1981). It is given by:

$$T = K\sigma R = KS/\sigma \quad (2)$$

where  $T$  = aquifer transmissivity,  $h$  = aquifer thickness,  $\rho$  = aquifer resistivity,  $K$  = hydraulic conductivity,  $R = h\rho$  = transverse resistance of the aquifer, and  $S = \frac{h}{\rho}$  = longitudinal conductance.

One of the problems we encountered in the study area was the paucity of pumping test data at all the VES locations. The pumping test data can be used to generate aquifer parameters at known borehole locations, but the cost is usually high. To overcome this challenge, we applied the empirical relation developed by Niwas and Singhal (1981) to estimate various aquifer parameters at all the sounding locations, including areas where no boreholes exist. In these instances, we extracted  $K$  values from pumping tests at sites with boreholes and used those values to estimate  $K$  for other areas without boreholes.

## 6 Results and Interpretation

### 6.1 Comparison of Geoelectrical Section with Lithology Log at Eke Ettem Market Square, Ikwo

The first geoelectric layer (Fig. 3) with an apparent resistivity of 135  $\Omega\text{m}$  correlates well with a moist reddish clayey overburden on the lithology log. The second geoelectric layer has a resistivity of 265  $\Omega\text{m}$  and corresponds to a hard dark grayish shale. The third geoelectric layer has a resistivity of 59.7  $\Omega\text{m}$  and correlates with a semi-hard shale layer on the lithology log. The fourth geoelectric layer with a resistivity of 17.2  $\Omega\text{m}$  correlates with a moist grayish shaley layer on the lithology log. The fifth geoelectric layer with a resistivity of 12.6  $\Omega\text{m}$  correlates with a fractured shale aquifer at a depth of 38.4 m. The aquiferous layer is underlain by a hard shale layer with a resistivity of 797  $\Omega\text{m}$ . The processed curve is shown in Fig. 4.

### 6.2 Comparison of Geoelectrical Section with Lithology Log at Ekpelu

The first geoelectric layer with an apparent resistivity of 733  $\Omega\text{m}$  coincides with the reddish brown lateritic overburden. The second (340  $\Omega\text{m}$ ) and third (32.1  $\Omega\text{m}$ ) geoelectric layers correlates with yellowish and moderately soft shale layers, respectively. The fourth geoelectric layer with an apparent resistivity of 46.9  $\Omega\text{m}$  correlates with the fractured dark shale layer, which serves as the aquifer, while the last geoelectric layer has an apparent resistivity value of 458  $\Omega\text{m}$  and corresponds with the hard grayish shale layer in the lithology log (Fig. 5). The processed curve is shown in Fig. 6.

### 6.3 Comparison of Geoelectrical Section with Lithology Log at Elugu Ettem, Ikwo

The first geoelectric layer has an apparent resistivity of value of 875.9  $\Omega\text{m}$  and correlates with a reddish brown lateritic overburden on the lithologic log. The second and third layers have resistivity values of 136.8 and 48.15  $\Omega\text{m}$ , respectively. These layers correspond to a light grayish hard shale and mottled shale layers on the lithology log. The fractured shale

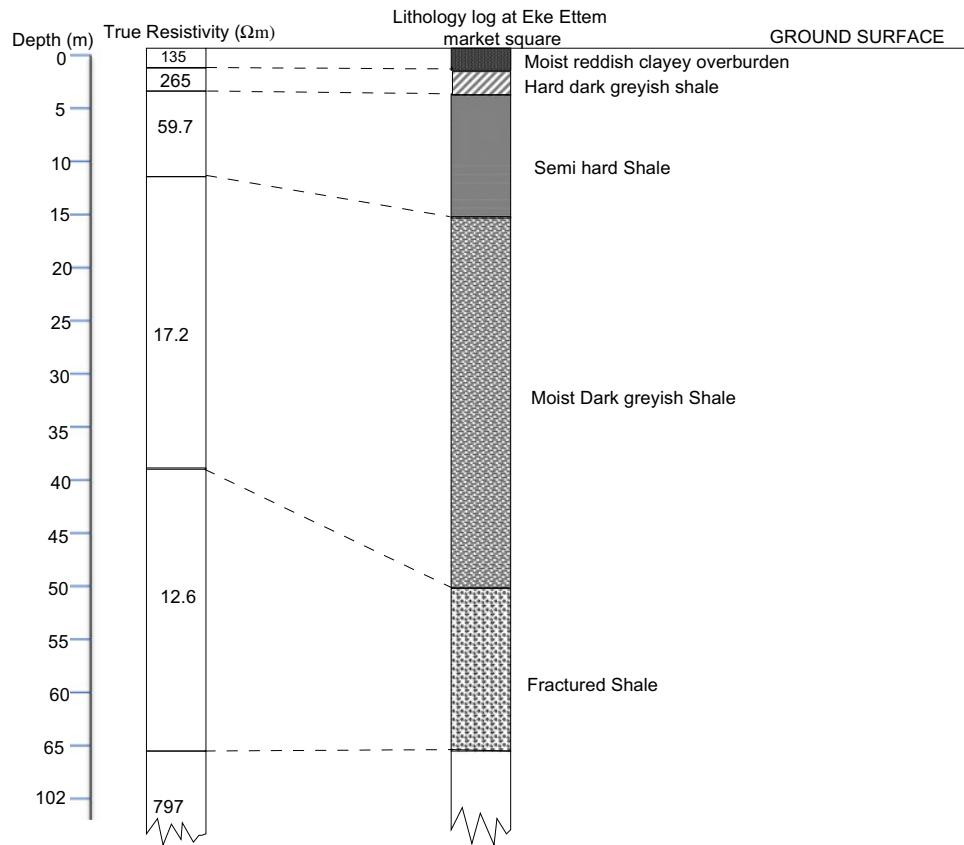


Fig. 3 Comparison of geoelectrical section with lithology log at Eke Ettem market square, Ikwo

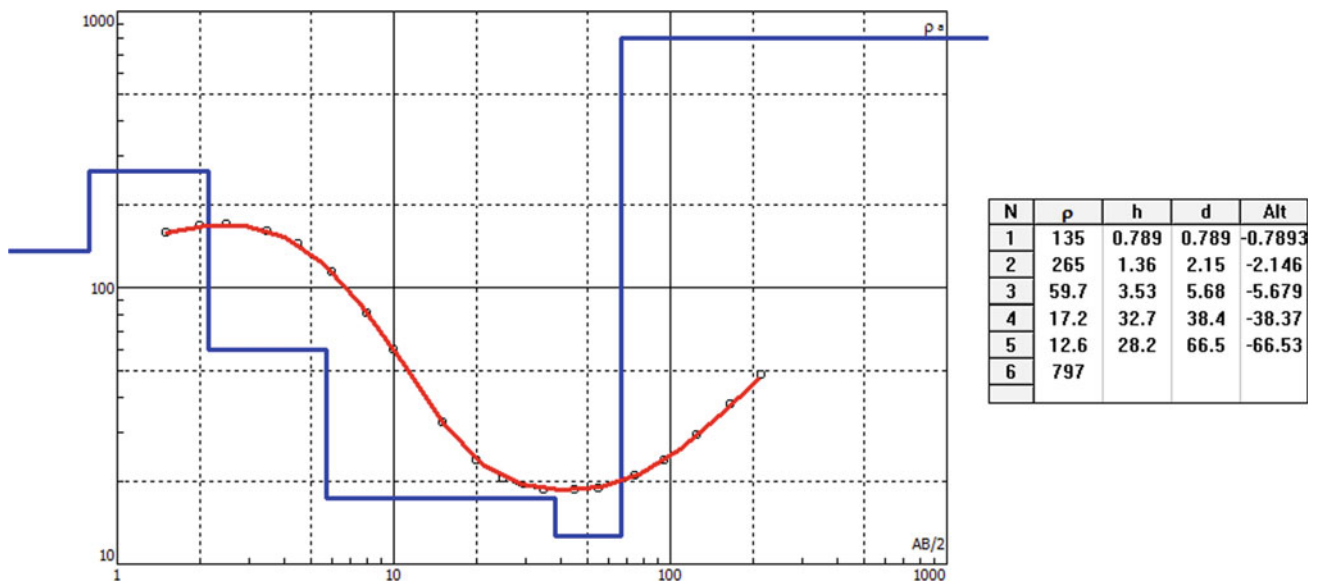


Fig. 4 Processed vertical electrical sounding result at Eke Ettem market square, Ikwo

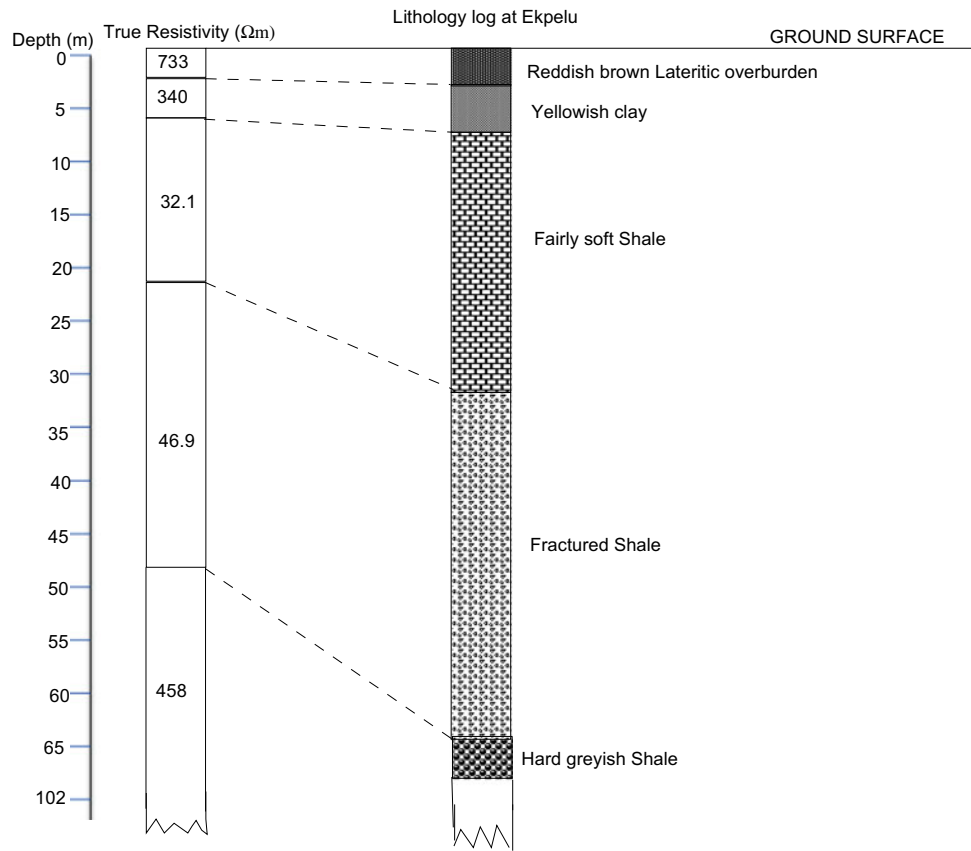


Fig. 5 Comparison of geoelectrical section with lithology log at Ekpelu, Ikwo

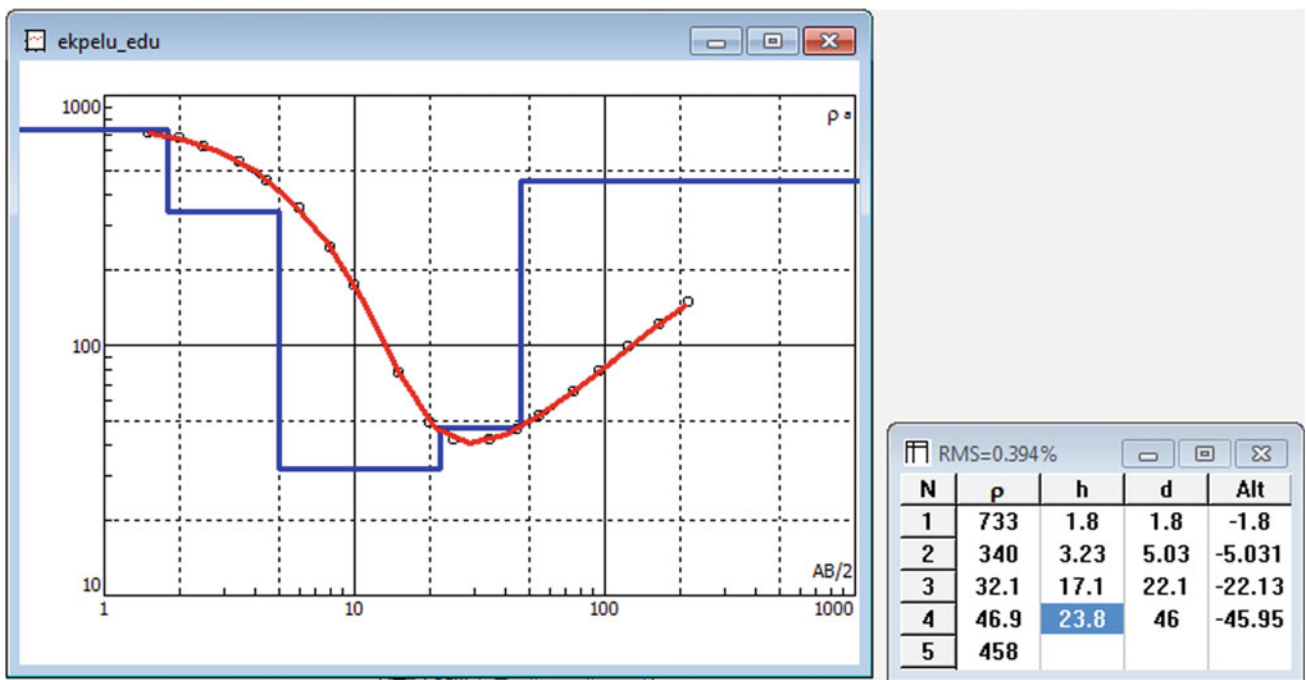


Fig. 6 Processed vertical electrical sounding result at Ekpelu, Ikwo

layer which serves as the aquifer has an apparent resistivity value of 26.26  $\Omega\text{m}$ . The aquiferous layer is underlain by a dark hard shale layer of indeterminate thickness and a resistivity of 300.9  $\Omega\text{m}$  (Fig. 7). The processed curve is shown in Fig. 8.

### 6.4 Comparison of Geoelectrical Section with Lithology Log at Amainyima, Ikwo

Five geoelectric layers (Fig. 9) were delineated with the first two layers correlating with a reddish brown lateritic

**Fig. 7** Comparison of geoelectrical section with lithology log at Elugu Ettem borehole, Ikwo

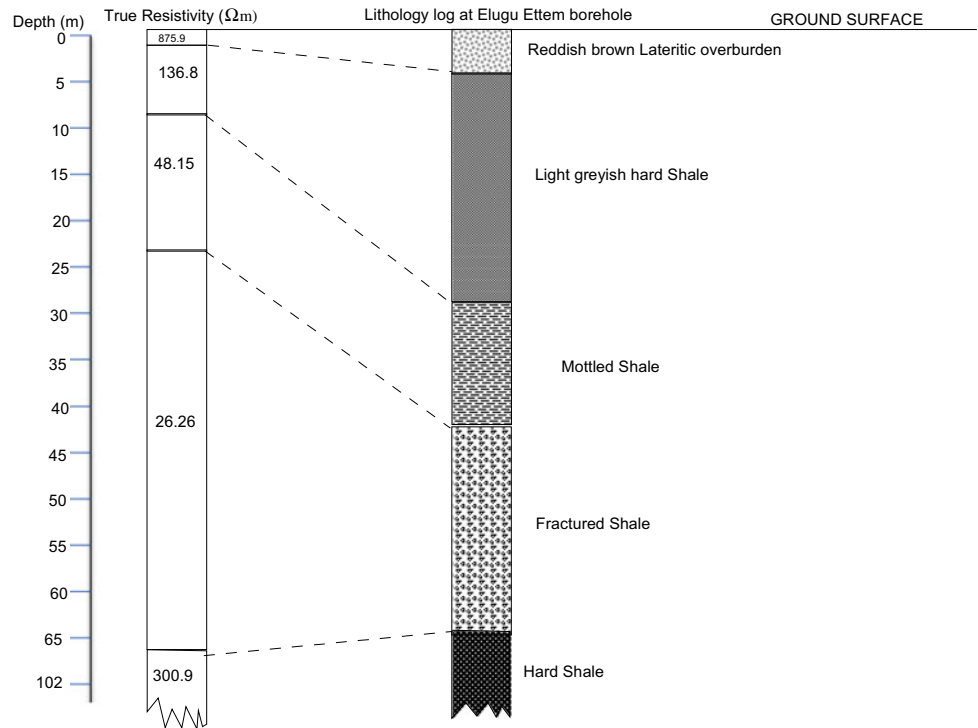


**Fig. 8** Processed vertical electrical sounding result at Elugu Ettem, Ikwo

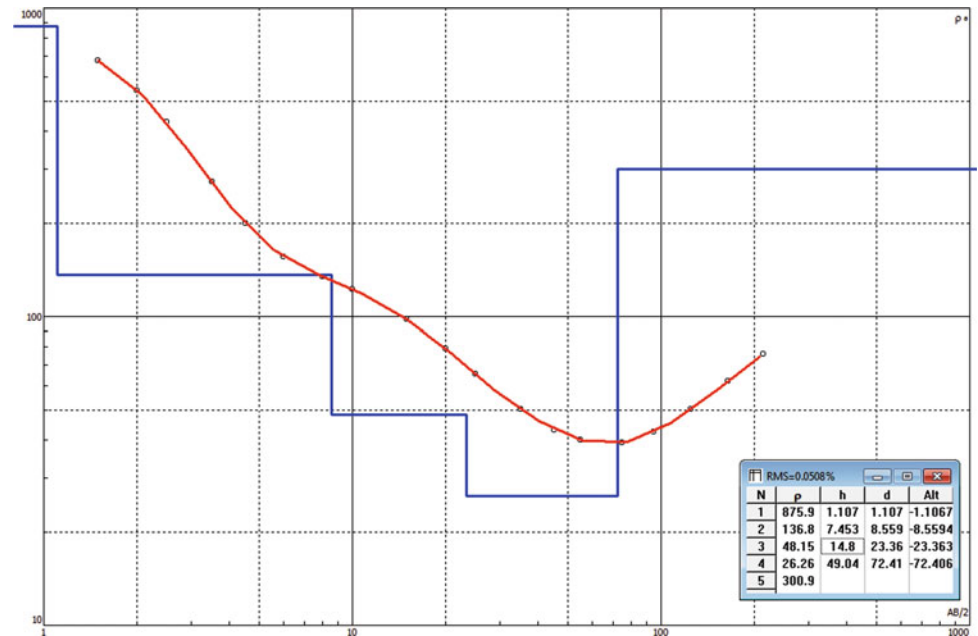
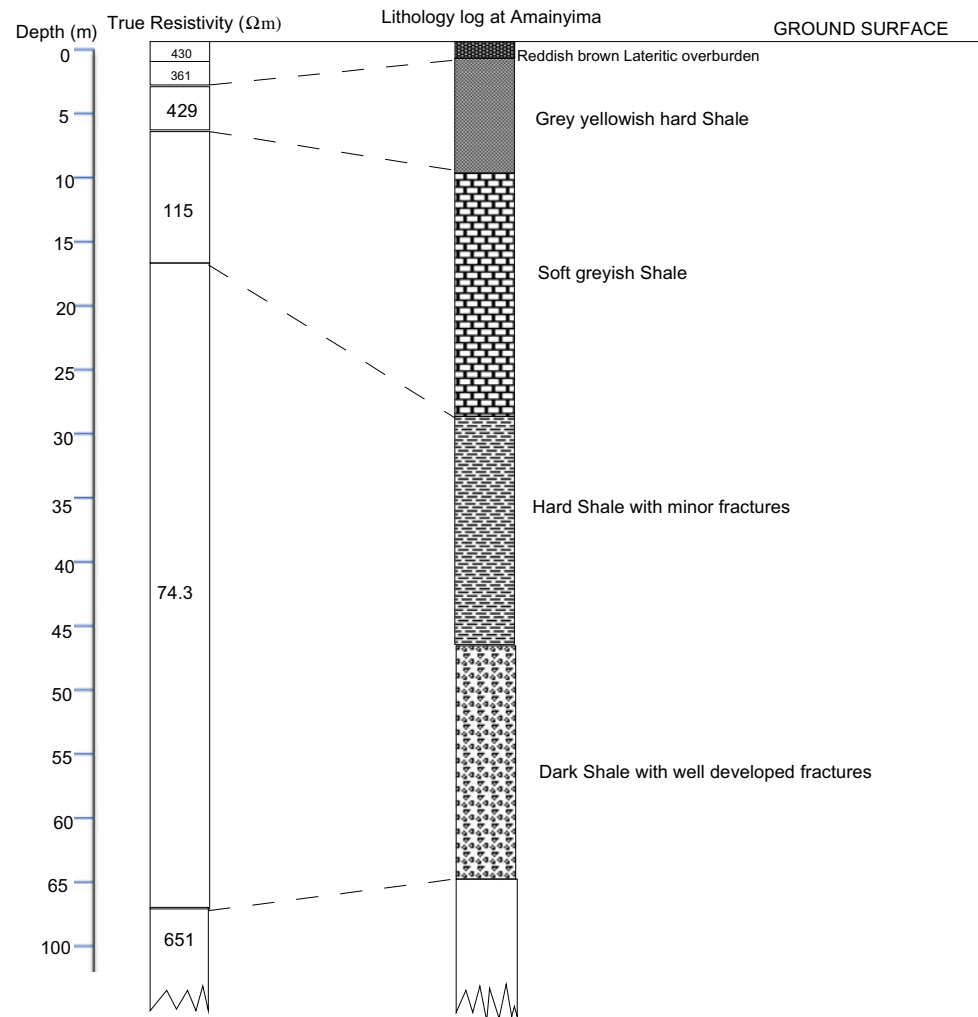




**Fig. 9** Comparison of geoelectrical section with lithology log at Elugu Ettem borehole, Ikwo



overburden with a resistivity of 430  $\Omega\text{m}$ . The third geoelectric layer with a resistivity of 429  $\Omega\text{m}$  correlates with a yellowish gray hard shale on the lithology log. The resistivity value dropped to 115  $\Omega\text{m}$  in the fourth layer which corresponds to a soft grayish shale layer. The aquiferous layer has a resistivity of 74.3  $\Omega\text{m}$  with an upper layer corresponding to a hard dark shale with minor fractures which is underlain by a dark shale layer with well-developed fracture framework. The aquiferous layer is underlain by a hard dark shale layer of undefined thickness and a resistivity of 651  $\Omega\text{m}$ . The processed curve is shown in Fig. 10.

## 7 Aquifer Parameters from Geosounding Data

The depth to the fractured shale aquifer ranges from 22.1 to 54.9 m at Ekpelu and Ndufu Alike, respectively, while aquifer thicknesses varies from 19 m at Ndufu Alike to 56.4 m at Amainyima. Hydraulic conductivity varies

between 0.0047 m/day at Ndufu Alike I and 0.3 m/day at Onyikwa Playground, while transmissivity varies between 0.0893  $\text{m}^2/\text{day}$  at Ndufu Alike Ikwo and 9.78  $\text{m}^2/\text{day}$  at Onyikwa Playground (Table 1).

## 8 Discussion and Conclusion

The results compare well with those obtained from pumping tests and other statistical analysis methods from other research works in Abakaliki area and environs (Ozoko, 2012; Ozoko, 2014; Onwe et al., 2020). The obtained aquifer parameters are compared well with earlier results by MacDonald et al. (2005). This shows that electrical resistivity survey is a useful technique for understanding the hydraulic characteristics of the aquifer system within the study area. Computer-modeled interpretation techniques were used to resolve the true thicknesses, resistivities, and depths to the fractured shale aquifers. The depth to the fractured shale aquifer ranges from 22.1 to 54.9 m at Ekpelu

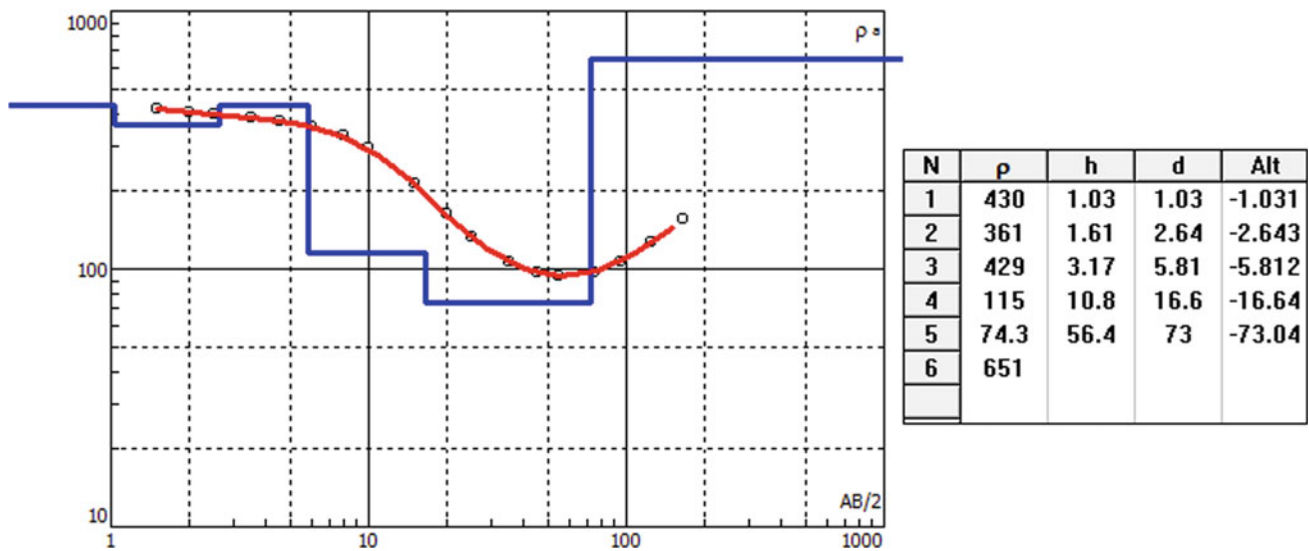


**Fig. 10** Comparison of geoelectrical section with lithology log at Elugu Ettem borehole, Ikwo

**Table 1** Derived aquifer parameters of the study area

VES No.	Location	Depth to water (m)	Aquifer thickness b (m)	Aquifer resistivity, $\rho$ ( $\Omega\text{m}$ )	Transverse resistance, $\rho b$ ( $\Omega\text{m}^2$ )	K from wells m/day	$K\sigma$	$K\sigma_{AVE}$	K from geosounding data m/day	T/m <sup>2</sup> /day
1	Ndufu Alike 1	48.4	19.0	14.6	277.4			0.0032	0.0047	0.0893
2	Enyim Ogidiga road (Ndufu Alike II)	54.9	19.0	22.6	429.4			0.0032	0.0723	1.3737
3	Ekpa Omaka	34.8	23.7	13.4	317.58			0.0032	0.0429	1.0167
4	Comm. Prim. school Ohatekwe	38.8	27.5	10.3	283.25			0.0032	0.0330	0.9075
5	Onyikwa playground	54.1	32.6	93.9	3061.14			0.0032	0.3000	9.7800
6	Comm. Pri. school Igweledoha	33.2	26.3	38.9	1023.07			0.0032	0.1245	3.2744
7	Eke Ettem market square	38.4	28.2	12.6	355.32	0.0564	0.0045	0.0032	0.0403	1.1365
8	Elugu Ettem playground	23.36	49.04	23.26	1140.67	0.0542	0.0023	0.0032	0.0744	3.6486
9	Ekpelu	22.1	23.8	32.1	763.98	0.1282	0.0040	0.0032	0.1027	2.4440
10	Amainyima	25.8	56.4	25.8	1795.68	0.0484	0.0019	0.0032	0.0826	4.6586

(VES 9) and Ndufu Alike II (VES 2), respectively, while aquifer thicknesses vary from 19 m at Ndufu Alike I and II (VES 1 and 2) to 56.4 m at Amainyima (VES 10). Hydraulic conductivity varies between 0.0047 m/day at Ndufu Alike I (VES 1) and 0.300 m/day at Onyikwa playground (VES 5),

while transmissivity varies between 0.0893 m<sup>2</sup>/day at Ndufu Alike I (VES I) and 9.780 m<sup>2</sup>/day at Onyikwa playground (VES 5). We recommend that a hydrochemical study be carried out to determine the potability of the water for both industrial and domestic uses.

## References

- Ekwe, A. C., Nnodu, I. N., Ugwumbah, K. I., & Onwuka, O. S. (2010). Estimation of aquifer hydraulic characteristics of low permeability formations from geosounding data: a case study of Oduma Town, Enugu State. Online. *Journal of Earth Sciences*, 4(1), 19–26. <https://doi.org/10.3923/ojesci.2010.19.26>.
- Ekwe, A. C., Onu, N. N., & Onuoha, K. M. (2006). Estimation of aquifer hydraulic characteristics from electrical sounding data: The case of middle Imo River basin aquifers, southeastern Nigeria. *Journal of Spatial Hydrology*, 6(2), 121–132.
- Ekwe, A. C., & Opara, A. I. (2012). *Aquifer transmissivity from surface geo-electrical data: A case study of Owerri and environs*, South-eastern Nigeria
- Keller, G. V., & Frischnecht, F. C. (1979). *Electrical methods in geophysical prospecting* (pp. 91–135). New York: Pergamon Press.
- Loke, M. H., Chambers, J. E., Rucker, D. F., Kuras, O., & Wilkinson, P. B. (2013). Recent developments in the direct-current geoelectrical imaging method. *Journal of Applied Geophysics*, 95, 135–156.
- MacDonald, A.M., & Davies, J. (2000). *A brief review of groundwater for rural water supply in sub-Saharan Africa*. British Geological Survey Technical Report WC/00/33.
- MacDonald, A. M., Davies, J., & Peart, R. J. (2001). Geophysical methods for locating groundwater in low permeability sedimentary rocks: Examples from southeast Nigeria. *Journal of African Earth Sciences*, 32, 115–131.
- MacDonald, A. M., Kemp, S. J., & Davies, J. (2005). Transmissivity variations in Mudstones. *Ground Water*, 43, 259–269. <https://doi.org/10.1111/j.1745-6584.2005.0020.x>.
- Okonkwo, A. C., & Ezech, C. C. (2013). Aquifer hydraulics and delineation of groundwater quality zones using electrical resistivity method at Oduma and environs in Enugu State, Southeastern Nigeria. *International Research Journal of Geology and Mining (IRJGM)* (2276–6618), 3(1), 31–39
- Okonkwo, A. C., Ezech, C. C., Ugwu, G. Z., & Ogbonnaya, B. J. (2017). Georesistivity, aquifer hydraulic characteristics and groundwater potential zones of Mpu Town and Environs, Enugu State, Nigeria. *Elixir Geology*, 111, 48730–48736
- Obarezi, J. E., & Nwosu, J. I. (2013). Structural controls of Pb-Zn mineralization of Enyigba district, Abakaliki, Southeastern Nigeria. *Journal of Geology and Mining Research*, 5(11), 250–261.
- Omeje, M., Ebele, J. E., & Ugwuoke, P. E. (2015). Geophysical Analysis of Basement Terrain Groundwater Using Vertical Electrical Sounding: A Case Study of Parts of Abuja North Central Nigeria. *International Journal of Geophysics and Geochemistry*, 2(4), 92–97.
- Onuoha, K. M., & Mbazi, F. C. C. (1988). Aquifer transmissivity from electrical sounding data. The case of Ajali Sandstone Aquifers, South-West of Enugu. In: C.O. Ofoegbu (Ed.), *Ground water and mineral resources of Nigeria* (pp. 17–29). Wiesbaden: Fried-vieweg and Sohn.
- Onwe, M. R., Nwankwor, G. I., Ahirakwem, C. A., Abraham, E. M., & Emberga, T. T. (2020). Assessment of geospatial capability index for siting waste dump/landfill to control groundwater geopollution using geographic information system (GIS) approach: Case study of Abakaliki area and environs, Southeastern Nigeria. *Applied Water Science*, 10(12), 1–19.
- Opara, A. I., Onu, N. N., & Okerefor, D. U. (2012). Geophysical sounding for the determination of aquifer hydraulic characteristics from Dar-Zarrouk parameters: Case study of Ngor Okpala, Imo River Basin, Southeastern Nigeria. *Pacific Journal of Science and Technology*, 13(1), 590–603.
- Ozoko, D. C. (2014). Hydraulic properties of Abakaliki Shale-Regolith Aquifer, in Ebonyi State South Eastern Nigeria. *Journal of Environment and Earth Science*, 4(12), 95–105.
- Ozoko. (2012). Hydrogeochemical and Microbial Characteristics of Abakaliki Shales, Ebonyi State, Nigeria. *Journal of Environmental Hydrology*, 20(5), 1–9.
- Reyment, R. A. (1965). Aspects of the geology of Nigeria. University of Ibadan press, pp 145.
- Struckmeir, W. F., & Margarat, J. (1995). Hydrogeological maps: a guide and standard legend. *International Contributions to Hydrogeology: Vol. 17. International Association of Hydrogeologists*. Hanover: Heise.